Hurricane Surge Hazard Analysis: The State of the Practice and Recent Applications for Southeast Louisiana

prepared for

The Southeast Louisiana Flood Protection Authority—East

Task Order 02-03-006

prepared by

Bob Jacobsen PE, LLC

Baton Rouge, Louisiana

May 2013

Hurricane Surge Hazard Analysis: The State of the Practice and Recent Applications for Southeast Louisiana

prepared for

The Southeast Louisiana Flood Protection Authority—East

Task Order 02-03-006

prepared by

Bob Jacobsen PE, LLC

Baton Rouge, Louisiana

May 2013

Cover photographs taken from Figure 2, in *Hurricane Gustav (2008) Waves and Storm Surge: Hindcast, Synoptic Analysis, and Validation in Southern Louisiana* by J. C. Dietrich et al (Monthly Weather Review, Vol. 139, 2488 – 2522. See References for Part II)

Don't cross a river if it is four feet deep on average.

Nassim Nicholas Taleb
The Black Swan: The Impact of the Highly Improbable (2007)

…the amount of confidence someone expresses in a prediction is not a good indication of its accuracy—to the contrary, these qualities are often inversely correlated.

Nate Silver
The Signal and the Noise: Why So Many Predictions Fail, But Some Don't (2012)

Crying won't help you, praying won't do you no good.
Crying won't help you, praying won't do you no good.
When the levee breaks, mama, you got to move.

Kansas Joe McCoy and Memphis Minnie
When the Levee Breaks (1929)

This Report is dedicated to the families of New Orleans. Over the centuries we have reaped extensive benefits from hurricane surge risk management, but have endured tremendous suffering when this management has been inadequate. Today, thanks to federal investment, we enjoy greater hurricane surge risk reduction than millions of residents in other major port cities along the Gulf of Mexico and Atlantic coasts.

It is now increasingly up to us to maintain and improve surge risk management in the face of regional subsidence, coastal land loss, rising global temperatures and sea levels, changing and highly uncertain hurricane probabilities, levee settlement, and diminishing federal funding. Moreover, we must help confront severe surge risks to the residents of outlying communities and a fragile deltaic ecosystem. To meet these challenges, it is now up to us to ensure that we have the best surge hazard analysis and—just as importantly—that we understand and apply it.

About the Author

Bob Jacobsen is a 50-year resident of southeast Louisiana and his connection to the coast and New Orleans regional surge protection is both professional and personal.

Over the years Mr. Jacobsen has pursued education in both environmental policy and engineering, receiving Master's degrees from Louisiana State University in both Political Science and Civil Engineering. As time permits, he continues to work towards a PhD in Civil Engineering, with an emphasis on coastal hydrodynamics.

Mr. Jacobsen's 33-year career has focused on state-of-the-art planning studies and conceptual designs in environmental and water resource engineering and related program fields. During the first 20-years he worked on an array of major environmental contamination problems, including remediation of contaminated sediments for Superfund sites and scenic water bodies, removal of carcinogenic pollutants from important aquifers, and upgrading petrochemical wastewater treatment systems. Since 2001 he has specialized in hydrology/hydraulics issues in coastal Louisiana—encompassing both hurricane storm surge and coastal restoration. His wide ranging experience has allowed him to hone a blend of field, analytical, construction, and management skills, providing him with a unique perspective on south Louisiana environmental sustainability dynamics.

In the years following Hurricane Katrina Mr. Jacobsen worked on numerous coastal hydrodynamic projects for southeast Louisiana, including i) an hydraulic feasibility study for a proposed Mississippi River diversion near Garyville LA (lead author); ii) an analysis of the role played by the Mississippi River Gulf Outlet in conveying storm surge (lead author); iii) modeling of Lake Pontchartrain tidal exchange (lead author); iv) assessment of hurricane surge interactions with coastal landscape features (contributor); and v) an investigation of LIDAR topographic data accuracy and potential ADCIRC mesh improvements for the southeast Louisiana hurricane surge hazard analysis (contributor).[1] Between 2007 and 2011 he provided senior technical review on a surge hazard study for South Carolina and authored key reports for planning a surge hazard analysis for Georgia and Northeast Florida. In 2011 he started his own consulting practice in coastal hydrology and hydrodynamics.

Mr. Jacobsen has served on the local Baton Rouge Branch and Louisiana Section Boards for the American Society of Civil Engineers and is currently President-Elect for the Louisiana Section.[2]

His mother and sister still live in the Metairie house the family moved into in 1965, two weeks before Hurricane Betsy struck. He grew up wade fishing in Lake Pontchartrain and rekindles his love for Louisiana's unique coastal experiences with frequent summer forays to Grand Isle.

---

[1] The first and second tasks were completed for the (now) Louisiana CPRA; the third, fourth, and fifth under contracts with the USACE. The fourth and fifth were tasks within projects directed by Joseph Suhayda, PhD, a co-worker at the time. The fifth effort was part of the senior technical review of the USACE's southeast Louisiana surge hazard analysis led by Dr. Suhayda and completed in late spring of 2007. Mr. Jacobsen and Dr. Suhayda were subsequently employed by Taylor Engineering (beginning in late summer 2007), which performed some STWAVE modeling as part of the USACE/FEMA southeast Louisiana surge hazard analysis. Mr. Jacobsen and Dr. Suhayda did not participate in the Taylor Engineering STWAVE work.

[2] During post-Katrina forensic studies several senior Branch members participated on investigation teams sponsored by the National Science Foundation, the State of Louisiana, and the Society, including Louis Capozzoli, PhD PE; Gordon Boutwell, PhD PE; and Billy Prokaska, PE. These members reached similar profound conclusions regarding the failure of the New Orleans surge protection system.

Acknowledgements

The Southeast Louisiana Flood Protection Authority-East (SLFPA-E) volunteer board commissioners, including several whose tenures have ended, deserve credit for the idea of this Report. Their earnest desire and firm commitment that the New Orleans perimeter surge protection system design, and all its underlying analyses, be made completely open, transparent, understandable, and subject to comprehensive professional scrutiny is the only reason this Report was undertaken. It has been a career highlight to assist them in serving the citizens of Orleans, Jefferson, and St. Bernard Parishes.

The person most responsible for carrying out the Board's vision is its indefatigable Regional Director, Robert Turner, PE. Bob has maintained an unflinching demand for a thorough and independent Report. As with every aspect of his leadership at SLFPA-E, he has constantly pushed to get the science and engineering right and to listen to everyone with something to say.

Thanks are owed to the SLFPA-E staff, including Chief Engineer Stevan Spencer, PE; Special Assistant Sheila Grissett; Assistant Betty Vignes; GIS Specialist Roger Colwell; Contract Engineer Bill Fogle; and the Parish Levee District Directors—Gerry Gillen, PE; Fran Campbell; and Nick Cali. They provided timely support on countless occasions.

During this effort the Louisiana Coastal Protection and Restoration Authority (CPRA) initiated a parallel evaluation of the U.S. Army Corps of Engineers 2005-2009 hurricane surge hazard analysis for southeast Louisiana. This separate project has been overseen by CPRA Engineer Manager Rickey Brouillette, PE and led by project manager David Minton, PE. Joseph Suhayda, PhD serves as the senior technical expert for the team and he is supported by Nathan Dill, Pat Fitzpatrick, PhD, and Peter Vickery, PhD. All have made important contributions to understanding and improving surge hazard analysis. The SLFPA-E agreed that drafts of this Report should be shared with CPRA, and in turn the CPRA team has provided a much needed review, together with additional insights. No doubt some minor errors and confusing sentences remain—but hopefully no major ones. The responsibility for these, however, rests entirely with the author of this Report.

Executive Summary

ES.1. Background

The region encompassing the Southeast Louisiana Flood Protection Authority—East (SLFPA-E) jurisdiction has a five-fold unique and unfortunate vulnerability to extreme hurricane surge:

1st. The region lies at the heart of the central-northern Gulf of Mexico, which is exposed to a high landfall frequency of powerful hurricanes due to the very warm waters of the Loop Current. The Loop Current not only fuels hurricane intensification but also the growth of wind fields; moreover, it sustains slow moving storms.

2nd. The protrusion of the Mississippi River delta into the central-northern Gulf of Mexico raises counterclockwise wind-driven surge on the eastern flank and creates critical exposures for the regional "corner" formed by the intersection with Mississippi coast, the "funnel" produced by the junction of the GIWW and MRGO levees, and Lake Pontchartrain "filling and tilting."

3rd. The vast low-lying delta platform on which the region rests is fragmenting and subsiding—with some of the world's highest relative sea level rise magnifying surge inundation.

4th. Expanding shallow coastal shelves, sounds, bays, and lakes enable hurricane winds to push surge inland with more momentum. And,

5th. Declining coastal vegetation reduces the landscape frictional drag on surge momentum.

These five factors have combined to create surge heights in excess of 20 ft twice in less than 40 years.

Two major institutional tools for managing hurricane surge risk are flood insurance—offered under the National Flood Insurance Program (NFIP), administered by the Federal Emergency Management Agency (FEMA)—and perimeter protection systems. In the wake of Hurricane Katrina, the U.S. Army Corps of Engineers (USACE) was directed both to a) revise the regional surge hazard analysis—as part of a NFIP update to the regional Flood Insurance Study (FIS)—and b) design and construct a NFIP accreditable levee system, known as the Hurricane and Storm Damage Risk Reduction System, (HSDRRS).

It is important to recognize that the NFIP and HSDRRS are directed primarily at managing property damage risks. In managing flood property losses the NFIP focuses on an analysis of the 100-year hurricane surge hazard (100-yr average recurrence, or 1% annual chance). Thus, the HSDRRS is designed to minimize 100-yr overtopping—consistent with a level which avoids erosion issues and which also does not aggravate the residual interior flood hazard associated with severe rainfall events. While the 100-yr hazard level may seem to many like a stringent criteria, it is widely recognized as inadequate for addressing critical residual risks to property, community infrastructure and cultural assets, regional and national economic interests, as well as human lives and livelihoods.

Between 2005-09[3] the USACE undertook a ground-breaking hurricane surge hazard analysis to estimate the 100-yr surge hazard for the regional FIS and accreditable HSDRRS design. The analysis employed considerable professional, academic, and other technical resources and greatly advanced the state of scientific knowledge and the engineering practice. The USACE also used the FIS analysis to estimate

[3] The period from 2005-2009 represents the years in which the USACE made methodology decisions and performed the vast majority of the analysis. Many methodology choices are thus already over seven years old, and much of the analysis is over five years old. Documentation of the work is included in: IPET, *Performance Evaluation of the New Orleans and Southeast Louisiana Hurricane Protection System, Volumes I through VIII*, 2006-09; USACE, *Flood Insurance Study, Southeast Parishes of Louisiana, Intermediate Submission 2: Offshore Water Levels and Waves*, July 2008; USACE, *Elevations for Design of Hurricane Protection Levees and Structures*, Draft Report Version 4.0, August 18, 2010. USACE, *Louisiana Coastal Protection and Restoration, Final Technical Report*, June 2009.

500-yr surge for HSDRRS resiliency/armoring plans—to reduce breaching threats under more extreme events. In addition, the USACE and the Louisiana Coastal Protection and Restoration Authority (CPRA), have improvised on portions of the FIS analysis to assess residual 1,000-yr interior inundation hazards for HSDRRS polders and to study alternative future coastal protection and restoration scenarios.

Notably, the NFIP accepts programmatic, resource, cost, and schedule constraints on FIS surge hazard analysis consistent with its limited risk management goals. However, for regions with substantial surge risks, like SLFPA-E, it is appropriate for risk managers to employ more rigorous hazard analysis, updated more frequently to the most recent standards for accuracy and quantifying uncertainty.

ES.2. Objectives and Organization

This Report provides SLFPA-E with:

1. A comprehensive explanation of the evolving science and technical practice of hurricane surge hazard analysis. This review of surge hazard analysis and the encompassed methodologies is not restricted to the risk context of NFIP, but instead is undertaken from a broad risk perspective, congruent with the greater responsibilities of the SLFPA-E. To accomplish this objective this Report has been organized into five parts corresponding to the five major subjects (and tasks) in surge hazard analysis:

   Part I. Hurricane Climatology
   Part II. Modeling Hurricane Surge Physics
   Part III. Hurricane Surge Hazard Analysis
   Part IV. Hurricane Surge Hazard Analysis for Polders
   Part V. Hurricane Surge Hazard Analysis for Future Conditions

   Each part includes detailed technical information on the current approaches underlying each task, critical assumptions, and methodology limitations. Background information is taken not only from the USACE's southeast Louisiana study but from the scientific literature, other recent hazard studies, and several new analyses undertaken for this Report. For example, new information on Gulf of Mexico hurricane climatology is presented based on records through the 2011 season.

2. A review and evaluation of the USACE 2005-09 analysis within the context of the evolving state of the practice, in each part.

3. Recommendations for improving surge hazard analysis for southeast Louisiana.

In addition, this Executive Summary assesses implications of the above for the HSDRRS performance and provides recommendations for revising the HSDRRS design and improving surge risk management.

ES.3. Principal Findings on the State of the Practice for Surge Hazard Analysis

The state of the practice in hurricane surge analysis has rapidly evolved over the last five years in response to continued scientific and technical advances. These advances have largely been spurred on by a need for better surge forecasts, together with FISs for other locations along the Gulf of Mexico and Atlantic coasts. The USACE—both through New Orleans District and the Engineer Research and Development Center—has continued to play a crucial role in methodology improvements. **A major finding of this Report is that recent methodological advances provide for reduced systemic and local bias (error) in surge hazard analysis.** Five important advances include:

1. Understanding of the regional hurricane climatology has continued to progress since Hurricane Katrina (e.g., Hurricanes Gustav, Ike, and Isaac). Research on storm frequencies and characteristics is clarifying the importance of more factors to surge hazard, e.g., Holland B and Integrated Kinetic Energy. The particular role of the Loop Current and coastal water temperature in local hurricane return period, intensity, wind field extent, and dynamics is also becoming better understood, as is the surge threat of large, low intensity hurricanes.
2. Models have improved significantly regarding a) representation of physics in component wind, surge, and wave models; b) code developments (e.g., tight coupling with wave models); c) mesh resolution, quality, and node attributes (e.g., elevations and Manning's *n* values); and d) execution speed and the ability to complete extensive model performance tests (due to high performance parallel computing, HPPC, technology). Recent models are even more reliable, robust, and locally realistic than those developed five years ago.
3. HPPC speeds and capacity have multiplied many fold, which now allows the number of storms used in the joint probability analysis (JPA) to be greatly expanded and facilitates a Joint Probability Method with Optimal Sampling (JPM-OS) approach as opposed to a Surge Response-OS approach.[4]
4. Greater HPPC efficiency and improvements in JPM-OS further allow for a rigorous JPA of polder inundation hazards and residual risk management, moving beyond basic reach-by-reach overtopping hazard assessments.[5] This facilitates a full consideration of residual risk, uncertainties, and the "conservatism" of the design—i.e., a true "risk-based" design.
5. Greater HPPC efficiency also enable more sophisticated evaluations of future surge hazard scenarios, including such factors as varying regional response to relative sea level rise (RSLR), coastal land loss, and local settlement.

A second crucial finding is that despite advances in estimating surge hazards, uncertainties in surge hazard estimates remain very high, with the pace of future reduction likely to be very slow. Methods for quantifying uncertainties are well established and show that *overall surge hazard estimate uncertainty has a very large fractional magnitude, and non-normal distribution.* Applying a normal distribution to provide some indication of epistemic uncertainty magnitude, the 100-yr exterior surge

[4] There are two different approaches to hurricane surge JPA. In the JPM-OS approach the storm set is selected to represent both a) the hurricane climatology (i.e., each storm represents a fraction of the overall frequency of storms) and b) the surge response of the region. In this case the number and characteristics of storms in the set are typically optimized through a comparison with a "surge hazard benchmark"—a less refined surge analysis of the region. A "wind hazard benchmark" can also be used to aid in selecting the set. In the Surge Response-OS approach, the storm set is selected only according to "b." If surge-response is considered smooth then the set can be substantially reduced, and surge response extensively interpolated and extrapolated. For complex coasts—such as those dominated by sheltered water bodies—a Surge Response-OS requires more storms, negating its main advantage. A major disadvantage of Surge Response-OS is that it does not support polder inundation hazard analysis. HPPC improvements now allow for both the use of large JPM-OS sets and elaborate benchmark testing.

[5] A polder inundation JPA is required to assess whole-polder inundation hazards (e.g., 100-yr)—incorporating reach exposure *independence* and varying reach seepage, overtopping, breaching, rainfall, pumping and internal routing. Reach exposure independence means that a 100-yr reach overtopping volume has a much shorter return period when regarded as polder surge inundation volume. For a hypothetical polder consisting of two reaches having with independent exposures, the 100-yr reach overtopping hazard constitutes a 50-yr polder hazard. The IPET Report (Volume VIII) provided a planning-level evaluation of polder inundation hazards with some basic features of expanded JPA. The IPET polder inundation JPA was undertaken prior to the USACE finalizing the HSDRRS design.

estimates for southeast Louisiana have a 90% confidence interval of *at least* ± 4.3, 5.1, and 6.1 ft (43, 34, and 30%) on surges of 10, 15, and 20 ft, respectively. Additional aleatory uncertainty can have a similar magnitude but is far from normally distributed.6

ES.4. Principal Findings on the 2005-09 Southeast Louisiana Surge Hazard Analysis

Review of the southeast Louisiana 2005-09 surge hazard analysis in light of recent methodology advances indicates that the analysis has seven important potential bias factors, including four sources of low—under-estimation—bias:

1. **The evaluation of hurricane climatology does not take into account the influence of large, slow-moving, low intensity hurricanes on the 100-yr surge**.
2. **The surge model contains several superseded approaches and the mesh contains outdated topographic, bathymetric, land cover, and HSDRRS data.** These limitations produce local bias in sensitive areas within the region. The model validation—which was done by comparing a Hurricane Katrina hindcast to surge observations—acknowledged one example of significant local bias: a consistent under-representation of surge height by more than 1.5 ft along the south shore of Lake Pontchartrain. The model likely has additional locations of under-estimation bias, as well as some locations with an over-estimation bias.
3. **The Surge Response-OS approach and small 152-storm set overly smooth the interpolation and extrapolation of regional surge response to variations in hurricane characteristics (see Footnote 2). The set does not include sufficient scenarios of extreme landfalling hurricanes for estimating the 500-yr hazard**—e.g., no landfalling Category 5 hurricanes.
4. **The 2057 analysis for the future 100-yr condition only uses a uniform 1.0 ft RSLR around the entire perimeter and applies a uniform increase to estimated surge still water and wave heights for most of the east-bank**.

One small upward bias factor:

5. The approach used to compute the cumulative distribution function (CDF) modestly increases the 100- and 500-yr exterior surge hazard estimates—at one location by 0.4 and 1.1 ft, respectively.

And two factors that could be significant but are difficult to gauge at this point:

6. The method used in characterizing foreshore wave heights associated with the 100- and 500-yr surge conservatively assumes Rayleigh distributed wave heights, but also a possibly low breaker index of 0.4.
7. The JPA for the 2011 conditions does not re-simulate all the storms in the set, but chose to adjust some storm results from the previous JPA for the 2007 conditions.

[6] Uncertainty due to measurement and model imprecision is termed epistemic, while that due to natural variability is termed aleatory. For surge still waters of 10, 15, and 20 ft the estimated standard deviation for total epistemic uncertainty are *at least* 2.6 (26%), 3.1 (21%), and 3.7 ft (19%), respectively. Standard deviations can be equated to 80%, 90%, or 95% confidence intervals by multiplying by 1.28, 1.65, or 1.98, respectively. Thus, the 90% confidence interval for a 100-yr 10 ft surge exceeds ±4.3 ft. There is additional, large, aleatory asymmetric uncertainty associated with the short length of hurricane climatological and surge records.

Review of the state of the practice also identifies five important limitations in the 2005-09 analysis regarding the quantification of uncertainty in surge hazard estimates:

1. **Uncertainties associated with hurricane dynamics**—e.g., intensification, growth, and decay.
2. **Uncertainty in the combined wind/surge/wave modeling** indicated by other recent studies.
3. **Uncertainties in the JPA method and CDF integration,** which have not been examined.
4. **Uncertainties for interior polder inundation hazard factors** such as seepage, overtopping, breaching, rainfall, pumping, and internal routing, which have not been quantified.
5. **Most importantly, the HSDRRS design allowance for uncertainty in the local wave overtopping rates**, which does not reflect the actual statistical uncertainties. The Monte Carlo analysis used to compute the allowance a) employed much lower standard deviations for exterior surge still water than those estimated, and b) did not vary the wave height with depth, as stipulated in the design analysis.

These bias factors and uncertainty issues indicate that the 2005-09 analysis is outdated for SLFPA-E surge risk management purposes beyond the 2013 NFIP FIS and HSDRRS accreditation.

ES.5. Recommendations for Improved Surge Hazard Analysis for Southeast Louisiana

Based on these findings and conclusions, the Report provides two major recommendations for revising the southeast Louisiana surge hazard analysis:

1. **The southeast Louisiana hurricane current and future surge hazard analyses should be updated as soon as possible to provide higher quality median and exceedance level estimates of exterior surge, waves, overtopping, and polder inundation over a full range of hazard levels.** Table ES.1 provides a list of specific recommendations, addressing each of the five tasks, to bring the regional surge hazard analysis up to the state of the practice.

   SLFPA-E should share this recommendation (and the findings supporting them) with the CPRA, USACE, and other federal, state, and local agencies with surge and polder flood risk management missions, including NFIP responsibilities.

   Given that SLFPA-E and CPRA are responsible for managing a full range of surge risks (see the *Louisiana's Comprehensive Master Plan for a Sustainable Coast*, 2012) it is appropriate for them to assert strong leadership in regional surge hazard analysis. SLFPA-E should work with CPRA to establish and fund a permanent program to regularly revise the southeast Louisiana surge hazard analysis—encompassing all five tasks—as part of the state's Master Plan process. The permanent program should be a cooperative partnership with FEMA, USACE, and NOAA (if mutually agreeable), the recently created Water Institute of the Gulf, and leading academic researchers on the various tasks. The revisions should incorporate updates to hurricane and regional data, statistical methods, and modeling approaches and codes in order to meet the needs of federal, state, and local community and ecosystem planners for high quality surge hazard estimates over a wide range (e.g., 10-yr to 10,000-yr)—addressing exterior, overtopping, and inundation hazards and their uncertainties.

2. **SLFPA-E should support a cooperative partnership with CPRA, FEMA, USACE, and NOAA to encourage and fund research for improving regional surge hazard analysis.** Table ES.2 presents a list of research topics—such as investigating potential climate change impacts on the way the Loop Current influences regional hurricane climatology.

This partnership should also develop "living" technical guidance to enhance the consistency and quality of methodologies. This guidance should include incorporating lessons learned from other regional surge studies and identifying best practices for various applications.

Given significant rainfall-only and Mississippi River flood vulnerability in southeast Louisiana, improved analysis of these hazards is also crucial to coordinated residual flood risk management by SLFPA-E, CPRA, and other federal, state, and local agencies.

ES.6. Implications for the HSDRRS Performance

The USACE used the 2005-09 analysis in the HSDRRS elevation design to minimize current 100-yr surge wave overtopping of levees. Floodwalls were designed higher, to future 2057 100-yr overtopping conditions (with RSLR), due to the excessive cost of subsequent crown increase. The outdated methodologies of the 2005-09 analysis--associated bias factors and uncertainty issues—imply the following six conclusions regarding levee performance *as designed* (excluding settlement overbuild):

1. **Revising the analysis for Bias Factors Nos. 1 and 2 above will likely raise median estimates of the exterior 100-yr surge (versus the current FIS estimates) at many HSDRRS reaches, perhaps by two feet at some locations. However, a complete re-analysis is updated is needed to determine the combined influence of all the bias factors on the exterior 100-yr surge estimate.** The 100-yr freeboard—height of the crown above the 100-yr surge still water—varies depending on reach estimated wave conditions. It ranges from 3.0 ft for a reach fronted by forests in St. Charles Parish north of Airline Highway, to over 10 ft for some reaches near the IHNC/GIWW Barrier. Increases to the 100-yr surge estimates are not likely to exceed HSDRRS crowns, but for certain low freeboard reaches could reduce freeboard below the two feet minimum required by FEMA. Higher 100-yr surge estimates could substantially increase estimates of wave overtopping—by factors of two or more. If a reassessment of foreshore wave characteristics substantially increases wave breaker index, the 100-yr wave overtopping estimates could increase by much higher multiples.

2. **Revising the analysis for Bias Factors Nos. 1, 2, and 3 are even more likely to raise median estimates for 500-yr surge and overtopping throughout the region.** The most significant impact is on reaches with low 500-yr freeboard, where there could be a significant threat of free flow overtopping and interior-side erosion and breaching. For example, a reach in St. Charles Parish north of Airline Highway with only 0.5 ft of 500-yr freeboard could show a negative freeboard under a revised analysis.

3. **Revised quantification of uncertainty addressing the above issues will notably increase statistical confidence intervals for 100- and 500-yr surge, waves, and overtopping.** Revisions for both bias and uncertainty together can increase the estimate of current overtopping hazards at exceedance levels by *an order of magnitude.*

4. **Revised median and 10% exceedance estimates of the 100-yr overtopping rate at many reaches will likely surpass the specified 100-yr criteria in the HSDRRS design for interior-side erosion protection** (0.1 and 0..01 cfs/ft)**.** Meeting current criteria will require raising the design elevation to reduce overtopping. Alternatively, overtopping criteria could be increased and the segment erosion protection modified (e.g., through armoring). However, increasing allowable overtopping rate must also ensure that the higher overtopping *volume* does not adversely affect the polder inundation hazard. Ongoing research on wave overtopping erosion of levees may also revise the erosion criteria, which could be increased or reduced depending on specific levee and wave characteristics.

5. **Revising the analysis for the bias factors and uncertainty issues is also likely to raise the polder inundation risk. However, an improved JPA based on the final HSDRRS design is needed to determine the magnitude of increase.** The IPET "planning level" estimates of the 100-yr surge inundation for the New Orleans metropolitan polders—based on a preliminary HSDRRS design without the IHNC/GIWW and Seabrook Barriers and other upgrades—indicated that *100-yr inundation volumes are far lower for surge than for a rainfall-only event*. An improved polder inundation hazard analysis—applied to the final HSDRRS design—is required to reassess this preliminary indication, as well as to evaluate the residual 500- and 1,000-yr polder inundation hazards and their uncertainties.

6. **An updated future analysis addressing Bias Factor No. 4—which takes into account varying regional impact of RSLR, erosion, and land cover change (e.g., New Orleans East Land Bridge)—is likely to show significant spatially-varying impacts to future 100-yr and 500-yr surges and HSDRRS reach overtopping.** The 2057 design elevations will need to be adjusted to take into account higher overtopping at some reaches.

These six performance concerns indicate that HSDRRS levees as designed have significant shortcomings for the SLFPA-E's management of surge risks.

ES.7. Additional Recommendations for the HSDRRS

The following four HSDRRS recommendations derive from the above findings and recommendations for improved surge hazard analysis, and the implications for the HSDRRS design:

1. **SLFPA-E should work with CPRA and USACE to revise surge (still water level), wave, and overtopping exceedance levels to reflect the total statistical (including non-normal) uncertainty**. **SLPFA-E should then work with the CPRA and USACE on determining if a 10% exceedance level is appropriate** (i.e., 80% confidence interval).[7]

2. **SLFPA-E should work with CPRA and USACE to add three exceedance level design criteria:**

    a. A minimum freeboard for the 100-yr/exceedance surge, in addition to the NFIP required 2 ft minimum 100-yr/median freeboard. SLFPA-E, CPRA, and USACE should define an appropriate 100-yr/exceedance freeboard. The requirement will necessitate raising some reaches, such as a levee in St. Charles Parish north of Airline Highway, which currently has a crown design of 14.0 ft for a 100-yr surge of 10.8 ft—a freeboard of 3.2 ft. A 100-yr surge estimate at the 10% exceedance level accounting for total uncertainty is likely to be above 15 ft.

    b. Reach-specific 100-yr/exceedance wave overtopping rates. This would replace the current uniform 0.1 cfs/ft criteria and could be higher or lower depending on reach erosion control. The allowable rate would be based on latest erosion research but would not exceed a limit required to minimize polder inundation impact. Revised estimates of local 100-yr/exceedance surge and waves will likely require upgrading wave breaking or crown elevation, and/or interior-side erosion control, for many reaches.

[7] The NFIP does not require allowances for uncertainty in the delineation of local flood hazards, largely because the uncertainty in annual claims can be managed actuarially across the nationwide program . However, locally borne risks associated with levee failure imply the need to account for uncertainty at an appropriate interval. The USACE levee certification guidance (*Process for the NFIP Levee System Evaluation*, August 2010, EC_1110-2-6067) suggests an exceedance level of *at most* 10% (equivalent to an 80% confidence interval).

The uniform design criterion for the median 100-yr overtopping (0.01 cfs/ft) could be eliminated if it provides no needed benefit.

c. Reach-specific 500-yr (resiliency) still water levels, waves, exterior scour velocities, overtopping rates, and seepage rates—at appropriate exceedance levels. These should be based on reach-specific conditions and the latest performance research and should consider the full range of failure mechanisms. SLFPA-E should work with the CPRA and USACE to clarify the HSDRRS authorization, and modify as needed, to allow selecting and prioritizing resiliency projects from among a full range of alternatives—with the objective of optimizing reduction in polder residual risk. Resiliency projects should include the option of further raising reach crowns.

SLFPA-E should work with the CPRA and USACE to upgrade structural designs as needed to be consistent with revised hydraulic design.

3. **SLFPA-E should work with the CPRA and USACE to accelerate installation of reasonable resiliency measures which are not likely to be rendered obsolete in the near future** by revisions to surge hazard analysis, 100-yr and 500-yr exceedance level design criteria, and erosion research. If USACE construction funds are not available SLFPA-E should obtain state and/or local funding and expedite completion. Levee reaches with low freeboard (e.g., St. Charles Parish) should be prioritized for maintenance lifts.

4. **SLFPA-E should work with the CPRA and USACE to ensure a systematic approach to HSDRRS projects.** In general, the top priority should be minimizing 100-yr wave overtopping in accordance with design criteria at the specified exceedance level. The second priority should be 500-yr resiliency at an appropriate exceedance level. The third priority should be further upgrades to HSDRRS (e.g., the 2012 CPRA Master Plan "High Level" alternative). All polder HSDRRS components must be treated as equally important "links in a surge risk management chain."

ES.8. Additional Recommendations for Surge Risk Management

Finally, the SLFPA-E should also work with the CPRA, regional parish governments, the USACE, and other appropriate agencies on seven further surge risk management actions:

1. **Complete studies to identify cost-effective internal compartmentalization projects** to reduce or control inundation in the event of an HSDRRS breach. Possible projects include diverting water from the IHNC/GIWW sub-basin to the Central Wetlands; reinforcing I-walls along the IHNC; and improving legacy barriers at parish boundaries.

2. **Maintain and improve critical coastal "lines of defense,"** per the CPRA 2012 Master Plan, such as the New Orleans East and Bayou LaLoutre Land Bridges and Biloxi Marsh.

3. **Examine regional surge hazard/risk impacts and issues associated with Mississippi River and other levees below the HSDRRS** as part of the Mississippi River Hydrodynamic and Delta Management Study.

4. **Continue to evaluate potential cost-effective Lake Pontchartrain Barrier alternatives that avoid adverse ecological and surge hazard impacts**.

5. **Conduct a state-of-the-practice "all flood" hazard analysis for the New Orleans region**. This analysis should be used to optimize surge risk management given other sources of flood hazard. In order to reduce polder 100-yr flood hazards, expanding interior drainage and pumping capacity and non-structural measures may take precedence over raising HSDRRS crowns. In order to reduce 1,000-yr flood hazards, attention may need to shift from HSDRRS improvements to Mississippi River levee upgrades.
6. **Upgrade polder infrastructure and revise building codes consistent with future polder "all flood" hazard analysis and sound risk management**.
7. **Implement reasonable policies to incentivize a broader segment of property owners to purchase flood insurance under the NFIP**.

Table ES.1. Recommendations for Updating the Southeast Louisiana Surge Hazard Analysis

Task	Recommendation
I. Hurricane Climatology	1. Revise the joint probability expression—and associated uncertainty—for southeast Louisiana regional hurricane landfall as a function of latest data on hurricane frequency, core intensity, core size, forward speed, and track, including hurricanes of any intensity. 2. Use an appropriate data record; reassess evidence for a Gulf of Mexico climate cycle. 3. Address scatter in relationship of central pressure deficit and maximum wind speed in joint probability expression. 4. Address wind field distribution variability—e.g., Holland B, Integrated Kinetic Energy, etc.—for the full range of hurricane core intensities and sizes, in a revised joint probability expression. 5. Address variability in intensification—associated with passage over the Loop Current/Eddies—and pre-landfall decay (infilling) for the full range of hurricane intensities, sizes, wind-field distributions, and forward speeds. in a revised joint probability expression. 6. Re-evaluate the return period for regional landfall of a Hurricane Katrina and evaluate the return periods for Hurricanes Gustav and Isaac. 7. Incorporate results of studies on future hurricane climatology as a function of climate change into estimates of uncertainty regarding future hurricane probabilities.
II. Modeling Hurricane Surge Physics	1. Revise the finite element mesh layout and resolution; refine fidelity of linear feature alignments (e.g., break lines); provide for reasonable consistency in resolution of similar landscapes and key landscape conveyance features. 2. Revise mesh (node and interior weir boundary) elevations consistent with a current regional digital elevation model, including current applicable NAVD88 epoch. 3. Revise other mesh attributes (e.g., Manning's *n*, surface canopy coefficient, surface directional roughness, eddy viscosity) consistent with current landscape information. 4. Use a tightly coupled surge-wave code with full plane wave modeling and include all relevant physics terms. While SWAN-ADCIRC is the current state-of-the-practice HPPC surge code, alternatives should be evaluated as they become available. 5. Evaluate choice of fully explicit versus implicit-explicit numerical scheme, wetting-drying approaches and parameters; and air-sea drag formulation. 6. Support (e.g., sensitivity testing) decisions that vary from established guidance/state-of-the-practice. 7. Provide model calibration/validation using Hurricanes Katrina, Gustav, and Isaac; explain choice of parameters that are/are not employed in calibration. 8. Evaluate residual instabilities and local mass conservation errors in final calibration/validation. 9. Evaluate potential local bias in final calibration/validation results and provide methods for correcting bias in the use of the model. 10. Revise the estimate of uncertainty in regional surge modeling.

Table ES.1. Recommendations for Updating the Southeast Louisiana Surge Hazard Analysis (Continued)

Task	Recommendation
III. Hurricane Surge Hazard Analysis	1. Employ a true JPM-OS approach with a much expanded set size (e.g., hundreds of storms) in the surge JPA. The JPM-OS should be determined using appropriate regional wind and surge benchmarks. The surge benchmark should sufficiently capture critical nonlinear responses and surge hazard conditions—particularly around large sheltered water bodies. Sensitivity tests should be used to examine the scope of regional nonlinear surge response and surge hazard conditions.. Alternatively, the revised surge JPA can employ a Monte Carlo JPM. 2. Rigorously validate the surge JPA versus tide gauge-based return frequency analyses to evaluate potential bias in JPA results. 3. Employ an integration method which provides the median estimated CDF. Sensitivity tests should be conducted on possible variations to the integration method to identify the best approach. 4. Define and quantify all sources of normally and non-normally distributed uncertainty contributing to the overall uncertainty in the surge hazard analysis, including uncertainties in the hurricane climatology, wind/surge/wave model, the selected surge JPA method, and set size. Prepare uncertainty intervals for the estimated CDF based on all sources of uncertainty.
IV. Hurricane Surge Hazard Analysis for Polders	1. Incorporate the improvements in the hurricane climatology, surge modeling, and exterior surge hazard analysis discussed in the Recommendations for Parts I, II, and III. 2. Provide a joint probability analysis (JPA) of polder inundation hazards, expanding on the IPET approach, and estimate the residual 100-, 500-, and 1,000-yr inundation hazards. 3. Base the polder inundation JPA on the larger JPM-OS set of storms as identified in the Part III recommendations. 4. Include a realistic quantification of the range of breach I-L cases and associated fragility conditions for each storm. 5. Estimate local wave conditions and HSDRRS wave overtopping with the state-of-the-practice methods that better account for local peak wave conditions during hurricane peak surge. 6. Further expand the inundation JPA to encompass the nonlinear influence of additional key probabilistics—such as exterior SWL and wave height—on inundation volume. 7. Examine the full influence of uncertainties—associated with the hurricane climatology, the exterior hurricane surge and local wave model, seepage, overtopping, breaching, rainfall, pumping, internal routing, and particular JPMs—on the inundation hazard estimate. Such treatment should be developed to allow estimating a range of confidence intervals—e.g., 80, 90, 95%. 8. Update estimates of the wave overtopping hazard for the HSDRRS design at each reach in accordance with No.5, and update confidence intervals using full uncertainties for surge and wave conditions.
V. Hurricane Surge Hazard Analysis for Future Conditions	1. Follow the recommendations in Parts II, III, and IV for improved model development, exterior surge hazard analysis, and polder inundation hazard analysis. 2. Re-evaluate the future conditions hazards at appropriate intervals (e.g., Years 10, 25, 50, and 100) based on *all* recognized applicable coastal landscape trends—e.g., RSLR, coastal erosion, vegetation changes, perimeter system degradation, and polder subsidence—when the current exterior surge and interior polder inundation hazards analyses are revised. 3. Re-run all JPM-OS storms for the future conditions JPAs instead of using a small subset of storms to adjust the estimate of future hazard. 4. Use specific storm scenarios—e.g., a Katrina-like hurricane—to provide additional insight and aid public understanding of impacts to future surge hazard.

Table ES.2. Research Topics for Improving Southeast Louisiana Surge Hazard Analysis

Task	Recommendation
I. Hurricane Climatology	1. Update information on various traditional and new characteristics for Gulf of Mexico and landfall hurricanes, as the historical record expands. 2. Conduct more rigorous statistical analysis of data on these characteristics; particularly clarification of confidence intervals (i.e., uncertainty) in estimates of hurricane characteristics and correlations between characteristics, e.g., (CPD:Vmax2). 3. Improve the joint probability expressions for Gulf of Mexico hurricanes, and landfalling regional hurricanes, including estimation of uncertainty. 4. Revisit the selection of a representative GoM hurricane data record, taking into account quality of observations and accepted findings on GoM climate cycles. 5. Investigate factors influencing the particular hurricane return frequencies for southeast Louisiana, especially the Loop Current and associated eddies. 6. Further expand the joint probability expression to include additional important hurricane attributes contributing to surge, such as wind field asymmetry and banding. 7. Assess the influence of secular climate trends on the Loop Current and other factors influencing GoM hurricanes.
II. Modeling Hurricane Surge Physics	1. Update Louisiana LIDAR DEMs, coastal water body bathymetry, raised feature topography, and land cover data sets. 2. Acquire wind (at a range of averaging periods), SWL, current, and wave time-series data across a wide range of coastal landscape locations during hurricanes, as well as during normal tides and seasonal meteorological events. 3. Improve and refine H*Wind files (10-min average) for surge calibration and validation. 4. Improve treatment of surge physics, such as depth-variable hydrodynamic friction (e.g., Manning's n), the air-sea drag, wetting and drying, wave shoaling/breaking, and local time-varying rainfall. 5. Further application of higher order steep-slope wave modeling, including capability of coupling with 2D SWL models. 6. Advance numerical methods, codes (SWAN+ADCIRC and others), and HPPC techniques and systems. 7. Incorporate 3D models for baroclinic analysis where needed to improve accuracy. 8. Address significant raised feature erosion and other landscape dynamics during actual surge events where needed to accurately simulate surge and waves. 9. Expand sensitivity analyses assessing the implications of model settings (e.g., numerical methods, modification of acceleration terms, time step, etc.), mesh resolution, node attributes, forcing data, coupled models, and other model aspects on runtime, stability, and performance.

Table ES.2. Research Topics for Improving Southeast Louisiana Surge Hazard Analysis (Continued)

Task	Recommendation
III. Hurricane Surge Hazard Analysis	1. Expand the number of high quality long-term regional gauge records. Long-term records for several regional USGS and USACE gauges can be enhanced by addressing datum and gap issues. 2. Further evaluate appropriate return frequency distribution equations for the analysis of tide gauge records. In particular, equations should provide reasonable treatment of extreme historical observations. 3. Examine nonlinear surge response and surge hazard conditions for complex coastlines, including sheltered water bodies, particularly for southeast Louisiana. 4. Assess JPM approaches and set size optimization, Cumulative Distribution Function integration techniques, and the estimation and treatment of hazard uncertainty. 5. Study JPM wind field (10-min average) representation of surge forcing conditions
	6. Investigate methods for wave hazard analysis; such as the appropriate application of 1D overland wave modeling (WHAFIS transect selection and attribution, local wind-wave boundary conditions, wave transformation parameters, etc.) and determining those locations and conditions where more advanced modeling (2D, Boussinesq, etc.) should be applied.
IV. Hurricane Surge Hazard Analysis for Polders	1. Further research on local wave, seepage overtopping, breaching, rainfall, pumping, and interior routing processes, including laboratory and field studies to evaluate empirical formulations and coefficients. High priority issues include: • Appropriate wave height distributions for short duration surge peaks. • Appropriate breaker parameters or wave transformation models that can be applied to HSDRRS foreshore regions. • The role of preferential seepage pathways in initiating collapse breaching and field investigations to locate and characterize such pathways. • The wave and direct (weir) overflow expressions and coefficients for all phases of hurricane surge overtopping and breaching, for a variety of structures and conditions, including both average and instantaneous rates. • Exterior- and interior-side wave-induced, and free-flow induced, scour and breach initiation and development. • Wind setup and wave equations/models applicable to sheltered southeast Louisiana water bodies (e.g., Lake Borgne and Pontchartrain, Breton Sound, Barataria Bay, Mississippi River, etc.) and inundated polders and sub-basins (e.g., IHNC/GIWW and outfall canals). 2. Improve coupling of exterior surge, local wave, seepage, overtopping, breaching, rainfall, pumping, and internal routing models. 3. Further expand and enhance the inundation JPA to make it less speculative. 4. Better the analysis of non-surge polder flood hazards—such as rainfall-only events and overtopping/breaching during a Mississippi River flood—which are critical to evaluating the risk implications of surge inundation hazards
V. Hurricane Surge Hazard Analysis for Future Conditions	1. Assess the influence of climate cycles and secular climate change on the CN-GoM hurricane climatology, SLR, and seasonal steric conditions, including influences mediated by the Loop Current. As part of assessing future hurricane climatology for the CN-GoM provide suitable JPM-OS sets for various future surge hazard evaluations. 2. Improve trend analyses for regional subsidence, coastal erosion, and vegetation conversion; elevation changes to perimeter systems and polder interiors; and HSDRRS fragility.

Table of Contents

Part V. Hurricane Surge Hazard Analysis for Future Conditions

General Technical Note 1, Concepts in Flood Return Frequency Analysis

General Technical Note 2, Elevation Data for Hurricane Surge Hazard Analysis

List of Acronyms

AMO	Atlantic Multi-decadal Oscillation
CDF	Cumulative Distribution Function
CEM	Coastal Engineering Manual (USACE)
CLs	Confidence Limits (UCL/LCL—Upper/Lower Confidence Limits)
CN-GoM	Central-Northern Gulf of Mexico
CP	Central pressure
CPD or ΔP	Central pressure deficit
CPRA	Coastal Protection and Restoration Authority
CV and CV(RMSE)	Coefficient of variation and coefficient of variation for RMSE
ENSO	El Niño-Southern Oscillation
EST	Empirical Simulation Technique
FEMA	Federal Emergency Management Agency |
FIRM	Flood Insurance Rate Map
FIS	Flood Insurance Study
NFIP	National Flood Insurance Program
ft	Feet
GIS	Geographic Information System
GMH	GoM Major Hurricane
GMH/L	Which Makes Landfall at Any Category
GMH/LMH	Which Makes Landfall as a Major Hurricane
-500	Along 500-mi CN-GOM Coast
-151	Along 151-mi (2½° Latitude) Segment below New Orleans
-60	Along 60-mile (1° Latitude) Segment below New Orleans
GoM	Gulf of Mexico
GTN	General Technical Note (see Table of Contents)
H_s	Significant Wave Height
HHI	Hurricane Hazard Index
HII	Hurricane Intensity Index
HPPC	High Performance Parallel Computing
HSDRRS	Hurricane and Storm Damage Risk Reduction System
HSI	Hurricane Surge Index
IKE	Integrated kinetic energy
IKE_H and IKE_{TS}	IKE out to the extent of hurricane and tropical storm force winds
IPET	Interagency Performance Evaluation Task Force
JONSWAP	Joint North Sea Wave Project
JPA	Joint Probability Analysis
JPM and JPM-OS	Joint Probability Method and JPM with Optimal Sampling
km	Kilometer
LOI	Location of Interest
LaCPR Study	Louisiana Coastal Protection and Restoration Study (USACE)
MEOW	Maximum Envelop of Water
MJO	Madden–Julian Oscillation
MOM	Maximum of the Maximum
mph	Mile per hour
MPI	Maximum Probable (or Possible) Intensity
mb	Millibar

m	Meters
MsCIP	Mississippi Coastal Improvement Plan
NLCD	National Land Cover Database
NOAA	National Oceanic and Atmospheric Administration
CPC	Climate Prediction Center
CSC	Coastal Services Center
GFDL	Geophysical Fluid Dynamics Laboratory
HRD	Hurricane Research Division
NCDC	National Climate Data Center
NHC	National Hurricane Center
NRL	Naval Research Laboratory
NAO	North Atlantic Oscillation
PBL Model	Planetary Boundary Layer Model
PD	Pressure deficit
PDF	Probability Density Function
PJ	Petajoules
PMH	Probable Maximum Hurricane
r	Radial distance from the storm center
R^2	Coefficient of determination values
R_H and R_{TS}	Radius of hurricane and tropical storm force winds
R_{max}	Radius of maximum winds from the storm center
RFA	Return frequency analysis
RMSE	Root mean square error
RSLR	Relative sea level rise
s	Seconds
SDPI	Surge Damage Potential Index
SI	Scatter Index
SLFPA-E	Southeast Louisiana Flood Protection Authority—East
SLR	Sea level rise
SPH	Standard Project Hurricane
SSS	Saffir-Simpson Scale
SST	Sea surface temperatures
SWEs	Shallow Water Equations
SWL	Still water level
T_p	Peak wave period
TCHP	Tropical Cyclone Heat Potential
TJ	Terajoules
USACE	U.S. Army Corps of Engineers
V_f	Forward speed
V_{max}	Maximum sustained wind velocity
WDPI	Wind Damage Potential Index
yr	Year
θ	Heading angle
η	Difference between SWL and LMMSL; equal to the setup/setdown
μ and σ	Mean and Standard deviation

Introduction

This Introduction provides a background overview of six important topics in hurricane surge risk management for southeast Louisiana:

1. The concepts of hurricane surge hazard and risk;
2. Basic public and private tools for hurricane surge risk management;
3. The National Flood Insurance Program and perimeter surge protection;
4. The authorized New Orleans regional Hurricane and Storm Damage Risk Reduction System;
5. The 2005-2009 hurricane surge hazard analysis; and
6. Uncertainty in surge hazard estimates.

The purpose of this Report in supporting regional surge risk management is then described.

I.1 Hurricane Surge Hazard and Risk

Hurricane surge risk is the product of two components: the probability of given hurricane surge conditions at a location—i.e., the surge hazard—and the consequence of that surge.

For any particular surge still water and wave height (see Section 6 for definition of surge components) there is a quantifiable probability—given as a percent—that these can occur at a specific location in any year. For example, a surge of 15 feet or greater may have a two percent chance of occurring each year at a given location. This probability is also called a two percent *return frequency*, and is equivalent to the expectation that a surge of 15 ft or greater will occur at least one time out of every 50 years, *on average.* This 50-yr time frame is referred to as an *average* recurrence or return period. A one percent return frequency is equivalent to a 100-yr return period; a 0.2 percent chance to a 500-yr return period; and a 0.1 percent chance to 1,000-yr return period. The same still water level can have different return periods at different locations—e.g., at West End versus Little Woods along Lake Pontchartrain versus Shell Beach along Lake Borgne. A hurricane making landfall in southeast Louisiana will produce varying regional still water peaks, with varying return periods.

A local 100-yr surge hazard is not guaranteed to recur exactly on a 100-yr interval, but to recur on average once every 100 years over a very long time frame—e.g. about 10 times over 1,000 years. Probabilities can be computed for single occurrences over shorter (and longer) time frames than 100 years, as well as for multiple occurrences over various time frames. For example, a local surge at or above the 100-yr hazard has a 26% probability of occurring during the course of a 30-yr mortgage.

In any given year, a surge with a *local* 100-yr return period is twice as likely to occur as a *local* 200-yr surge, at any point. When considering surge hazard around the exterior of a polder (a Dutch work to describe the area within a continuous perimeter surge protection system) it is important to consider the *whole-perimeter* hazard. For polders, the relationship between local surge exposures is important to understanding *inundation hazard*. If the exposure at points all around a polder are highly dependent, a particular hazard level (e.g., 100-yr) at all locations is likely to be associated with the same storm. However, if the exposures are independent, the hazard at each location would be associated with separate storms. If a polder has two independent surge exposures, the combined probability of a 100-yr surge happening at one or the other location in a given year is close to 2%, or a 50-yr return period. (See General Technical Note 1 for a further discussion of return frequency concepts in hydrology.) Thus, a polder can be exposed to overtopping volumes much more frequently than the local hazard indicates.

A *surge hazard analysis* estimates the still water and wave heights associated with a full range of return periods at every location within a region. This analysis is typically presented in the form of a cumulative distribution function curve, as illustrated in Figure I.1. A surge hazard analysis also estimates the uncertainties associated with the proposed curve.

Estimates can also be developed for full range of consequences that can occur throughout a region with each local surge hazard level. These might include the number of people not evacuating who are likely to be killed; the number of residents suffering various physical and emotional illnesses; residential and commercial property damages; temporary and permanent business, employment, and personal income losses; impacts to historical and cultural assets and local ways of life; etc. A *surge risk analysis* presents the range of consequences as a function of return probability—e.g., graphs of cumulative distribution function curves for estimated deaths, housing units destroyed, insured property losses, uninsured property losses, decline in one year local gross domestic product, etc.

Assessing surge risk—hazard plus consequences—provides a rigorous way of describing the probability and magnitude of disasters for a given location, facilitating comparisons between types of disasters (e.g., a surge flood event versus a rainfall-only flood event) and locations, and supporting informed decisions about how to best manage risk.

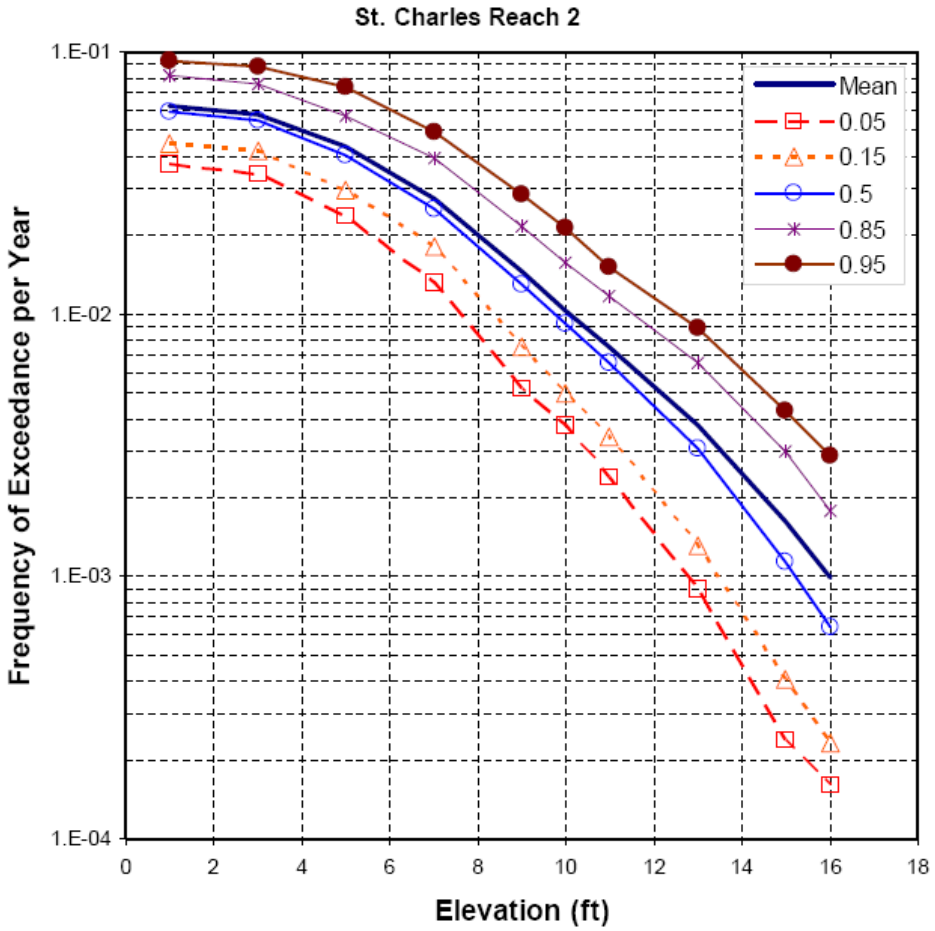

Figure I.1. Example of Surge Hazard Analysis with Confidence Limits

IPET 2009

I.2. Public and Private Hurricane Surge Risk Management

There are six principal governmental tools for surge risk management:

1. The Federal Emergency Management Agency (FEMA) sponsored National Flood Insurance Program (NFIP) covering both residential and commercial property damage. Other FEMA programs address local infrastructure losses.
2. Risk reduction by a perimeter levee/floodwall surge protection system. Perimeter systems may be sponsored by federal-local partnerships or they may be local-only projects. Those designed and constructed by the U.S. Army Corps of Engineers (USACE) in southeast Louisiana are done under a cost share partnership with the State of Louisiana Coastal Protection and Restoration Authority (CPRA), with long-term operations and maintenance provided by a local agency, such as the Southeast Louisiana Flood Protection Authority-East (SLFPA-E), with local funds.
3. Risk reduction through maintained and enhanced coastal "lines of defense"[8]—such as barrier islands, ridges, land bridges, and wetlands.
4. Risk reduction by maintained local infrastructure, such as internal drainage systems and compartmentalization structures within a polder;
5. Risk reduction through laws and regulations governing building standards, such as local zoning ordinances and building codes, buyouts, and subsidized elevation, some of which are required and some of which are voluntary under the NFIP.
6. Risk mitigation through emergency response and recovery programs, including, evacuation, flood fighting, flood recovery, rebuilding grants and loans, etc.

The residual risks—uninsured property damages; economic disruption; loss of life; health effects; loss of historic and cultural treasures; changes to a "way of life;" etc—are borne by individuals, volunteer organizations, businesses, and society at large.

Government sponsors must clearly define objectives and practical implications for the public tools. The public surge risk management must be understandable to the whole community—so that private residual risk management considerations can be properly weighed.

Proper application of public surge risk management tools by government agencies requires rational decision-making based on:

1. Scientifically Sound and Complete Information. For example, surge hydrologic boundaries must take precedence over political jurisdictions. Moreover, decision makers require good evaluations not just for surge hazards and consequences, but also for other related flood hazards—e.g., rainfall-only and Mississippi River. Agencies must also commit to re-analyzing hazards and risks to account for changing conditions, e.g., demographics, land use, climate, surge hazards, etc.
2. Rigorous Treatment of Uncertainties—in scientific information, hazard levels, consequences, and the performance of risk management tools. *The apparent precision of sophisticated analyses and plans can provide a false sense of security.* Agencies need to adopt straightforward ways of referencing and communicating fundamental surge risks and uncertainties.

[8] See Lopez, J. A., *The Multiple Lines of Defense Strategy to Sustain Louisiana's Coast*, Lake Pontchartrain Basin Foundation December 12, 2005

3. Complete Life-Cycle Cost-Benefit Evaluation. The risk reduction and other benefits afforded by each tool must justify commitment of the sponsor resources necessary for the complete long-term development and sustainment of that tool. For example, a successful perimeter system requires the associated financial, human, political, and organizational resources not only for the initial construction phase, but also for anticipated additional construction phases, operations, and maintenance. Long-term opportunity and environmental costs must also be accurately identified and accounted for in the evaluation.
4. Consistency and Synergy. All the components must support the risk management objective, with no "weak or gold-plated links." For example, structures in a perimeter system should not be under-designed or excessively over-designed. Difficulties also arise when policies undermine risk management, such as providing local shelters when evacuation is mandated; encouraging "free riders;" and subsidizing a community's perimeter system.

The performance of the above tools is a third factor in the final calculation of surge risk. For the New Orleans area, in addition to organized evacuation, two important public institutional tools for surge risk management are the NFIP and the USACE designed perimeter surge protection system.

I.3. The NFIP and Perimeter Surge Protection

The federally administered NFIP provides property owners with an affordable way to manage threats of severe flood damage to their property, and communities with a way to reduce the risk that a critical mass of viable property owners can be wiped out. The NFIP requires that mortgages for homes subject to 100-yr flood (including surge) hazards be secured by flood insurance. Premiums for this insurance are generally below a fair market price, but nevertheless cost hundreds of dollars per month. Outside the 100-yr flood hazard the NFIP provides optional flood insurance to mortgagees and property owners, at premiums as much as 90 percent lower than for those exposed to the 100-yr hazard.[9] An artifact of the NFIP 100-yr threshold is a sharp transition in the value of homes located outside the 100-yr flood zone versus those in the 100-yr flood zone, with the latter often lowered by tens of thousands of dollars.

Risk management from the community perspective is greatly enhanced if most property owners not subject to the insurance mandate (either because the property is not under a commercial mortgage or the property is outside the 100-yr flood zone) nevertheless purchase optional flood insurance. NFIP flood insurance outside the 100-yr hazard offers an extremely good risk reduction value from a community perspective. However, individual owners are often not sufficiently motivated to take advantage of the value.

The NFIP currently has subsidized premium costs for flood insurance both inside and outside the 100-yr hazard, dramatically enhancing the attractiveness of flood insurance both to policy holders and for *local* risk management. However, under the recently passed Biggert-Waters Flood Insurance Reform and Modernization Act of 2012 subsidies are scheduled to decline significantly. Premiums for insuring a home inside the 100-yr hazard zone are expected to increase several fold, depending on the potential depth of a 100-yr flood. Despite the reduced subsidies, flood insurance remains the most important tool for managing flood damage risks to property.

[9] It is important to note that the NFIP (which also includes a Community Rating System that adjusts local premiums based on community actions to reduce flood risks) strives to achieve many goals, some of which are not consistent—including conserving floodplains and minimizing development impacts; making flood insurance affordable; reducing flood claims; and maintaining a national actuarially sound insurance system.

To complement the NFIP, a reasonable surge risk management tool for a densely populated urban area is to construct a perimeter system that eliminates contribution of surge to the 100-yr flood hazard. An interior 100-yr flood hazard remains inside the polder for rainfall-only events. For southeast Louisiana, such systems can dramatically reduce the 100-yr (and 500-yr) flood zones with the polder. The *combination* of the NFIP together with a perimeter system can enhance property values, make housing more affordable, increase local discretionary spending, raise the attractiveness of the community to businesses, and support growth.[10]

For a critical urban region such as metropolitan New Orleans, coupling a 100-yr perimeter system with the NFIP is an especially effective tool in managing not only residential property damage risks, but important risks to the long-term viability of the community itself. *This is particularly true if property owners not subject to the NFIP mandate purchase flood insurance.* If the NFIP were eliminated, a higher perimeter protection system—likely at a much greater cost to the community—would be required to achieve the same level of risk management.

I.4. The New Orleans Hurricane and Storm Damage Risk Reduction System

In the wake of catastrophic loss of life and property from surge inundation during Hurricane Katrina in 2005, previous planning, design, and maintenance of New Orleans regional perimeter surge protection were severely criticized. The Interagency Performance Evaluation Task Force (IPET), the State of Louisiana, the Independent Levee Investigation Team, the American Society of Civil Engineers, and the National Academy of Engineers produced five major reports on the subject—the first three providing detailed forensic analyses, the last two primarily providing comments on the IPET report.[11] The foremost recommendation of these reports was for sound risk-based design and maintenance.

---

[10] These and other economic benefits are typically weighed against the total construction, maintenance, operation, opportunity, and environmental costs of the perimeter system, over a long term, as part of evaluating the feasibility of such systems. Interestingly, if the NFIP were based around a graduated flood hazard/risk analysis (i.e., not tied to the 100-yr threshold), the feasibility of perimeter systems could be reasonably evaluated for a range of surge risk management objectives. This might be very helpful to smaller communities.

[11] IPET, *Performance Evaluation of the New Orleans and Southeast Louisiana Hurricane Protection System, Volumes I through VIII*, 2006 - 2009.

Team Louisiana (van Heerden, I. L. et al), *The Failure of the New Orleans Levee System During Hurricane Katrina, A Report Prepared for Louisiana Department of Transportation and Development*, Baton Rouge, Louisiana, December 18, 2006.

Independent Investigation Levee Team (Seed, R. B. et al), *Investigation of the Performance of the New Orleans Flood Protection Systems in Hurricane Katrina on August 29, 2005, Final Report*, supported, in part, by the National Science Foundation, July 31, 2006.

American Society of Civil Engineers Hurricane Katrina External Review Panel (Andersen, C. F. et al), *The New Orleans Hurricane Protection System: What Went Wrong and Why*, 2007.

National Academy of Engineering and National Research Council of the National Academies, *The New Orleans Hurricane Protection System, Assessing Pre-Katrina Vulnerability and Improving Mitigation and Preparedness*, 2009.

The U. S. Congress authorized[12] the USACE to revise the southeast Louisiana FIS and rebuild the regional New Orleans hurricane surge perimeter protection system to a 100-yr level of hurricane surge protection, consistent with the NFIP. While this hazard objective affords some increased protection of lives over a lesser objective, federal, state, and local officials remain committed to comprehensive evacuation as the primary tool for saving lives. Given its objective primarily as a property damage risk management tool, the USACE renamed the New Orleans perimeter surge protection network as the Hurricane and Storm Damage Risk Reduction System (HSDRRS). The HSDRRS configuration and associated polders are shown in Figure I.2.

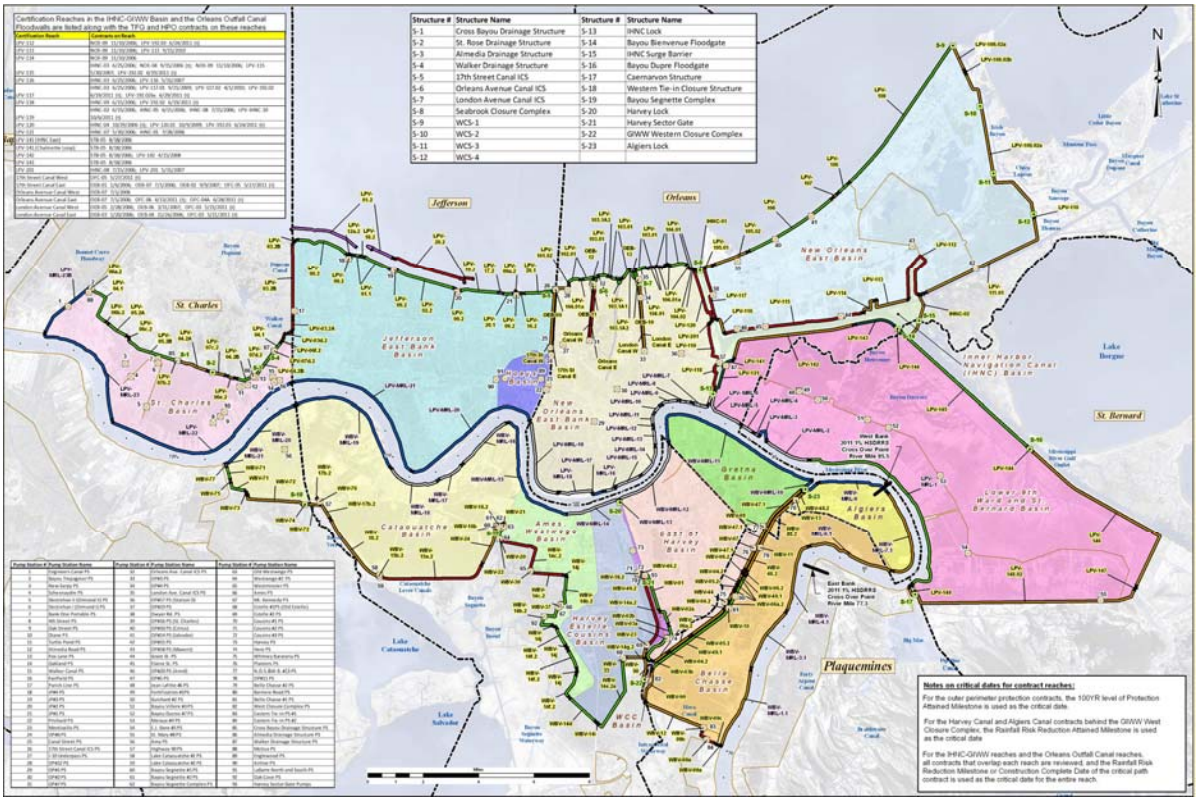

Figure I.2. The Hurricane and Storm Damage Risk Reduction System and Polders[13]
USACE

[12] See Construction headings of Chapter 3, Title II of the Emergency Supplemental Appropriations Act for Defense, the Global War on Terror, and Hurricane Recovery of 2006, and Chapter 3, Title III of the Supplemental Appropriations Act of 2008, (Public Laws 109-234 and 110-252, or the 4th and 6th Construction Supplementals); the Energy and Water Development Appropriation Act of 2006 and the Department of Defense Appropriations Act of 2006 (Public Laws 109-103 and 109-148).

[13] SLFPA-E encompasses three polders: New Orleans East, 9th Ward-St. Bernard, and East Jefferson-New Orleans Metro. Portions of St. Charles Parish between the Bonnet Carré Spillway and East Jefferson are currently part of the latter polder. With the addition of two closure structures—the Inner Harbor Navigation Canal (IHNC) structure east of Paris Road and the Seabrook structure at Lake Pontchartrain, the three polders are essentially subsumed within one large polder for primary surge protection purposes. The three polders continue to function somewhat independently for internal drainage and secondary surge protection purposes, although they all discharge to, and are exposed to, the IHNC/GIWW sub-basin. Additional drainage sub-basins exist within each polder.

To achieve the HSDRRS objective the USACE worked with FEMA to also revise the Southeast Louisiana Flood Insurance Study (FIS) which provides estimates of regional surge hazard for NFIP purposes.

Numerous federal, state, and local agencies, as well as community and business leaders (e.g., the Flood Protection Alliance), and professional organizations have urged that an HSDRRS based primarily on the NFIP and managing property damage risks is not sufficient. Problematic evacuation and loss of life; the critical regional/national role of the local port, oil and gas production, refining, chemical manufacturing, fisheries, tourism, and other infrastructure and economic activity; a large renter population; as well as the presence of unique historic/cultural assets are cited as good reasons for a 500- or 1,000-yr level of surge hazard protection. [14]

In addition to the 100-yr HSDRRS, Congress therefore authorized the USACE to undertake a comprehensive Louisiana Coastal Protection and Restoration Study (LaCPR Study) of HSDRRS enhancements and other long-term surge risk management measures. The LaCPR Study, completed in 2009, included three alternatives for improving the east-bank HSDRRS:

- Upgrade the HSDRRS to a 400-yr level, considered by the Study to be equivalent to a repeat of a Hurricane Katrina, with allowances for alternate tracks;
- Install barriers at the mouth of Lake Pontchartrain to achieve the 400-yr level; and
- Install barriers at the mouth of Lake Pontchartrain to achieve 1,000-yr level, considered equivalent to the surge risk for a strong Category 5[15] hurricane;

The LaCPR Study also included alternatives for building controls and coastal lines of defense. These alternatives were evaluated on the basis of number of residents affected (but without regard to an estimate of non-evacuees), mitigation of property and infrastructure damage, reduced economic impairment, and lessened impacts to historic/cultural assets. The alternatives were also assessed for cost, schedule, and environmental benefits (in the case of coastal restoration projects) and damages (in the case of new structures). The evaluation process eliminated an upgraded HSDRRS as cost inefficient.

The USACE produced a final array of five plans for the New Orleans area—plus one with a variation covering Plaquemines Parish. The five plans included one with coastal restoration measures only; three with coastal restoration and alternate polder building control plans (targeted at the 1, 0.25, and 0.1 percent risk levels); and one with coastal restoration and the Lake Pontchartrain barrier. Congress has not funded, and there is no current schedule, for further USACE investigation, evaluation, or detailed development of these five or other plans.

The CPRA, through development of *Louisiana's Comprehensive Master Plan for a Sustainable Coast, 2012*, has continued to evaluate HSDRRS enhancements—e.g., a "High Level" plan and possible Lake Pontchartrain Barrier Project—together with coastal "lines of defense," such as the New Orleans East Land Bridge, the Bayou LaLoutre Land Bridge, and the Biloxi Marsh. The 2012 Master Plan also calls for evaluating multiple Mississippi River diversion sites in Plaquemines Parish, which could also address. removal of long stretches of Mississippi River levees, potentially reducing surge hazards in the New Orleans area.

---

[14] See the post-Katrina studies noted above; *Flood Protection and Coastal Restoration, Transition New Orleans Task Force*, Presented to Mayor-elect Mitch Landrieu, City of New Orleans, April 2010; the Louisiana Section of the American Society of Civil Engineers *2012 Report Card for Louisiana's Infrastructure*; and www.levees.org

[15] See Section 1 for a discussion of hurricane categories.

I.5. The 2005-2009 Hurricane Surge Hazard Analysis

Sophisticated hurricane surge hazard analyses have been undertaken as part of coastal FISs for several decades and consist of three tasks:

1. Characterizing regional hurricane climatology. A thorough scientific review of hurricanes approaching landfall in the region of interest is the basis for a probabilistic analysis of various characteristics influencing surge. In turn, these are used to examine the joint probability conditions of regional hurricanes and to produce a large representative set of synthetic hurricanes which can be used in the hazard analysis.
2. Developing hydrodynamic models. The modelers must capture the relevant scope and scale of hurricane surge still water and wave physics, including complex interactions with coastal features, as well as validate the models to demonstrate their capability to simulate the conditions produced by historic hurricanes and conditions of interest.
3. Analyzing hurricane surge hazard. The hurricane joint probability information is combined with the surge model to estimate the various return period exterior surge still water and waves (e.g., 50-, 100-, 500-, 1,000-yr, etc.) throughout the region.

Each task includes documentation of methodologies, presentation of results, and evaluation of results and uncertainties.

The NFIP FIS, IPET Study, HSDRRS design, and LaCPR Study all relied on a surge hazard analysis undertaken by the USACE between 2005 and 2009. Tasks 1, 2, and 3 were performed by a joint USACE-FEMA surge team.[16] The USACE performed a fourth task to provide input to the HSDRRS planning and design and IPET Risk and Reliability Report:

4. Evaluating the surge hazards for polders. The USACE analyzed 100-yr overtopping conditions at HSDRRS reaches to establish design requirements. The 100-yr design objective does not eliminate overtopping but requires that it be reduced to rates consistent with preventing erosion and impacting interior rainfall-only hazards. The HSDRRS design also has a resiliency requirement to provide for withstanding 500-yr overtopping. The USACE has also undertaken preliminary assessments of polder inundation hazards and risks as part of a 2009 IPET residual risk assessment and ongoing resiliency design.[17]

The USACE added a fifth task to support the LaCPR Study:

5. Assessing surge hazards for future conditions, including the influence of alternative future hurricane climatology, sea level rise, polder systems, regional subsidence, and coastal landscape scenarios on the 100-yr, 400-yr, and 1,000-yr surge hazards.[18]

---

[16] Led by Donald T. Resio of the USACE Engineer Research and Development Center and Joannes J. Westerink of the University of Notre Dame; documented in the FEMA/USACE, *Flood Insurance Study, Southeast Parishes of Louisiana, Intermediate Submission 2: Offshore Water Levels and Waves*, July 2008.

[17] The design elevation effort led by Nancy Powell of the USACE New Orleans District with support from Royal Haskoning; documented in USACE New Orleans District, *Hurricane and Storm Damage Risk Reduction System, Design Elevation Report*, Draft Report Version 4.0, August 18, 2010. The evaluation of polder hazard led by Jerry Foster, USACE Headquarters; documented in IPET Volume VIII, 2009. Resiliency design is still in progress.

[18] Led by Donald T. Resio and Joannes J. Westerink. Task 5 is documented in USACE, *Louisiana Coastal Protection and Restoration, Final Technical Report*, June 2009.

In preparing the 2012 Master Plan, the Louisiana CPRA has also made extensive use of the 2005-09 surge hazard analysis.

It is important to note that the NFIP and its concentration on the 100-yr property risks can impose programmatic, resource, cost, and schedule constraints on flood hazard analysis. However, the multiple post-Katrina programs, spurred the USACE to employ considerable professional, academic, and other technical resources in conducting the 2005-09 effort. As a result, the USACE demonstrably enhanced the state of scientific knowledge and the state of practice for surge hazard analysis.

As part of this effort the USACE engaged a senior review team to suggest improvements.[19] The National Academy of Engineers' report also included comments on the USACE analysis. The USACE adopted suggestions of the peer review team which were deemed consistent with program requirements.

I.6. Uncertainty in Surge Hazard Estimates

As noted above, rational surge risk management must not only be mindful of the probability for surge events and consequences, but must also allow for uncertainty in estimating these probabilities and consequences. Compared to rainfall/riverine flood hazard estimates, surge hazard estimates are based on shorter historical records and generally involve more variables—with more complex interactions and subject to significant unknowns. Uncertainties can involve the precision of observations, measurements, and models (epistemic) and the sampling of natural variability (aleatory).

The NFIP does not require that local 100-yr flood hazards be defined with allowances for uncertainty. In part this is because risks associated with uncertainty to the NFIP can be managed actuarially across the entire national program. However, locally focused risk management does require accounting for the risk associated with uncertainty in hazard estimates. Given the multiple purposes of the 2005-09 surge hazard analysis, the USACE incorporated some analysis of uncertainty, including allowances for uncertainty in the HSDRRS design

For simplicity, epistemic uncertainty in a surge hazard estimate has been described with a normal distribution. Figure I.3.a presents a series of normal distribution curves around a median surge estimate of 15 ft. The series of curves illustrates that for higher relative standard deviations (i.e., the standard deviation as a percent of the median estimate) the distribution becomes wider. Figure 1.3.b. shows that for these curves, the 90% confidence interval also becomes much wider. The large uncertainty in surge hazard variables leads to wide uncertainty intervals in surge hazard estimates. The standard deviation for epistemic uncertainty alone for a 15 ft 100-yr surge estimate can be above 2.6 ft (21%), yielding a 90% confidence interval greater than 4.3 ft (34%).

Treating uncertainties as normally distributed may be supportable for certain purposes. However, over reliance on the assumption of a normal distribution can be misleading. Figure 1.3.c illustrates that a symmetrical distribution does not have to be normal, and can in fact have much "fatter tails," implying much higher probabilities for extreme events. Furthermore, critical uncertainties related to return frequency are not symmetrical. Figure 1.3.d compares a normal versus a skewed distribution. (See General Technical Note 1 for a further discussion of uncertainty.)

While there is extensive research on methods for quantifying uncertainties there have been no studies to guide the selection of appropriate confidence intervals for surge risk management.

---

[19] The review was led by led by Joseph N. Suhayda, Ph. D and is documented in USACE/FEMA, *Southeast Louisiana Joint Surge Study, Independent Technical Review, Final Report*, October 15, 2007.

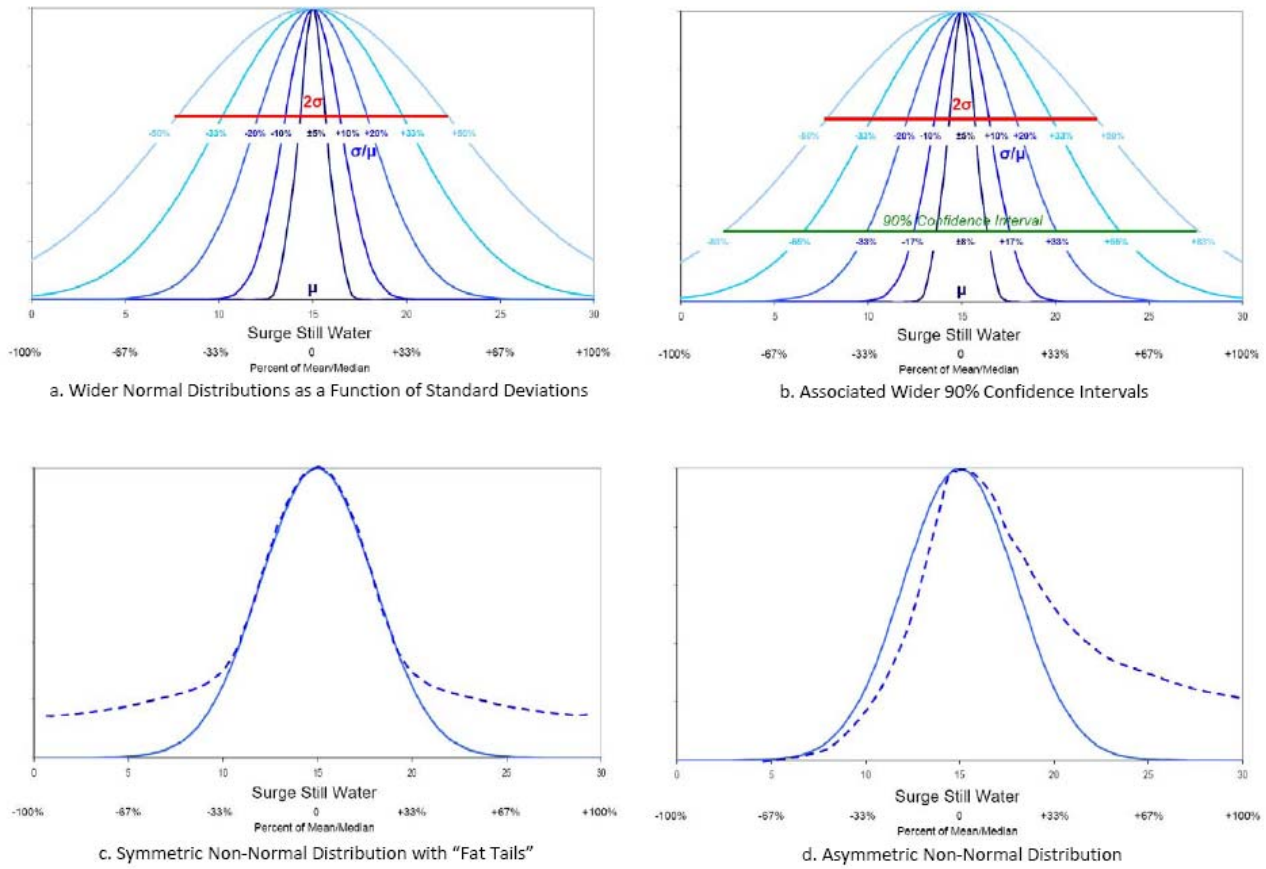

a. Wider Normal Distributions as a Function of Standard Deviations

b. Associated Wider 90% Confidence Intervals

c. Symmetric Non-Normal Distribution with "Fat Tails"

d. Asymmetric Non-Normal Distribution

Figure I.3. Normal and Non-Normal Distributions

I.7. This Report

*The SLFPA-E has a broad hurricane surge risk management missio*n. Unlike the NFIP, the SLFPA-E surge risk management decisions are not limited to property protection and controlled by the 100-yr hazard, but encompass concern for the full range of surge consequences and probabilties.

SLFPA-E's primary focus is on perimeter protection, including working with CPRA and USACE to:

1. Ensure that the HSDRRS design is capable of meeting the 100-yr overtopping criteria through planning, design, and construction review, as well as maintaining and operating the HSDRRS.
2. Ensure that the HSDRRS design is capable of meeting 500-yr HSDRRS resiliency through planning, design, and construction review, as well as maintaining and operating the HSDRRS.
3. Identify projects to further enhance HSDRRS risk reduction performance.

However, the SLFPA-E's mission also encompasses working with an array of federal, state, and local agencies and partners to plan and implement key actions on the other five public surge risk management tools. *Given its broad mission, a state-of-the-practice analysis of surge hazards and uncertainties is critical to the mission of the SLFPA-E.*

Since the USACE 2005-09 effort, approaches to the various tasks in hurricane surge hazard analysis have continued to evolve rapidly. Advances have been especially spurred on by research for hurricane surge forecasting and by coastal FISs for Mississippi, Texas, North Carolina, South Carolina, Georgia/Northeast Florida, and Florida-Big Bend, West Coast Florida and Northwest Florida/Alabama. These advances have improved the estimation of surge hazards and the treatment of uncertainties, and have important ramifications for southeast Louisiana surge risk management.

Bob Jacobsen PE, LLC has prepared this Report, entitled *Hurricane Surge Hazard Analysis: the State of the Practice and Recent Applications for Southeast Louisiana*, in accordance with a Task Order from the SLFPA-E. The objective of this Report is to provide a comprehensive explanation of the evolving technical approach to hurricane surge hazard analysis and an evaluation of the USACE 2005-09 effort in the context of this evolution, including those steps critical to the USACE's HSDRRS design.

To accomplish this objective, this Report is organized into five parts, corresponding to the five surge hazard analysis tasks:

Part I. Hurricane Climatology
Part II. Modeling of Hurricane Surge Physics
Part III. Hurricane Surge Hazard Analysis
Part IV. Hurricane Surge Hazard Analysis for Polders
Part V. Hurricane Surge Hazard Analysis for Future Conditions

Each part provides a detailed discussion of the current state of the practice for the respective tasks—including the approaches, assumptions, and limitations. As Tasks 1 and 2 are the basis for the entire surge hazard analysis, Parts I and II include an extensive background for these subjects. Background information is taken not only from the USACE's southeast Louisiana hazard study but from other recent wind and surge hurricane hazard studies, the relevant scientific and technical literature, and several significant new analyses of these subjects conducted for this Report.

Each part examines the USACE's application of the respective task to southeast Louisiana, as well as other recent applications, including the State of Louisiana's 2012 Comprehensive Master Plan for a Sustainable Coast. Key comments from the USACE senior technical review are incorporated into the discussion. Each part is concluded with a list of essential findings and recommendations.

The recommendations include revising the 2005-09 surge hazard analysis to a) remedy significant biases resulting from outdated methods and b) better describe uncertainties. In addition, the recommendations note important research opportunities to significantly advance the current state of the practice. The final section of this Report's Executive Summary also addresses implications of these revisions for the HSDRRS design and other surge risk management actions.

Part I.
Hurricane Climatology

NOAA 2005

Hurricanes occur often in the Gulf of Mexico (GoM), with a total of 249 recorded over the 161-year period from 1851 through 2011.[1] Of these, 87 made landfall along a roughly 500 mile east-west portion of the central-northern GoM (CN-GoM) centered on southeast Louisiana and stretching from Sabine Pass at the Texas-Louisiana border to the Bay-Gulf County border just east of Panama City FL. A strong hurricane makes landfall in this region many times over the average human life-span, producing some of the most severe local surges seen in the coastal United States.

This Part I presents the state of the practice in quantifying hurricane climatology for the CN-GoM, and in particular southeast Louisiana, including four topics:

Section 1., the six hurricane characteristics which influence surge and associated waves (which are often lumped together as surge for the purposes of this Part I) at a landfall location—core intensity, core size, wind field geometry, dynamics, track angle, and forward speed;

Section 2., the influence of seasonal and climate cycles and climate change on these characteristics;

Section 3., hurricane landfall probabilities; and

Section 4., hurricane joint probabilities;

These sections discuss the established scientific literature and ongoing research, including methods, assumptions, and limitations. The USACE evaluation of southeast Louisiana hurricane climatology, done in support of their 2005-09 surge hazard analysis, is among the work reviewed. In addition to the work of others, the sections incorporate results from a *new* analysis of the hurricane record updated through 2011. Afterwards, a list of conclusions is presented, together with recommendations for improving our understanding of hurricane climatology for southeast Louisiana. Part II addresses the physics of hurricane surge and the development of hydrodynamic models to capture the physics. Part III describes how joint probability analysis for hurricanes is combined with the hydrodynamic modeling to evaluate hurricane surge hazards.

[1] Based on National Oceanic and Atmospheric Administration, National Climatic Data Center, International Best Track data, Basin.NA.ibtracs_wmo.v03r02.csv ,downloaded on September 30, 2011. Supplemented with 2010 and 2011 data. ftp://eclipse.ncdc.noaa.gov/pub/ibtracs/v03r03/all/csv/basin

Section 1. Hurricane Characteristics

Before modern weather satellites, coastal radar, and aircraft missions, hurricane data were comprised of coastal weather station and shipboard observations. The surge produced by a hurricane at any given point of interest along the coast was commonly considered in terms of four characteristics at, or just prior to, landfall. These included two cyclonic characteristics—the intensity (wind speed and central pressure) and size (eye diameter), both measured at the cyclone's core—and the storm's track (which encompassed its landfall location and approach heading to the coast) and forward speed. With advances in the spatial coverage and frequency of hurricane observations, especially offshore, scientists no longer consider a snapshot of core intensity and size—at or just prior to landfall—to be sufficient for understanding the cyclonic influences on surge. Scientists are now also examining the role of two additional characteristics: the extended wind field and storm evolution.

The National Oceanic and Atmospheric Administration (NOAA) through a variety of divisions—e.g., Climate Prediction Center (CPC), Coastal Services Center (CSC), Geophysical Fluid Dynamics Laboratory (GFDL), Hurricane Research Division (HRD), National Climate Data Center (NCDC), and National Hurricane Center (NHC)—publishes tropical cyclone related data and research for the Atlantic basin. These data encompass nearly 1,700 tropical cyclones (870 hurricanes) for the 161-yr period beginning in 1851 and extending through 2011. Information on historical hurricanes is not static and is often revised as a result of ongoing research. Scientists have used historic data to assess the recurrence, correlations, and trends (see GTN-1 for an explanation of these terms) in Atlantic basin tropical cyclone characteristics. To avoid potential bias associated with the incompleteness or inaccuracy of records prior to the advent of satellite and aircraft reconnaissance many scientists choose to only use more recent observations (e.g., Toro uses data beginning from 1940, Toro 2008).

1.1. Core Intensity

A tropical cyclone features a center of low atmospheric pressure, which induces a counterclockwise circulation of winds in the northern hemisphere. The differential atmospheric pressure measured between the low pressure at the cyclone center, and the higher far-field ambient pressure (typically about 1020 millibars, mb) is the central pressure deficit (CPD or ΔP). In mature hurricanes the low pressure center forms an "eye" with relatively light winds and clear skies. The maximum sustained wind velocity (V_{max}) is usually found at the eyewall.[1] The eye CPD and eyewall V_{max} are traditional and convenient ways of summarizing a storm's intensity and facilitate characterization of the most destructive wind and pressure hazards to coastal buildings. CPD and V_{max} are highly transient and localized properties—they indicate a storm's greatest intensity but only for a specific time and location.

[1] Maximum sustained surface winds are defined as the average wind speed over a 1 minute period at an elevation of 10 meters above the ground at an unobstructed location (e.g., over open water). Wind speeds observed at flight level are reduced (using a factor of 65 to 90%) to estimate surface winds. Some atmospheric models that develop wind circulation patterns from regional atmospheric pressure conditions provide winds as 30-minute averages. For wind stress applied to water, hydrologists use a 10-minute average wind. Meteorologists and structural engineers often also refer to the 3 second gust. Generalized conversions between wind averages can be applied at various coastal regions. Well offshore some coversions are: 10-min/30-min = 1.03 to 1.09; 1-min/30-min = 1.11 to 1.24; and 3-sec (gust)/1-min = 1.11 to 1.3; the higher end of the range was used in the southeast Louisiana FIS (USACE 2008) while the lower end was recommended by Harper et al 2008.

A hurricane's CPD and V_{max} are important to its potential to generate surge. Hurricane wind is the most significant surge force, typically accounting for at least 80% of the increase in the SWL (Kurian 2009). Low atmospheric pressure also contributes a direct SWL increase near the core. Each 10 mb drop in central pressure translates into a SWL rise of about 4 inches. Surge SWL correlates with core intensity—with CPD linearly and with V_{max}^2—with all other hurricane attributes and coastal landscape factors (see Part II) being equal (Resio et al 2007).

Since its development in 1971 meteorologists have employed the familiar Saffir-Simpson Scale (SSS), shown in Table 1.1, to rank a hurricane's changing core intensity over its history. The SSS, consisting of five categories of hurricanes, was originally developed to rate potential wind damage. Hurricanes of Category 3 and higher are considered major hurricanes. As with core intensity the SSS is effective in rating surge potential if other hurricane attributes and coastal landscape factors are equal. However, the remaining attributes and coastal factors play critical parts in surge hazard and the SSS should not be used alone to judge surge potential (Fitzpatrick et al 2010). For example, Category 5 Hurricanes Camille (1969) and Category 3 Katrina (2005) both made landfall near Bay St. Louis MS but the surge of the latter exceeded the former by many feet.

Table 1.2 presents the number and percentage of recorded Atlantic basin and GoM hurricanes by SSS. A total of 88 GoM major hurricanes (GMHs) have occurred, or nearly 29% of all recorded Atlantic Basin major hurricanes. Over the 161-yr record this equates to a simple average of 55 GMHs per century. Table 1.2 also provides the number of hurricanes making landfall in the CN-GoM at Category 3 or higher. Thirty out of 88 GMHs, have struck the CN-GoM at major status, a simple average of 19 per century. These 30 hurricanes account for **over one-third of all GMHs and *nearly 10% of all Atlantic major hurricanes.*** GMH landfalls in the CN-GoM are discussed further in Section 3.

Table 1.1. Saffir-Simpson Scale[2]

Category	V_{max}			Central Pressure	
	mph	m/s	knots	mb	CPD mb (ambient at 1020 mb)
Tropical Depression	< 39				
Tropical Storm	39-73	17 - 33		< 1,000	> 20
1	74-95	33-42	64-82	< 980	> 41
2	96-110	43-49	83-95	979-965	41- 56
3	111-130	50-58	96-113	964-945	56 - 75
4	131-155	59-69	114-135	944-920	76 - 100
5	156+	70+	136+	< 920	>100

[2] This Part I Report was prepared in early 2012. Later in the year, prior to the 2012 hurricane season, NOAA slightly modified the wind categories for major hurricanes. The renamed Saffir Simpson Hurricane *Wind* Scale now provides Category 3 as 111-129 mph (96-112 kt); Category 4 as 130-156 mph (113-136 kt); and Category 5 as 157 mph or higher (137 kt).

Table 1.2. Number of Hurricanes by Saffir-Simpson Scale (1851 to 2011)

Category	Atlantic Basin	GoM	At CN-GoM Landfall	GoM / Atlantic Basin	At CN-GoM Landfall / GoM
1	338	103	39	30.5%	37.9%
2	224	58	18	25.9%	31.0%
3	170	44	22	25.9%	50.0%
4	106	34	7	32.1%	20.6%
5	32	10	1	31.3%	10.0%
All	870	249	87	28.6%	34.9%
per century	540	155	54		
Major	308	88	30	28.6%	34.1%
per century	191	55	19		

The ten GoM hurricanes reaching Category 5 and their GoM peak V_{max} (mph) were:

- 2005 Katrina, 172.5
- 2005 Rita, 178.25
- 2004 Ivan, 161
- 1980 Allen, 189.75
- 1977 Anita, 172.5
- 1969 Camille, 189.75
- 1967 Beulah, 161
- 1961 Carla, 172.5
- 1960 Ethel, 161
- 1924 Not Named, 166.75

Of these, ***half*** (Ethel, Camille, Ivan, Katrina, and Rita), made landfall in the CN-GoM. However only one, Camille actually made landfall in the CN-GoM at Category 5 strength.

Figure 1.1 presents the cumulative number of GoM hurricanes by SSS recorded from 1851 through 2011. The cumulative rates for all categories do not indicate any dramatic changes over the 161-yr period. Some minor step increases are apparent in the 1880s and 1930s, presumably associated with improved observations. Figures 1.2.a and 1.2.b present the linear trends in hurricane and GMH cumulative frequency for the overall 1851-2011 period, and a more recent 1940-2011 period. The overall linear rates for hurricanes and GMHs for 1851-2011 are 153 and 52 per century (the latter being slightly less than the simple average noted above), with coefficient of determination values (R^2) of 0.998 and 0.978. The post-1940 trend for all hurricanes is nearly identical, with an R^2 value of 0.995. However, the post-1940 trend for GMHs is 44% higher, at 75 per century, with an R^2 value of 0.964.

The 1851-2011 GoM data includes a peak V_{max} value for each hurricane (but not CPD), and can be used to evaluate the observed relative and cumulative frequency for core intensity.[3] Figure 1.3 presents the relative frequency for hurricane peak V_{max} for the GoM at 5.75 mph (5 knot) increments. Figure 1.4 illustrates the cumulative frequency. The V_{max} distribution is very asymmetric, consistent with the decreasing frequency of higher intensity storms.

[3] See GTN-1 for definitions and discussion of relative frequency, cumulative frequency, return frequency, return period, and probability distribution functions.

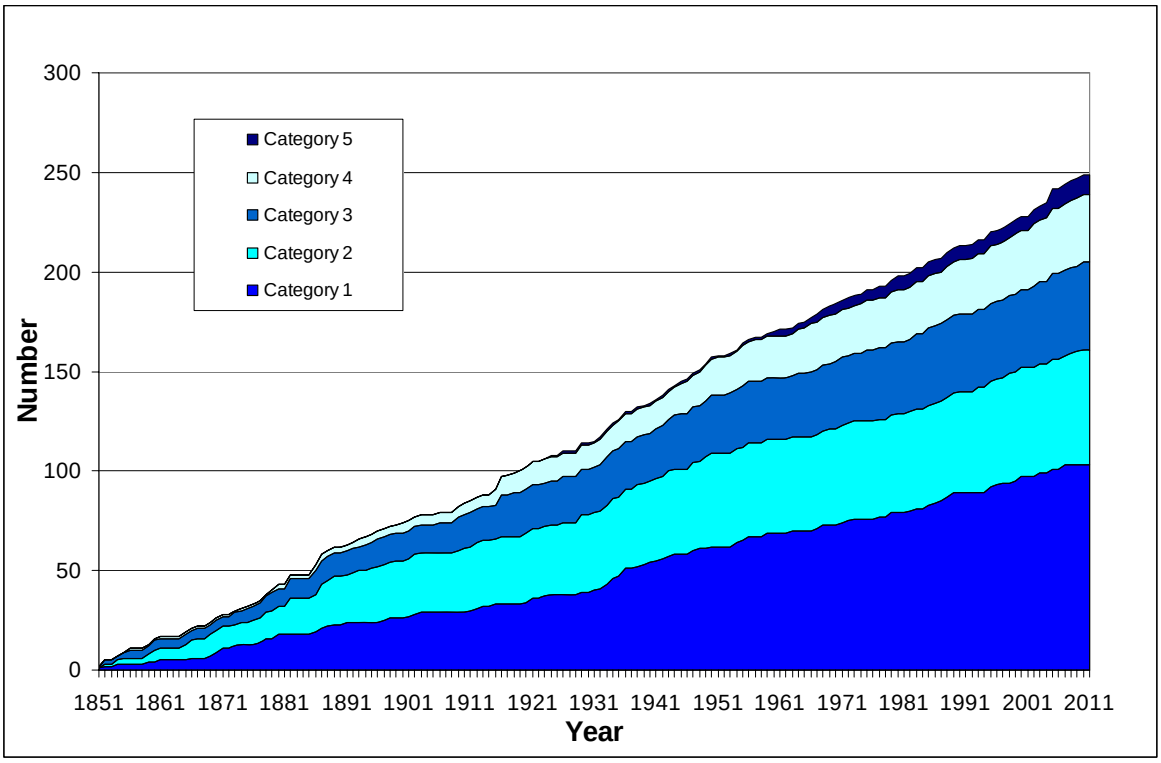

Figure 1.1. Cumulative Number of GoM Hurricanes by Saffir-Simpson Scale

Figure 1.5.a graphs the same GoM hurricane V_{max} information in the form of observed return period using a log transformation. The highest V_{max} (189.75 mph) was recorded twice out of 249 GoM hurricanes in 161 years, giving it an observed frequency of 0.68% and *T* of 95 years.[4] Figure 1.5.b depicts the observed return period V_{max} data compared to three probability distribution functions often used for highly skewed datasets: Log-normal, Gumbel, and Log Pearson Type III. As is typical, the distribution functions show some deviations from the observed frequencies and each other. [5]

Using the Gumbel distribution, the estimated return period for Category 3+, 4+, and 5 hurricanes in the GoM are 1.8, 4.2, and 13.9 years, respectively. The return period for GMHs corresponds to a frequency of 56 per century, close to the simple average noted above.

Figure 1.6 provides extrapolations of the three distribution functions. The estimated V_{max} values for the 500-yr hurricane are 207, 228, and 237 mph, respectively, and for the 1,000-yr hurricane are 217, 242, and 254 mph. However, simple extrapolation of probability functions to estimate extreme hurricane intensity ignore physical limitations of hurricane strength (see section below).

---

[4] Return Frequency (F_R) is calculated as (Rank – 0.3)/249.4 and T = (161/249) * (1/ F_R). If F_R is calculated using Rank/250 then F_R = 0.8% and T = is 81 years.

[5] As discussed in GTN-1, reliable estimates for extreme events require very long records extending many times the return period of interest.

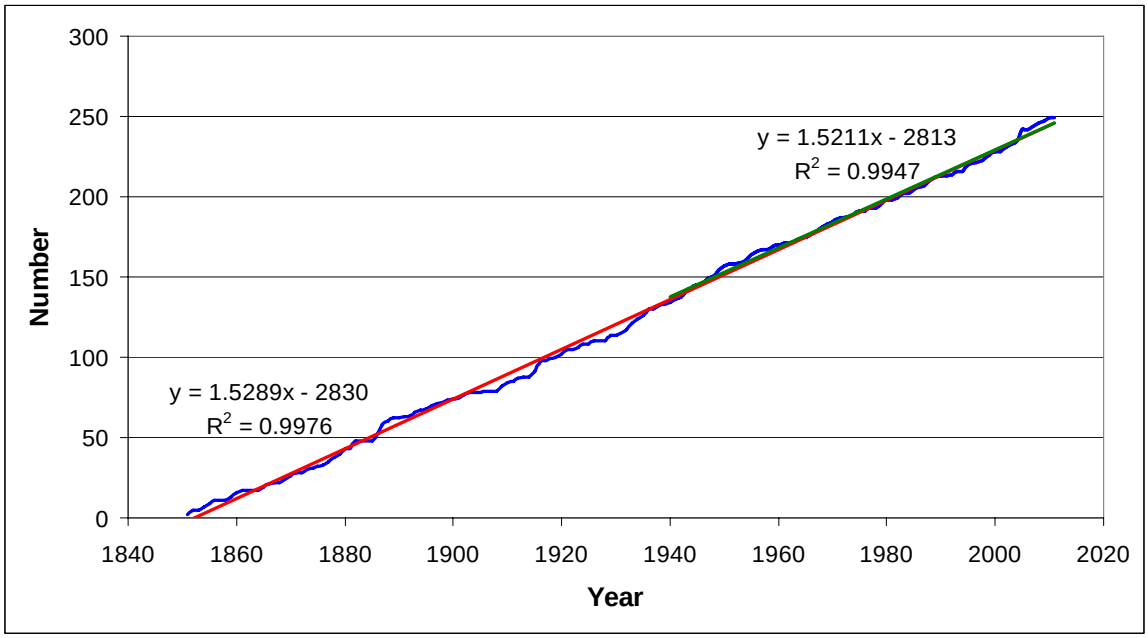

a. All Hurricanes 1851-2011 and 1940-2011

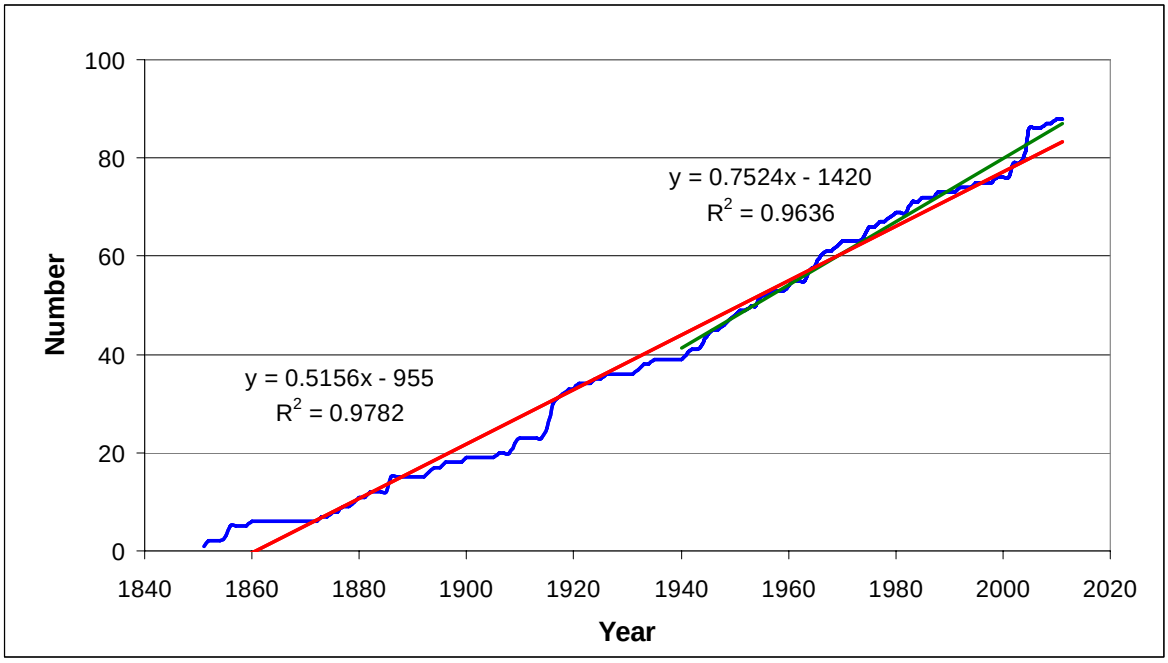

b. Major Hurricanes 1851-2011 and 1940-2011

Figure 1.2. Cumulative Number of GoM Hurricanes

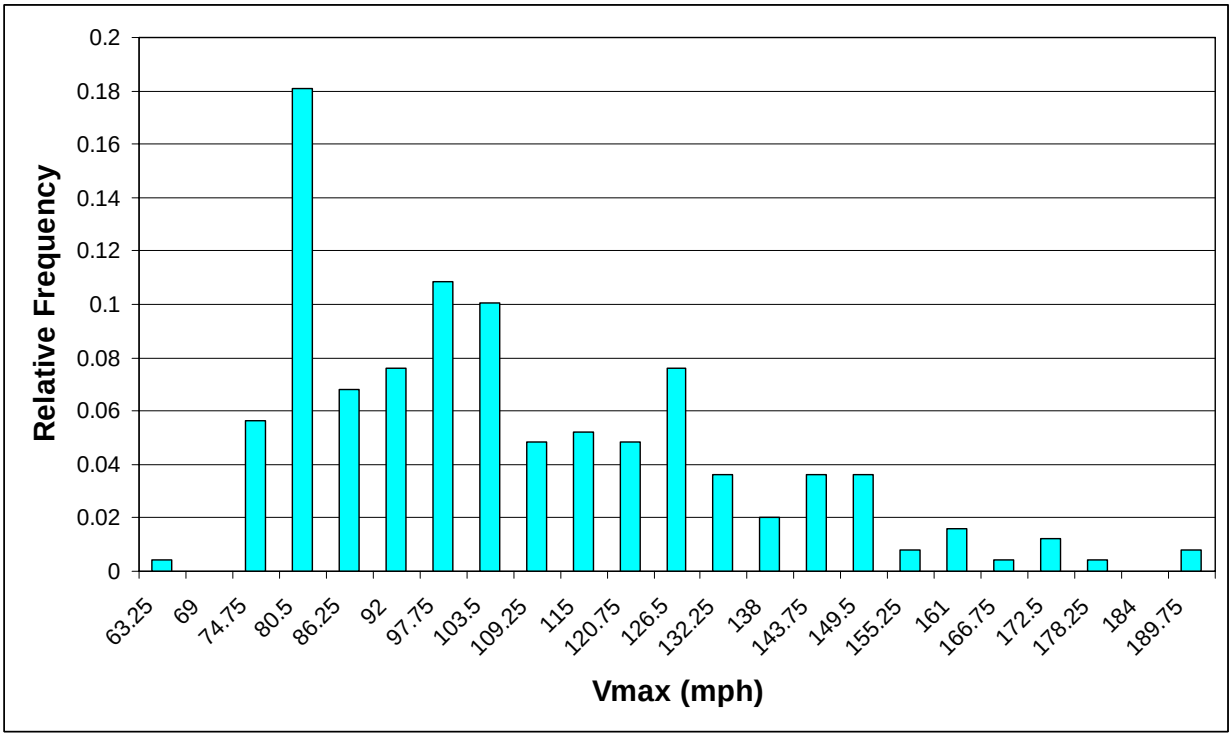

Figure 1.3. Relative Frequency of Hurricane V_{max} for the GoM (1851-2011)

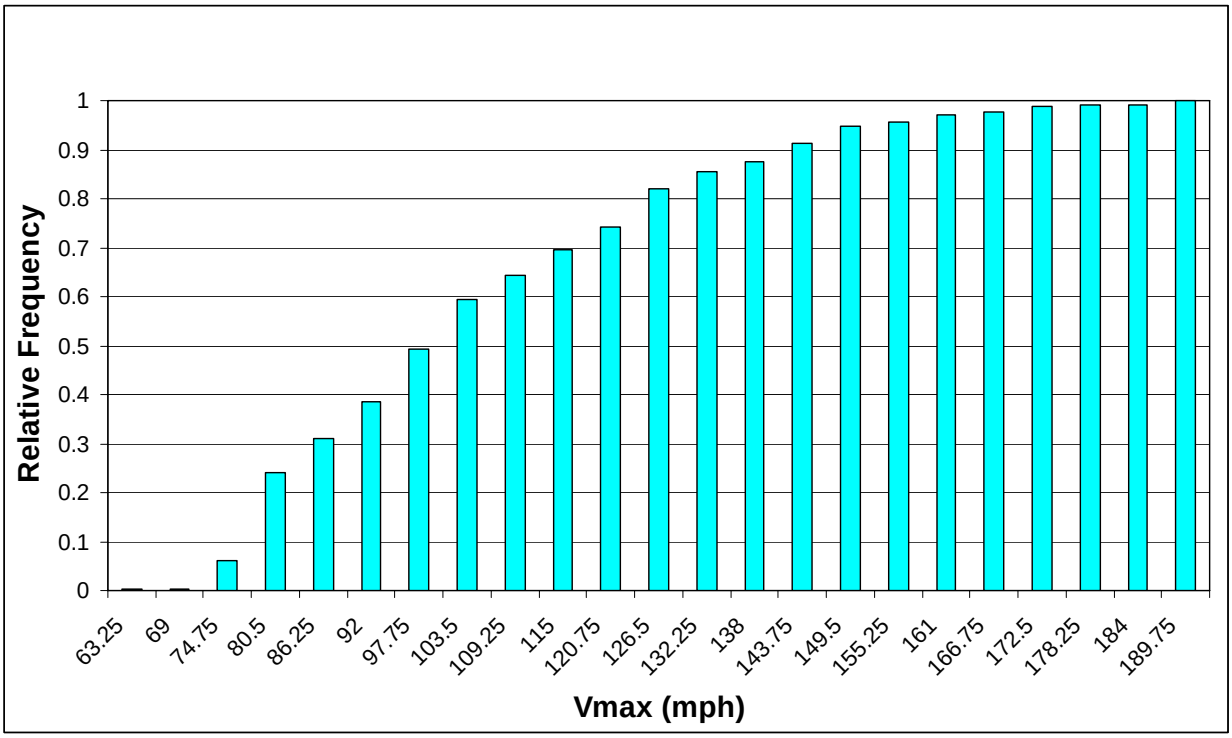

Figure 1.4. Cumulative Frequency of Hurricane V_{max} for the GoM (1851-2011)

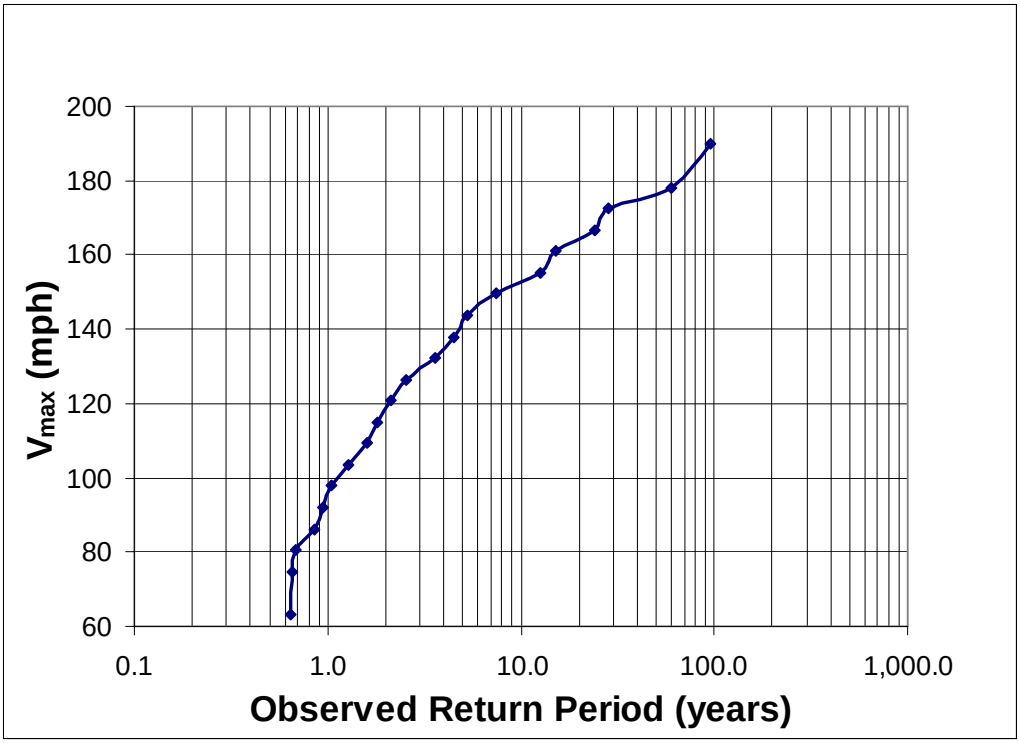

a. Observed Return Period

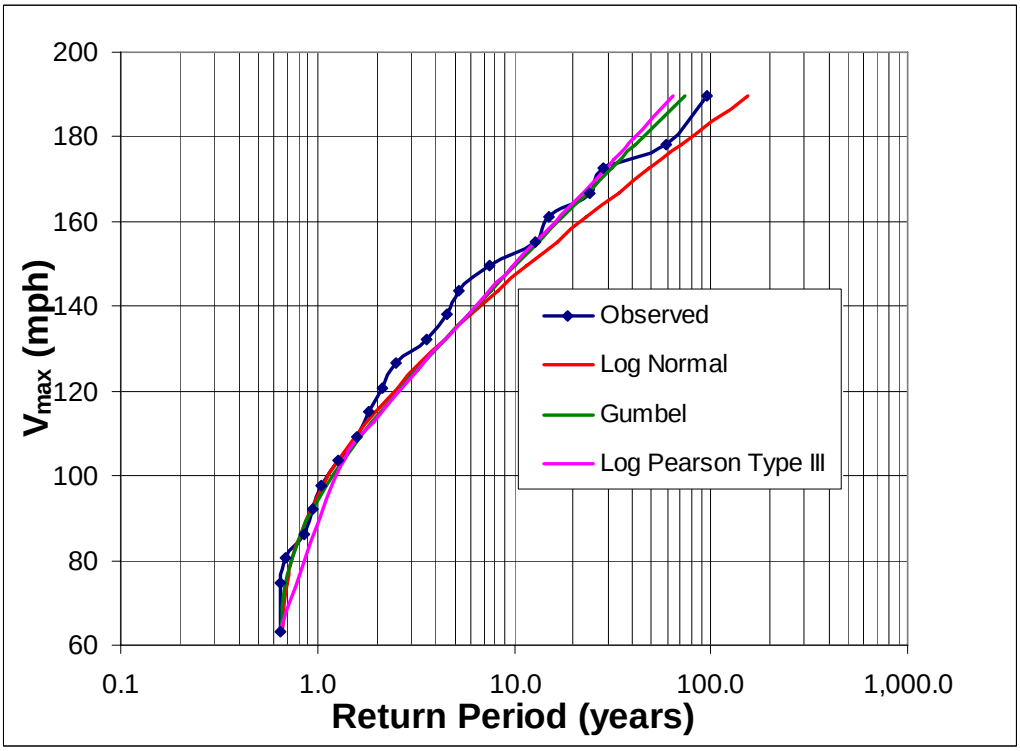

b. With Three Probability Distribution Functions

Figure 1.5. Return Period for GoM Hurricane V_{max}

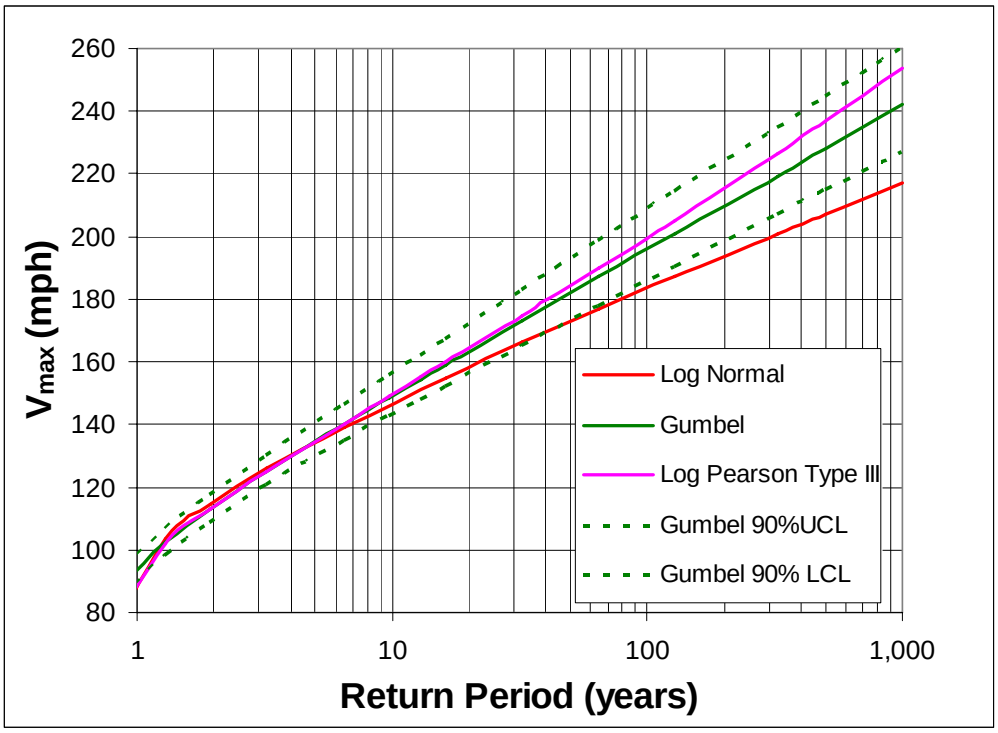

Figure 1.6. Extrapolation of Return Period for Hurricane V_{max} for the GoM

Importantly, for skewed distribution functions the confidence limits are also asymmetric. The lower confidence limit, mean estimate, and upper confidence limit for the 100-, 500-, and 1,000-yr return hurricane V_{max} (mph) using the Gumbel distribution are:

- 100-yr: 186, 196, and 209
- 500-yr: 215, 228, and 245
- 1,000-yr: 227, 242, and 260

Thus, at the 500-yr return, the lower confidence limit is 13 mph lower than the mean, while the upper confidence limit is 17 mph higher.

Hurricane scientists have examined the relationship between the two core intensity characteristics, V_{max} (mph) and CPD (mb). The SSS reflects a simple linear relationship: $V_{max} \approx CPD + 54$. Knaff and Zehr (2007) reviewed various CPD:V_{max}^2 correlations and, using 15 years of data and over 3,800 points, developed an improved equation:

$$V_{max} = 18.63 - 14.96S - 0.76\varphi - 0.52CPD + 9.74\sqrt{CPD} + 1.5c^{0.63}$$

for V_{max} in knots, Φ - latitude, S - a size parameter, and c - storm translation speed. Figure 1.7 compares the equation results and the data. The R^2 is 0.935 with a root mean square error (RMSE) of 9 mph.[6]

[6] See GTN-1 for a discussion of correlation analysis, R^2, and RMSE.

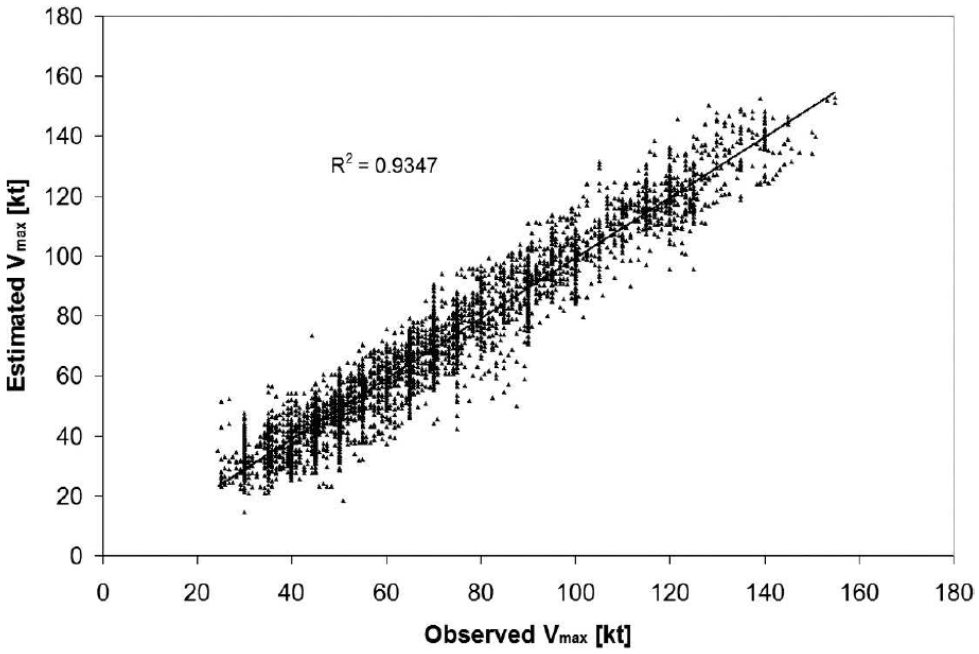

Figure 1.7. Observed V_{max} versus V_{max} Estimated as a Function of CPD
Knaff and Zehr, 2007

1.2. Core Size

Hurricane core size affects surge, as a larger core causes the strong eyewall winds to exert their stress over longer fetches of open water, setting larger areas of water in motion. Thus, large storm cores can create more expansive domes of water that compress into higher SWLs at the coastal shoreline (Irish et al 2008). The traditional and convenient short-hand for hurricane size has also been associated with the eye, in this case the radial distance from the center to the location of V_{max} (R_{max}), which is often approximated as the radius of the hurricane eye.

Observers have noted that extreme hurricane intensification and eye contraction tended to go hand-in-hand—much like a figure skater drawing in her arms and spinning faster. As small to moderate sized storms extract energy from warm ocean waters under supportive atmospheric conditions they can "spin up"—Hurricanes Ethel in 1960 and Camille in 1969 being two classic examples. Thus, there is an inverse correlation of intensity (e.g., CPD) and R_{max} for such individual hurricanes undergoing intensification. (Shen 2006a). In the past hurricane scientists thought that large storms were less capable of spinning up and only recently have they observed conditions conducive to large, intense hurricanes (e.g., Katrina, Rita). Consequently, they are now re-examining the physical mechanisms for hurricanes to become both large and extremely intense. (Shen 2006b)

While a CPD-R_{max} relationship has been shown for individual storms, the correlation between CPD and R_{max} across hurricanes is much less clear due to the wide variety of conditions associated with initial development and intensification. Using a subset of 59 US hurricanes, Louisiana State University researchers documented mean R_{max} and standard deviation values of 51 and 26 km for Category 3 storms, and 48 and 40 km for Category 4 storms, (Hsu and Yan 1998).

Cardone and Cox assessed the relationship of R_{max} and central pressure at peak intensity for 52 Category 2 and higher hurricanes (CPD >40) in the GoM (Resio et al 2007). Figure 1.8 shows that the range of observed R_{max} is fairly large, with R_{max} between 5 and 120 nautical miles. Some decline in R_{max} with lower central pressure (CP ≈ 1020 – CPD) can be seen in the figure. From this data they estimated a linear relationship of R_{max} = 14 + 0.3*(110-CPD), with a standard deviation (normal distribution) at 44% of the estimate, consistent with considerable scatter.

In a separate analysis Vickery (Appendix E, Resio et al 2007) analyzed flight data and surface wind files for selected GoM storms through 2005 (see Figure 1.9), and developed the following slight inverse exponential relationship: R_{max} (in km) = $3.859 - 7.7 \times 10^{-5}$ (CPD^2) . The R^2 for this relationship was 0.29. Figure 1.9 illustrates the wide scatter at ± two standard deviations.

Toro (G. R. Toro 2008) examined the correlation of CPD (referred to as DP) and R_p and, as depicted in Figure 1.10, also found a slight inverse relationship with considerable residual uncertainty. (R_p in Figure 1.10 is associated with the radial profile of the pressure deficit and essentially equal to R_{max}.)

One important factor which tends to distort a relationship between hurricane intensity and R_{max} is eyewall replacement. Following initial intensification and eye contraction, if conditions are conducive to further strengthening, hurricanes can undergo formation of a second, outer eyewall. When the inner wall breaks down, the hurricane intensity can temporarily drop until the second eyewall goes through its contraction cycle. Thus, major hurricanes can be associated with a range of eye diameters, including the possibility of two eyewalls. Hurricane Katrina appeared to be undergoing such a replacement as it made landfall and the complex distribution of the outer winds contributed to a very high surge in Pascagoula MS, 50 miles east of the landfall at Waveland MS (Blackwell et al 2008).

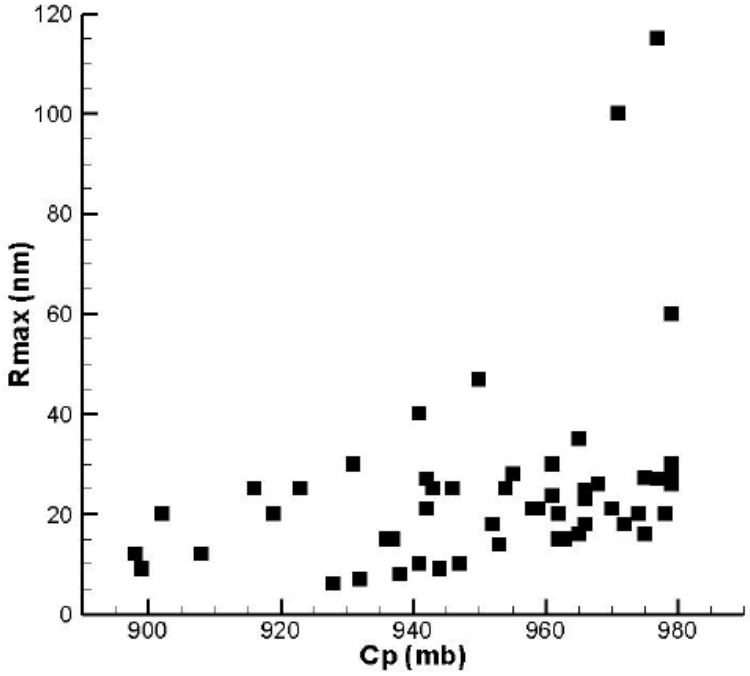

Figure 1.8. R_{max} versus Central Pressure
Cardone and Cox in Resio et al 2007

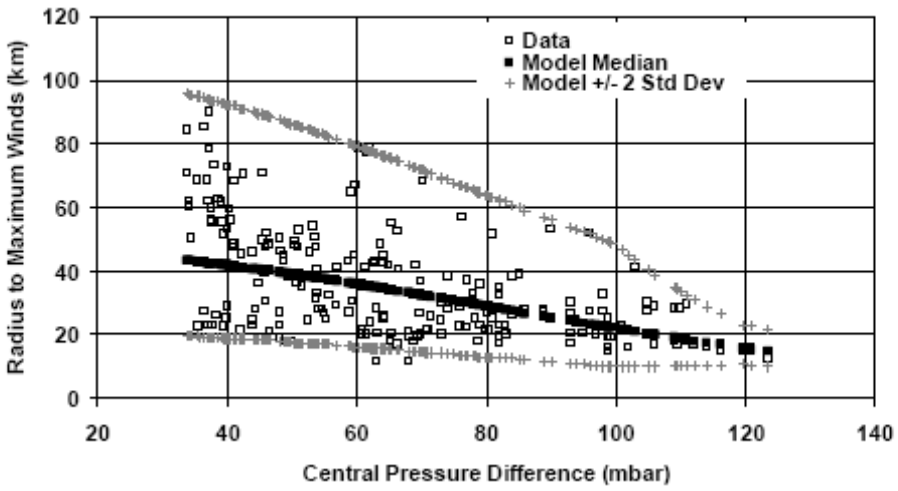

Figure 1.9. R_{max} versus CPD

Vickery in Resio et al 2007

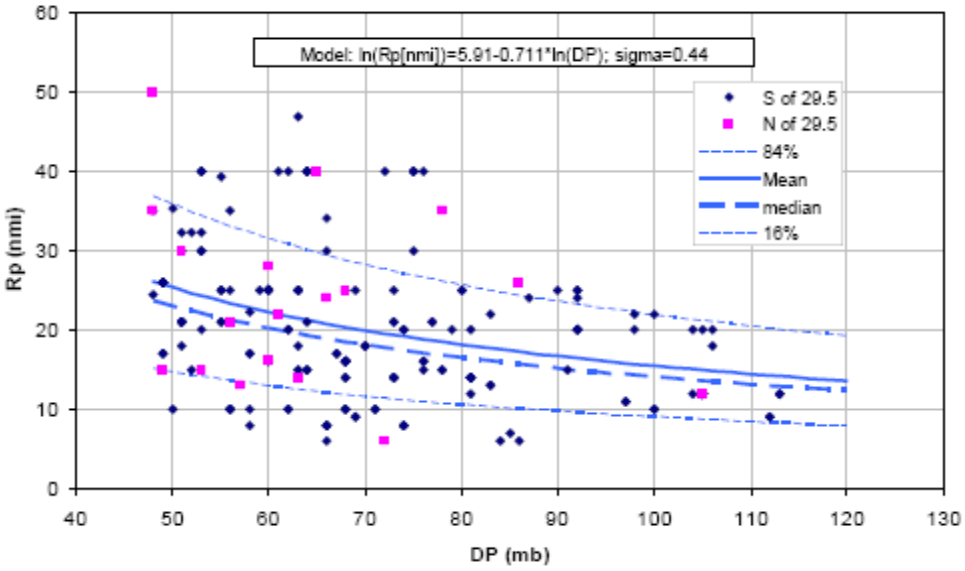

Figure 1.10. R_p versus CPD

G. R. Toro 2008

1.3. Wind Field Geometry

In addition to the size and strength of the eye wall winds, the extent and strength of the total wind field influence surge. For many decades NOAA has been collecting flight level wind data throughout tropical cyclones at frequent intervals. Since 1994, NOAA has employed this data, together with surface wind observations from buoys, ships, and land stations, to produce surface wind field analyses, generally at three hour intervals, termed H*Winds files. Figure 1.11 depicts several H*Winds snapshots for Hurricanes Katrina, Rita, and Gustav. To better indicate the wind field size, storms are often described in terms of the radius of hurricane force and tropical storm force winds (R_H and R_{TS}). The R_H and R_{TS} at peak GoM intensity for several recent hurricanes are shown in Table 1.3.

Figure 1.11 illustrates that the radial wind profile in hurricanes of equal category can vary dramatically. Figure 1.12 shows wind field snapshots for Hurricanes Gustav and Ike at which both storms had nearly identical V_{max} values of 105 mph. However R_H in the northeast quadrant for Hurricane Ike was 86% farther than for Gustav, at 141 versus 76 miles. In the same quadrant, the extent of tropical storm force winds was about 27% higher, at 290 versus 228 miles. The Hurricane Gustav H*Winds at 1930 UTC (Figure 1.11) illustrate that the radial profile can also be quite asymmetric, with hurricane force winds ranging between 76, 47, 41, and 60 miles in the four quadrants.

It is important to recognize at least four potential issues with H*Wind files:

1. Quality and spatial limits of wind measurements; while H*Winds are fitted to actual wind data, there are usually very few observations relative to the wind field area; near coast and on-land peak wind observations are often not available due to station damage;
2. Interpolation and extrapolation of surface winds from flight level data;
3. Lack of sufficient data to characterize wind field structures—such as secondary eyewalls, banding, asymmetry, etc—that are observed in other sources (e.g., satellite, radar, etc.); and
4. Lack of sufficient data to characterize wind field dynamics—such as infilling and sheltering.

These issues often lead to extensive review of surface wind field accuracy. For example, because hindcasts of historic hurricanes rely on surface winds to force the surge and wave model (see Part II) modelers will modify the wind data to improve surge simulation accuracy when there is reasonable justification (see model validation for Hurricanes Betsy and Camille, FEMA 2007).

Table 1.3. Examples of Extent of Hurricane and Tropical Storm Force Winds

Name	Year	Peak Category	Peak V_{max} (mph)	R_{max} (miles)	R_H (miles)	R_{TS} (miles)
Isadore	2002	3	126.5	14	49	181
Lili	2002	4	143.75	10	61	183
Ivan	2004	5	161	25	90	213
Dennis	2005	4	143.75	9	25	174
Katrina	2005	5	172.5	21	105	227
Rita	2005	5	178.25	12	52	202
Gustav	2008	4	138	18	52	189
Ike	2008	2	109.25	61	136	297

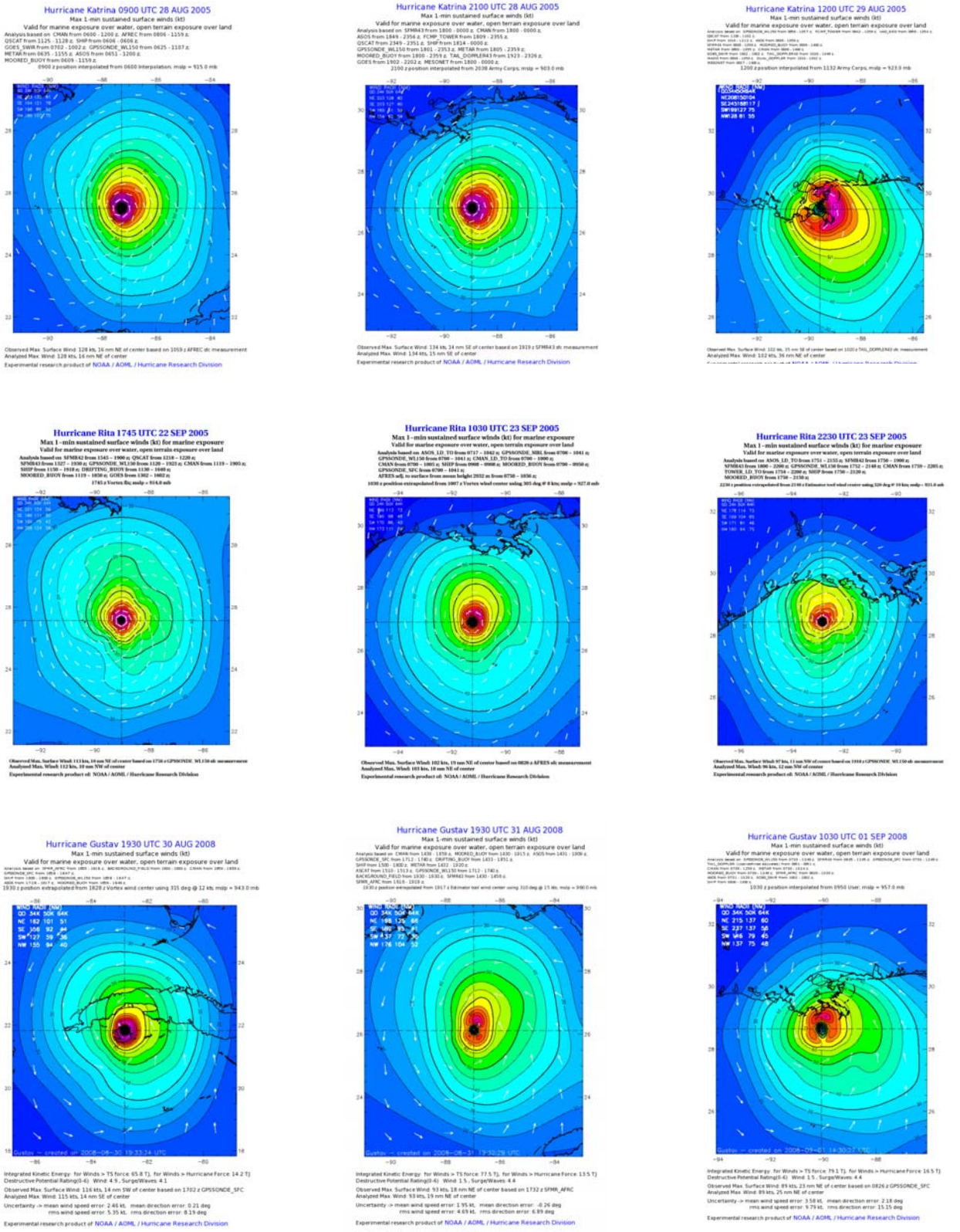

Figure 1.11. Example H*Wind Snapshots

NOAA-HRD, http://www.aoml.noaa.gov/hrd/data_sub/hurr.html

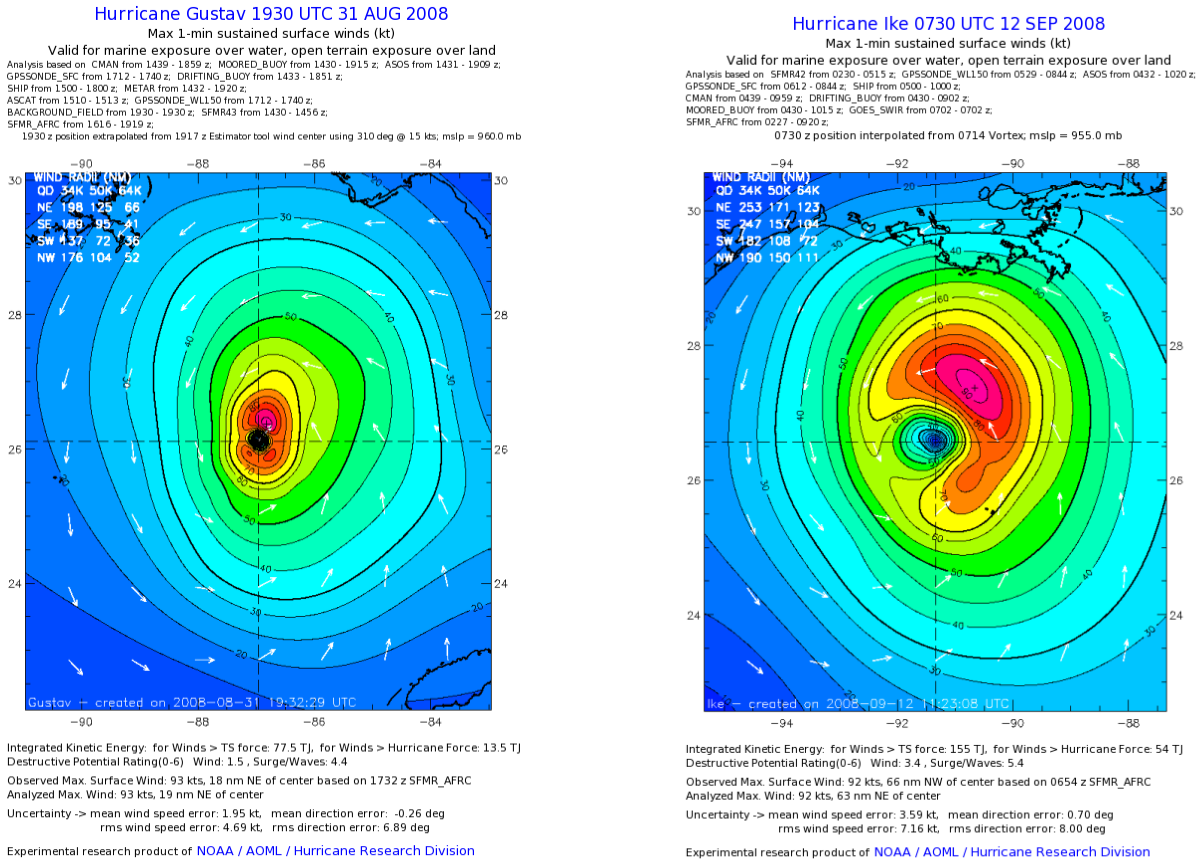

Figure 1.12. Comparison of Hurricane Gustav and Ike Wind Fields at Similar V_{max}
NOAA-HRD, http://www.aoml.noaa.gov/hrd/data_sub/hurr.html

In 1980 Holland proposed using an exponential function to describe the radial drop off in intensity (pressure deficit, PD) with distance from the storm center (r) (Holland 1980):

$$PD = CPD * \exp - \left(R_{\max} / r\right)^{B}$$

The Holland B parameter ranges from 0.5 to 2.0 and adjusts the peakedness in the radial intensity decline, with higher Holland B values providing a more gradual radial drop off. Vickery et al showed that Holland B could be used to accurately describe hurricane radial wind profiles using a modified approach to estimating the parameter from flight data (Vickery et al 2000). Vickery's 2007 analysis of flight level data and H*Wind files showed that increasing Holland B is weakly correlated with decreasing R_{max} and latitude (i.e., Coriolis force) and with increasing CPD (Resio et al 2007). Figure 1.13 illustrates the correlations, all of which showed considerable residual scatter. The strongest correlation was between higher Holland B values and higher sea surface temperatures (SST), supporting the physical theory that larger hurricane wind fields require greater ocean energy. Vickery suggested that large (higher R_{max}) intense (low CP) hurricanes likely have a Holland B upper limit of about 1.2.

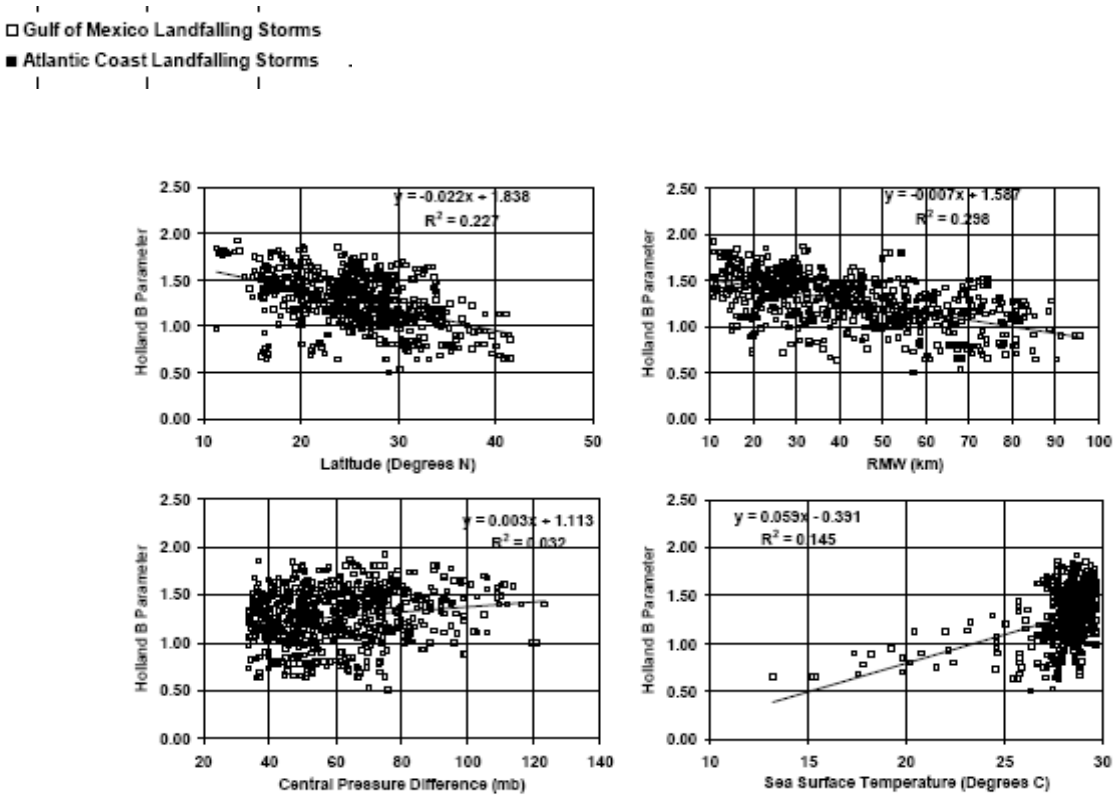

Figure 1.13. Holland B Parameter versus Latitude, R_{max}, CPD, and SST
Vickery in Resio et al 2007

To better account for hurricane asymmetry the Holland B parameter can be specified by wind field quadrant. The research described above addresses only correlations involving the average Holland B value.

In 2007 Powell and Reinhold proposed characterizing hurricanes on the basis of the total wind *integrated kinetic energy* (IKE) contained over the tropical cyclone area at any point in time (Powell and Reinhold 2007). The kinetic energy at any point in the wind field is a function of the velocity squared (V^2), which better correlates to actual wind hazard and surge generation physics. IKE thus better describes a hurricane's overall areal wind and surge strength. The IKE is usually measured over the area for which winds exceed some threshold, e.g., tropical storm force (IKE_{TS}), hurricane force (IKE_H), etc. The IKE for large lower category hurricanes can exceed those for higher category storms. Hurricanes Ike and Katrina had peak V_{max} of 109 and 172 mph, respectively, but peak IKE_{TS} of 120 and 117 terajoules (TJ) respectively (Powell and Reinhold 2007). Fritz examined the correlation of IKE_{TS} to R_{TS} and V_{max} for multiple observations of 139 U.S. landfalling hurricanes (1988 to 2008) and found that size was more important in predicting IKE_{TS} than core intensity, with R^2 of 0.94 and 0.29 respectively (see Figure 1.14).

Because IKE does not scale strongly with the core intensity it does not give a good indication of the landfall area surge peak. To account for both core intensity and IKE, Fitzpatrick proposed using a new characteristic based on $IKE^{1/2} \cdot V_{max}$ (which thus has the form of a velocity squared) to evaluate surge generating potential at landfall (Fitzpatrick et al 2010).

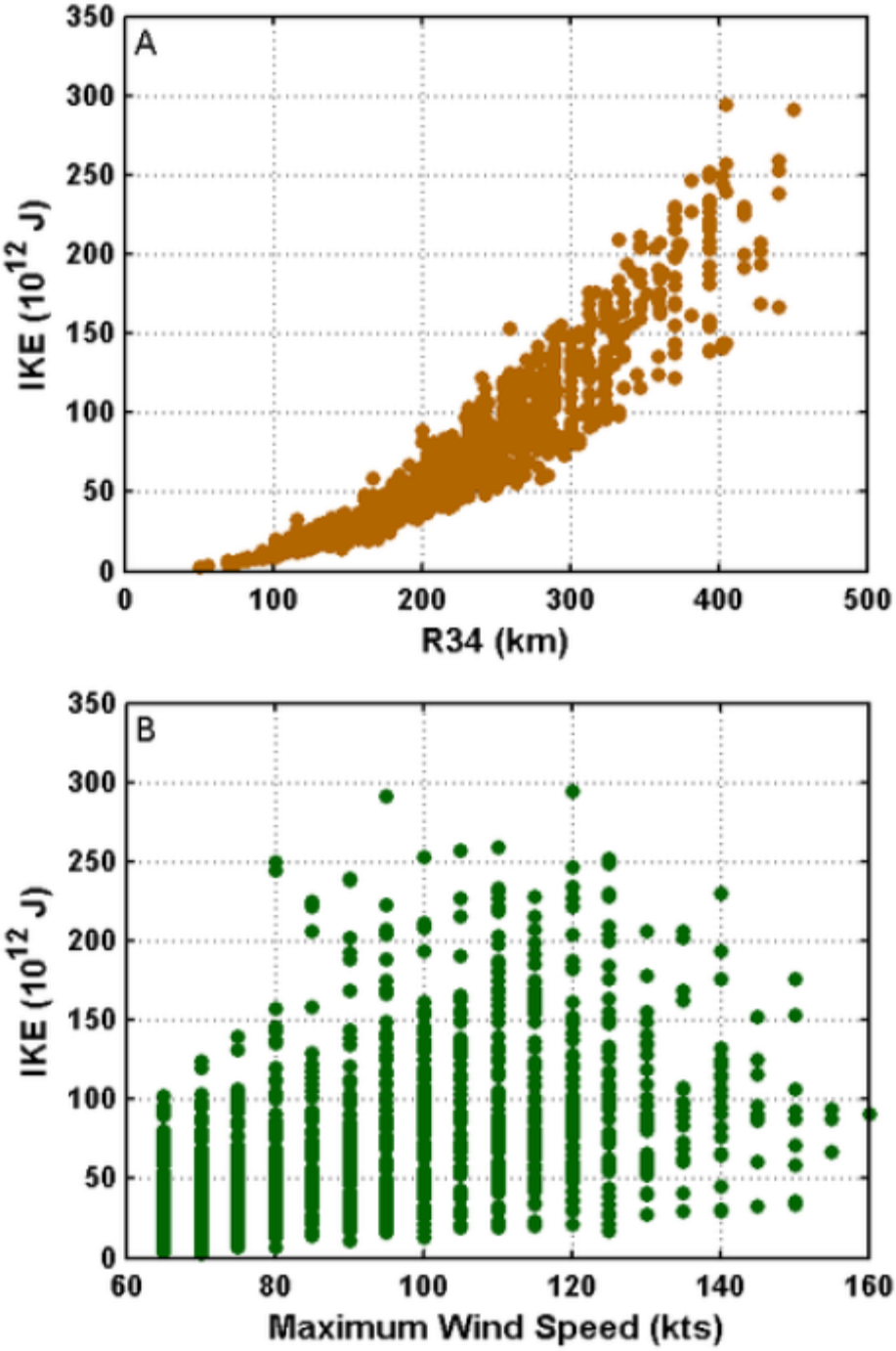

Figure 1.14. Relationship of IKE with R_{TS} and V_{max}
Fritz 2009

Other scientists have proposed alternatives for indicating the combined influence of wind field intensity and geometry, including wind velocity squared or cubed (see Kantha 2008). Five additional indices are:

- Hurricane Intensity Index (HII) = $(V_{max}/74)^2$
- Hurricane Hazard Index (HHI) = $(V_{max}/74)^3 * (R_H /R_{H0})$
- Hurricane Surge Index = $(V_{max}/74)^2 * (R_H /R_{H0})$
- Wind damage potential (W_{DP}) Index (0.1-5.9)
- Surge damage potential (S_{DP}) Index (0.1-5.9)

Powell and Reinhold developed the latter two based on IKE values (Powell and Reinhold 2008). Table 1.4 presents values for the IKE_{TS}, IKE_H, $IKE_{TS}^{1/2} * V_{max}$ and the above five indices for selected storms, and highlights the top three ranked storms according to each index. (For Powell and Reinhold analysis R_{H0} was the radius of hurricane force winds for Hurricane Andrew.)

The reinsurance industry uses the Carvill Hurricane Index (CHI, see Carvill undated):

$$CHI = (V_{max}/74)^3 + 1.5 * (R_H /R_{H0}) * (V_{max}/74)^2$$

where V_{max} is in mph and R_{H0} is a reference R_H. The CHI for several landfalling storms is shown in Table 1.5.

[In August 2012, following preparation of this Part I Report, Category 1 Hurricane Isaac made landfall in southeastern Louisiana , with tropical storm force winds extending out over 200 miles. Hurricane Isaac produced extremely high surges in several locations—in Braithwaite LA exceeding those from Hurricane Katrina. This further illustrates that the wind field distribution is a critical hurricane characteristic in evaluating the potential for severe storm surge.]

1.4. Hurricane Dynamics

Hurricanes making a CN-GoM landfall generally traverse the GoM in less than four days, during which time their intensity, size, and wind field distribution can undergo major changes.[7] Increasing availability of satellite and long-range reconnaissance information has allowed scientists to evaluate the nature of hurricane genesis, development, intensification, and decay. Hurricane dynamics are critical not only to understanding the mechanisms, frequencies, and climatic trends of major hurricane occurrence (Merrill 1988), but also to potential surge hazards.

Surge hazards cannot simply be considered a function of a pre-landfall snapshot of hurricane conditions. Hurricane dynamics affect the cumulative energy directed at the coast during the days preceding landfall. Large hurricanes located hundreds of miles away from their landfall can initiate early SWL rises, termed forerunners, which can then be magnified during landfall. Figure 1.15 presents several hydrographs for local tide gauges which illustrate the forerunner of Hurricane Ike in 2008.

[7] Major hurricanes can take less than 72 hours to cross the GoM (e.g., Hurricane Katrina) and emergency planners thus require forecasts well in advance of entry into the GoM.

Table 1.4. Examples of Alternative Hurricane Ranking Indices

Powell and Reinhold 2007, Kantha 2008

Storm	Year	R_{max} (miles)	CP (mb)	V_{max} (mph)	R_{TS} (miles)	R_H (miles)	SSS	IKE_{TS} (TJ)	IKE_H (TJ)	$IKE_{TS}*V_{max}$ (PJ-m/s)	HII	HHI	HSI	W_{DP}	S_{DP}
Andrew	1992	12	922	152	119	48	5	20	7	1.4	5.2	11.9	5.2	5	2.5
Camille	1969	9	909	145	143	68	5	63	31	4.1	5	15.8	7.1	5.2	4
Charley	2004	4	941	141	97	25	4	11	2	0.7	4.1	4.3	2.1	4.1	1.9
Dennis	2005	6	946	114	184	21	3	40	2	2.0	2.7	1.9	1.2	0.3	3.4
Emily	2005	15	948	121	181	53	3	70	14	3.8	3	5.8	3.4	1.7	4.2
Fabian	2003	42	941	114	236	86	3	123	40	6.3	3	9.3	5.4	3.7	5.1
Frances	2004	32	960	103	198	86	2	94	29	4.3	2	5.1	3.6	2.5	4.7
Hugo	1989	23	934	130	197	91	4	95	25	5.5	3.5	12.4	6.6	4.7	4.7
Iris	2001	5	948	96	103	23	4	5	1	0.2	3.8	3.6	1.8	0.1	1.3
Isabel	2003	54	957	105	331	133	2	174	42	8.2	1.9	7.3	5.3	3.4	5.6
Ivan (AL)	2004	22	946	110	203	80	3	81	26	4.0	2.7	7.4	4.5	2.2	4.4
Ivan (Jamaica)	2004	11	925	157	195	75	4	95	32	6.7	3.8	11.6	6	5.6	4.7
Jeanne	2004	30	950	103	197	81	3	73	21	3.4	2.7	7.5	4.6	1.9	4.3
Katrina (FL)	2005	9	984	74	71	17	1	5	0	0.2	1.2	0.5	0.4	0.1	1.3
Katrina (LA)	2005	40	920	116	282	135	3	122	49	6.3	3	14.6	8.4	3.7	5.1
Katrina peak	2005	16	909	159	217	86	5	124	45	8.8	5.2	21.4	9.4	5.8	5.1
Keith (Belize)	2000	12	959	112	96	27	3	11	4	0.6	2.4	2.1	1.4	0.5	1.9
Michelle	2001	17	949	112	208	50	4	61	14	3.1	3.5	6.8	3.6	1.7	4
Opal	1995	61	942	112	219	105	3	119	38	6.0	2.4	8.2	5.3	3.5	5
Rita	2005	19	937	110	222	108	3	74	32	3.6	2.4	8.4	5.4	2.6	4.3
Wilma peak	2005	4	892	139	203	33	5	70	7	4.3	4.8	7.2	3.3	4.6	4.2
Wilma (FL)	2005	45	951	114	236	111	3	104	29	5.3	2.5	9.2	5.8	2.8	4.8
Wilma (Mexico)	2005	12	930	132	245	75	4	121	28	7.1	3.2	9	5	4.7	5.1

174	Ranked 1st on this Index
174	Ranked 2nd on this Index
174	Ranked 3rd on this Index

Table 1.5. Examples of Carvill Huricane Index

http://en.wikipedia.org/wiki/Carvill_Hurricane_Index

Name	Year	Landfall	NHC Advisory Number	V_{max}	R_H (miles)	SSS	CHI
Bonnie	1998	North Carolina	31B	115	115	3	10.7
Earl	1998	Florida	11	80	115	1	4.6
Georges	1998	Mississippi	51B	105	45	2	5.1
Bret	1999	Texas	17	140	40	4	10.4
Floyd	1999	North Carolina	34A	110	115	2	9.6
Irene	1999	Florida	9	75	30	1	1.8
Lili	2002	Louisiana	48A	100	60	2	5.2
Claudette	2003	Texas	27A	75	30	1	1.8
Isabel	2003	North Carolina	49A	100	115	2	7.7
Charley	2004	Florida	18	145	30	4	10.4
Frances	2004	Florida	44A	105	75	2	6.6
Ivan	2004	Alabama	55B	130	105	3	13.5
Jeanne	2004	Florida	49B	115	70	3	8
Dennis	2005	Florida	25B	120	40	3	6.9
Katrina	2005	Florida	9	75	15	1	1.4
Katrina	2005	Louisiana	26A	145	120	4	19
Rita	2005	Texas	26B	120	85	3	9.9
Wilma	2005	Florida	36	125	90	3	11

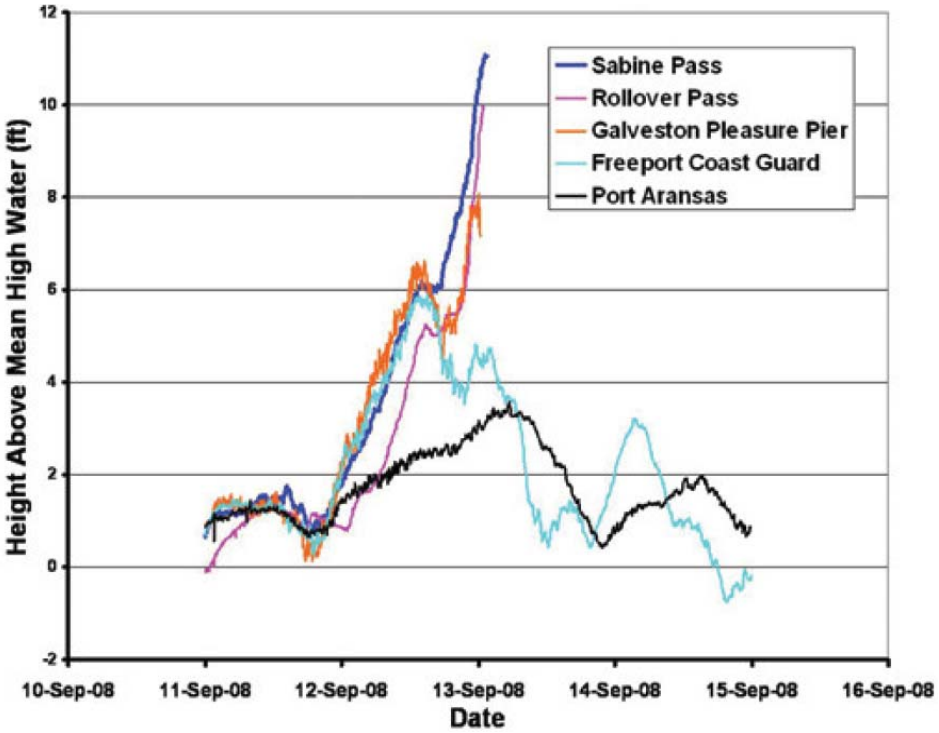

Figure 1.15. Hurricane Ike Forerunner

Watson 2009

Intensification

Hurricanes which intensify and grow during their trek across the GoM are likely to become some of the most powerful surge producing hurricanes in the Atlantic basin. Figure 1.16 illustrates values for R_{max}, Holland B, V_{max}, and CPD for Hurricane Katrina and Rita over the days leading up to landfall. The most rapid intensification on record for the Atlantic basin—also termed deepening of CPD or core—occurred with Hurricane Wilma in 2005 in the Caribbean, which dropped from 954 mb to 901 mb in less than 5.5 hours, with V_{max} rising from 150 mph to 184 mph.

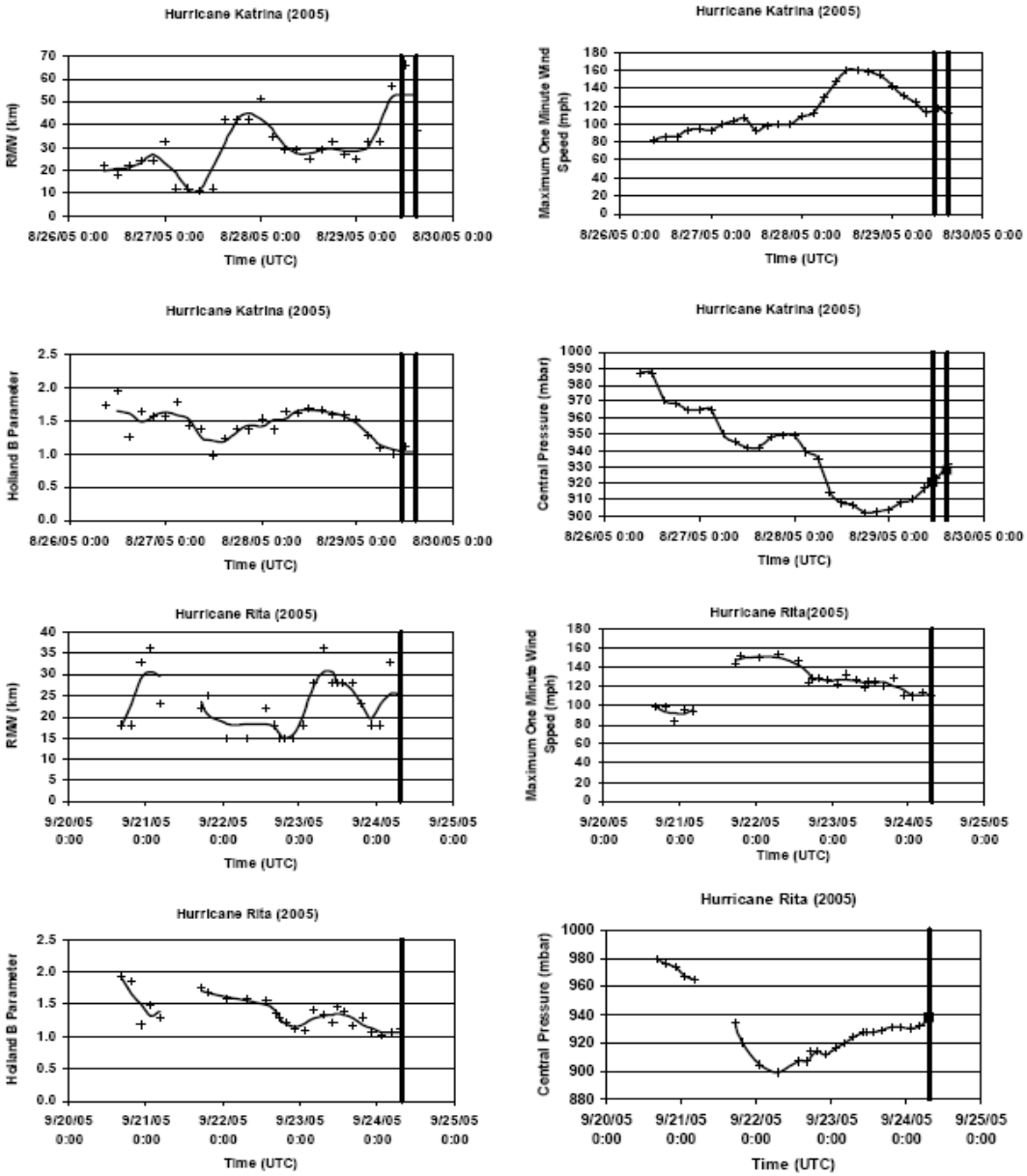

Figure 1.16. Intensification of Hurricanes Katrina and Rita

Vickery in Resio et al 2007

Currently, hurricane scientists have less confidence in forecasting a hurricane's intensity than track (Pasch 2011). Intensity and geometric transformations are largely governed by three interactions:

1. Land masses. Hurricanes which avoid prolonged crossings of larger mountainous Caribbean islands (e.g., Hispaniola and Cuba) are more likely to emerge into the GoM with stronger circulation centers. There is some evidence that while interaction with Caribbean islands can contribute to a diffusion of the wind field, this can also result in eventual hurricane enlargement, as in Hurricane Ike's interaction with Cuba (Fritz 2009).
2. Sea surface temperature (SST). Hurricanes which pass westward from the southern Florida peninsula or Strait across the GoM can draw energy from the higher water temperatures of the Florida and/or Loop Currents, as illustrated in Figure 1.17. Hurricanes coming from the Yucatan Strait or western Cuba can pass over large warm eddies which periodically break off from the Loop Current. Hurricanes that traverse lower water temperatures do not have these sources of energy. Importantly, if a hurricane stalls, the energy in surface waters can be exhausted, with upwelling colder deep water actually cause weakening. The depth limit of warm ocean water is considered a natural "braking" mechanism on the intensity and size of hurricanes.
3. Atmospheric conditions. Hurricane stability and growth are inhibited by encounters with a) masses of cool dry air (which are readily sucked into the core and then interfere with convection and cyclonic circulation); b) regional environments with high wind shear (which disrupt the wind field); or c) interfering upper level pressure systems.

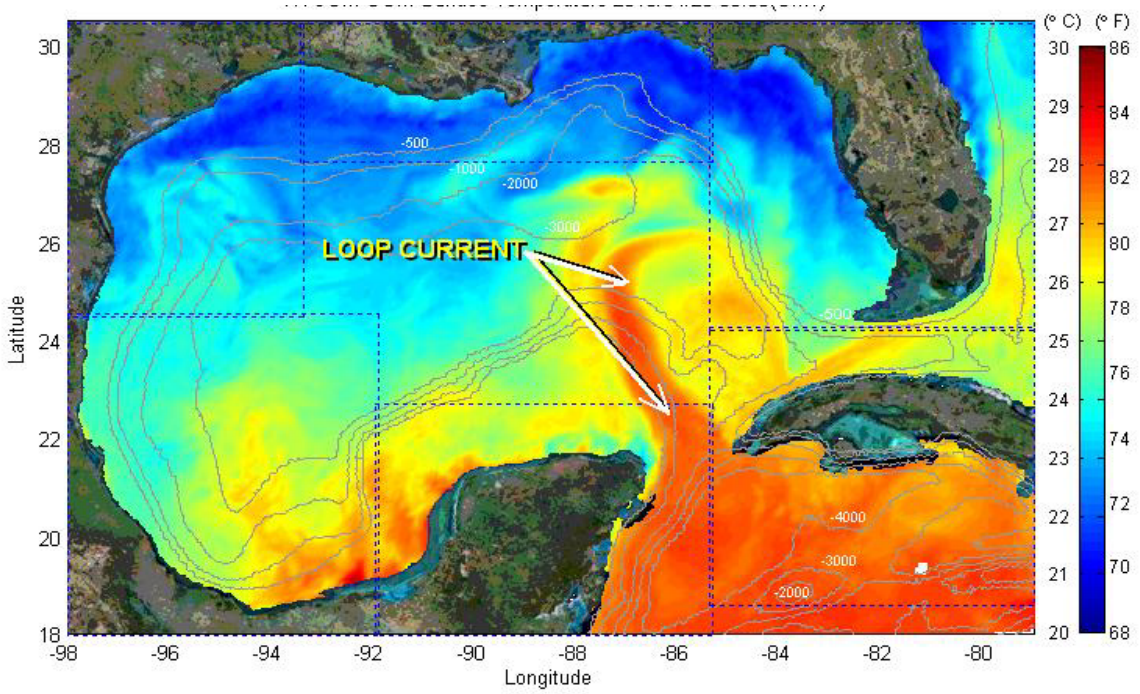

Figure 1.17. Example of the GoM Loop Current
WAVCIS Laboratory, Coastal Studies Institute, Louisiana State University

Scientists have examined the correlation between higher SST and intensity. Vickery et al (2000) noted a weak linear correlation of CPD to SST for GoM storms in geneal, due to the confounding influence of atmospheric conditions, but a stronger correlation for more intense storms (see Figure 1.18). In general, CPD above 80 mb required SSTs greater than 28.5° C. Recently, scientists have proposed that hurricane development and strengthening depends not just on SST, but on local depth averaged sea temperature. Studies are evaluating the relationship of intensification to the total available ocean energy—termed Tropical Cyclone Heat Potential (TCHP)—as evidenced by the correlation illustrated between TCHP and central pressure illustrated in Figure 1.19 (Wada and Usui 2007).

To better understand regional atmospheric influences on hurricane genesis, intensification, and resiliency—and to improve intensification forecasts—meteorologists are increasingly employing high resolution regional atmospheric models. (Shen 2005, Shen et al 2006b). In addition, hurricane meteorologists are studying detailed flight data to gain insights on hurricane wind field structures (e.g., primary circulation broadness, vertical alignment/tilting, etc.) and internal mechanisms of intensification and resiliency (Mallen et al 2005).

Decay

Powerful hurricanes can lose strength and symmetry as they approach landfall and move onshore. As the winds circulate counterclockwise into the forward right and then forward left quadrant (with respect to the track) they pass over land, encounter resistance, become disrupted, and decline in strength. The winds can rebuild again as they circle around the eye over water. The wind disruptions in the forward quadrants lead to intrusion of drier, higher pressure, overland air, which reduces the central pressure deficit and the engine for wind circulation—a process known as "filling" (see NOAA-NWS 1987 and Kimball 2006). Two examples of powerful storms which underwent rapid decay are Hurricanes Ethel (1960) and Lili (2002). Figure 1.20 summarizes the rise in central pressure for 22 post-1940 intense hurricanes (central pressure less than 955 mb) making landfall along the coast of the northern GoM (Resio et al 2007) Weakening in the last 6 to 24 hours prior to landfall was also characterized by an increase in R_{max} and decrease in Holland B. A 2010 study also found that GMHs typically undergo pronounced decay with landfall approach (Rappaport et al 2010).

Importantly, there has been no research on decay for less intense storms. Warm coastal waters may reduce decay for lower intensity storms. [Slow moving 2012 Hurricane Isaac is an example.]

1.5. Track and Forward Speed

For any given landfall location surge hazard also depends on a hurricane's track and forward speed along the track. Over a hurricane's course, the NHC pinpoints the center of circulation and provides wind field descriptions at frequent (typically 3-hour) intervals. Five critical junctures along the track for GoM storms are:

1. Entry into the GoM,
2. Maximum Intensity or maximum IKE,
3. Near coast prior to the onset of in-filling and decay,
4. Landfall, and
5. Inland following shifts and reduction in coastal winds.

The changing cyclonic characteristics between these five locations describe storm dynamics, which can influence surge through forerunner and other effects.

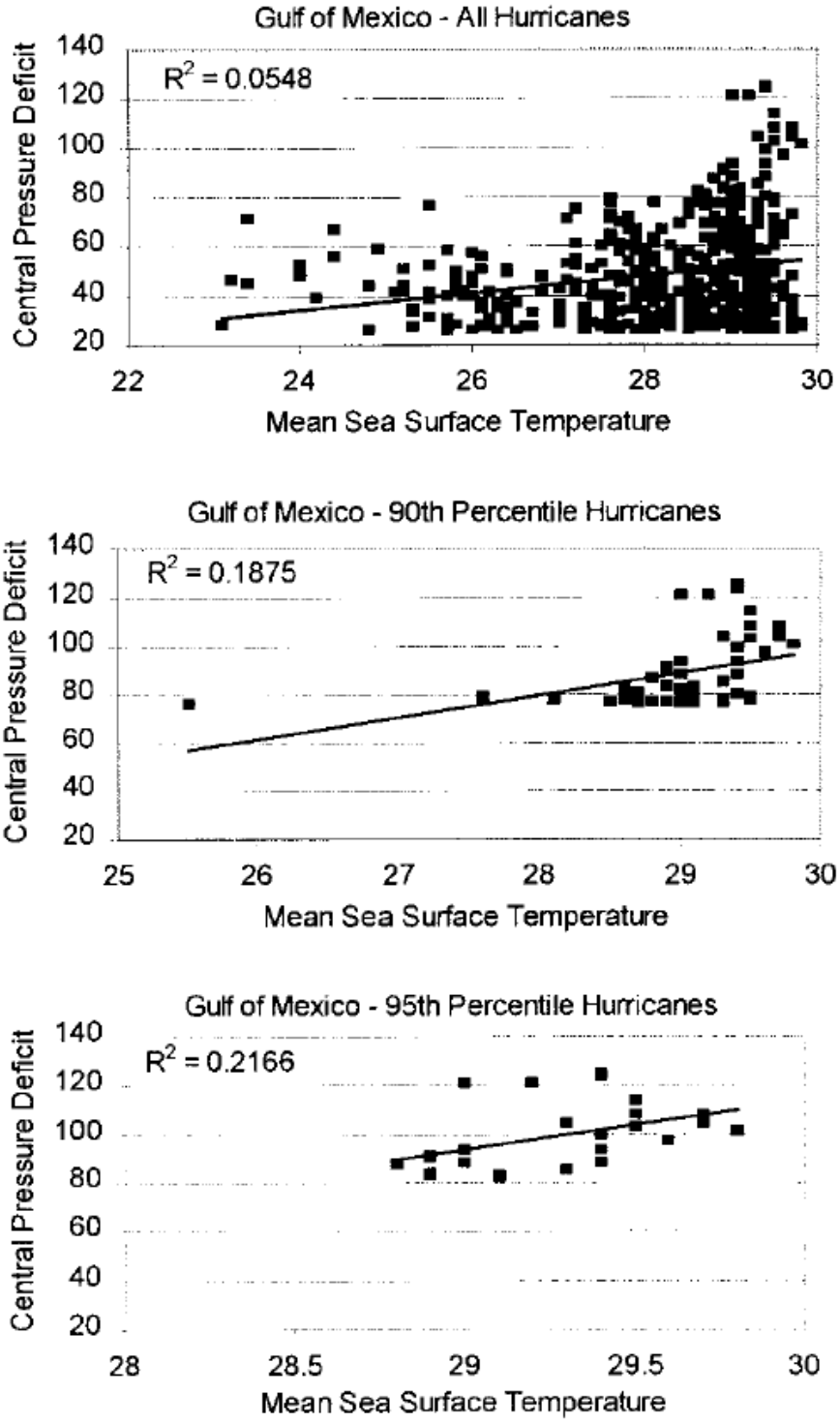

Figure 1.18. Correlation of Hurricane Intensity with SST

Vickery et al 2000

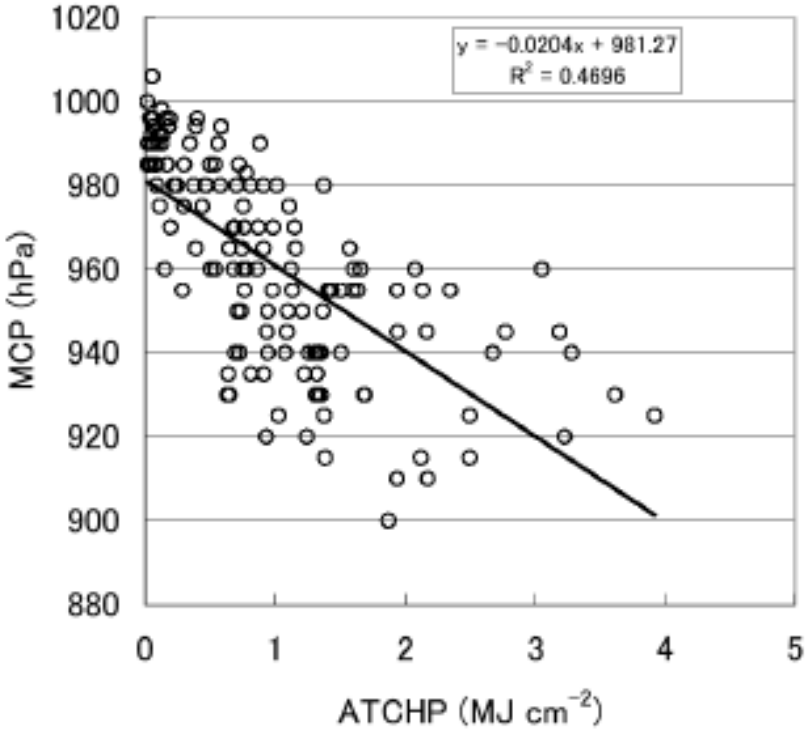

Figure 1.19. Correlation of Hurricane Intensity with Accumulated TCHP
Wada and Usui 2007

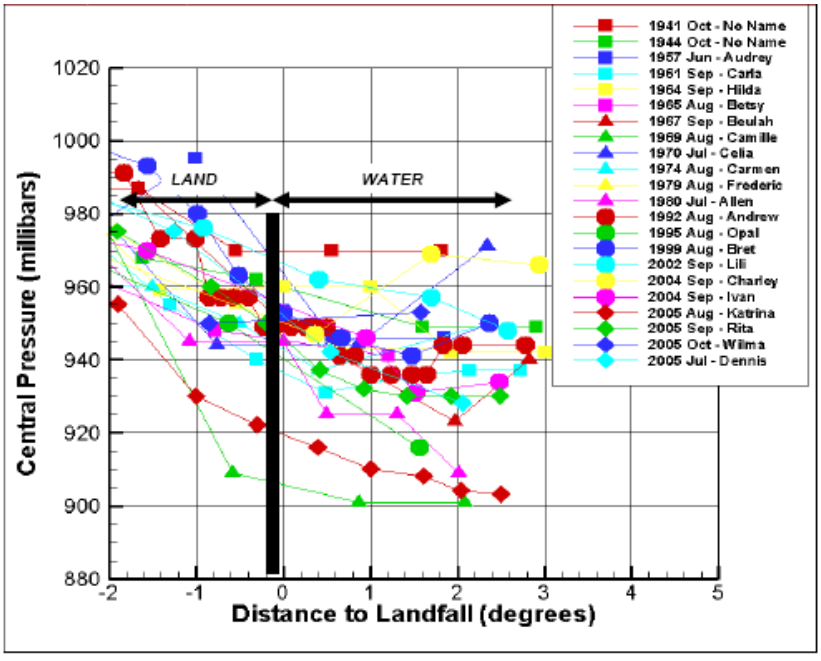

Figure 1.20. Rise in Hurricane Central Pressure Prior to Landfall
Resio et al 2007

Hurricanes can make multiple landfalls in the Atlantic basin. Hurricanes Betsy (1964), Andrew (1992), and Katrina (2005) all struck the east coast of Florida before crossing into the GoM and making landfall in Louisiana. Hurricane Ivan (2004) made a Gulf Coast landfall near Gulf Shores AL as a strong Category 3 storm and moved inland. It later emerged as a low pressure center in the mid-Atlantic Ocean, re-intensified as a tropical cyclone, traveled south along the U.S. Atlantic coast, crossed the Florida peninsula, re-entered the GoM, and made a second Gulf Coast landfall near Cameron LA as a tropical storm, one week after its previous Gulf Coast landing (see Figure 1.21). Hurricanes can even make multiple landfalls in the GoM—Hurricane Katrina made landfall near Buras LA followed by re-entry into Breton/Mississippi Sounds and landfall near Waveland MS.

As illustrated in Figure 1.22, hurricane wind and surge impacts depend greatly on the distance and direction to the landfall location. The strongest of the counterclockwise circulating winds produced by a landfalling hurricane are usually the landward winds in the forward right quadrant. These winds drive the correspondingly highest surge onshore in this quadrant. For a generic planar (regular seaward sloping) east-west shoreline, the highest coastal surge is concentrated immediately to the east of landfall and tapers eastward. West of the landfall, surge is more modest with some drawdown possible at landfall.

Figure 1.21. Track of Hurricane Ivan (2004)l
National Hurricane Center

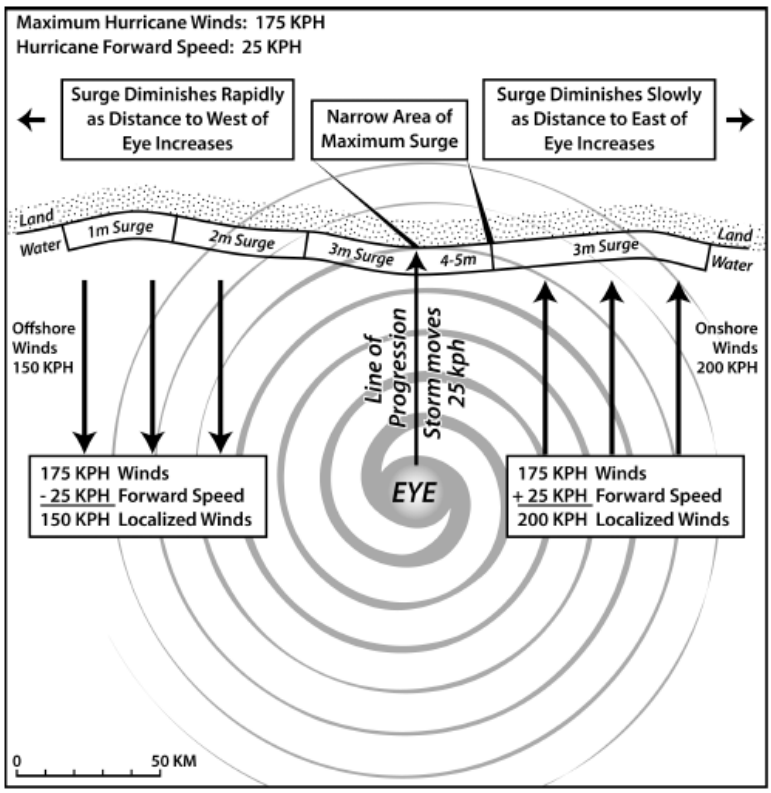

Figure 1.22. Generalized Schematic of Hurricane Storm Surge at Landfall

(Note Wind speeds are in kilometers per hour and surge is in meters)
Needham and Keim 2011

Certain GoM tracks have the potential for producing greater CN-GoM surge, including those: a) bringing a cyclone over the Loop Current or associated eddy, thus favoring intensification; and b) moving east to west across the GoM allowing for greater forerunner development and providing a longer, shallow surge fetch along the continental shelf east of the Mississippi River delta (see Part II).

Track locations in the 12 hours prior to and following landfall describe the heading (angle) θ, at which the cyclone core makes landfall. Storms approaching an east-west planar beach from the southwest (easterly θ) tend to trap and amplify surge, compared to those approaching from the southeast (westerly θ). The actual influence of landfall location and track θ greatly depends on the local variations in shoreline shape and bathymetry (see Part II).

Forward speed (V_f) along the track has two countervailing influences on surge. Storms with higher V_f at landfall approach (the last 12 hours leading up to landfall) deliver a stronger wind punch—because forward speed is added to the radial wind speed east of the storm center—leading to extreme surge compression against the coast. On the other hand, storms which have a slower V_f prior to landfall—especially those with higher IKE—may cause greater areal inundation due to the build up of forerunners (Rego and Li 2009) and longer wind durations. However, a slow V_f can cause a storm to deplete the underlying ocean thermal energy and lose intensity.

Attachment 1 provides the tracks for the 39 GMHs which struck along the 500-mile CN-GoM over the last 161 years—30 of which maintained major hurricane strength to landfall.

Section 2. The Influence of Seasonal and Climatic Trends

The frequency of tropical cyclones, major hurricanes, and particular genesis regions and tracks tends to correlate with the time of year and known inter-annual to multi-decadal climatic variations affecting ocean temperature and atmospheric conditions. Climatologists are examining these trends closely, as well as the potential influence of rising global temperature on hurricane frequency and characteristics.

2.1. Seasonal Trends

Atlantic basin tropical cyclones develop primarily between May and December in association with the formation of low pressure centers over warm ocean waters (generally above 26.5° C, 80° F) under modest shear and other conducive atmospheric conditions. Often these low pressure centers originate from waves of hot rising Sahara Desert air that propagate off the coast of West Africa in the intertropical convergence zone beginning in mid-to-late summer. The peak of hurricane season is from late September through early October. The NHC website on tropical cyclone climatology (NOAA-NHC) summarizes observations regarding seasonal hurricane trends, including:

- The observed tropical cyclone seasonal frequency (per 100 years) in the Atlantic basin (see Figure 2.1.a).
- Typical points of origin by 10 day periods (e.g., Figure 2.1.b).
- Typical tracks by month (e.g., Figure 2.1.c).

2.2. Climate Cycles

Dating back to the mid 1980s and the pioneering work of Dr. William Gray, climatologists have observed short- and long-term regional cycles that tend to influence SST/TCHP and atmospheric conditions—which in turn affect Atlantic Basin hurricane development and intensification. Four important cycles—also referred to as oscillations—are:

- The Madden–Julian Oscillation (MJO), a 30-90 day intra-seasonal cycle in which large alternating regions of enhanced versus suppressed convection propagate eastward around the globe within the tropical zone. The former supports while the latter inhibits tropical cyclone development. This pattern contributes to the inverse tropical cyclone activity level in the western-north Pacific versus the north Atlantic basins (Klotzbach 2010).
- The inter-annual El Niño-Southern Oscillation (ENSO), with warming (El Niño) versus cooling (La Niña) cycles (generally lasting a year or two at most) in the equatorial eastern Pacific Ocean, which induce increased (decreased) wind shear in western Atlantic basin (Gray 1975, Gray 1984, Bove et al 1998, Saunders et al 2000, Elsner et al 2001, Elsner 2003, Jagger et al 2001, Elsner and Jagger, 2005, Klotzbach 2011).
- The Atlantic Multi-decadal Oscillation (AMO), with periods (overall 50 to 90 years) of oscillating North Atlantic SSTs, with warmer cycles increasing the potential for tropical cyclone development and intensifications (Saunders and Harris 1997, Bell and Chelliah 2005, Chylek and Lesins 2008). The AMO initiated a warm period in 1995 which is expected to last until 2015 to 2035, possibly peaking around 2020 (Enfield and Cid-Serrano 2010).

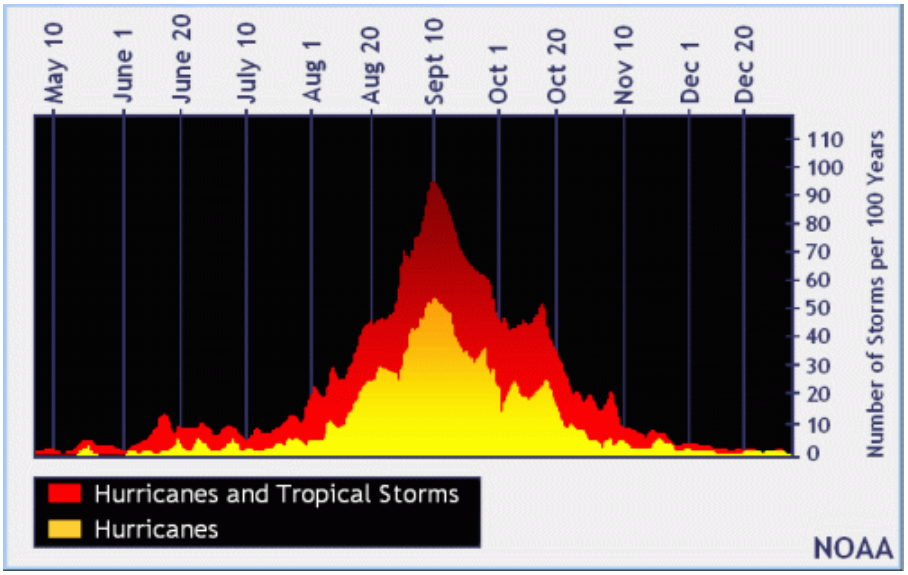

a. Seasonal Frequency of Tropical Cyclones

b. Example Origin of Tropical Cyclones by 10-Day Calendar Period

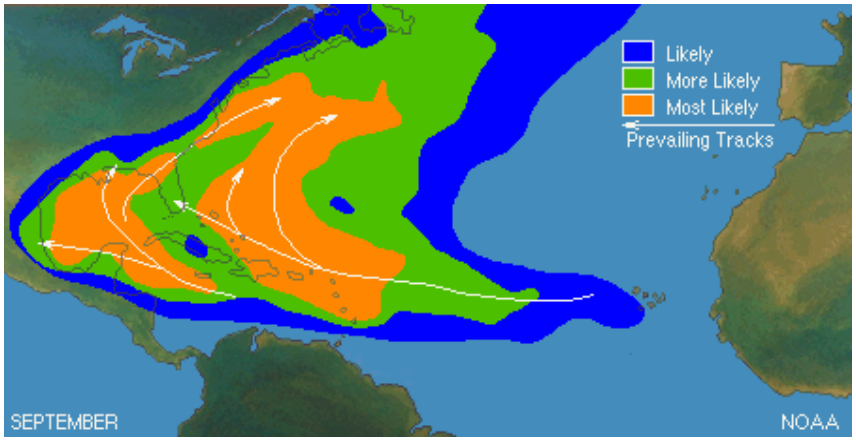

c. Example Typical Tracks by Month

Figure 2.1. Seasonal Trends in Atlantic Hurricanes
NOAA-NHC

- The North Atlantic Oscillation (NAO), in which the centers of mid-Atlantic high and low atmospheric pressure—generally centered near the Azores and Iceland, respectively—shift and strengthen/weaken. The NAO influences tropical cyclone development off the west coast of Africa and the re-curving of Atlantic hurricanes versus tracking on toward the GoM. The NAO has significant seasonal and inter-annual variability. (Elsner and Kocher 2000, NOAA-CPC).

Researchers have used both historic and paleo-records (McCloskey and Knowles 2009, Wallace and Anderson 2010) and regional and global atmospheric and sea temperature models of increasing complexity and resolution (Zhao et al 2009, Kim and Webster 2010, Chen and Lin 2011, Schultz 2011) to study the influence of these climate cycles on temporal trends in hurricane frequencies and characteristics.[1] Researchers have also studied if correlations among individual hurricane characteristics persist as seasonal characteristics for climate cycles. For example, a 2011 investigation (S. Quiring et al 2011) found the negative correlation between core intensity and core size held up for mean annual V_{max} and R_{max}. They also identified a positive correlation between mean annual R_{max} and R_{TS}.

Researchers have investigated correlations of GoM hurricane activity to climate cycles and found both the MJO and ENSO and to be important (Maloney and Harmann 2000). Resio and Orelup examined variability in the total annual peak kinetic energy of GoM hurricanes for 1941 to 2005 and identified two periods of higher hurricane activity—1957 to 1970 and post-2000. They evaluated the influence of trends in sea level atmospheric pressure and SST on this variability and suggested a roughly 40-year climate cycle in GoM hurricane activity, depicted in Figure 2.2 (Resio and Orelup 2006, not published).

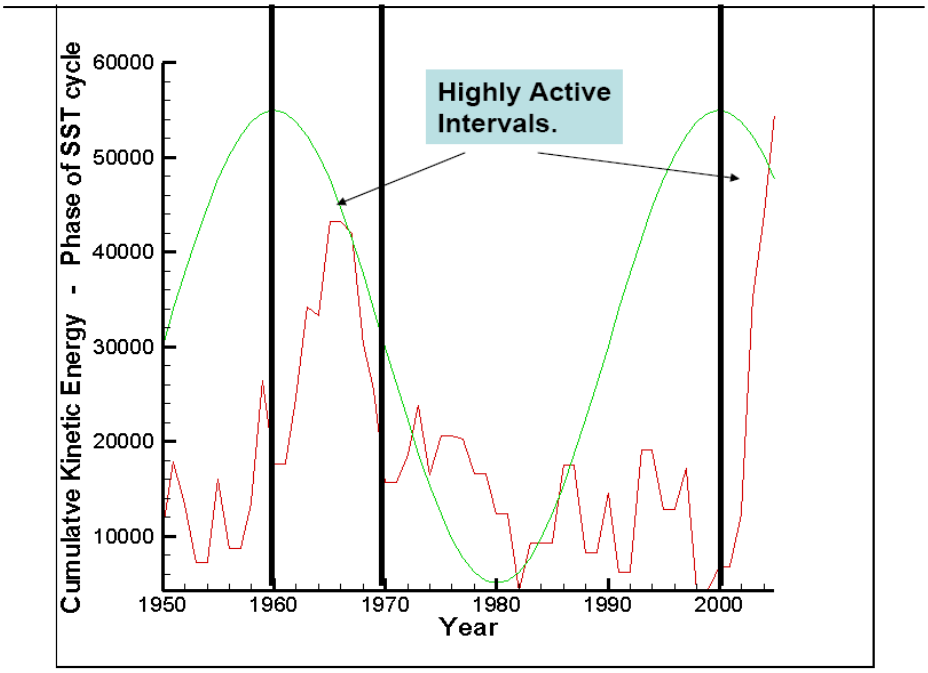

Figure 2.2. Cycle in Total Annual Peak Kinetic Energy for GoM Hurricanes
Resio and Orelup 2006

[1] Other climate variations include solar activity; stratospheric quasi biennial oscillations, Caribbean sea-level pressures; 200mb zonal winds; and African West Sahel rainfall activity (Elsner and Jagger 2008, Landsea et al 1999).

Figure 2.3 shows a rolling 5-year average for the number of hurricanes and GMHs from 1851 to 2011, together with the long-term average based on the linear trends previously noted—1.53 and 0.52 per year. Evidence of extended durations of lower/higher hurricane and major hurricane activity can be observed but there is no obvious indication of cyclic pattern.

2.3. Climate Change

Scientists have also begun to evaluate the influence of rising global temperature on hurricane frequency and intensity. In 2006 Elsner described the potential linkage between global warming and hurricanes as follows:

> The power of Atlantic tropical cyclones is rising rather dramatically and the increase is correlated with an increase in the late summer/early fall sea surface temperature over the North Atlantic. A debate concerns the nature of these increases with some studies attributing them to a natural climate fluctuation, known as the AMO, and others suggesting climate change related to anthropogenic increases in radiative forcing from greenhouse-gases. Here tests for causality using the global mean near-surface air temperature (GT) and Atlantic SST records during the Atlantic hurricane season are applied. Results show that GT is useful in predicting Atlantic SST, but not the other way around. Thus GT "causes" SST providing additional evidence in support of the climate change hypothesis. Results have serious implications for life and property throughout the Caribbean, Mexico, and portions of the United States. (Elsner 2006a)

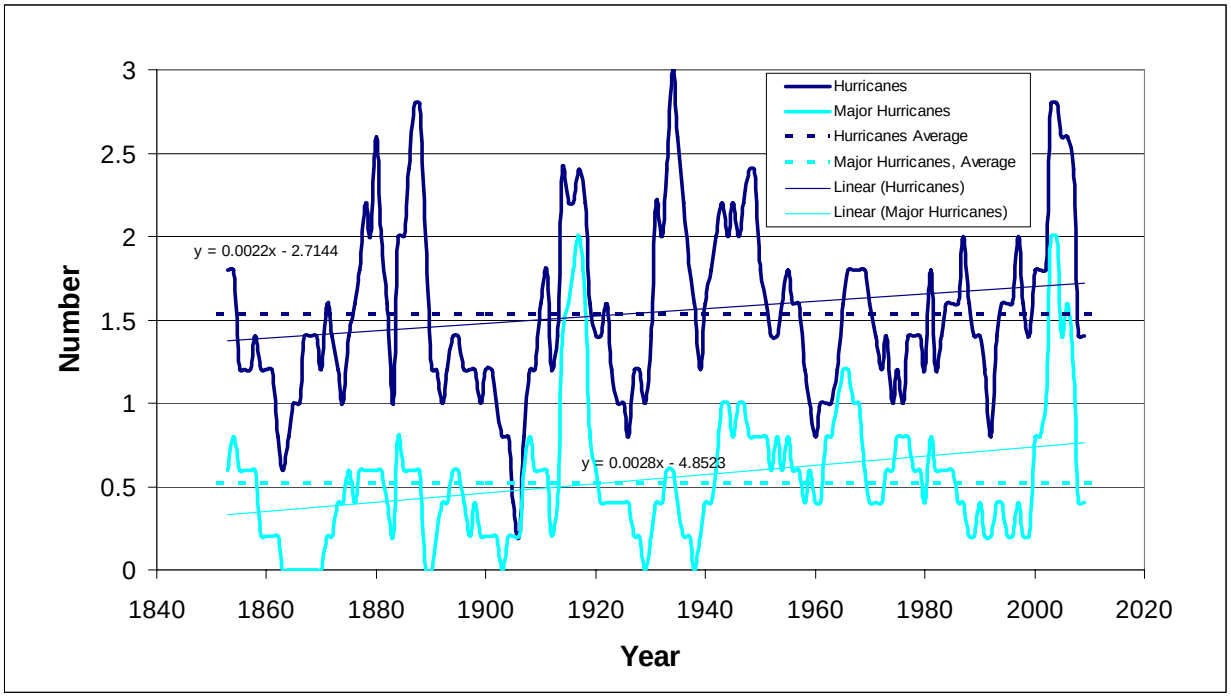

Figure 2.3. Rolling Average for GMHs

The NOAA-GFDL website "Global Warming and Hurricanes," summarizes recent research on the influence of climate change on hurricanes. Figure 2.4 illustrates the frequency of hurricanes in the Atlantic Basin from 1851 to 2006. Researchers are utilizing high resolution, regional and global climate models—which incorporate atmospheric physics, ocean temperature, and hurricane genesis potential—to simulate secular trends in hurricane frequency. Figure 2.5 compares observed trends in hurricane frequency for 1980 to 2006, which indicates an average increase of 1.5 hurricanes per decade, to a recent model for the same period, which produced an average increase of 2.1 hurricanes per decade.

Researchers are using these same models to predict potential future changes in tropical storm frequency and intensity associated with secular climate trends. One important difficulty they face is distinguishing the recent rise in Atlantic ocean temperatures and hurricanes due to the current AMO cycle from those that might be attributable to global warming (Enfield and Cid-Serrano 2010). Another challenge is ensuring that the models can also address the potential for future conditions that might be unfavorable to hurricane development (e.g., increased shear).

A 2010 paper to which many leading hurricane climatologists contributed stated the following:

> Whether the characteristics of tropical cyclones have changed or will change in a warming climate—and if so, how—has been the subject of considerable investigation, often with conflicting results. Large amplitude fluctuations in the frequency and intensity of tropical cyclones greatly complicate both the detection of long-term trends and their attribution to rising levels of atmospheric greenhouse gases. Trend detection is further impeded by substantial limitations in the availability and quality of global historical records of tropical cyclones. Therefore, it remains uncertain whether past changes in tropical cyclone activity have exceeded the variability expected from natural causes. However, future projections based on theory and high-resolution dynamical models consistently indicate that greenhouse warming will cause the globally averaged intensity of tropical cyclones to shift towards stronger storms, with intensity increases of 2–11% by 2100. Existing modeling studies also consistently project decreases in the globally averaged frequency of tropical cyclones, by 6–34%. Balanced against this, higher resolution modeling studies typically project substantial increases in the frequency of the most intense cyclones, and increases of the order of 20% in the precipitation rate within 100 km of the storm center. For all cyclone parameters, projected changes for individual basins show large variations between different modeling studies. (Knutson et al 2010)

A research team employing a high-resolution dynamic climate model, led by Done and Holland, presented a paper at the 2011 Offshore Technology Conference in Houston Texas and estimated that tropical cyclone activity will increase in the North Atlantic Basin by up to three storms per season by 2100 due to global warming influences on genesis potential (Done et al 2011).

Figure 2.3 includes the 161-year linear trend in the 5-year rolling averages for both GoM hurricanes and GMHs. Both show only very slight increases—less than 0.3 per century—indicating no current evidence for a long-term secular trend in GoM hurricane activity. The notable 44% increase in the post- versus pre-1940 rate of GMHs associated with improved observations, shown in Figure 1.2 b, may contain some climate influence but these have not been investigated except for the cycle suggested by Resio and Orelup. In analyzing the 1941 to 2005 total annual peak kinetic energy of GoM hurricanes (Figure 2.2), Resio et al noted that there was no indication of a long-term secular trend (Resio et al 2007).

There have been no investigations to date of future hurricane climatology specific to the CN-GoM. As noted in Sections 1, the Loop Current and associated eddies are crucial to the specific high hazard of this region. A 2012 paper by Liu et al suggests—consistent with other research on the Florida Straits Current and Gulf Stream—that global climate change could reduce the Loop Current by up to 25%, significantly *cooling* the GoM. This scenario would likely *reduce* the landfall frequency of powerful hurricanes along the CN-GoM, and particularly southeast Louisiana, and *lower* the 100-yr and higher surge hazards. More research on this and related topics is therefore needed.

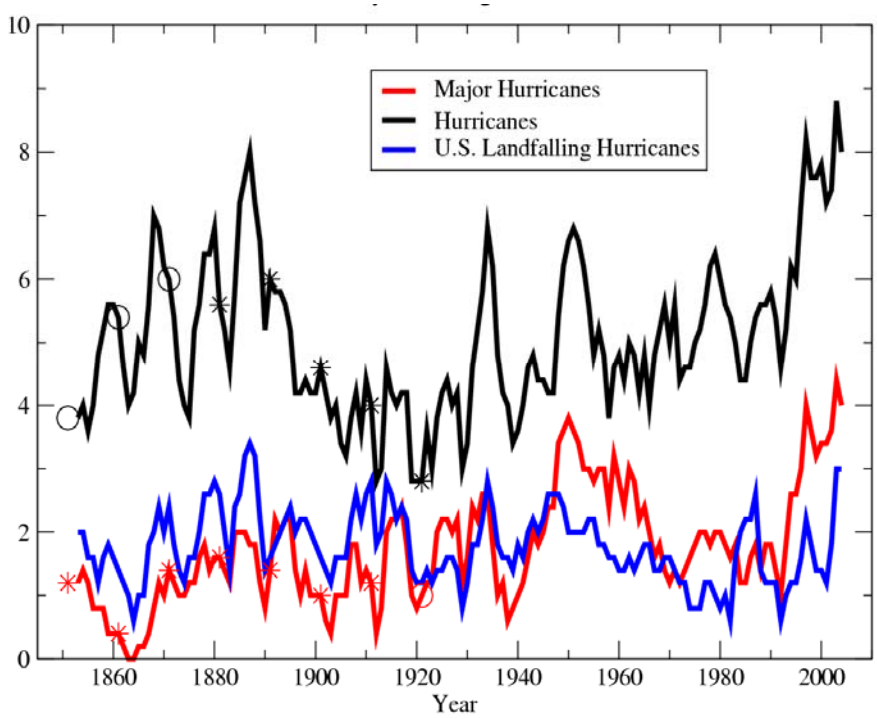

Figure 2.4. Atlantic Basin Hurricane Counts, 5-year Running Mean
NOAA-GFDL

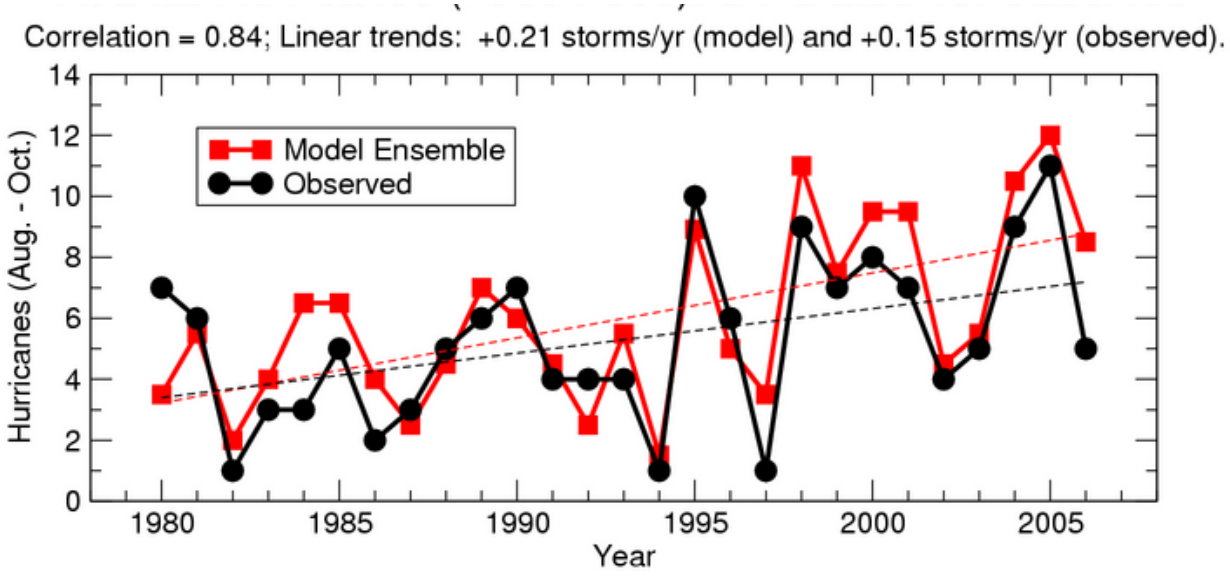

Figure 2.5. Atlantic Basin Hurricane Counts, Simulated versus Observed
NOAA-GFDL

Section 3. Hurricane Landfall Probabilities

Due to the significant wind and surge hazards associated with close proximity to a hurricane strike, concerned coastal citizens and government officials have sought scientific analyses of local frequencies, correlations, and trends in landfalling hurricanes. As discussed in Section 1, hurricanes of various core intensity (CPD, V_{max}) occur with varying frequency in the GoM versus the overall Atlantic basin. Importantly, given tendencies in tracks, genesis, intensification, and decay, coastal meteorologists also observe differences in the landfall characteristics of hurricanes for different coastal regions.

To assess local hurricane climatology researchers divide the coastline into segments with reasonably uniform strike probabilities. Segment lengths must not be so large as to contain obvious geographic differences in hurricane frequency (e.g., Florida to Maine on the Atlantic coast is too long a segment) but must not be so short as to include only a small number of observations. Many studies have chosen segments based on coastal county/parish boundaries, or centered on coastal communities.

In recent years researchers have evaluated the observed return frequency of hurricanes according to core intensity—as given by the landfall CPD—and applied probability distributions to hurricane landfall core intensity to estimate extreme events. Much of the focus of CN-GoM landfall return frequency has been on GMHs only. The following notation is employed in summarizing return periods for various sub-cateogries of GMHs (see Figure 3.1):

L-500—landfalling *at any category* somewhere within the 500 mi CN-GoM segment as a whole.

LMH-500—landfalling *at Category 3 or higher* within the 500 mi CN-GoM segment.

L-151—landfalling *at any category* within the 151 mi (2.5° longitude) segment below New Orleans.

LMH-151—landfalling *at Category 3 or higher* within the 151 mi (2.5° longitude) segment below New Orleans.

L-60— landfalling *at any category* within the 60 mi (1° longitude) segment below New Orleans.

LMH-60—landfalling *at Category 3 or higher* within the 60 mi (1° longitude) segment below New Orleans.

Researchers have not studied return frequencies for GMH/LMHs core size, Holland B, decay, θ, and V, but have instead investigated correlations between GMH/LMH CPD and these characteristics. They have also studied potential seasonal and climate trends on landfalling storms.

Importantly, there is no recent research on return periods for GoM hurricanes that never attain Category 3 but which have large wind fields. As noted in Section 1.3, these storms can generate significant surge.

3.1. Return Frequency for Landfall Intensity

Beginning in the 1960s, hurricane researchers employed long-term coastal meteorological data to analyze the relative frequency of landfalls along the nation's shore according to simple classifications of tropical storm intensity. In 1971 Simpson and Lawrence used observations from 1886 to 1970 (85 years) to evaluate the frequency of three categories of storms: tropical storms of all magnitude, those which achieve hurricane strength, and those which became strong hurricanes—with 125 mph maximum sustained winds and greater (Simpson and Lawrence 1971). To quantify shoreline crossing frequency they divided the U.S. GoM and Atlantic coastline into 58 50-mile segments. The authors counted a crossing event for both the landfall segment and the next eastward segment.

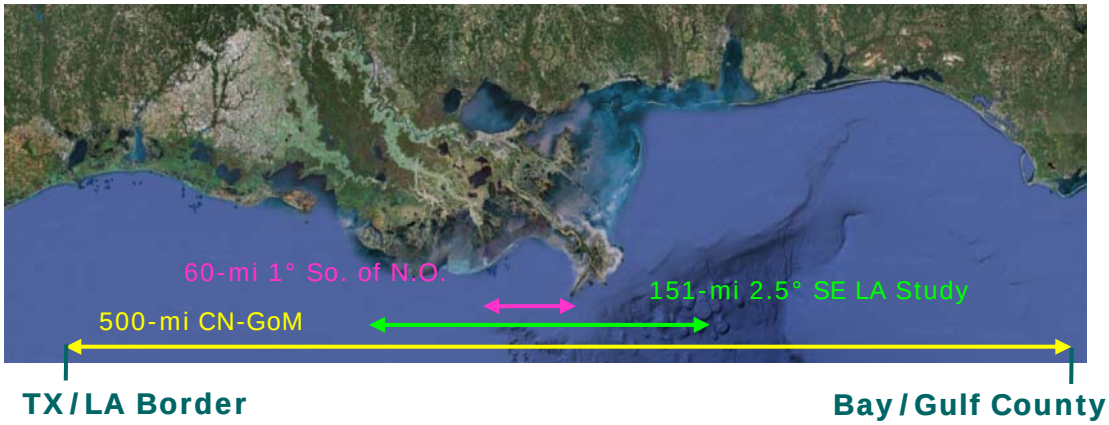

Figure 3.1. Hurricane Landfall Regions

Nine segments (Nos. 7 to 15) comprise the CN-GoM. The range of annual crossing frequencies for each of these individual nine segments in this region were:

Tropical storms and hurricanes	12 to 21%
Hurricanes	6 to 14%
Strong hurricanes	0 to 4%

The approximate combined landfall annual frequencies for the entire region (summing occurrences for all nine segments and dividing the total by two because events were counted for two segments) were 72.9%, 42.3%, and 6.9% for the three categories respectively. Simpson and Lawrence did not develop any probability distributions for the data or estimate extreme return period magnitudes.

U.S. landfall frequency for the Atlantic basin has since been revisited periodically. In 1987 NOAA-NWS evaluated varying landfall hurricane climatology at 100-mi intervals along the Atlantic and GoM coasts to support joint probability analysis for FIS (NOAA-NWS 1987). The evaluation provided cumulative probability distributions for CP, R_{max}, V_f, and θ. In 1999 Elsner and Kara examined landfalls on a county by county basis using data from 1900 to 1996 (Elsner and Kara 1999). Following the prominent 2005 season—in which hurricanes Emily, Katrina, Rita, and Wilma all reached Category 5 intensity—and the NHC's web-based delivery of comprehensive hurricane data—publication of landfall frequency information has expanded.

In 2007 Keim[1] et al, calculated observed landfall return periods for 45 U.S. GoM and Atlantic coast locations, including eight along the CN-GoM—Cameron LA, Morgan City LA, Boothville LA, Gulfport MS, Dauphin Island AL, Pensacola FL, Destin FL, and Panama City Beach FL (Keim et al 2007). The analysis used the NHC data set for the 105-yr period from 1901 to 2005, broken down by tropical storms of all magnitude, hurricanes of all magnitude, and major hurricanes (Category 3 and above). The authors' analysis encompassed strikes of 194 tropical storms, 117 Category 1/2 hurricanes, and 57 major hurricanes. Of the 368 total storms 14 were non-landfalling storms that grazed the coast.

[1] Dr. Barry Keim is the Louisiana State Climatologist.

For each storm, the authors identified the maximum sustained winds that occurred after the storm approached within 50 miles of landfall. Given the absence of size and wind distribution data for older storm records, the authors generated a generic wind field—extent of major hurricane, hurricane, and tropical storm force winds to the right and left of the landfall point—using generalized "swath" assumptions for each of the three types of events. The authors then determined observed return periods by analyzing the 368 synthetic wind fields at each of the 45 landfall locations. They did not attempt to fit observed return periods to probability distributions or estimate magnitudes for extreme return periods. The relative return period results for the eight CN-GoM locations are shown in Table 3.1.

A 2008 study by Parisi and Lund estimated return periods for hurricane strikes by category for the entire U.S. coastline and the Texas to Alabama region using 1900-2006 data (Parisi and Lund 2008). The data encompassed landfall wind and central pressure data for 214 strikes, including bypassing storms which produced coastal hurricane force winds but did not make landfall. Table 3.2 summarizes the results. The authors also determined national return periods for the landfall core V_{max} and central pressures for several notable hurricanes (Table 3.3). Return periods for the core V_{max} versus central pressure for individual storms differed widely—ranging from Camille, where the V_{max} return period exceeded central pressure return period by a factor of 5.8, to Katrina , where central pressure return period exceeded V_{max} return period by a factor of 3.4. This discrepancy is consistent with the wide scatter in V_{max} associated with CDP noted earlier.

Table 3.1. Observed Return Period (Years) for Landfalling Tropical Storm, Hurricane, and Major Hurricane Winds Along the CN-GoM

Keim et al 2007

	Cameron	Morgan City	Boothville	Gulfport	Dauphin Island	Pensacola	Destin	Panama City Beach
Tropical Storm	3	3	3	4	3	3	3	4
Hurricane	15	10	7	10	8	6	8	8
Major Hurricane	52	26	26	52	21	21	35	105
Hurricanes (1900 – 1996)	12	9	9	12	10	10	11	8
Hurricanes (1886 – 1970)	17	7	10	17	7	7	7	14

The NHC website on hurricane climatology (NOAA-NHC Tropical Cyclone Climatology) contains updated information on observed hurricane strikes. Figure 3.2. shows the number of recorded hurricane strikes by county while Figures 3.3.a and b depict hurricane and major hurricane return periods for landfall within 50 nautical miles of numerous points along the U.S. Atlantic basin.

Table 3.2. Observed Return Period (Years) for Hurricane Landfall Categories

Parisi and Lund 2008

Category	Nationwide	Texas, Louisiana, Mississippi, and Alabama
1	0.9	1.6
2	1.3	2.1
3	2.0	2.8
4	4.7	5.6
5	23.1	37.1

Table 3.3. Observed Nationwide Return Period (Years) for Selected Hurricane Landfall Core Intensity Conditions

Parisi and Lund 2008

Storm Name	Year	V_{max} (mph)	Return Period (years)	Central Pressure (mb)	Return Period (years)
New Orleans	1915	150	13.7	931	6.3
Labor Day	1935	184	265.3	892	101.6
Betsy (Louisiana)	1965	121	2.9	948	2.9
Beulah	1968	127	3.7	950	2.7
Camille	1969	167	62.9	909	35.7
Hugo	1989	138	6.7	934	5.3
Andrew (Florida)	1992	167	62.9	922	10.9
Charley	2004	150	13.7	941	3.8
Katrina	2005	127	3.7	920	12.7

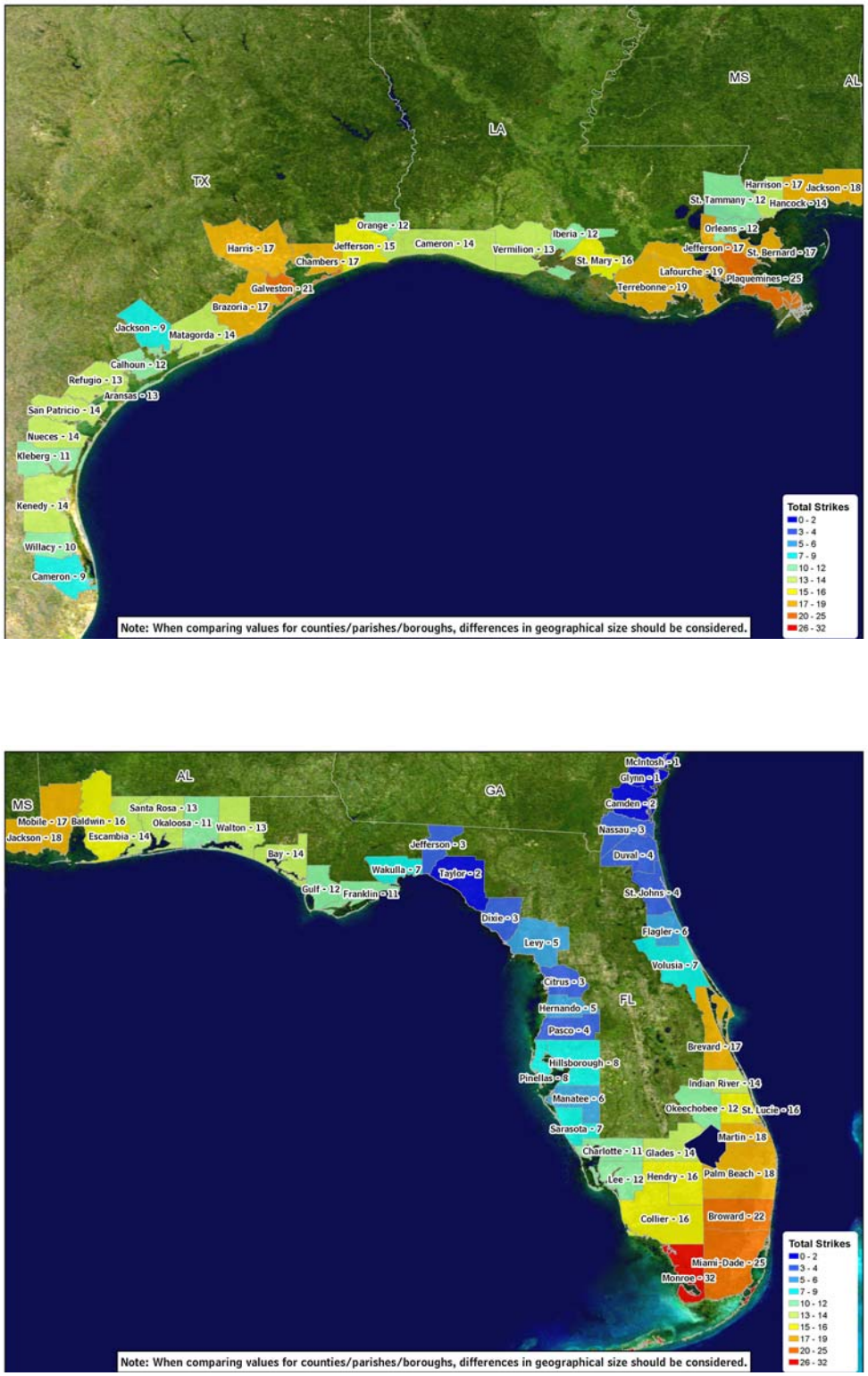

Figure 3.2. Total Number of Recorded Hurricane Strikes (1900 to 2010)
NOAA-NHC

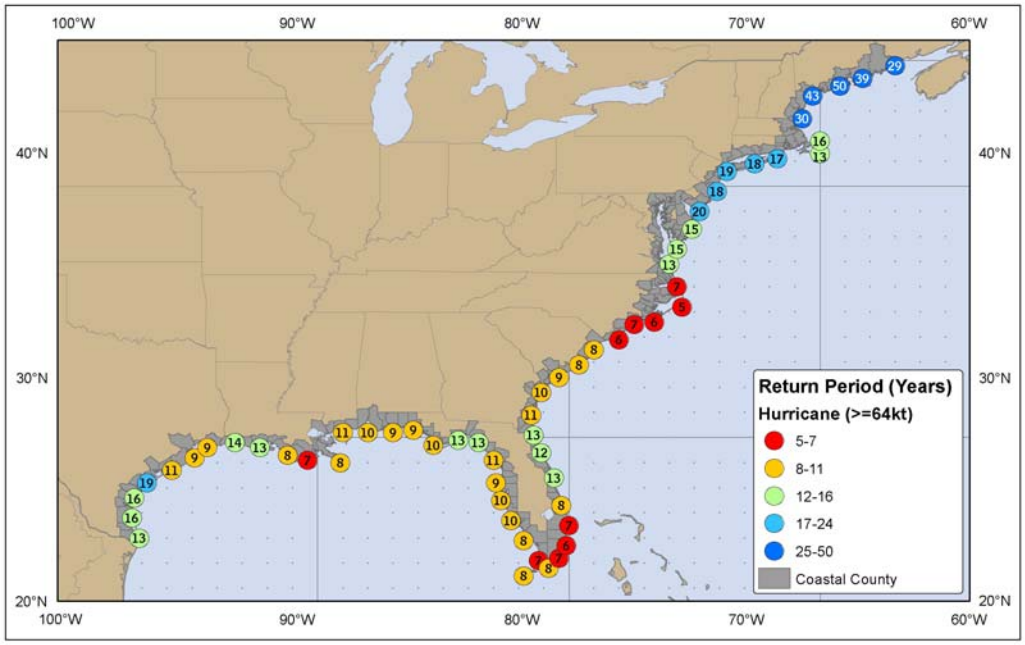

a. Hurricanes

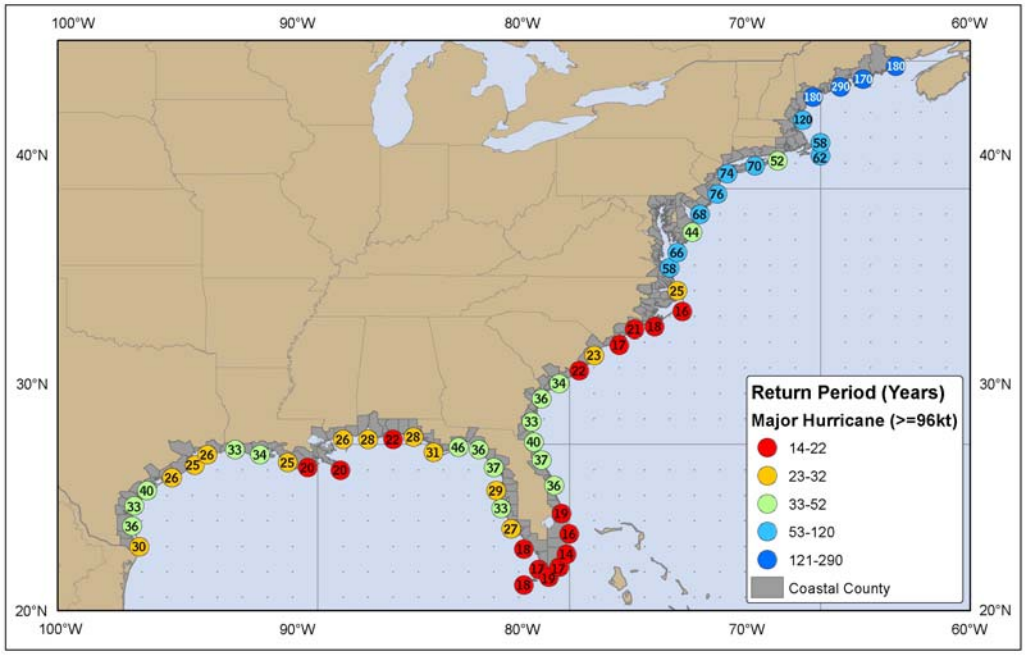

b. Major Hurricanes

Figure 3.3. Observed Return Period (Years) for Hurricanes and Major Hurricanes Passing Within 50 Nautical Miles of U.S. Coastal Locations

NOAA-NHC

In 2007 Resio et al analyzed landfall intensity frequency and characteristics for 1° longitudinal segments (approximately 60 miles) along the CN-GoM and Texas. The researchers employed geostatistical methods to derive landfall trends at this high resolution. In addition, they utilized the storm record from 1941 to 2005 (65 years) to account for a balance in their purported hurricane activity cycle.[2] The scientists examined the frequency of hurricane landfall for storms that peaked in the GoM at central pressures below 955 mb (mid Category 3), based on a set of 22 post-1940 GMHs (see Figure 1.20 for list). Figure 3.4 shows that Resio et al estimated return period for a GMH/L-60 storms is about 16 years. The Resio et al landfall rate for a storm at hurricane strength in this segment is 0.0486 per year or a return period of 20.6 years.

Resio et al evaluated the landfall central pressure return frequency data with a Gumbel distribution. Figure 3.5 shows the estimated landfall CPs corresponding to 50-, 100-, and 500-yr return periods along the CN-GoM (seven segments, Nos. 4 to 10). Figure 3.6 provides the CP versus return period for the 1° segment below New Orleans. The CPs for the 50-, 100-, and 500-yr return periods are 963, 940, and 912 mb respectively. The return period for Hurricane Katrina's 920 mb CP landfall at Buras LA is estimated at about 280 years within this segment. This CP is close to the Category 4/5 borderline; however Katrina's landfall winds of 126.5 mph were at a strong Category 3, which is the official basis for categorization (see Section 1). Uncertainties with the Gumbel-fitted estimates were not provided.

Toro (2008) evaluated the probability distribution of CPD (referred to as DP is his report) within a 124 mile radius of a point centered near Bay St. Louis MS, based on 1940 to 2005 hurricanes of Category 2 and higher. Figure 3.7 illustrates his results, which employed a Weibull distribution, including uncertainty bands. A CPD of 100 mb (equivalent to ambient and central pressures of 1020 and 920 mb) has a median return period of about 24 years (1/0.043). Note that exceedance probability is presented on a log scale and there is noticeable asymmetry in the uncertainty bands (here represented as ± one standard deviation about the 50th percentile) with ± one standard deviation at about 8 and 111 years. The difference in the return period for 100 mb CPD between Resio et al and Toro—300 years versus 24 years is due to their spatial samples sizes and orientation—a 60 mile longitudinal line versus a 124-mile radial area. The Resio et al and Toro research efforts were closely coordinated as part of a regional flood insurance study and Resio et al stated that the results of the two studies seemed fairly consistent.

Resio et al and Toro focused on the return period for central pressure and not V_{max} (to provide the appropriate input to atmospheric vortex models). In 2006 Elsner et al looked at nearshore (not strictly landfall) return period for V_{max} in the GoM from Texas to Alabama. They found that Hurricane Katrina winds of 159 mph in this region had an expected return period of 21 years, with 95% confidence limits of 10 and 50 years (Elsner et al 2006b).

As previously noted, the 161-yr period from 1851 through 2011 includes 249 total GoM hurricanes, 93 striking the 500-mile CN-GoM, 87 striking the CN-GoM at hurricane strength. The record also includes 39 GMH/L-500 storms—a simple average of 24.2 per century, one every 4.1 years—and 30 GMH.LMH-500s—a simple average of 18.6 per century, one every 5.4 years. Table 3.4 lists the 39 GMHs/L-500 and indicates their peak and landfall intensity, as well as their landfall location. Figure 3.8 depicts the tracks of these 39 GMH/L-500 hurricanes.

[2] In accordance with their hypothesized cycle, Resio et al used a full 40-year cycle (10 higher followed by 30 lower activity years) from 1960 to 2000. To compensate for including the higher activity years of 2001-2005 they included the lower activity years for 1941-1960.

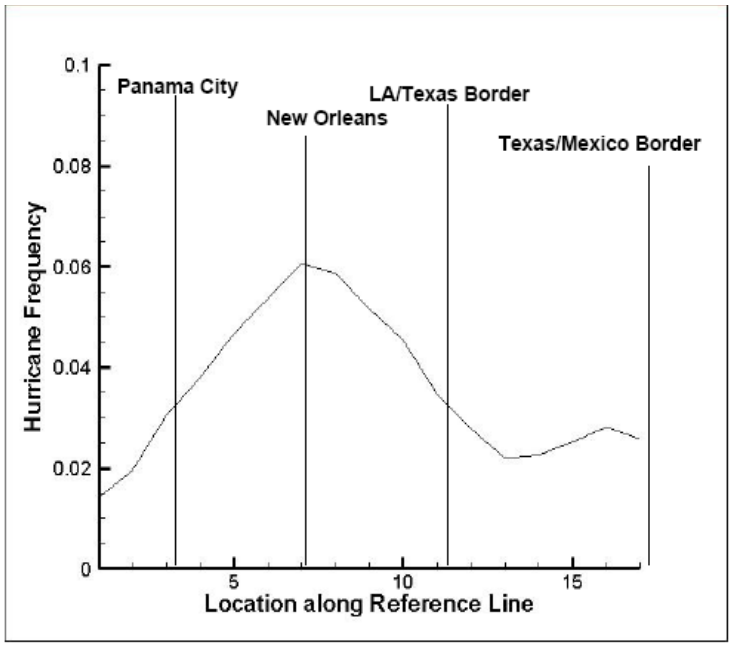

Figure 3.4. Landfall Return Frequency (per Year) for GoM Hurricanes Peaking at Central Pressures <955 mb

Resio et al 2007

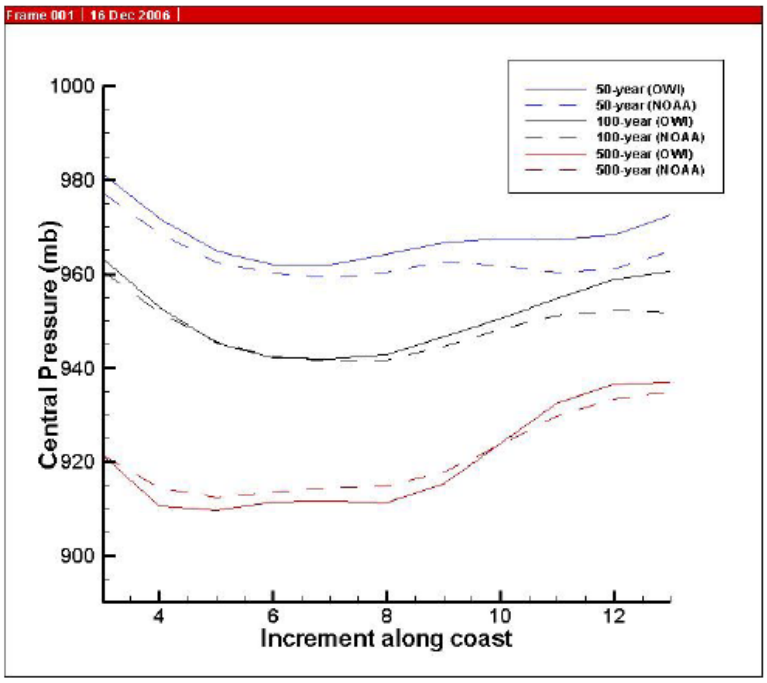

Figure 3.5. Observed 50-, 100-, and 500-yr Return Periods for Landfall Central Pressures at Segments Along CN-GoM

Resio et al 2007

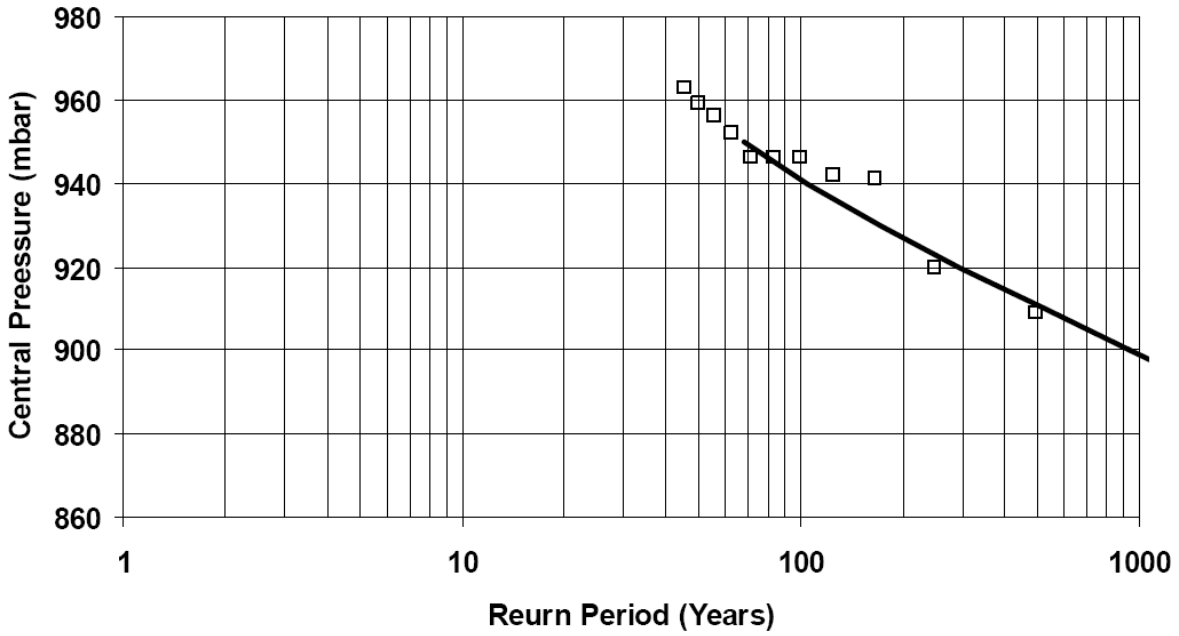

Figure 3.6. Return Period Probability Distribution for Landfall Central Pressure for 1° Longitude (60-mi) Segment South of New Orleans

Resio et al 2007

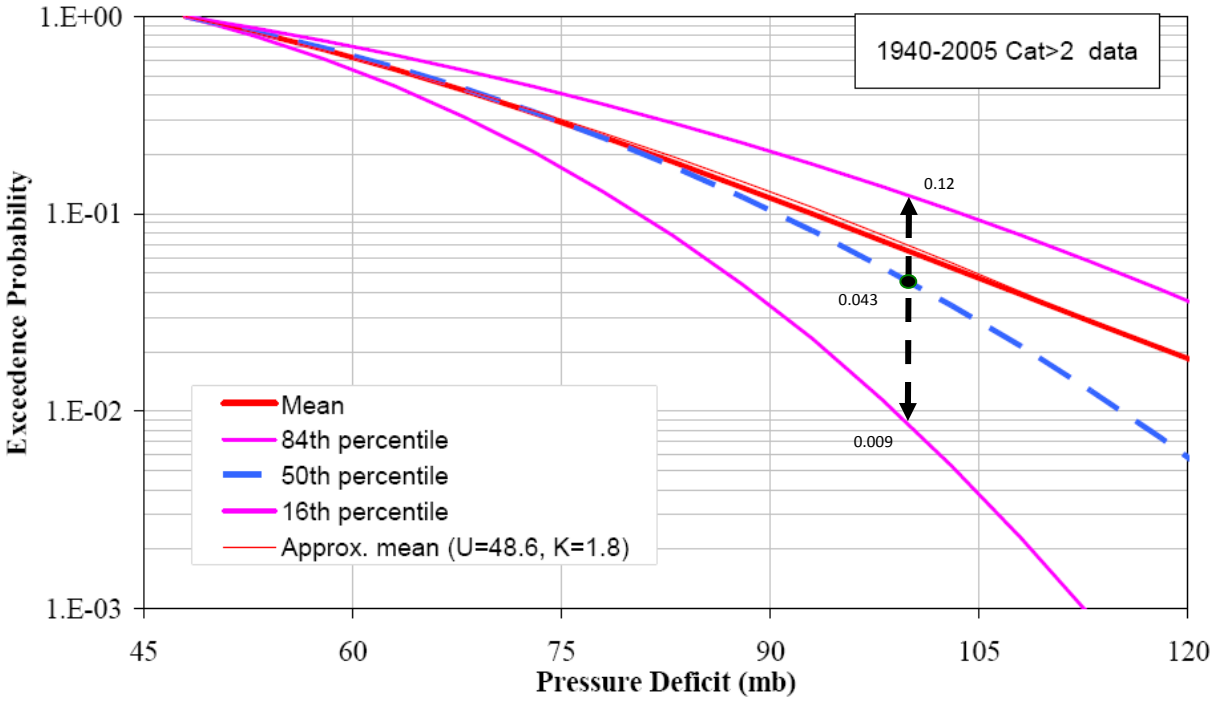

Figure 3.7. Return Frequency Probability Distribution for Landfall CPD for 124-mile Radius Centered Near Bay St. Louis MS

Toro 2008

Table 3.4. List of GMHs/L-500

Name	Year	Peak			Landfall			
		Cat	V_{max} mph	CPD mb	Cat	V_{max} mph	CPD mb	Location
Gustav	*2008*	*4*	*138.0*	*70*	*2*	*109.3*	*65*	*Timbalier Is LA*
Katrina	**2005**	**5**	**172.5**	**118**	**3**	**126.5**	**100**	**Buras LA**
Rita	2005	5	178.3	123	3	115.0	85	Johnsons Bayou LA
Dennis	2005	4	143.8	85	3	126.5	78	Santa Rosa Is FL
Ivan	2004	5	161.0	96	3	120.8	77	Gulf Shores AL
Lili	2002	4	143.8	80	1	92.0	58	Intracoastal City LA
Isidore	**2002**	**3**	**126.5**	**86**	**TS**	**63.3**	**36**	**Grand Isle LA**
Opal	1995	4	149.5	101	3	126.5	80	Santa Rosa Is FL
Andrew	*1992*	*4*	*143.8*	*83*	*4*	*138.0*	*65*	*Morgan City LA*
Elena	1985	3	126.5	66	3	115.0	61	Ship Is MS
Kate	1985	3	120.8	66	2	92.0	45	Mexico Beach FL
Frederic	1979	4	132.3	77	4	132.3	70	Dauphin Is AL
Eloise	1975	3	126.5	65	3	126.5	65	Panama City FL
Carmen	*1974*	*4*	*149.5*	*83*	*4*	*149.5*	*83*	*Morgan City LA*
Camille	*1969*	*5*	*189.8*	*111*	*5*	*189.8*	*111*	*Venice LA*
Betsy	**1965**	**4**	**155.3**	**79**	**4**	**143.8**	**77**	**Grand Isle LA**
Hilda	1964	4	149.5	79	3	109.3	61	Franklin LA
Ethel	*1960*	*5*	*161.0*	*NA*	*1*	*86.3*	*NA*	*Chandeleur Is LA*
Audrey	1957	4	143.8	74	4	143.8	74	Johnsons Bayou LA
Florence	1953	3	126.5	52	1	80.5	35	Destin FL
Not Named	1926	3	126.5	NA	2	109.3	65	Fort Morgan AL
Not Named	1918	3	120.8	70	3	120.8	65	Cameron LA
Not Named	1917	4	138.0	NA	3	115.0	71	Fort Walton, FL
Not Named	1916	3	120.8	70	3	120.8	70	Dauphin Is AL
Not Named	**1915**	**4**	**143.8**	**NA**	**3**	**126.5**	**76**	**Grand Isle LA**
Not Named	1909	3	120.8	NA	3	120.8	68	Grand Isle LA
Not Named	1906	3	120.8	67	2	109.3	62	Horn Is MS
Not Named	1894	3	120.8	NA	3	120.8	NA	Panama City FL
Not Named	**1893**	**4**	**132.3**	**72**	**4**	**132.3**	**72**	**Cheniere Caminada LA**
Not Named	1886	3	120.8	NA	3	120.8	NA	Johnsons Bayou LA
Not Named	1882	3	115.0	71	3	115.0	71	Santa Rosa Is FL
Not Named	1879	3	126.5	NA	3	126.5	NA	Morgan City LA
Not Named	1877	3	115.0	NA	3	115.0	NA	Panama City FL
Not Named	**1860**	**3**	**126.5**	**NA**	**3**	**126.5**	**NA**	**Grand Isle LA**
Not Named	1856	4	149.5	86	4	149.5	86	Last Island, LA
Not Named	1856	3	115.0	NA	2	115.0	NA	Panama City FL
Not Named	**1855**	**3**	**126.5**	**NA**	**3**	**126.5**	**NA**	**Buras LA**
Not Named	1852	3	115.0	NA	3	115.0	59	Horn Is MS

Seven in **bold** crossed a 1° (60 mi) segment south of New Orleans; five additional in *italics* crossed 2.5° (151 mi) segment; CPD assuming an ambient pressure of 1020 mb; wind speeds converted from knots.

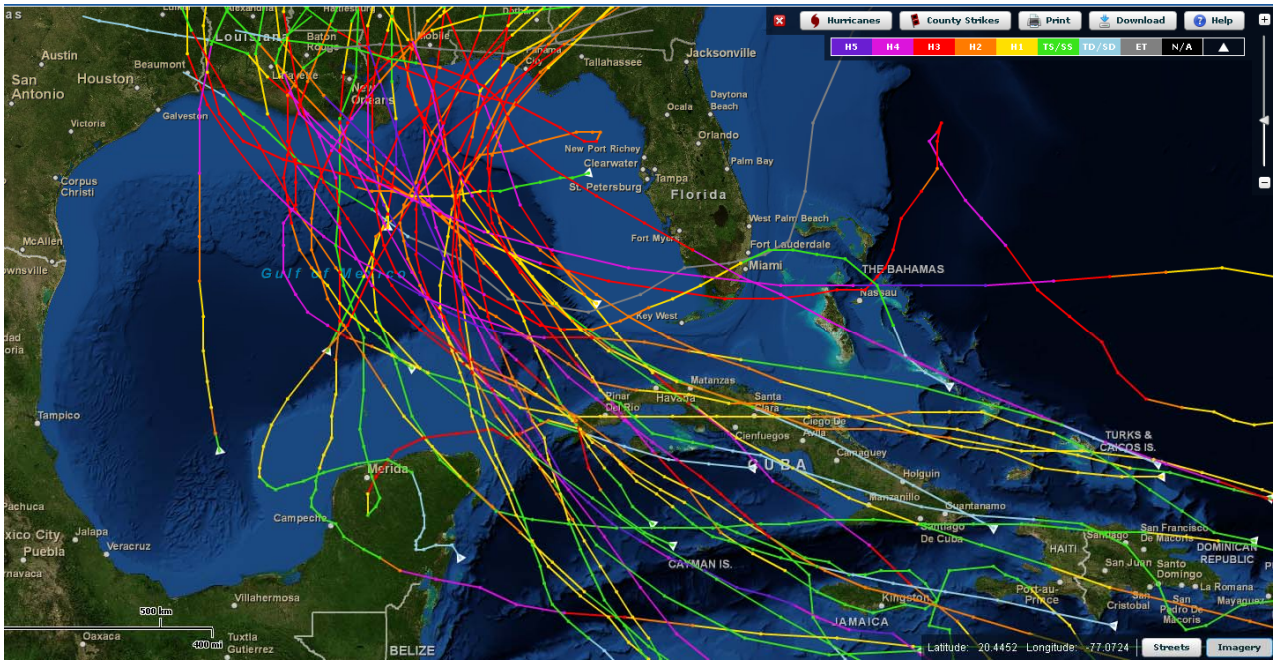

Figure 3.8. Tracks of 39 GMHs Striking the CN-GoM

http://www.csc.noaa.gov/hurricanes/#app=3d30&3e3d-selectedIndex=2

Figures 3.9 and 3.10 graph the cumulative number of GMHs/L-500 and GMHs/LMH-500 versus time. The overall linear 161-yr trend lines are 20.2 and 16.1 per century, one every 5 and 6.2 years, respectively, both a bit lower than the simple averages (R^2 of 0.97 and 0.96).

Figure 3.11 illustrates the return period for V_{max} for the 39 GMHs/L-500, together with three probability distribution functions, log-normal, Gumbel, and Log Pearson Type III, and the uncertainty bands for the Gumbel distribution. The Gumbel distributions assigns a return period of 6.5 years to the landfall of a 111 mph hurricane (Category 3) along the CN-GoM, a bit longer than the simple average of 5.4 years. The return period for Hurricane Camille's 190 mph landfall V_{max} is very long for all three distributions, at 794, 510, and >1,000 years respectively, compared to the observed return period of 232 years (using the method described in Footnote 4).

The lower confidence limit, mean estimate, and upper confidence limit for the 100-, 500-, and 1,000-yr return V_{max} for landfall in the CN-GoM using the Gumbel distribution are:

- 100-yr: 157, 163, and 169 mph
- 500-yr: 181, 189, and 199 mph
- 1,000-yr: 191, 201, and 212 mph

The Gumbel distribution confidence intervals for the return period estimates are asymmetric. For example at the 100-yr return of 163 mph the 90% confidence interval spans roughly from -33% to + 50%, or from 66 years to 150 years. At the 500-year return the 90% confidence interval spans roughly from -50% to + 100%, or from 250 years to 1000 years.

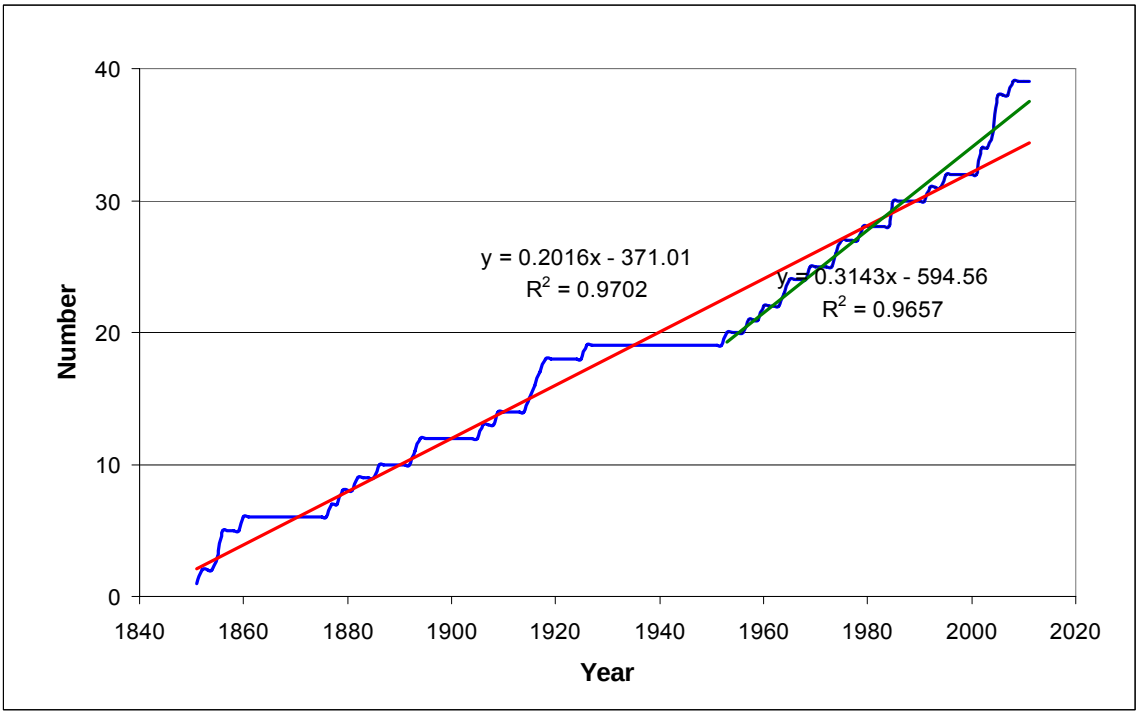

Figure 3.9. Cumulative Number of GMHs/L-500

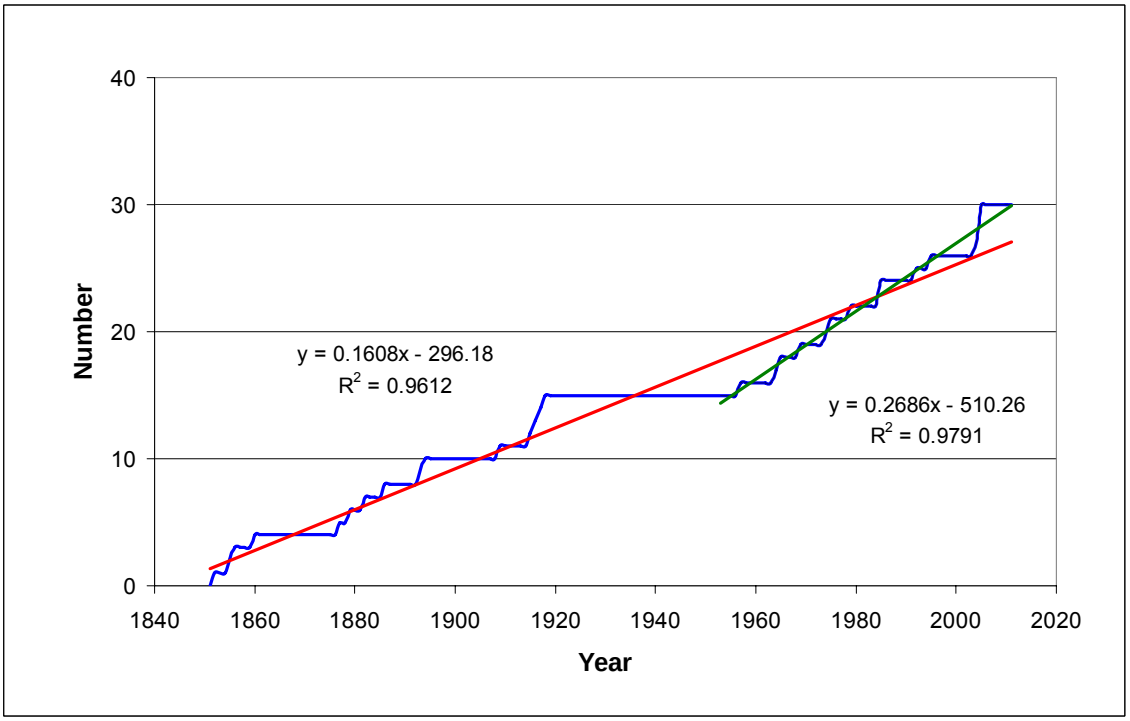

Figure 3.10. Cumulative Number of GMHs/LMH-500

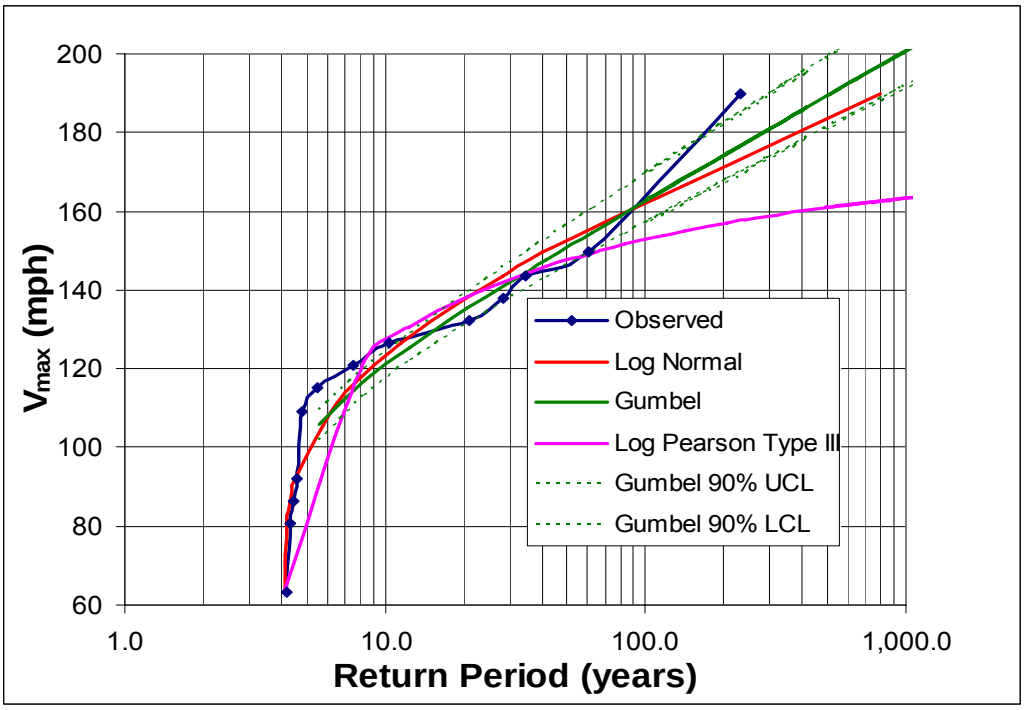

Figure 3.11. Return Period Distribution for L-500 V_{max}

Of the 39 GMH/L-500 hurricanes, twelve were L-151 and seven were L-60, as highlighted in Table 3.4. Of these, nine and six were LMH-151 and LMH-60. Table 3.5 summarizes the return periods for GMHs by segment and category: 4.1 and 5.4 years (L-500 and LMH-500), 13.4 and 17.9 years (L-151 and LMH-151), and 23.0 and 26.8 years (L-60 and LMH-60). Confidence intervals for these return periods have been suggested based on Figure 3.11. A 90% confidence interval for GMH/L-60 and GMH/LMH-60 return period may be on the order of -23% to +30%. The 26.8-year return period for LMH-60 is consistent with the Keim et al finding of a 26-year return period for Boothville LA.

Table 3.5 shows that GMHs approaching the 60-mile New Orleans segment are more likely to remain at major category through landfall (6 out 7, or 86%) compared to the 500-mile CN-GoM or 151-mile segment (which are very similar at 77 and 75%). While the L-500- and L-151 GHMs have nearly identical length-adjusted landfall rates, as do LMH-500- and LMH-151, the 60-mile New Orleans segment has much higher length-adjusted rates for both classes of landfalls, 50 and 67% higher. These higher landfall rates for the 60-mile segment are consistent with the higher rate depicted in Resio et al's Figure 3.4. A higher hurricane landfall activity for the 60-mile segment may be attributable to the interactions with the Loop Current and associated eddies for hurricanes tracking toward this segment.

Figure 3.12 illustrates using the larger population of CN-GoM GHMs to estimate GMH/L-60 return periods and adjusting for the latter's higher frequencies [using a factor of, 1/{(60/500)*(1.5 to 1.67, see Table 3.5)}]. The Resio et al distribution from Figure 3.6 has also been included on Figure 3.12 by using V_{max} values which generally correspond to the CP values. Figure 3.12 shows that the two curves match up reasonably well, with the Resio et al distribution assigning shorter return periods for V_{max} above 125 mph. This shorter return period reflects the Resio-Orelup proposed 40-yr cycle in GoM hurricane activity.

Table 3.5. 161-Yr Record GMH Landfall Rates by Segment and Landfall Category

	L-500	LMH-500	L-151	LMH-151	L-60	LMH-60
Number in 161-yr Record	39	30 (77%)	12	9 (75%)	7	6 (86%)
Return Period (yr)	4.1	5.4	13.4	17.9	23.0	26.8
Suggested 90% Confidence Interval	-16.7 to +20%	-16.7 to +20%	-20 to +25%	-20 to +25%	-23 to +30%	-23 to +30%
Frequency (per century)	24.2	18.6	7.5	5.6	4.3	3.7
Length Adjusted Frequency (per century-mi)	0.048	0.037	0.049	0.037	0.072	0.062
500-mi/60-mi Length Adjusted Frequencies					1.5 (0.072/0.048) i.e. 50%	1.67 (0.062/0.037) i.e. 67%

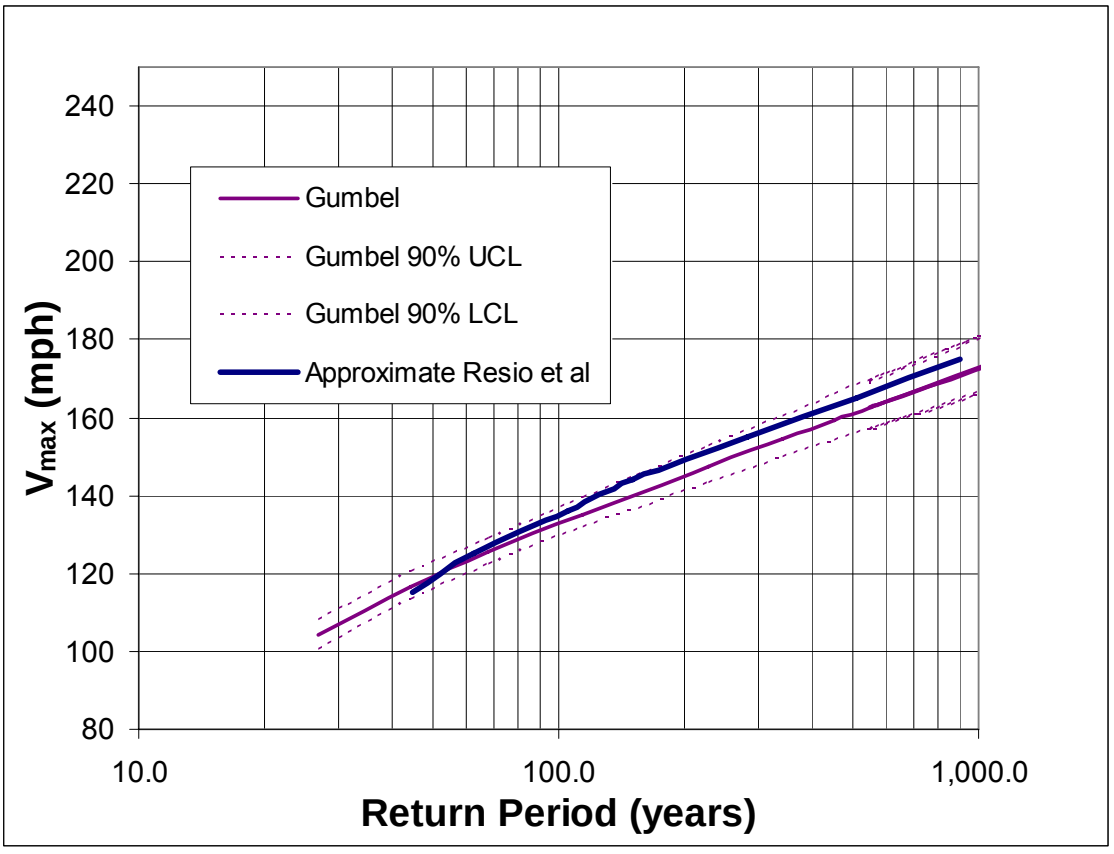

Figure 3.12. Return Period Distribution for GMH/L-60 V_{max}

As V_{max} can vary considerably for a given CPD, it is important to evaluate the return period for both landfall winds and landfall CPD. As previously noted, Katrina's borderline Category 4/5 CPD at landfall of 100 mb has an L-60 return period of about 280 years according to Figure 3.6. The Figure 3.12 Gumbel distribution for L-60 V_{max} indicates that a borderline Category 4/5 V_{max} has a return period of about 340 years. However, Figure 3.12 indicates that both the Gumbel distribution and the Resio et al curve place Katrina's actual strong Category 3 126.5 mph landfall V_{max} at a return period of closer to 63 years.

Coastal geologists are employing much longer records—encompassing the entire late Holocene (up to 5,000 years before present)—to evaluate highly localized recurrence of intense hurricane landfall in the CN-GoM/Texas.[3] Evidence of hurricane landfalls is obtained from detailed soil cores at coastal lakes and bays. Sediment overwash data for Lake Shelby AL, Western Lake FL, Pearl River Marsh MS, Atchafalaya Marsh LA, and Laguna Madre TX have led to estimates of long-term average return periods for intense hurricane landfall—at the much smaller spatial scale of a coastal bay or lake—of 350, 400, 450, 133 and 217 years, respectively. Intermittent periods of considerably higher frequencies are also noted. (Liu and Fearn 2000, Wallace and Anderson 2010).

3.2. Landfall Characteristics

Since 2005, landfalling hurricane characteristics have also been the subject of numerous correlation studies. The following findings are pertinent to landfalls in the CN-GoM:

- *Core intensity measurements of V_{max} versus CPD*. Figure 3.13 plots landfall V_{max} versus central pressure for the 30 hurricanes listed in Table 3.4 for which both data are available. Figure 3.13 includes a linear equation fitted to the data, with an R^2 of 0.71, and confidence limits. The amount of residual scatter in the central pressure versus V_{max} relationship is substantial—approximately ±20 mph at ± two standard deviations.
- *Core intensity versus core size*. For landfall hurricanes along the Gulf coast Vickery noted that no statistically significant correlation exists between the R_{max} and either latitude or CPD (in Resio et al 2007). He estimated a Log-Normal probability distribution of R_{max} (in km) with a mean value ln (R_{max}) of 3.558 and a standard deviation ln (R_{max}) of 0.457.
- *Wind field distribution.* No research has identified possible correlations between the extent of hurricane/tropical force winds, Holland B, IKE, or other wind field indices with core intensity, R_{max}, track, or V_f characteristics specific to landfall.
- *Intensification*—CPD versus SST. Vickery (Vickery et al 2000) employed a collection of empirical storm tracks to simulate an average of 8.4 Atlantic storms/yr (standard deviation of 3.56 storms/yr) over a synthetic 20,000-yr period. Core intensity along the randomly selected track for each of the 168,000 storms was estimated using the correlation of CPD and SST (see above) and typical regional ocean SSTs. The model produced estimates of CPD frequency for storms making landfall along the U.S. coast. Figure 3.14 shows that simulated mean CPD and variance corresponded well to observed values. Vickery used this model—together with a wind model—to estimate return period coastal peak gusts.

[3] This research field goes by the name of paleotempestology.

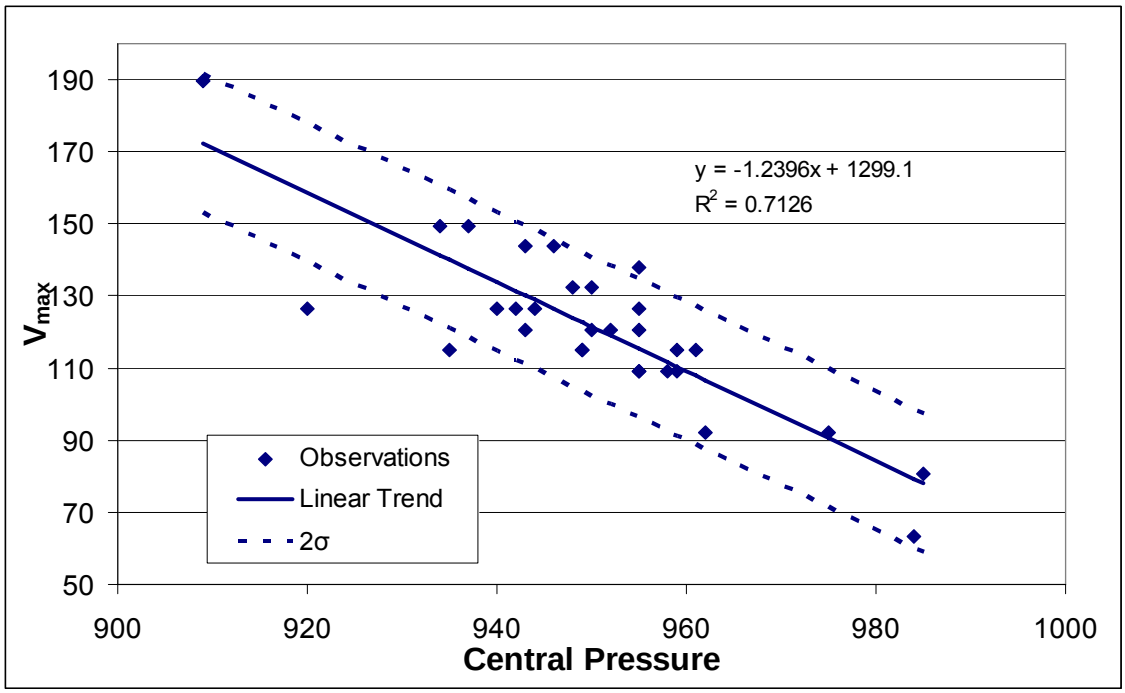

Figure 3.13. GMHs/L-500 Central Pressure versus V_{max}

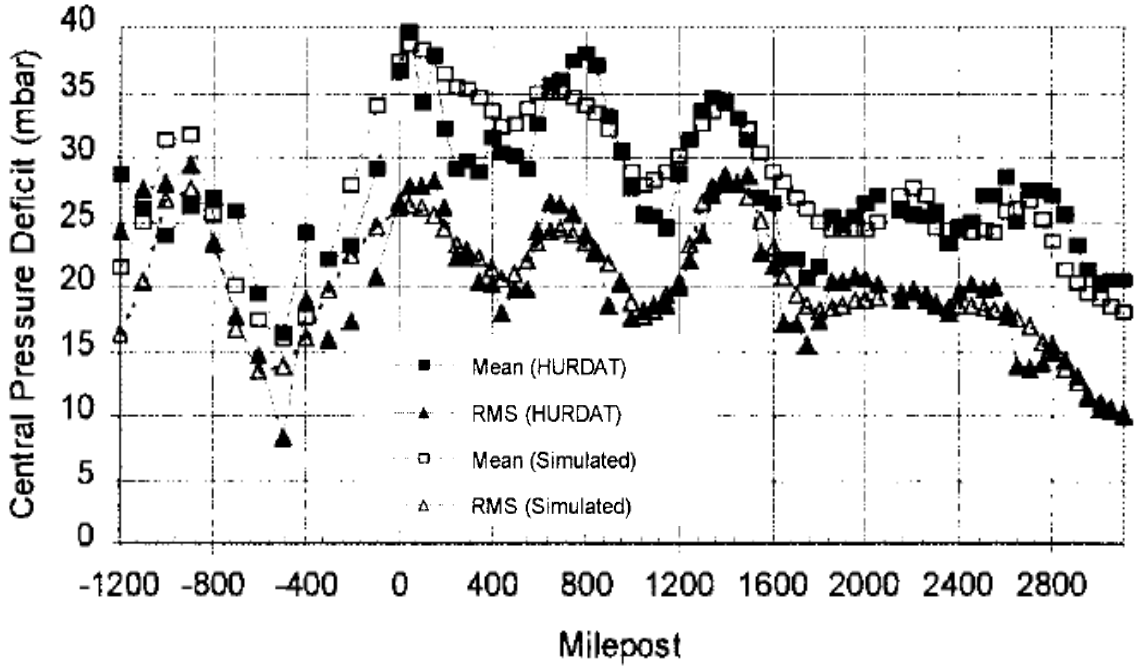

Figure 3.14. Predicted versus Observed Landfall Central Pressure

Vickery et al 2000

- *Decay prior to landfall*. Recent research on GMH weakening prior to landfall has produced estimates of decay rates. Resio et al in 2007 suggested a linear decay of CPD between 90 nm offshore and landfall. The total reduction in CPD depends on the offshore R_{max} and equals ($R_{max\text{-}offshore}$ – 6 nm), but is restricted to minimum/maximum CPD reductions of 5/18 mb. For storms with offshore R_{max} > 10 nm, the R_{max} increases from $R_{max\text{-}offshore}$ to 1.3 * $R_{max\text{-}offshore}$ at landfall. For those with higher Holland B, a decrease in Holland B (to 1.0) is suggested. No uncertainties regarding these estimates were provided.

  Table 3.4 shows that with improving observations, a greater percentage of GMHs are found to decay prior to CN-GoM landfall. Prior to 1900 there were no records of GMHs decaying as they approached landfall. Between 1900 and 1985 seven out of sixteen GMHs decayed by at least one category prior to landfall. However, beginning in 1985 detailed V_{max} records show that all 11 GMHs experienced V_{max} decay prior to CN-GoM landfall (including two striking south of New Orleans)—ranging from 12 to 63 mph with an average of 34 mph, or 4 to 50% with an average of 23.5%.

- *Decay following landfall.* Further decay after landfall has also been studied. A continuation of the linear rate of pre-landfall decays are considered appropriate for two hours following landfall (Toro 2008), after which CPD decay is exponential (Vickery and Twisdale 1995).

- *Track.* Figure 3.8 illustrates that only 6 of the 39 GMH-$L_{500/161}$ originated in the GoM and five in the northwestern Caribbean Sea. The majority were born in the Atlantic or central and eastern Caribbean Sea. Nearly all of the 39 GMH-$L_{500/161}$ are distinguished by their passage through the region dominated by the very warm SST of the Loop Current, as depicted in Figure 1.17. (The western-most storm, Hurricane Audrey of 1957, may have encountered a warm eddy, which can break off from the Loop Current and drift west.)

- *Approach Heading*. Scientists have found landfalling θ in the CN-GoM to be independent of CPD (Resio eta al 2007). They have suggested normal distributions for θ along 1° east-west coastal segments. The estimated mean and standard deviation (positive θ for west of due north) are shown in Figure 3.15. The mean hurricane landfall θ for Segment 7, which corresponds to the Louisiana coastline south of New Orleans, is about 16° west of north,with a standard deviation of about 21°. Researchers have suggested a correlation between higher V_f and more easterly θ, attributable to recurving conditions caused by landfalling storms encountering westerly atmospheric steering currents. Hurricane Betsy was an important exception.

  A similar study by Toro for a 124 mile segment along coastal Mississippi found a Beta distribution (more peaked symmetrical distribution than a normal distribution) of θ with a mean of 12.4 degrees (westerly) and standard deviation of 37.5 degrees (Toro 2008).

- *Forward Speed*. Researchers have also found the V_f of landfalling hurricanes in the CN-GoM to be independent of CPD (Resio et al 2007). Toro has suggested that the V_f of hurricanes with CPD > 48 mb making landfall in the CN-GoM follows a log-normal distribution as shown in Figure 3.16.

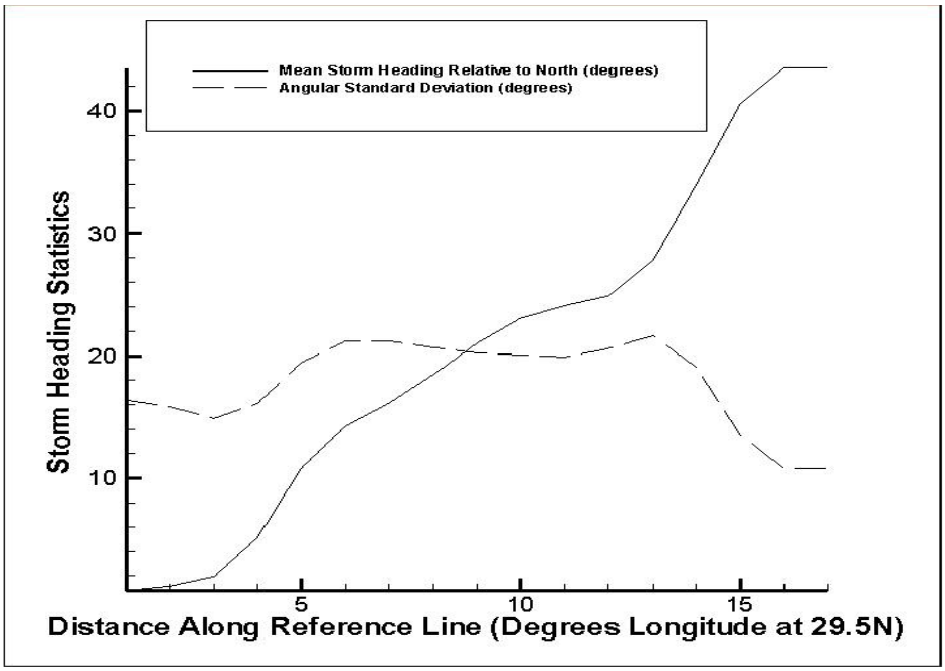

Figure 3.15. Hurricane Landfall Headings Along the CN-GoM/Texas Coast

Resio et al 2007 (see Figure3.4 for reference locations)

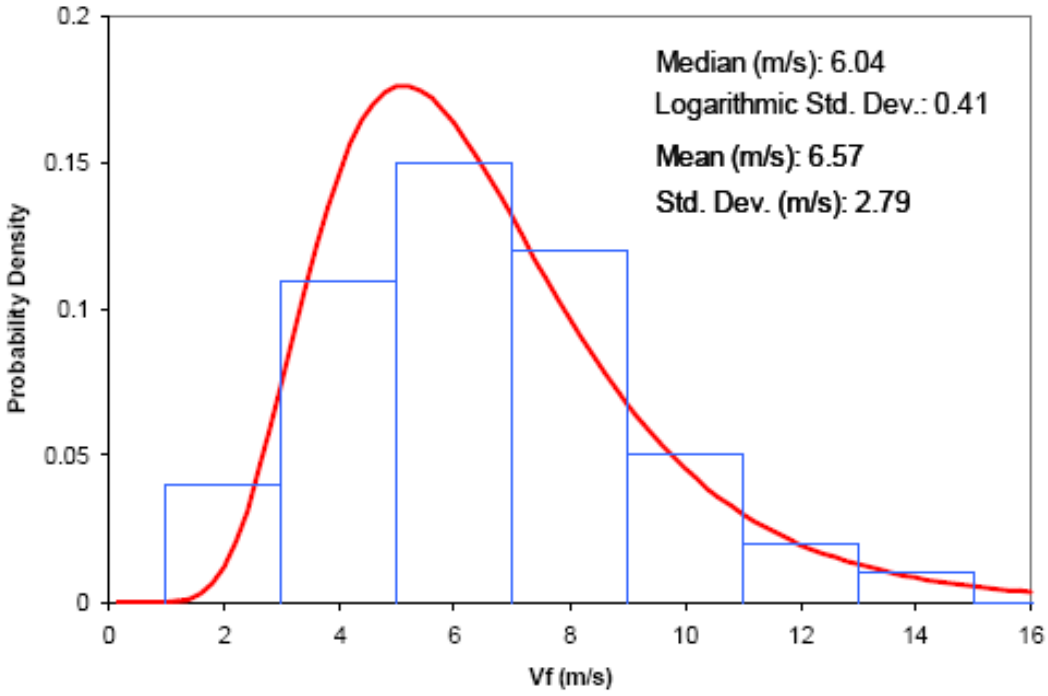

Figure 3.16. Forward Velocity of GMHs/LMH-500

Toro 2008

3.3. Landfall Climatic Trends

As part of their evaluation of relative return frequencies for tropical storms, hurricanes, and major hurricanes at 45 locations, Keim et al compared their 1901-2005 computed hurricane return periods with those calculated for 1886-1970 by Simpson and Lawrence and for 1900-1996 data by Elsner and Kara. Comparisons for the eight CN-GoM locations are shown in Table 3.1. Keim et al ascribed major variations between studies to differences in multi-decadal phases in Atlantic SST and upper atmospheric pressure conditions. In their 2008 review of U. S. hurricane landfall frequencies Parisi and Lund examined the influence of climatic cycles and long-term trends but found no great impacts on return period estimates.

Figure 3.17 illustrates a 2-yr rolling average for the 161-yr record of GMHs/L-500. Several periods of prolonged landfall inactivity (zero landfalls) are evident. Figure 3.17 reveals three periods of higher activity in GMH-$L_{500/161}$—1855-56 (three in two years), 1916-18 (three in three years), and 2002-5 (six in four years). The higher activity of 2002-05 period has been associated with conducive hurricane genesis conditions, higher Atlantic/GoM SSTs, and favorable La Nina (Cooper and Stear 2006). The long-term linear trend in the 2-yr running average has a slope of 0.08 storms per century, indicating the long term secular trend is very stationary, but with a high degree of scatter in the 2-yr averages (R^2 is only 0.01)

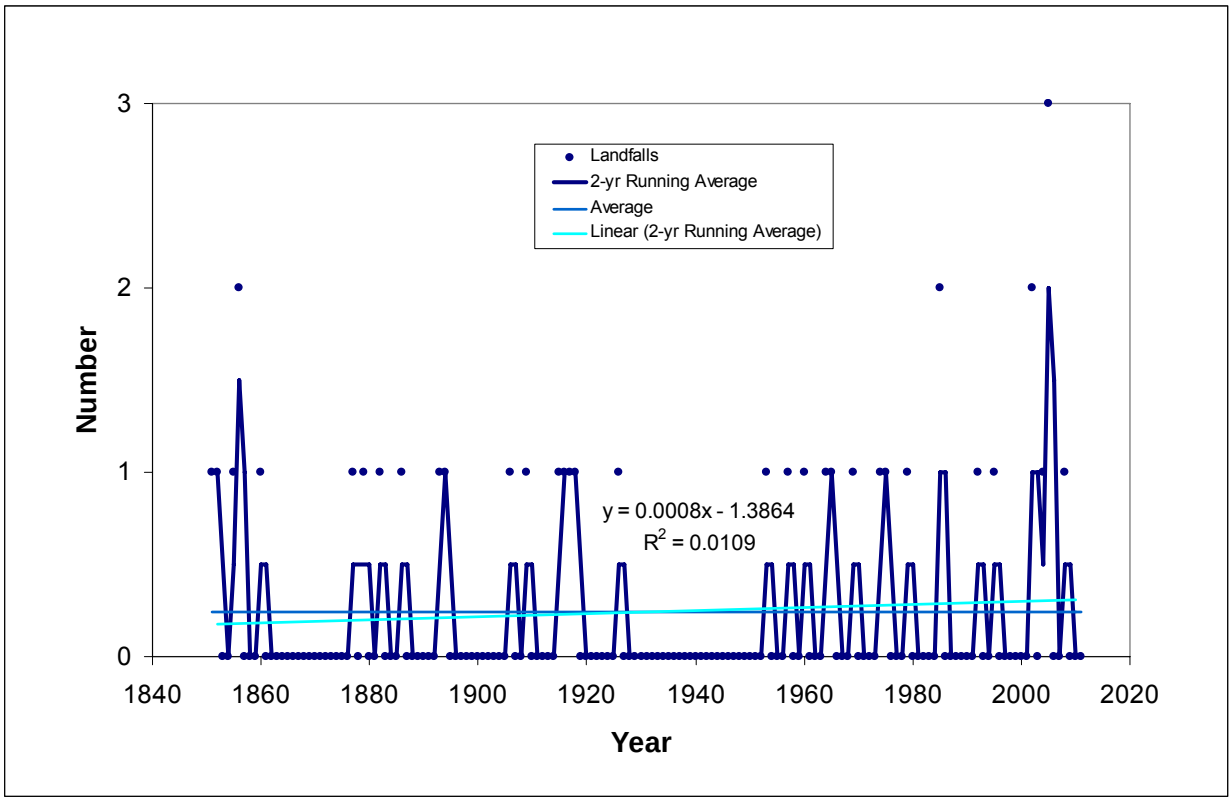

Figure 3.17. Rolling Average for GMHs/L-500

As with the graph of cumulative GMHs in Figure 1.2 b, Figures 3.9 and 3.10 indicate escalations in GMH/L-500 and GMH/LMH-500 over recent decades, in these cases a 60-yr period since 1952. The GMH/L-500 60-yr linear trend shown in Figure 3.9, is 31.4 per century compared to the 161-yr linear trend of 20.2 per century, an increase of 55%. The 60-yr trend for GHM/LMH-500, illustrated in Figure 3.10, is 26.9 per century, 67% higher than the 161-yr trend of 16.1 per century.

Toro suggested that the increasing hurricane activity over recent decades may be due to improved observations beginning with World War II coastal aerial reconnaissance, while Resio and Orelup suggested that it may reflect a 40-yr GoM climate cycle. In contrast to a period beginning in 1952, both Toro and Resio et al suggested that a period beginning in the early 1940s is appropriate. However, Figures 3.9 and 3.10 show that starting a record in the early 1940s adds many low activity years to the record. Resio et al proposed that a 1941-2005 record provides a balanced representation of the active and inactive phases of a 40-yr climate cycle.

Table 3.6 presents estimates of recent (based on the 60-yr record) return periods obtained by simply applying the 55 and 67% escalators to the 161-yr record return periods (Table 3.5) for the three segments and two landfall categories. The shorter recent return periods are: 2.7 and 3.2 years (L-500 and LMH-500), 8.6 and 10.7 years (L-151 and LMH-151), and 14.9 and 16.1 (L-60 and LMH-60).[4] Table 3.6 suggests the size of possible confidence intervals for these return period estimates—based on the 161-yr period Gumbel distribution for the entire CN-GoM. However, larger confidence intervals may be warranted due to the smaller record.

Table 3.6 also includes escalated length-adjusted landfall rates by segment and landfall category. In addition, Table 3.6 shows the observed return periods and length-adjusted landfall frequencies for GoM Category 5 hurricanes (GMH-5) in all three segments over the 60-yr record. With the caveat that the sample size is relatively small, five Category 5 hurricanes in 60 years, the length-adjusted rate appears to be much higher for the 151- and 60-mile segments.

The shorter, recent L-60 and LMH-60 return periods imply a revision to Figure 3.12 and the estimated Hurricane Katrina's landfall return period noted previously. Figure 3.18 multiplies the L-60 Gumbel distribution for V_{max} return periods by 0.62 (i.e., 1/1.6) to account for the recent escalation. The revised return periods are now noticeably shorter than the corresponding Resio et al values. A major reason is the inclusion of the low activity 1941 to 1952 period by Resio-Orelup in their proposed GoM hurricane activity cycle.

According to the escalated Gumbel distribution in Figure 3.18, the recent 100-yr return period L-60 V_{max} is just above 140 mph, while for the Resio et al curve it is approximately 135 mph. Hurricane Katrina's 126.5 mph V_{max} and 100 mb CPD landfall now have revised estimated return periods (based on the Figure 3.18) of closer to 40 and 212 years, compared to previous estimates of about 63 and 340 years from Figure 3.12 (based on the total 161-yr record). The estimated return periods of 40 and 212 years for strong Category 3 and borderline Category 4/5 are much shorter than the Resio et al estimated return period of 63 and 280 years. According to the Gumbel distribution the 90% confidence interval for these return period estimates are about -25 to +33% and -33 to + 50%.

[4] The actual 60-year record for L-60 and LMH-60 is three and two respectively over the 60-year record; thus the observed return periods are 20 and 30 years; the results of applying the escalators to the 161-year record for GMH/L-60 and GMH/LMH-60—14.9 and 16.1 years—may be more representative.

Table 3.6. Recent GMH Landfall Rates by Segment and Landfall Category

	L-500	LMH-500	GMH-5/ L-500	L-151	LMH-151	GMH-5/ L-151	L-60	LMH-60	GMH-5/ L-60
Total (161-yr) Record Return Period (yr) (from Table 3.5)	4.1	5.4		13.4	17.9		23.0	26.8	
Escalator (60 vs 161-yr record)	1.55	1.67		1.55	1.67		1.55	1.67	
Recent Return Period (yr)	2.7	3.2	12*	8.6	10.7	20*	14.9	16.1	60*
Suggested 90% Confidence Interval	-16.7 to +20%	-16.7 to +20%	-20 to +25%	-20 to +25%	-20 to +25%	-23 to +30%	-20 to +25%	-20 to +25%	-25 to +33%
Frequency (per century)	37.5	31.1	8.3	11.6	9.3	5.0	6.7	6.2	1.7
Length Adjusted Frequency (per century-mi)	0.075	0.062	0.017	0.077	0.062	0.033	0.112	0.103	0.028

* These are observed return periods for Category 5 GoM hurricanes, based on Table 3.4.

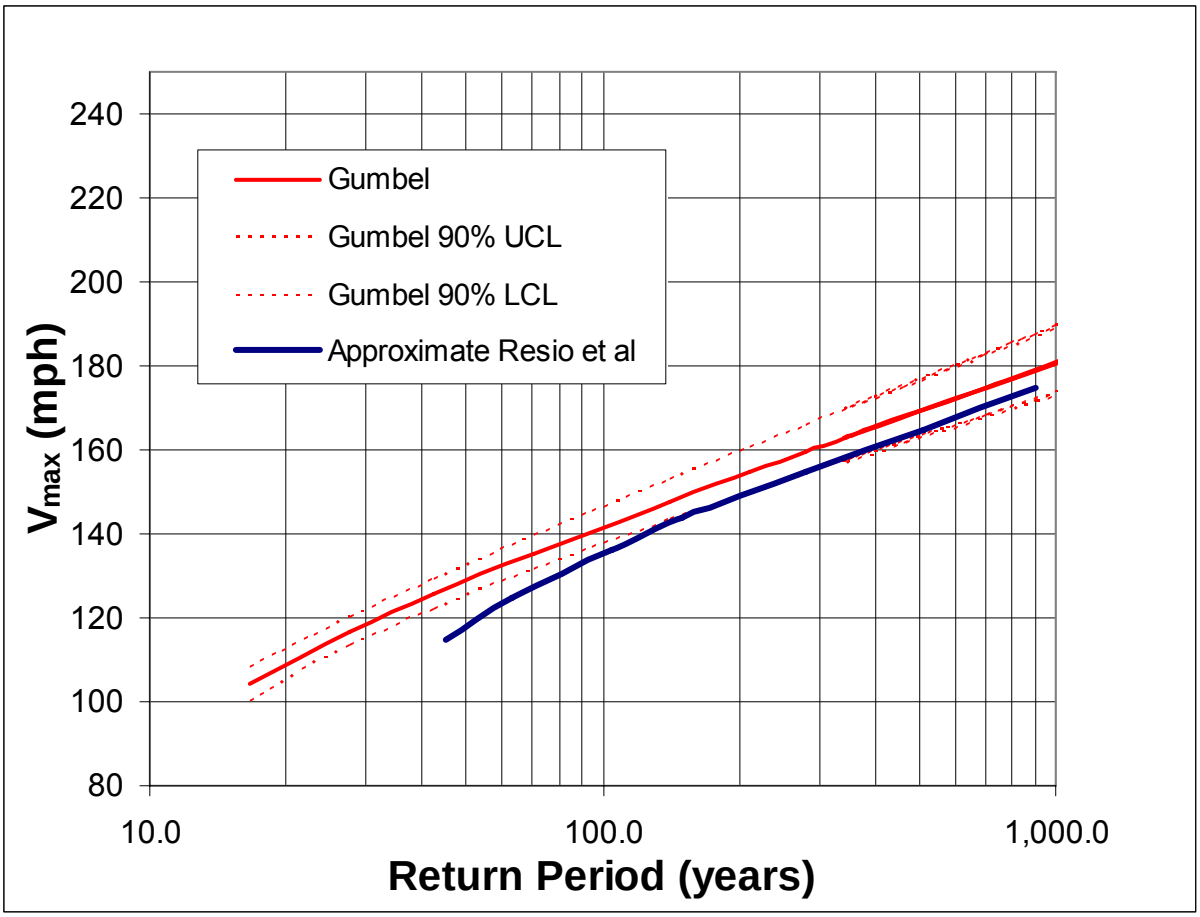

Figure 3.18. Recent Return Period Distribution for GMH/L-60 V_{max}

Section 4. Hurricane Joint Probability Analysis

4.1. Overview of Hurricane JPA

As discussed in Section 1, five hurricane attributes—core intensity (CPD or V_{max}), R_{max} , wind field distribution, V_f, and track θ —and their dynamics along the track, contribute to surge hazard associated with any particular landfall point, combining in highly nonlinear ways. Figure 4.1 illustrates a joint observed occurrence for two hurricane attributes, IKE and V_{max} , with a three-dimensional contour depiction. Fritz prepared the illustration, which depicts the joint occurrence for the entire U.S. coastline, as part of recent Master's thesis. Similar 3D contour figures can be used to illustrate the joint observed occurrence, or computed joint probability, of any two characteristics.

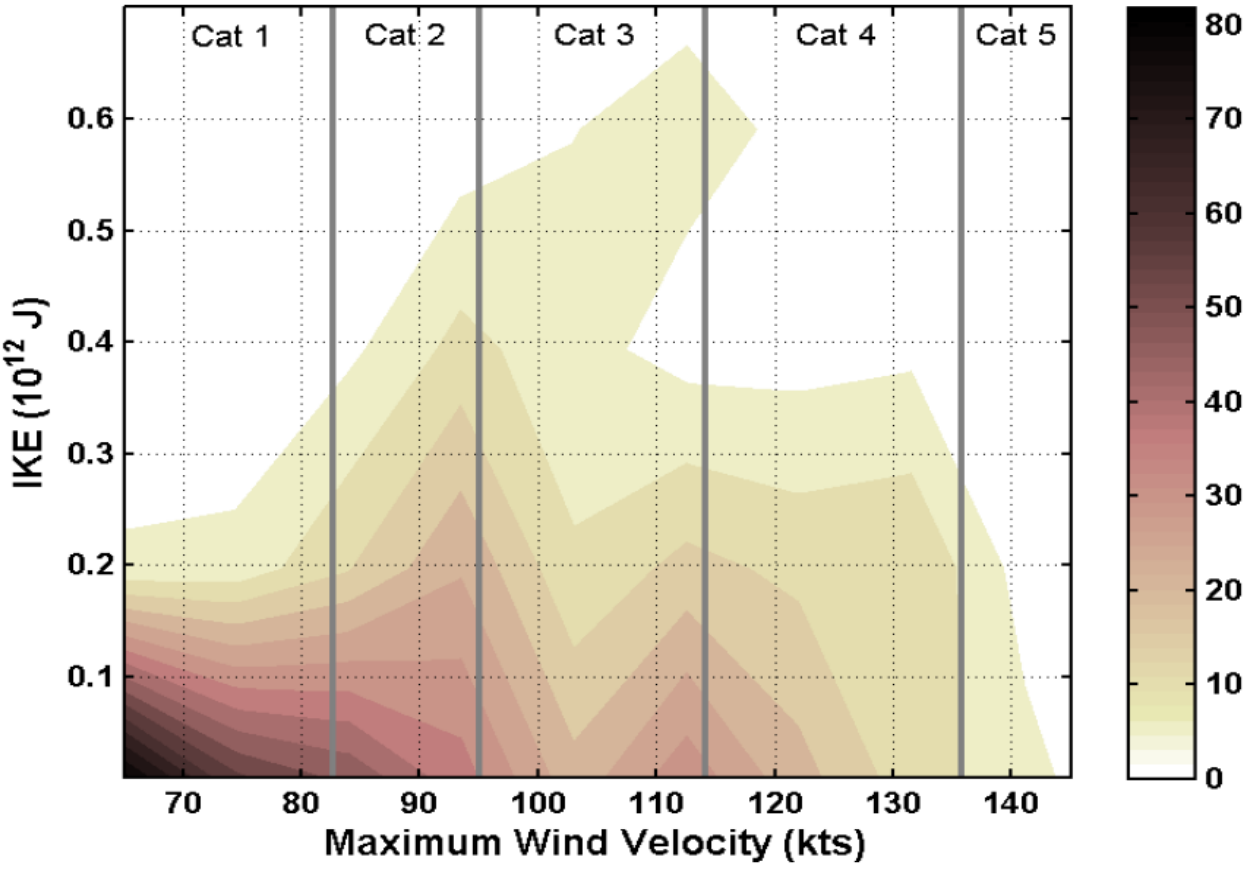

Figure 4.1. Joint Occurrence for Hurricane IKE and V_{max}
Fritz 2009

Due to the limited number of recorded hurricanes in any coastal region, joint occurrences alone are inadequate to describing joint probabilities. For example, the joint occurrences for IKE and V_{max} shown in Figure 4.1 are not fully representative of the joint probability. Irish (2011) has noted that return period estimates for hurricane joint characteristics based only on historic records can have unsatisfactory uncertainty bands. Thus, to improve the statistical representation of regional hurricane climatology scientists combine the available probability expressions for each hurricane attribute, such as those described in Sections 1 and 3, into a joint probability analysis (JPA).[1] In this way scientists can mathematically compute joint probabilities for any attribute combination.

Three important sources of potential error/uncertainty in a hurricane JPA and its applications include:

1. The hurricane attributes excluded in the analysis;
2. The established uncertainty in the probability distributions and functional relationships for selected attributes;
3. The representativeness of the historical data for the attribute probability distributions, functional relationships, and confidence limits. These "unknown unknowns" can only be described through reasoned hypothetical adjustments and sensitivity analysis (see GTN-1).

A JPA can be undertaken to examine the influence of future changes in hurricane characteristics and uncertainty. In this case the probability expressions for the individual attributes are modified to reflect a trend analysis or hypothesis, and the joint probabilities are recomputed. An example might include the effect of hypothesized changes in average CPD peaks and scatter in 2050 years based on higher future SSTs. To date there has been no future conditions JPA for GoM hurricanes.

Evaluations of hurricane wind and surge hazards requires a stochastic approach coupling a JPA of hurricane climatology with deterministic wind and hydrodynamic models. This approach is accomplished by developing a synthetic set of storms to represent the hurricane climatology JPA and then simulating each storm's conditions with the wind and/or hydrodynamic model.

Synthetic sets, which that are considerably larger than the historic record, can be developed using two basic approaches: the Empirical Simulation Technique (EST) and the Joint Probability Method (JPM).

The EST employs the joint probabilities evidenced in the historical record with some adjustments. A larger, artificial dataset is created by randomly drawing more storms from the historical record and introducing some modifications to historic storms to increase the range of attributes and attribute-track combinations. Additional track variations are developed by offsetting empirical (observed) tracks. Missing values for characteristics along the track are interpolated from existing data points, or developed from other statistical relationships. The constraint of the EST largely to minor adjustments in observed joint occurrences may not address the numerous combinations of hurricane attributes and tracks which should be considered. Recent advances in understanding the probabilities and correlations for CPD, V_{max} , R_{max}, V_f, and θ allow the JPM to create a larger universe of synthetic storms (NOAA-NWS 1987, Divoky and Resio 2007).[2]

---

[1] The concept of joint probability and techniques for JPA, as well as stochastic analysis, are explained in GTN-1.

[2] Certain statistical techniques, discussed below, can be used to reduce the synthetic dataset for the JPM, just as techniques can be used to expand the range of the EST; thus the relative advantages and disadvantages of these two approaches can be made to converge.

In a *full JPM* the synthetic hurricane set includes a range of values for all attributes. For example, a full JPM set for a particular CN-GoM landfall location might be developed using four attributes—peak CPD and R_{max} in the GoM and the V_f , and θ at landfall (if other attributes like Holland B are ignored)—with respective probability density functions (PDFs).[3] The ranges for each of the four independent characteristics might be divided into five equally spaced values. For example five values for CPD could be 50, 70, 90, 110, and 130 mb. Calculation of the joint probability for each of the 625 combinations (5^4) for that one landfall location is straightforward using the respective functions. In addition to the four JPM characteristics, tracks would be selected based on track tendencies shown in Figure 3.8, and intensification and decay could be based on typical conditions/rates for the GoM. The relative error in full JPM synthetic set can be reduced by increasing the number of values for each attribute. However, as the number of increments in each attribute increases, the synthetic set size increases dramatically. The deterministic modeling of large synthetic sets can exceed the capacity of computational resources.

Evaluating the hurricane wind or surge joint probability distribution along a coastal region requires replicating the full JPM synthetic set at some spacing of landfall locations. The relative error for characterizing wind or surge hazards at intermediate locations can be evaluated through a sensitivity analysis of landfall spacing.

In a *Monte Carlo JPM* (see GTN-1) the synthetic set for each landfall location is randomly selected to represent a time period of interest. Thus, a synthetic 1,000-yr hurricane record for a location which experiences an average of 16 hurricanes per century would contain 160 randomly selected storms. Probability distributions of attributes within the synthetic set can be assessed and the set can be lengthened to stabilize the distributions at key return periods—e.g., a 100-yr return combination of CPD and R_{max}. Depending on the synthetic record length required, the Monte Carlo JPM may reduce the set size and computation resources for deterministic modeling. For example, the 1,000-yr Monte Carlo set of 160 storms is much less than the 625-storm full JPM set and adequate for characterizing a 100-yr return event at a given landfall location.

The Monte Carlo technique can be readily employed to incorporate the effect of attribute distribution uncertainties—such as for the number of storms per year and their CPD. More random draws are added to sample from storm frequency and CPD distribution uncertainty bands. However, employing the Monte Carlo technique to account for attribute uncertainty will expand the set size.

When deterministic modeling computations are extremely expensive, further reduction of the synthetic set size may be desired—albeit with increased potential error in representing the hurricane climatology. Researchers have devised techniques for developing an optimized subset (or optimized sample, OS) of the full JPM, referred to as a *JPM-OS* (Resio et al 2007 and Toro et al 2008; also see GTN-1). The use of OS in hurricane surge JPA is addressed in Part III, Section 13.

4.2. Recent Hurricane JPA

In the late 1980s hurricane climatologists began compiling storm attribute probability information to facilitate JPA (NOAA-NWS 1987). Since then hurricane JPAs have been used to support studies of hurricane hazards. The historic 2005 season stimulated new research on hurricane frequency and attributes, which has been employed in recent JPAs.

[3] Additional probabilistic characteristics could be considered, such as wind field asymmetry, Holland B, etc.

Two teams have recently developed hurricane JPAs for a portion of the CN-GoM. Resio et al (2007) effort focused on coastal Louisiana and was part of multi-purpose hurricane surge study responding to catastrophic damage inflicted by Hurricanes Katrina and Rita in 2005. The Resio team work is documented in the southeast Louisiana FIS (USACE 2008), HSDRRS design (USACE 2010), Louisiana Coastal Protection and Restoration Study (USACE 2009), and the IPET Risk and Reliability Analysis (IPET 2009).

Resio et al employed the GoM hurricane record from 1941 to 2005 as representative of their hypothesized 40-yr climate cycle (see Section 2) and developed probability equations for CP, R_{max}, V_f, and θ. Figure 4.2 presents the individual PDFs.[4] Thus, the joint probability, $\boldsymbol{p}(CP, R_{max}, V_f, \theta, X)$, where X is the distance to hurricane landfall, represents the hurricane climatology in the vicinity of any location of interest.

Toro (2008) employed the nearly identical period, from 1940 to 2005, for defining attribute PDFs for a coastal Mississippi study. Figure 4.3 lists Toro's probability distributions and associated coefficients.

Resio et al used the joint expression for CP and R_{max} to estimate the L-60 joint probability of Hurricane Katrina—as a 398-year return period event. Thus, the Katrina's large R_{max} (40 miles at landfall) increases the return period almost 120-years, or 42 percent, versus the 280-year Resio et al return period for Hurricane Katrina's borderline Category 4/5 CP alone (Figure 3.6). Resio et al did not provide a confidence interval for the 398-year joint probability estimate.

As noted in Section 3, Hurricane Katrina's landfall V_{max} of 126.5 mph corresponds to a strong Category 3 hurricane. Resio et al (Figure 3.6) placed the return period of a strong Category 3 hurricane at about 63 years, and a 42% increase to account for overall joint probability would equate to 89 years. A factor of 42% may be too high to account for joint probabilities for a strong Category 3 63 year return period, so the overall return period may be lower. If the escalated return period estimates (see Figure 3.18) for Hurricane Katrina landfall CP and V_{max}—212 and 40 years—were used instead of the Resio et al estimates (280 and 63 years) the joint probability return period with R_{max} would be lower.

The nearly five-fold difference between a joint probability return period based on CP versus one based on V_{max} illustrates the need for a JPA that directly addresses:

- V_{max} as an attribute of core intensity—especially as it is more directly correlated to hurricane hazards, including surge;
- Variability in Holland B, or other wind field distribution parameter (e.g., IKE), to incorporate the influence of extended hurricane and tropical storm force winds (e.g., on forerunners); and
- Greater varying of attributes over the course of a hurricane's GoM trek, beginning at GoM entry.

Toro did not evaluate the return period of Hurricane Katrina.

[4] Unfortunately the coefficient values for these expressions are not presented in a straightforward manner in the documentation and individual JPA calculations cannot be replicated.

$$p(c_p \mid x) = \frac{\partial F[a_0(x), a_1(x)]}{\partial c_p} = \frac{\partial}{\partial x}\left\{\exp\left\{-\exp-\left[\frac{c_p - a_0(x)}{a_1(x)}\right]\right\}\right\} \text{ (Gumbel Distribution)}$$

$$p(R_p \mid c_p) = \frac{1}{\sigma(\Delta P)\sqrt{2\pi}} e^{-\frac{(\bar{R}_p(\Delta P) - R_p)^2}{2\sigma^2(\Delta P)}}$$

$$p(v_f \mid \theta_i) = \frac{1}{\sigma\sqrt{2\pi}} e^{-\frac{(\bar{v}_f(\theta_i) - v_f)^2}{2\sigma^2}}$$

$$p(\theta_i \mid x) = \frac{1}{\sigma(x)\sqrt{2\pi}} e^{\frac{(\bar{\theta}_i(x) - \theta_i)^2}{2\sigma^2(x)}}$$

Figure 4.2. Probability Density Functions for Louisiana Hurricane Attributes

Resio et al 2007

Rate(ΔP >48 mb) = 2.88E-4E-4 storms/km/yr
Rate (ΔP 31-48 mb) = 2.57E-4 storms/km/yr
Can treat distance as uniformly distributed
Heading:
- i. ΔP >48 mb, Beta ($r = 10.229$, and $t = 11.747$)
- ii. ΔP 31-48 mb, normal (mean= -9.9 deg, σ =58.7 deg; truncate at ± 90 degrees)

ΔP : three-parameter Weibull
- i. ΔP >48 mb, U = 48.6 mb, k = 1.8 (see Equation (3-5))
- ii. ΔP 31-48 mb, U = 46.6 mb, k = 1.95 (see Equation (3-7))

R_p given ΔP : lognormal
- i. Greater storms
  1. mean (nmi): $406.2\Delta P^{-0.711}$
  2. sigma (nmi): $187.7\Delta P^{-0.711}$
- ii. Lesser storms
  1. mean (nmi): $79.58\Delta P^{-0.33}$
  2. sigma (nmi): $36.78\Delta P^{-0.33}$

Vf: lognormal
- i. Greater storms
  1. mean (m/s); 6.6
  2. sigma (m/s): 2.8
- ii. Lesser storms
  1. mean (m/s); 5.5
  2. sigma (m/s): 2.5

Figure 4.3. Probability Density Functions for Mississippi Hurricane Attributes

Toro 2008

In addition to Louisiana and Mississippi, hurricane JPAs are currently being conducted for seven other GoM and south Atlantic regions as part of FEMA coastal FISs. Ongoing studies and the lead technical team include:

- Texas, the Resio et al team that completed the Louisiana JPM-OS;
- North Carolina, Vickery team that completed the coastal wind study;
- South Carolina, the Toro team that completed the Mississippi JPM-OS;
- Florida—Big Bend, the Toro team that completed the Mississippi JPM-OS;
- Northwest Florida/Alabama, the Toro team that completed the Mississippi JPM-OS;
- Northeast Florida/Georgia, a Baker-AECOM team; and
- Central Florida—Atlantic, a Baker-AECOM team.

These studies are all employing the standard hurricane climatological attributes used in the Louisiana and Mississippi JPA, with $\boldsymbol{p}(CP, R_{max}, V_f, \theta, X)$. The North Carolina study includes variations in Holland B within the JPA. No studies to date have introduced IKE into the joint probability. Details on the individual PDFs for each study, and methods for their derivation, have not yet been published but are presumed to be very similar to those used in Louisiana and Texas.

4.3. Recent Application to Coastal Wind Hazard Studies

Peter Vickery and his associates have coupled hurricane JPA and atmospheric vortex modeling to evaluate U.S. coastal wind return periods. Vortex models such as the Hurricane Boundary Layer (HBL) model (Vickery et al 2009a) produce a dynamic wind/pressure field based on inputs for the hurricane core track, ambient pressure, CPD, and R_{max}. Hurricane wind field dynamics are simulated by varying these parameters along the track, reflecting intensification in areas of high sea surface temperature and decay with landfall approach. More sophisticated synthetic wind and pressure fields can be created to account for Holland B (or IKE) and intensification/decay dynamics. Asymmetric wind fields can also be created. Three issues with vortex models are accounting for:

1. Wide scatter in maximum core wind speeds (V_{max}) associated with hurricanes of given CPD;
2. Scatter in intensification, decay, Holland B, and asymmetry values assigned on the basis of correlations with other values (e.g, decay as a function of R_{max} and CPD); and
3. Wind field variations, such as banding and secondary eyewalls.

A 2009 update to a 2000 study (Vickery et al 2009b, Vickery et al 2000) employed a large synthetic hurricane set—equivalent to a record of 100,000 years in order to examine return periods as long as 2,000 years. To generate the synthetic record they used the Monte Carlo approach of randomly selecting combinations of hurricane tracks (varied slightly from historical tracks which included V_f) and probability-based attributes (initial CPD, R_{max}, Holland B). They improved their 2000 intensification and decay algorithms to adjust CPD, R_{max}, and Holland B along the track. They also utilized the Monte Carlo technique to propagate input uncertainties for CPD and Holland B. The result of the joint probability for coastal winds—e.g., 50- to 2,000-year return winds—were determined at coastal points every 57.5 miles (50 nautical miles) (Vickery et al 2009b). The authors do not provide the joint probability results for hurricane attributes themselves, i.e., CPD (or V_{max}), R_{max}, Holland B, and V_f.

In validating the wind field model the team identified a bias of 3 percent (under-prediction) for 100-year coastal winds. After correction for bias, Vickery et al estimated the coefficient of variation in 100-year GoM winds at 6 percent (see GTN-1 for a discussion of bias and uncertainty).

Figure 4.4 presents the return frequency for overland wind gust (mph) at a location east of New Orleans (coastal St. Bernard Parish). The 100- and 500-year return gusts are about 125 and 150 mph—roughly equivalent to 96 and 115 mph 1-minute sustained winds. The 100-yr 125 mph gust can readily occur with less than Category 3 hurricane--which has a V_{max} of 111 mph, an equivalent maximum gust of roughly 144 mph gust. The coefficient of variation for wind gusts translates into a ±2σ range of 84.5 to 107.5 mph for the 100-year sustained winds at this location.

The estimated return period for a 125-mph gust of 100 years has a 90% confidence interval spanning from about -50% to +100%, or 50 to 200 years, due to the asymmetric distribution. This confidence interval for a single point return period is much larger than the one that applies for L-60 (see Section 3).

Figure 4.5 shows the return frequency for the whole Louisiana state coast line (m/s). The 100-year return gust for the state as a whole is estimated at 70 m/s or 156 mph, or a 1-minute wind of 120 mph.

Figure 4.6 excerpts Vickery's 50- to 1,000 return period wind gust contours for the CN-GoM. The contour shapes support the previously noted higher landfall frequency for southeast Louisiana.

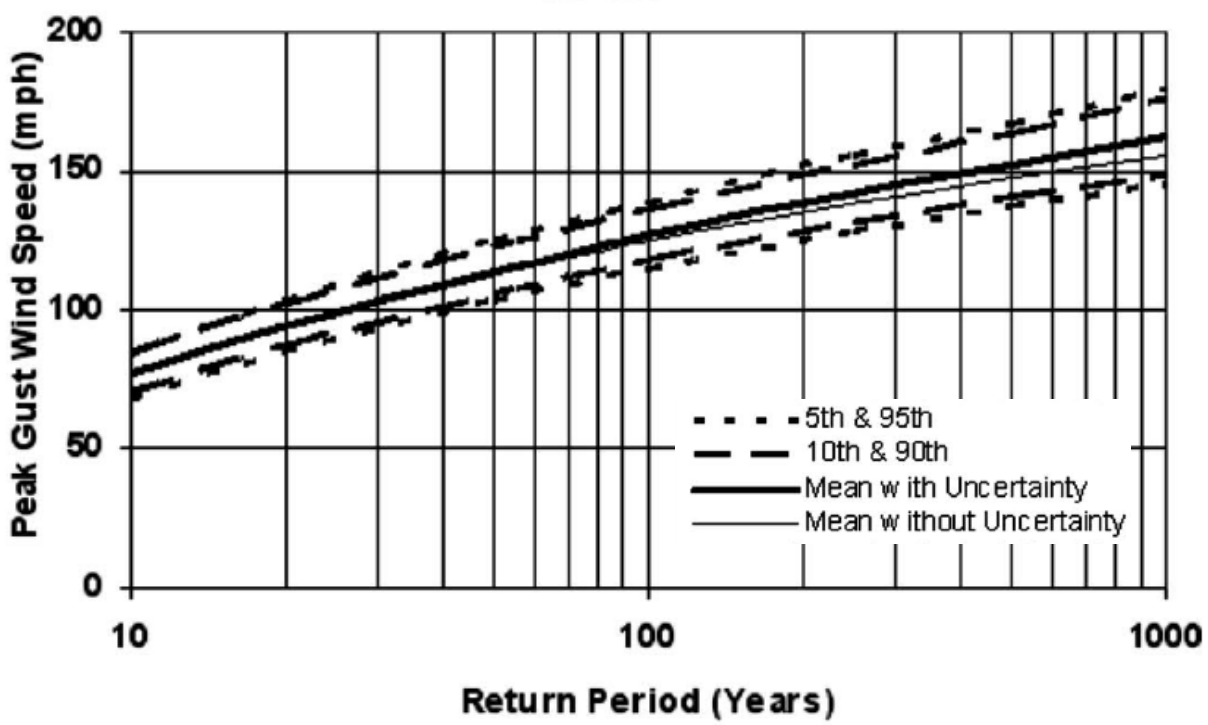

Figure 4.4. Return Period Wind Gusts for St. Bernard Parish LA
Vickery et al 2009b

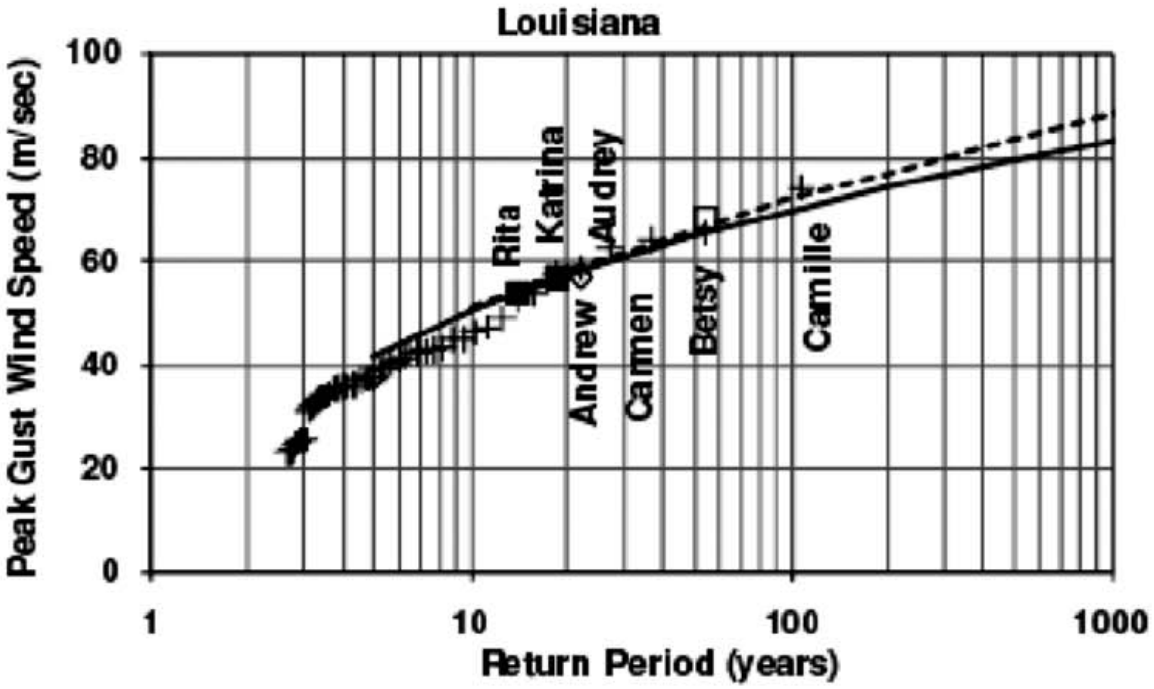

Figure 4.5. Return Period Wind Gusts for the State of Louisiana
Vickery et al 2009b

The American Society of Civil Engineers and coastal states has employed Vickery's results in developing building codes for wind loads. Hurricane Katrina's maximum sustained winds at landfall (Buras LA) are reported as 126.5 mph, roughly equating to 164.5 mph 3-second gusts (at a 1.3 gust factor). This would put Hurricane Katrina's Buras winds as approaching a 500-year return period. Using Figure 4.4 as an indication, accounting for logarithmic uncertainty could place this as low as a 200-year return period.

Vickery's input range and variation, (and consequently large data set size), and treatment of uncertainty for joint probability as well as CPD and Holland B inputs, provide an important current benchmark in hurricane joint probability analysis. Nonetheless it is important to reiterate the residual uncertainty associated with the overall joint probability analysis—±12 percent for two standard deviations for the 100-year return frequency along the GoM coast. (The uncertainty at higher return periods was not given.) This ±12 percent reflects uncertainties Nos. 1 through 4 above.

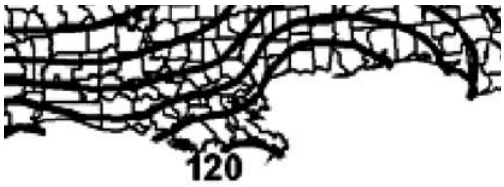

50-Year Return Period

100-Year Return Period

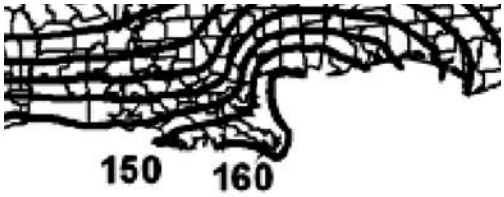

500-Year Return Period

1,000-Year Return Period

Figure 4.6. Return Period Wind Gusts for the CN-GoM (mph)
Vickery et al 2009b

Part I. Conclusions and Recommendations

Conclusions

Our current understanding of hurricane climatology for southeast Louisiana is founded on extensive research by many teams of professional scientists, particularly in the wake of the 2005 hurricane season, and on a new analysis based on the 1851 to 2011 (161-year) record. This information supports the following important conclusions regarding hurricanes characteristics and their landfall joint probabilities for southeast Louisiana:

1. Overall hurricane recurrence in the GoM appears to be near stationary over the entire record.
2. Post-1940 recurrence of GMHs is 50% higher than the 161-year average. A major causes of this increase is improved observations.
3. GoM correlations between the two core intensity parameters, CPD and V_{max}^2, and between CPD and R_{max}, both have considerable scatter; Holland B, V_f and θ appear to be randomly distributed. The literature provides scatter estimates for both GoM maximum and landfall conditions.
4. Recent research supports the importance of the wind field profile attribute—e.g., Holland B and radius of hurricane and tropical storm force winds—as well as IKE. New indices have been proposed based on IKE and $IKE^{1/2} \cdot V_{max}$ but statistical analyses of these indices for the GoM have not yet been produced. Hurricanes which never reach SSS Category 3, but which have large wind fields, can generate significant surge.
5. Scientific understanding of basic mechanisms of hurricane intensification (and the role of SST and TCHP), interference (landforms and atmospheric conditions), and landfall decay (infilling) are becoming more robust. While powerful hurricanes are very likely to decay prior to landfall, decay trends for low intensity hurricane have not been established.
6. In addition to seasonal influences, extensive research shows that four major climate cycles—MJO, ENSO, AMO, and NOA—affect Atlantic basin hurricane activity. Resio and Orelup suggest there may be a 40-year cycle for GoM hurricane activity but research on climate cycle influence on GoM hurricanes is limited.
7. Return periods for GMH landfall over the 161-year record, by segment by category (L-500, LMH-500, L-151, LMH-151, L-60, and LMH-60) are reasonably well defined—4.1, 5.4, 13.4, 17.9, 23.0, and 26.8 years—with suggested confidence intervals approaching a maximum of -23 to +30%.
8. The recent (1952-2011 60-year) period shows a 55% increase in frequency of GMH/L-500 and a 67% increase for GMH/LMH-500. These escalations shorten return period estimates by segment by category to: 2.7, 3.2, 8.6, 10.7, 14.9, and 16.1 years.
9. Recent (60-year) Category 5 return periods by segment are 12, 20, and 60 years.
10. Comparison of length-adjusted frequencies for GMH/LMH shows that the rate for the 60-mile segment south of New Orleans is 67% higher than for the 151- or 500-mile segments. Also the percentage of GMH/L-60 which are LMH are higher (86%) than for the 151- and 500-mile segments (75 and 77%)
11. The Loop Current and associated eddies likely cause hurricanes tracking toward the center of the CN-GoM (i.e., L-60) to be more intense, and cause major hurricanes to remain at major category through landfall. They also likely contribute to the more frequent regional landfall of

hurricanes exhibiting larger cores, more expansive wind fields, and less decay. *Importantly, the landfall frequency of lower intensity hurricanes with large wind fields has not been studied*.

12. The influence of improved observations and recognized climate-cycles during the past 60 years of the 161-yr record offer reasonable explanations for the secular trend in GMH frequency. Researchers have not demonstrated climate change influence on the post-1952 50% increase in GMHs, the 55% increase in GMH/L, and the 67% increase in GMH/LMH (across the full CN-Gom) apart from these influences. Researchers modeling the influence of greenhouse gas increases on global climate and SST are suggesting potential increases in the frequency of more intense hurricanes, but possibly also atmospheric shear conditions which could inhibit hurricane. No research on future hurricane climatology specific to the CN-GoM has been undertaken. However, an investigation has proposed that climate change could reduce the Loop Current by 25%, producing a *cooling* effect on the GoM.
13. Directly solvable analytical expressions for the joint probability of hurricane attributes have been formulated—$\boldsymbol{p}(CP, R_{max}, V_f, \theta, X)$—incorporating current individual attribute probability equations. To date, Holland B, IKE, intensification, and decay have not been incorporated into GoM hurricane joint probability expressions.
14. Assessing Hurricane Katrina's L-60 intensity (only) return period requires distinguishing between its 126.5 mph V_{max}—ranked at a strong Category 3—versus its 920 mb CP—which is analogous to a borderline Category 4/5 hurricane. According to the recent (escalated) post-1952 distribution, the return periods are about 40 years for the former and 212 years for the latter. The Resio et al return periods, which are based on the 1941-2005 period (which reflect a proposed GoM cycle and incorporate additional low hurricane activity years) are 63 and 280 years.
15. Resio et al evaluated the joint probability of Hurricane Katrina's borderline Category 4/5 CP plus 40-mi R_{max} landfall and estimated the return period at 398 years, a 42% increase over the 280-year return period for CP alone. However, a similar increase applied to the 63-year return period based on strong Category 3 V_{max} landfall intensity yields a return period of 89 years. If the escalated return period estimates are used in place of the Resio et al estimates the joint probability return periods would be lower. The over four-fold difference between a joint probability return period based on CP versus one based on $\boldsymbol{V_{max}}$ illustrates the need for an improved joint probability approach.

Recommendations

Conclusions based on the review and new analyses presented above indicate that the 2006 hurricane climatology is outdated. They also provide the basis for recommendations to improve the analysis of hurricane climatology for southeast Louisiana. Six specific updates should include :

1. Revise the joint probability expression—and associated uncertainty—for southeast Louisiana regional hurricane landfall as a function of latest data on the frequency of hurricanes of varying CP, R_{max}, V_f, and θ, including hurricanes of any intensity.
2. Use an appropriate data record; reassess evidence for a Gulf of Mexico climate cycle.
3. Address scatter in relationship of central pressure deficit and maximum wind speed in the joint probability expression.
4. Address wind field variability—e.g., Holland B, Integrated Kinetic Energy, etc.—for the full range of hurricane core intensities and sizes, in a revised joint probability expression.

5. Address variability in intensification—associated with passage over the Loop Current/Eddies—and pre-landfall decay (infilling) for the full range of hurricane intensities, sizes, wind-field distributions, and forward speeds. in a revised joint probability expression.
6. Re-evaluate the return period for regional landfall of a Hurricane Katrina and evaluate the return periods for Hurricanes Gustav and Isaac.
7. Incorporate results of studies on future hurricane climatology as a function of climate change into estimates of uncertainty regarding future hurricane probabilities.

The Louisiana CPRA, together with federal partners, should fund critical research to improve the analysis of hurricane climatology, including:

1. Update information on various traditional and new (e.g., IKE and $IKE^{1/2} \cdot V_{max}$) characteristics for Gulf of Mexico and landfall hurricanes, as the historical record expands.
2. Conduct more rigorous statistical analysis of data on these characteristics; particularly clarification of confidence intervals (i.e., uncertainty) in estimates of hurricane characteristics and correlations between characteristics, e.g., ($CPD:V_{max}^2$).
3. Improve the joint probability expression for Gulf of Mexico hurricanes and landfalling regional hurricanes, including estimation of uncertainty.
4. Revisit the selection of a representative GoM hurricane data record, taking into account quality of observations and accepted findings on GoM climate cycles.
5. Investigate factors influencing the particular hurricane return frequencies for southeast Louisiana, especially the Loop Current and associated eddies.
6. Further expand the joint probability expression to include additional important hurricane attributes contributing to surge, such as wind field asymmetry and banding.
7. Assess the influence of secular climate trends on the Loop Current and other factors influencing GoM hurricanes.

It is important to recognize the large uncertainty that remains in estimating hurricane return frequency. Much of this uncertainty is associated with the still relatively brief hurricane record. In the near-term, methodological improvements and research are not likely to yield major reductions in uncertainty.

Part I. References

Bell, G. D., and M. Chelliah, Leading Tropical Modes Associated with Interannual and Multidecadal Fluctuations in North Atlantic Hurricane Activity, Journal of Climate, Vol. 19, February 2006.

Blackwell, K. G., A. Wimmers, C. Velden, P. J. Fitzpatrick, P. J., and B. Jelley, Hurricane Katrina's Eyewall Replacement Cycle over the Northern Gulf and Accompanying Double Eyewalls at Landfall: A key to the Storm's Huge Size and Devastating Impact Over a Three-state Coastal Region. 28th Conference on Hurricanes and Tropical Meteorology, April 28 to May 2, 2008, Orlando, FL http://www.drfitz.net/Selected_Presentations.php

Blanton, B. O., P. J. Vickery, North Carolina Coastal Flood Analysis System: Hurricane Parameter Development, A Draft Report for the State of North Carolina, Floodplain Mapping Project, Technical Report TR-08-06 September 12, 2008.

Bove, M.C., J. J. O'Brien, J B. Elsner, C. W. Landsea, and X. Niu, X. Effect of El Niño on U.S. Landfalling Hurricanes, Revisited. Bulletin of the American Meteorological Society, Vol. 79, 1998.

Carvill, Carvill Hurricane Index: an Index to Measure the Destructive Potential of Hurricanes, http://www.cmegroup.com/trading/weather/files/WEA_chi_whitepaper.pdf

Chen, J-H, S-J Lin. The remarkable predictability of inter-annual variability of Atlantic hurricanes during the past decade. Geophysical Research Letters 38:11, L11804 2011,

Chylek, P. and G. Lesins, Multidecadal Variability of Atlantic Hurricane Activity: 1851–2007, Journal of Geophysical Research Vol. 113, 2008.

Cooper, C. and J. Stear, Hurricane Climate in the Gulf of Mexico, Offshore Technology Conference, 1 May-4 May 2006, Houston, Texas.

Divoky, D. and D. T. Resio, Performance of the JPM and EST Methods in Storm Surge Studies, 10th International Workshop on Wave Hindcasting and Forecasting and Coastal Hazard Symposium, Hawaii, November 11 – 16, 2007.

Done, J., G. J. Holland, C. Bruyere, and A. Suzuki-Parker, Effects of Climate Variability and Change on Gulf of Mexico Tropical Cyclone Activity, Offshore Technology Conference, 2011.

Elsner, J. B. and A.B. Kara, Hurricanes of the North Atlantic: Climate and Society, Oxford University Press, 1999.

Elsner, J. B. and B. Kocher, Global Tropical Cyclone Activity: A Link to the North Atlantic Oscillation, Geophysical Research Letters, Vo. 27 No. 1, January 2000.

Elsner, J. B., B. H. Bossak, and X-F Niu, Secular Changes to the ENSO-U.S. Hurricane Relationship, Geophysical Research Letters, Vol. 28, 2001.

Elsner, J. B. Tracking Hurricanes, Bulletin of the American Meteorological Society, March 2003,

Elsner, J. B. and T. H. Jagger, Prediction Models for Annual U.S. Hurricane Counts, Journal of Climate, Vol. 19, Issue 12, 2005.

Elsner, J. B., Evidence in Support of the Climate Change–Atlantic Hurricane Hypothesis, Geophysical Research Letters Vol. 33, 2006a.

Elsner, J. B., T. H. Jagger, and A. A. Tsonsis, Estimated Return Period for Hurricane Katrina, Geophysical Research Letters, Vol. 33, Issue 8, 2006b.

Elsner, J. B. and T. H. Jagger, Comparison of Hurricane Return Levels Using Historical and Geological Records, Journal of Applied Meteorology and Climatology, Vol. 47, 2007.

Elsner, J. B. and T. H. Jagger, United States and Caribbean Tropical Cyclone Activity Related to the Solar Cycle, Geophysical Research Letters, Vol. 35, 2008.

Enfield, D. B., and L. Cid-Serrano, Secular and Multidecadal Warmings in the North Atlantic and Their Relationships with Major Hurricane Activity, International Journal of Climatology, Vol. 30, 2010.

Federal Emergency Management Agency (FEMA), Mississippi Coastal Flood Hazard Project, Calibration and Validation of Model Report, November 19, 2007.

Fitzpatrick, P. J., N. Tran, Y. Li, Y. Lau, and C. M. Hill, A Proposed New Storm Surge Scale, Geosystems Research Institute, Mississippi State University, BLDG 1103, Room 108, Stennis Space Center, MS 39529 USA. June 2010. http://www.drfitz.net/uploads/fitz_ocean_surge_scale_ieee_certified.pdf

Fritz, A. M., North Atlantic Tropical Cyclones: A Kinetic Energy Perspective, In Partial Fulfillment of the Requirements for the Degree Master of Science in the School of Earth and Atmospheric Science Georgia Institute of Technology, August 2009.

Gray, W. M., Tropical Cyclone Genesis, Atmospheric science paper No. 234, Department of Atmospheric Science, Colorado State University, Fort Collins, CO., 1975

Gray, W. M., Atlantic Seasonal Hurricane Frequency, Part I: El Nino and 30 mb quasi-biennial Oscillation Influences, Monthly Weather Review, Vol. 112, 1984.

Harper, B. A. Harper, J. D. Kepert and J. D. Ginger,Guidelines for Converting Between Various Wind Averaging Periods in Tropical Cyclone Conditions, World Meteorological Organization, October 2008.

Holland, G. J., An Analytical Model of the Wind and Pressure Profiles in Hurricanes, Monthly Weather Review, Vol. 108, August 1980.

Holland, G. J. and P. J. Webster, Heightened Tropical Cyclone Activity in the North Atlantic: Natural Variability or Climate Trend? Philisophical Transactions of the Royal Society, Vol. 365, 2007.

Hsu, S. A., and Z. Yan, A Note on the Radius of Maximum Wind for Hurricanes, Journal of Coastal Research, Vol. 14, Issue 2, 1998.

Interagency Performance Evaluation Task Force (IPET), Performance Evaluation of the New Orleans and Southeast Louisiana Hurricane Protection System, Volumes VIII, Engineering and Operational Risk and Reliability Analysis, U.S. Army Corps of Engineers, June 2009.

Irish, J. L., D. T. Resio, J. J. Ratcliff, The Influence of Storm Size on Hurricane Surge, Journal of Physical Oceanography, Vol. 38, p. 2003, September 2008.

Irish, J. L., D. T. Resio, and D. Divoky, Statistical Properties of Hurricane Surge Along a Coast, Journal of Geophysical Research. Vol, 116, C10007, 2011.

Jagger, T. H., J. B. Elsner, and X. Niu, A Dynamic Probability Model of Hurricane Winds in Coastal Counties of the United States. Journal of Applied Meteorology, Vol. 40, 2001.

Kantha, L., Comment: Tropical Cyclone Destructive Potential by Integrated Kinetic Energy, Bulletin of the American Meteorological Society, February 2008.

Keim, B. D. and R. A. Muller Hurricanes of the Gulf of Mexico, Louisiana State University Press, 2009.

Keim, B. D., R. A. Muller, and G. W. Stone, Spatiotemporal Patterns and Return Periods of Tropical Storm and Hurricane Strikes from Texas to Maine, Journal of Climate, Vol. 20, July 2007.

Kim, H.-M. and P. J. Webster, Extended-Rrange Seasonal Hurricane Forecasts for the North Atlantic with a Hybrid Dynamical-Statistical model, Geophysical Research Letters, Vol. 37, 2010.

Kimball, S. K., A Modeling Study of Hurricane Landfall in a Dry Environment, Monthly Weather Review, Vol. 134, July 2006.

Klotzbach, P. J., El Niño-Southern Oscillation's Impact on Atlantic Basin Hurricanes and U.S. Landfalls. Journal of Climate Vo. 24, 2011.

Klotzbach, P. J., On the Madden-Julian Oscillation—Atlantic Hurricane Relationship, Vol. 23 Journal of Climate, January 2010.

Knaff, J. A. and R. M. Zehr, Reexamination of Tropical Cyclone Wind–Pressure Relationships, Weather and Forecasting, 22, 71–88, February, 2007.

Knutson, T. R., J. L. McBride,J. Chan, K. Emanuel, G. Holland, C. Landsea, I. Held, J. P. Kossin, A. K. Srivastava, and M. Sugi, Tropical Cyclones and Climate Change, Nature Geoscience Vol. 3, 2010.

Kurian, N. P., N. Nirupama, M. Baba, and K. V. Thomas, Coastal Flooding Due to Synoptic Scale, Meso-Scale and Remote Forcings. Natural Hazards, 48, 259-273, 2009.

Landsea, C.W., R. A. Pielke, Jr., A. M. Mestas-Nunez, and J. A. Knaff, Atlantic Basin Hurricanes: Indices of Climate Changes. Climatic Change, Vol. 42, 1999.

Levinson, D. H., Vickery, P. J., and Resio, D. T., A Review of the Climatological Characteristics of Landfalling Gulf Hurricanes, for Wind, Wave, and Surge Hazard Estimation, Ocean Engineering Vol. 37, p. 13–25, 2010.

Liu, K-B and M. L. Fearn, Holocen History of Catastrophic Hurricane Landfalls Along the Gulf of Mexico Coast Reconstructed from Coastal Lake and Marsh Sediments, in Current Stresses and Potential Vulnerabilities: Implications of Global Change for the Gulf Coast Region of the United States (Z. H. Ning and K. K. Abdollahi, Eds.), Gulf Coast Regional Climate Change Council, Franklin Press, Baton Rouge LA, 2000.

Liu, Yanyun, S. K. Lee, B. A. Muhling, J. T. Lamkin, D. B. Enfie, Significant reduction of the Loop Current in the 21st Century and its Impact on the Gulf of Mexico, Journal of Geophysical Research: Oceans, Vol. 117, No. C5, May 2012.

Mallen, K. J., M. T. Montgomery, B. Wang, Reexamining the Near-Core Radial Structure of the Tropical Cyclone Primary Circulation: Implications for Vortex Resiliency, Journal of the Atmospheric Sciences, Vo..62, February 2005.

Maloney, E. D. and D. L. Hartmann, Modulation of Hurricane Activity in the Gulf of Mexico by the Madden-Julian Oscillation, Science, March 2000.

McCloskey, T. A and J. T. Knowles, J. T., Migration of the Tropical Cyclone Zone Throughout the Holocene, In Elsner, J. B. and T. H. Jagger, Hurricanes and Climate Change. New York: Springer, 2009.

Merrill, R. T., Environmental Influences on Hurricane Intensification, Journal of the Atmospheric Sciences, Vo. 45 No. 11, June 1988.

Needham, H., and B. D. Keim, Storm Surge: Physical Processes and an Impact Scale, in A. Lupo, Recent Hurricane Research - Climate, Dynamics, and Societal Impacts, InTech, April 2011.

Pasch, R. J., Hurricane Intensity Forecast Improvement: Is it Possible?, Presentation, National Hurricane Conference, Atlanta, GA, 21 April 2011, http://www.nhc.noaa.gov/outreach/presentations/2011_IntensityForecastingImprovement_Pasch.pdf

Powell, M. D., and T. A. Reinhold, Tropical Cyclone Destructive Potential by Integrated Kinetic Energy, Bulletin of the American Meteorological Society, April 2007.

Quiring, S., A. Schumacher, C. Labosier, and L. Zhu, Variations in mean annual tropical cyclone size in the Atlantic, Journal of Geophysical Research, 116, D09114, doi:10.1029/2010JD015011. 2011.

NOAA-CPC, North Atlantic Oscillation, http://www.cpc.ncep.noaa.gov/data/teledoc/nao.shtml

NOAA-CSC, Historical Hurricane Tracks, http://www.csc.noaa.gov/hurricanes/#

NOAA-GFDL, Global Warming and Hurricanes, http://www.gfdl.noaa.gov/global-warming-and-hurricanes

NOAA-HRD, Surface Wind Field Analysis, http://www.aoml.noaa.gov/hrd/data_sub/hurr.html

NOAA-NCDC, International Best Track Data for the North Atlantic Basin, Basin.NA.ibtracs_wmo.v03r02.csv, downloaded on September 30, 2011. Supplemented with 2010 and 2011 data. ftp://eclipse.ncdc.noaa.gov/pub/ibtracs/v03r03/all/csv/basin

NOAA-NHC, Tropical Cyclone Climatology, http://www.nhc.noaa.gov/climo/

NOAA-NWS, Meteorological Criteria for Standard Project Hurricane and Probable Maximum Hurricane Windfields, Gulf and East Coasts of the United States, NOAA Technical Report NWS 23, 1979.

NOAA-NWS, (Ho, F. P., J. C. Su, K. L. Hanevich, R. J. Smith, and F. P. Richards) Hurricane Climatology for the Atlantic and Gulf Coasts of the United States, NOAA Technical Report NWS 38, April 1987.

Parisi, F. and R. Lund, Return Periods of Continental U.S. Hurricanes, Notes and Correspondence, Journal of Climate, Vol. 21, January 2008.

Pielke, R. A., Jr., and R. A. Pielke Sr., Hurricanes: Their Nature and Impacts on Society. Wiley, 1997.

Rappaport, E. N., J. L. Franklin, A. B. Schumacher, M. DeMaria, L. K. Shay, and E. J. Gibney, Tropical Cyclone Intensity Change before U.S. Gulf Coast Landfall. Weather Forecasting, Vol. 25, 1380–1396, 2010.

Rego, J. L. and C. Li, On the importance of the forward speed of hurricanes in storm surge forecasting: A numerical study, Geophysical Research Letters, Vol. 36, 2009.

Resio, D. T., S. J. Boc, L. Borgman, V. J. Cardone, A. Cox, W. R. Dally, R. G. Dean, D. Divoky, E. Hirsh, J. L. Irish, D. Levinson, A. Niederoda, M. D. Powell, J. J. Ratcliff, V. Stutts, J. Suhada, G. R. Toro, and P. J. Vickery, White Paper on Estimating Hurricane Inundation Probabilities, U.S. Army Corps of Engineers, ERDC-CHL, 2007.

Resio, D. T. and L. Orelup, Climatic Variations in Hurricanes and Their Potential Effects on Waves and Surges in the Gulf of Mexico, 2006.
ftp://ftp.wmo.int/Documents/PublicWeb/amp/mmop/documents/JCOMM-TR/J-TR-34-9th-waves-workshop/Presentations/Resio.pdf

Saunders, M. A., R. E. Chandler, C. J. Merchant, and F. P. Roberts, Atlantic Hurricanes and NW Pacific Typhoons: ENSO Spatial Impacts on Occurrence and Landfall, Geophysical Research Letters Vol. 27 Issue 8, 2000.

Saunders, M. A., and A. R. Harris, Statistical Evidence Links Exceptional 1995 Atlantic Hurricane Season to Record Sea Warming, Geophysical Research Letters, Vol. 24 Issue 10, 1997.

Schultz, C., Next generation atmospheric model improves hurricane forecasting, Eos Transaction of the American Geophysical Union, 92, , 2011.

Shen, B-W., A simple prediction model of hurricane intensity Quarterly Journal of the Royal Meteorological Society, Vol 131, pp. 2887–2906, 2005.

Shen, B-W., Does the size of hurricane eye matter with its intensity? Geophysical Research Letters, Vol. 33, 2006a.

Shen, B-W., R. Atlas, O. Reale, S. J. Lin, J. D. Chern, J. Chang, C. Henze, and J. L. Li, Hurricane forecasts with a global mesoscale-resolving model: Preliminary results with Hurricane Katrina (2005), Geophysical Research Letters, Vol. 33, 2006b.

Simpson, R. H. and M. B. Lawrence, Atlantic Hurricane Frequencies Along the U.S. Coastline, NOAA Technical Memorandum NWS TM SR-58, June 1971.

Toro, G. R., Joint Probability Analysis of Hurricane Flood Hazard for Mississippi, Final Report, Revision 1. Prepared for URS Group, Tallahassee, FL, in support of the FEMA-HMTAP, Flood Study of the State of Mississippi, Risk Engineering, Inc. 4155 Darley Avenue, Suite A Boulder, CO 80305. June 23, 2008.

USACE, Flood Insurance Study, Southeast Parishes of Louisiana, Intermediate Submission 2: Offshore Water Levels and Waves, July 2008.

USACE (New Orleans District), Hurricane and Storm Damage Risk Reduction System, Design Elevation Report, Draft Report Version 4.0, August 18, 2010.

Vickery P. J., P. F. Skerlj, and L. A. Twisdale, Simulation of Hurricane Risk in the U.S. Using Empirical Track Model, Journal of Structural Engineering, October 2000.

Vickery, P. J., and L. A. Twisdale, Wind-field and Filling Models for Hurricane Windspeed Predictions.'' Journal of Structural Engineering, ASCE, Volume 121 No. 11, 1700–1709, 1995.

Vickery, P. J., D. Wadhera, Statistical Models of Holland Pressure Profile Parameter and Radius to Maximum Winds of Hurricanes from Flight-Level Pressure and H*Wind Data. Journal of Applied Meteorology and Climatology, Vol. 47, 2497–2517, 2008.

Vickery, P.J., D. Wadhera, M.D. Powell and Y. Chen, A Hurricane Boundary Layer and Wind Field Model for Use in Engineering Applications, Journal of Applied Meteorology and Climatology, Vol. 48, p. 381, 2009a.

Vickery, P. J., D. Wadhera, L. A. Twisdale, Jr., and F. M. Lavelle, U.S. Hurricane Wind Speed Risk and Uncertainty, Journal of Structural Engineering, Vol. 135, p. 301, 2009b.

Wada, A. and N. Usui, Importance of Tropical Cyclone Heat Potential for Tropical Cyclone Intensity and Intensification in the Western North Pacific, Journal of Oceanography, Vol. 63, pp. 427 to 447, 2007.

Wallace, D. J, and Anderson, J. B., Evidence of similar probability of intense hurricane strikes for the Gulf of Mexico over the late Holocene, Geology, Volume 38, p. 511-514, June 2010.

Watson, R. L., Evaluation of coastal response to Hurricane Ike through pre-storm and post-storm aerial photography, Shore and Beach, Vol. 77, No. 2, Spring 2009,
http://texascoastgeology.com/papers/shoreandbeachpub.pdf

WAVCIS Laboratory, Coastal Studies Institute, Louisiana State University, http://wavcis.csi.lsu.edu/

Zhao, M. I. M. Held, S. Lin, and G. A. Vecchi, Simulations of Global Hurricane Climatology, Interannual Variability, and Response to Global Warming Using a 50-km Resolution GCM, Journal of Climate, Volume 22, Issue 24, December 2009.

Attachment 1

Tracks for Gulf of Mexico Major Hurricanes Making Landfall in Central-Northern Gulf of Mexico

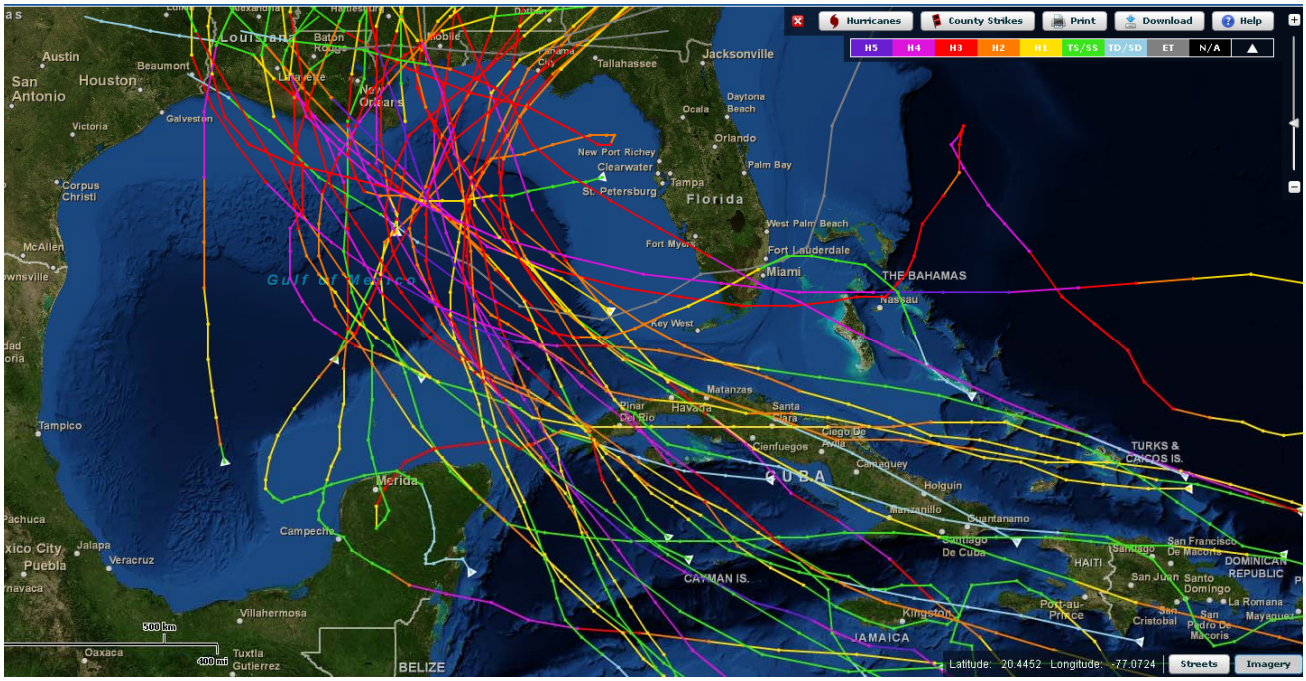

Source: National Oceanic and Atmospheric Administration, Coastal Services Center

http://www.csc.noaa.gov/hurricanes/#app=3d30&3e3d-selectedIndex=2

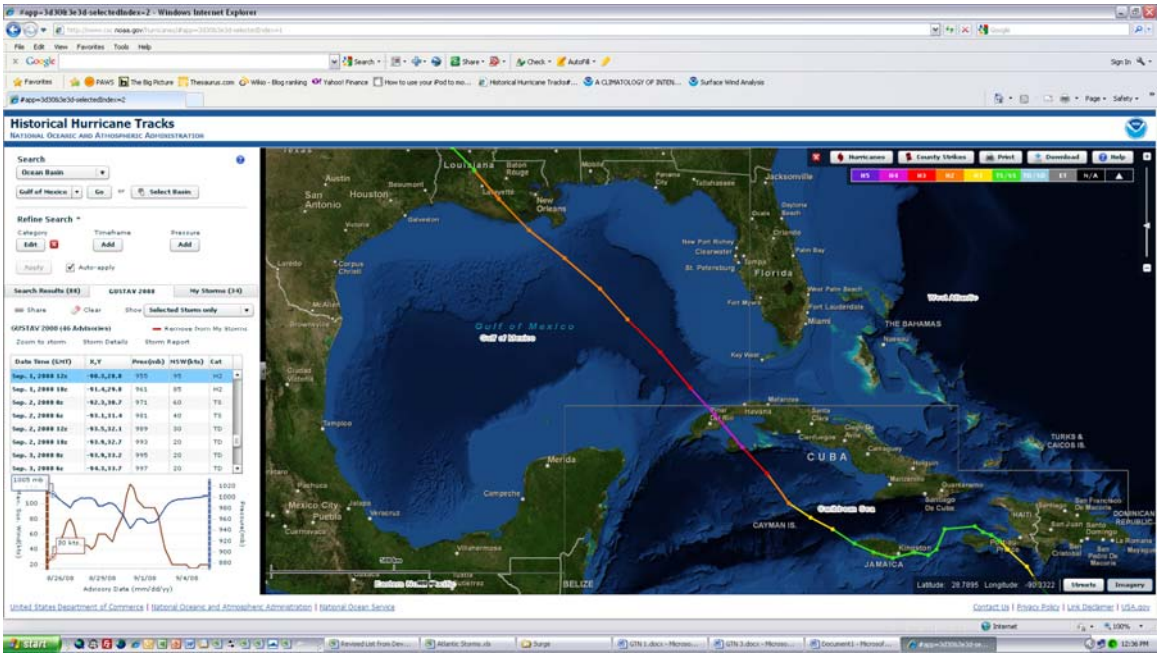

Hurricane Gustav, 2008

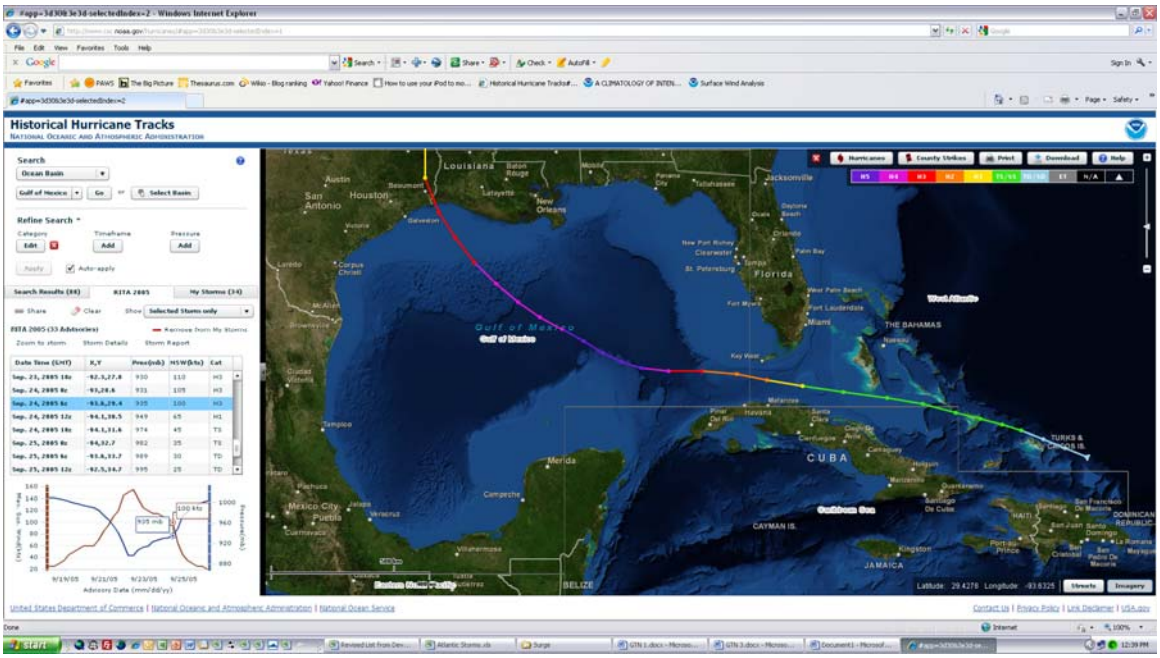

Hurricane Rita, 2005

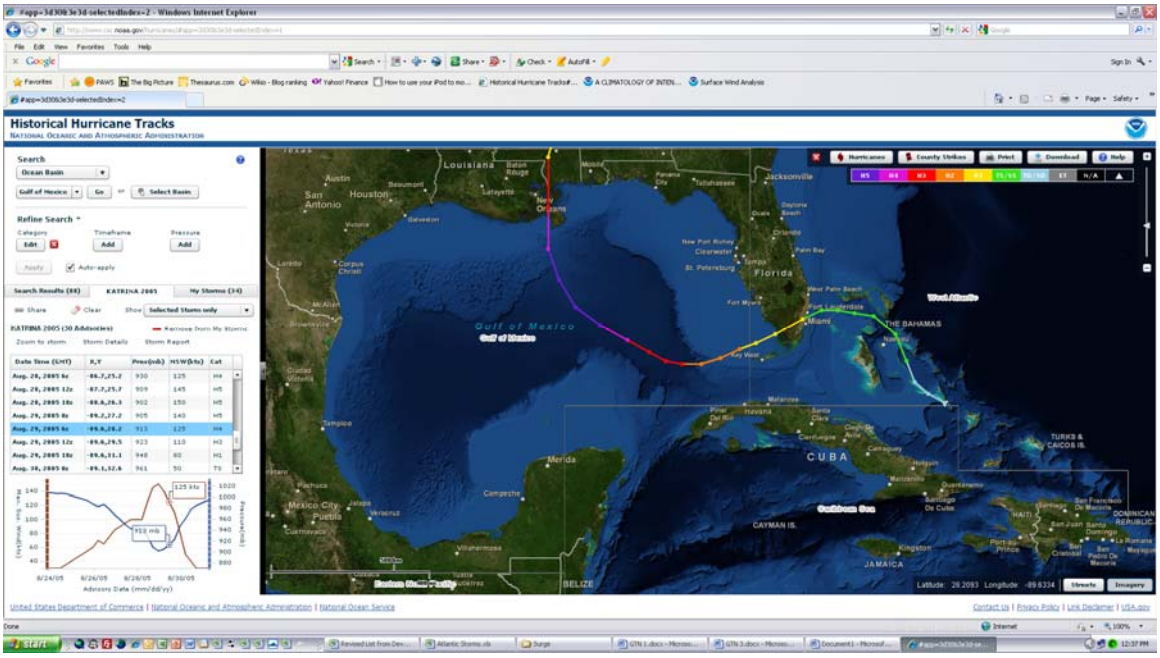

Hurricane Katrina, 2005

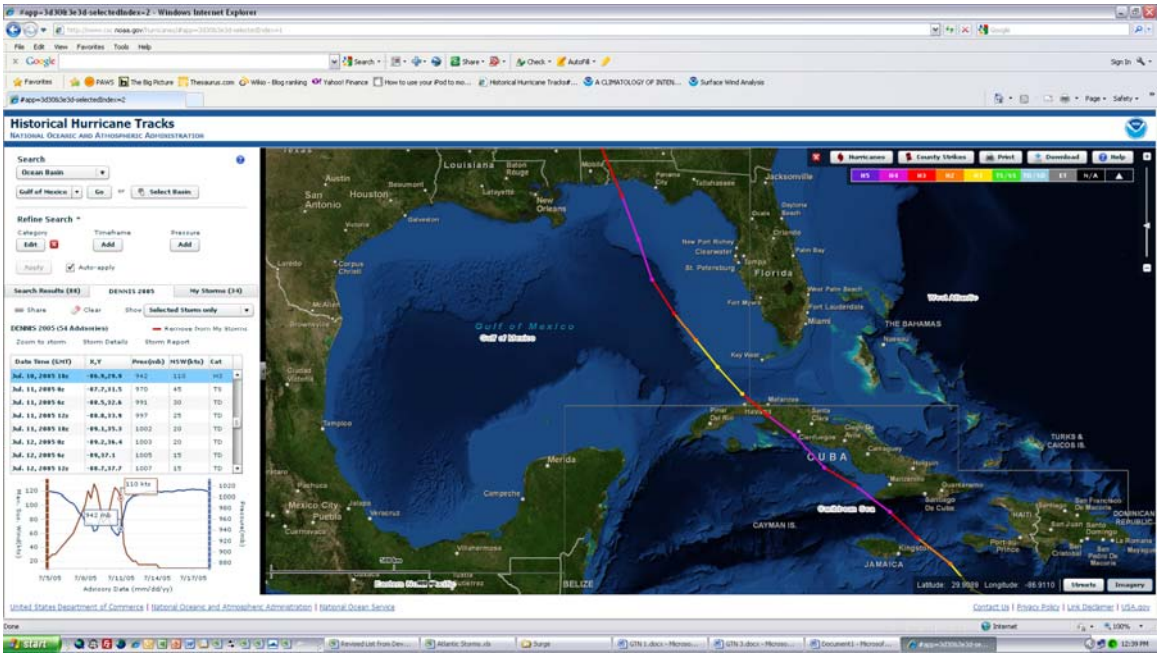

Hurricane Dennis, 2005

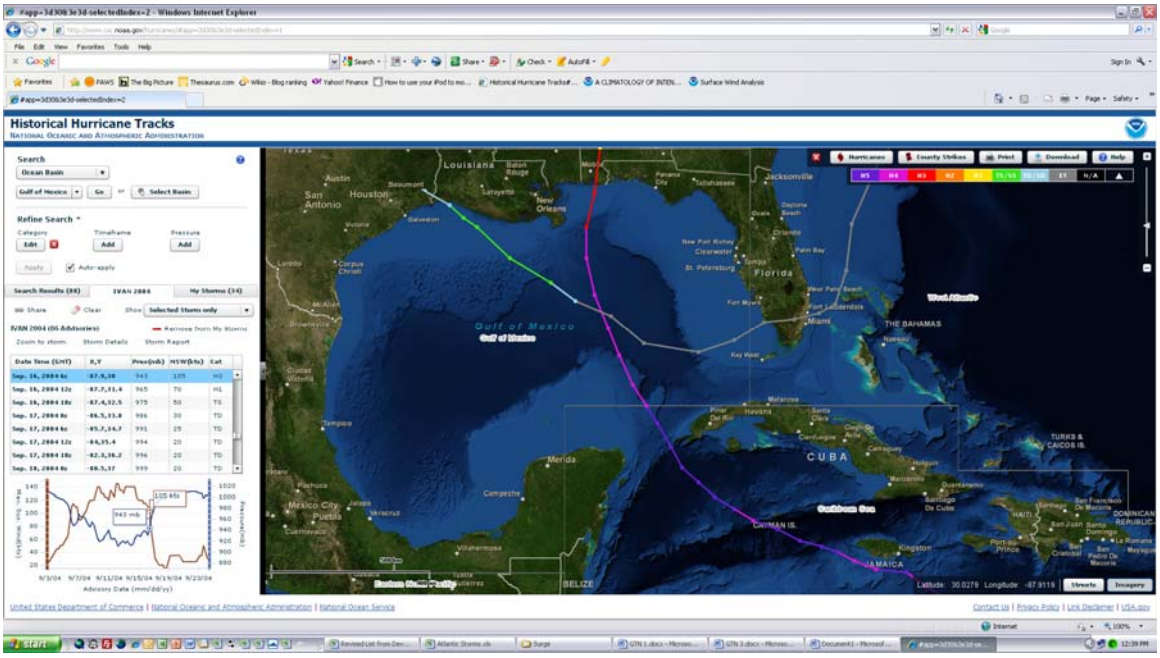

Hurricane Ivan, 2004

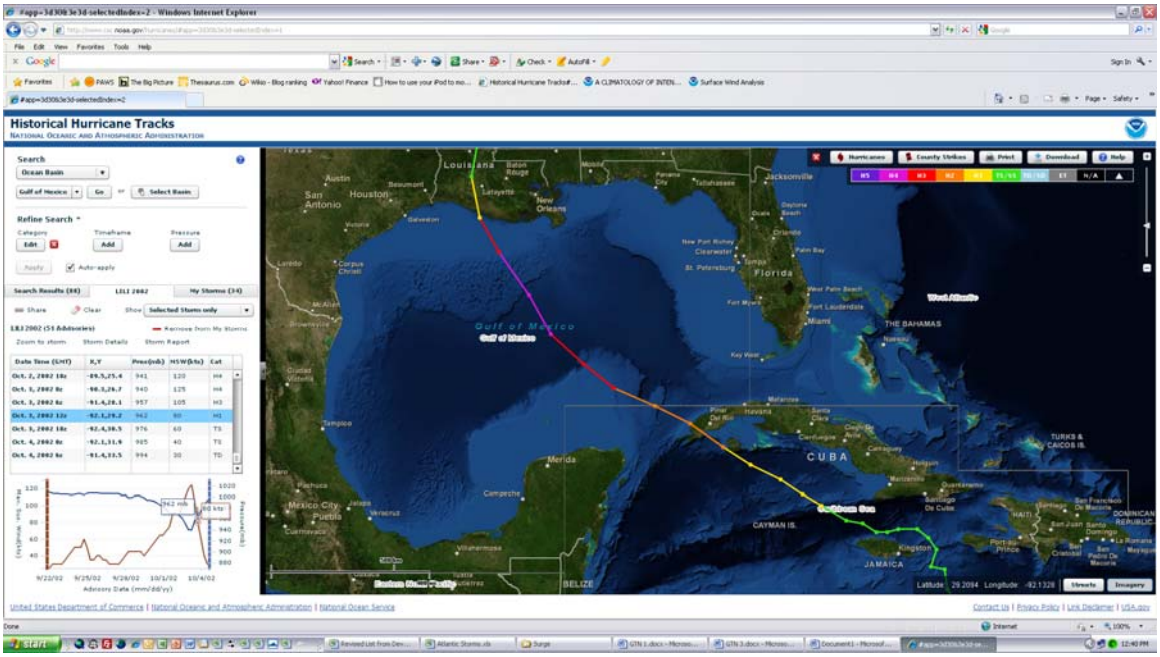

Hurricane Lili, 2002

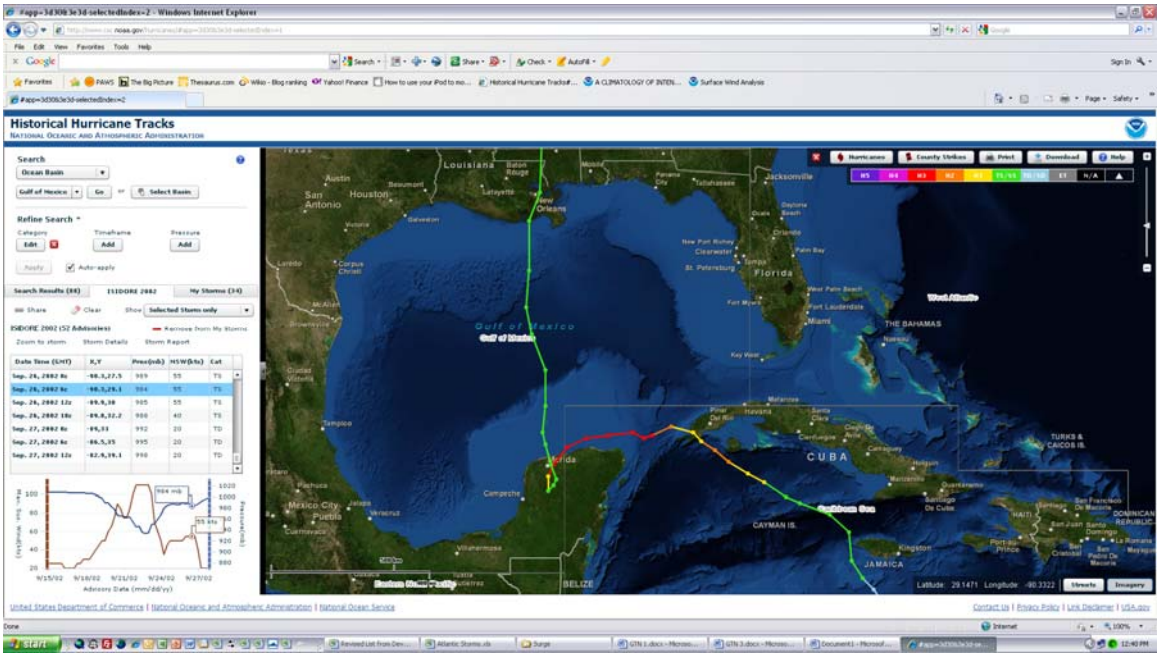

Hurricane Isadore, 2002

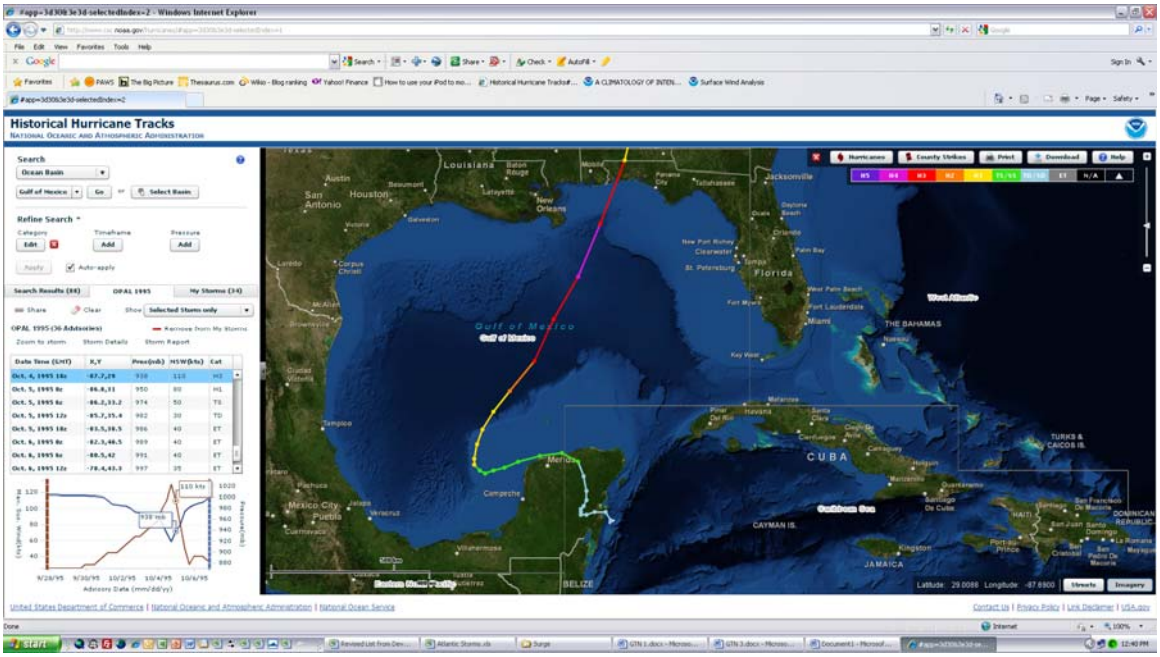

Hurricane Opal, 1995

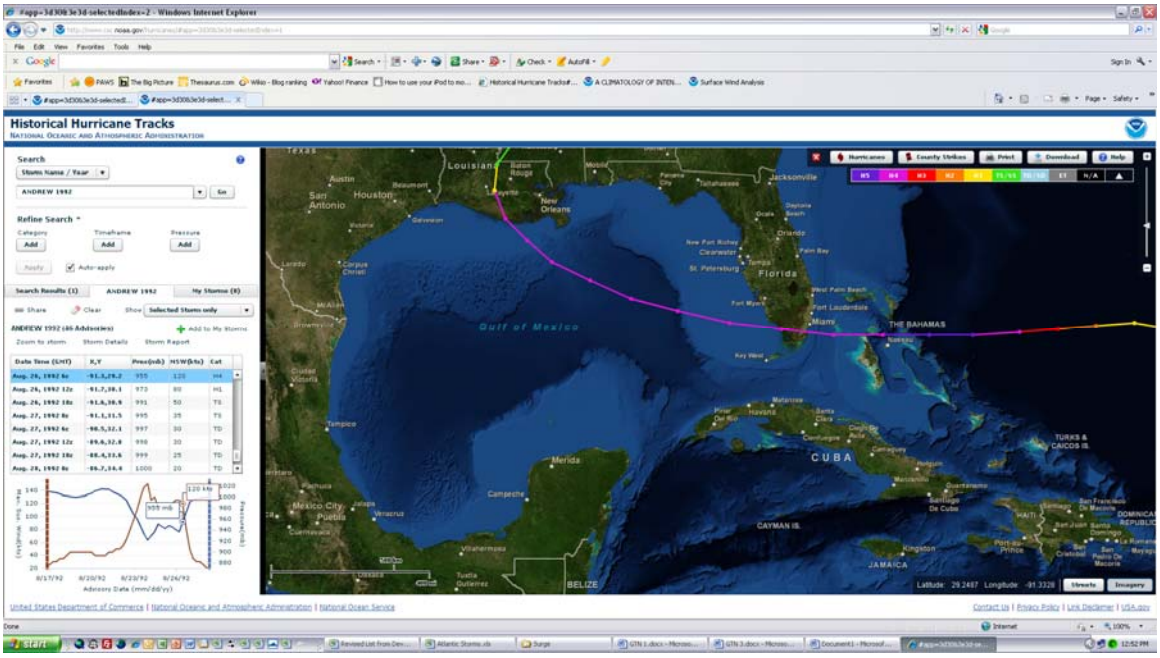

Hurricane Andrew, 1992

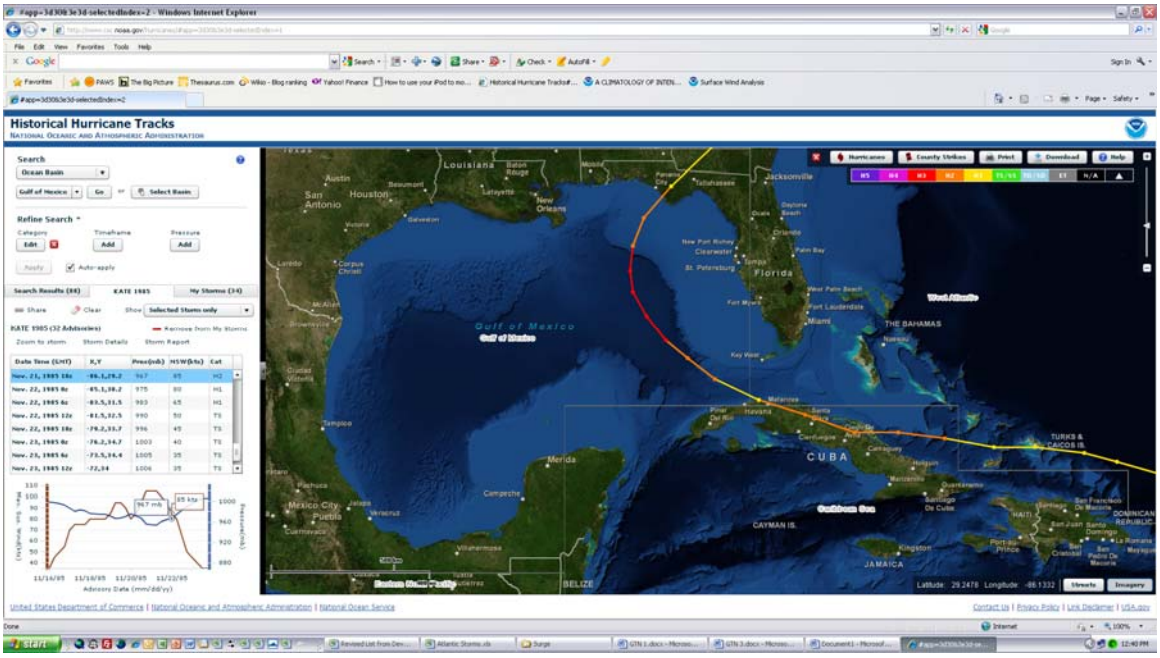

Hurricane Kate, 1985

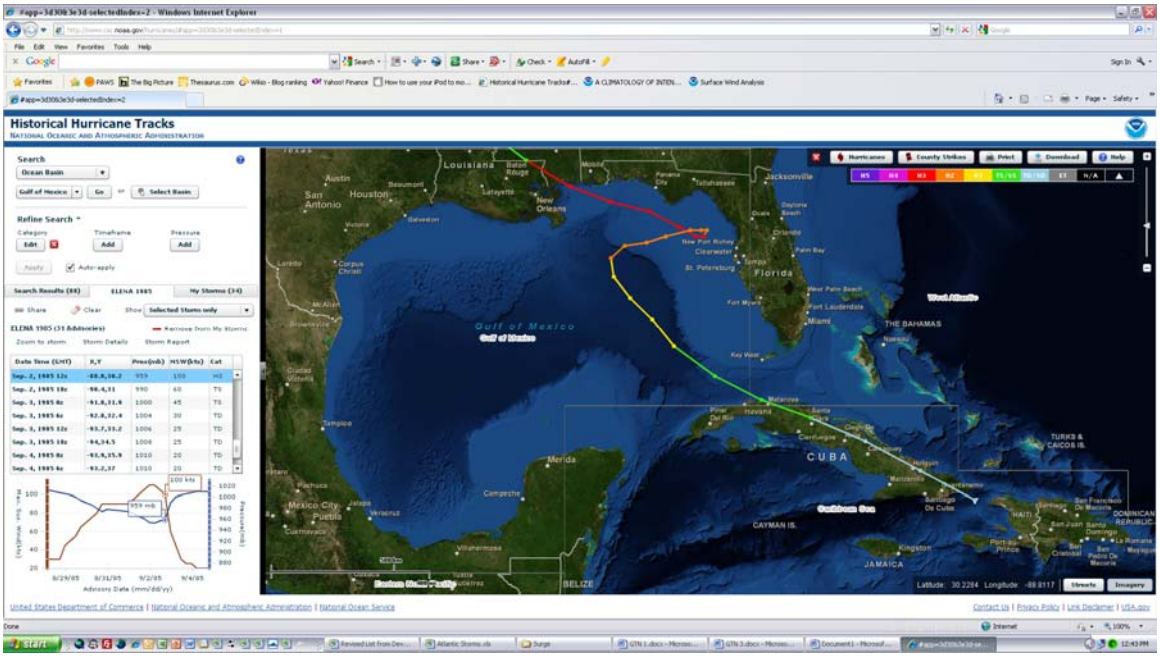

Hurricane Elena, 1985

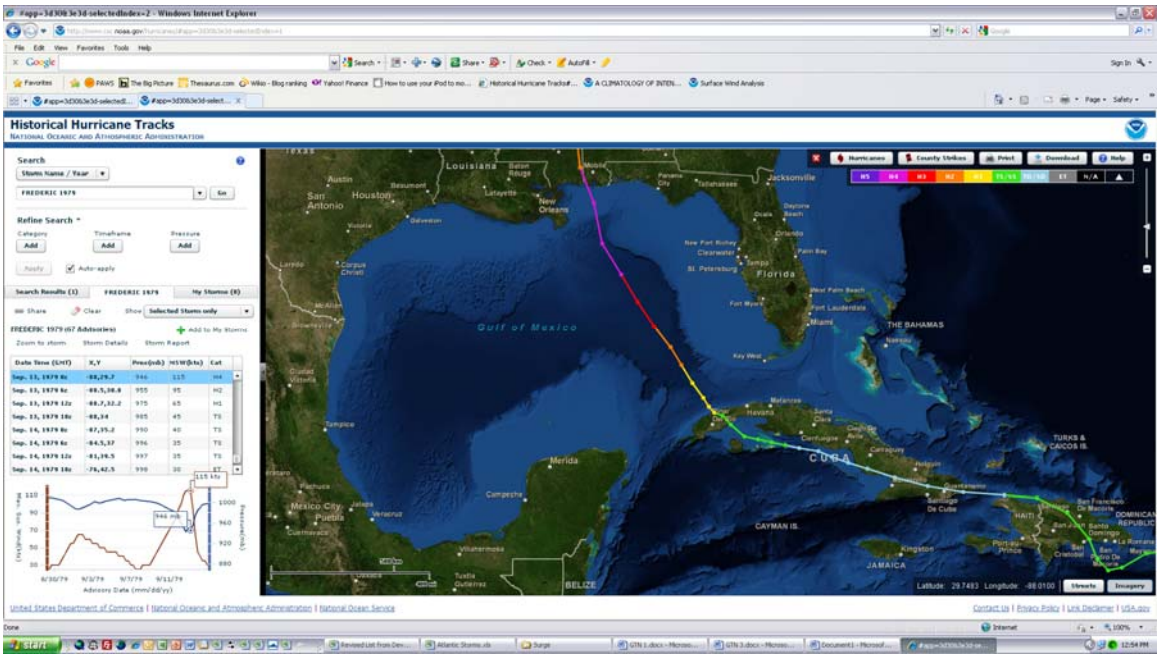

Hurricane Frederic, 1979

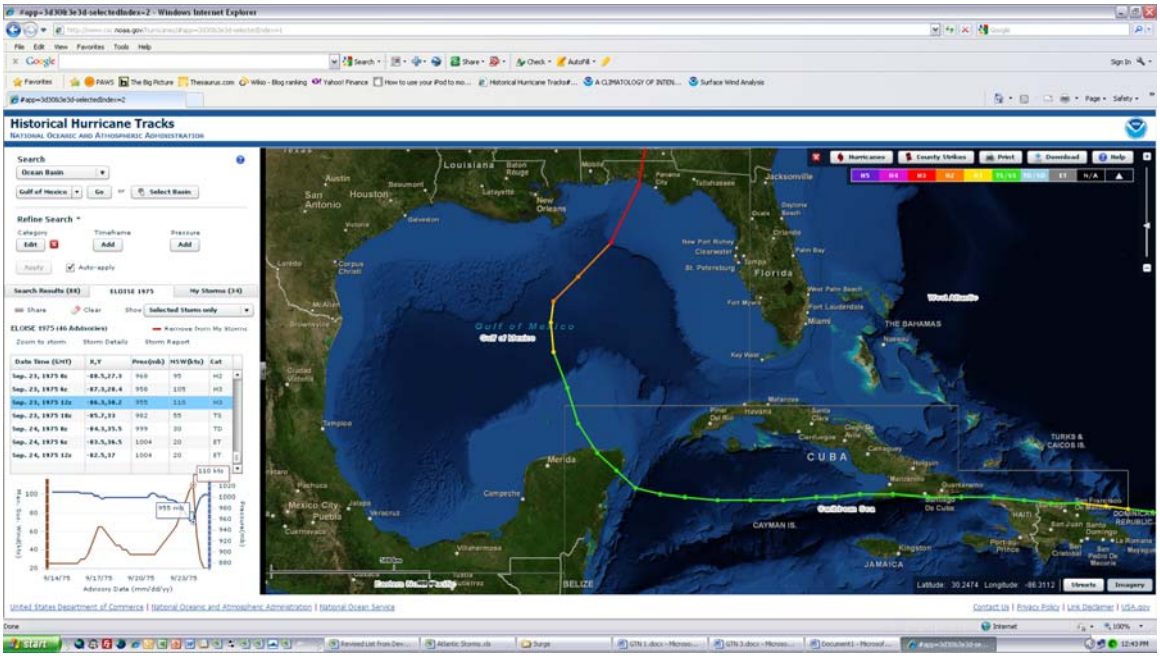

Hurricane Eloise, 1975

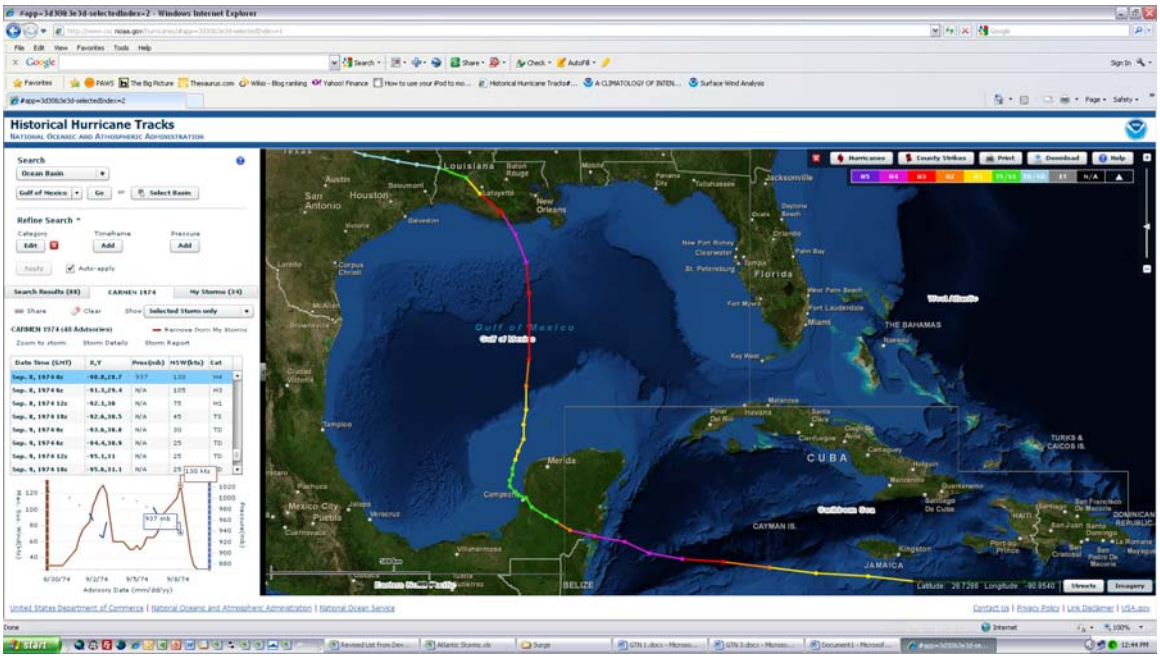

Hurricane Carmen, 1974

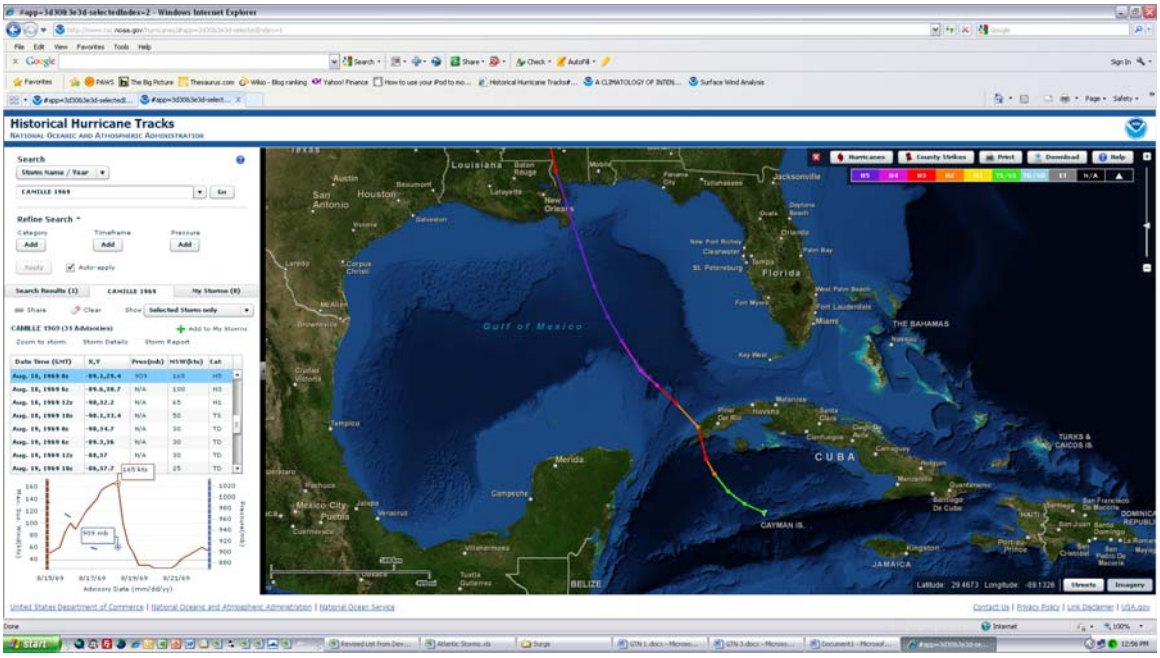

Hurricane Camille, 1969

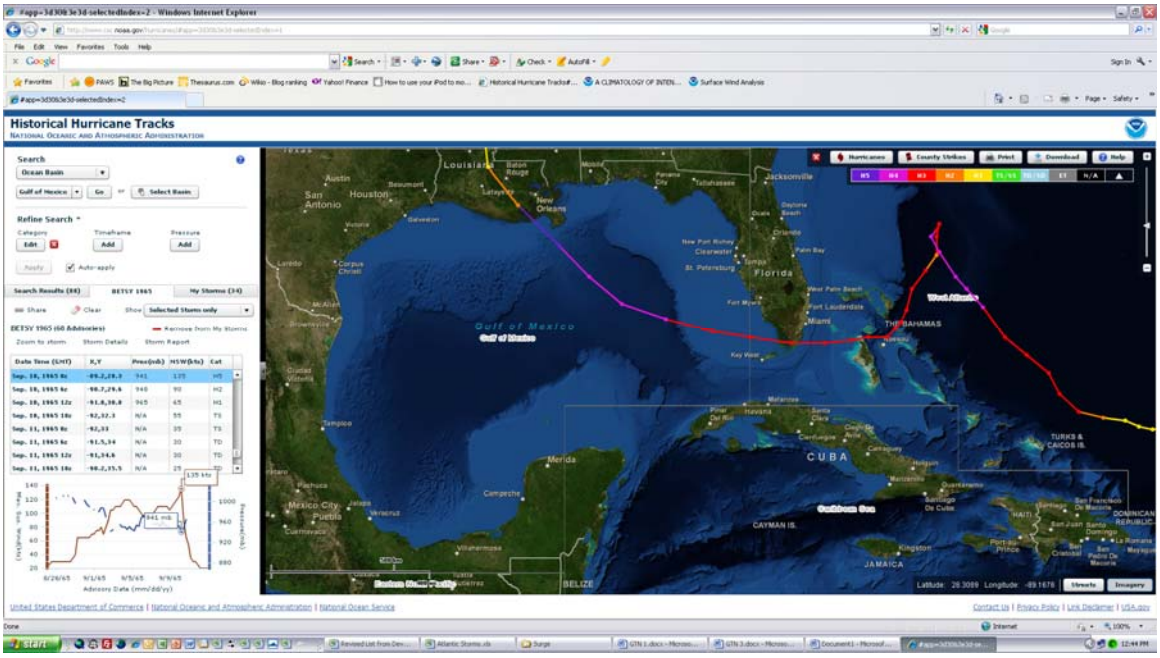

Hurricane Betsy, 1965

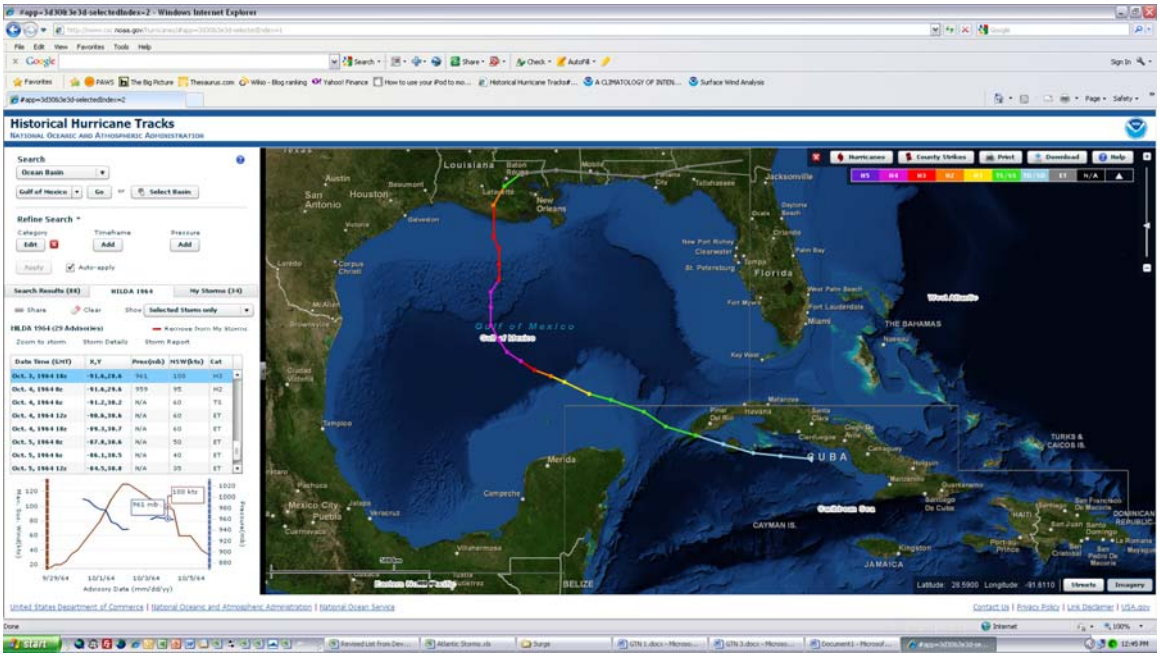

Hurricane Hilda, 1964

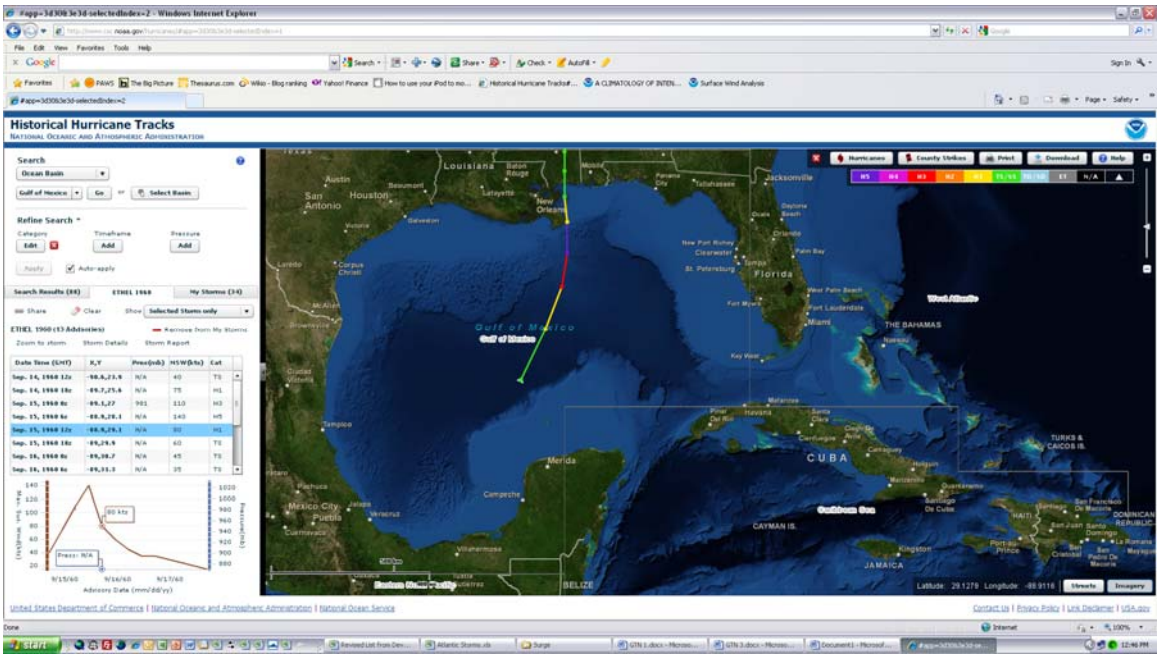

Hurricane Ethel, 1960

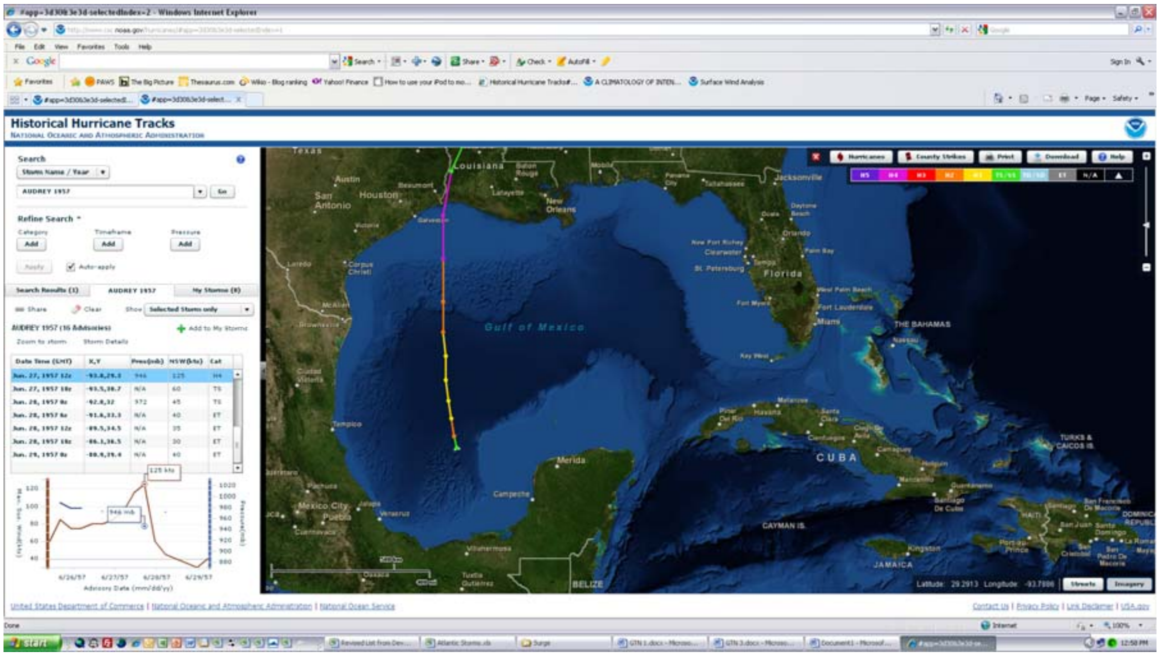

Hurricane Audrey, 1957

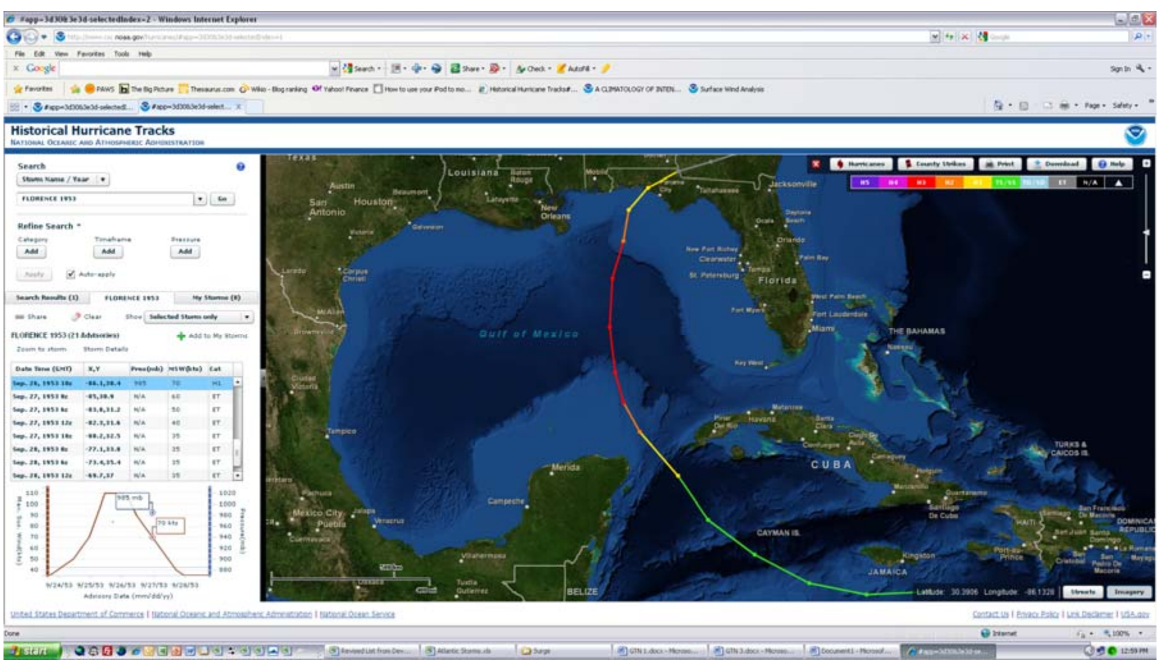

Hurricane Florence, 1953

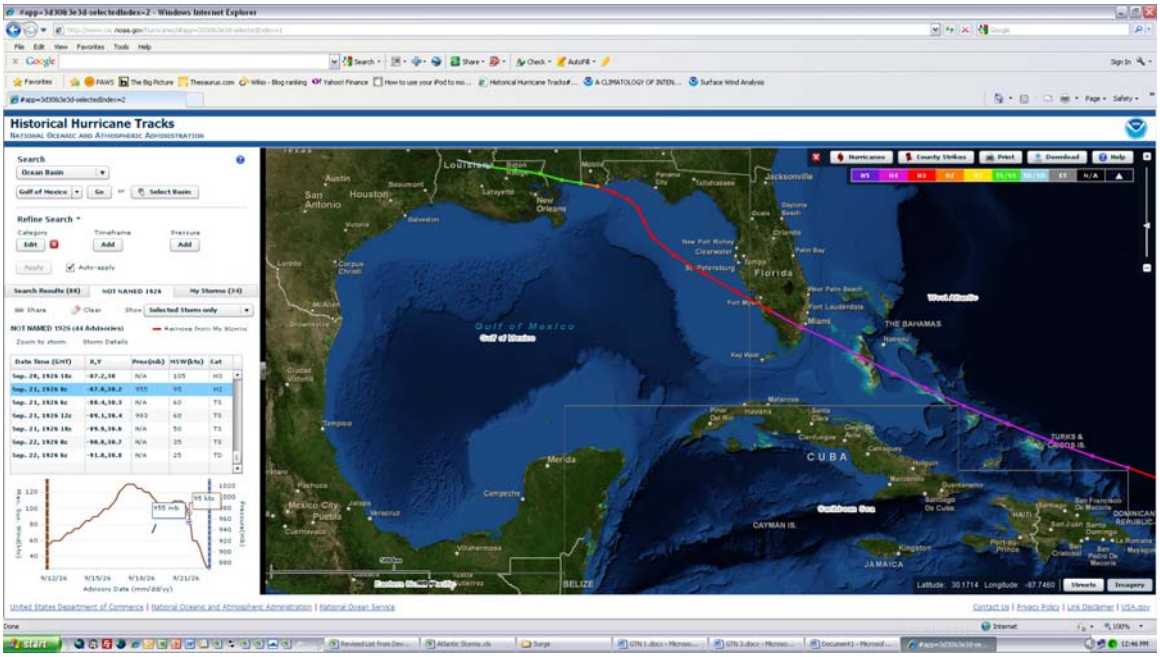

Hurricane Not Named 1926

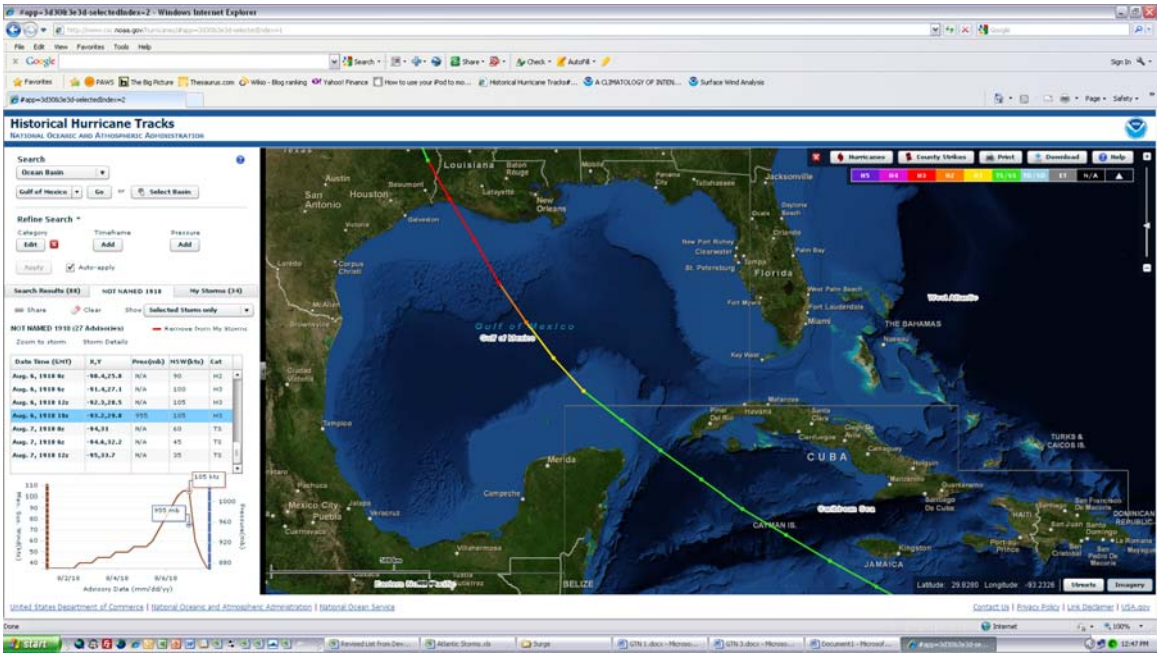

Hurricane Not Named, 1918

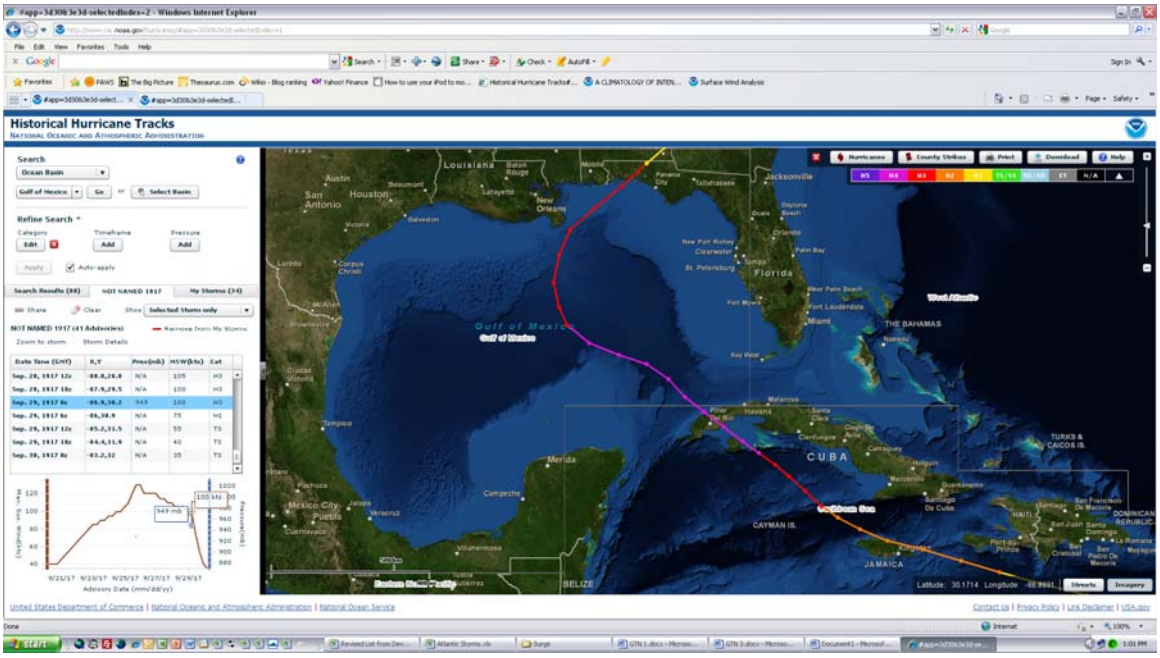

Hurricane Not Named, 1917

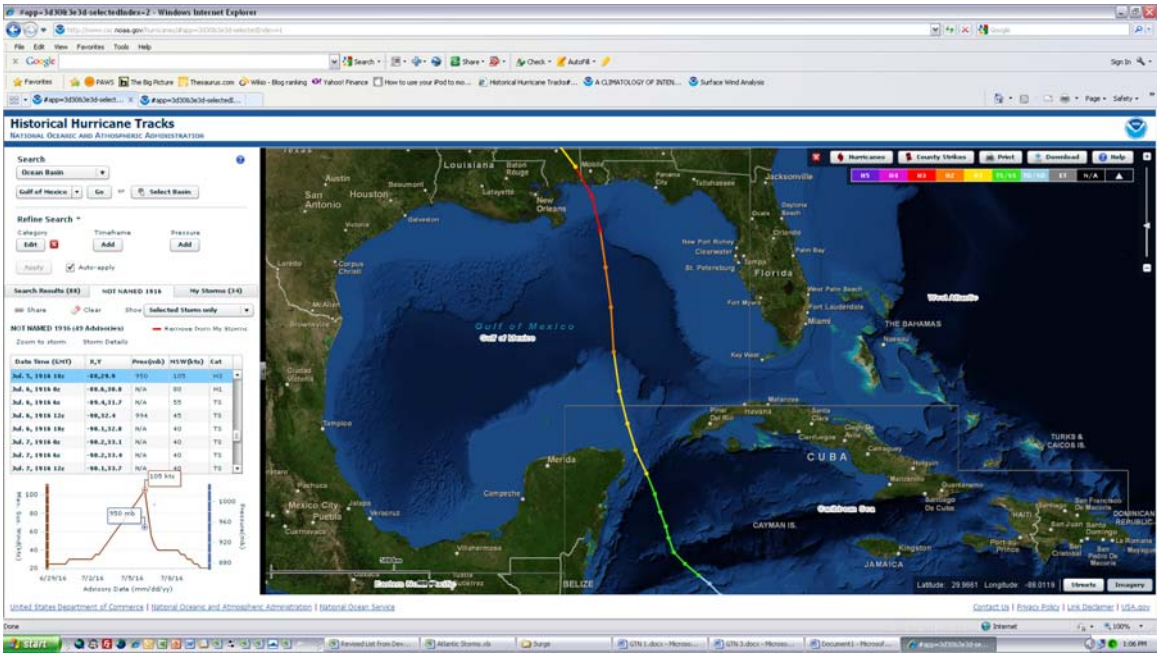

Hurricane Not Named, 1916

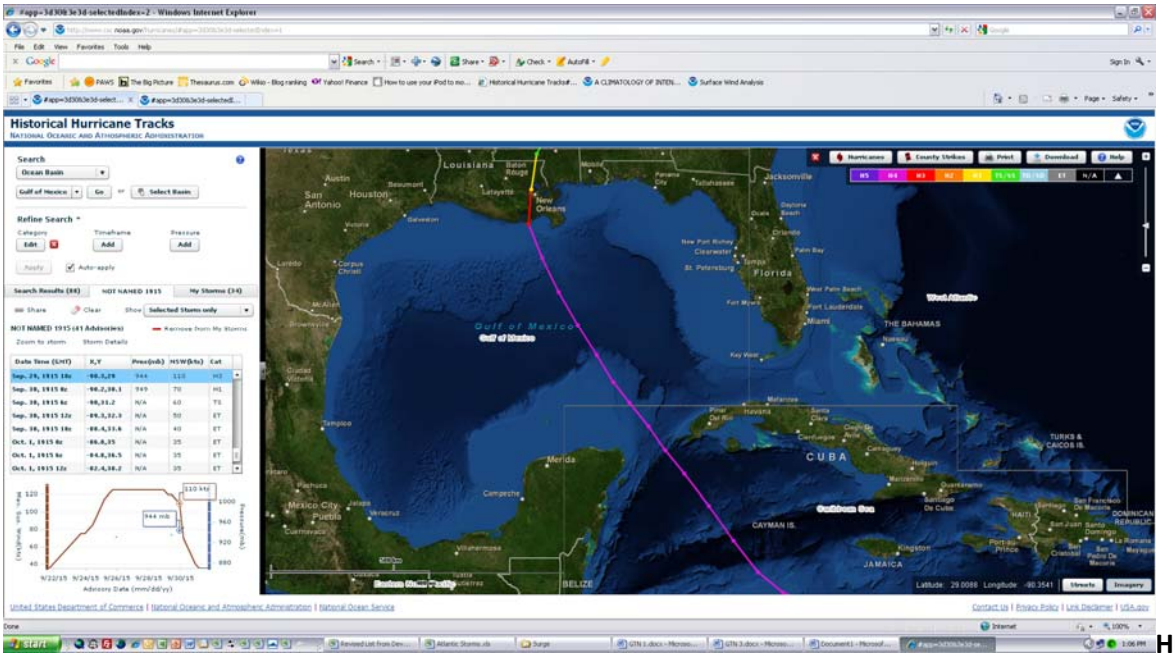

Hurricane Not Named, 1915

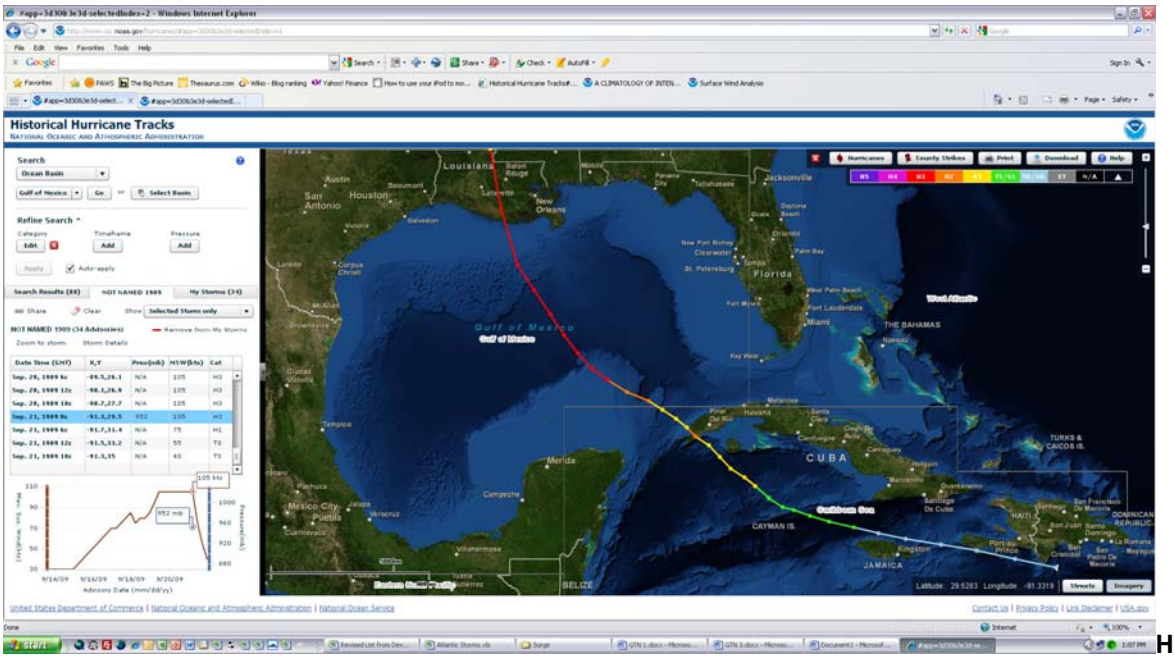

Hurricane Not Named, 1909

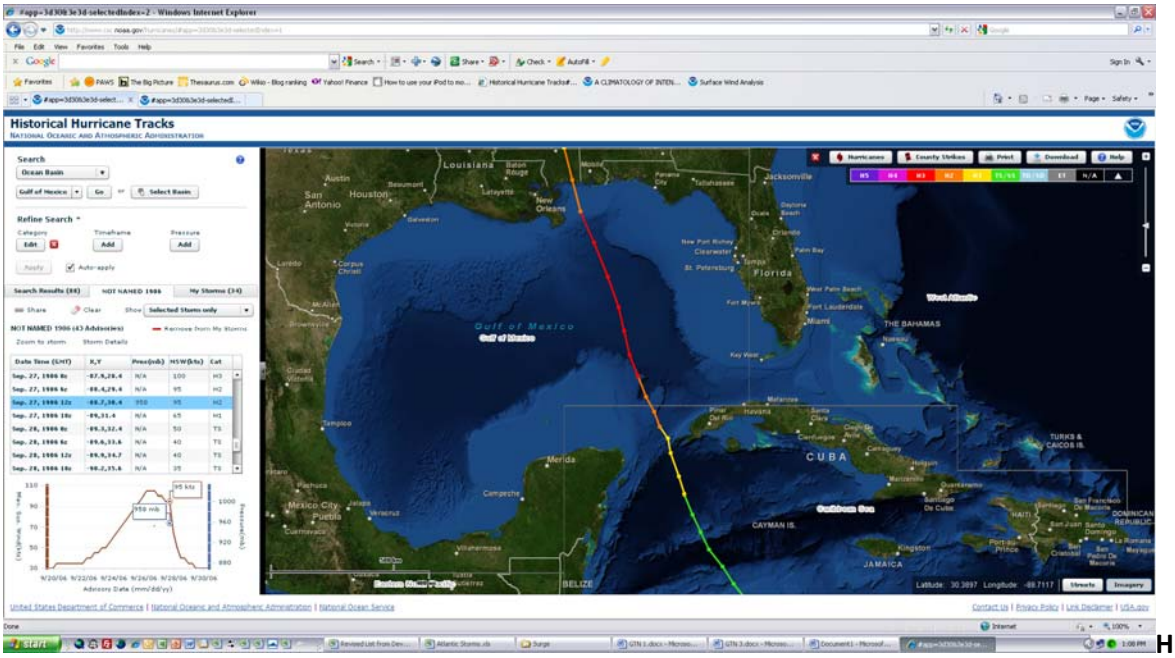

Hurrica

Hurricane Not Named, 1906

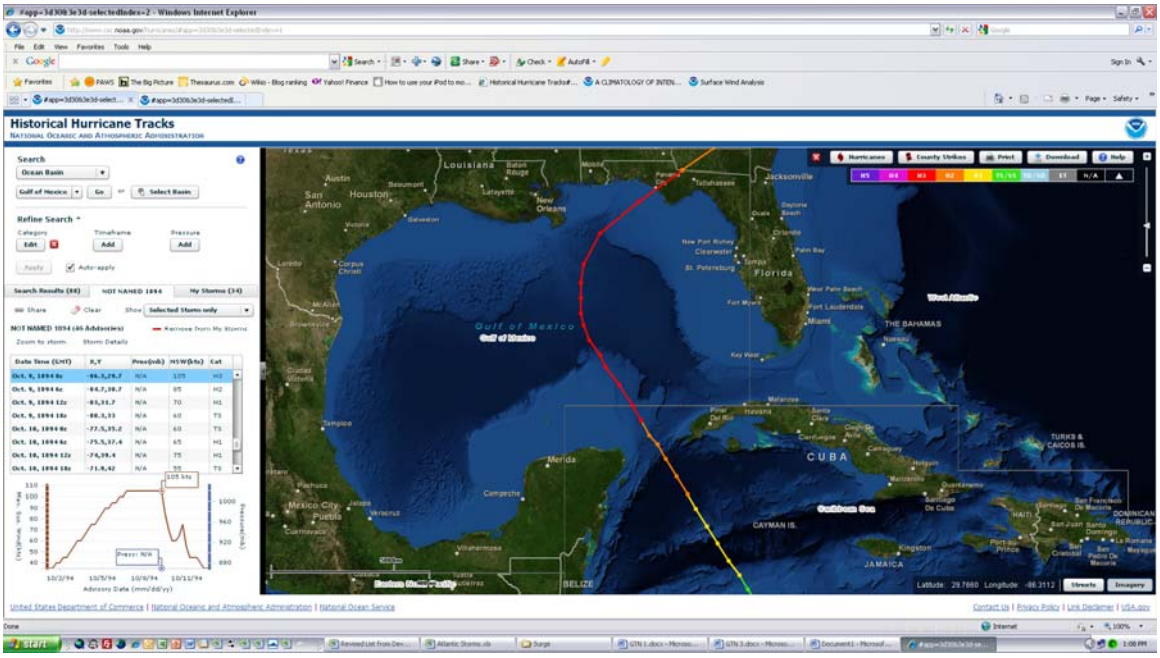

Hurricane Not Named, 1894

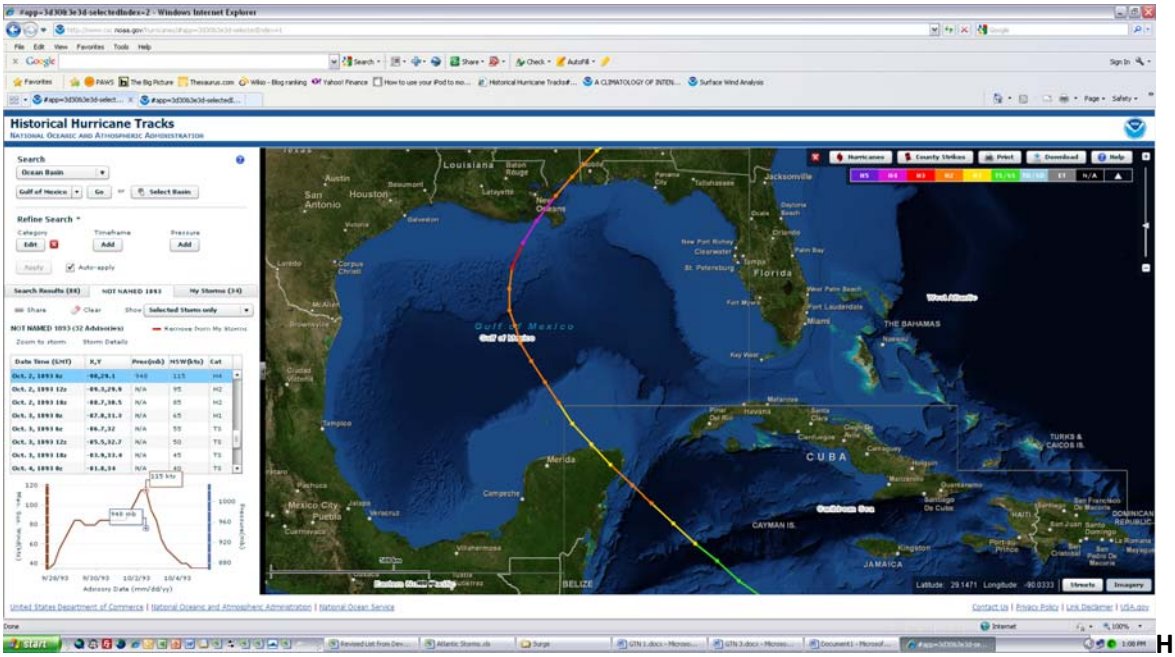

Hurrica

Hurricane Not Named, 1893

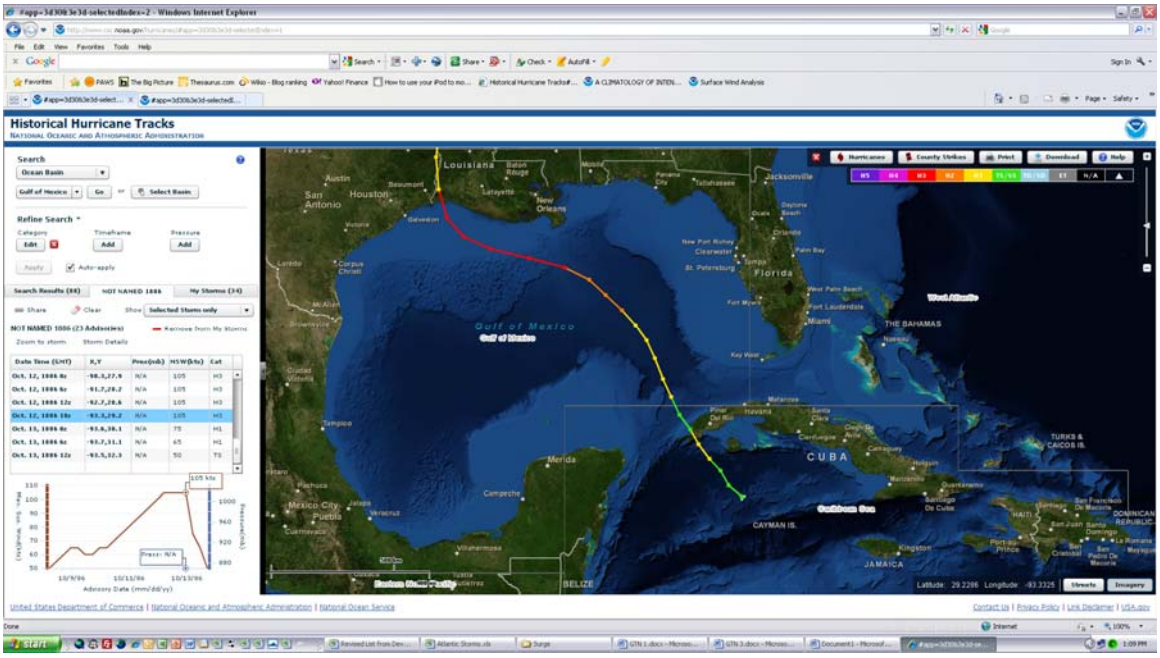

Hurricane Not Named, 1886

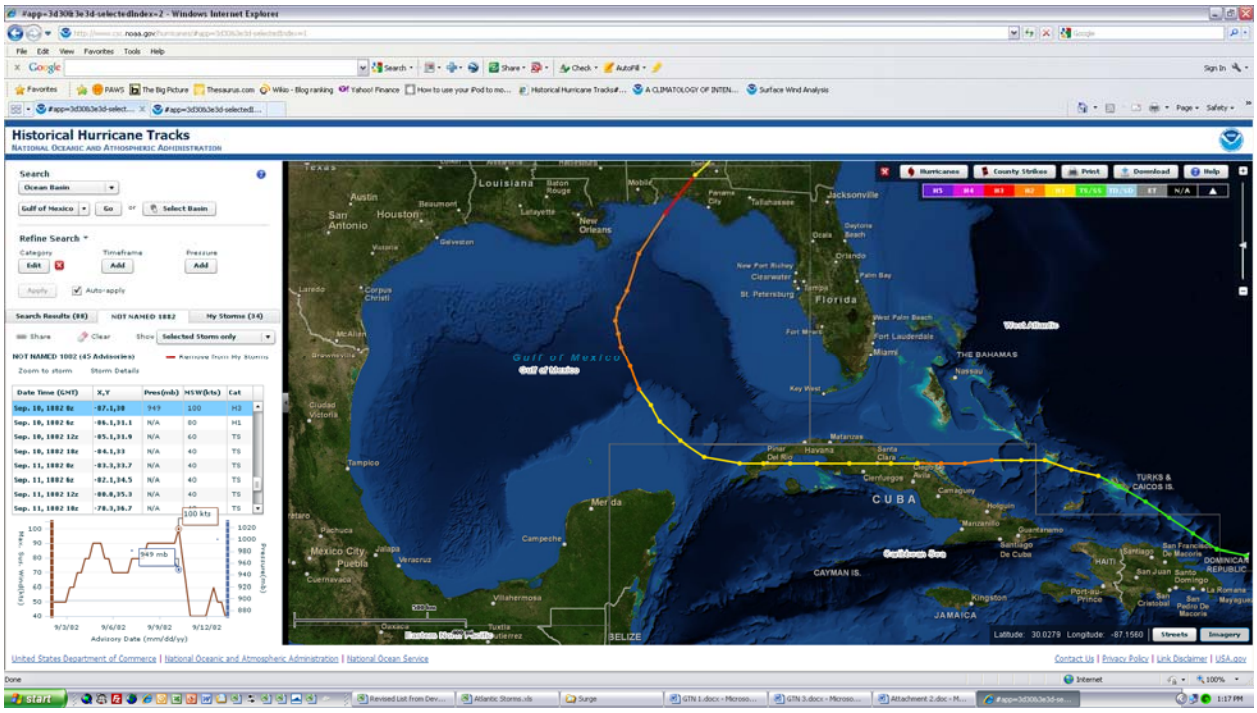

Hurricane Not Named, 1882

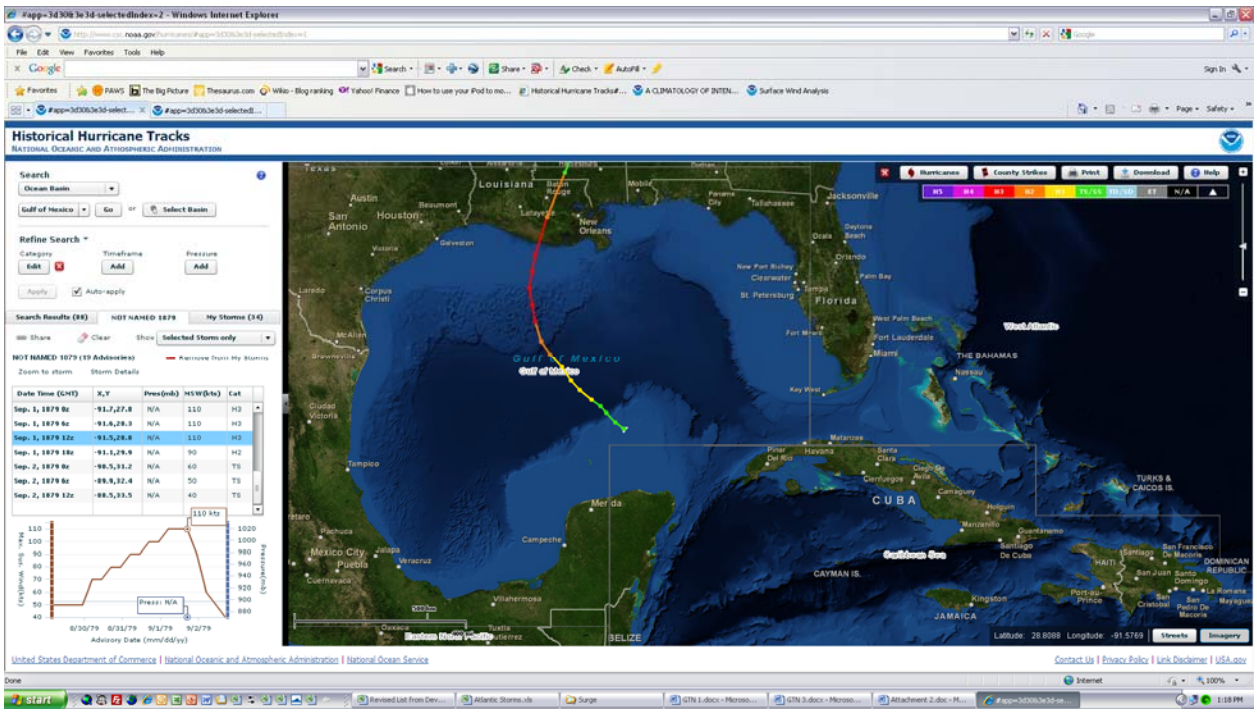

Hurricane Not Named, 1879

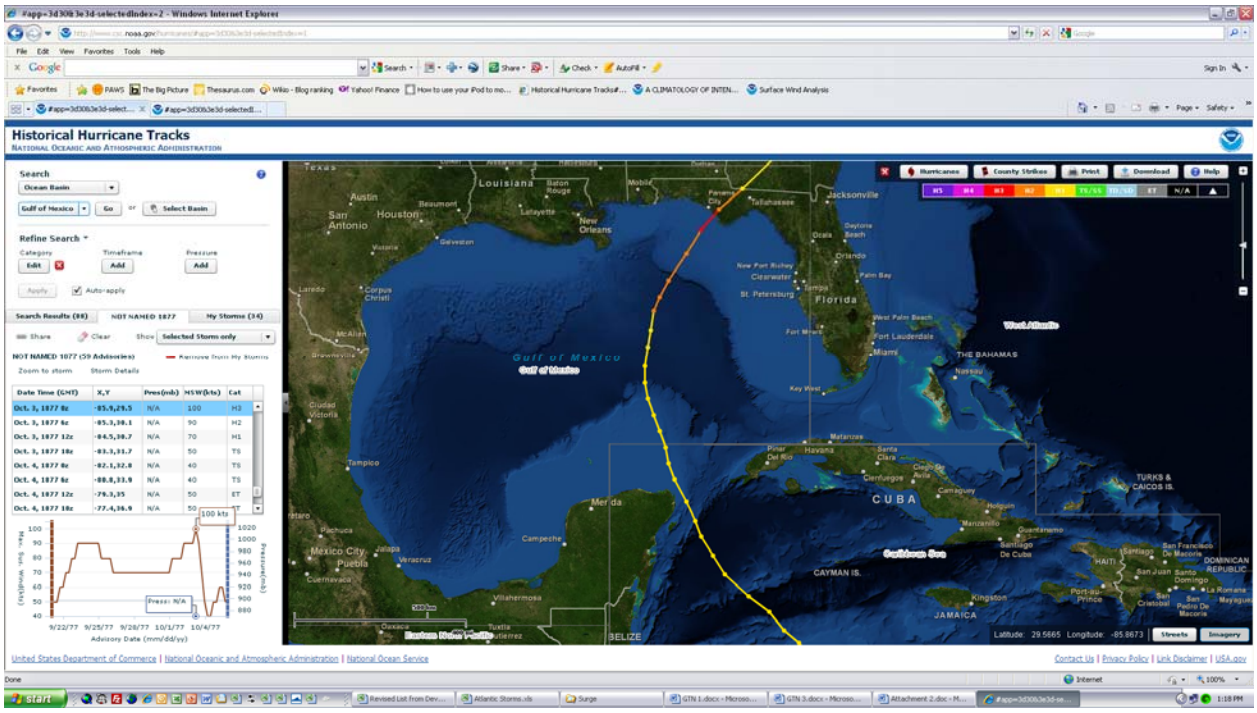

Hurricane Not Named, 1877

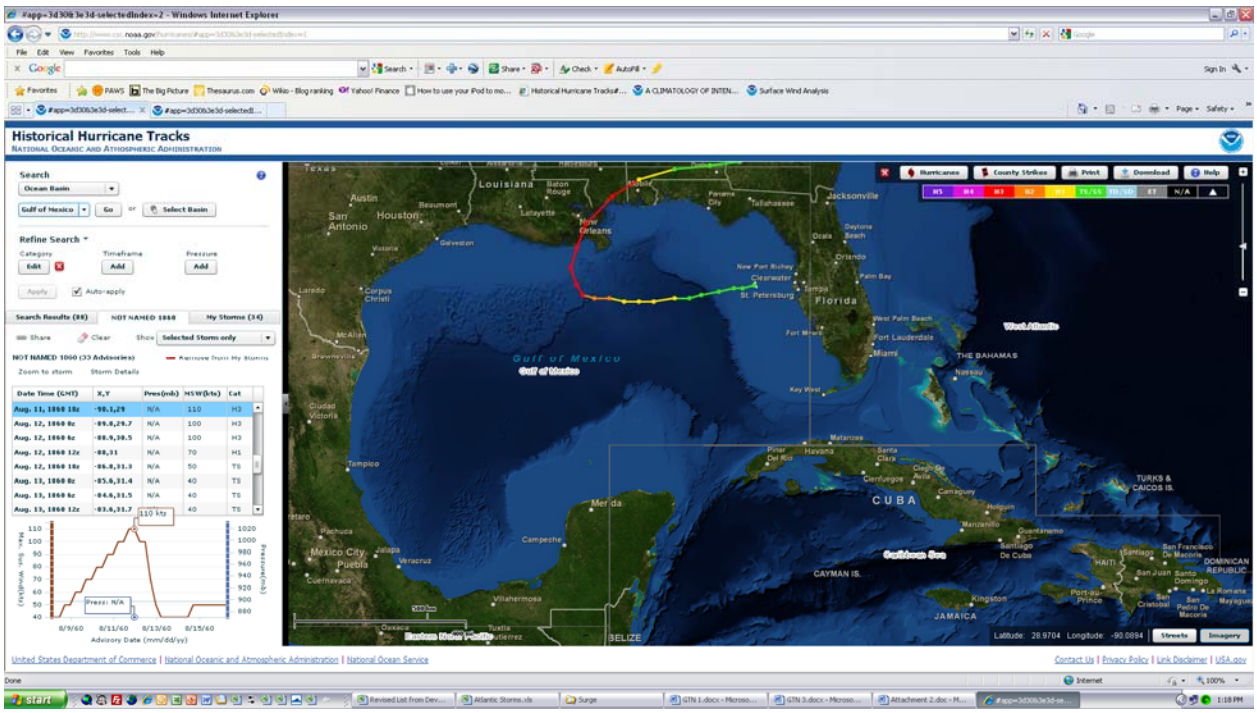

Hurricane Not Named, 1860

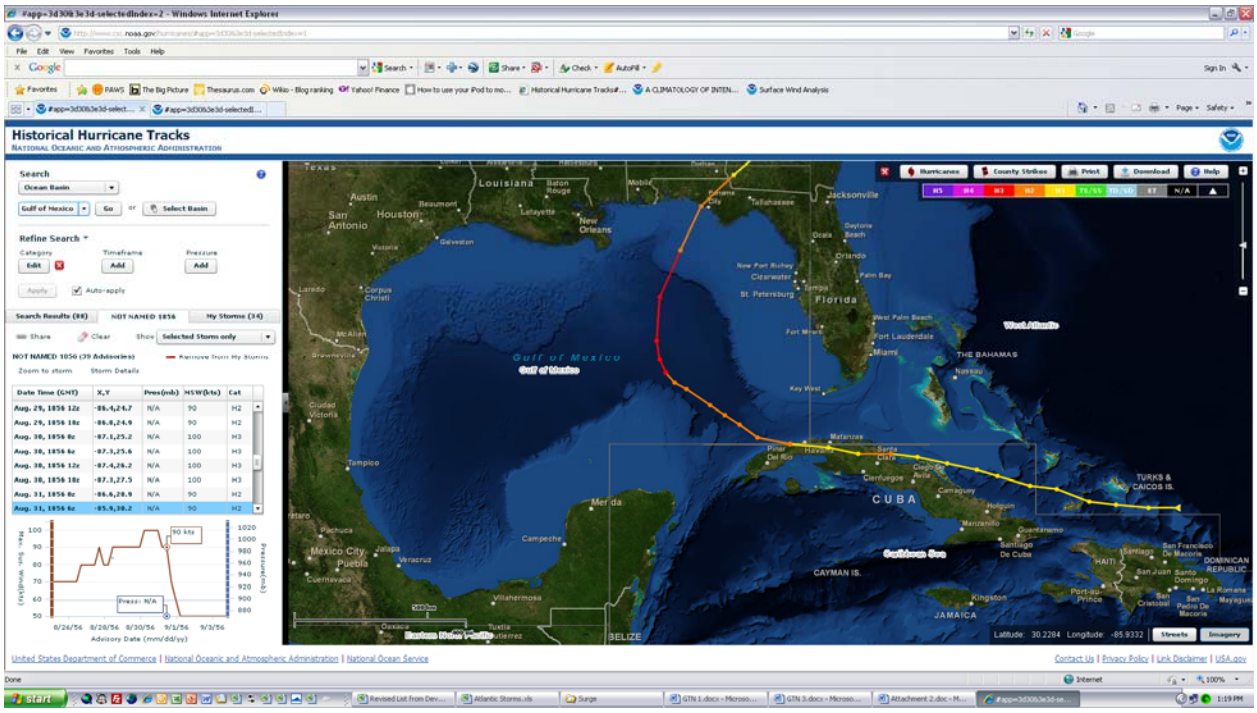

Hurricane Not Named, 1856

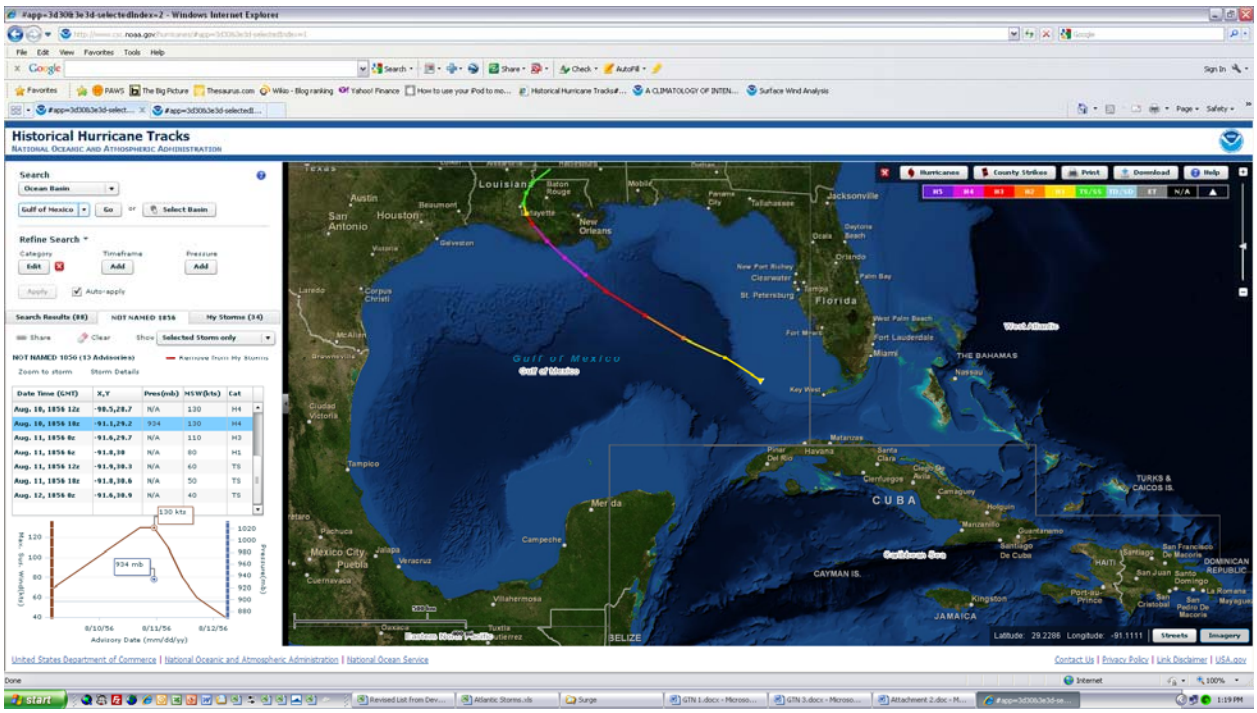

Hurricane Not Named, 1856

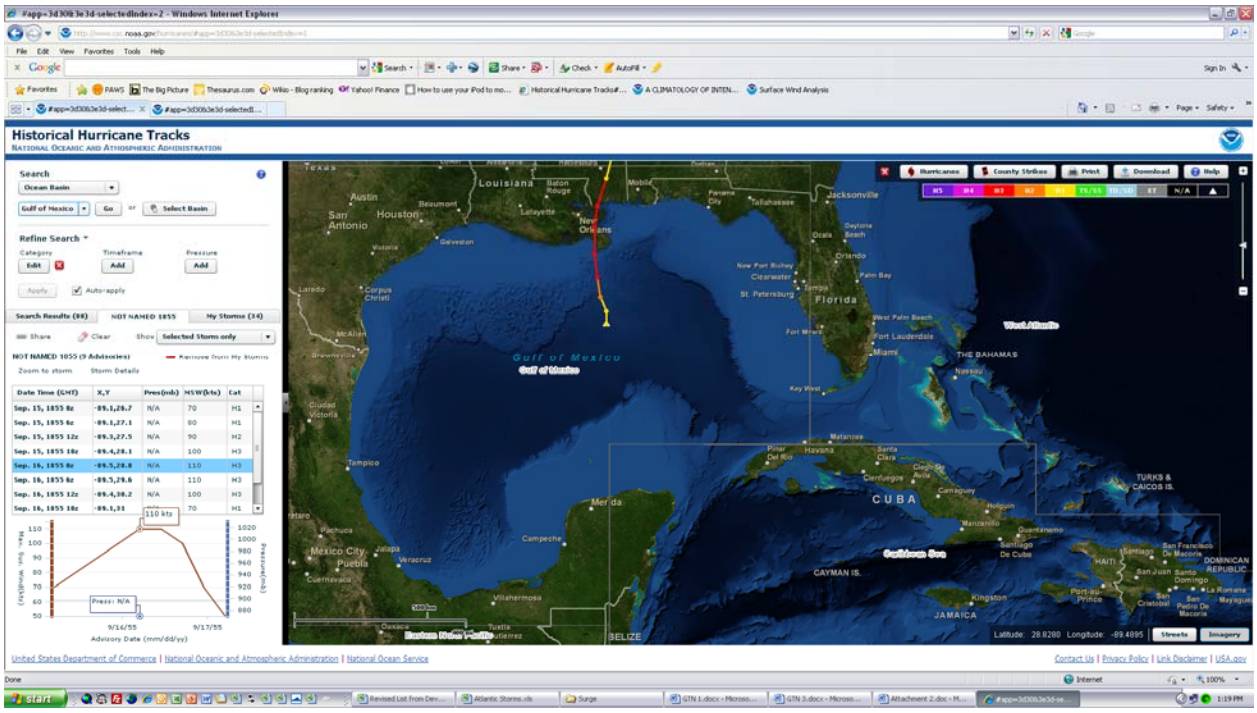

Hurricane Not Named, 1855

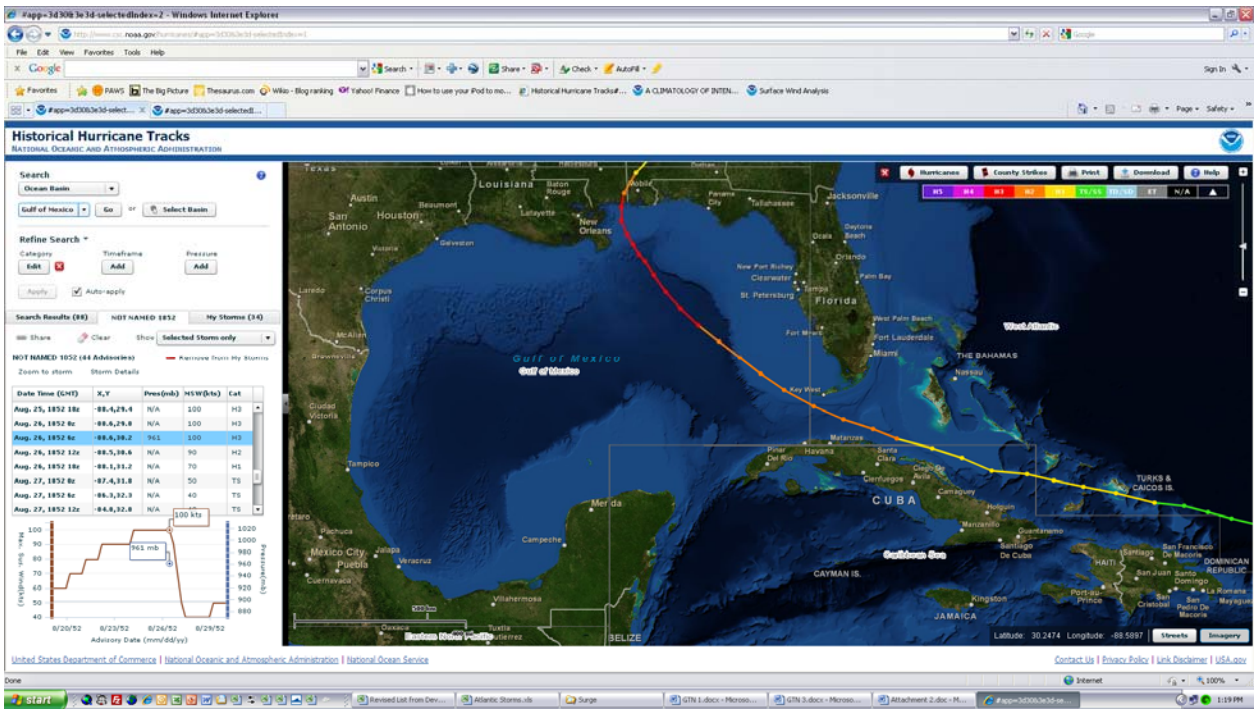

Hurricane Not Named, 1852

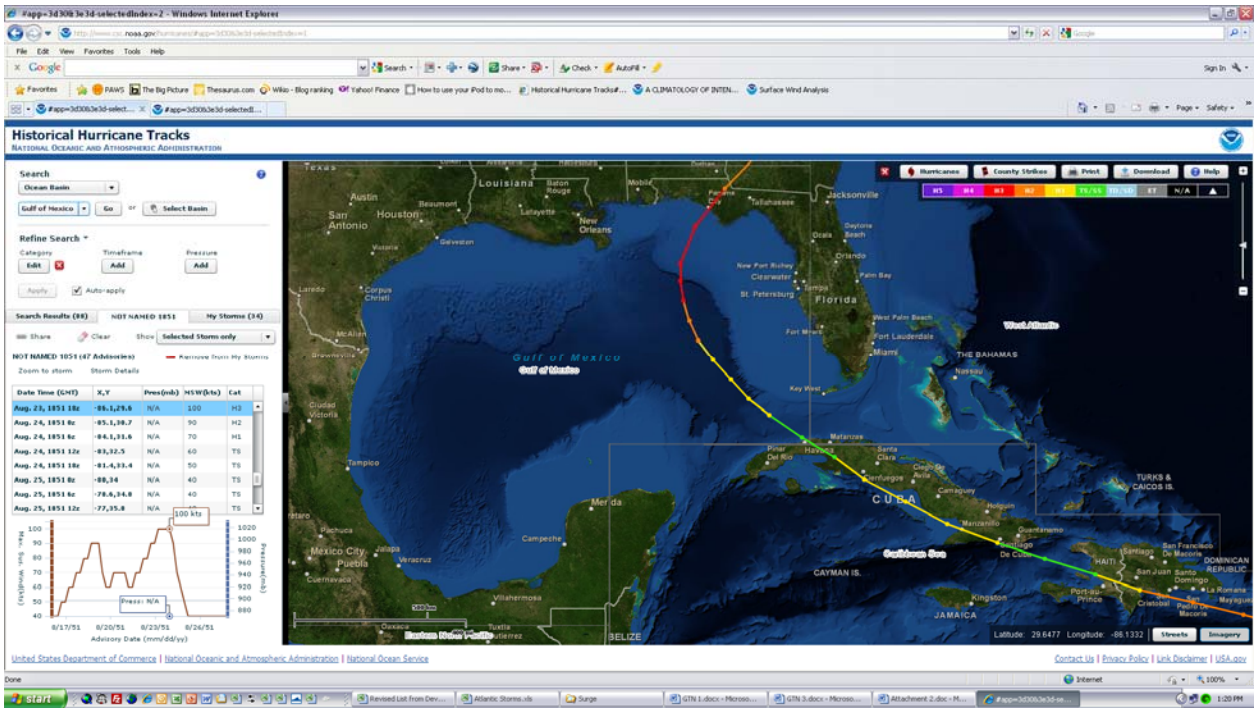

Hurricane Not Named, 1851

Part II.

Modeling Hurricane Surge Physics

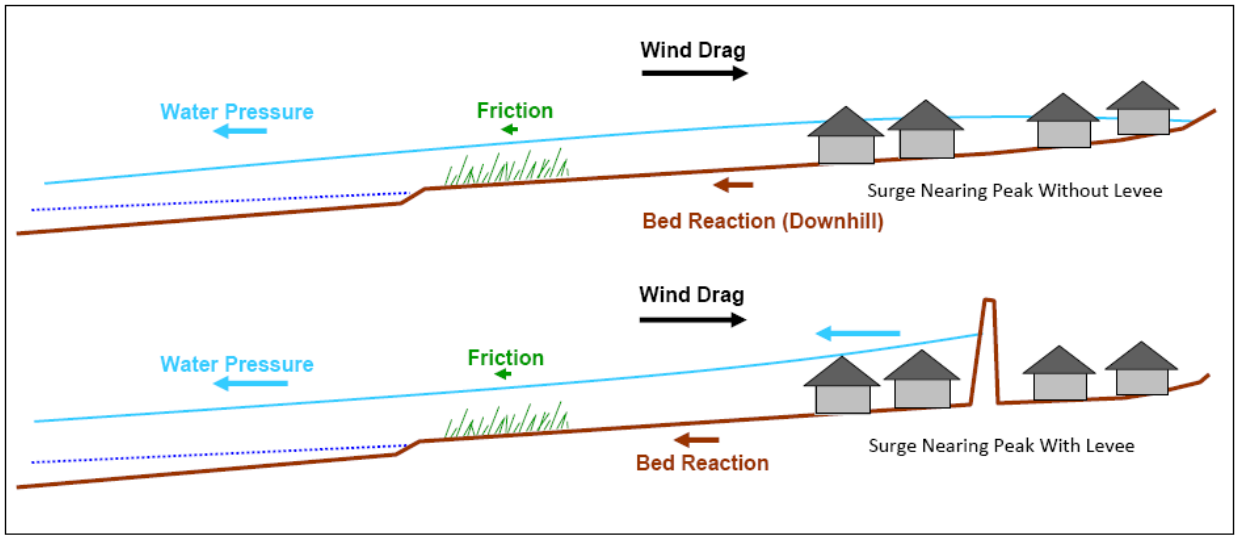

Subpart A. Hurricane Surge Physics

A hurricane reaches Category 3 or higher in the Gulf of Mexico, on average, every other year, with over 40 percent making landfall along a 500-mile stretch of the central-northern coast. These hurricanes possess a range of core intensities (indicated by the central pressure deficit and maximum eyewall winds), core sizes, wind field distributions, forward speeds, and tracks. Part I of this Report reviewed the current science on hurricane climatology of the CN-GoM. This information provides the basis for present return frequency estimates for hurricanes exhibiting various joint characteristics. For example, the landfall of storms with intensities at strong Category 3 and borderline Category 4-5 are estimated to have a return periods on the order of 40 and 212 years for a 1° latitude segment south of New Orleans LA (see Section 4).

The landfall of major hurricanes near the middle of this region—along the unique coastal conditions of southeast Louisiana—creates the most extreme surge inundation hazards in the United States, as typified by Hurricanes Betsy in 1965, Camille in 1969, and Katrina in 2005. This Part II, Subpart A reviews the scientific basis for these hazards by examining the three following subjects:

Section 5., the components of hurricane surge and the surge dynamics[1];

Section 6., the physics of hurricane surge;

Section 7., the interaction of hurricane surge with regional coastal landscape features; and

This subpart primarily provides a qualitative discussion of these concepts. Part II, Subpart B addresses surge hydrodynamic modeling—state-of-the-practice methods which can be used by risk managers to estimate surge dynamics for any specific hurricane. Part III then summarizes the approach to combining hurricane joint probabilities and surge modeling in analyzing hurricane surge hazards.

[1] *Surge dynamics* refers to the changing shape of the SWL surface during the course of hurricane landfall. This is distinguished from *coastal or landscape morphodynamics* which refers to changes in terrain and bathymetric features associated with the surge. Examples of landscape morphodynamics include barrier island and headland dune erosion, shoreline erosion, widening and deepening of coastal passes, expansion of shoals adjacent to passes, and loss of vegetation.

Section 5. Surge Components and Dynamics

5.1. Surge Components

As illustrated in Figure 5.1, surge is basically an extensive dome of water with surface waves. The dome is created primarily by the hurricane wind field acting on the water and secondarily by the storm's CPD (see Section 6). The surge dome typically extends many tens of miles—occasionally exceeding 100 miles—and its passage can take over a day along the open coast and longer for inundated areas and shelter water bodies. Figure 5.1 shows that as the storm approaches the coast and depths decline, the hurricane wind action produces a taller dome.

The elevation of the surge dome is compared to *Local Mean Sea Level (LMSL)* and *Local Monthly Mean Sea Level (LMMSL)*. LMSL is a very long-term (on the order of 19 year) average coastal sea surface elevation which factors out the effect of astronomical tide cycles, as well as short-term and seasonal meteorolological and hydrodynamic events. Gradual changes in the LMSL based on multi-decade gauge data can be used to estimate sea level rise. NOAA computes LMSL at coastal locations throughout the United States, including the CN-GoM. LMSL can also be estimated for inshore locations—such as coastal passes (e.g., Rigolets), lakes (e.g., Borgne and Pontchartrain.), bays (e.g., Barataria, Eloi), and sounds (e.g., Chandeleur, Breton, and Mississippi)—using long-term data from other (e.g., USGS, USACE) gauges. Using high quality local control information tide gauge data is converted to the North American Vertical Datum of 1988, in the appropriate epoch (see GTN-2 for a discussion of geoid vertical referencing). Stable regional coastal hydrodynamic factors—such as slight differences in gravity, river base inflow, and ocean currents create variations in LMSL referenced in NAVD88. LMSLs at Grand Isle LA and near West End in Lake Pontchartrain are 0.2 and 0.5 feet NAVD88-2006.81, respectively (NOAA 2011).

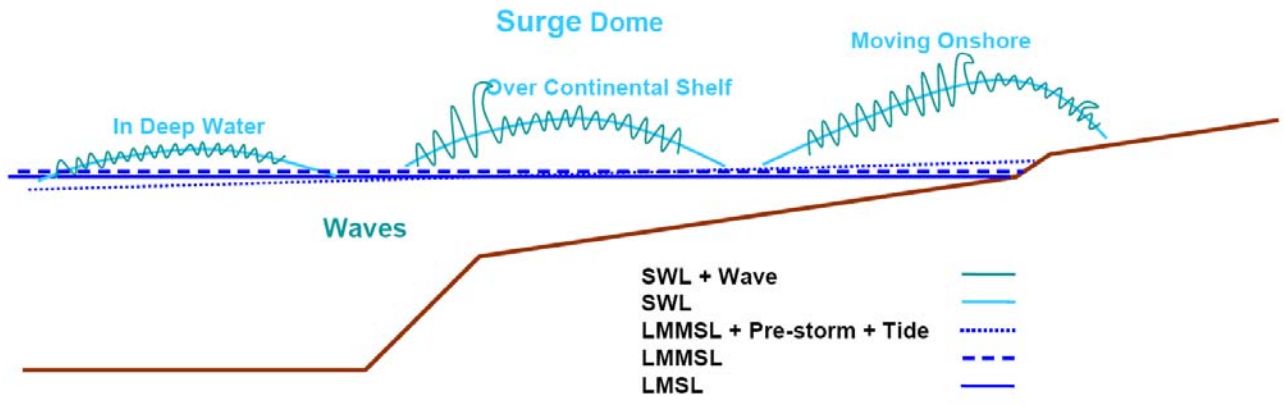

Figure 5.1. Typical Surge Components Moving From Deep Water to Onshore
(not to scale)

LMMSL is the average montly water surface elevation that would be present without the astronomical tides and individual short-term meteorological events. LMMSL reflects seasonal meteorological trends—e.g., regional runoff and persistent wind setup associated with frontal passages or centers of low/high barometric pressure—and steric effects (thermal expansion/contraction of Gulf of Mexico sea water). During late summer/early fall the LMMSL along the southeast Louisiana coast is about six inches above the LMSL. (USACE 2008). Computation of a LMMSL also requires gauge data for many years.

Along coastal southeast Louisiana astronomical tides are dominated by the diurnal (daily) as opposed to semi-diurnal (twice daily) gravitational affects of the sun and moon acting on the ocean waters, and highly dampened compared to the Atlantic coast. Six major constituents include the K_1, O_1, Q_1, and P_1 diurnal and the M_2 and S_2 semi-diurnal constituents. Amplitudes (and phases) have been established by NOAA from long-term tide station data. For example at a Shell Beach LA in Lake Borgne 0.453, 0.42, 0.085, 0.138, 0.079, 0.062, or a total of just over 1.2 ft (NOAA Tides and Currents). The southeast Louisiana tide range can exceed 2.5 ft along the open coast and up to 6 inches in Lake Pontchartrain.

Figure 5.2 illustrates gauge data for one month at Grand Isle LA. The figure shows the predicted astronomical tide (blue), observed gauge data with tides (red), and the data with tides filtered out (green). The tide-filtered stage shows the influence of non-tropical weather events. Factoring in tides, seasonal effects, and the occasional non-tropical weather event generating strong coastal winds, the local sea level along coastal southeast Louisiana at any time typically ranges within ±3 ft of LMSL.

Together, the LMMSL, astronomical tide, pre-storm influence, and the surge dome, are called the *storm tide*. The measured elevation of the storm tide or *total surge* (referred to henceforth as simply surge) is termed the *still water level* (SWL) because it removes the influence of high frequency waves. [Wave scientists often use SWL to refer to a totally undisturbed water surface—e.g., in an experimental flume prior to creation of waves—and mean water level (MWL) to refer to the wave-filtered elevation at any point. However, hydrologists use the term "still," as in SWL, to simply refer to the wave-filtered level.]

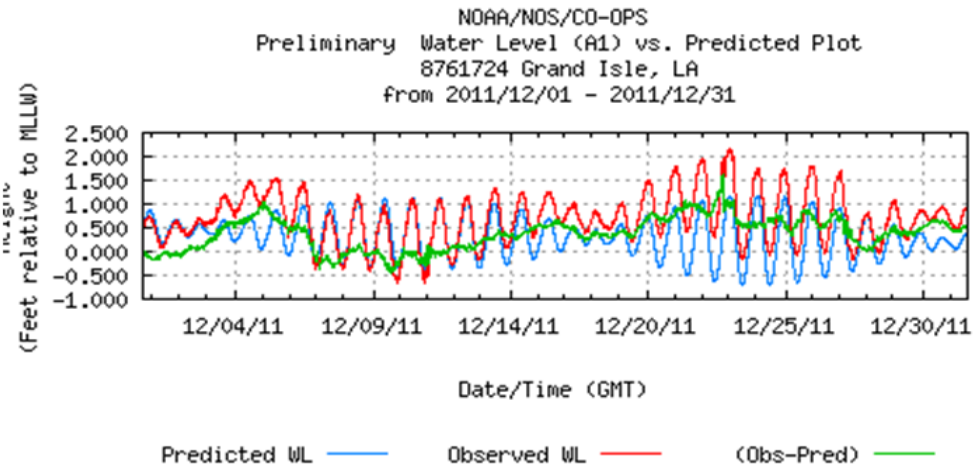

Figure 5.2. Example of Tides Filtered Out from Daily Tide Gauge Data
NOAA 2011

SWL data can be obtained from stage data recorded with the use of stilling basin or from data that is smoothed (i.e., with high-frequency waves filtered out). The red lines on the two NOAA graphs in Figure 5.3 illustrate surge SWL data (the green line is the astronomical tide component). Overland SWL measurements can be derived from post-storm high water marks (HWMs) within building interiors. As illustrated in Figure 5.3, for an extreme hurricane such as Katrina, the peak two feet of surge lasts for many hours on the open coast and for a few hours along interior lakes and bays, (but longer in confined areas where receding is delayed).

The high-frequency waves have periods measured in seconds and oscillate about the SWL as shown in Figure 5.1. The wavelengths are measured from peak to peak (the period is the time required for passage of one wave, peak to peak) and heights are measured from trough to peak. Offshore wave lengths are much greater than heights and waves are nearly symmetric about the SWL (approximating a sine function). With shoaling wave heights increase and lengths decrease. With the approaching shoreline, as depth (SWL minus the bathymetric elevation) continues to decline below increasing wave height, waves become increasingly steep and asymmetric until they break. Thus, in the nearshore and over inundated areas the surge depth controls the maximum height of waves, and the greatest wave heights generally, but not always, occur with maximum SWL.

Different wave conditions typically dominate different zones as waves from a deeper region reach a breaking zone, and then waves with new characteristics regenerate and move further shoreward. Some typical zone transitions include:

- The deeper open Gulf of Mexico to the Continental Shelf;
- The Continental Shelf to the nearshore zone of barrier islands and headlands;
- Open water in larger sounds, bays, lakes, and channels to their nearshore zones; and
- Smaller bays, lakes, channels, and submerged coastal wetlands to the nearshore (foreshore) of natural and artificial embankments.

Hurricane waves are irregular—meaning the height (H), period (T), and direction of individual waves vary within a wave field. Wave heights do not vary in a normal distribution but are instead typically characterized by the skewed (i.e. asymmetrical) Rayleigh distribution as shown in Figure 5.4. In this distribution two important conditions are *the significant wave* (H_s, the average of the upper one-third waves), and *the 1% wave* (the wave that occurs once out of every 100 waves on average).[1] These statistical conditions within a wave field change during the course of a storm as SWL rises and falls and as winds rise/fall and shift direction. Over the course of a two-hour SWL peak a wave field with an average period (T_{avg})[2] of 8 seconds will produce a total 900 waves. If the wave field contains a representative number of the various waves, nine 1% waves will occur. However, the probability of any single two-hour wave field containing nine (or more) 1% waves is actually 54%.

Obtaining accurate wave spectrum data requires a very high frequency capture rate platform- or buoy-mounted gauge. Compared to SWL data there is a significant dearth of hurricane coastal wave data in all zones. The peak elevation of SWL-plus-wave for inundated areas can sometimes be gleaned from HWMs along open exposed walls or from floating debris left in trees or along embankments.

---

[1] $H_{avg} = 0.625H_s \approx 5/8\ H_s$; $H_P = .705H_s\ (-\ln P)^{1/2}$, where P is the Percentile, e.g., $H_{1\%} = 1.52H_s$ and $H_{0.1\%} = 1.9H_s$

[2] T_{avg} and T_p refer to the wave periods (1/frequency) containing the average and peak wave energy.

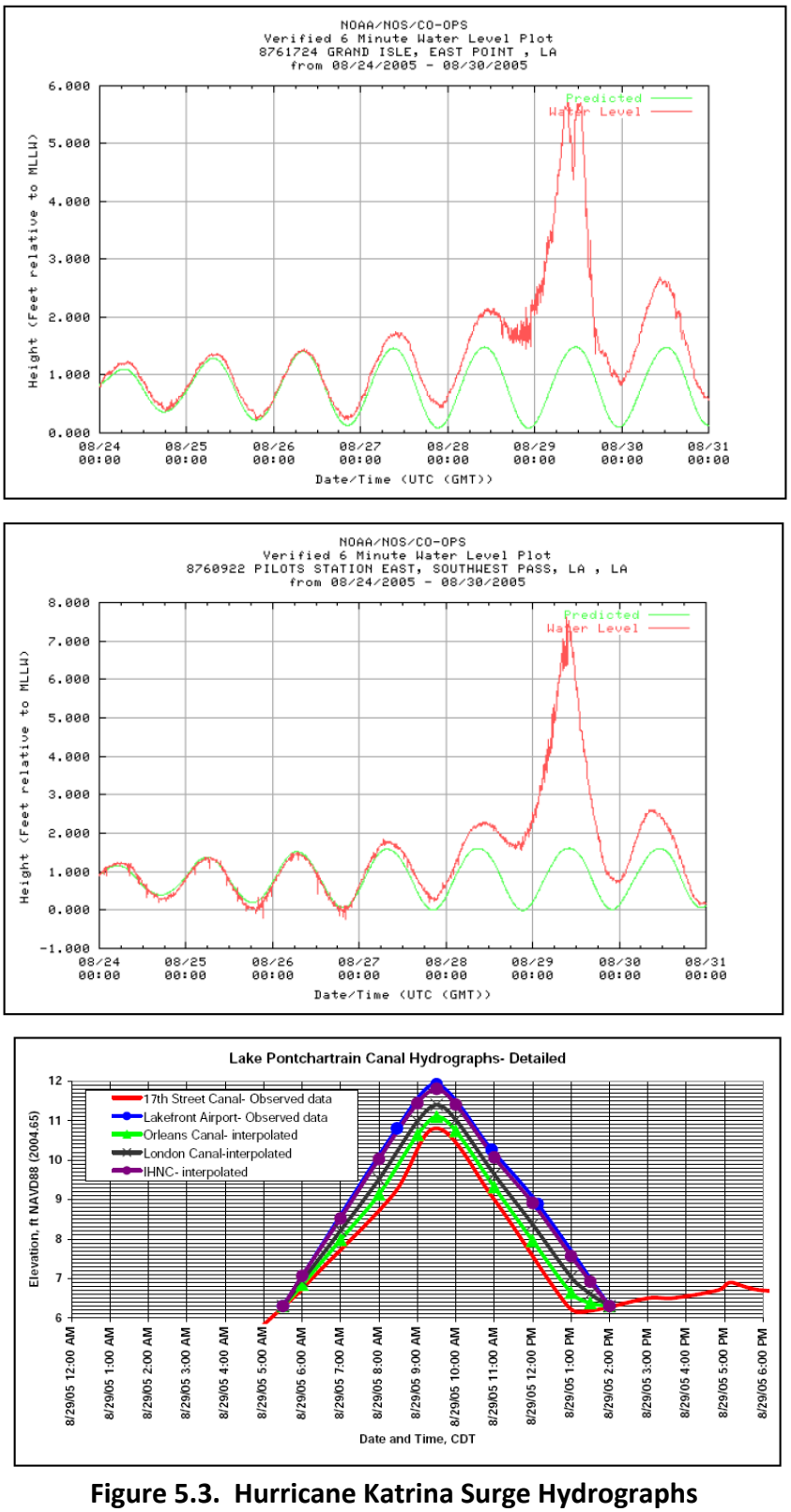

Figure 5.3. Hurricane Katrina Surge Hydrographs
IPET 2006

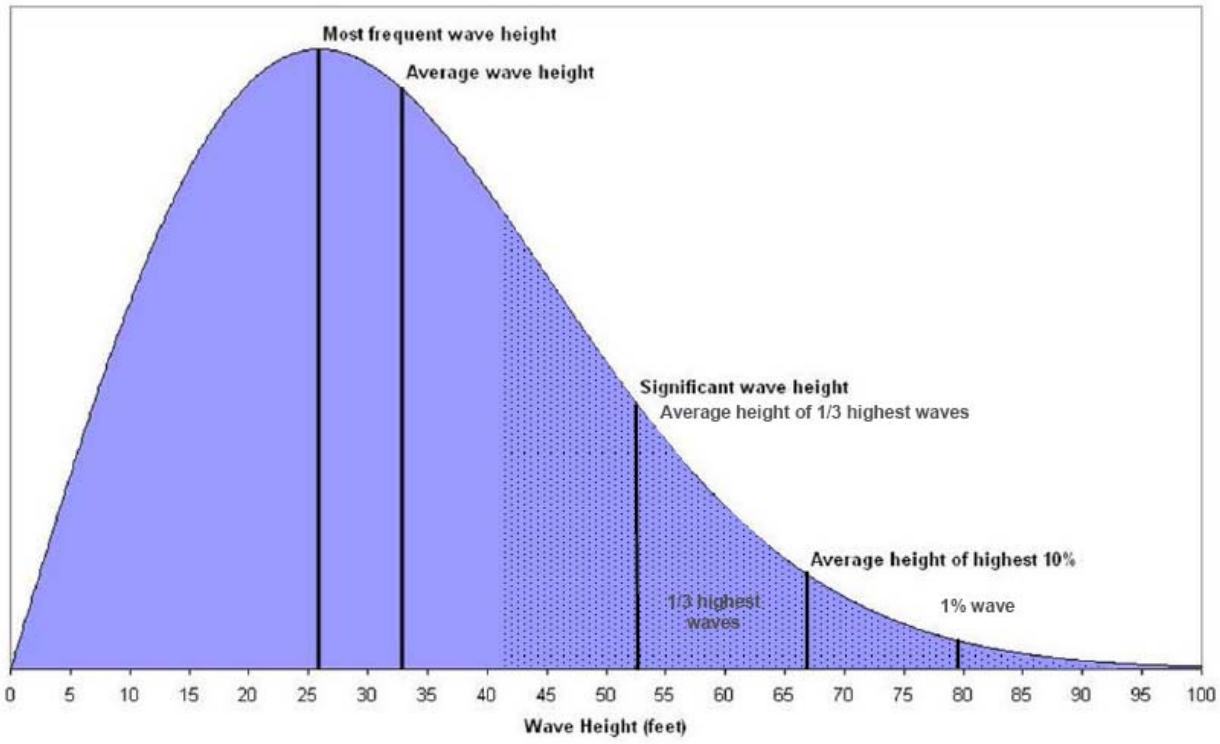

Figure 5.4. Rayleigh Distribution for Hurricane Ivan Waves at Buoy 42040
NOAA, http://www.vos.noaa.gov/MWL/aug_05/nws.shtml

5.2. Surge Dynamics

The surge dome shape changes as it approaches landfall, depending on the individual hurricane core intensity and size, wind field, dynamics, forward speed, and track and specific interactions with the local coast. The spatially varying surge SWL above LMMSL at any snapshot in time is termed the *setup* (η). Over expansive open water and inundated land with flat bathymetry the *setup slope* can be less than half a foot per mile. But with declining depth, the wind stress raises the dome height and the setup slope. When the surge encounters elevated obstructions, the dome is also squeezed, further steepening the setup slope, sometimes reaching two feet per mile. Variations in landscape compression of surge domes are analogous to the different effects of spilling a large drum of water in the middle of a room, versus close to a wall, or near a corner.

The varying magnitude and direction of winds contained in a hurricane wind field produce widely varying surge effects. The rise and fall of surge is fastest with the landfall of the dome peak, typically just to the right of the hurricane center. At this location the SWL is capable of rising several feet per hour. To the left of landfalling dome the offshore winds can produce a SWL s*etdown* below LMMSL (negative η). Secondary eyewalls and wind banding can cause irregularities in regional setup/setdown.

Landfalling surge domes exhibit elongation, turning, and fingering as they are forced over and around the coastline and its natural and artificial barriers. Figure 5.5 depicts surge dynamics for Hurricane Katrina in a series of plan views based on a computer simulation (USACE 2008). Peak SWLs actually reached above 18 ft (NAVD88-2004.65) in eastern St. Bernard Parish (Reggio) and in excess of 13 ft along Lake Pontchartrain in Little Woods in eastern Orleans Parish (URS 2006).

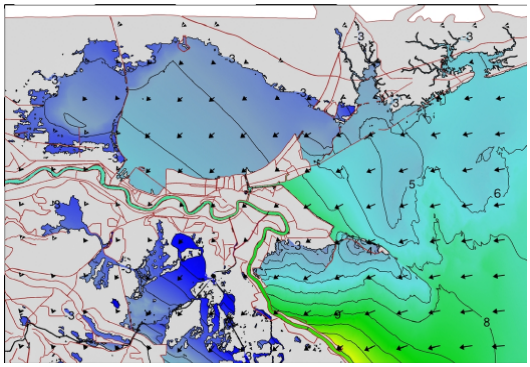

2 am CDT August 29, 2005

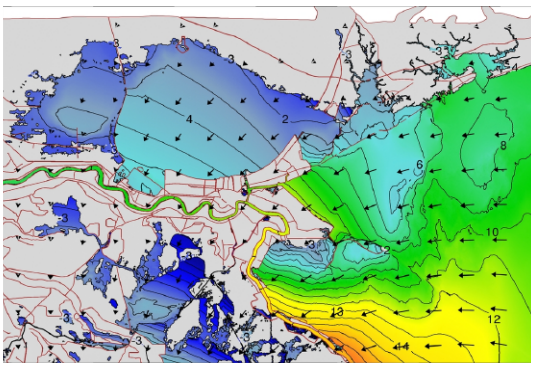

5 am CDT August 29, 2005

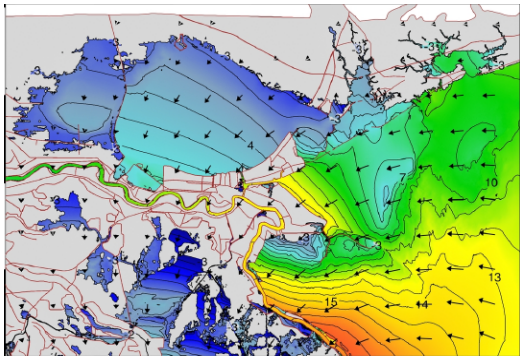

6 am CDT August 29, 2005

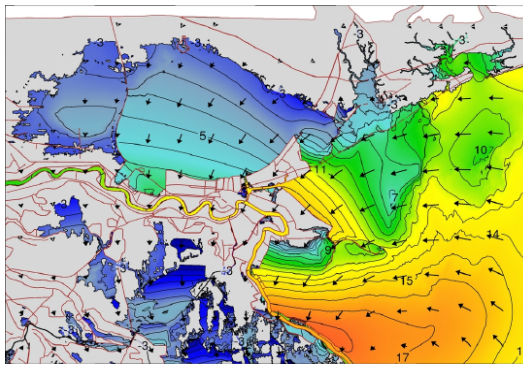

7 am CDT August 29, 2005

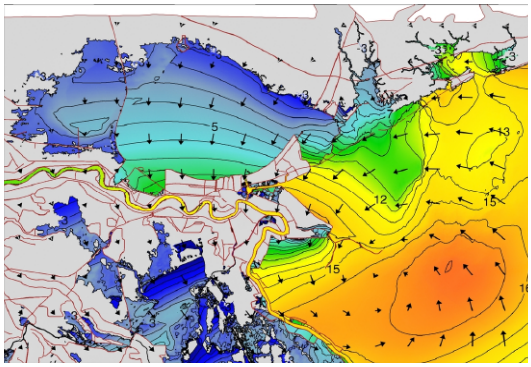

8 am CDT August 29, 2005

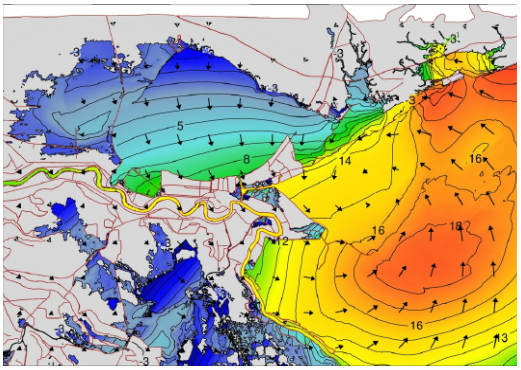

9 am CDT August 29, 2005

Figure 5.5. Hurricane Katrina Surge Dynamics
(approximated using computer simulation)
USACE 2008

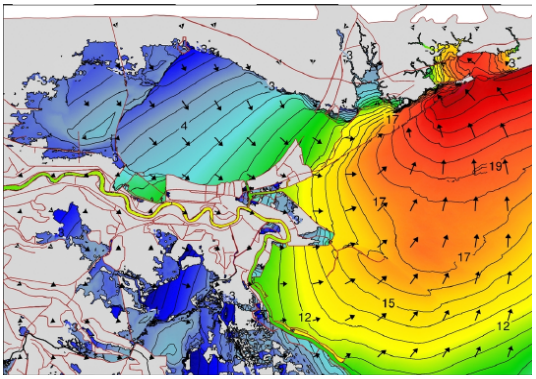

10 am CDT August 29, 2005

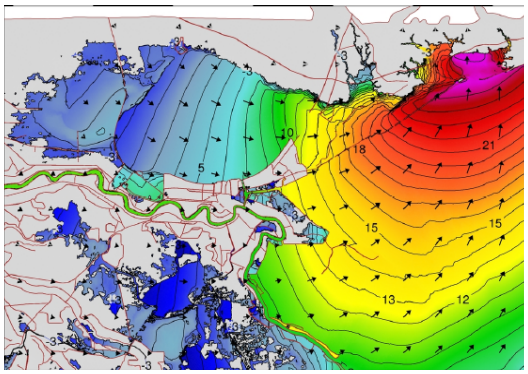

11 am CDT August 29, 2005

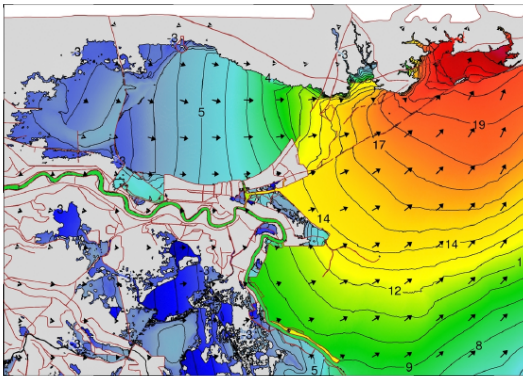

12 pm CDT August 29, 2005

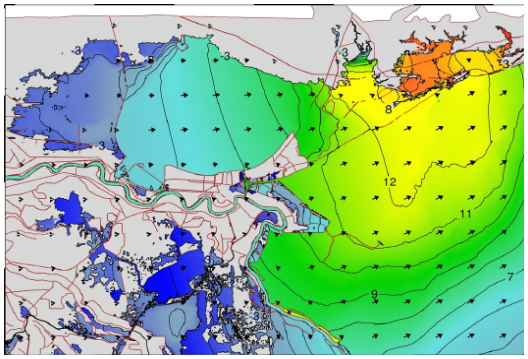

3 pm CDT August 29, 2005

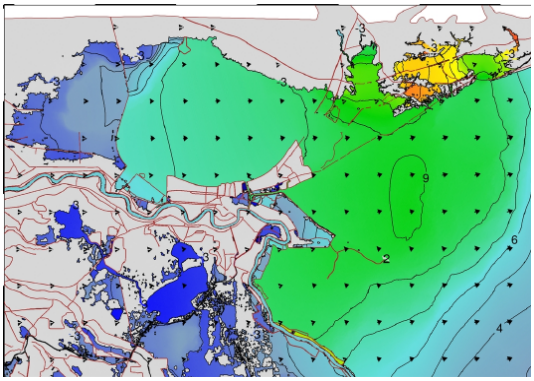

6 pm CDT August 29, 2005

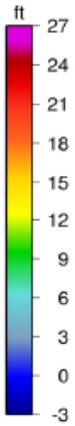

Surge Elevation (NAVD88)

Figure 5.5. (continued) Hurricane Katrina Surge Dynamics
(approximated using computer simulation)
USACE 2008

Section 6. Surge Physics

6.1. Surge SWL Physics

The particular surge dynamics of an individual hurricane are governed by fundamental physical hydrodynamic laws (see Resio and Westerink 2008). The total surge domain at any point in time can be considered as a vast collection of individual vertical columns of water (much like the way a flat image is composed of pixels) The treatment of a water body as a set of vertical columns allows for a two-dimensional (2D, i.e., *x* and *y*) analysis of surge SWL physics in which all exchanges, forces, velocities, and acceleration are considered only in the lateral direction, with a depth averaged value at each column.[1] These physical interactions are governed by three basic laws:

1. Conservation of mass dictates that 1) over the entire domain and duration of the event the total volume of water must remain equal to the initial volume; [2] and 2) over any increment of time the change in water depth (i.e., SWL or η) within each individual water column must equal the amount of water exchanged with the surrounding columns or the atmosphere.
2. Conservation of momentum requires that the net lateral forces acting on each individual column at any *instant* of time must be balanced by the sum of the column's two inertial conditions—the column average lateral acceleration (i.e., rate of change in lateral velocity) with respect to time and space—multiplied by the column's mass (proportional to water depth). If the net forces zero out, then the column has no acceleration. Over any *increment* of time, a change in the net forces on an individual column must equal a change in the mass times acceleration—either the mass, the acceleration, or both.
3. The conservation of energy requires—as with a pendulum—that the kinetic energy of the oncoming surge wave prior to landfall must be translated into to a combination of a) increases in surge potential energy (i.e., rising onshore inundation; b) outgoing wave energy; and c) energy spent on friction and erosion. In equation forms momentum and energy conservation for surge closely mirror each other so reference is typically made simply to the momentum, or force, equation.

The 2D momentum conservation law encompasses ten forces acting on each column. The magnitude and direction of forces are defined in terms of input variables and empirical coefficients (parameters).[3] The first three of the ten lateral forces are familiar from basic open channel flow dynamics and include:

1. *Water pressure,*[4] which is proportional to the difference in depth between adjacent columns.

---

[1] A rigorous analysis decomposes the water body into three-dimensional blocks and considers physical interactions in the vertical as well. The 2D physics are then derived from the 3D on the basis of simplifying assumptions. All applied (as opposed to research) studies currently employ a 2D treatment of hurricane surge physics.

[2] The domain boundary is set far enough away that it is assumed to be unaffected by the hurricane.

[3] Empirical coefficients are obtained from scientific/engineering literature based on experiments or analysis of event data. Input variables are either those generally taken as constants, such as the acceleration of gravity and the specific gravity and viscosity of air and seawater, or those based on measurements or assumptions associated with a particular scenario (e.g., wind conditions). Variables to be solved include the water depth and velocity.

[4] Some forces are commonly expressed in terms of pressure and stress, which are simply forces per unit area (normal and tangential, respectively) to the line of force.

2. *The lateral component of the bed reaction force*—proportional to the bathymetric slope and gravity (and sometimes referred to as a gravity component)—in the direction of downhill. The first two forces can be combined, into a single force proportional t0 the change in η.

3. *Friction,* a drag force (or shear stress) which is exerted laterally in opposition to moving water by bottom roughness and obstructions. Friction is proportional to the water column lateral *velocity squared (V^2)* and an empirical *friction coefficient*. Hydraulic analysis frequently uses a simplified one-dimensional (i.e., channel) equation ignoring water pressure (the Manning's Equation) which estimates a setdown (call a headloss in hydraulics) in the direction of flow proportional to the V^2, the *friction coefficient squared (n^2)*, and the flow path *length*, and inversely proportional to the *depth raised to the four-thirds power*.[5] The combination of the last three terms is called the *conveyance*. The Manning's *n* coefficient depends on the type, density, and submergence of vegetation and other obstructions.

Extensive research on riverine flooding over vegetated floodplains has verified the use of momentum balances involving water pressure, gravity, and friction and provides the basis for Manning's *n* values. However, appropriate Manning's *n* values for surge events are still a subject of ongoing research both in the open ocean, Continental Shelf (Kennedy et al 2011), and overland. For example, as submergence increases the Manning's *n* value for flow over a marsh can drop by up to an order of magnitude. This difference in the friction coefficient can have a significant effect because headloss is proportional to n^2.

A fourth lateral force is added when channel hydraulics are considered in 2D:

4. *Turbulent stress*, which accounts for horizontal eddies (swirls) in the flows that laterally diffuse momentum. This force describes momentum spreading between adjacent columns that is not captured by the other terms depicting momentum transfer at larger scales. The rate of spreading can be considered proportional to an eddy viscosity coefficient and the local velocity gradient. The eddy viscosity coefficient, in turn, can be considered a function of the column width and local velocity gradient condition (after Smagorinsky).

Empirical coefficients for quantifying the influence of horizontal turbulence in momentum balances are not well defined, especially for surge events, and research is needed to improve methods of representing turbulent stress.

Two more lateral forces considered in coastal hydrodynamics are:

5. *Astronomical tides*, which are created by gravitational effects of the sun and moon. The magnitude and direction (onshore versus offshore) of tides are well established and can be readily interpolated to each column.

6. *Coriolis force*, which is caused by the earth's rotation and deflects moving bodies of water to the right in the northern hemisphere in proportion to the latitude

During hurricanes and other storms three additional lateral forces act on the coastal water column:

7. *Atmospheric pressure*, which produces a direct rise of about 4 inches in water level for every 10 mb drop in overlying air pressure with respect to the far field ambient pressure. However, the hurricane CPD primarily influences surge not through the direct rise but by inducing a wind vortex (see Part I).

[5] For narrow channel flow the hydraulic radius is used in place of depth.

8. *Wind drag*, which is a shear stress that moves the water column in the direction of the circulating hurricane winds. Wind drag is a function of the *wind* V^2 [6] and an empirical *air-sea drag coefficient*. The air-sea drag coefficient, in turn, depends on the roughness of the water surface (i.e., wave field). Adequate characterization of hurricane air-sea drag coefficients has been hampered by lack of observations for wave fields and surge velocity. (Powell et al 2003). In onshore areas, wind drag is reduced by sheltering from trees and buildings. In a simple equation wind driven setup is proportional to wind drag and *fetch* (the wind path length over open water) and, importantly, inversely proportional to water depth. The wind drag is responsible for most of the surge SWL rise (Kurian 2009).

   All other factors being equal, maximum storm surge SWL is generally proportional to the wind V_{max}^2—which in turn is generally proportional to hurricane core CPD, (Resio et al 2007). (Part I describes several proposed alternatives to the Saffir-Simpson Scale based on V_{max}^2. For two hurricane storms with equivalent V_{max}^2 but different R_{max}, the larger core storm will exert its wind drag over a larger area. Figure 6.1 illustrates the combined role of core intensity (as measured by CPD) and R_{max} in producing a peak surge for a generic, straight, shallow planar shoreline (Irish et al 2008), with all other hurricane attributes held equal.

9. *Radiation stress* exerted by waves. A dramatic spatial variation in wave heights—such as from nearshore wave shoaling and breaking (see next section)—creates a steep spatial gradient in the radiation stress. The radiation stress gradient is balanced by a corresponding setdown in SWL at the wave breaking point and a setup at the shoreline. These are referred to as *wave setdown and setup* (see Figure 6.2) and contribute to η. The wave setdown at breaking is on the order of 5 percent of the breaking significant wave height. The wave setup is up to 20 percent of the breaking significant wave height. For a breaking significant wave height equivalent to 50% of the depth, the setdown and setup are 2.5% and 10% of the breaking depth. Depending on the local breaking depth at peak surge, the wave setup can contribute about 10 to 30 percent of η along the open coast shoreline (Resio et al 2007). Shoreline geometry and bathymetry can create notable long shore gradients in wave setup, thereby inducing long shore currents.

The 2D physics encompassing these nine forces are “barotropic” as opposed to “baroclinic,” which must add addition equations to describe lateral variations in water temperature and salinity, and thus, density. Researchers are studying three dimensional (3D) surge physics, incorporating vertical density variations as well as a tenth force, (see Resio and Westerink 2008, Dresback et al 2010, Weaver and Luettich 2010, Weisberg and Zheng 2008):

10. *Buoyancy,* which drives relative movement of lighter (warmer, fresher) and heavier (colder, saltier) layers—particularly near coastal passes with high temperature and salinity gradients.

The 3D analysis can be *hydrostatic*, addressing only depth variations in 2D forces and acceleration, or fully 3D, considering actual vertical components of forces and acceleration.

[6] See Section 1, Footnote 1 for a discussion of hurricane wind averaging periods, e.g., 30-, 10-, 1-minute, and 3-s gusts.

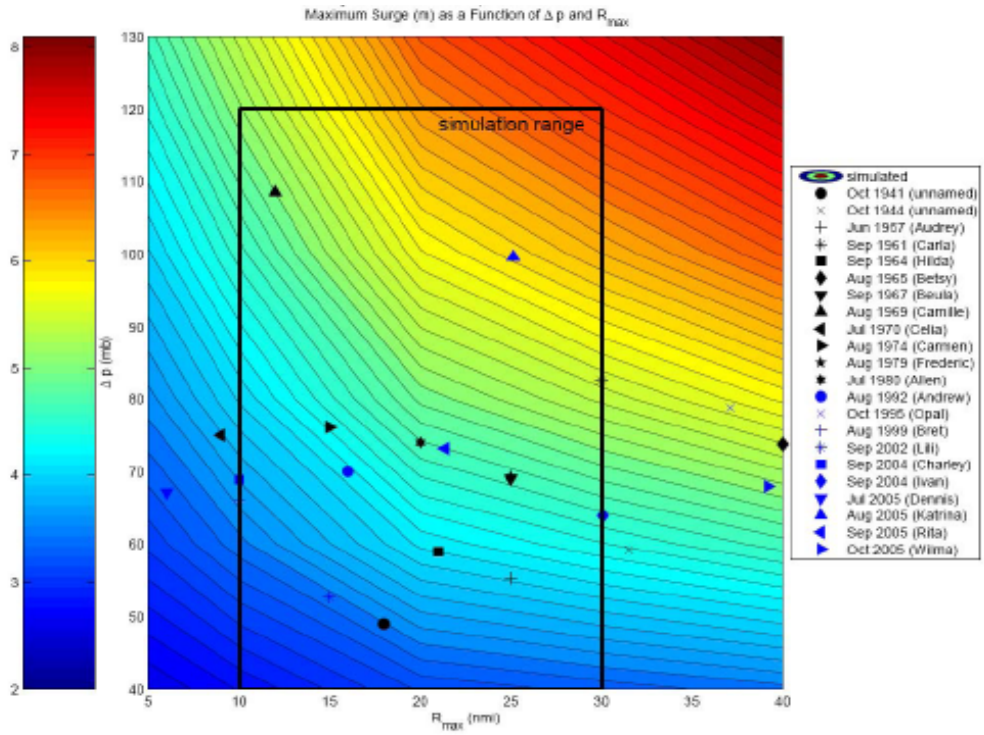

Figure 6.1. Combined Influence of Hurricane Core Intensity and Size on Surge
Irish et al 2008

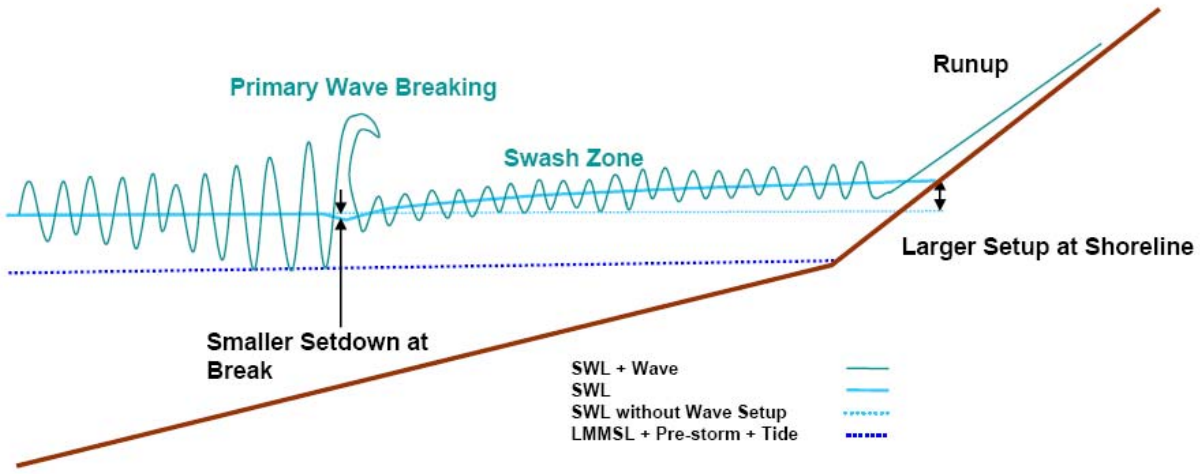

Figure 6.2. Nearshore Wave Setdown and Setup Influence on SWL
(not to scale)

Figures 6.3.a. through d. present a simplified schematic of 2D surge physics, including the shoreward wind drag, seaward bed reaction, and overland friction resistance. With advancing overland surge (Figure 6.3.b.) the landward forces (primarily wind drag and water pressure) are countered by friction and bed reaction. As the surge approaches its inland peak (Figure 6.3.c. or d.) the friction force declines (due to the reduced velocity near peak) and the landward wind drag is balanced by seaward water pressure and gravity. As illustrated in Figures 6.3.c. and d., coastal surge barriers compress the advancing surge and adjust the balance, with landward conveyance obstruction coming at the expense of higher flood-side setup.[7] This aspect of surge physics is clearly shown in Figure 5.5, which shows the setup induced by the southeast Louisiana regional hurricane protection system at various times during Hurricane Katrina.

6.2. Wave Physics

Estimating the potential contribution of waves to hurricane hazards—both to SWL setup as noted above and through the waves themselves—requires understanding wave physics. Eight important wave physical processes include (see Dean and Dalrymple 1991):

1. Open ocean wave generation, which depends on wind velocity and fetch and provides the basic deep water irregular wave field conditions (H_s, T_p) prior to waves entering the Continental Shelf zone.
2. Wave shoaling, in which wave heights increase and wavelengths shorten due to reduced depth. As Hurricane Ivan (2004) crossed from the deep Gulf of Mexico onto the Continental Shelf (east of the Mississippi River delta) significant wave and maximum wave heights were estimated to exceed 60 and 120 feet, respectively (Wang et al 2005).
3. Friction, (e.g., muddy bottoms, wetland vegetation for inundated coasts) which can reduce wave heights through energy dissipation (Anderson et al 2011)
4. Wave breaking at limiting depths. As depth declines, waves reach a point at which they break. H_s:depth ratios have been proposed at 0.4 to 0.7 depending on local conditions (USACE 2010). Nearshore wave data collected along the Texas coast during Hurricane Ike (2008) showed that breaking H_s was about half the SWL depth (Kennedy et al 2010). For overland waves in inundated vegetated terrain, a ratio at the lower end of the range would be expected, but research for such conditions is very limited. Research is also limited on characterizing wave height distributions in various post-break environments.
5. Wave regeneration in interior bays, lakes, and large channels.
6. Wave field transformations (H_s, T_p) due to interactions with surge currents.
7. Wave field refraction (bending due to incident angle interaction with the general bathymetry), diffraction (bending around obstacles and after passage through openings, such as barrier islands, passes, and headland points), and reflection. These processes can cause wave energy to become focused at particular locations.

[7] A detailed study of surge dynamics in southeast Louisiana absent the current regional hurricane protection system has not been undertaken.

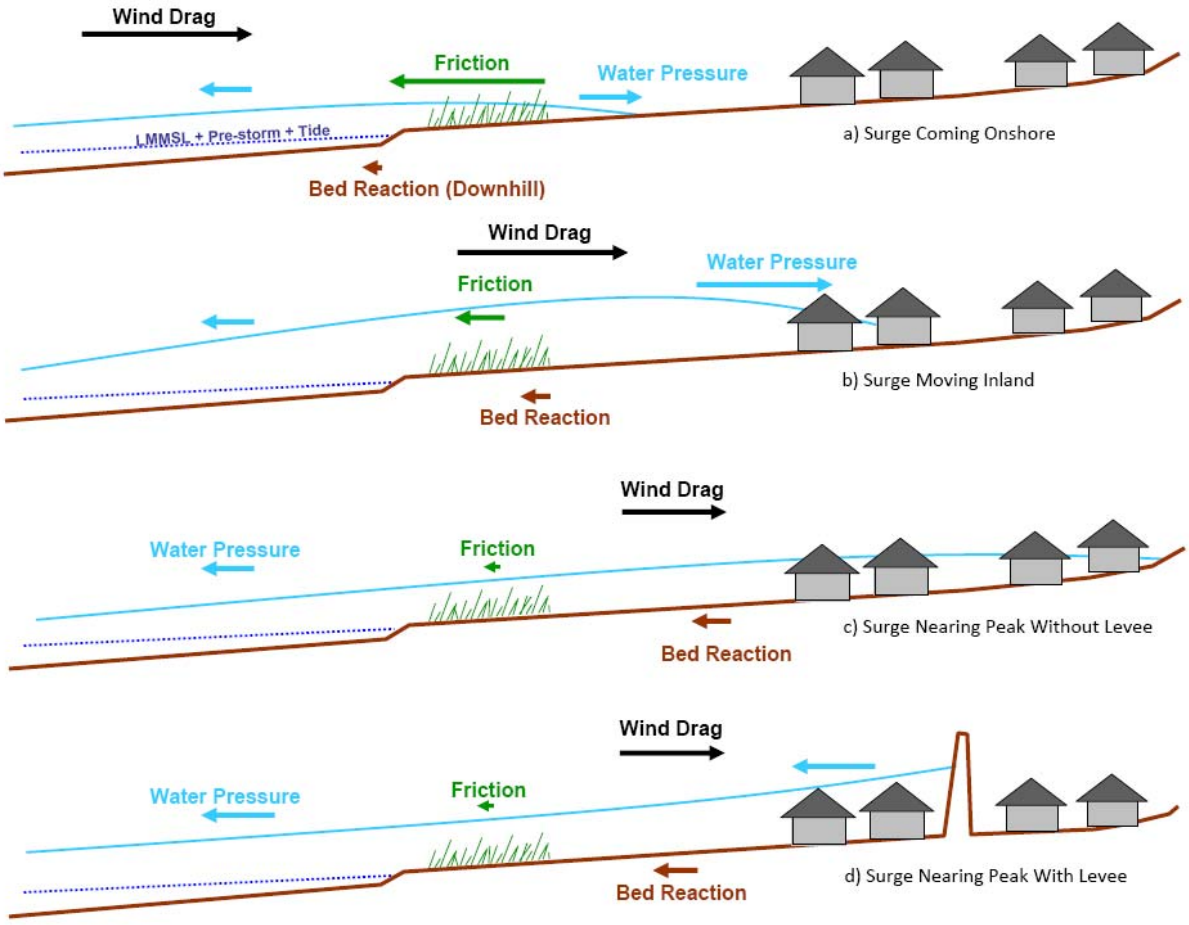

Figure 6.3. Simplified Schematic of Surge Physics
(not to scale)

8. Wave runup, which occurs when a broken wave rolls up the shore face. The wave momentum pushes water up the slope to a height greater than that of the nearshore pre-break wave (see Figure 6.2). The runup height depends on the pre-break wave height, wave steepness, shore slope, and slope roughness. The runup height of the maximum wave is referred to as the maximum runup.

Data depicting wave processes in shallow interior water bodies and over land during hurricanes is very sparse. Available empirical equations describing these processes rely primarily on idealized laboratory experiments or observations for nearshore conditions less dynamic and less extreme than hurricanes. In addition, the short time over which peak surge conditions occur may reduces the applicability of empirical generalizations derived for near-steady wave fields. Thus, extensive research on hurricane wave conditions is required to improve confidence in their mathematical representation.

Section 7. Surge and Coastal Landscape Interactions

Surge dynamics result from a hurricane's attributes (core intensity, size, wind field distribution, forward speed, and track) setting a quantity of Gulf of Mexico water in motion, and the interaction of that large moving mass of water with the landfall area coastal landscape features, as governed by the physics of mass and momentum conservation. Coastal landscape features interact with three specific aspects of the regional and local surge physics: wind setup, surge conveyance, and wave processes (see Interaction of Hurricane and Coastal Landscape Features: A Literature Review, Suhayda and Jacobsen 2007). Coastal landscape features occur at a range of scales—regional to local--and often influence two, or even all three, aspects of surge physics.

7.1. Features Influencing Wind Setup

Coastal features influence wind setup through sheltering (reducing wind) or by affecting fetch or water depth. Such features are present at a wide range of spatial scales, with the largest features having the greatest potential impact. An important large-scale, coastline geomorphologic feature influencing wind setup is the presence of an extensive, shallow Continental Shelf, such as in the northeastern Gulf of Mexico. The counterclockwise winds of hurricanes approaching Mississippi River Delta will exert a westward drag across the lengthy fetch of the relatively shallow shelf fronting the Mississippi/Alabama/Florida Panhandle, shown in Figure 7.1. The combination of an intense westward wind drag, long fetch, and shallow depth creates the potential for significant wind setup along the eastern flank of the Delta. The wind setup is enhanced in those cyclones that enter the eastern Gulf of Mexico and traverse westward, e.g., Hurricanes Betsy (1965) and Katrina (2005). Even hurricanes that make landfall in southwest Louisiana or eastern Texas can drive significant surge into the eastern Delta and Lake Pontchartrain if they exert a sustained and heavy wind drag along this portion of the Continental Shelf. e.g., Hurricanes Rita (2005) and Ike (2008).

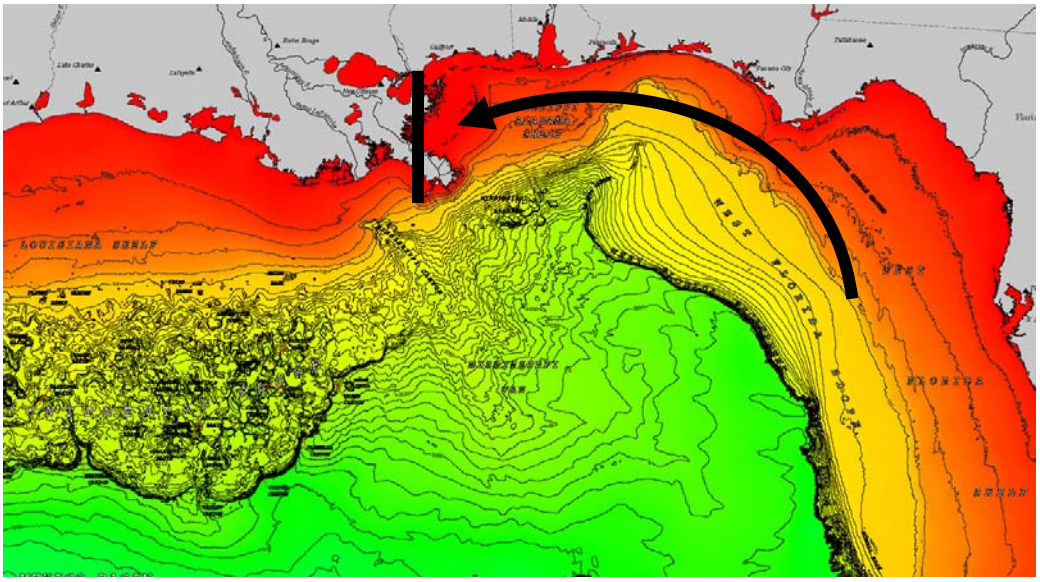

Figure 7.1. Bathymetry of the Gulf of Mexico Continental Shelf
http://ngdc.noaa.gov/mgg/ibcca/images/1234.jpg

In 2010 Fitzpatrick et al evaluated surge differences for a hypothetical coastline—with a range of shelf bathymetric slopes over a perpendicular offshore distance of 200 miles—for a variety of hurricanes. As illustrated in Figure 7.2, they found that shallow shelves can produce surge more than twice as high as deep shelves, consistent with wind setup physics. The authors further evaluated the role of shelf bathymetry with a combined hurricane size-intensity factor ($IKE^{1/2} * V_{max}$, see Part I) on surge. Figure 7.3 indicates that surge approximates a linear function of the size-intensity factor at various bathymetries.

It is important to note that the influence of shelf bathymetry on surge is different than for a tsunami. For hurricane surge, a long shallow shelf amplifies the wind setup which results from wind drag acting across many tens of miles of water surface. A tsunami wave is generated at a particular offshore location and propagates toward the coast. Against a steeper coastal bathymetry the tsunami compresses more rapidly and produces a higher SWL; whereas a shallow shelf causes the tsunami to dissipate energy, producing a lower SWL over.

Large scale coastal protrusions like the Mississippi River Delta also affect hurricane winds. As storms approach landfall near those protrusions, winds rotating into the left front quadrant experience increase land drag, which can lead to storm infilling and decay (see Part I). Similarly, expansive forested coastal landscapes can produce more infilling than open marsh. The core intensity of major hurricanes are more likely to be affected by land-wind interaction than less powerful storms.

Two significant types of local scale wind setup features include:

1. Barrier islands and long headland spits, ridges, and cheniers (e.g., Grand Isle, Caminda Headland, Bayou La Loutre, Chenier Caminda). These features, particularly when densely forested, can reduce wind drag in leeward sounds, bays, lakes, and inundated areas.

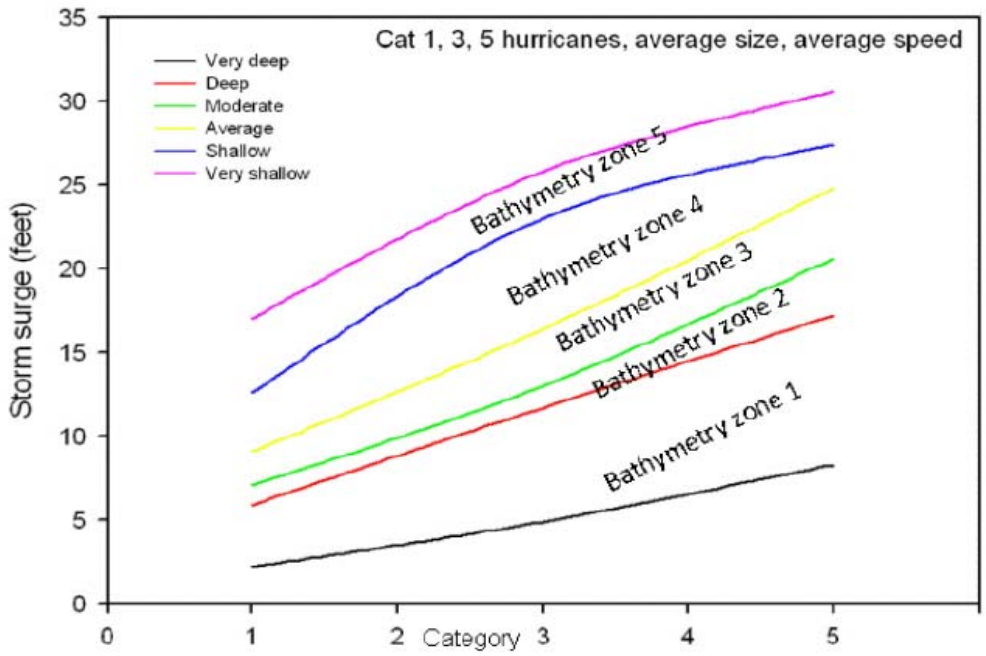

Figure 7.2. Influence of Shelf Bathymetry on Surge for Hurricanes by Category
Fitzpatrick et al 2010

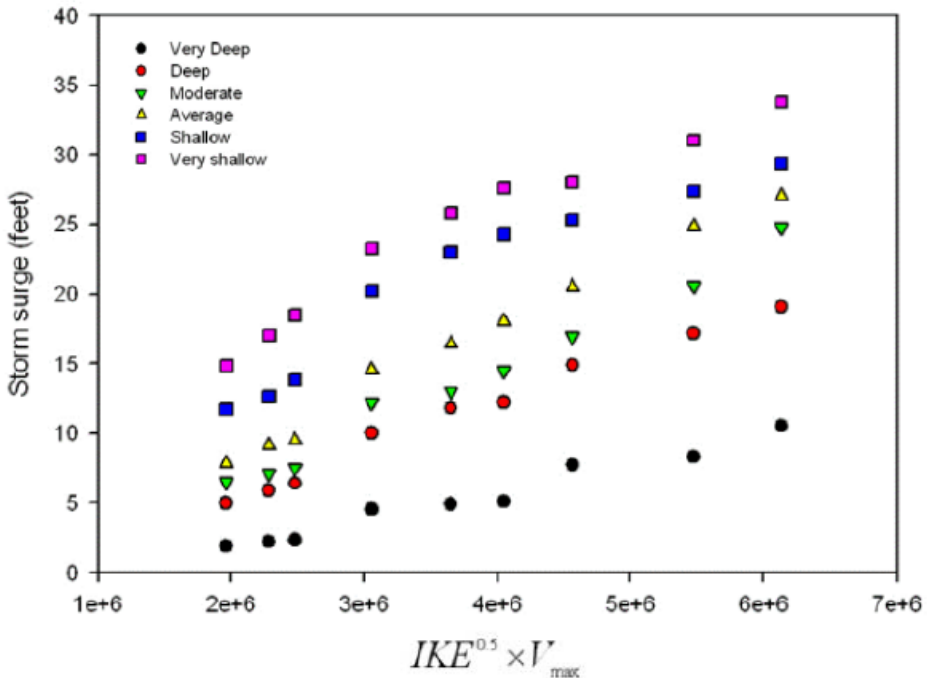

Figure 7.3. Influence of Shelf Bathymetry on Surge for Hurricanes by IKE-Vmax Factor
Fitzpatrick et al 2010

2. Large, shallow sounds, bays, and lakes. Hurricane winds readily "fill and tilt" Lakes Borgne, Pontchartrain, and Maurepas. Hurricane Katrina first filled Lake Pontchartrain, raising SWL to about 5 ft, and then exerted strong northerly winds over the lake as it passed just to the east, tilting water up onto the south shore to elevations over 12 ft. In 1979 Crawford employed the newly developed Sea, Lake, and Overland Surge from Hurricanes (SLOSH) model to study the varied impacts of hurricane winds acting across Lake Pontchartrain based on track, see Figure 7.4.

The effect of local features depends on the particular wind field strength, duration, and orientation.

7.2. Features Influencing Conveyance

Conveyance features—through variations in the flow length, depth, and friction coefficient (Manning's *n*)—divert surge movement. The exponents of the conveyance headloss variables—length, depth$^{4/3}$, and Manning's n^2—influence their relative importance. Five important categories of conveyance features are illustrated in Figure 7.5, and include:

1. Flood protection and other hydraulic control structures. These structures are purposefully designed to obstruct and divert the movement of surge. In reducing flood depths on the protected side they necessarily increase flood side setup. Regional examples of flood protection and other hydraulic control structures include:

   - HSDRRS levees and floodwalls;
   - Navigation locks. e.g., IHNC, Algiers, Harvey;
   - Floodgates, e.g., Gulf Intracoastal Waterway (GIWW) and Seabrook; and
   - Channel weirs/closures, e.g., Mississippi River Gulf Outlet (MRGO) at Bayou La Loutre.

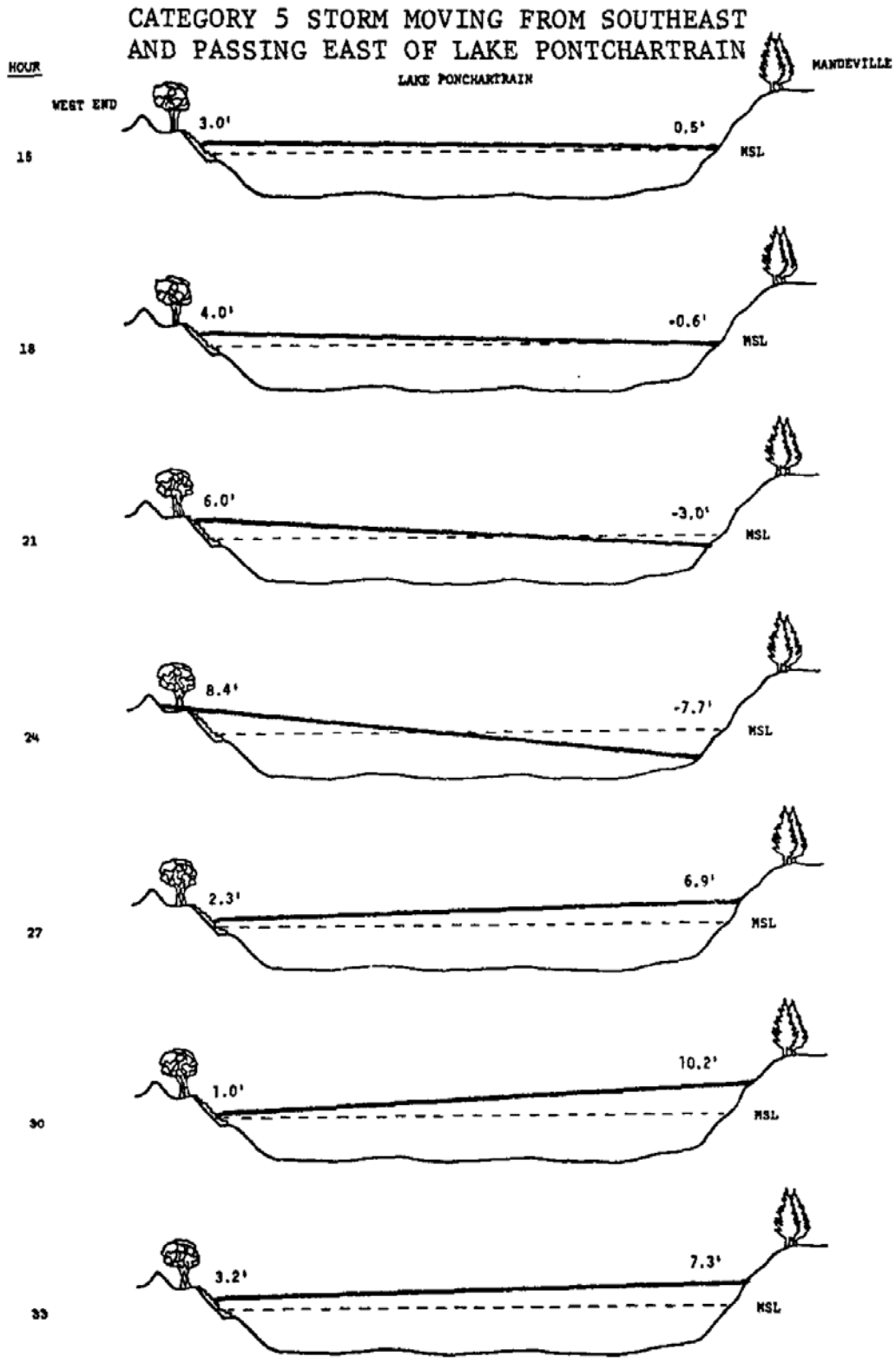

Figure 7.4. Tilting of Lake Pontchartrain in Response to Strong Hurricane
Crawford 1979

a. Hurricane Protection Levee: Plaquemines Parish Levee at Braithwaite LA, Hurricane Gustav

b. Hurricane Protection Floodwall: Industrial Canal Floodwall, Hurricane Gustav

Figure 7.5. Photographs of Coastal Conveyance Features

c. Hydraulic Structure: Mississippi River Gulf Outlet Closure Structure

d. Railroad Embankment: CSX Railroad Crossing, New Orleans East
(U.S. Army Corps of Engineers photo)

Figure 7.5 (continued) Photographs of Coastal Conveyance Features

e. Barrier Islands: Chandeleur Islands

f. Coastal Headland: Caminada Headland

Figure 7.5. (continued) Photographs of Coastal Conveyance Features

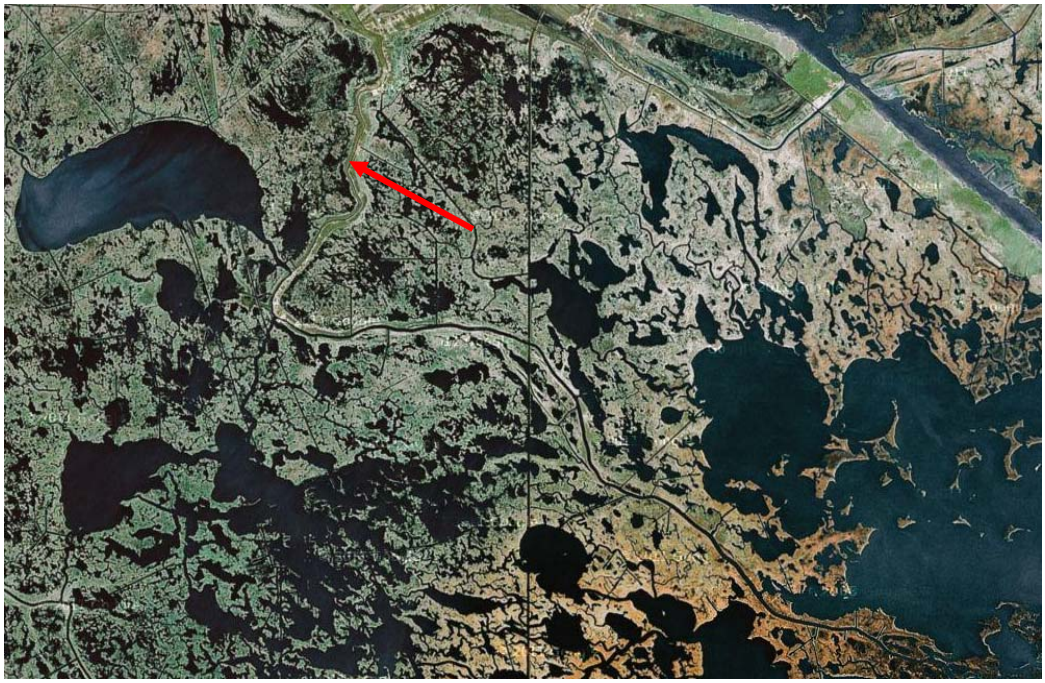

g. Coastal Ridge: Ridge Along Bayou Terre aux Boeufs

h. Coastal Pass: Chef Menteur Pass

Figure 7.5. (continued) Photographs of Coastal Conveyance Features

i. Coastal Forest: Maurepas Swamp

j. Coastal Marsh: Delacroix Marsh

Figure 7.5. (continued) Photographs of Coastal Conveyance Features

k. Coastal Channel: Mississippi River Gulf Outlet Reach 2
looking east at Bayou La Loutre

l. Interior Channel: Junction of Mississippi River Gulf Outlet Reach 2 (Left) and Gulf Intracoastal Waterway (Foreground) and Reach 1 (Extending under the Paris Road Bridge), "The Funnel"

Figure 7.5. (continued) Photographs of Coastal Conveyance Features

2. Other man-made embankments. These features consist primarily of built-up earthen subgrades for roads, railroads, and bridge approaches and are potentially important to surge conveyance when they transect low-lying coastal marshes and swamps. Examples include:

   - The CSX and Norfolk-Southern railroad embankments in New Orleans East;
   - The Canadian Northern railroad embankment along Lake Pontchartrain in St. Charles Parish;
   - US Highway 90 in New Orleans East; and
   - Louisiana Highways 46 and 300 in eastern St. Bernard and Plaquemines Parishes

3. Natural topographic barriers. Significant natural topographic barriers include:

   - Barrier islands, e.g., Chandeleur and Breton Islands;
   - Headland dune complexes, e.g., Caminada Headland;
   - Cheniers, e.g., Chenier Caminada; and
   - Inland ridges and remnant distributary natural levees, e.g., Bayou LaLoutre Ridge in St. Bernard Parish. Extended ridges, known as *land-bridges*, particularly those that are accompanied by man-made roads or railroad embankments, are important conveyance obstructions. Examples include the New Orleans East and Manchac land-bridges.

   As with flood protection structures, road/railroad embankments and natural topographic barriers can obstruct and divert the movement of surge. The degree of conveyance control exerted by these features depends on:

   - Barrier Length. Given the size of a surge long wave, short features have little effect on surge events;
   - Elevation. To be effective as a surge barrier the feature cannot be submerged;
   - Gaps. Numerous or large openings substantially reduce the effect on surge;
   - Erodibility. Features made of fine sands, silts, or noncohesive organic material may not withstand surge hydrostatic, wave, and overtopping forces; and
   - Armoring. Man-made embankments that are hardened (e.g., asphalt and concrete roads, rip rap armored slopes) and natural ridges that are well vegetated are more likely to withstand erosion.

4. Land cover. Lengthy flow paths with high friction can absorb significant surge energy, ultimately reducing the inland setup (Loder 2008). The Manning's *n* value for densely vegetated wetlands (e.g., forested swamps with heavy underbrush) can be up to five times greater than for broken marsh and up to ten times greater than for open water.

5. Preferential conveyance pathways. These include:

   - Passes and inlets, e.g., Caminada, Barataria, Rigolets and Chet Menteur Passes;
   - Large coastal/estuarine waterbodies, such as sounds, (e.g., Breton, Chandeleur, and Mississippi), bays (e.g., Barataria, Terrebonne), and lakes (e.g., Borgne, Pontchartrain, and Maurepas);
   - Coastal channels, e.g., the Mississippi River below Venice and the MRGO Reach 2 (see discussion below on impact relative to surge conditions);
   - Interior channels, e.g., the Mississippi River above Venice, MRGO Reach 1.

A very important large-scale conveyance feature in southeast Louisiana is the eastbank Mississippi River Delta—comprised of the remnant marshes and ridges in St. Bernard delta (e.g., Biloxi and Delacroix marsh), Plaquemines delta, and Beliz delta. As shown in Figure 7.1, hurricanes that create massive westerly wind setup along the northeastern Continental Shelf (see above) squeeze surge against the eastern flank of the southward extending Delta. Such surges are further trapped and compressed by the extension of the Biloxi Marsh and New Orleans East land-bridges across the mouths of Lakes Borgne and Pontchartrain. The overall effect is that surge is pushed into a "corner"—much like a drum of water spilled into the corner of a room—with the communities of Waveland and Bay St. Louis at the vertex. In addition to this large-scale corner, there are local corners including the junction of HSDRRS structures along the MRGO and GIWW at the IHNC Surge Barrier, and the junction of the HSDRRS levee with the Mississippi River Levee at Caernarvon.

7.3. Features Influencing Wave Processes

Wave features influence one or more of the seven processes described above and can be located in any of the various zones. The most important class of wave features are those that affect breaking and regeneration. Figure 7.6 provides examples of wave features. Seven important categories include:

1. Offshore expansive shoals, reefs, mud lumps, and submerging barrier islands, which can transform and possibly break the large ocean waves, (e.g., Ship Shoal, Chandeleur Islands);
2. Barrier islands and long headland spits and ridges (e.g., Grand Isle, Caminada Headland, Bayou La Loutre Ridge) which reduce surface winds and leeward wave regeneration.
3. Non-flood protection embankments and natural topographic barriers, which act as inland breakwaters (e.g., roads, railroads, ridges).
4. Large shallow coastal/estuarine water bodies over which winds can generate substantial waves (e.g., Lakes Borgne, Pontchartrain, and Maurepas).
5. Land cover and water bottom. The same friction sources that reduce conveyance can also dampen waves, enhance wave breaking, and reduce wave regeneration when they are not overly submerged, e.g., forest swamps with heavy underbrush (Loder 2008). In addition, the presence of a thick layer of viscous mud can transform waves.
6. Breakwaters (continuous or segmented). They are typically located in the nearshore (e.g., Fourchon, and Grand Isle) or foreshore (e.g., the south shore of Lake Pontchartrain).
7. Shoreline erosion stabilization. These features are designed to mitigate erosion by direct wave attack and long shore currents, and manage the transport and deposition of sediments. Coastal sediment controls include jetties, groins, and foreshore armoring. Major regional jetties include those at the mouth of the MRGO and Barataria, Caminada, and Fourchon Passes. Examples of shore armoring include foreshore rip rap (e.g., Lakes Borgne, Pontchartrain, and numerous other water bodies), concrete stepped seawalls (e.g., Lakefront Park in New Orleans), and sheet pile bulkheads (primarily along the banks of developed properties). These features reinforce the shoreline and hold the slope and foreshore in place. When the shoreline become submerged armoring can play a role in wave breaking, particularly if it is elevated above the shore.

These features also affect local hurricane waves through wave refraction, diffraction, and reflection, as well as interactions with surge currents. Local coastal features can produce complex variations in wave heights (up to several feet) and wave setup (greater than one foot) over short distances.

a. Breakwater: Fourchon Beach

b. Jetty: Belle Pass

Figure 7.6. Photographs of Coastal Wave Features

c. Shoreline Armoring: Foreshore Protection Along Lake Pontchartrain

d. Shoreline Bulkhead

Figure 7.6. (continued) Photographs of Coastal Wave Features

7.4. Impact of Coastal Features Relative to the Surge Conditions

Crucially, the particular influences of coastal features are affected by the specific surge conditions. Drowning of a feature during extreme surge events significantly diminishes its impact, compared with its influence for smaller surges or tides alone. Employing the analogy of the drum of water spilled on the floor, the bulk of the spill can only be controlled by large continuous features—small raised bumps and cracks in the floor will not divert the water until the depth gets down to a thin film.

As noted earlier, the surge flow resistance and wave breaking by coastal marshes and forest underbrush are significantly affected by the degree submergence. (Forest trees themselves can be too widely spaced to influence surge but may reduce wave transmission and regeneration.) Simple reductions in surge per distance traveled over marsh—e.g., the old "rule of thumb" of one foot of surge reduction per 2.7 miles of marsh—are not reliable (Suhayda and Jacobsen 2007, Resio and Westerink, 2008).

Loder (2008) modeled the influence of marsh—bottom elevation, depth-independent friction, and continuity—on surge SWL and wave heights in an idealized domain. Loder found SWL reduction was highly sensitive to surge magnitude, even without taking into account Manning's *n* depth-dependency. Increasing *n* from 0.002 to 0.2 reduced inland SWL, but these reductions varied between 35 and 76% as levels of inundation were reduced. At constant *n* of 0.005, the SWL reduction varied between 2 and 52% depending on depth alone. However, H_s reduction over marsh was much less sensitive to surge magnitude, with consistent 60+% reduction.

Wamsley et al (2009) provided a preliminary assessment of the influence of marsh conditions on surge. Using the Caernarvon Marsh, the authors applied a simple fixed adjustment to the regional topography, and thereby modified the associated percentage of land cover types (based on elevation). The authors used three topographic/land cover scenarios (base, degraded, and restored). Due to the basic scope of their investigation they only used constant (not depth dependent) Manning's *n* values for each land cover type. They then compared surge results for two hypothetical hurricane simulations on identical tracks—a large moderate storm (similar to Hurricane Hilda) and a large intense storm (similar to Hurricane Katrina). Figure 7.7 shows the results for reduced peak surge and maximum waves for the base versus degraded condition. In this analysis, the degraded marsh had surge heights up to 90% higher, and maximum wave heights up to three feet higher, than the base condition for the intense storm. Given the basic analysis, the authors were not able to distinguish between the contributions of topography and land cover modifications. Additional research is needed on the effects of changing topography and land cover, incorporating depth-dependent Manning's *n*.

The role of coastal channels surrounded by expansive low-lying marsh in conveying surge is also stage dependent. An important and often misunderstood example is the influence of the coastal MRGO Reach 2, as compared to the interior Reach 1 (Figures 7.5k and l), during Hurricane Katrina (Jacobsen and Suhayda 2006, Ebersole et al 2010). Coastal channel conveyance is very significant during low to moderate surge events—as it is for typical tide and weather mediated exchange. However, during more extreme surges the vast majority of flow is likely to occur overland and the importance of the channel conveyance diminishes. Similarly, embankments and natural ridges can mitigate low-to-moderate surge but may provide very little reduction of extreme surges.

The lesser relative impact of certain coastal features on extreme surge is an important consideration in prioritizing wetland "multiple lines of defense" for urban surge protection, shown in Figure 7.8 (see Lopez 2008). Features which do not sufficiently contribute to high hazard protection may not warrant investment for urban flood protection. However, for less urbanized coastal communities, enhancement

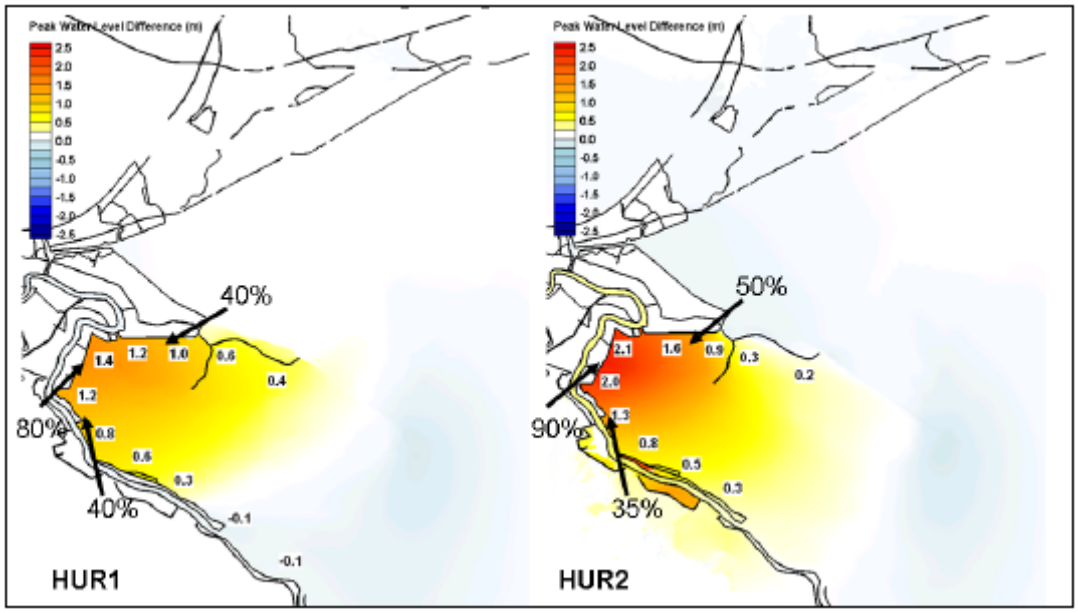

a. Peak Surge Difference

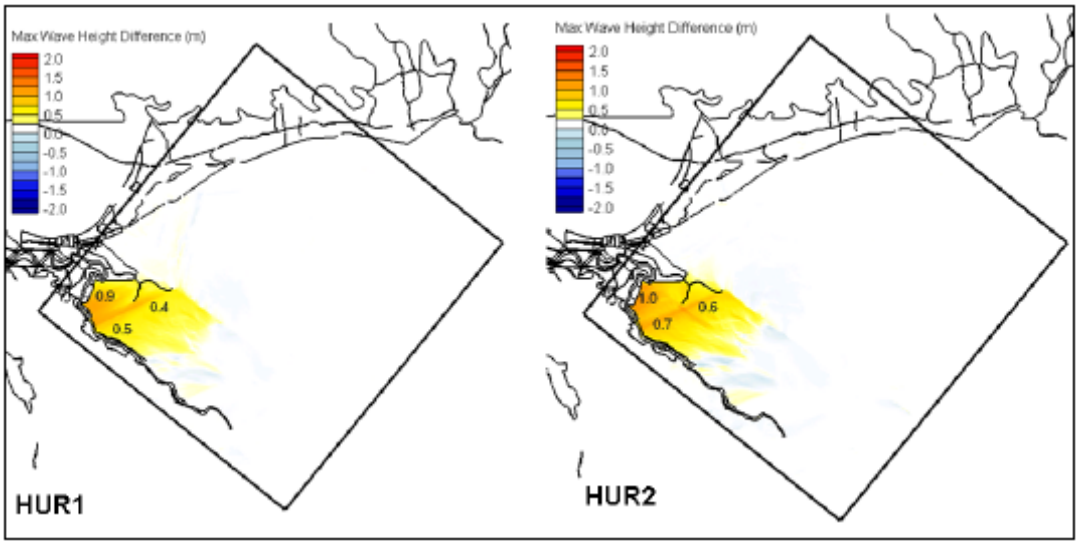

b. Maximum Wave Height Difference

Figure 7.7. Difference Between the Degraded and Base Caernarvon Marsh Conditions
Hurricane 1—Large, Moderate (Hilda); Hurricane 2—Large, Intense (Katrina)
(Wamsley et al 2009)

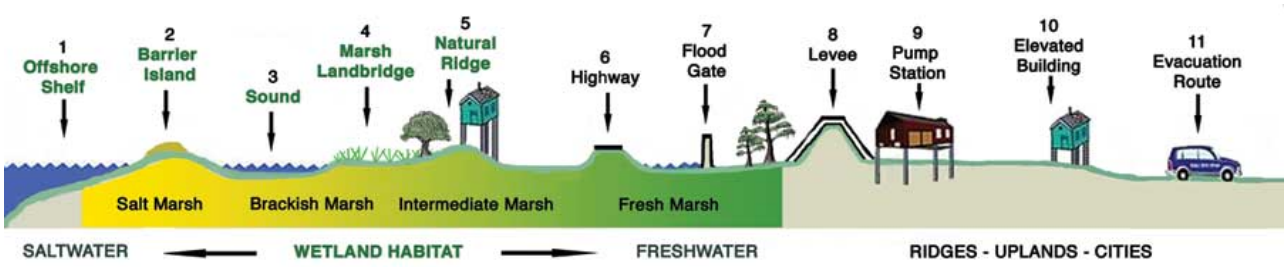

Figure 7.8. Multiple Lines of Defense Strategy
Lopez 2008

of low-lying features may provide cost-effective protection against lower (typically more frequent) surges. Low-lying features may also be cost-effective in mitigating the assaults of recurring modest surges on fragile ecosystems, such as shoreline erosion and saltwater damage along the MRGO Reach 2.

Massive urban surge protection systems can have significant negative coastal ecosystem impacts. The higher setup created by these systems (see Figure 6.3.d) can alter coastal circulation, erosion, and deposition patterns associated with storm surges. An example is the erosion in the Canaervon Marsh during Hurricane Katrina. Depending on their design, these systems can also disrupt normal estuarine tidal flow and water quality (e.g., see discussions regarding the proposed Morganza to Gulf Project, http://www.mvn.usace.army.mil/prj/mtog/feasibility_study_documents/mtog_index.htm).

Importantly, coastal features can have very different impacts depending on a storm's track and associated surge orientation. Surge setup against Grand Isle was from Barataria Bay (on the north side of island) during Hurricane Katrina, but from the Gulf of Mexico (on the south side) during Hurricane Gustav. Thus, shoreline breakwaters, enhanced dunes, and other features on Grand Isle have different impacts depending on whether surge is approaching from the north or south.

Impacts can also vary over the course of a storm as wind direction reverses. Prior to its closure at Bayou La Loutre, the MRGO Reach 2 (Figures 7.5c and k) conveyed early surge from Breton Sound toward New Orleans. But at the time surge peaks at the confluence with Reach 1 and the GIWW (called "the funnel," Figure 8.4l), Reach 2 conveyed surge outward to Breton Sound (see Jacobsen and Suhayda 2006). Figure 8.9 illustrates the reversal in the SWL difference along Reach 2 with and without Reach 2 closure for a storm similar to Hurricane Betsy (the green line is the headloss without the closure, the orange line is with the closure). The headloss reverses several hours prior to the peak at the upper end of Reach 2 (at the Paris Road Bridge). In this example Reach 2 closure raises peak SWLs in upper Reach 2 (the red line peak is higher than the blue line peak). As expected though, the effect of Reach 2 closure in raising the Paris Road peak SWL is small given that most of the regional conveyance is outside the MRGO. (The analysis was done prior to construction of the IHNC Surge Barrier.)

The complexity of surge-landscape interactions means that careful analysis is required in planning for coastal improvements.

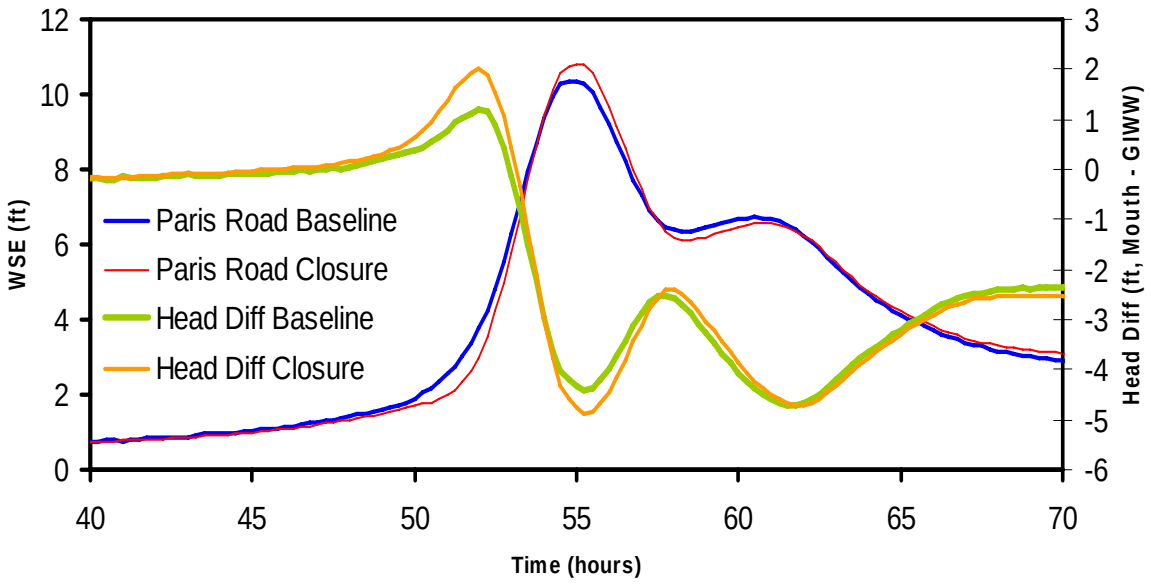

Figure 7.9. Changes in Paris Road SWL and MRGO Reach 2 Headloss with Reach 2 Closure for Betsy-Like Hurricane
(prior to construction of IHNC Surge Barrier)

Subpart B. Hurricane Surge Modeling

Leading scholars in the field of coastal hydrodynamics have developed sets of mathematical equations to capture the physics-based descriptions of hurricane surge dynamics presented in Part II Subpart A. To solve these equations in the context of subtle surge-landscape interactions they have researched methods for producing highly detailed representations of coastal conditions (e.g., topography and friction at a scale of tens of meters). Scholars have also addressed the severe numerical, coding, and computational challenges associated with solving time-varying surge SWL and wave equations for a large high resolution domain. One key advancement has been the porting of models to High Performance Parallel Computing (HPPC) systems. Together, these hydrodynamic equations, landscape representations, codes, and numerical and computational methods constitute what are called hurricane surge models. Furthermore, since all models are necessarily approximations of actual surge phenomena,[1] scholars have examined the effects of simplifying physics (e.g., ignoring buoyancy forces), generalizing landscape conditions (e.g., smoothing terrain), and selecting particular computational techniques.

Following the disastrous hurricane seasons of 2004-05, which saw seven major hurricanes in the Gulf of Mexico, four of which made landfall at major status along the CN-GoM, practical applications of high resolution surge modeling have been sought by surge risk managers, including those at FEMA (for FISs), the USACE (for flood protection and coastal restoration planning and design), and other public agencies and private parties. Governmental agencies have partnered with universities and the engineering community to provide modeling approaches which satisfy project requirements. These partners are also continuously working to improve modeling techniques.

This Part II Subpart B discusses the following topics:

> Section 8., technical approaches and general issues associated with high resolution modeling of surge SWL physics;
>
> Section 9., technical approaches and general issues associated with high resolution modeling of surge wave physics;
>
> Section 10., the ADvanced CIRCulation (ADCIRC) model—and its coupling with wind field and wave models—which FEMA and the USACE primarily rely on to characterize surge and wave hazards throughout the Gulf of Mexico and South Atlantic; and
>
> Section 11., recent applications of high resolution surge models and quality of hindcast results.

These sections address both current and evolving methodologies in high resolution modeling. A key source of information for these sections is a recent summary by Jacobsen et al (2010) for FEMA

The reader is encouraged to consult GTN-1 for an introduction to concepts involved in evaluating model accuracy and precision, and sensitivity, calibration, and validation testing for model performance.

The ensuing Part III addresses how information on regional hurricane climatology (presented in Part I) is combined with surge modeling (addressed herein) to provide hurricane surge return frequency analysis.

---

[1] The famous saying: "essentially, all models are wrong, but some are useful," (by the statistician George E. P. Box) emphasizes the point that models have to simplify reality to some degree and their potential weaknesses in accuracy and precision (see GTN-1) should be understood before employing them.

Section 8. SWL Modeling

8.1. General Background

Hurricane surge SWL (or η) modeling is an extension of coastal hydrodynamic modeling for tidal and meteorological driven circulation. *History of Coastal Inundation Models* (Massey et al 2007) reviews the evolution of these models. FEMA in support FISs, NOAA in support hurricane emergency evacuation and response, the USACE for planning hurricane protection systems, and the Navy for support of nearshore operations have been the principal sponsors for the development and application of surge SWL models in the United States. These agencies frequently coordinate on aspects of surge modeling, funding leading university researchers and sharing code developments. In particular, the USACE—through its Coastal and Hydraulics Laboratory (CHL)—has worked closely with FEMA on regional surge studies (such as the surge hazard analysis for southeast Louisiana).

The hurricane wind field is the primary force responsible for generating surge SWLs and waves, with atmospheric pressure deficit and wave radiation stress gradients also contributing to η. Hurricane SWL and wave modelers typically use NOAA H*Wind files—as described in Part I—and atmospheric pressure data to perform hindcasts, including those undertaken for sensitivity, calibration, and validation testing. For synthetic hurricane surges, modelers create wind and pressure fields with vortex models—also described in Part I—which are based on inputs for the track, the central pressure deficit (CPD), the radius to maximum winds (R_{max}), the wind field profile (Holland B), asymmetry, intensification, and decay. Uncertainties with H*Wind files and vortex models can have a major influence on surge modeling results, as wind setup is proportional to wind velocity squared. Thus, a ten percent error in wind speed can easily translate into a twenty percent error in the estimated setup.

Currently, surge hazard analysis employ surge models representing 2D physics using one equation for mass conservation and two for momentum (one for the east-west, x, direction and one for the north-south, y, direction). The three equations are known as the Shallow Water Equations (SWEs), and are partial differential equations written in the mathematical language of calculus. Specific formulations are developed to incorporate the various terms (described in Section 6) and used to solve for the three dependent variables throughout the geographic domain over which surge is being evaluated: the SWL setup (η) and two depth-averaged velocity components (u and v).[1]

Surge SWL modeling requires translating the SWEs into numerical approximations—using finite algebraic terms—that can be solved with a computer. The algebraic equations are incorporated into engineering software code that simultaneously solves for η and depth-averaged u and v at each surge water column, for any point time. These models are termed *dynamic* (or *unsteady, transient,* or *time-dependent*) as they seek to describe conditions as they vary during the course of the event.

2D surge codes simulate hydrodynamic processes—which are *naturally continuous,* spatially and temporally—as a series of *artificially discretized* spatial and temporal steps. The lateral spatial intervals

[1] In ocean physics the 3D Navier-Stokes equations form the basis for a complete physical analysis. The SWEs, also known as the Saint Venant equations, are derived from the 3D Navier-Stokes equations assuming hydrostatic conditions, negligible, baraoclinic forces, and applicability of depth-averaging (for example, see Dawson and Mirabito, 2008). 3D analysis is primarily the focus of academic research (e.g., under funding by the U.S. Navy Research Laboratory, NRL, and other agencies). A full 3D analysis may reveal localized variations in surge SWL not described in 2D, such as those associated with sharp vertical gradients in salinity and temperature driven buoyancy forces (Weisberg and Zheng 2008, Resio and Westerink 2008, Dresback et al 2010, Weaver and Luettich 2010, Sheng et al 2010).

(the columns) are defined by points, termed nodes. Modelers create a data file containing the node locations in a horizontal coordinate system (e.g., latitude/longitude).

Starting with an initial condition, the 2D code computes SWL and velocity vectors at each node at each subsequent specified time-step as a function of the translated equations and five sets of input values:

1. Initial conditions, i.e., the starting water surface elevation and velocity (x and y) throughout the domain (at each node);
2. Lateral boundary conditions, i.e., the water surface elevation or velocity for those nodes along the perimeter, which must be specified for all time-steps. These include river flows into the domain and the tides at the open ocean boundary.
3. SWL gains/losses (rainfall, evaporation) at each node.
4. Forces with specified magnitudes (e.g., gravity) at each node.
5. Nodal attributes governing unspecified force magnitudes, such as bathymetric/ topographic elevation of each node, the friction coefficient, the eddy viscosity coefficient, the wind sheltering coefficient, and the air-sea drag coefficient.

Depending on the code, node inputs can be spatially uniform or variable, as well as temporally constant or variable. Spatially and temporally variable inputs can themselves be computed according to a specified rule (code subroutines) using other inputs (e.g., date/time dependent tides, latitude dependent Coriolis force), the current solution (e.g., depth dependent friction coefficient, velocity shear dependent eddy viscosity), or coupled models (e.g., atmospheric pressure and wind speeds from a vortex model and radiation stress gradients from a wave model). The influence of major uncertainties in input values (e.g., friction coefficient, wind field, etc.) are assessed with sensitivity analyses (see below).

8.2. Model Numerical Methods

Discretization of space and time leads to two fundamental modeling challenges. The first challenge is determining the number and spacing of nodes to represent the physical domain, which is akin to selecting the megapixel resolution for a digital camera. Node arrangements vary in the fidelity of their representation of the real domain terrain and landscape properties (e.g., friction and other coefficients). In principle, higher resolution supports better surge modeling detail and accuracy, but at the expense of greater computational resources. However, some surge models may not improve with greater terrain and landscape detail, due to other uncertainties or model limitations, just as poor lighting can obviate the advantage of a higher resolution digital camera.

The second challenge is devising the algaebraic algorithms for solving conditions at each node which approximate the PDEs. Numerical translations of surge PDEs are equations with an infinite series of algebraic terms, usually listed in order of greater accuracy refinement. All numerical methods must choose a point at which to truncate these translations, introducing what is termed as truncation error. Higher order solutions necessarily include more terms and less truncation error, but are more computationally expensive. Solutions with only “first order” accuracy have a truncation error that typically introduces significant artificial smoothing (also termed numerical dissipation or dampening). “Second order” solutions have higher accuracy but less dampening, and consequently are more susceptible to instabilities—spurious errors which can become compounded over time. The algorithms are analogous to computer animation tools which apply rules of motion to a still frame. The more rules of motion—tailored to each object in the still frame and to the changing conditions of each object—the more realistic the animation.

Simple domains can be modeled with *structured grids* composed of rectangles or smooth regular curvilinear quadrilaterals. Structured grids accommodate the generally more direct numerical solutions known as *finite difference* methods. Two well known codes which rely on structured grids and finite difference numerical methods are Sea, Lake, and Overland Surge from Hurricanes (SLOSH), which is often used by NOAA and the USACE in emergency planning, and FEMA Surge, which was formerly used in coastal FISs. Figure 8.1 illustrates a structured curvilinear grid for southeast Louisiana.

The alternative to a structured grid is an unstructured grid, or mesh. A triangular (or quadrilateral) mesh can have tighter (i.e., denser) node spacing along irregular coastlines, interior floodplains, and raised topographic features to better resolve physical processes in these areas. Conversely, the same mesh can have coarser spacing over areas where de-resolving hydrodynamic processes is suitable (e.g., the open ocean and flat expansive marsh). By employing variable node spacing, unstructured, triangular meshes can better optimize the location and number of nodes to represent complex coastal domains. Figure 8.2 illustrates an unstructured triangular mesh.

Solutions for an unstructured mesh require less direct, more sophisticated *finite element* numerical methods. Finite element methods encompass a range of approaches but typically have greater computational requirements for a given number of nodes. However, for a given target refinement in an area of interest, the unstructured mesh may contain significantly less nodes, in which case the combination of the unstructured mesh and finite element method may be more computationally efficient. Finite element methods have been routinely applied to floodplains for two decades to cost-effectively capture complex hydrodynamic patterns. The combination of an unstructured mesh with the finite element method has become more attractive in the last ten years as computational costs have drastically declined and the demand has increased for better resolution of domain landscape features.

Both finite difference and finite element numerical methods are designed to conserve mass over the global domain at each time step within machine precisions. However, an important difference is that finite difference methods conserve mass on a node by node basis, while finite element methods conserve mass over patches of nodes. The absence of strict mass conservation at the node level in the finite element method is not typically a problem unless sources of instabilities are present (see below) or surge flow become supercritical (e.g., shallow flow down steep slopes). The unstructured mesh for a finite element model can be further refined to improve mass conservation (to an acceptable tolerance) over particular small areas of interest, and remain (depending on the degree of refinement) more computationally efficient than a corresponding finite difference model. A third type of numerical scheme, *finite volume*, employs unstructured meshes but imposes strict mass conservation over each triangular mesh element (e.g. FVCOM, ADCIRC-DG). However, finite volume methods are much more computationally demanding, and without higher order numerical schemes tend to introduce considerable dampening.

Finite difference and element methods can be either fully explicit, fully implicit, or a blend. Explicit methods solve the 2D equations for SWL and velocity at each node for the current time-step solely based on results from the previous time-step; i.e., the current time-step solution is only dependent on

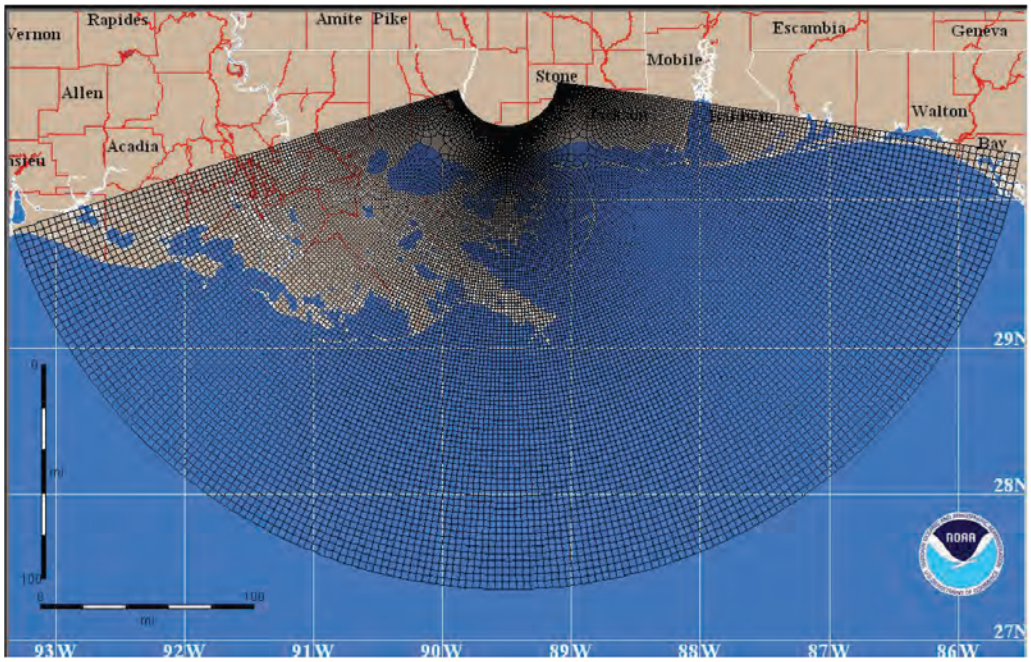

Figure 8.1. Example of a Structured Curvilinear Grid
Glahn et al 2009

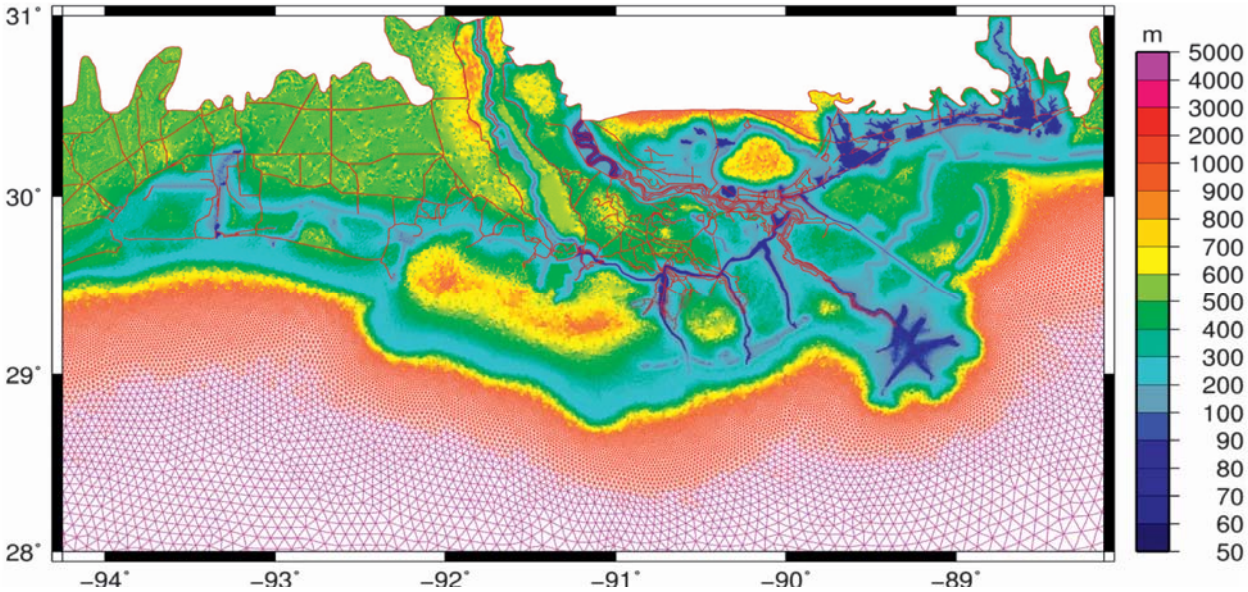

Figure 8.2. Example of an Unstructured Grid, or Mesh
(Legend is node spacing)
Bunya et al 2010

pre-determined values. Implicit methods solve equations for SWL and velocity at each node by also incorporating results for adjacent nodes at the current time-step. These latter values are obviously not determined prior to the model marching to the current time-step. In contrast to explicit methods, implicit methods require the use of more computationally intensive iterative techniques (which in turn require specification of iteration limitations and/or convergence criteria). Explicit methods are subject to Courant instabilities while implicit methods can be strained by wetting and drying fronts (see below).

With declining computer processing costs, 2D hydrodynamic codes are being been written to take advantage of parallel computer processing architecture. Some codes can only use the additional processors on a single workstation, while others can be used with High Performance Parallel Computing (HPPC) systems employing hundreds of computer cores. Academic research of surge hydrodynamics has utilized HPPC systems for nearly a decade (Westerink 2004). Since the destructive 2005 hurricane season, HPPC systems have seen wider practical application in FEMA and USACE surge modeling due to increased availability, speed, and cost-efficiency of the HPPC systems, as well as the demand for higher spatial and temporal resolution of surge physics, which requires vastly more computational steps.

Table 8.1 provides a list of 2D hydrodynamic codes which have been applied to regional scale, high resolution hurricane surge studies and notes several key characteristics and limitations. (Codes that are applied primarily to local-scale studies, such as bridge scour evaluations, are not included.) The code providers noted in Table 8.1 continue to work on a range of improvements, including 3D physics; full baroclinic forcing; better parameterization of turbulence stress and friction; updates to wind vortex models; coupling with wave models (see Section 9); more robust wetting and drying schemes; more efficient and accurate numerical methods; and better computational efficiency. One recent advancement in two finite element codes (ADCIRC and ADH) is automatic mesh refinement to enhance local mass conservations and restrict local instabilities.

8.3. Node Attribute Data

Modelers require domain geometry (topographic and bathymetric) and land cover data in order to establish node elevations and coefficients for wind sheltering and friction. Modelers typically obtain these data at two scales: large coverage (e.g., at scales of U.S. Geological Survey, USGS, quarter quadrangle to county-wide) and feature-specific (e.g., at scales of particular water bodies and land features). Large coverage topographic data sets are increasingly available through federal-state-coordinated efforts (e.g., USGS, NOAA, and FEMA sponsored topographic data and digital elevation models, DEMs, derived from Light Detection and Ranging, LIDAR). Coordinated survey efforts produce data and DEMs for regional bathymetry. The U.S. Fish and Wildlife Service (USF&WS) and other agencies sponsor updates to the National Land Cover Data (NLCD). Large coverage sources typically provide the bulk of the required data.

Key coastal landscape features (see Section 7) may not be adequately represented in large coverage data sets. Large coverage data sets may be outdated—such as with an accreted shoal, eroded shoreline or barrier island, urbanized landscape, dredged channel, expanded jetty, etc. In some cases, the large coverage data may be current but may not adequately resolve small features with potential significant impact, such as a LIDAR DEM not capturing the height of a floodwall crest. In these instances mesh development and attribute assignment need to incorporate feature-specific geometry and cover information. Some coastal features require detailed investigations and surveys to provide adequate node information.

Table 8.1. 2D Hydrodynamic Codes for Hurricane Surge SWL Studies

Code	Developer	Open Source	Wave Setup	Numerical Method	HPPC Compatible	Licensing
Adaptive Hydraulics (ADH)	ERDC USACE	Yes	Yes; loose coupling with wave model (e.g., STWAVE)	Finite element with adaptive mesh	Yes	Parallel version licensed from USACE (CHL)*
Advanced Circulation (ADCIRC)	ADCIRC Development Group	Yes	Yes, tightly coupled version with SWAN	CG - Finite element; DG -finite volume with adaptive mesh and numerics	Yes	Parallel version licensed from USACE Coastal and Hydraulics Laboratory (CHL)/ADCIRC Development Group*
Coastal Modeling System M2D	ERDC USACE	Yes	Yes; loose coupling with STWAVE	Finite difference	Yes	Parallel version licensed from USACE (CHL)*
Delft	Deltares	Yes	Yes	Finite difference	Yes	Licensed from Deltares
FEMA Surge	FEMA	Yes	No	Finite difference	No	Not in general use since the 1990s
Finite Volume Coastal Ocean Model (FVCOM)	University of Massachusetts, Dartmouth	Yes	Yes; tightly coupled version with SWAN	Finite volume	Yes	Not licensed for commercial applications
MIKE21	Danish Hydraulic Institute	No	Yes	Finite difference or finite volume	Limited to cores on workstation	Must be purchased from DHI
Regional Ocean Modeling System (ROMs)	Rutgers Ocean Modeling Group	Yes	Yes; tightly coupled version with SWAN	Finite difference	Yes	Free license including commercial applications.
Sea, Lake, and Overland Surge from Hurricanes (SLOSH)	FEMA/USACE/ NOAA	Yes	No	Finite difference	No	Generally shared within the emergency planning community for establishing flood envelopes; not typically available for commercial applications
SELFE	Oregon Health and Science University	Yes	Yes; coupled with WaveWatch Model II	Finite element	Yes	Free license including commercial applications.
Telemac	The TELEMAC Consortium	Yes	Yes; coupled with TOMAWAC	Finite element	Yes	Free license including commercial applications.

*Serial version licenses can be obtained with Surface-water Modeling System (SMS) user interface software from Aquaveo, LLC.

Source data for the nodal attributes should be:

- Complete with regard to the domain;
- Representative of conditions appropriate to the hurricane being simulated (e.g., historic landscape conditions for Hurricane Betsy; late summer/early fall vegetation conditions for synthetic storms);
- Accurate, with acceptable limits of uncertainty;
- Sufficiently spatially resolved to support interpolation to the particular mesh node spacing;
- Compatible, in cases where multiple, overlapping data sources must be used.

Limitations in nodal attribute data are often a major source of model inaccuracy and overcoming them requires substantial effort during model development. For example, topographic/bathymetric elevation data from numerous sources having different applicable dates, vertical references, and levels of uncertainty must be reconciled. (GTN-2 discusses issues related to appropriate vertical referencing for coastal Louisiana.)

Figure 8.3 illustrates some nodal attribute data for the unstructured mesh shown in Figure 8.2

8.4. Instability Issues

The very nature of numerical methods (simplified algebraic approximations of complex PDEs, spatial/temporal discretization, truncation of higher order terms, precision limits, convergence criteria, iteration restrictions, etc.) entails accuracy limitations. Furthermore, as a model progresses through time-steps computational methods can cause mass conservation errors at particular nodes to compound drastically, creating local solution instabilities and extremely unphysical results (e.g., high “mountains” or low “depressions” in the water surface). As the simulation proceeds, some instabilities can create mass conservation discrepancies large enough to exceed the modelers preset tolerance for terminating the simulation. “Non-fatal” instabilities can propagate below termination tolerances, “contaminating” local results, and can only be identified by a careful inspection of output. Figure 8.4 presents peak surge elevation profile along an inland river and illustrates an instability in an implicit versus an explicit simulation.

Modelers can try four “quick fixes” to reduce model instabilities.

1. Select a different numerical method or scheme (e.g., explicit versus implicit).
2. Alter the treatment of one or both momentum terms. For example, removal of acceleration terms in the momentum equation would impose a pseudo steady, gradually varied flow solution. However, this would not be suitable for depicting large, rapid surges through narrow inlets.
3. Reduce the model time-step. However, reducing the time step increases model runtime, roughly proportionately.
4. Increase the nodal eddy viscosity value (see Section 6). Higher eddy viscosity values boost local momentum diffusion, smoothing local velocity gradients (see below). However, higher eddy viscosity values can lead to unrealistically sluggish hydrodynamics.

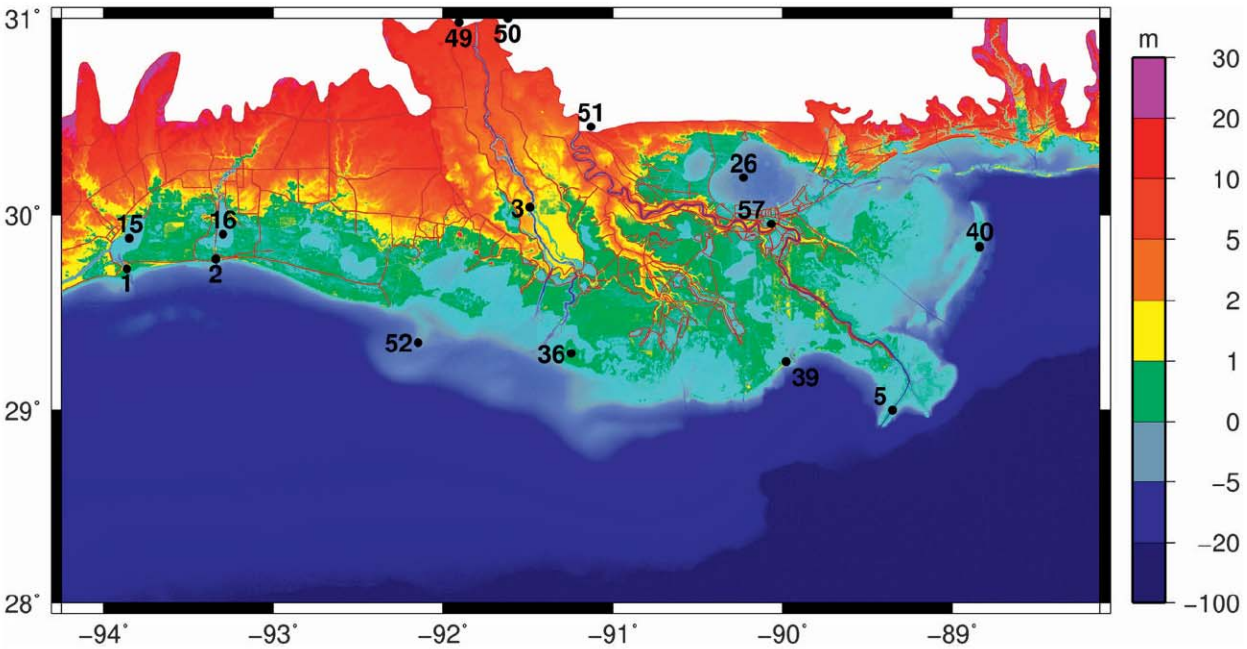

a. Topography and Bathymetry

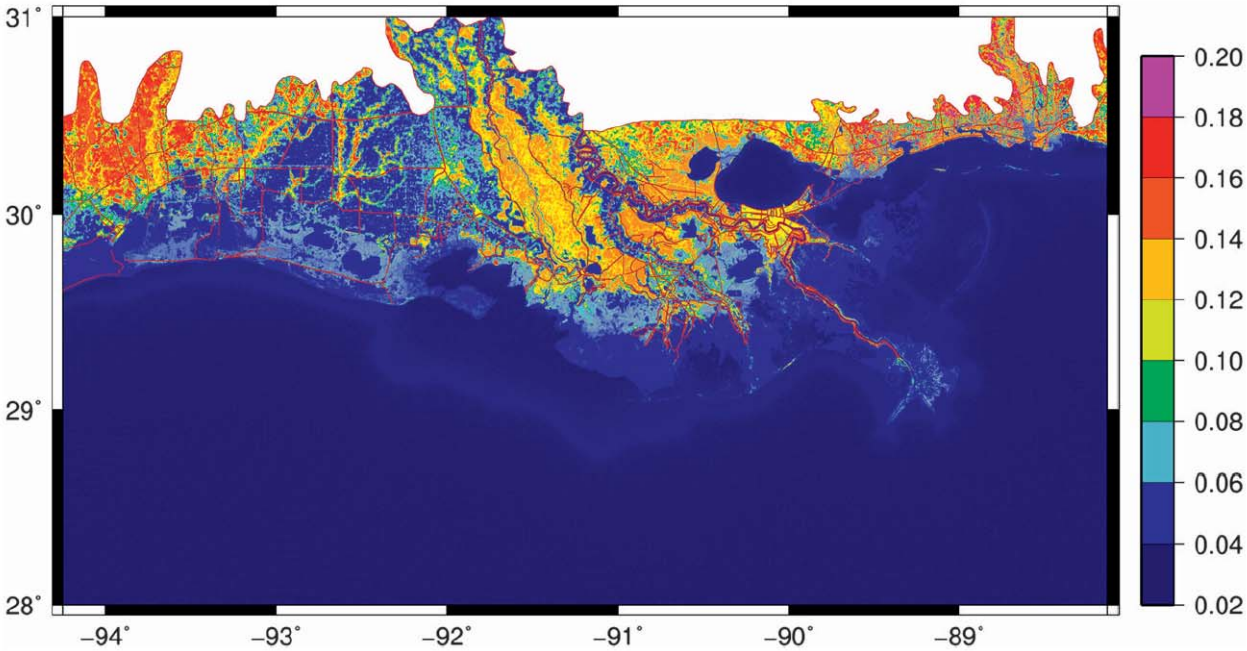

b. Manning's n Friction Coefficient

Figure 8.3. Example of Node Attributes for Unstructured Mesh
Bunya et al 2010

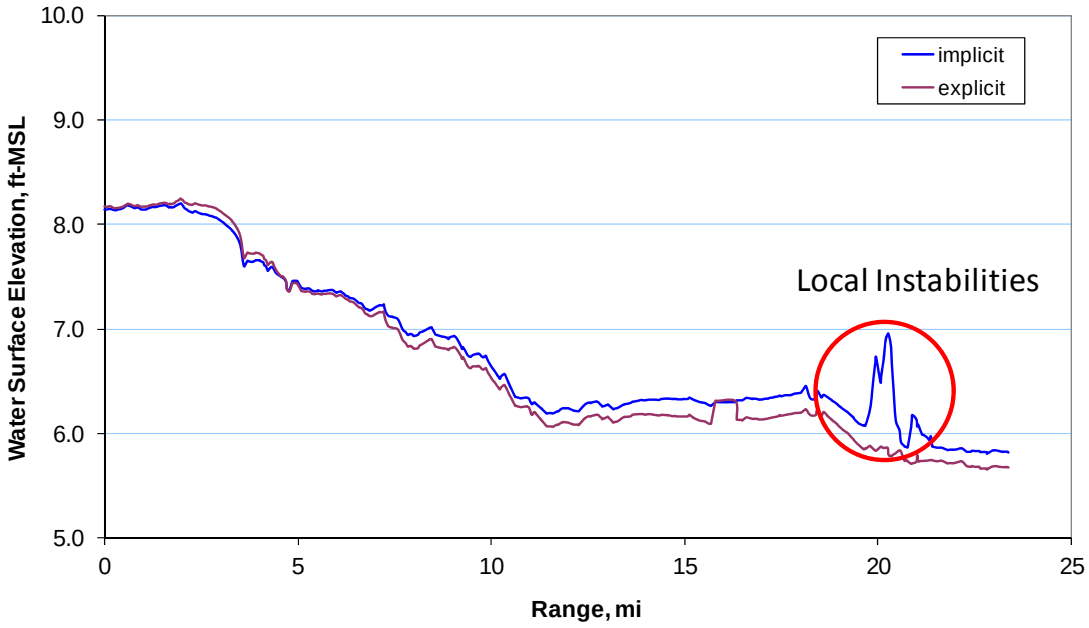

Figure 8.4. Example of Instability in an Implicit versus and Explicit Simulation Comparison of Peak Surge Elevation Profiles Along an Inland River
Jacobsen et al 2010

To avoid the potential drawbacks associated with these quick fixes, experienced modelers will usually investigate potential mesh sources of instabilities and make revisions to mitigate them. Four significant sources of instability associated with mesh arrangements and their potential solutions include:

1. The Courant stability condition. This condition, critical with explicit numerical schemes, requires that the maximum physical velocity at which a perturbation in the SWL (e.g., a wave) propagates be much less than the velocity at which the numerical solution propagates (node spacing / time-step, or *dx/dt*). Surge perturbation velocity in nearshore areas and overland is the same as shallow water wave celerity [$(gh)^{½}$ where *h* is water depth]. The value of $(gh)^{½} * (dt/dx)$ should generally remain less than 0.5 throughout the model domain and over the course of the simulation. For example, at dt = 1 s, the value of $(dx)^2/h$ (units of feet) should exceed 130. Thus, improving Courant stability requires mesh de-refinement or time-step reduction.

2. Mesh quality. Numerical stability in unstructured meshes is improved by using mild area transitions between adjacent elements and by avoiding small interior angles (i.e., for triangles the more nearly equilateral the better). The former requirement tends to increase node density while the latter tends to decrease it.

3. Force and velocity gradients. Solutions with smooth force and velocity gradients tend to remain stable. Smoothness is improved by a) designing meshes with element edges that follow attribute contours (e.g., elevation, Manning's n, and other attributes affecting force generation); and b) reducing perturbations in, and the steepness of, attribute gradients (i.e., smoothing the contours); and c) refining the mesh in areas of high gradients. Approaches a) and c) tend to increase mesh resolution, while b) tends to decrease mesh resolution.

4. Wetting and drying fronts. Wetting and drying are a significant source of instabilities in surge modeling (See Dietrich et al 2005, and Massey and Blain 2008). 2D models can advance wetting/drying fronts subject to certain thresholds—e.g., water depth and velocity. These logical (on-off) conditions help to control wetting/drying oscillations, which numerical methods can exacerbate. Models, however, must also avoid steep, irregular wetting/drying fronts. The three approaches to alleviating steep, irregular velocity gradients can also be used to address problematic wetting/drying.

In addition to adjusting the mesh and nodal attributes to relieve these force gradient and wetting/drying sources of instabilities, the modeler can use refinement to impose greater local mass conservation. However, in refining a mesh, the modeler must recognize that the Courant condition may require a time-step reduction, particularly for mesh refinement in areas of deeper water. If reducing the time step is not practical, the modeler may need to coarsen the mesh and smooth the attribute gradient. Models with longer time-steps and coarser meshes often have much lower development and production costs, and faster schedules, but sacrifice domain fidelity and possibly simulation accuracy.

Model codes with higher numerical accuracy—i.e., lower truncation error and thus lower numerical dampening—will typically face more instability problems. However, such codes provide the modeler with control over optimizing model stability with fidelity to terrain and land cover conditions. This optimization involves extensive manual adjustments to node positions and attributes, which are extremely tedious and time consuming. Testing these adjustments can require numerous simulations.

8.5. Model Performance Testing

GTN-1 provides an introduction to testing of model performance for accuracy (bias) and precision (uncertainty)—including sensitivity, calibration, and validation testing. Due to complex surge dynamics, performance evaluation of surge models requires high quality surge data—both for HWMs and hydrographs—over a broad area. However, federal and state agencies have not had adequate plans for collecting such data until recently. For southeast Louisiana, data prior to 2005 have also had significant problems with vertical referencing (see GTN-2).

Surge model performance is also typically evaluated for tides, as there is usually greater availability of numerous high quality tide time series compared to surge events. Modelers usually evaluate the tidal constituents themselves, which requires harmonic analysis of tide station data. Importantly, inshore areas are likely to be much more sensitive to conveyance conditions for evaluations of tidal propagation versus extreme surge events. Modelers must therefore consider potential differences in bottom friction (e.g., Manning's *n*) for tides versus surge events.

Surge SWL model sensitivity tests examine the relative influence of various model settings (e.g., mesh layout, modification of acceleration terms, time-step), initial and boundary conditions, and inputs (e.g., nodal attributes, wind values, etc.) on the model efficiency (i.e., runtime), stability, and the quality of results. Thus, sensitivity tests provide important information on what is called model robustness: the simulation conditions for which particular settings and parameters can be applied. Sensitivity tests can use actual tide and surge events or hypothetical/synthetic conditions. When employing the latter the tests are often termed "numerical experiments."

Calibration tests simulate actual tides and surge events. The modeler compares the simulation results for SWLs and velocities to the observed values and adjusts parameters (those which have been found to be highly sensitive) within accepted ranges to achieve a best fit. Calibration often requires judgment on whether or not to "tune" a parameter—such as the friction coefficient (Manning's *n*)—to improve the

simulation of a particular event. For example, it may not be appropriate to apply a shallow marsh Manning's *n* value that supports tidal calibration to extreme surge events.

Following calibration, a validation test is performed on an additional separate hindcast to assess the selected settings and parameters. If the model is not calibrated, the validation test relies on the modeler's experience and judgment (based on previous models) for settings and parameter values. As discussed in GTN-1, validation results are used to identify model bias (inaccuracy) and precision (uncertainty). In employing the validated SWL model to simulate a range of possible hurricane scenarios any residual bias requires application of suitable correction factors (Dean et al 2004).

Models which employ coarse structured grids and finite difference codes (e.g., SLOSH), and which simplify surge physics by ignoring wave setup, have the advantage of being very simple, fast, and inexpensive to operate (e.g., simulating a few storm days on a desktop computer in less than an hour).[2] Figure 8.5 plots simulated versus observed SWL for the SLOSH model over several storms. The results show that SLOSH hindcast models can simulate SWLs above 15 ft within ±20% but are less accurate for lower surges, where detailed landscape features become important.

Models which incorporate a fuller physical description (e.g., wave setup) and higher resolution, may require hundreds of computer cores to simulate the same event, but usually provide better validation results, particularly at the lower SWLs affected by the coastal landscape. Figure 8.6 illustrates the ADCIRC model validation results for Hurricanes Katrina.

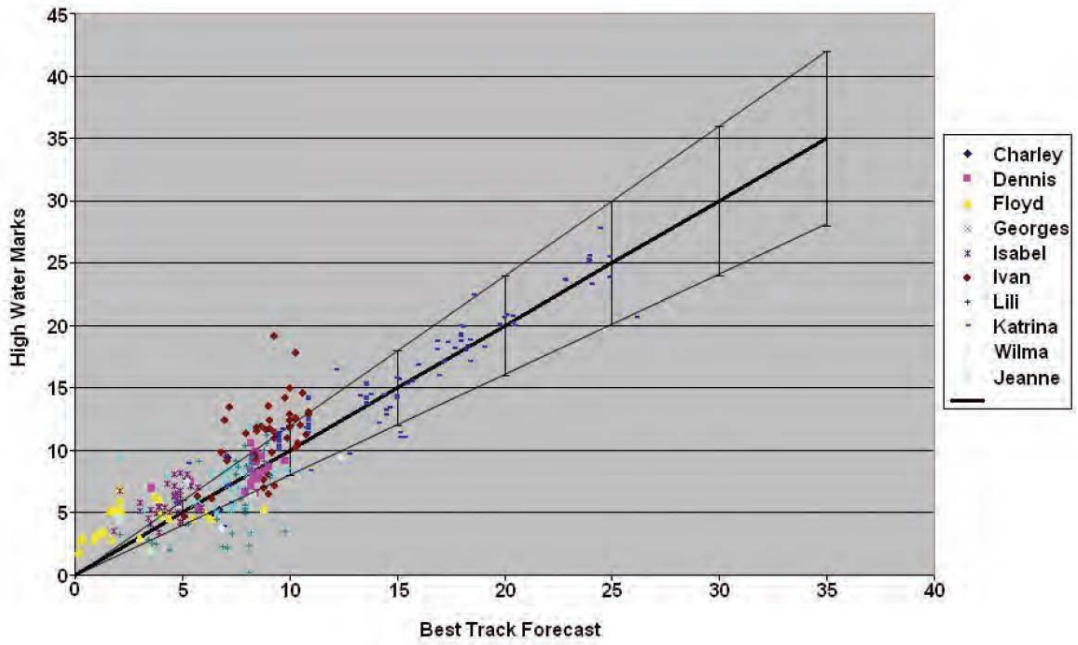

Figure 8.5. Comparison of SLOSH Model Predictions to Observed High Water Marks (With ±20% Error Bands)
Glahn et al 2009

[2] Due to rapid run-time demands and other exigencies, application of surge models like SLOSH to real-time forecasting, necessitates greater simplification than planning/design applications. A detailed discussion of simplifications in real-time surge forecast techniques, and their implications, is beyond the scope of this report

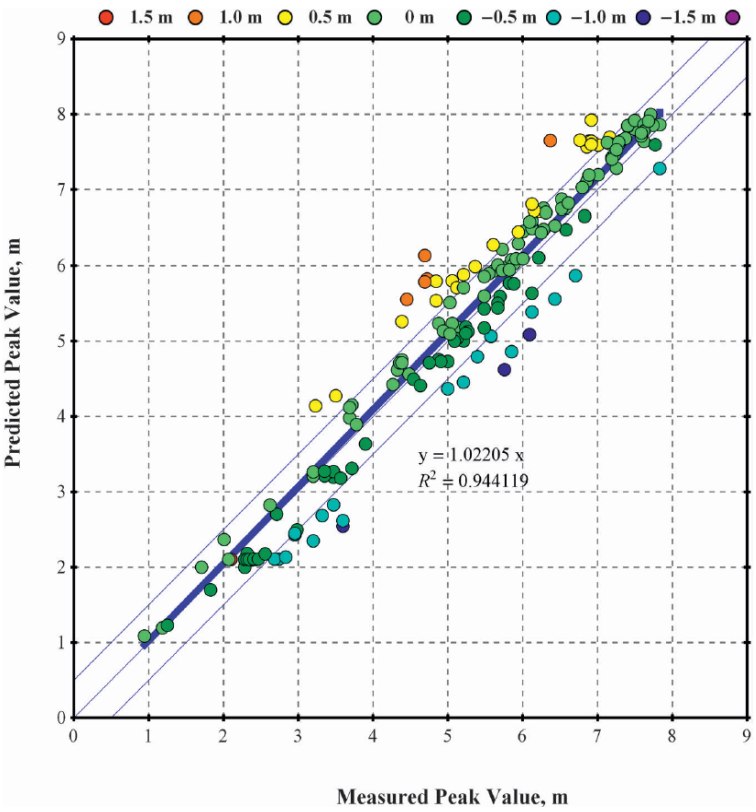

Figure 8.6. Comparison of ADCIRC Model Predictions to Observed High Water Marks Hurricane Katrina (With ±0.5 m Error Bands)

Bunya et al 2010

Section 9. Wave Modeling

9.1. Open Ocean and Nearshore Waves

Modeling the generation of hurricane wave fields (H_s, T_p) in the open ocean, and the propagation and transformation of these fields to the nearshore zone fronting barrier islands and headlands is crucial in order to evaluate the radiation stress gradients which provide wave setup contribution to SWL (see Section 6). Modeling of these waves and associated physical processes is similar to SWL modeling (Section 9) in the need to:

- Employ spatial and temporal discretization of governing equations and numerical methods;
- Develop grids or meshes;
- Assess coefficients and node attribute data (bathymetry and wave friction coefficient);
- Input transient conditions affecting waves—e.g., wind fields, SWLs, currents—as well as initial and boundary wave condition; and
- Address stability issues.

Prior to 2005 the USACE developed separate finite difference codes to model the open ocean irregular wave field generation—WAve Prediction Model (WAM)—and nearshore transformation—Steady State Spectral Wave (STWAVE). The models were designed to use separate grids—with the WAM model using a much coarser (1- 10s km scale) ocean basin grid—and STWAVE using a higher resolution (100s m scale) nearshore regional grid. This nearshore grid resolution captures the shoaling of large ocean waves as they pass over the Continental Shelf, and the breaking of these waves—and associated radiation stress gradients—as they approach the open coastline. For hurricane events the USACE utilizes WAM to simulate generation of hurricane wave spectra in the open ocean and these results are employed as boundary conditions for nearshore wave modeling with STWAVE.

STWAVE is limited to modeling transformation conditions along mild bathymetric slopes—thus it is suitable for the Continental Shelf and nearshore regions but is not used to simulate wave breaking over inundated levee foreshores. To assess transient wave conditions, STWAVE is run as series of separate steady-state simulations. STWAVE can be run with full 2D (full plane) multi-directional waves, or uni-directional wave (half plane) waves. STWAVE provides for wave energy dissipation through friction but does not address wave diffraction. The USACE is working on wave code improvements, including modeling transient conditions and use of finite element methods and unstructured meshes.

Another common used finite difference code for wave modeling is Simulating WAves Nearshore (SWAN), developed by Delft Technical University. SWAN provides for transient simulations. After 2005, SWAN code authors developed a finite element version capable of running on an unstructured mesh, improving the efficiency of modeling open ocean wave generation together with higher resolution nearshore transformations. In addition, they have begun incorporating wave diffraction processes.

Even more so than with SWL data for surge models, there is a paucity of nearshore wave data for developing, calibrating, and validating nearshore wave models. In one of the only hurricane wave studies to date, Bender et al ran several STWAVE simulations (see Figure 9.1 for example output), with modified bottom friction values, for nearshore Hurricane Ike (2008) waves along the Texas coast and compared the model results to wave measurements. The results, illustrated in Figure 9.2, showed that the STWAVE open water bottom friction value needed to be almost three times higher than the value used in SWL modeling (Bender et al 2010) to avoid over-predicting wave heights.

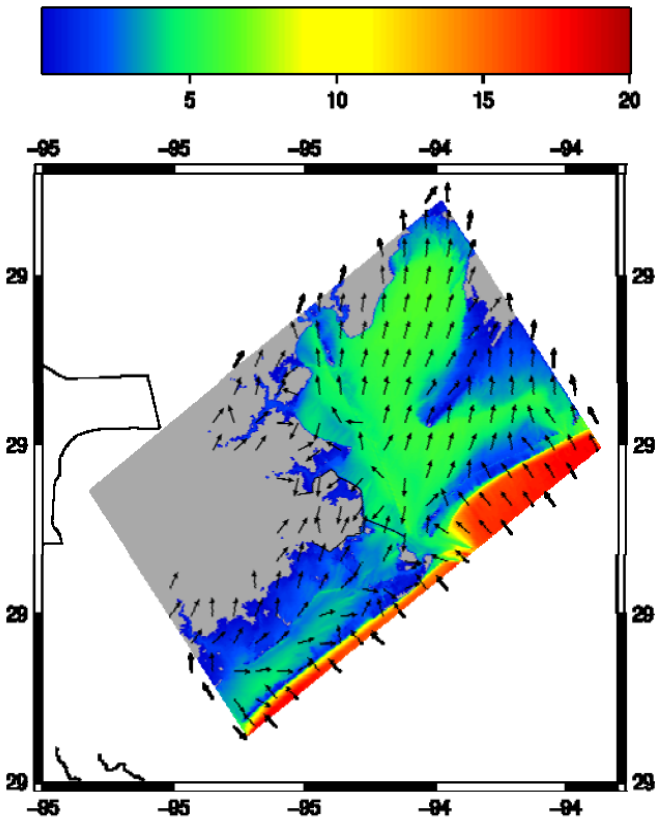

Figure 9.1. STWAVE Output, Hurricane Ike Maximum Wave Height (ft) at Galveston Bay TX
Bender et al 2010

Future hurricane wave data will no doubt allow further understanding of nearshore wave model physics, parameterization, and numerical representation.

9.2. Interior Waves

Following breaking in the nearshore zone seaward of barrier islands and headlands, residual waves propagate into and over coastal sounds, bays, lakes, and inundated wetlands. Local wind fields also energize these interior waves. Modeling the propagation and transformation of interior waves, particularly their interaction with local coastal features and surge induced currents (see Sections 6 and 7) requires higher resolution and smaller time steps. During peak SWL, which can add more than 10 feet of water depth, locally generated wind waves in large inland lakes and bays (e.g., Lakes Borgne and Pontchartrain) can reach breaking heights exceeding 10 feet. Wave setup from such locally generated interior waves can contribute to local SWL and thus need to be modeled.

Investigators of local hurricane wave conditions have employed detailed 2D STWAVE and SWAN models. For example, researchers used SWAN to evaluate local wave conditions for Hurricanes Ivan (2004) and Katrina (2005) within coastal bays that led to the uplifting and collapse of bridge spans (Douglass et al 2004, Chen et al 2009).

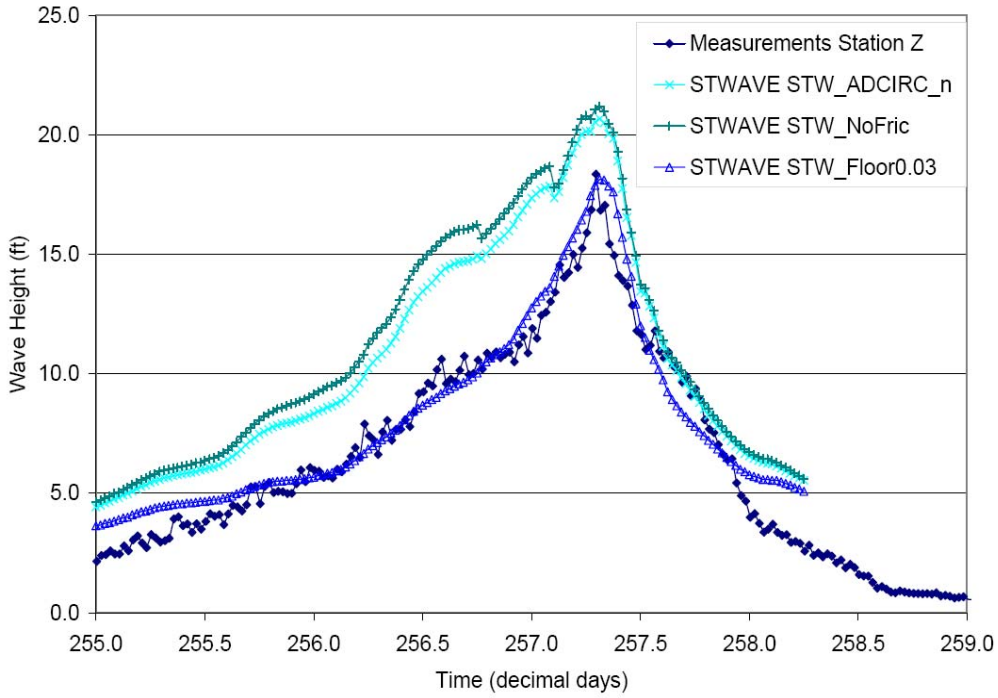

a. Wave Height versus Time (Decimal Days)

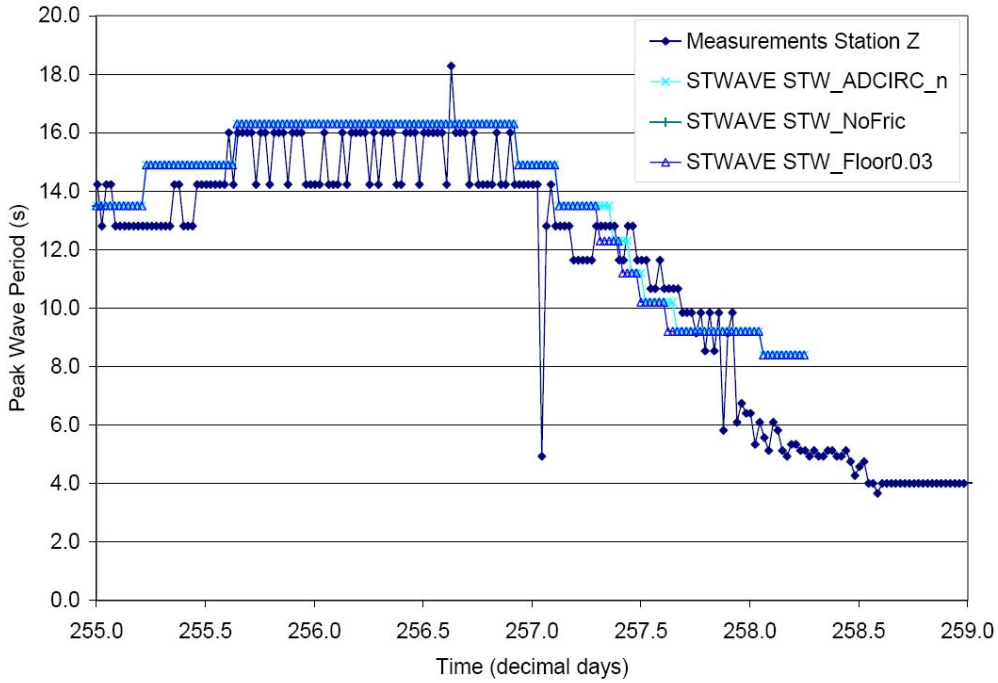

b. Wave Period versus Time (Decimal Days)

Figure 9.2. Hurricane Ike Nearshore Waves, Measured versus Model Results
Bender et al 2010

Modeling the propagation and transformation of larger waves and wave setup contribution in areas of complex shore terrain, especially steep waves and water bottom slopes, requires special treatment of non-linear PDEs terms, such as Boussinesq analysis (see Kennedy et al 2000 and Chen et al 2000). The USACE performed 2D Boussinesq modeling (COULWAVE) of wave conditions associated with Hurricane Katrina at several locations (in three Orleans Parish outfall canals, the IHNC, and along the MRGO Reach 2, New Orleans East, and Mississippi River levees, see IPET 2006, Volume IV, Appendix 15). Figure 9.3 depicts the results of a Boussinesq model for the 17th Street Outfall Canal. Lynette has also recently used Boussinesq modeling to evaluate Hurricane Katrina wave conditions along the MRGO Reach 2 levee (Lynette et al 2010).

While local scale 2D hurricane wave models for the coastal interior, including Boussinesq models, offer improved resolution, physics, and numerical methods, evaluations to date with respect to measured data have been very preliminary. More hurricane wave observations—particularly those associated with relatively short-term peak conditions—are required to assess model performance and to determine appropriate ranges for friction and other coefficients. This research is especially important for locations subject to significant locally generated wave setup (e.g., Lake Pontchartrain).

The Wave Height Analysis for Flood Insurance Studies model (WHAFIS, see FEMA 1988) is used to determine basic approximations of interior wave height transformations along transects under assumed steady-state condition. Importantly, the NFIP addresses 1% waves and assumes an upper limit on 1% wave heights at 0.78*Depth. WHAFIS solves only simple linear shoaling and energy dissipation (from vegetation or muddy bottoms) equations. Transects can be established in any direction at a representative spacing, with nodes for key topographic and landscape transitions. Wave heights at a location can be evaluated using multiple transects with different orientations over the same region. For example, evaluation of wave conditions over an inundated Grand Isle can examine Gulf of Mexico waves (from a hurricane passing to the west, e.g., Hurricane Gustav) and Barataria Bay waves (from one passing to the east, e.g., Hurricane Katrina). Most WHAFIS applications utilize standard coefficients. As a simple shoaling model, FEMA uses WHAFIS to adjust hazard elevation estimates (above the SWL) for inundated interior coastal areas also exposed to wind-driven waves. [1]

9.3. Coupling of 2D SWL and Wave Models

Because accurate 2D SWL modeling requires the input of accurate wave radiation stress gradients, and because accurate wave modeling requires input of accurate SWLs and velocity, modelers have sought ways to couple SWL and 2D wave models. Table 8.1 lists the coupling approaches employed with high resolution 2D SWL codes.

In *loose coupling* the 2D SWL and wave models are run separately for an interval over which wave conditions are nearly steady. The SWL model may be running at time-steps on the order of seconds, while the interval for loose coupling may be on the order of tens of minutes. At the start of an interval SWL and current values are input into the wave model—the results of the SWL model at the end of the previous interval. The wave model then computes the wave conditions and radiation stress gradients

[1] Modelers apply a given SWL to the WHAFIS transect nodes. The estimated wave heights along the transect are highly sensitive to transect selection and input conditions and coefficients. Several southeast Louisiana parishes are currently appealing FIS estimated hazard elevations due to concerns over WHAFIS modeling. WHAFIS is not a tool for analyzing complex radiation stress gradients or wave setup associated with critical wave breaking issues along interior shorelines.

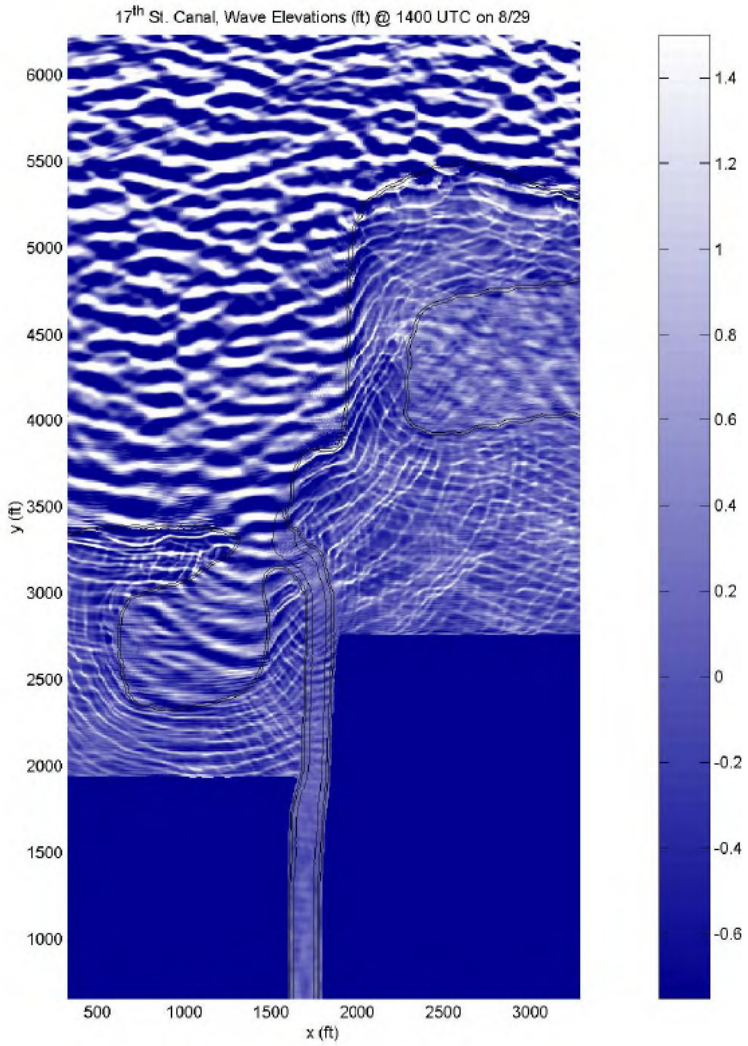

Figure 9.3. Boussinesq Model Results for Hurricane Katrina Waves. 17th Street Outfall Canal
IPET 2006

for the present interval. These gradients are input into the SWL model, which then steps through the present interval. After running the SWL model for the present interval its ending SWL and currents are used as the new starting SWL for the wave model's next interval. Depending on accuracy, cost, schedule, and other constraints, the modeler may adjust the coupling intervals. Loosely coupled models do not have to share the same mesh. The SWL code can use a finite element mesh and the wave code a finite difference grid, in which case results from one have to be interpolated to the other.

In *tight coupling* the SWL and wave models are combined into a single code which employs a single mesh (or grid). Tight coupling allows for other dynamic feedbacks, such as the effect of waves on SWL air-sea drag, and facilitates spatial and temporal refinement of wave processes in a computationally efficient way. In the future, as mesh resolutions become finer, and as these codes becomes more efficient and computational costs decline, tightly coupled 2D modeling will be able to resolve more of the interior coastal wave processes.

Section 10. ADCIRC Surge Modeling

10.1. ADCIRC Code

ADCIRC is a 2D/3D finite element hydrodynamic code which utilizes an unstructured mesh (Luettich and Westerink 2004). The ADCIRC code is an open source product of the ADCIRC Development Group (http://www.adcirc.org), a cooperative endeavor among several university researchers[1] sponsored by the USACE (see Dean et al 2004), FEMA, NRL, and NOAA. ADCIRC employs a higher order (second-third) finite element scheme which exhibits low artificial dampening. The 2D and 3D code equations allow inclusion of the relevant momentum terms but do not currently address rainfall/evaporation.

The ADCIRC code is unique among those listed in Table 8.1 for its many years of applications with HPPC systems. In parallel computing ADCIRC decomposes the model domain into subdomains, with each subdomain assigned to a separate computer core. Figure 10.1 illustrates the domain decomposition. With HPPC systems consisting of hundreds of cores, ADCIRC modelers can easily handle meshes exceeding one million nodes. In an optimal range, increasing the number of cores proportionally reduces runtime (Dietrich et al 2011a). ADCIRC's HPPC scalability, together with accelerating improvements in core performance, enable modelers to advance the spatial and temporal refinement of surge processes to improve the quality of hindcasts, forecasts, and scenario simulations. Parallel computation also allows ADCIRC 2D to employ a very large domain with an open boundary at the mid-Atlantic to reduce resonance and other boundary effects. These benefits of HPPC-based modeling have led FEMA and the USACE to select ADCIRC 2D for hurricane surge studies.

ADCIRC provides a choice between a fully explicit scheme and a scheme which combines an implicit solution for the nonlinear terms with an explicit solution for linear terms. As with any explicit scheme, ADCIRC is subject to the Courant instability condition (see Section 8). ADCIRC's authors have designed the two schemes to achieve similar high orders of accuracy (based on truncation error). Consequently, both ADCIRC schemes do not introduce substantial artificial dampening (an approach inherent in less

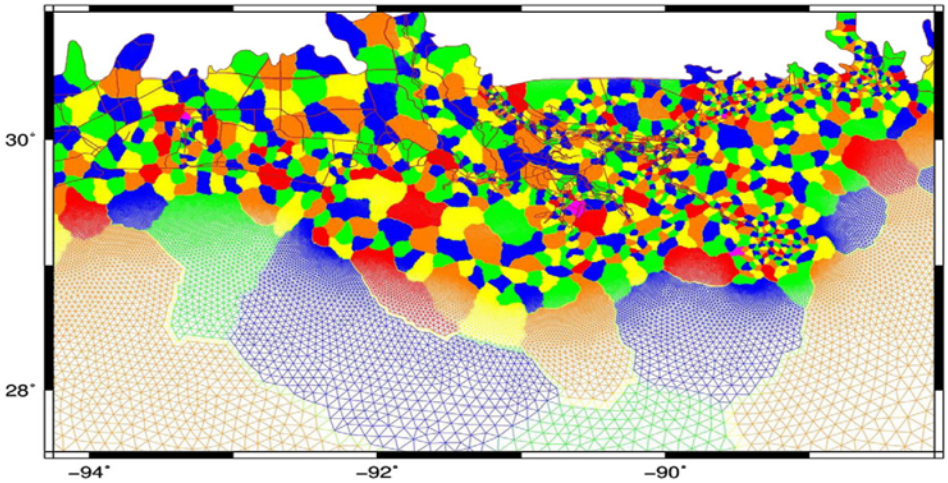

Figure 10.1. ADCIRC Mesh Domain Decomposition for HPPC

Dietrich et al 2011a

[1] Richard A. Luettich (University of North Carolina), Joannes J. Westerink (University of Notre Dame), Clint N. Dawson (University of Texas), and Randall L. Kolar (Oklahoma University).

accurate codes). This aspect of ADCIRC can allow numerical instabilities to propagate, necessitating attention to techniques for reducing instabilities (see Section 8). ADCIRC modelers also have some options in the treatment of acceleration terms. ADCIRC modelers have performed important surge studies with both schemes and with various modifications to the treatment of acceleration.

The ADCIRC finite element numerical scheme incorporates a weighted combination of two mass conservation expressions, one of which employs stronger local mass conservation. The weighting factor (termed tau_0)—emphasizing one or the other expression—can be preset globally or allowed to vary spatially by node. A spatially varying tau_0 can also be allowed to adjust automatically with temporal changes in nodal depth or bottom shear stress. ADCIRC modelers typically employ automated tau_0 to reduce instabilities that can develop at high stress gradients and wetting and drying fronts.

As an open source code ADCIRC facilitates ongoing research on several topics:

- Rainfall and evaporation inputs on a node basis;
- 1D conveyance features within the 2D model to simulate fine scale channels;
- Alternative numerical methods to provide strict mass conservation at the node level (i.e., a finite volume method); with the option of automatic mesh refinement and modifications to the algebraic algorithms to improve numerical accuracy and reduce unwanted dampening. (Kubatko et al 2009 and Dawson et al 2010).
- The application of 3D ADCIRC to surge, particularly the influence of baroclinic forcing associated with salinity and temperature gradients (Resio and Westerink 2008, Dresback et al 2010, Weaver and Luettich 2010); and
- Computational efficiency improvements to take advantage of new chip architectures, such as graphics processing units.

Code versions are sometimes subject to issues of limited documentation and code quality assurance.[2] However, users can readily inspect the source code.

10.2. ADCIRC SWL and Wave Coupling

Since 2005, surge study teams have loosely coupled ADCIRC 2D with STWAVE and SWAN to provide wave radiation stress gradient contributions to SWL and circulation. In 2006 the ADCIRC Development Group and the USACE CHL undertook significant development of ADCIRC-STWAVE loose coupling to meet needs for accurate hindcasts of Hurricanes Katrina and Rita and surge hazard analysis (Smith 2007 and Dietrich et al 2010). Figure 10.2 shows the estimated contribution of wave setup to Hurricane Katrina maximum SWLs and Figure 10.3 presents computed Hurricane Katrina wave heights for Lake Pontchartrain. ADCIRC-STWAVE loose coupling has also been employed in a recent Texas coastal FIS. (See Section 11 for a further discussion of ADCIRC-STWAVE hindcasts for southeast Louisiana and Texas.)

Researchers have also loosely coupled ADCIRC and SWAN, such as to evaluate wave conditions affecting a coastal bridge collapse during Hurricane Katrina (Chen et al 2009).

[2] For example, recently an error was discovered with a utility program that assigns 12 directional wind roughness coefficients at each node on the basis of land cover data, allowing computation of downwind wind reductions. The error caused the coefficients to be assigned in an order different from what the ADCIRC code required.

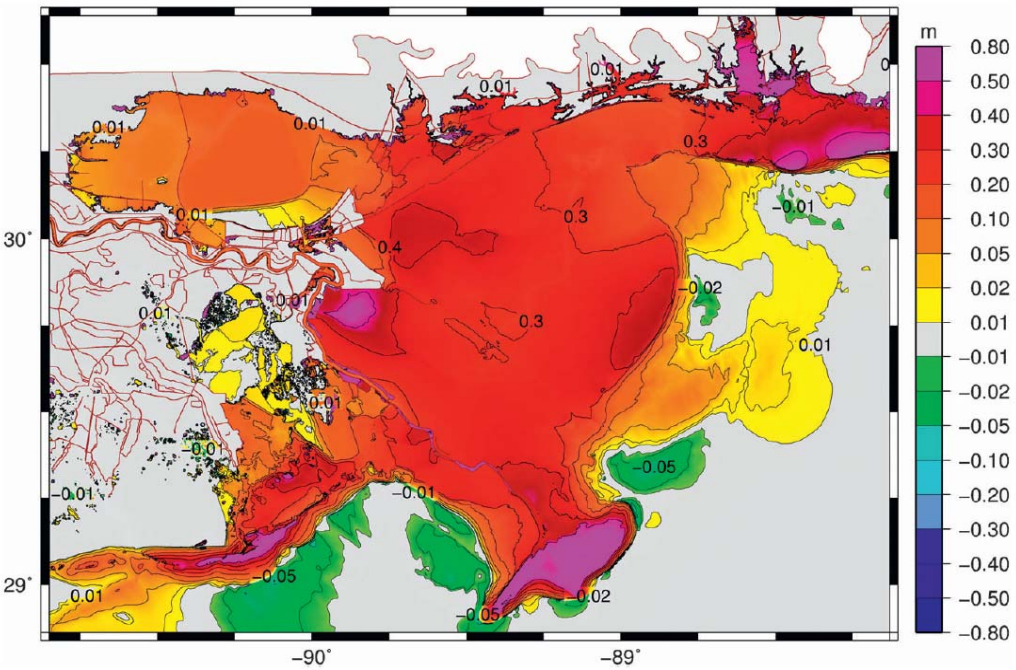

Figure 10.2. Contribution of Wave Setup to Maximum SWL for Hurricane Katrina
Dietrich et al 2010

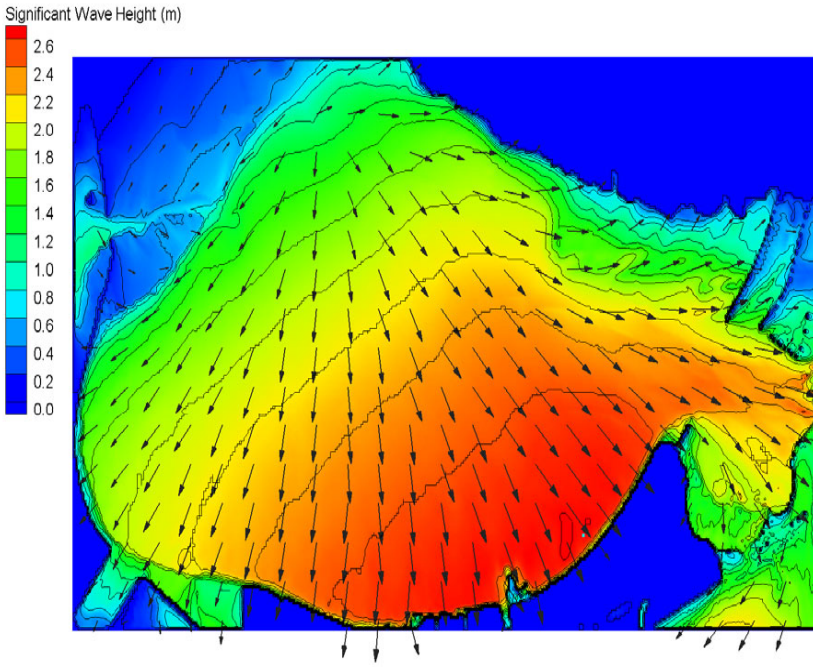

Figure 10.3. Maximum Modeled Significant Wave Heights in Lake Pontchartrain for Hurricane Katrina
Smith 2007

Recently, the ADCIRC Development Group upgraded ADCIRC 2D to provide tight coupling with SWAN in a single SWAN+ADCIRC version (Dietrich et al 2011a). The tightly coupled version uses the ADCIRC unstructured mesh. The combined code runs for each sub-domain on the assigned computer core. The SWAN subroutine develops output generally on 10 minute intervals (which can be adjusted by the modeler), which updates the ADCIRC radiation stress gradients at the equivalent of about 600 time steps (assuming a 1 second ADCIRC time step). The modeler specifies settings for the SWAN subroutine, including parameters for wave bottom friction (which can be developed from nodal Manning's *n* values), energy dissipation from white-capping, air-sea drag, and wave breaking. With nearshore zone mesh node spacing on the order of 100m, the SWAN subroutine can resolve wave refraction. SWAN does not address diffraction or reflection.

10.3. ADCIRC Mesh Development

An ADCIRC mesh is typically laid out with the aid of special mesh design software (e.g., Surface-water Management System, SMS, (www.aquaveo.com/sms) and Geographic Information Systems (GIS) software for managing attribute data. Table 10.1 lists the key steps and capabilities involved in preparing an ADCIRC mesh for coastal surge modeling. Given the large ADCIRC mesh sizes, and that the size of study area data sets often exceed terabytes, the production and editing techniques needed for these steps are especially challenging.

Specific nodal physical attributes which the modeler assigns in ADCIRC 2D surge modeling include:

- Elevation of the land and water bottom surface with respect to the geoid, which, with a water surface elevation, allows computation of water depth and the effects of various forces on the water column;
- Surface Canopy Coefficient, which allows for computation of surface wind reduction due to the presence of local trees, buildings, and other wind sheltering features, versus the standard wind field input value, which is at 10 meters (m) above the surface;
- Surface Directional Roughness Length, which allows for computation of wind speed reduction downwind of the node, depending on wind direction due to the presence of trees, buildings, and other wind drag features;
- Friction Coefficient, which allows for computation of momentum reduction due to bottom roughness, vegetation, and other sources of friction; and
- Horizontal Eddy Viscosity Coefficient, which allows for computation of inter-node momentum diffusion.

The coastal landscape elevation and friction characteristics have a significant influence the mesh design. Mesh node arrangements must resolve surge dynamics in accordance with varying spatial changes in bottom elevation, canopy, sheltering, and friction. Meshes are generally coarser over large areas of uniform terrain and cover (e.g., open water with smooth bathymetry, vast marshes) and become progressively finer near important coastal landscape features which exhibit locally varying terrain and cover. Careful meshing of coastal landscape conveyance features (see Section 7) is especially crucial, including raised features (flood protection and other hydraulic control structures, artificial embankments, and natural barriers) and preferential flow pathways.

Table 10.1. Typical ADCIRC Mesh Development Steps

Steps
1. Set up Geographic Information System (GIS) hardware systems, communication bandwidth, operating framework, procedures, file structures, protocols, metadata requirements, quality control, etc. which will allow storage and efficient retrieval, sharing, serving of terabyte sized data sets to all project team GIS users; users must be able to efficiently load, view, pan, write, etc with multiple large coverage data sets.
2. Acquire large coverage geometry (LIDAR and bathymetry), land cover, and aerial/satellite imagery data sets, together with detailed data sets on coastal features, all of which must be evaluated for: a. Completeness—the data should encompass the entire FIS study area; b. Currency—the data should represent existing conditions for the FIS; c. Accuracy—the limits of uncertainty should be understood and acceptable for an FIS; d. Resolution—data resolution should exceed that of the mesh; and e. Compatibility—metadata for multiple geometry and land cover data sources should be reconcilable. Metadata include referencing methods (e.g., vertical datum), classification schemes (e.g., land cover types), and methodologies for data acquisition, processing, etc.
3. Implement automated quality assurance checks of source data sets and maintaining/tracking evolution of key versions.
4. Prepare a seamless study area digital elevation model (DEM) and land cover map, both of which are in raster format: a. Join adjacent large coverage data sets into seamless study area coverage; b. Combine data in overlapping coverages into a single data set using customized precedence rules; and c. Incorporate data on small coastal features (specific geometry and land cover data) into the study area data sets where the large coverage data sets lack sufficient accuracy (e.g. elevations of narrow crested features missed by LIDAR data).
5. Work with study area DEM and land cover data sets: a. Analyze raster data sets (e.g., DEMs) to produce vector information (e.g., Digital terrain Models (DTMs), Triangulated irregular Networks (TINs), linear terrain features, and land class polygons, etc.); b. Work with other raster and vector data sets to refine/analyze DEM and Land Cover data (e.g., subdivide water land class based on navigational status from National Oceanic and Atmospheric Administration (NOAA) electronic charts); c. Query and analyze data sets to find locations with individual or combined characteristics of interest; and d. Interpolate raster and vector data sets to different resolutions; and e. Apply various conversions to geometry data sets to achieve a common reference.
6. Generate Mesh (programs such as SMS facilitate many of the following steps): a. Extract key mesh lines (Feature Arcs), especially for significant features (e.g., dune ridges, shorelines, channel thalwags) from study area data sets and higher resolution data, where appropriate; b. Extract key mesh polygons (e.g., land cover areas)) from study area data sets; c. Manually digitize and refine key lines and polygons to establish mesh regions/features of interest; d. Establish the appropriate node spacing targets for each mesh region and feature (e.g., along key lines and within polygons); e. Identify features to be represented by internal boundaries (i.e., weirs); and f. Layout mesh nodes and elements using triangle quality constraints (minimum interior angles, area transition, etc.).
7. Populate mesh with attribute data: a. Convert of study area land cover data sets to study area nodal attribute (coefficient) data sets; b. Interpolate final study area elevation and attribute data sets to study area mesh; c. Evaluate mesh quality, fidelity to study area data, at significant features; d. Identify and evaluate mesh locations with potential stability, fidelity, or economy (i.e., impact time-step) issues; e. Manually adjust node arrangements and attributes to address stability, fidelity, and economy requirements; and
8. Conduct trial simulations (tidal and storm surge) to assess mesh stability and accuracy; revise mesh as dictated by trial simulations.
9. Analyze and document the accuracy of final mesh versus study area DEM and attribute data sets.

Raised features which can divert flow—such as those shown in Figure 7.5—should be depicted in the mesh with good horizontal and vertical accuracy. To accomplish this the mesh should provide a continuous line of triangle edges to represent the general alignment of the feature crest. A coarser mesh creates the potential for greater horizontal offsets and errors in crest elevation, particularly for features with irregular alignments and crests. Coarse representation may suffice if the structure is either not overtopped or is substantially drowned under subject scenarios, and if the error in the inundation area and local conveyance is small. Finer meshes can more smoothly and accurately depict the advance of flooding and the overtopping of steeper, higher features. To avoid excessive mesh refinement of steep features (e.g., floodwalls, levees, and high road and railroad embankments) ADCIRC allows internal boundary weir functions to represent raised features. Representing raised features as internal weir boundaries also provides a numerically stable and economical way to accommodate overtopping.

The resolution of preferential flow paths is a significant issue in meshing inland coastal regions. Navigation channels strongly influence the validation of models to inland tide and low-to-moderate surge hydrographs. Figure 10.4 illustrates the difference in meshing a channel with two, three, four, or six cross-channel nodes. In order to accurately capture conveyance as a function of SWL, particularly with respect to overbanking, channel cross sections would ideally be represented by six nodes.

In recent years, the typical ADCIRC mesh resolution has increased significantly because of:

- Greater scientific and public scrutiny of tide and surge processes and predictions in the face of catastrophic storms (Ivan, Katrina, Rita, and Ike), projected sea level rise, continued coastal development, and planning for surge protection. This scrutiny, in turn, heightens demand for more accurate and more confident modeling.
- Continuing advances in HPPC technology, which make higher resolution of the spatial scales of surge physics economical. Over the last five years, ADCIRC modelers have increased the resolution of inshore features from on the order of 100 meters (m) to less than 50 m, more than quadrupling the mesh density (number of nodes per m^2)[3] for these regions.
- Availability of high quality, high resolution, large coverage inshore topography data (e.g., LIght Detection And Ranging, LIDAR, topographic data) and land cover information (e.g., National Land Cover Data, NLCD) to support dense mesh development.
- Continuing improvements in the ADCIRC code (e.g., coupling with wave modeling) which increase the sensitivity of results to mesh resolution relative to the mathematical representation of the physics.

For a triangular mesh the average node spacing equals $1.075/(\text{mesh density})^{½}$. Thus, reducing node spacing in an area of interest by half will nearly quadruple the number of nodes. Increased mesh refinement must be approached carefully to avoid issues of computational stability. Resolving instabilities in large meshes can require numerous, time consuming adjustments to nodes arrangements and attribute assignments (see Section 8).

[3] For a triangular mesh, mesh density ≈ 1.15 **/** (average node spacing)^2 .

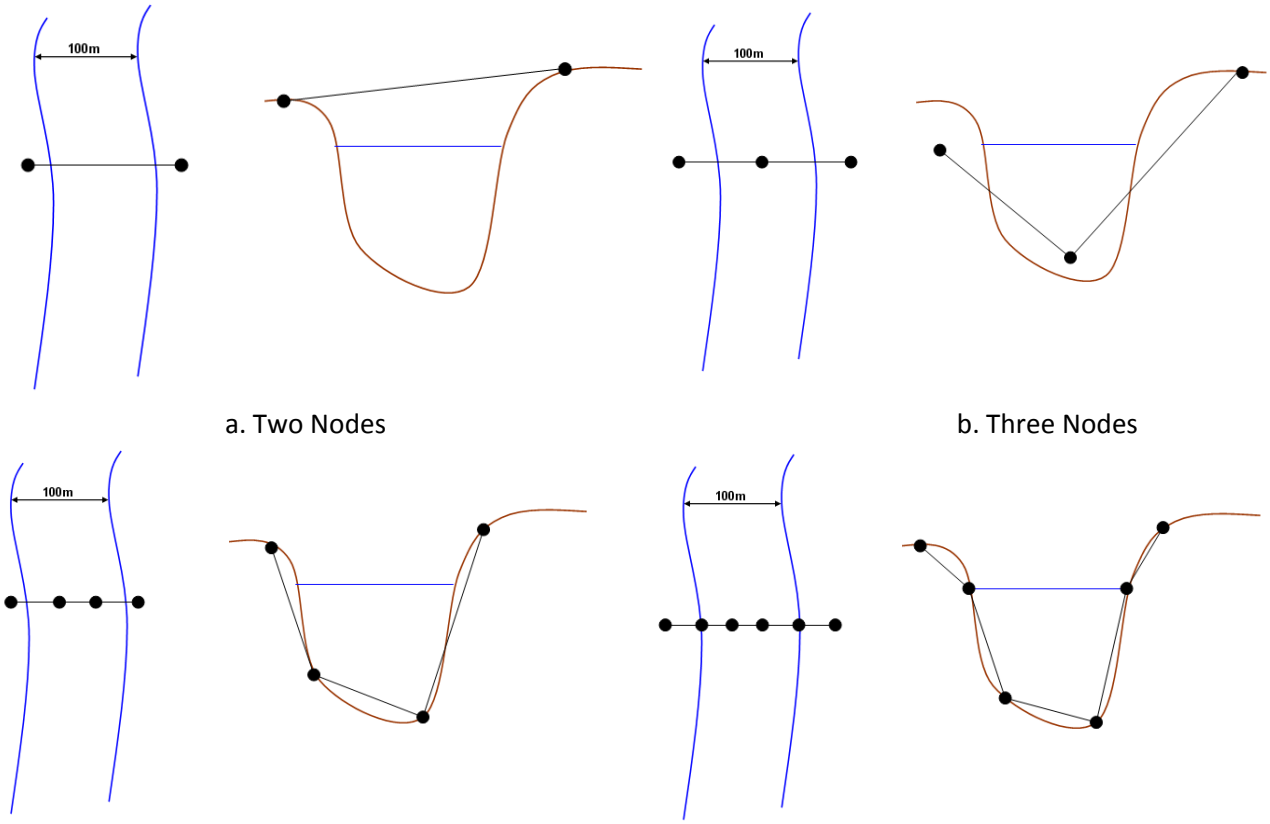

a. Two Nodes b. Three Nodes

c. Four Nodes d. Six Nodes

Figure 10.4. Alternative Number of Cross Channel Nodes
Jacobsen et al 2010

10.4 Influence of Key ADCIRC Parameters and Mesh Resolution

In 2010 Jacobsen et al, under funding from FEMA, investigated the influence of ADCIRC settings/parameters and mesh resolution on surge and tide model performance. The researchers employed the South Carolina coastal FIS ADCIRC SWL model validated for Hurricane Hugo for sensitivity tests entailing 16 surge and 2 tide simulations. Sensitivity tests examined ADCIRC explicit versus implicit solution method, modifications to the treatment of acceleration, and selected variations of time-step, eddy viscosity, and mesh resolution. The researchers prepared four modifications to the base South Carolina mesh to evaluate adjustments in the resolution of conveyance and raised topographic features. Simulations assessed effects on model runtime, stability, and accuracy. Major findings of the study were:

- Use of the explicit (as opposed to the implicit) solver for ADCIRC surge application that meet Courant stability condition is generally recommended as it reduces runtime, moderately increases wetting stability, and provides no significant difference in accuracy.
- No modification in the treatment of acceleration terms is generally recommended. The unmodified version does not significantly affect runtime or stability. Modification would be acceptable if it eliminates persistent instabilities with relatively minor influence on results,

e.g., at key inlets. A sensitivity test is recommended if modifying the acceleration terms is being considered.

- Eddy viscosity value should be less than 100 m^2/sec. Lower values (including nodal variable values where convenient) improve surge conveyance accuracy and should be employed consistent with model stability.
- Reducing model time-step increases runtime, increases stability (reduces the Courant number) and improves accuracy. The experimental mesh with high mesh resolution (50 m node spacing of key features) proved stable at a 1 s time-step while the very high resolution (30 m) required a reduction of time step from 1 to 0.5 s.
- For the subject meshes the compute time increased nearly proportional with mesh size.
- Increasing conveyance mesh resolution does not create significantly instability (when coupled with an appropriate time-step) and improves surge modeling accuracy in critical areas for floodplain fidelity (see Figure 10.5). Drastic changes in mesh resolution along the course of a channel reduce stability and accuracy.
- Increasing overland mesh resolution does not create significant instability (when coupled with an appropriate time-step) and improves the horizontal accuracy of localized inundation. Increases in overland mesh resolution which do not substantially change regional overland surge conveyance do not affect accuracy.
- For tidal simulations, increasing conveyance mesh improves accuracy, particularly for the low water portion of tide hydrograph, subject to other conveyance properties.

The researchers noted that sensitivity test conclusions were all consistent with ADCIRC model theory.

10.5. Project Considerations

Given the extreme size and complexity of large high resolution meshes,[4] development of an ADCIRC coastal surge model faces several important project considerations, including:

- Multiple objectives for the ADCIRC surge model (e.g., forecasting, forensic analysis, FIS, surge protection planning and design, coastal landscape management, etc.). Different projects can impose different mesh refinement and model validation requirements. In particular, different projects may focus modeling efforts on different surge hazard levels, necessitating different mesh development actions.
- Participation of local stakeholders, such as local agency officials and private interests, may urge resolution requirements for particular conveyance and raised topographic features and aspects of surge inundation.
- Availability and quality of mesh attribute data;
- Availability of surge hydrodynamic modeling and GIS professionals with appropriate mesh development experience.

[4] Similar mesh development problems apply with any code for HPPC application—such as ADH and FVCOM (see Table 10.1).

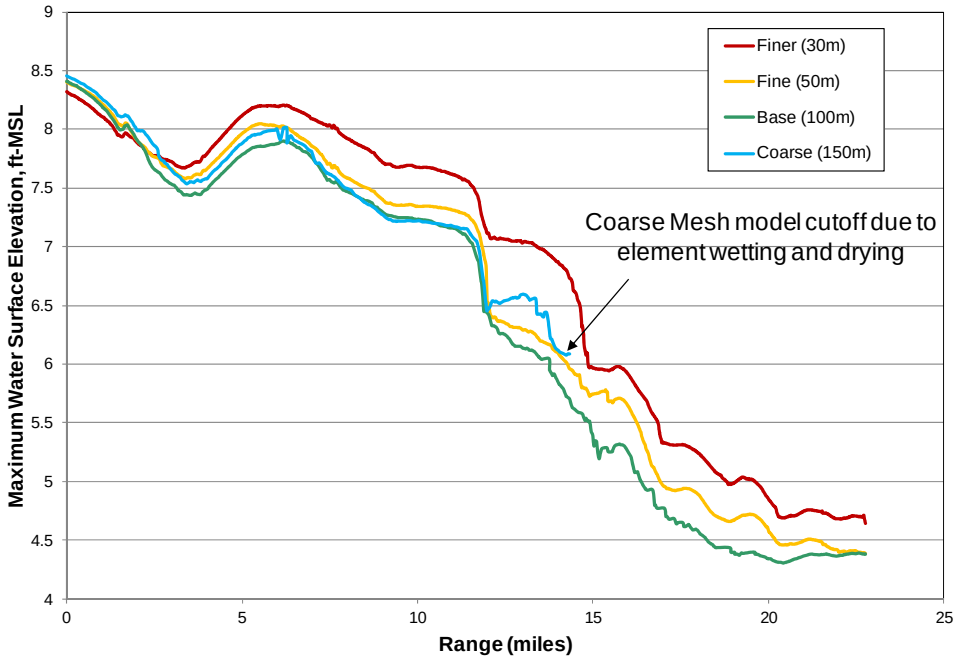

Figure 10.5. Example of Surge Sensitivity to Resolution of Preferential Conveyance Feature
(Figure shows the modeled peak surge profiles along the Ashley River in South Carolina)
Jacobsen et al 2010

- Coordination of a large dispersed group of modeling professionals.
- Limited budgets and schedules for mesh development, testing, and validation. Development of a stable and accurate mesh entails a lengthy, tedious process. In some cases the task of mesh development has been contracted to university laboratories, in which case the lower labor costs (compared to private contractors) and particular research objectives may allow (as schedules permit) for increased mesh experimentation.
- Suitable HPPC resources, which should provide for a) a sufficient number of appropriate compute, writer, head, and back-up cores, together with communication and storage hardware, on a single system assigned for the duration of the project;[5;] b) supervisory personnel with expertise in the setup and operation of ADCIRC; and c) availability on a priority basis throughout the lengthy mesh development, validation, and production periods. In some cases mesh development contracts with university laboratories have allowed for the use of their research HPPC systems. Figure 10.6 depicts the decision-making process for determining HPPC costs.
- Acceptable error and uncertainty and implications of model performance limitations, which necessarily reflect compromises, for the use of model results.
- Potential code improvements that could enhance model performance for the project.

[5] Slight differences in model results can occur when simulations are completed on HPPC systems with differing number of cores and subdomains.

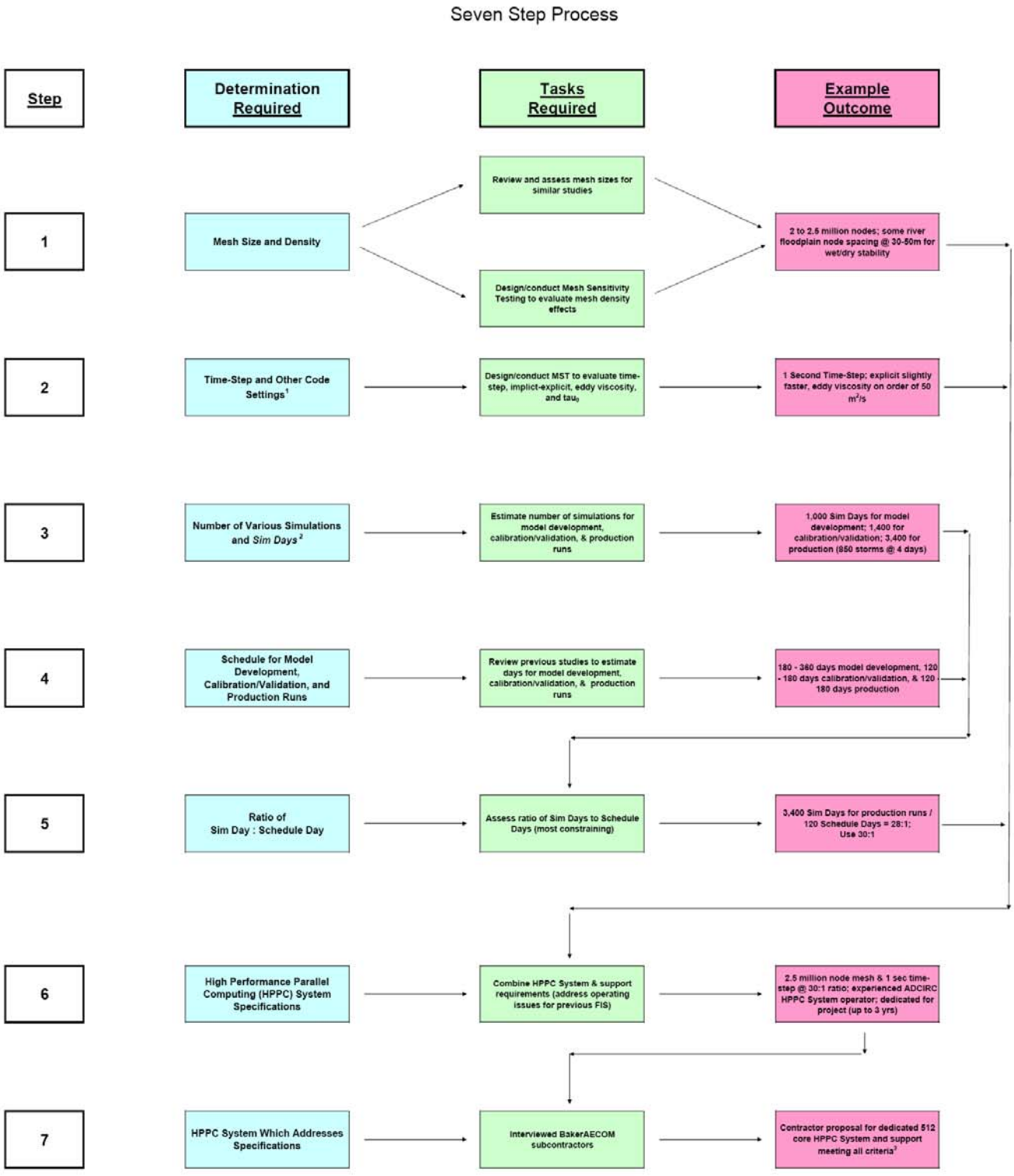

[1] The tightly coupled SWAN+ADCIRC version of the code, which is assumed to run at about 1/2 the speed of ADCIRC alone.

[2] A *Sim Day* is one day of storm or tide conditions; a typical hurricane hindcast simulation period is four to five days plus spin up for tides of up to 20 days; a tidal simulation may be up to 40 days.

[3] 5,800 total Sim Days = 139,200 hours; @ 30:1 = 4,640 HPPC System hours; @ 512 cores = 2.4 million core-hours; typical core-hour "phone quote" is on order of $1.00/core-hour; thus for larger projects it may make sense for the sponsor to purchase partial or full interest in an HPPC system.

Figure 10.6. Determining ADCIRC Computing Requirements and Costs

Section 11. Recent Applications of Hurricane Surge Modeling

This section reviews surge SWL and wave 2D modeling applications undertaken by the USACE and others since 2005, primarily in support of FEMA FISs. These applications all entail high resolution meshes and SWL codes executed on HPPC systems. The principal SWL code has been ADCIRC, with a few research investigations employing FVCOM. This section focuses on the hindcast demonstrations of these 2D models and summarizes the results of sensitivity, calibration, and/or validation testing to assess model performance in capturing the relevant surge and nearshore wave physics. Part III reviews applications of validated high resolution models in the return frequency analysis for SWLs and nearshore waves. Applications of overland wave modeling (e.g., WHAFIS) to assess potential waves associated with a particular return SWL are also discussed in Part III. Applications of additional analysis to hurricane protection structures and polders are examined in Part IV.

11.1. Overview of Post-2005 Surge Models

Jacobsen et al 2010 summarized six surge models prepared since 2005 by FEMA and partnering state/regional flood management agencies for south Atlantic and GoM coastal areas—for revised NFIP mapping. The six studies included Florida-Big Bend, Louisiana,[1] Mississippi, North Carolina, South Carolina, and Texas. Of these six, formal model reports have only been issued on Louisiana and Mississippi. Preliminary information on model parameters and mesh has been obtained for the other four. The six models all utilize 2D ADCIRC (see Section 10), which incorporates all of the relevant physics (excluding buyouancy). Table 11.1 summarizes basic information regarding various model settings and the high resolution meshes. Additional FIS modeling studies using 2D ADCIRC have also been initiated for Northeast Florida/Georgia, Central Florida-Atlantic, and Northwest Florida-Panhandle.

The six models employed different SWL numerical methods, treatment of acceleration terms, time steps, and eddy viscosity values to balance accuracy, stability, and efficiency considerations, given mesh resolution. (See Sections 8 and 10 for a discussion of these factors and an assessment by Jacobsen et al of their influence on model performance.) They have also used different wave coupling approaches, with a South Carolina study using the recently available tightly coupled SWAN+ADCIRC code. The six models all utilize node spacing well below 100 m to resolve coastal conveyance features, with North Carolina providing geometry detail below 10 m.

Jacobsen et al compared the node densities of the six meshes—which encompassed a total of 40 coastal and 77 inland counties—for 28 land/water classifications. They identified twelve classifications which contributed significantly to mesh size:

- Three wetland—Palustrine Forested, Palustrine Emergent, Estuarine Emergent—and three inshore water classifications—Inshore Navigable, Inshore Deep, and Inshore Shallow. These six classifications accounted for over 60 percent of inshore nodes for coastal counties.
- Two nearshore water classifications (from shoreline to 30 m depth) also contribute significantly to coastal county mesh size—Nearshore Deep and Nearshore Shallow.
- Four classifications account for over 50 percent of the nodes for the interior counties—Cultivated Land, Pasture/Hay, Palustrine Forested Wetland, and Inshore Shallow Water.

[1] The Louisiana surge model was developed for a multi-purpose effort also encompassing metropolitan New Orleans HSDRRS design and the LaCPR Study of future coastal restoration and protection alternatives.

Table 11.1. Summary of Six Recent FIS 2D ADCIRC Models

Jacobsen et al 2010

	Florida-Big Bend	Louisiana	Mississippi	North Carolina	South Carolina	Texas
Status	Ongoing	Complete	Complete	Ongoing	Ongoing	Ongoing
Lead	State of Florida	FEMA VI	FEMA IV	State of North Carolina	State of South Carolina	FEMA VI
ADCIRC Modeler	U of Central Florida	U of Notre Dame	URS Corporation	U of North Carolina	Taylor Engineering	U of Notre Dame
Multi-Purpose Study?	Not Determined	Yes	No	Not Determined	No	Not Determined
HPPC System	UCF 256 cores/run more cores available	USACE >1,000 cores 256 cores/run	URS 256 cores	RENCI 4,096 cores 512 cores/run maximum	URS 128 cores	USACE >1,000 cores 256 cores/run
Numerical Method	Implicit/ Explicit	Implicit/ Explicit	Implicit/ Explicit	Fully Explicit	Implicit/ Explicit	Implicit/ Explicit
Spatial/Temp Accel Modified?	Yes/Yes	Yes/Yes	Yes/Yes	No/No	No/No	Yes/Yes
Time Step	1	1	1	0.5	2	1
Eddy Viscosity (m^2/s)	Variable (2 – 50)	Uniform 50	Uniform 50	Variable (2 – 12)	Uniform 50	Variable (2 – 50)
Mesh Nodes	855,445	2,137,978	900,450	517,049	528,401	3,323,388
Weirs	No	Yes	Yes	No	No	Yes
Tightest Node Spacing (m)	17.8 - 24.1	27.0 - 33.1	32.8 - 43.0	6.8 - 9.5	58.5 - 69.2	25.9 - 32.9
Wave Model Coupling	SWAN Loose	WAM/ STWAVE Loose	SWAN Loose	Wave Watch III/SWAN Loose	SWAN+ ADCIRC Tight	WAM/ STWAVE Loose

However, as illustrated in Figure 11.1, the node spacing for land/water classifications in both coastal and inland counties varied widely, both within and across these recent studies. Some of this variation could be due to the presence of topographic features. At this time the scientific literature does not provide guidance on mesh resolution or the effects of resolution inconsistency. Jacobsen et al prepared a mesh recommendation for the Northeast Florida/Georgia FIS based on targeting mesh density for each of the land/water classifications at the upper 25th percentile for the 40 coastal and 77 inland counties.

11.2. USACE 2006 Louisiana Surge Model

As noted in Section 10.2, in 2006 a team comprised of the ADCIRC Development Group (led by Joannes Westerink), the USACE CHL (led by Bruce Ebersole and Jane Smith), and several contractors, developed a loosely coupled 2D ADCIRC-STWAVE model for coastal Louisiana in support of a multi-purpose effort encompassing state-wide FEMA FIS (USACE 2008), metropolitan New Orleans HSDRRS design (USACE 2010), and the LaCPR study of future coastal conditions.[2] As noted in Table 11.1 the modelers used the implicit/explicit numerical method, modified the spatial and temporal acceleration terms, and set eddy viscosity values to a uniform 50 m^2/s. The modelers conducted hindcast validations for Hurricanes Katrina and Rita, which are documented in the FIS report and also in Bunya et al 2010.

The full southeast Louisiana FIS mesh (SL15v3_2005_r09) extends to the mid-Atlantic ocean. Figures 8.2 and 8.3 illustrate the coastal Louisiana portion of the ADCIRC mesh. As described in Section 7, coastal southeast Louisiana includes a variety of landscape features which influence how wind setup and conveyance affect surge, all of which are reflected to some extent in the mesh.

Figures 11.2.a. and b. further depict the ADCIRC mesh topography/bathymetry, and node spacing, with Figures 11.3.a. and b. showing details of two areas—in Houma LA and New Orleans LA. The mesh includes the use of internal boundaries (weirs) to represent levees, floodwalls, and raised coastal roads and railroads. Mesh topography was developed primarily from 5-m LIDAR DEMs (see GTN-2). In areas without LIDAR coverage topography was estimated from the USGS 30-meter DEM where applicable. Where both DEMs lacked coverage the modelers used the National Land Cover Data (NLCD) set to assign elevations based on land cover type (e.g., for coastal marsh). Elevations for levees, floodwalls, roads, and railroads were obtained from feature survey data.

Mesh features—particularly raised features—have some minor planimetric (horizontal offset) errors, principally associated with node density limitations. More importantly, however, the mesh has extensive topography and bathymetry errors. Elevation errors are due primarily to 1) outdated bathymetric data for many coastal water bodies (some of which has been updated since 2006); and 2) problematic vertical referencing of the LIDAR and USGS DEMs and other sources of topographic and bathymetric data used at the time of mesh development (see GTN-2).

Of the 2.1 million nodes in the mesh, close to 926,000 (43%) are located in the coastal Louisiana parishes, with 727,000 inshore and 199,000 in the nearshore region. Almost 446,000 nodes (21%) are located in inland parishes. The remaining 766,000 nodes (36%) are located over adjacent states and the open GoM and Atlantic ocean. Table 11.2 provides a breakdown of node spacing and node percentages within coastal and inland parishes by land/water classifications. As indicated in Figure 11.1, there was considerable variation between parishes for similar classifications.

[2] The team has also used the Hurricane Katrina hindcast to support USACE forensic investigations, see IPET 2006 and Ebersole et al 2010.

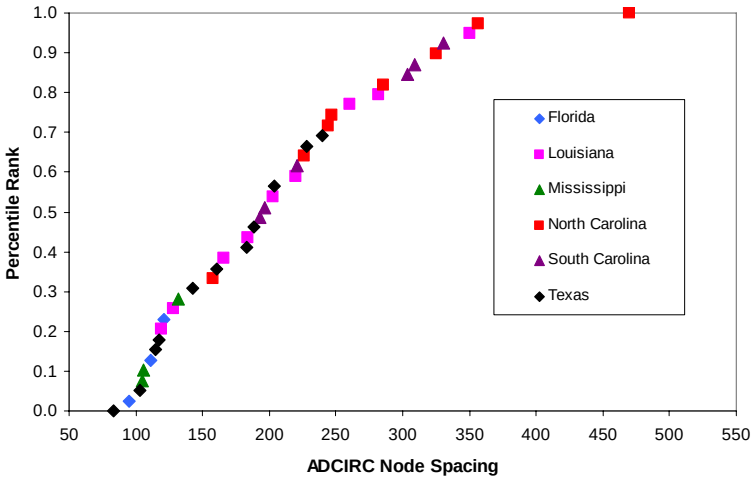

a. Estuarine Emergent Wetland (40 Coastal Counties)

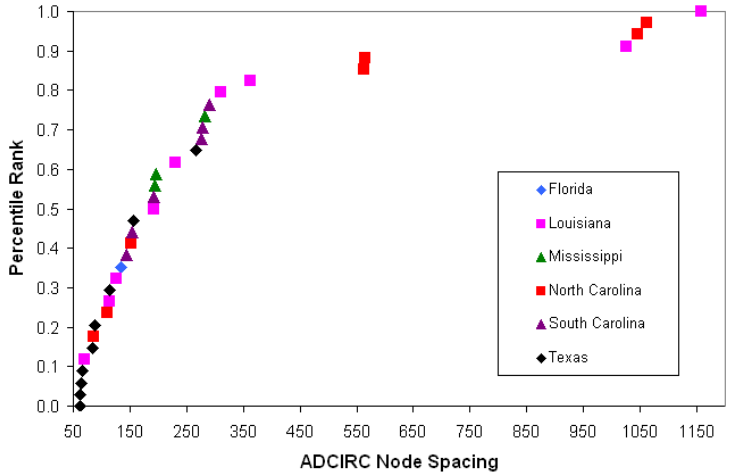

b. Deep Water (40 Coastal Counties)

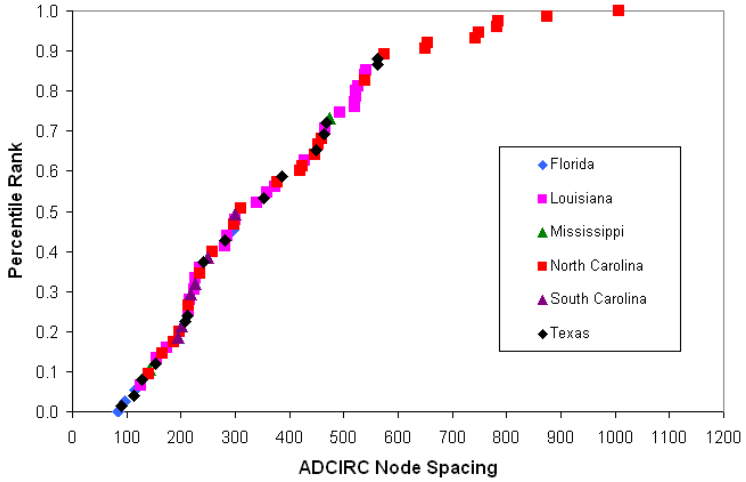

c. Palustrine Forested Wetland (77 Interior Counties)

Figure 11.1. Example Distributions of Node Spacing for Land/Water Classification
Jacobsen et al 2010

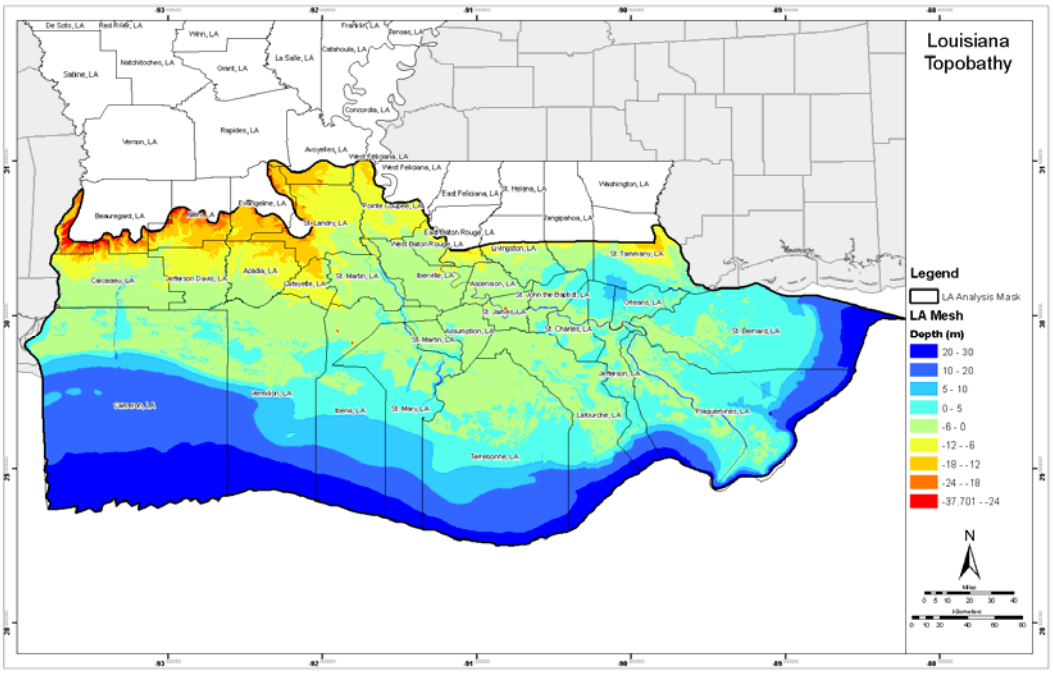

a. Mesh Topography/Bathymetry

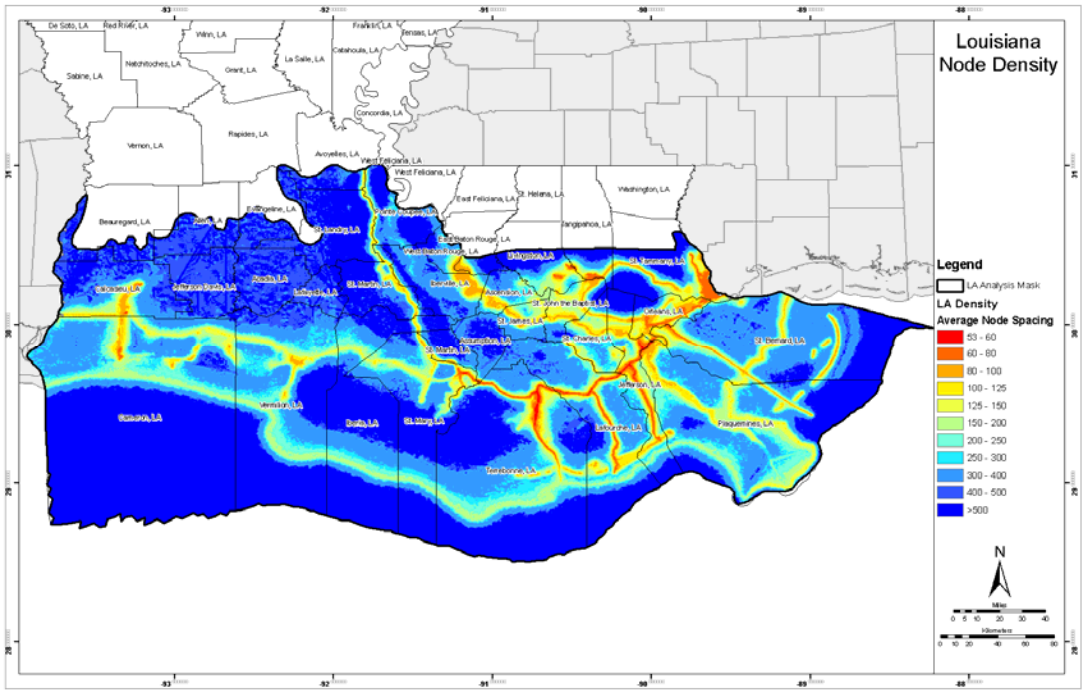

b. Mesh Node Spacing

Figure 11.2. Louisiana ADCIRC Mesh

Jacobsen et al 2010

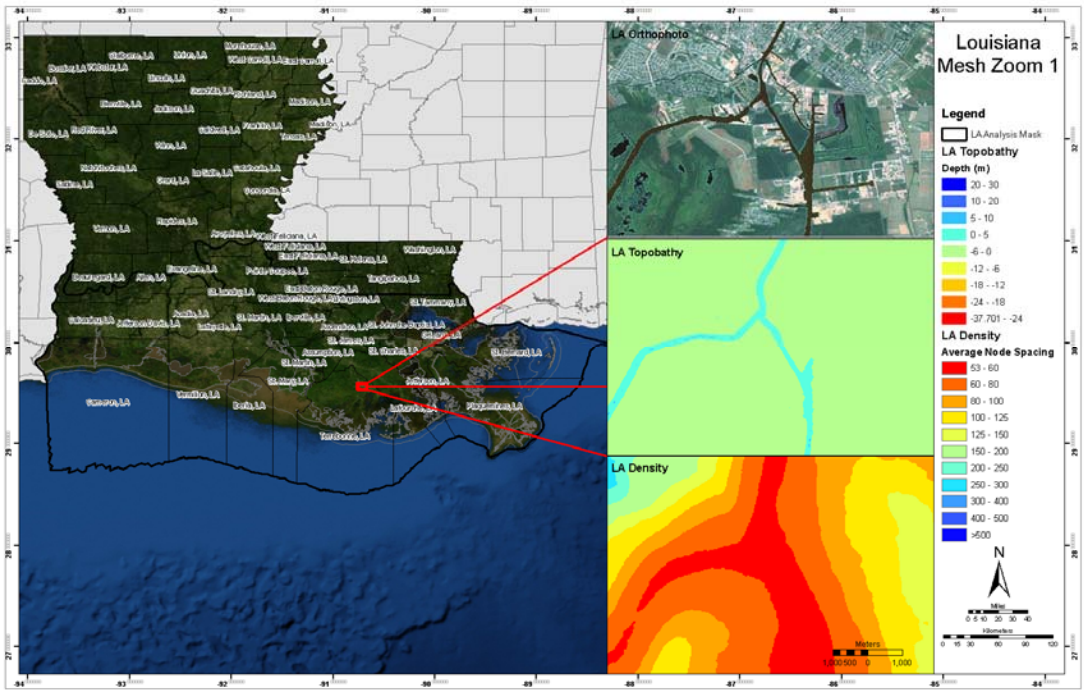

a. Mesh of Houma LA

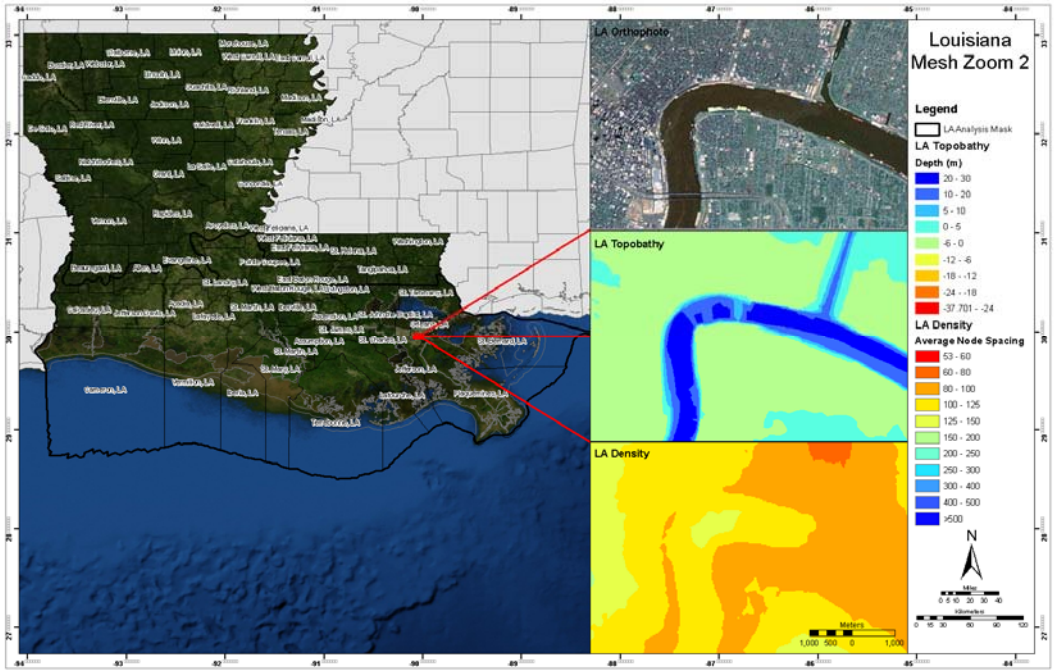

b. Mesh of Mississippi River Near New Orleans LA

Figure 11.3. Louisiana ADCIRC Mesh Details

Jacobsen et al 2010

Table 11.2. Southeast Louisiana ADCIRC Mesh Nodes

Jacobsen et al 2010

	Coastal Parishes		Interior Parishes	
	Avg Node Spacing (m)	Percentage of Nodes	Avg Node Spacing (m)	Percentage of Nodes
High Intensity Developed	118	1.0%	166	1.5%
Medium Intensity Developed	132	1.2%	204	2.1%
Low Intensity Developed	157	3.9%	239	6.7%
Open Spaces Developed	157	0.3%	262	0.8%
Cultivated Land	302	4.5%	361	13.0%
Pasture/Hay	215	2.3%	350	4.9%
Grassland	258	0.2%	421	0.8%
Deciduous Forest	188	0.1%	335	0.0%
Evergreen Forest	232	0.0%	449	1.6%
Mixed Forest	163	0.0%	421	0.1%
Scrub/Shrub	177	0.4%	450	1.4%
Palustrine Forested Wetland	212	9.0%	290	27.1%
Palustrine Scrub/Shrub Wetland	175	1.6%	245	2.0%
Palustrine Emergent Wetland	220	12.3%	202	5.7%
Estuarine Forested Wetland				
Estuarine Scrub/Shrub Wetland	159	0.1%	134	0.1%
Estuarine Emergent Wetland	237	19.0%	116	9.7%
Unconsolidated Shore	226	1.1%	179	0.2%
Bare Land	236	0.0%	347	0.0%
Dunes	158	0.3%	191	0.1%
Palustrine Aquatic Bed	211	0.4%	233	0.2%
Estuarine Aquatic Bed	255	0.5%	110	0.0%
Inshore Navigable Water	106	1.6%	117	1.3%
Inshore Deep Water	252	5.1%	196	5.0%
Inshore Shallow Water	242	35.4%	181	15.7%
		100.0%		100.0%
Nearshore Navigable Water	296	0.3%		
Nearshore Deep Water	471	82.7%		
Nearshore Shallow Water	329	17.0%		
		100.0%		

The modelers assigned constant friction coefficient values (Manning's *n*) on the basis of land cover data. Table 11.3 lists the values that were used for Louisiana GAP land cover data. Water bottom friction values were 0.02 for open ocean and large inland lakes; 0.025 for sheltered estuaries and deep channels and rivers; and 0.045 for shallow channels. While Manning's *n* values for water bottoms are likely to remain steady with increased SWL, values for flow over marsh would likely decrease significantly with surge depth (see Section 7).

The modelers spent considerable effort in mesh refinement to improve local depiction of surge dynamics, (and improve stability). However, they did not calibrate the model—typically done by "tuning" Manning's *n* values. Their rationale was as follows:

> It can happen that adjusting a parameter such as Manning *n* compensates for other modeling deficiencies. Such a tuned model may better match the data for a specific storm, but for the wrong reason. The model may then not work well for other storms or certainly when the modeled storm transcends the data set. Typically, in regions where model results do not match the data, there are geometric details that have been neglected. We want to avoid ad hoc tuning of parameters and, instead, add grid resolution to capture the missing geometric details. Using grid resolution to improve the model is a more robust method of making corrections.

Table 11.3. Manning-n Values for Louisiana Gap (LA-GAP) Classification

USACE 2008

NLCD Class	Description	Manning's-n
1	Fresh Marsh	0.055
2	Intermediate Marsh	0.05
3	Brackish Marsh	0.045
4	Saline Marsh	0.035
5	Wetland Forest-Deciduous	0.14
6	Wetland Forest–Evergreen	0.16
7	Wetland Forest–Mixed	0.15
8	Upland Forest–Deciduous	0.16
9	Upland Forest–Evergreen	0.18
10	Upland Forest–Mixed	0.17
11	Dense PineThicket	0.18
12	Wetland Scrub/Shrub–Deciduous	0.06
13	Wetland Scrub/Shrub–Evergreen	0.08
14	Wetland Scrub/Shrub–Mixed	0.07
15	Upland Scrub/Shrub–Deciduous	0.07
16	Upland Scrub/Shrub–Evergreen	0.09
17	Upland Scrub/Shrub–Mixed	0.08
18	Agriculture Crops–Grass	0.04
19	Vegetated Urban	0.12
20	Non-Vegetated Urban	0.12
21	Wetland Barren	0.03
22	Upland Barren	0.03
23	Water	0.02 - 0.045

The FIS documentation does not provide sensitivity analyses for Manning's *n* (or other model settings and parameters that could be modified) to assess the potential affect of selected values. Section 7.4 described Wamsley et al's 2009 analysis showing that surge results could be highly sensitive to marsh elevation; Section 10.4 discussed results of selected sensitivity tests for model settings performed by Jacobsen et al using a South Carolina mesh.

In addition to mesh attributes, the ADCIRC 2D model included:

- A LMSL of 0.44 ft NAVD88-2004.65[3] and LMMSL adjustment (for steric effect, see Section 5.1) of 0.34 to 0.49 ft for August to September.
- The tidal boundary and forcing for K_1, O_1, Q_1, M_2, S_2, N_2, and K_2 constituents. (P_1., which typically has a higher amplitude than the semi-diurnal constituents, was not included).
- Boundary inflows for the Mississippi/Atchafalaya Rivers, which closely approximated actual flows during Hurricanes Katrina and Rita (167,000/70,000 and 181,000/79,000 cfs).
- Wind and atmospheric pressure provided by H*Wind files and interpolations from CPD-ambient pressure data. Bunya noted that the match line between the buoy data (as depicted in Figure 11.4) and the H*Wind files had a slope of 0.99 with an R^2 of 0.93, though No. 42007 near Mississippi Sound was out of service during the passage of the eye. Uncertainties with the H*Wind wind field, which have a significant influence on SWL and wave height, were not evaluated (see Section 1.3).
- Radiation stress gradients at 30-minute intervals from the loosely coupled STWAVE model.

Smith set up four STWAVE grids (see Figure 11.5), three larger overlapping half-plane grids along the coast and a fourth full plane, grid for Lake Pontchartrain. The four STWAVE models were forced with H*Wind data and boundary and initial wave conditions taken from a regional WAM model.

All four STWAVE grids contained 200 m resolution, with a bathymetry interpolated from the ADCIRC mesh. Smith performed a sensitivity analysis of bathymetry, using degradation of the Chandeleur Islands. The tests indicated that changing from emergence to submergence had a significant influence on leeward waves, but relative changes to submergence had much less effect.

Although not stated in the FIS documentation, STWAVE appears to have been run without energy dissipation from friction (see Smith 2007). Under this condition Smith analyzed the sensitivity of the Lake Pontchartrain grid to resolution (down to 50 m) and found that finer resolution was not warranted. Sensitivity analysis for bottom friction by Smith showed that spatially variable friction, as well as dynamic change in friction (e.g., associated with damaged vegetation), both could affect hindcasts of Katrina waves (Smith 2007). The modelers also assessed the sensitivity of wave results to wind speed—finding that a 5% change in wind speeds could produce a 1-ft change in wave heights.

[3] This value is about 0.2 ft higher than the current LMSL value of about 0.1 to 0.3 NAVD88-2006.81 along the southeast Louisiana coast, see GTN 2.

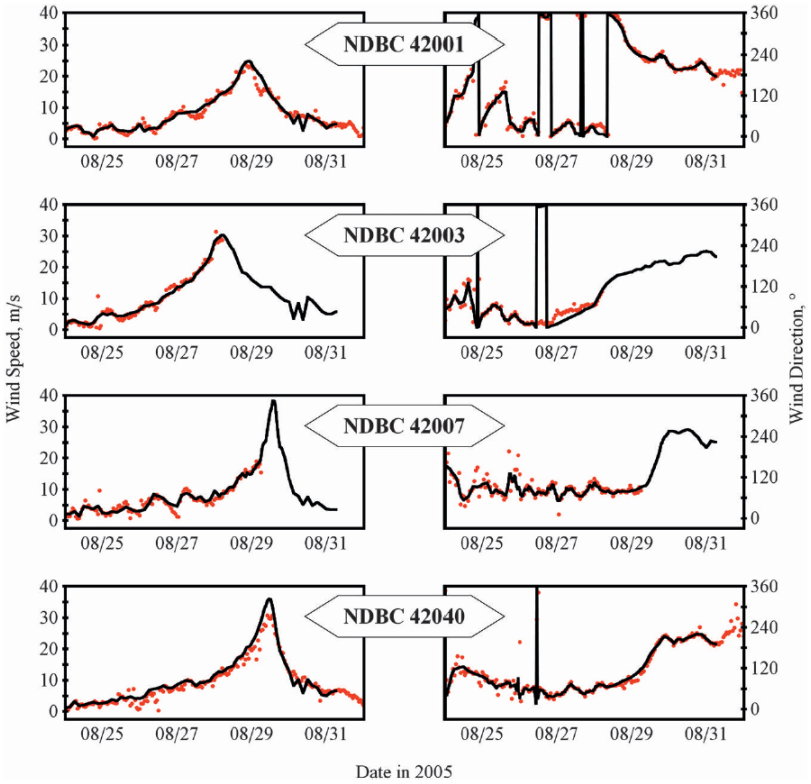

Figure 11.4. Hurricane Wind Measurements versus H*Wind File
Bunya 2010

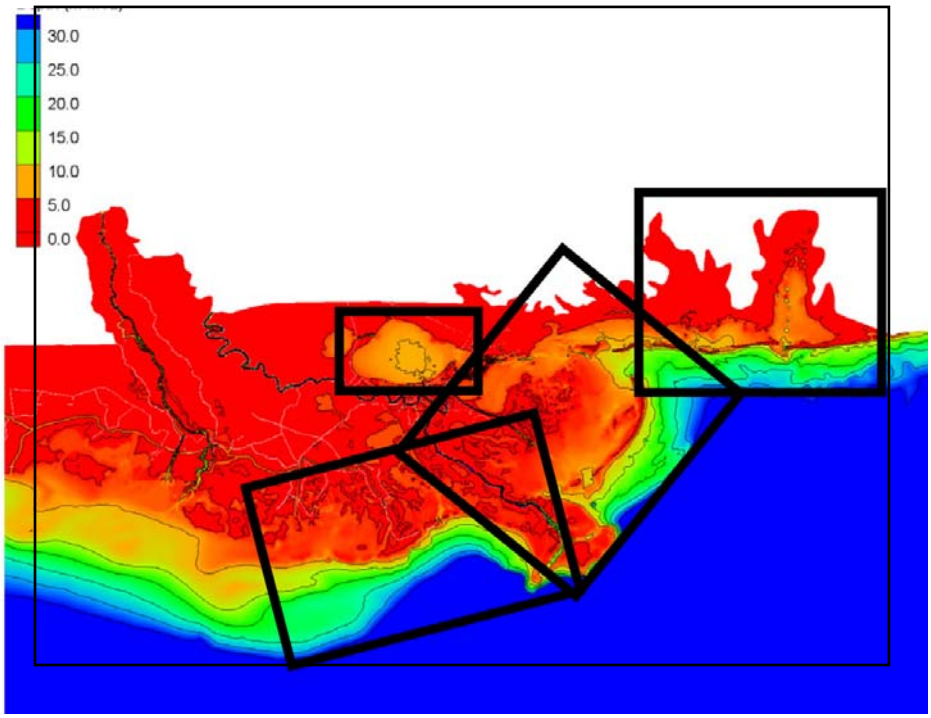

Figure 11.5. Louisiana STWAVE Grids
Smith 2007

Results of Tidal Validation

The ADCIRC modelers compared the results of a tidal simulation (45-day spin up, including river inflow and tide ramps, followed by a 60-day simulation) for the seven included constituents with harmonic analysis of the same constituents at numerous NOAA Gulf of Mexico tide stations. As shown in Figure 11.6, predicted versus observed amplitudes for 15 Louisiana stations were generally within ±0.1 ft. Computed K_1 and O_1 amplitudes at several seaward stations were consistently higher than observed, possibly indicating a lack of inland tidal conveyance. The most noticeable error was in the phases for the small K_2 constituent. Simulating the inland propagation of low amplitude tides in southeast Louisiana can be hampered by poor mesh resolution, physical and numerical dampening, the absence of baroclinic forcing, and insufficient tidal data (see Jacobsen and Dill 2007).

Results of Hurricane Katrina Validation

Figure 5.5 depicts the 2006 ADCIRC 2D SWL model results for Hurricane Katrina surge dynamics. Figures 11.7.a. and b. compare ADCIRC results with 206 observed SWL HWMs obtained by the USACE and 193 HWMs obtained FEMA. The overall matches for both data sets were reasonable, with slopes of 0.99 and 1.05 and R^2 values of 0.92 and 0.94. Modeled peak SWLs were within ±1.5 feet at 63 percent of USACE HWMs and within ±3.0 feet at 96 percent. Modeled peak SWLs were also within ±1.5 feet at 75 percent of the FEMA HWMs and within ±3.0 feet at 98 percent. These results imply a relative error of about 10% for HWMs greater than 15 ft.

The ADCIRC modelers noted a cluster of SWL results under-predicted by 1.5 to 3 feet along the south shore of Lake Pontchartrain. Figures 11.8.a. and b. show the locations of these under-predictions. The modelers suggested that poorly resolved wave setup in this region was a reason for the model bias. Three other possible sources of error not considered by the modelers may be 1) stronger wind setup in the shallow lake due to inaccurate characterization of local winds or air-sea drag; 2) a higher lake LMMSL not accounted for in the model; and 3) local drainage discharges along the south shore of Lake Pontchartrain not included in the model.

Figure 11.9 presents the modelers' comparison of nine modeled versus observed surge SWL hydrographs. The hindcast agrees reasonably well in shape and timing of hydrograph peaks. The modelers did not provide a statistical measure of the agreement (e.g., R^2). The modeled amplitude in Lake Pontchartrain (Pass Manchac and Bayou LaBranche) is generally lower, by more than one foot. The under prediction at the 17th Street Canal is partially attributed to under-resolution of south shore wave setup (Bunya 2010).

The ADCRIC validation for Hurricane Katrina demonstrates that the model reasonably captures general surge response to forcing conditions and major coastal terrain features. The model results in Figure 5.5 clearly illustrate the role of the regional hurricane protection system in diverting surge. Figure 11.10 a) and b) show the locations for a handful of USACE and FEMA HWMs that were measured east of New Orleans, outside the hurricane protection levees, in the coastal wetlands of St. Bernard and Plaquemines Parishes. The absence of extensive HWM data in this region prevents a validation of the highly dynamic surge response to variations in local coastal wetland conditions.

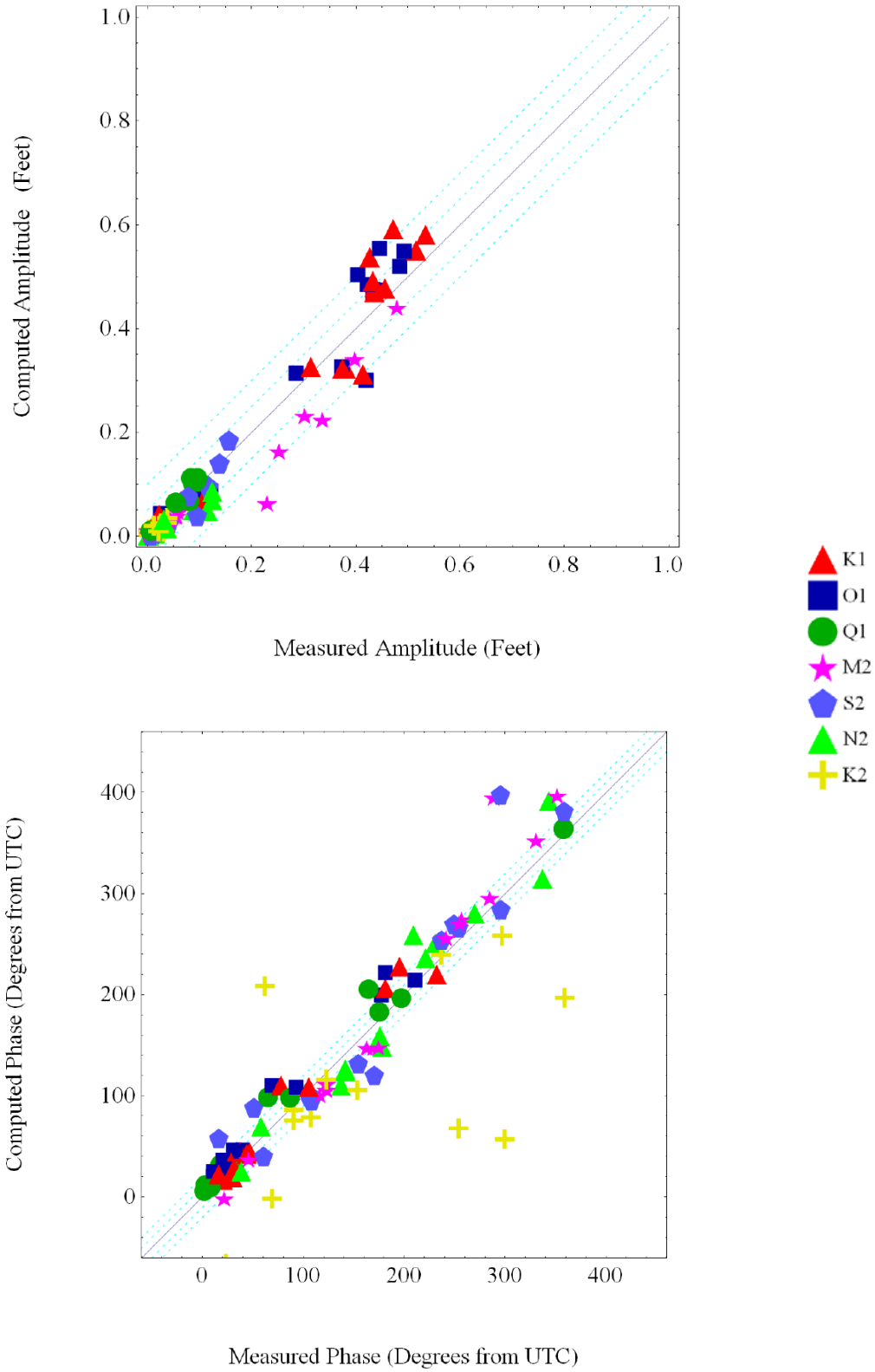

Figure 11.6. Tidal Validation for Louisiana Stations

USACE 2008

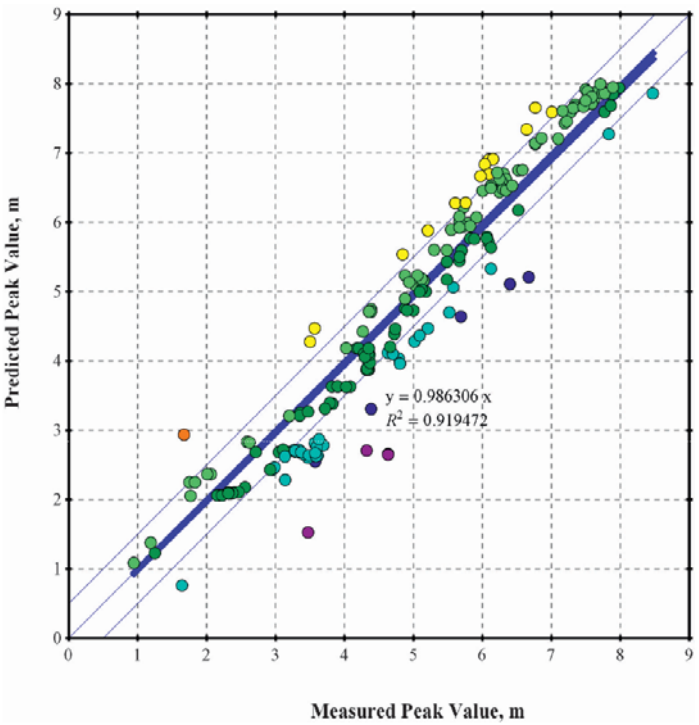

a. USACE HWMs

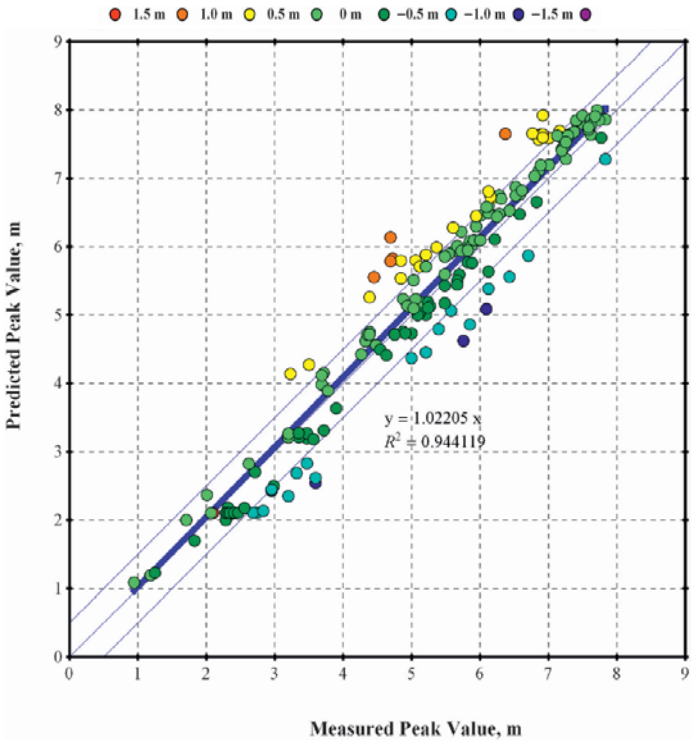

b. FEMA-URS HWMs

Figure 11.7. Hurricane Katrina Modeled Peak SWL versus Observed HWMs With ±0.5 m Error Bands

Bunya et al 2010

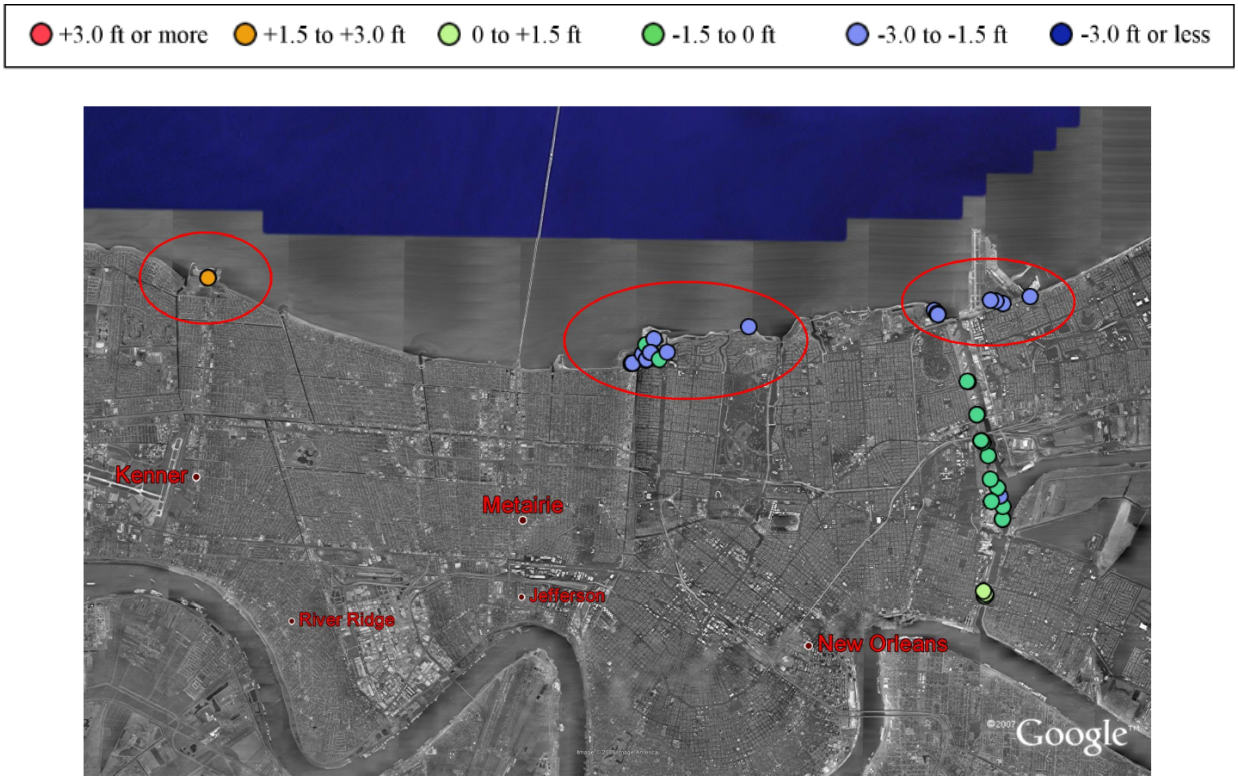

a. USACE HWMs

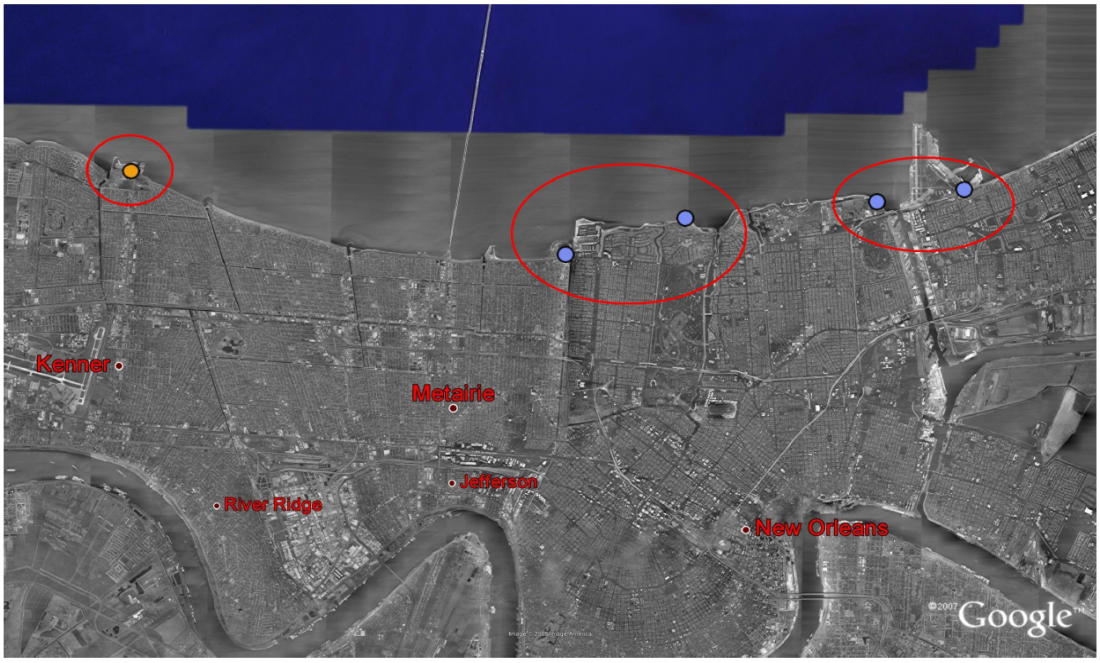

b. FEMA-URS HWMs

Figure 11.8. Under-Predicted Hurricane Katrina Peak SWLs Along Lake Pontchartrain South Shore

USACE 2008

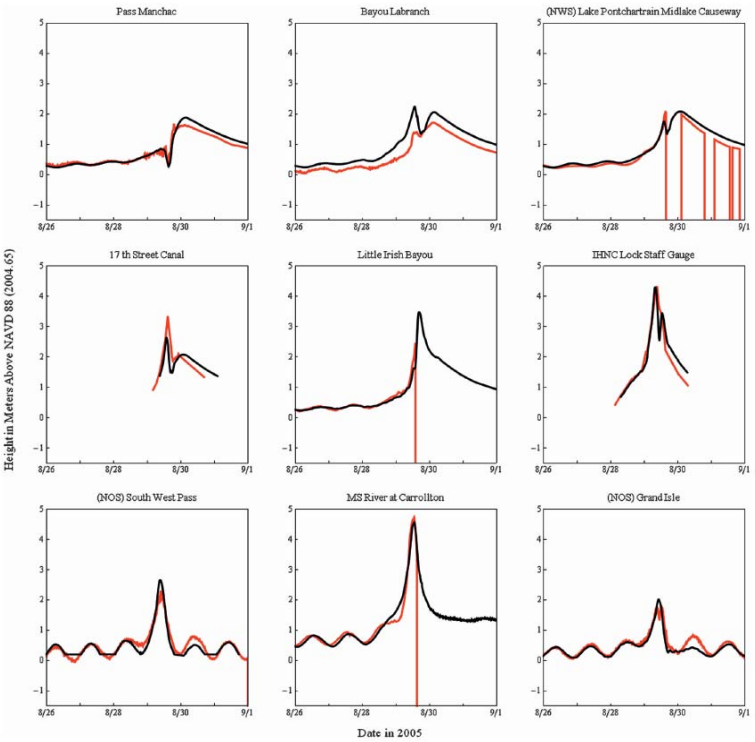

Figure 11.9. Hurricane Katrina Modeled (black) **versus Observed** (red) **Hydrographs**

Bunya 2010

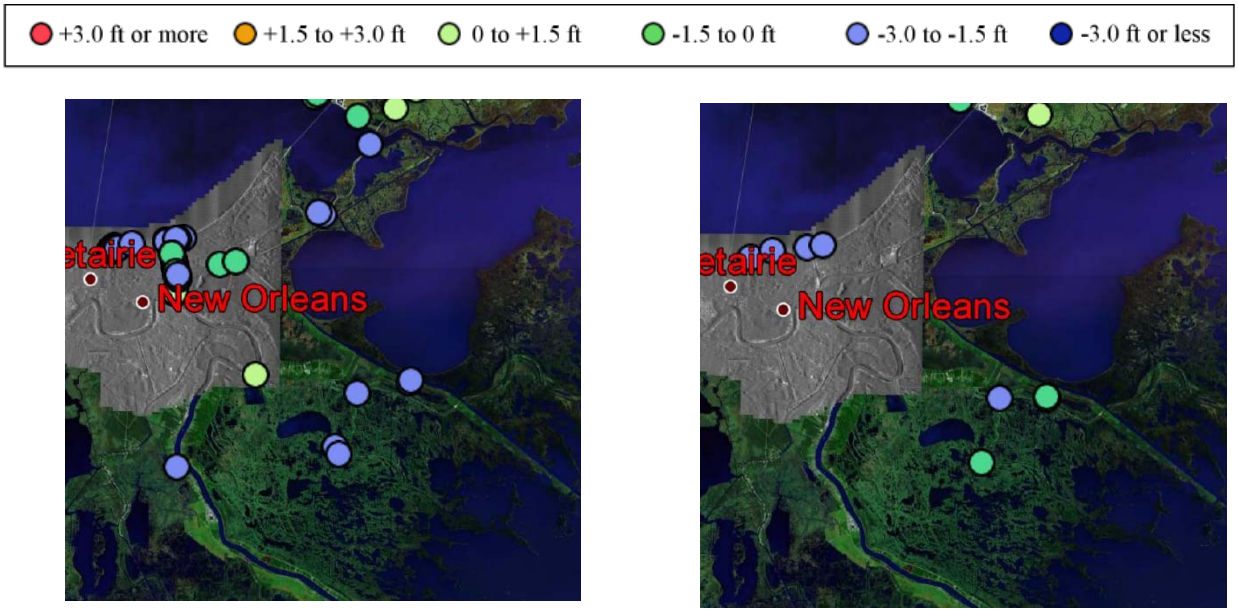

a)USACE HWMs b) FEMA HWMs

Figure 11.10. Hurricane Katrina HWMs in Eastern St. Bernard and Plaquemines Parishes

USACE 2008

Figure 11.11 compares the STWAVE results for Hurricane Katrina significant wave heights in Lake Pontchartrain to measurements obtained from deployed buoys. The buoys were placed in about 12 feet of water, with No. 22 north of the 17th Street Canal and No. 23 about one half mile to the west, and set to record wave data every 8.5 minutes. Smith suggests that buoy data are unreliable at the storm peak. The blue points and lines provide running 3-record averages at 25.5 minutes. Modeled significant wave heights appear to be about a foot lower during the growth phase than the observed heights.

The FIS model documentation does not analyze the sensitivity of Hurricane Katrina SWL validation results to the 2D ADCIRC model settings, parameter values, mesh resolution, mesh accuracy, or local mass balance errors or "non-fatal instabilities" that might have been present during the simulation.[4] The FIS model documentation does not provide a recommended bias correction to account for the noted error in matching Lake Pontchartrain SWLs, attributed to additional wave setup that cannot be represented in the model. Concerns related to sensitivity analyses, calibration, mass balance error analysis, and explicit bias correction have been raised by independent technical reviewers (Dean et al 2004 and USACE 2007). The USACE/FEMA currently regard the validation as sufficient for NFIP purposes (per email correspondence with Matthew M. DuBois, FEMA Region VI Engineer, August 10, 2011).

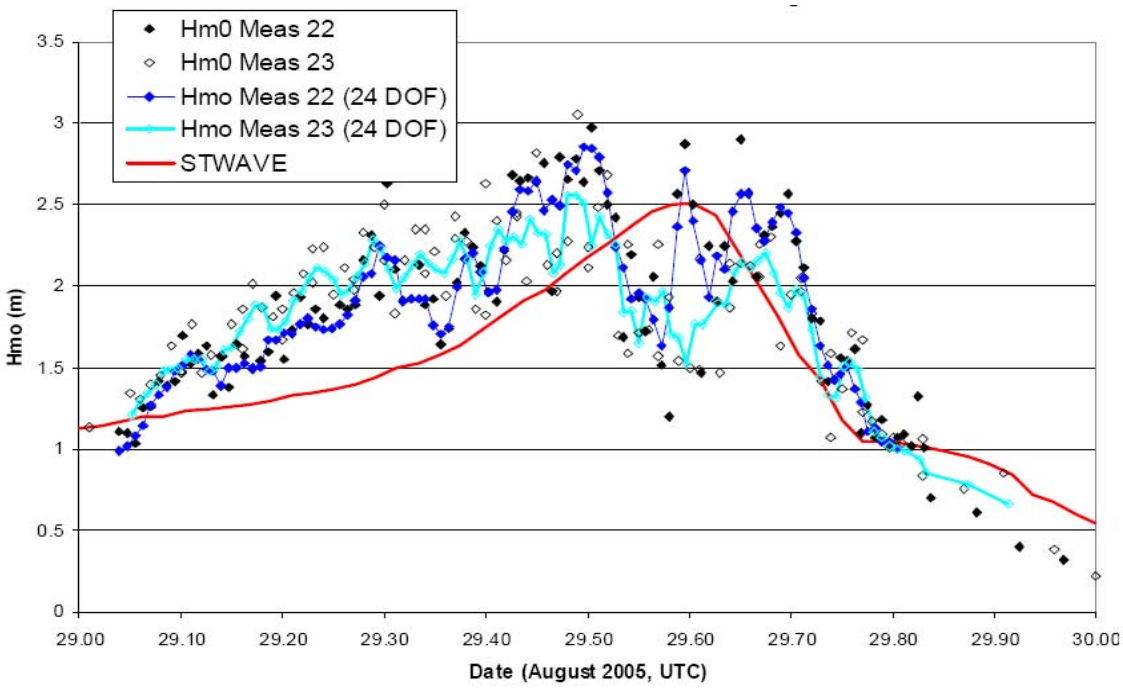

Figure 11.11. Hurricane Katrina Observed versus Modeled Significant Wave Heights in Lake Pontchartrain

Smith 2007

[4] The FIS documentation (USACE 2008) addresses mass conservation errors for one synthetic storm used in the return frequency analysis. Over each time-step (1 s) an average of 6% of the domain area had a relative mass conservation error exceeding ±0.01%. Further breakdown of this error was not provided.

Results of Hurricane Rita Validation

Figure 11.12 depicts the 2006 ADCIRC 2D SWL model results for Hurricane Rita surge dynamics along the southwest Louisiana coast. A key aspect is the peak compression of the surge long wave against the coast with landfall at approximately 3 am CDT September 24, 2005, followed by the continued landward spreading of the surge wave for hours after landfall. Thus, inland areas of southwest Louisiana, e.g., along the Calcasieu River near Lake Charles, experienced peak surge several hours after landfall.

The surge dynamics along the southeast Louisiana coast are illustrated in Figure 11.13. Hurricane Rita's large size and westward track across the GoM pushed a significant surge against the eastern Mississippi River delta flank and into Lake Pontchartrain. Surge levels for Hurricane Rita along the western Lake Pontchartrain shore were much higher for Hurricane Rita than for Hurricane Katrina.

Figure 11.14 presents the comparison of observed SWL HWMs and modeled SWL peaks, showing a slope of 0.98 and an R^2 of 0.74. The higher scatter for Hurricane Rita than Hurricane Katrina is consistent with lower peak SWLs, generally between 3 and 15 ft (NAVD88). Modeled peak SWLs were within ±1.5 feet at 33 of 62 HWM locations. The modelers noted higher residual error (under-prediction of SWL) in the Vermilion Bay region along the eastern portion of the landfall region (flagged in red in Figure 11.14). The poor match is associated with a cluster of twelve observations generally observed at 12 ft but predicted at about 10 ft. The modelers attributed this error to possible misrepresentation of conveyance geometry resolution and/or poor resolution of wave setup and provided a second trend line with a slope of 1.04 slightly a 0.86 R^2. As with the Hurricane Katrina hindcast for Lake Pontchartrain, additional factors could be inaccurate localized wind setup and pre-storm meteorological conditions.

The modelers compared computed versus observed hydrographs for several USGS recording stations. Figure 11.15 shows that surge timing and magnitude were reasonably well matched. In some cases, the mesh channel and overland conveyance were not sufficiently resolved. The modelers noted that the close fit with surge recession trends for several locations indicated good representation of frictional resistance.

For Hurricane Rita, ADCIRC was again loosely coupled with a regional WAM/coastal STWAVE model, in this case with bottom friction. The modelers compared the STWAVE hindcast maximum significant wave height of 6.6 ft to the observed value of 6 ft from an LSU WAVCIS station in Acadiana Bay. No other peak storm data were available for comparison. No sensitivity analyses were presented for the Hurricane Rita STWAVE model.

The FIS model documentation does not analyze the sensitivity of Hurricane Rita SWL validation results to the 2D ADCIRC model settings, parameter values, mesh resolution, mesh accuracy, or local mass balance errors or "non-fatal instabilities" that might have been present during the simulation. The FIS model documentation does not provide a recommended bias correction to account for the noted error in matching Vermilion Bay SWLs, possibly attributable to additional wave setup that cannot be represented in the model. Concerns related to validation sensitivity, calibration, mass balance errors, and explicit bias correction have been raised by independent technical reviewers (Dean et al 2004 and USACE 2007). As part of their FIS review, experts for Cameron Parish noted numerous mesh and attribute errors capable of introducing significant local bia s(Lonnie G. Harper and Associates 2009). These errors were subsequently addressed by the USACE.

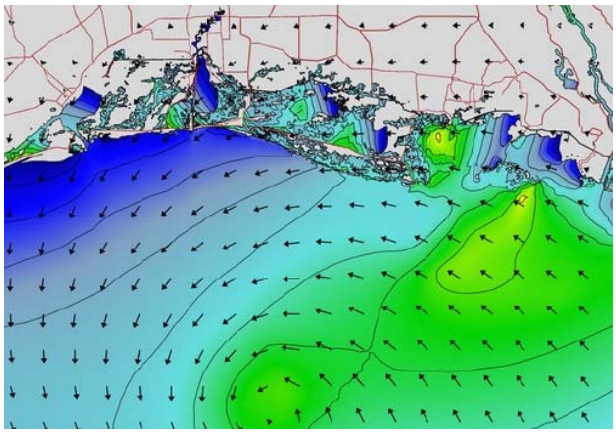

7 pm CDT September 23, 2005

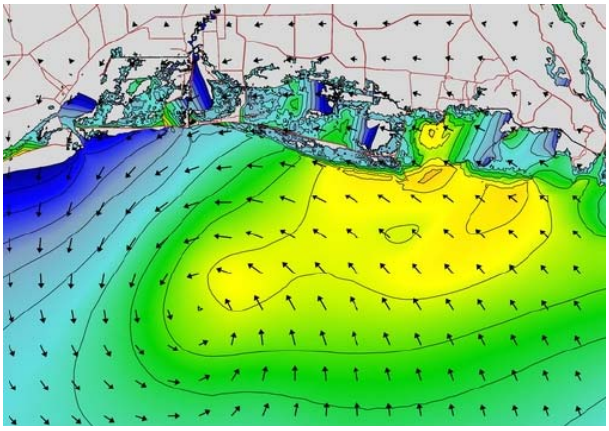

10 pm CDT September 23, 2005

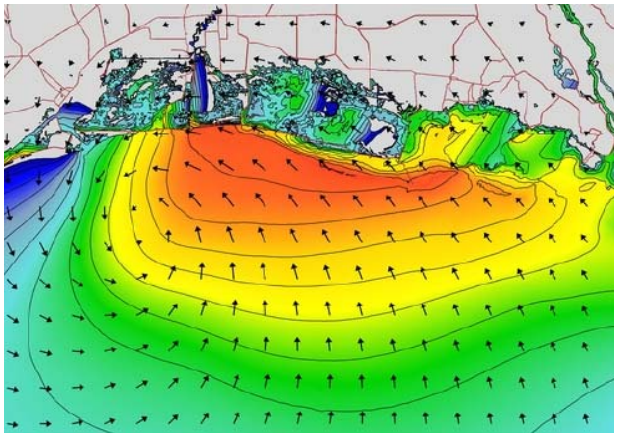

1 am CDT September 24, 2005

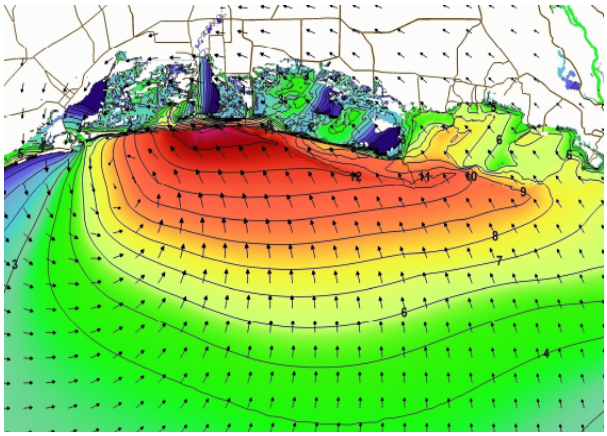

2 am CDT September 24, 2005

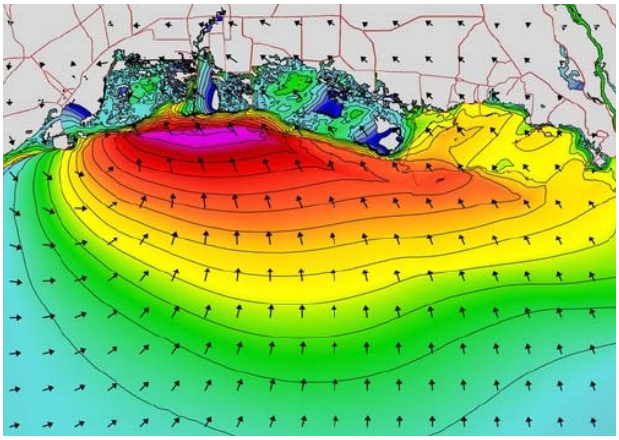

3 am CDT September 24, 2005

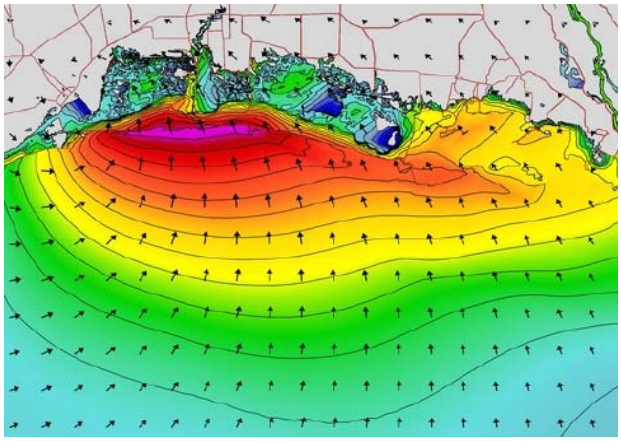

4 am CDT September 24, 2005

Figure 11.12. Hurricane Rita Surge Dynamics, Southwest Louisiana
USACE 2008

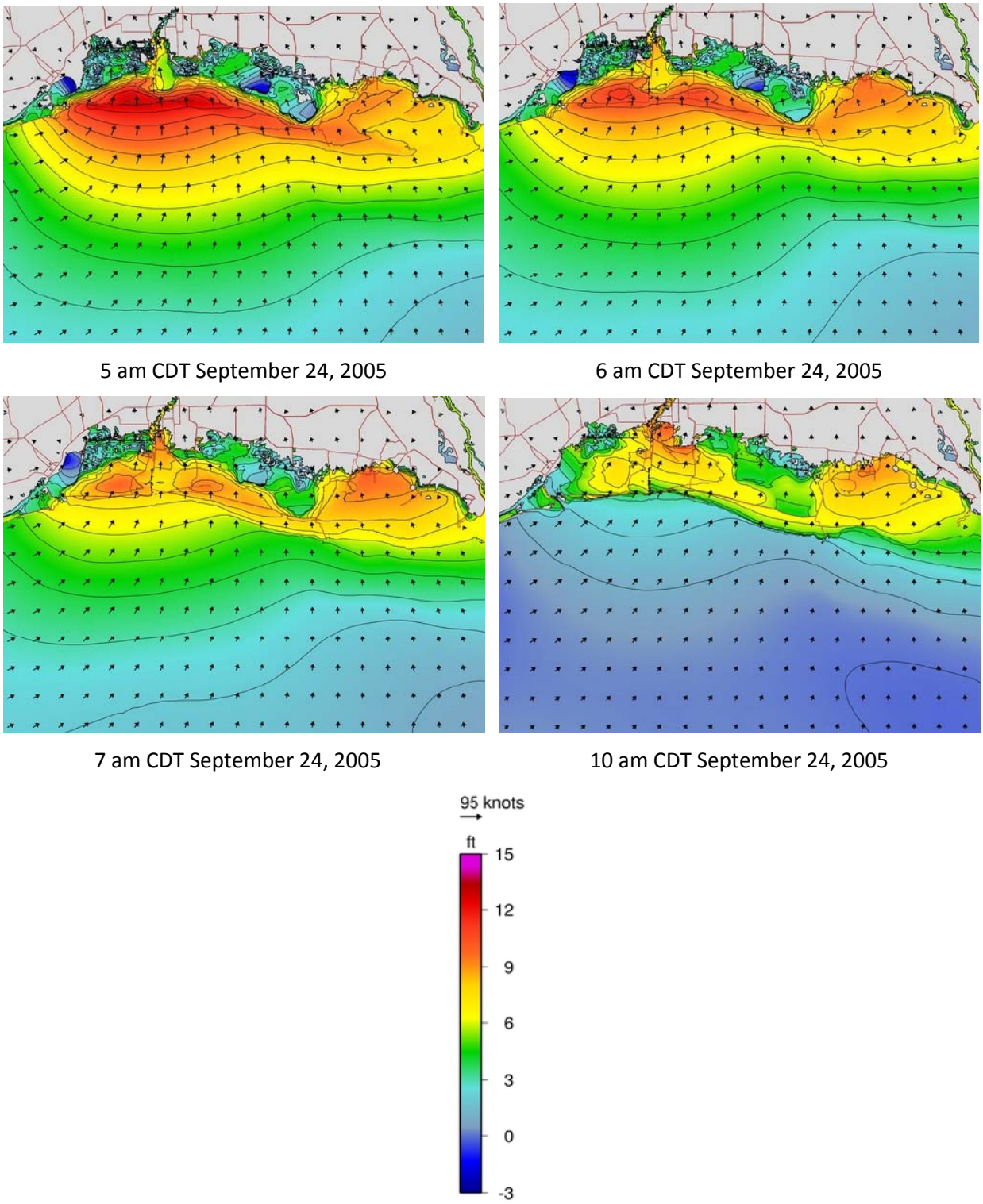

Figure 11.12. (Continued) Hurricane Rita Surge Dynamics, Southwest Louisiana
USACE 2008

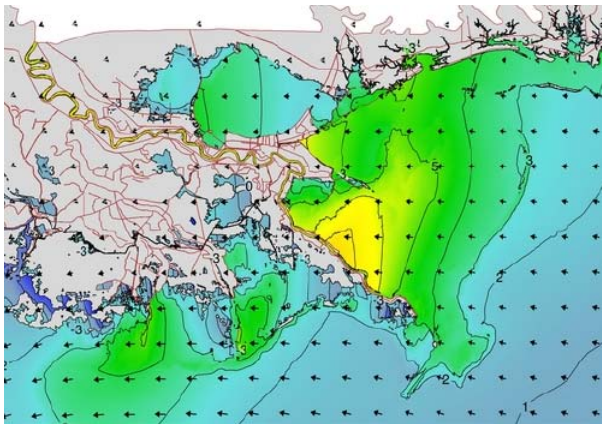

7 am CDT September 23, 2005

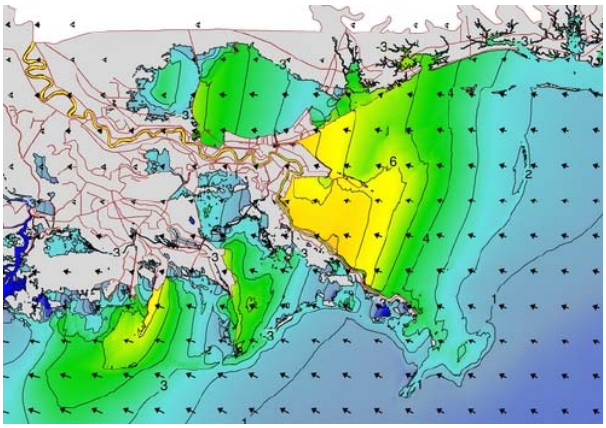

1 pm CDT September 23, 2005

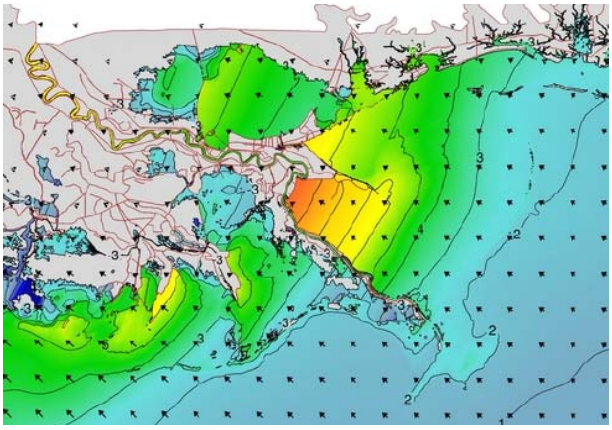

7 pm CDT September 23, 2005

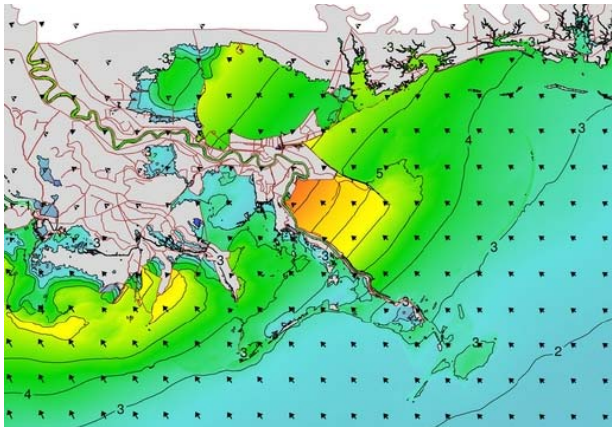

1 am CDT September 24, 2005

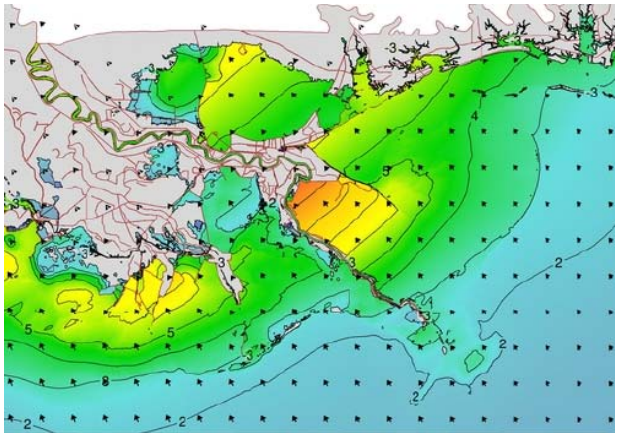

5 am CDT September 24, 2005

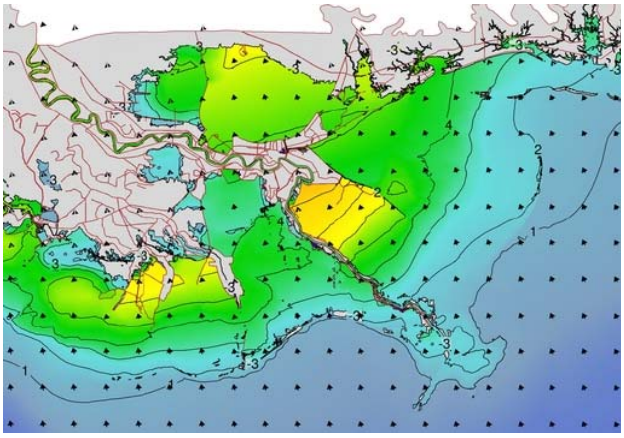

10 am CDT September 24, 2005

Figure 11.13. Hurricane Rita Surge Dynamics, Southeast Louisiana
USACE 2008

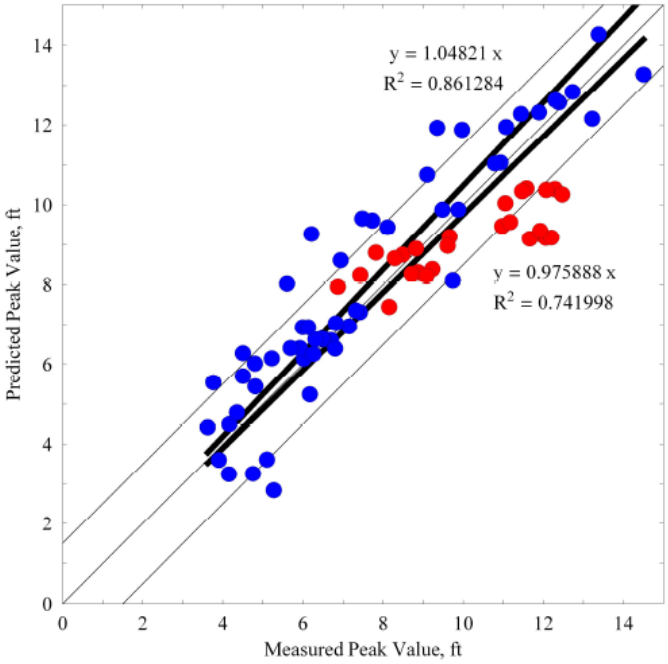

Figure 11.14. Hurricane Rita Modeled Peak SWL versus Observed HWMs
USACE 2008

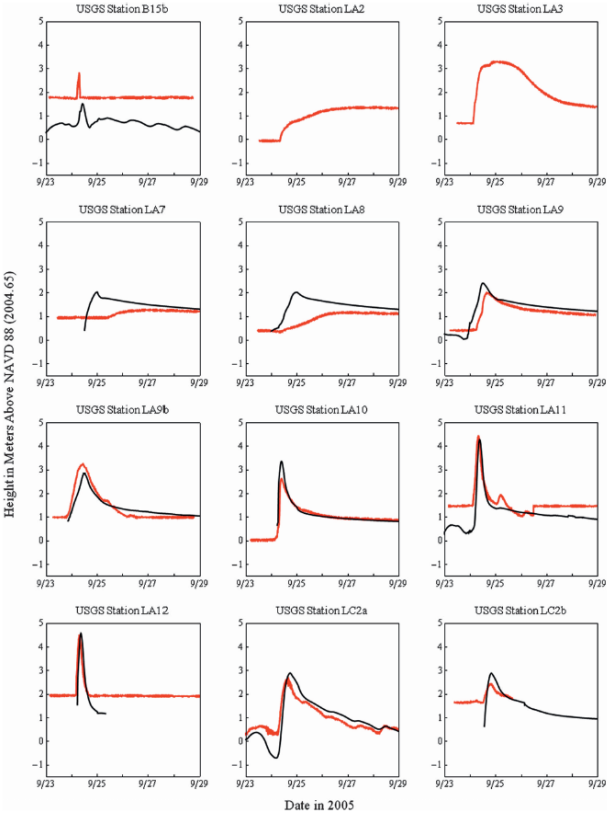

Figure 11.15. Hurricane Rita Modeled (black) **versus Observed** (red) **Hydrographs**
Bunya 2010

11.3. Other FIS Surge Models

Table 11.1 describes the 2D ADCIRC models used in five other FIS, three of which are in the northern GoM (Florida—Big Bend, Mississippi, and Texas), and two of which are along the south Atlantic (North and South Carolina). At the time of the Jacobsen et al report, final model testing documentation was available for only the Mississippi FIS. Limited preliminary test information was available for South Carolina and Texas FISs.

The Texas FIS has reportedly examined the sensitivity of hindcasts to Manning's n, wind sheltering, and directional roughness nodal attributes. In evaluating the Hurricane Ike hindcast, the Texas FIS modeling team identified an issue of matching Hurricane Ike's surge "forerunner"—a SWL rise that began about 20 hours in advance of the main landfall associated surge (see Figure 1.15). The forerunner contributed significantly to the overall SWL in northeast Texas and southwestern Louisiana. As depicted in Figure 11.16, the modelers identified the role of the Coriolis force in augmenting the landward velocity component of pre-landfall along-shore currents (Kennedy 2011). This landward current induces a cross-shore SWL gradient, termed an Eckman setup. The magnitude of the Eckman setup was found to be sensitive to the open ocean bottom friction and modelers reduced Manning's *n* for these regions from 0.02 to 0.01. However, this analysis has indicated a need for further evaluation of applicable air-sea drag coefficient values.

The Mississippi, South Carolina, and Texas studies have conducted sensitivity tests of the wave models used in coupling with the ADCIRC model. The wave model sensitivity tests consist primarily of comparing STWAVE and SWAN results and have shown that the two models are in reasonable agreement.

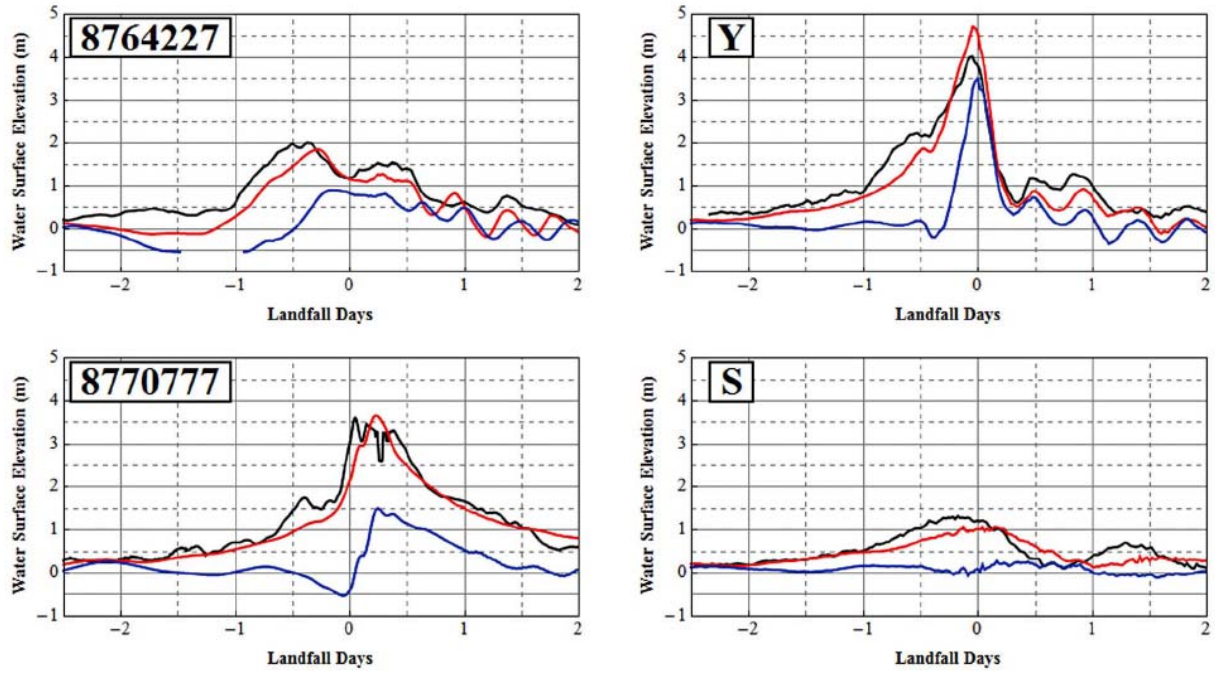

Figure 11.16. Hurricane Ike Forerunner Modeling

Observations (Black), Without Coriolis Force (Blue), With Coriolis Force (Red)

Kennedy et al 2011

Only the Mississippi FIS, which employed 2D ADCIRC loosely coupled with SWAN, has produced a formal calibration analysis (FEMA 2007b). The modelers compared ADCIRC results for Hurricane Katrina, having evaluated and adjusted the hurricane wind field to provide a reasonable agreement with general SWL trends. The modelers then compared modeled peak SWL values with 135 observed high water marks (HWMs) and adjusted Manning's n and directional roughness values so that at least 70 percent of the modeled values were within +/- 1.5 ft of the observed HWMs (see Figure 11.17; note no statistics on the match were provided). The vast majority of the HWMs, 90 percent, were greater than 15 ft. The modelers then validated the model against two older storms, Hurricanes Betsy and Camille. After adjusting the wind fields for these two storms (actual wind data were extremely sparse) more than 70 percent of the modeled surge peaks were within +/- 1.5 ft of selected HWMs.

At the time of this report, the Florida—Big Bend, Texas, North Carolina, and South Carolina FISs have not produced final calibration and validation documentation. The South Carolina modelers are using a tightly coupled SWAN+ADCIRC model with the coarsest coastal landscape resolution of any of the six meshes—about 60 m. The North Carolina model uses the full explicit 2D ADCIRC with unmodified acceleration terms, loosely coupled with SWAN version, but with much higher coastal resolution—to about 10 m. The South Carolina team is currently evaluating agreement with three storms: Hugo, Hazel, and Ophelia. Due to significant resolution differences in regions of mesh overlap, the South Carolina and North Carolina modelers are assessing the similarity of results for storms which affect both models. The Texas modelers are evaluating ADCIRC model agreement with five storms: Hurricanes Bret, Allen, Carla, Rita, and Ike. Once test results become available for Florida-Big Bend, Texas, North Carolina, and South Carolina FISs—as well as for new FISs of Northwest Florida/Alabama, Northeast Florida/Georgia, and Central Florida—Atlantic—these should provide an expanded basis for assessing the magnitude and nature of bias and uncertainty associated with 2D ADCIRC surge modeling.

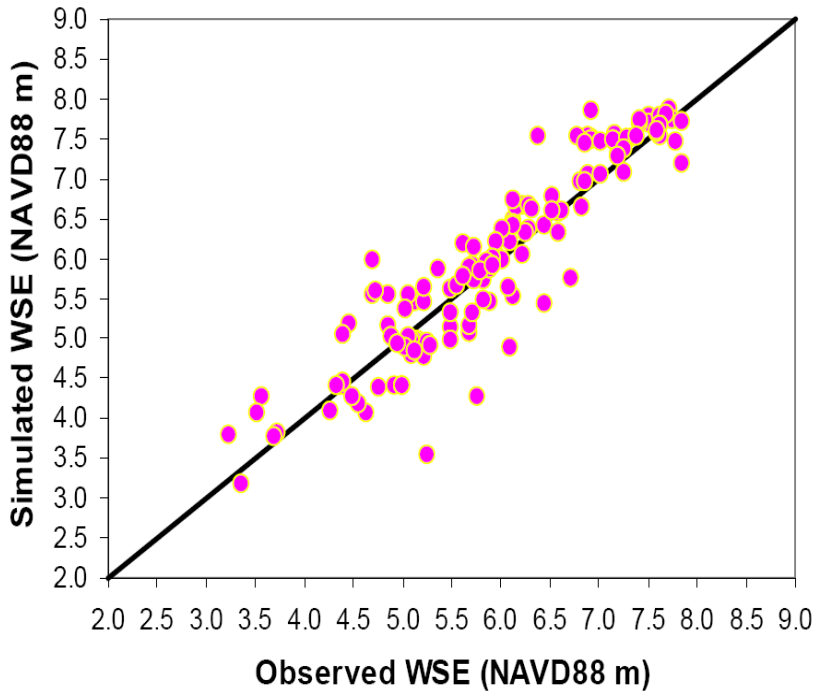

Figure 11.17. Hurricane Katrina Modeled Peak versus Observed HWMs for Mississippi FIS

FEMA 2007b

11.4 Other Applications

In addition to the FISs there have been six other notable applications of high resolution 2D models to studies of CN-GoM surge and tidal hydrodynamics, including the 2012 Louisiana Coastal Master Plan.

Dietrich

Dietrich et al (2011a) have evaluated hindcasts of Hurricanes Katrina and Rita using a tightly coupled SWAN+ADCIRC version, run on the same unstructured mesh described above. The authors noted that the error statistics for the SWAN+ADCIRC version were very similar to those for the loosely coupled ADCIRC/STWAVE model for both hindcasts.

Dietrich et al (2011b) provided further hindcast assessments for Hurricanes Katrina, Rita, Gustav and Ike (2008) using the tightly coupled SWAN+ADCIRC and an improved SL16 mesh with over 5 million nodes (more than twice the size of the FIS mesh) and node spacing approaching 20 m for some coastal features. Figure 11.18.a) presents the comparison of modeled SWL peaks versus observed SWL HWMs and hydrograph peaks for Hurricanes Gustav and Ike. Figure 11.18.b) shows the locations for the observations. Figure 11.19 reproduces the authors' tabulation of statistical measures of bias and precision (see GTN-1) for the four hindcasts, for SWL (ζ), H_s, and T_p. Figure 11.19 shows the slope (m) of the line of best fit (modeled versus observed), the R^2 for the fit, the overall bias (a normalized mean error), and scatter around the bias (a normalized standard deviation of errors). The results for Hurricanes Katrina and Gustav show similar bias (14% under-prediction), with the results for Hurricane Gustav having slightly higher scatter around the bias (24% versus 19%). The latter is consistent with Gustav's lower surge level and declining model precision at lower surge. The authors did not discuss if the larger 5 million node mesh improved the hindcasts for Hurricane Katrina and Ike compared to the earlier 2.1 million node mesh.

Chen

Chen led teams of researchers in utilizing 2D ADCIRC loosely coupled with SWAN to hindcast SWLs for Hurricanes Georges (1998), Ivan (2004), and Katrina (2005) in the Mobile AL area. A Hurricane George hindcast (Chen et al 2007) was performed with a local mesh of the Mobile Bay and Continental Shelf area (about 36,000 nodes). Hindcasts of Hurricanes Katrina and Ivan (Chen et al 2008) were undertaken with a regional shelf mesh (about 32,000 nodes) extending from Grand Isle LA to Panama City FL. Radiation stress gradients were analyzed with SWAN and incorporated into the ADCIRC model, together with tides and wind data. Bottom friction was handled with a uniform drag coefficient (0.0025), that was allowed to increase for surge depths below 1 m. Eddy viscosity was set to 30 m^2/s. For Hurricane Georges, modeled and observed hydrographs matched reasonably at three Mobile Bay tide station locations, with R^2 values all above 0.95. The excellent match may be attributable in part to the high quality local wind data and the straightforward conveyance dynamics of the single bay model. In the case of Hurricanes Ivan and Katrina, modeled and observed hydrographs matched reasonably at five regional tide gauge station locations, with overall RMSEs of 0.85 and 0.59 ft, respectively, for Hurricanes Ivan and Katrina. The R^2 values were not provided.

A subsequent analysis of Hurricane Katrina surge along the Mississippi coast (Chen et al 2009) found reasonable agreement of modeled peak SWLs versus observed HWMs. Figure 11.20 presents the authors' results along side the FIS results given previously in Figure 11.17. The R^2 value for Chen's modeled peaks SWL was 0.81, which is consistent with Dietrich's R^2 values shown in Figure 11.19.

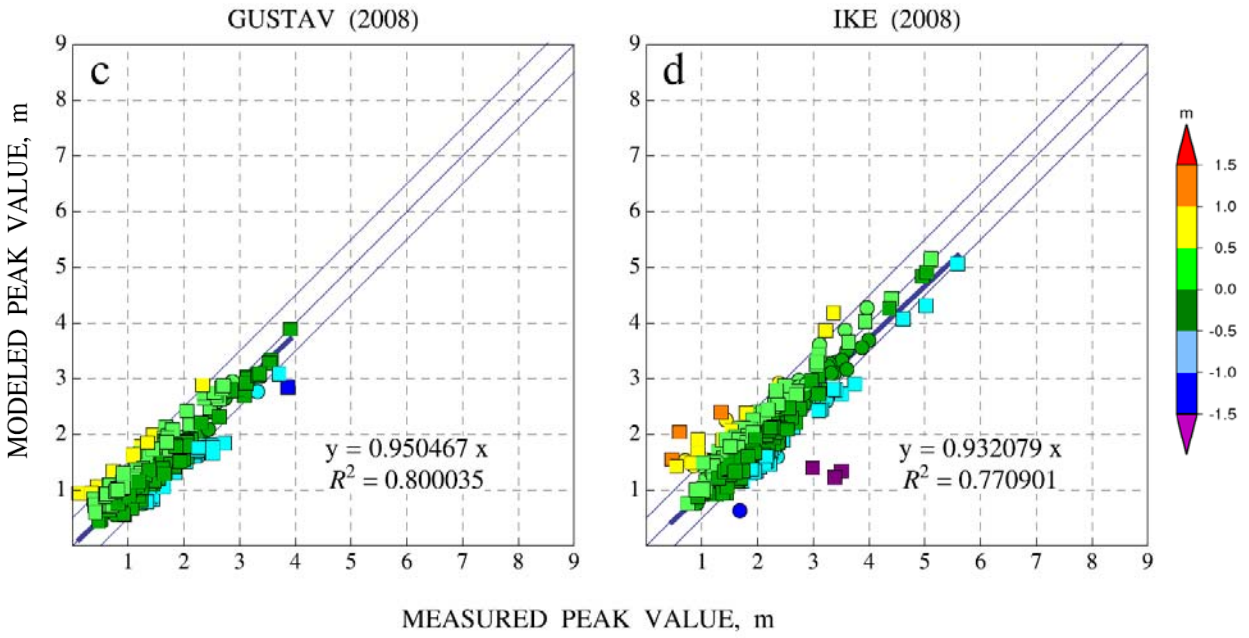

a. Modeled SWL versus Observations

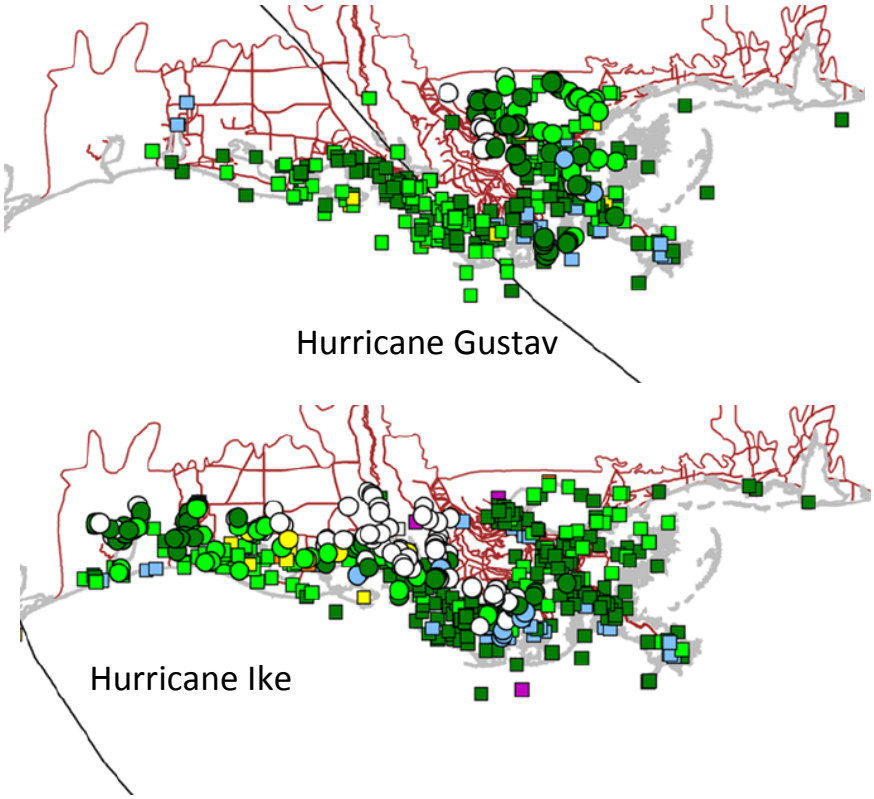

b. Observation Locations

Figure 11.18. Hurricanes Gustav and Ike Observed HWMs (circles**) Peak SWLs (**squares**)**
Dietrich et al 2011b

			Katrina	Rita	Gustav		Ike	
					All	Subset	All	Subset
Water levels	ζ	m	1.01	1.09	0.95		0.93	
		R^2	0.93	0.79	0.80		0.77	
		SI	0.19	0.28	0.24		0.16	
		Bias	0.14	0.15	0.14		−0.07	
Waves	H_s	*SI*	0.23	0.23	0.34	0.32	0.29	0.21
		Bias	0.05	0.43	0.35	0.22	0.09	−0.05
	T_p	*SI*	0.22	0.25	0.53	0.39	0.57	0.23
		Bias	0.07	0.25	−0.03	−0.01	0.02	0.04

Figure 11.19. Statistical Measures for Hindcasts of Hurricanes Katrina, Rita, Gustav, and Ike Using Tightly Coupled SWAN+ADCIRC and 5 Million Node Mesh

Dietrich et al 2011b

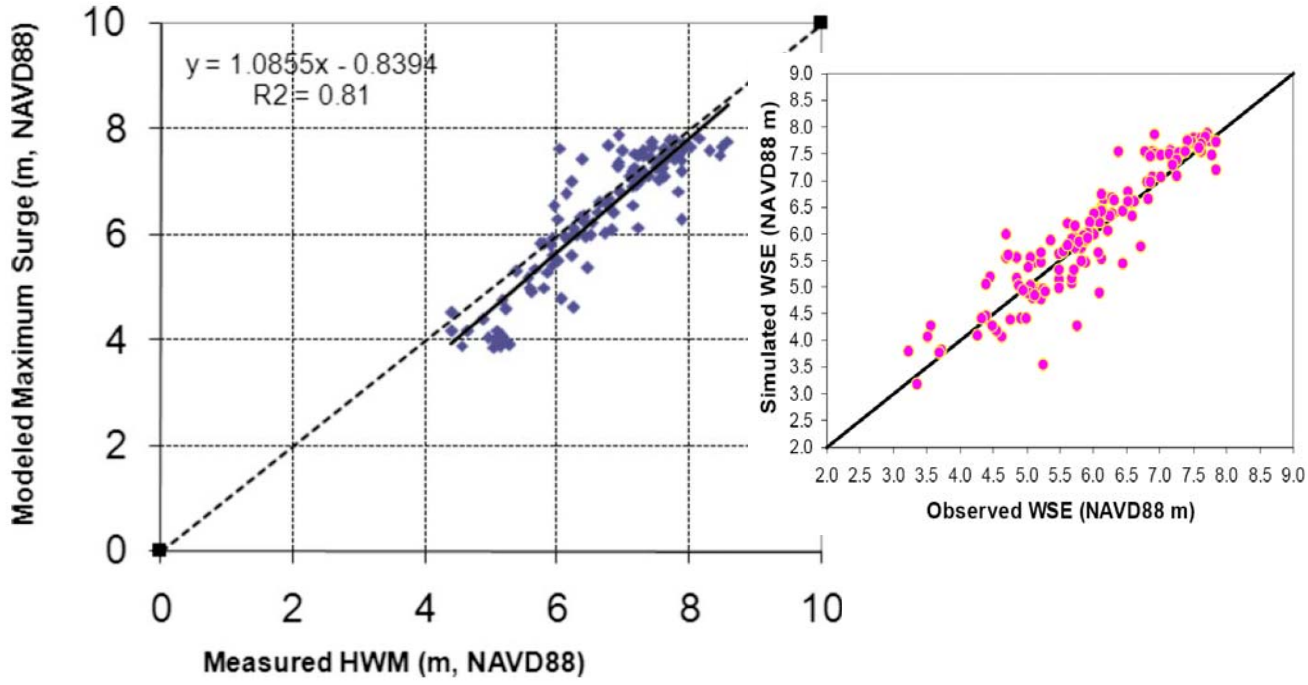

Figure 11.20. Hurricane Katrina Modeled Peak versus Observed HWMs

Chen et al 2009

Rego and Li

Rego and Li (2009) employed FVCOM in two vertical layers—essentially a 2D approach—with non-linear terms; an unstructured mesh of the northwestern-northcentral GoM—with over 90,000 nodes and node spacing approaching 200 m along the southwest Louisiana coast; wind forcing based on H*Winds; uniform, constant bottom drag coefficient (0.004); eddy viscosity after Smagorinsky; and nine tidal constituents to hindcast Hurricane Rita. Wave coupling was not included. Figure 11.21 shows model results versus observed hydrographs obtained from six temporary USGS gauges. The authors noted that model SWL peaks were generally within 5% of the observed peaks.

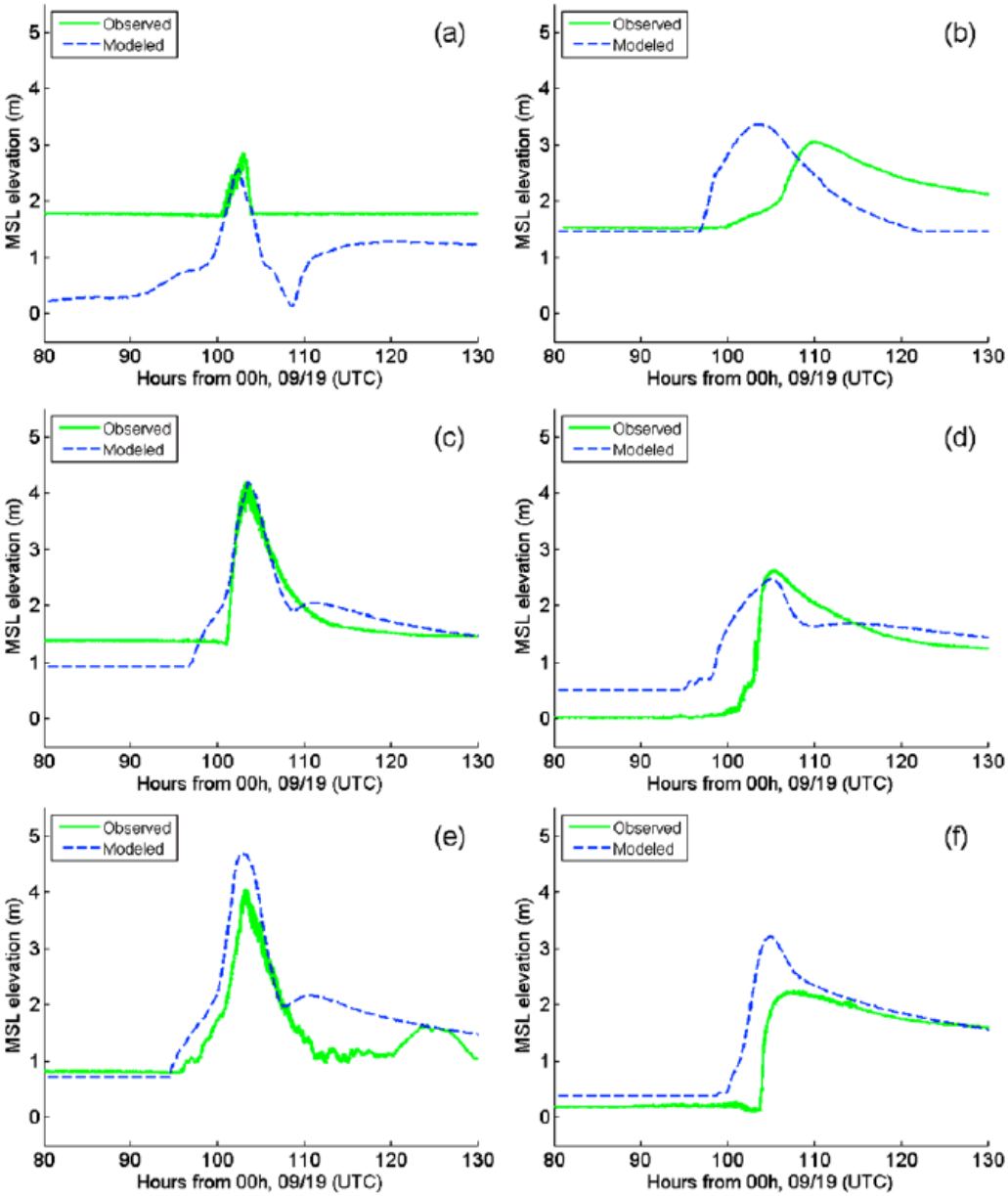

Figure 11.21. Hurricane Rita Modeled versus Observed Hydrographs
Rego and Li 2010

Jacobsen and Dill

Jacobsen and Dill (2007) used 2D ADCIRC and a portion of the SL15v3_2005_r09 mesh to simulate tidal propagation in Lakes Borgne and Pontchartrain, which are low in amplitudes (less than one foot). The authors report also included a companion study by McCorquodale et al (2007) which utilized FVCOM to study the local tidal prism. The authors found that dissipation associated with hydrodynamic models—either inherent in the numerical scheme (e.g., FVCOM) or associated with eddy viscosity (e.g., at 50 m^2/s in the FIS ADCIRC model)—can make it difficult to accurately capture modest tidal signals. The authors showed that reducing eddy viscosity in the ADCIRC model to 1 m^2/s (a value which may be impractical for surge simulations) improved tidal representation. For southeast Louisiana's extensive coastal marshes, representation of such tidal signals is indicative of a model's ability to accurately represent landscape influences on conveyance at lower SWLs (see Section 7).

Forbes

Research is also being conducted for high resolution 2D surge modeling forecast applications. Forbes et al (2010) simulated Hurricane Gustav (2008) surge under a variety of track and wind forecasts and hindcasts to evaluate suitable forecast techniques. Simulations were performed with the 2D ADCIRC FIS model, mesh, and nodal attributes; a LMSL and LMMSL adjustment of 1.2 ft (slightly higher than that employed in the FIS); river inputs for the Mississippi and Atchafalaya Rivers; and eight tidal constituents—the seven previously noted plus P_1. Wave setup was not included, as a tightly coupled version of ADCIRC was not available at the time and, moreover, the computational requirements of wave coupled simulations were considered impractical for forecasting. Full hindcasts were undertaken with three different wind files: an asymmetric vortex model based on basic hurricane parameters (CPD, R_{max}, Holland B); the 12 km resolution North American Mesoscale model; and post-storm H*Winds. Hydrographs from the three hindcasts were compared to observed hydrographs at 21 stations. The results indicated that an asymmetric vortex model with higher winds could compensate in forecast mode for the lack of wave setup..

2012 Louisiana Coastal Master Plan

In support of the 2012 Louisiana coastal Master Plan ARCADIS modified and validated a tightly coupled ADCIRC-SWAN model for the period from July 25 through September 14, 2008, which encompassed a 30+ day tidal spin-up followed by Hurricanes Gustav and Ike (see Appendix D24 in Louisiana CPRA 2012). The model revised an SL18 mesh (6.8 million nodes) to provide a project mesh (OCPR2012) with 1.15 million nodes. The OCPR2012 mesh incorporated SL18 node refinements in coastal Louisiana with spacing to 15 m for some features. The SL18 and OCPR2012 also included updated elevation, Manning's n, and wind drag mesh attributes, with values assigned in a manner similar to that described for the southeast Louisiana FIS. The OCPR2012 ADCIRC model employed the implicit/explicit solution, a one second time step, and eddy viscosity values ranging from 2 to 20 m^2/s. The documentation did not indicate the treatment of acceleration terms. The model forcing and boundary conditions included seven tidal constituents (K1, K2, M2, N2, O1, Q1 and S2). The model was initiated with a LMMSL of 0.91 ft NAVD88. ARCADIS compared model results for both storms to observed HWMs. Figures 11.22 and 11.23 show that nearly all model results were within ±2 ft of observed HWMs for both storms. The lines of best fit for the two storms had slight under-prediction slopes of 0.98 and 0.96, with R^2 values of 0.74 in both cases. These results showed slightly less under-prediction, but slightly greater residual scatter, than those of Dietrich presented above.

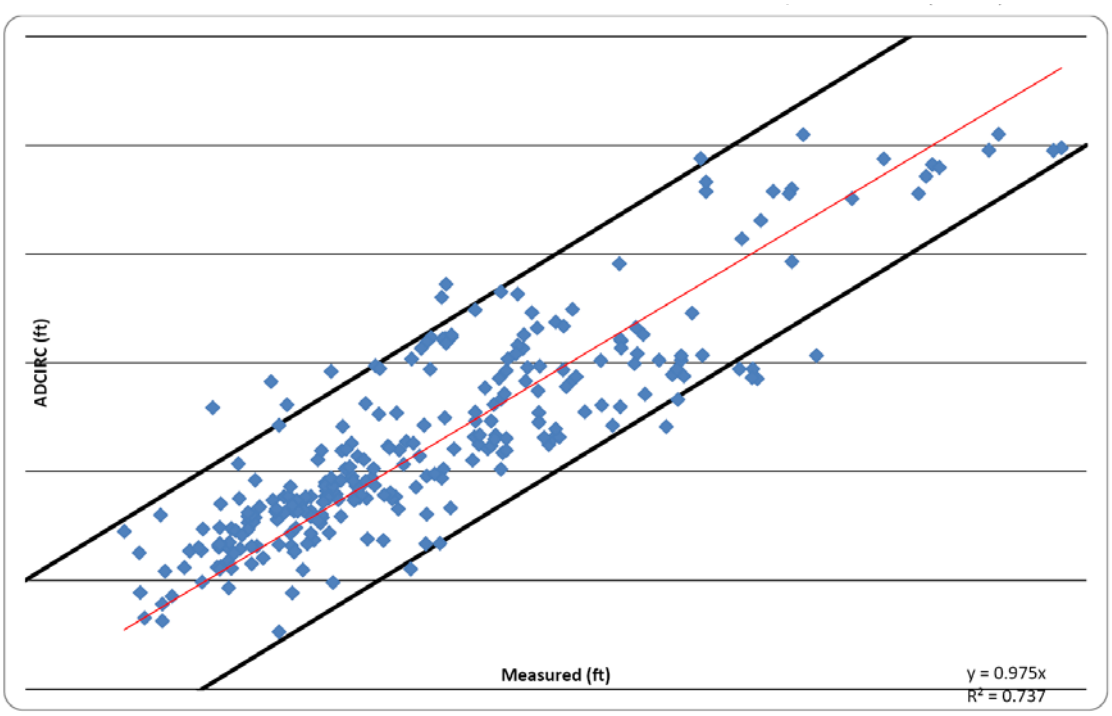

Figure 11.22. Hurricane Gustav Modeled versus Observed HWMs
ARCADIS in Louisiana CPRA 2012

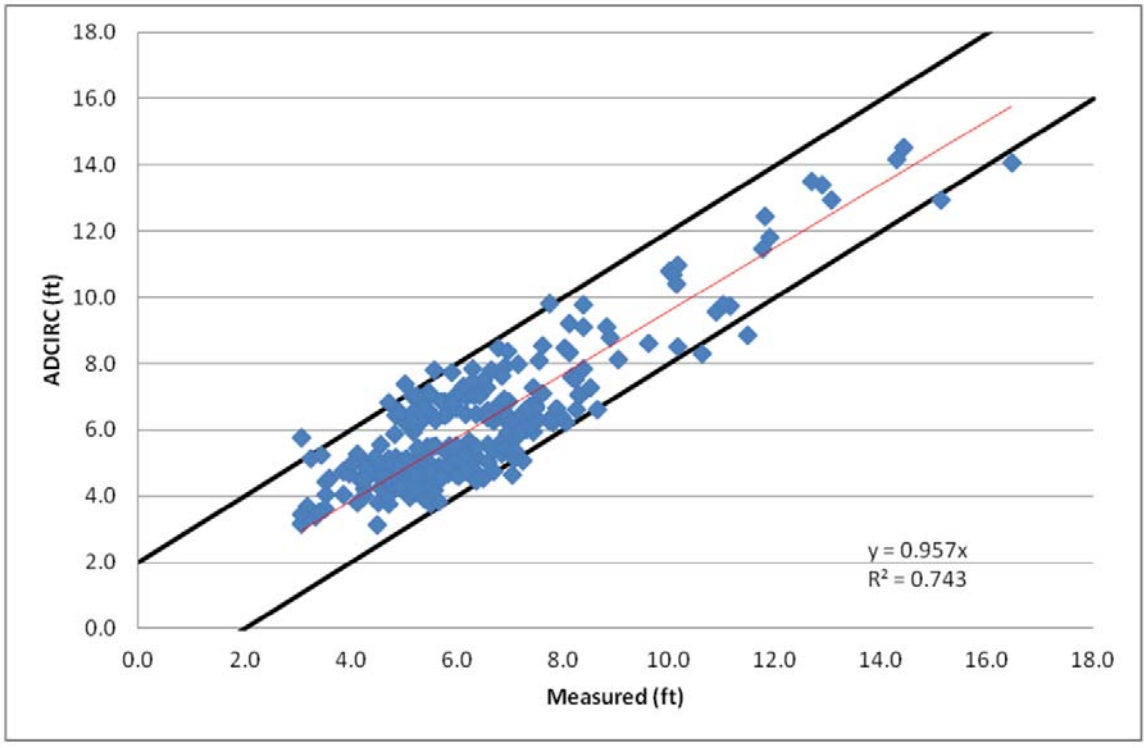

Figure 11.22. Hurricane Ike Modeled versus Observed HWMs
ARCADIS in Louisiana CPRA 2012

Part II. Conclusions and Recommendations

Conclusions

Part II has provided a review of scientific and technical literature, including available documentation for several FEMA surge FISs (Jacobsen et al 2010), together with original analyses, on surge physics and high resolution surge modeling. This information supports the following important findings:

Surge Physics

1. Hurricane surge can be considered in terms of several important components: LMSL, LMMSL, pre-storm meteorological conditions, astronomical tide, the "long" surge wave—the SWL "dome," and the irregular "short" wave field.
2. Surge dynamics are the unique product of the interaction of particular hurricane forcing conditions—associated with a hurricane's core intensity, core size, wind field distribution, dynamics, forward speed, and track—and the coastal landscape.
3. 2D surge physics can be understood through the application of laws of conservation of mass and momentum for a column of water. The latter entails two lateral acceleration terms and ten lateral forces.
4. Wind stress, wave radiation stress, water pressure, and atmospheric pressure provide the surge driving force while friction and bed reaction tend to resist surge. Turbulent stress diffuses momentum. The role of astronomical tide forcing depends on surge timing. Coriolis force can be important in generating surge "forerunner" through Eckman setup. Buoyancy force is typically ignored in 2D analyses.
5. Manning's *n*, particularly for overland flow, depends highly on inundation depth, but incorporation of depth-dependent Manning's *n* has been neglected to date.
6. Wave physics describe the generation and key transformations in irregular wave fields associated with shoaling, breaking, refraction, diffraction, and reflection. Breaking contributes a SWL setup—i.e., wave setup—primarily with the breaking of large ocean waves along the shallow Continental shelf. Breaking of locally generated waves in larger bays and lakes can also contribute significant local setup. Significant variations in local wave setup can arise from a range of wave-current and wave-feature interactions.
7. Coastal landscape features influence surge by affecting wind setup, conveyance, and/or wave conditions. Features are present at a range of scales (regional to local) and can produce a variety of effects that can depend greatly on surge conditions.
8. A crucial regional feature is the shallow Continental Shelf extending eastward of the Mississippi River Delta. GoM major hurricanes entering from Florida and tracking westward (e.g., Hurricanes Betsy, Katrina, Rita) create extreme wind setup against the Delta.
9. Fitzpatrick et al (2010) have shown that the combination of $IKE^{½} * V_{max}$ (see Part I) and shelf bathymetry is an excellent predictor of generic regional surge height.
10. Conveyance features—through variations in the flow length, depth, and friction coefficient (Manning's *n*)—divert surge movement. Conveyance headloss is proportional to length, $depth^{4/3}$, and Manning's n^2 . Thus, surge propagation is more sensitive to the depth and frictional roughness/obstructions.

11. Five important categories of conveyance features are flood protection and other hydraulic structures, other man-made embankments, natural topographic features, land cover, and preferential conveyance pathways. Numerous examples of all five categories are present at a variety of scales in southeast Louisiana.
12. The protruding Mississippi River Delta is a crucial regional conveyance feature, trapping surge in a "corner," with the communities of Waveland and Bay St. Louis MS at the vertex.
13. Coastal surge barriers enhance compression of the long wave, blocking landward conveyance at the expense of higher flood-side setup. Surge hazards are shifted not eliminated.
14. Coastal features that dampen waves and modify wave setup not only include designed breakwaters but a variety of embankments, shoreline stabilization and coastal sediment control structures, and land cover types.
15. The influence of coastal features on surge depends on
    - Surge stage—submergence, or "drowning," of embankments, land cover, and channels reduces their importance in controlling conveyance and wave breaking relative to the surrounding landscape;
    - Areal size and continuity—e.g., long embankments provide much greater surge diversion and wider forest bands provide greater frictional resistance;
    - Erodability—barrier islands and other raised features that disappear quickly as surge rises will exert less influence; appropriate armoring can enhance the strength of raised features.
16. The impact of a feature can vary with different hurricane tracks—e.g., Grand Isle experiencing higher seaward versus leeward setup depending on whether a hurricane passes to the west or east—and over the course of a hurricane event—e.g., channels providing seaward conveyance at storm surge peak.
17. The sensitivity of low-lying coastal feature performance to surge hazard magnitude implies a limited role for these features in major risk reduction.
18. It is important to note that massive surge protection systems can also have negative coastal environmental impacts.
19. There is a critical lack of surge hydrograph and wave data for parameterizing 2D surge SWL physics, particularly with respect to Manning's *n*, the air-sea drag coefficient, and wave shoaling/breaking parameters affecting wave setup.
20. In coastal areas subject to significant baroclinic forcing—with notable surge vertical circulation patterns due to the interaction of steep salinity, temperature, and bathymetric gradients—3D evaluation of surge physics is being initiated.

Surge Modeling

21. Hurricane surge models should be understood in totality as comprised of:
    - A set of SWEs for the physical mass and momentum conservation laws;
    - Numerical translations of these PDEs into algebraic expressions for discrete time steps and spatial intervals—at grid/mesh nodes;
    - A collection of boundary, initial, and dynamic forcing conditions;
    - Landscape representations for assigning parameter values at nodes; and
    - Computational codes and systems for executing the equations over an extended sequence of time steps.
22. State-of-the-art GoM 2D surge modeling extends to the mid-Atlantic Ocean but includes high coastal landscape resolution of landfall regions:
    - SWL is modeled with unstructured meshes and associated numerical methods taking advantage of HPPC platforms with hundreds of computer cores—e.g., ADCIRC and FVCOM.
    - Terrain and landscape data increasingly support extremely high node densities—with spacing approach 10 m and node totals numbering in the millions.
    - Waves are modeled with structured grid (e.g., STWAVE, SWAN), which is loosely coupled with the unstructured mesh SWL model for mutual feedback, allowing computation of wave radiation stress gradient contribution to setup.
    - Recently, code authors have developed a fully dynamic tight coupling of unstructured mesh version of SWAN with SWL models ADCIRC and FVCOM.
23. Important limitations include:
    - Restriction to 2D;
    - Possible modification of terms (e.g., acceleration);
    - The accuracy of the numerical method and residual numerical dampening;
    - Local mass conservation and “non-fatal” instabilities;
    - Modification of eddy viscosity and mesh characteristics to manage stability issues (Courant stability issues, steep local force gradients, wetting and drying);
    - Availability and accuracy of coastal landscape data for populating node attributes—e.g., elevation, Manning’s *n*, wind sheltering;
    - Fidelity of mesh and node attributes to coastal landscape; and
    - Applicability of wave models only to mild slopes—i.e., waves along the Continental Shelf and the nearshore area of larger coastal bays and lakes;
24. Sensitivity, calibration, and validation testing are crucial to evaluating model performance:
    - Sensitivity tests assess model robustness over a range of model settings (e.g., numerical method, excluded momentum terms, time-step), mesh lay out (e.g., node spacing and elevation), and parameter values (e.g., eddy viscosity, Manning’s *n*, and other nodal attributes). The tests typically examine effects on model runtime, stability, and accuracy.

- Calibration tests evaluate appropriate values for sensitive parameters (e.g., eddy viscosity, Manning's *n*) to provide accurate simulations of tides and surge hindcasts.
- Validation tests evaluate surge hindcast accuracy and precision, and provide appropriate corrections for any model bias.

25. 2D SWL model calibration and validation tests are hindered by the absence of sufficient high quality of surge event data (hydrographs and HWMs) and the uncertainty associated with wind forcing files (H*Winds). There is an even greater lack of surge event wave data.
26. Higher order Boussinesq methods are emerging to evaluate complex wave physics at steeper shorelines—e.g., the inundated foreshore of surge protection structures.
27. WHAFIS is a simple 1D shoaling/dampening model employed in coastal FISs for basic estimation of additional flood hazard elevations associated with overland waves. WHAFIS is not used for evaluating wave setup.
28. Over the last decade the ADCRIC Development Group, sponsored in part by USACE, FEMA, NOAA, and NRL, has continued to research and demonstrate key aspects of their open-source, 2D, high resolution, code, which enhances its suitability for regional hurricane surge modeling:
    - Interior weir boundaries for representing raised linear features;
    - Improved wetting and drying;
    - Spatially varying friction, eddy viscosity, and other nodal attributes;
    - Options for improved stability;
    - Tight coupling with SWAN;
    - HPPC scalability; and
    - Numerical method options for local mass conservation and higher numerical accuracy.

    The developers continue to research rainfall/evaporation inputs, coupling with 1D conveyance features; numerical methods; 3D modeling; and computational efficiency.
29. Recent 2D ADCIRC surge model sensitivity tests by Jacobsen et al (2010) provide insights into fully explicit versus implicit/explicit numerical method; modification of the treatment of acceleration terms; eddy viscosity value; time-step; and mesh resolution for landscape features.
30. 2D surge modeling efforts are subject to project considerations, including:
    - Programmatic objectives;
    - Stakeholder input;
    - Adequacy of landscape data;
    - Work team capacity;
    - Project schedule and budget;
    - HPPC resource availability; and
    - Acceptable error and uncertainty and implications of performance limitations and compromises for model use.

31. Six FEMA FISs (Louisiana, Mississippi, Texas, North Carolina, South Carolina, and Florida-Big Bend) have recently employed 2D ADCIRC, coupled with a wave model, for regional surge modeling—summarized in Jacobsen et al (2010); three additional surge FIS with 2D ADCIRC are underway (Northeast Florida/Georgia, Central Florida-Atlantic, Northwest Florida-Panhandle). Models vary in their numerical method, treatment of acceleration, eddy viscosity, time step, and mesh layout.
32. There is no current guidance on mesh development. According to 28 landscape categories node density varies widely both between and within FIS meshes.
33. The 2006 southeast Louisiana FIS 2D ADCIRC model, groundbreaking in scope at the time, used:
    - A mesh with 2.1 million nodes and resolution of selected coastal features to about 30 m;
    - The implicit/explicit numerical method;
    - A constant eddy viscosity value of 50 m^2/s and time step of 1 s; and
    - Node Manning's *n* and nodal wind sheltering coefficients assigned based on land cover data and associated values from technical literature.
34. Specific limitations of the 2006 southeast Louisiana FIS 2D ADCIRC model include:
    - The modelers chose to modify acceleration terms (in the mass conservation equation);
    - The mesh contains extensive elevation errors associated with outdated bathymetry sources and vertical referencing;
    - Model settings, mesh layout, and node attributes were simply presented as reasonable/practical for the time. Alternatives were not evaluated, possibly due to other project considerations. Sensitivity analyses for these selections were not provided; and
    - The model was not calibrated.
35. Modelers validated the 2006 southeast Louisiana FIS 2D ADCIRC model with tides and surge hydrograph and HWM data from Hurricanes Katrina and Rita. The hindcasts included:
    - Combined LMSL and LMMSL adjustments of 0.78 to 0.93 ft NAVD88-2004.65.
    - Tidal boundary and forcing for seven constituents (K_1, O_1, Q_1, M_2, S_2, N_2, and K_2);
    - Wind-forcing from H*Wind files;
    - Boundary inflows for the Mississippi and Atchafalaya Rivers; and
    - Radiation stress gradients at 30-minute intervals from a loosely coupled STWAVE model—run without friction for Hurricane Katrina and with friction for Hurricane Rita.
36. The validation results showed:
    - A reasonable match for coastal tide stations, but problematic propagation of interior low amplitude tides. Simulation of interior low amplitude tides is an important indicator that a model captures inland conveyance at lower, friction dominated, stages. Models often have difficulty matching low amplitude events due to mesh resolution limitations, numerical dampening, and/or eddy viscosity. Jacobsen and Dill (2007) subsequently showed that a 2D ADCIRC model with a much lower eddy viscosity (1 m^2/s, a value likely impractical for surge simulations) was better able to simulate interior low amplitude tide propagation.

- Reasonable capture of general surge response to Hurricane Katrina forcing conditions and major coastal terrain features. The results imply a relative error of about 10% for HWMs greater than 15 ft. *However, the validation showed a notable SWL bias (under-prediction greater than 1.5 ft) along the south shore of Lake Pontchartrain*. The STWAVE model validation was hampered by very limited data.
- Slightly more relative error for Hurricane Rita SWL response, consistent with the generally lower peak surges heights. Bias (under-prediction) was identified in the Vermilion Bay area and attributed to limited resolution of wave setup or poor mesh elevation data. The STWAVE model validation was also hampered by very limited data.

37. The 2006 southeast Louisiana FIS model validation limitations include:
    - Absence of sensitivity analyses for validation results to the model settings, parameter values, mesh resolution, mesh accuracy, or local mass balance errors or "non-fatal instabilities" that might have been present during the simulation;
    - Absence of a recommended bias correction to account for the noted 1.5+ ft error in matching Lake Pontchartrain SWLs, attributed to additional wave setup that cannot be represented in the model.
38. Concerns related to sensitivity analyses, calibration, mass balance error analysis, and local mesh attribute errors have been raised by independent technical reviewers and FIS appellants.
39. Five FIS are varying 2D ADCIRC model settings, wave model couplings, mesh density, and model performance testing:
    - A parallel Mississippi FIS model with 2D ADCIRC was loosely coupled with the SWAN wave model. In this study the modelers did calibrate the 2D ADCIRC model—using Hurricane Katrina data and adjusting wind input and Manning's *n* values. They validated the model with older data from Hurricanes Betsy and Camille. Relative error for the calibrated Mississippi model was similar to that for the southeast Louisiana model.
    - The Texas FIS 2D ADCIRC model has been calibrated using Hurricane Ike (2008)—with adjustments to offshore Manning's *n* value—to improve capture of Eckman setup in the surge forerunner.
    - The South Carolina model is using the tightly coupled SWAN+ADCIRC version.
    - The North Carolina model is using a fully explicit numerical method, without modifying the acceleration terms, and resolving coastal features in the mesh to a node spacing of 10 m.

    Final validation reports are not available for Texas, North Carolina, South Carolina, or Florida-Big Bend. Once available they should expand the basis for assessing the magnitude and nature of bias and uncertainty associated with 2D ADCIRC surge modeling.
40. Dietrich et al and ARCADIS each utilized a tightly coupled SWAN+ADCIRC version—with 5 million and 1.15 million node meshes, respectively—to hindcast Hurricanes Gustav and Ike. Both produced similar results for both storms, with slight under-prediction. Dietrich et al determined SI for the Hurricane Katrina, Rita, Gustav, and Ike hindcasts of 0.19, 0.28, 0.24, and 0.16, indicating that the state of the 2D surge modeling practice still entails considerable residual uncertainty.

Recommendations

The above conclusions indicate that the 2006 surge model is outdated, especially given the advances since 2006 in southeast Louisiana regional landscape elevation and land cover data, as well as model improvements indicated in other FISs and surge studies. They also provide the basis for recommendations to improve southeast Louisiana surge modeling. Ten specific updates to the current surge model should include:

1. Revise the finite element mesh layout and resolution; refine fidelity of linear feature (e.g., breakline) alignments; provide for reasonable consistency in resolution of similar landscapes and key landscape conveyance features.
2. Revise mesh (node and interior weir boundary) elevations consistent with a current regional digital elevation model, including current applicable NAVD88 epoch.
3. Revise other mesh attributes (e.g., Manning's *n*, surface canopy coefficient, surface directional roughness, eddy viscosity) consistent with current landscape information.
4. Use a tightly coupled surge-wave code with full plane wave modeling and include all relevant physics terms. While SWAN-ADCIRC is the current state-of-the-practice HPPC surge code, alternatives should be evaluated as they become available.
5. Evaluate choice of fully explicit versus implicit-explicit numerical scheme, wetting-drying parameters; and air-sea drag formulation.
6. Provide support (e.g., sensitivity testing) for decisions that vary from established guidance/state-of-the-practice.
7. Provide model calibration/validation using Hurricanes Katrina, Gustav, and Isaac; explain choice of parameters that are/are not employed in calibration.
8. Evaluate residual instabilities and local mass conservation errors in final calibration/validation.
9. Evaluate potential local bias in final calibration/validation results (such as the 1.5+ ft SWL bias for the south shore of Lake Pontchartrain if it remains) and provide methods for correcting bias in the use of the model.
10. Revise the estimate of uncertainty in regional surge modeling.

The Louisiana CPRA, together with federal partners, should fund critical research to improve surge modeling, including:

1. Update Louisiana LIDAR DEMs, coastal water body bathymetry, raised feature topography, and land cover data sets;
2. Acquire wind (at a range of averaging periods), SWL, current, and wave time-series data across a wide range of coastal landscape locations during hurricanes, as well as during normal tides and seasonal meteorological events;
3. Improve and refine H*Wind files (10-min average) for surge calibration and validation;
4. Improve treatment of surge physics, such as depth-variable hydrodynamic friction (e.g., Manning's *n*), the air-sea drag, wetting and drying, wave shoaling/breaking, and local time-varying rainfall;
5. Further application of higher order steep-slope wave modeling, including capability of coupling with 2D SWL models;

6. Advance numerical methods, codes, and HPPC techniques and systems;
7. Incorporate 3D models for baroclinic analysis where needed to improve accuracy; and
8. Address significant raised feature erosion and other landscape dynamics during actual surge events where needed to accurately simulate SWL and waves.
9. Expand sensitivity analyses assessing the implications of model settings (e.g., numerical methods, modification of acceleration terms, time step, etc.), mesh resolution, node attributes, forcing data, coupled models, and other model aspects on runtime, stability, and performance.

These recommendations can eliminate many sources of systemic and local errors (bias) in surge models, as well as work to reduce model uncertainty. However, many significant sources of hindcast imprecision are not amenable to reduction in the foreseeable future, and normally distributed uncertainty σ is likely to remain above 15%.

It is worth noting that improved surge modeling is crucial not only to better surge hazard analysis and risk management, but also to coastal ecosystem restoration and protection, in particular to a more rigorous understanding of the influence of coastal landscape features on hurricane surge dynamics. Furthermore, improvements in modeling surge hydrodynamic for a complex deltaic region such as southeast Louisiana can also lead to a better depiction of the river-tide-wind interactions driving daily estuarine circulation dynamics.

Part II. References

ADCIRC Development Group, 2009. Utility Programs, http://www.adcirc.org/Utility_ programs.html

Anderson, M. E., J. M. Smith, and S. K. McKay, Wave Dissipation by Vegetation. ERDC/CHL CHETN-I-82, September 2011

Bender, C. J., J. M. Smith, A. Kennedy, Hurricane Ike (2008) Nearshore Waves: Simulation and Measurements, Proceedings of the International Conference on Coastal Engineering, No 32, 2010.

Blanton, B., and R. Luettich, North Carolina Coastal Flood Analysis System Model Grid Generation: Renaissance Computing Institute (RENCI) Technical Report Series. Technical Report TR-08-05. Renaissance Computing Institute. Chapel Hill, NC. 2008.

Bunya, S., J. C. Dietrich, J. J. Westerink, B. A. Ebersole, J. M. Smith, J.H. Atkinson, R. Jensen, D. T. Resio, R. A. Luettich, C. A. Dawson, V. J. Cardone, A. T. Cox, M. D. Powel, H. J. Westerink, and H. J. Roberts, A High-Resolution Coupled Riverine Flow, Tide, Wind, Wind Wave, and Storm Surge Model for Southern Louisiana and Mississippi, Part I: Model Development and Validation, Monthly Weather Review, American Meteorological Society, Vol. 138, 345-377, 2010

Chen ,Q., J. T. Kirby, R. A. Dalrymple, A. B Kennedy, and A. Chawla, Boussinesq Modeling of Wave Transformation, Breaking, and Runup. Part II: 2D, Journal of Waterway, Port, Coastal, Ocean Engineering. Vol, 126, No. 1, 2000.

Chen, Q., L. Wang, H. Zhao, and S.L. Douglass, Prediction of Storm Surges and Wind Waves on Coastal Highways in Hurricane-Prone Areas. Journal of Coastal Research: Volume 23, Issue 5: pp. 1304 – 1317, 2007.

Chen, Q., L. Wang and R. Tawes, Hydrodynamic Response of Northeastern Gulf of Mexico to Hurricanes, Estuaries and Coasts, Volume 31, Number 6, 1098-1116, 2008.

Chen, Q., L. Wang, and Z. Haihong, Hydrodynamic Investigation of Coastal Bridge Collapse during Hurricane Katrina, Journal of Hydraulic Engineering, Vol. 135, No. 3, March 2009.

Crawfork, K., Hurricane Surge Potentials Over Southeast Louisiana as Revealed by a Storm-Surge Forecast Model: A Preliminary Study. Bulletin of American Meteorological Society, Vol. 60, pp. 422–429, 1979.

Dawson, C. and C. M. Mirabito, The Shallow Water Equations, Institute for Computational Engineering and Sciences, University of Texas at Austin, September 29, 2008 http://users.ices.utexas.edu/~arbogast/cam397/dawson_v2.pdf

Dawson, C. E.J. Kubatko, J.J. Westerink, C. Trahana, C. Mirabito, C. Michoskia, N. Pandaa, Discontinuous Galerkin Methods for Modeling Hurricane Storm Surge, Advances in Water Resources, Vol. 34, No.F 9, September 2011.

Dean, R. G. and R. A Dalrymple, Water Wave Mechanics for Engineers and Scientists, World Scientific Publishing Company, 1991.

Dean, R. G., M. Powell, and R. O. Reid, Review of the Application of the Numerical Model “ADCIRC” for Storm Surge Predictions in the New Orleans LA Vicinity, prepared for the USACE New Orleans District, January 31, 2004.

Dietrich, J.C. R. L. Kolar, and J. J. Westerink, 2005. Refinements in Continuous Galerkin Wetting and Drying Algorithms. Estuarine and Coastal Modeling, 2005.

Dietrich, J. C., S. Bunya, J. J. Westerink, B. A. Ebersole, J. M. Smith, J. H. Atkinson, R. Jensen, D. T. Resio, R. A. Luettich, C. Dawson, V. J. Cardone, A. T. Cox, M. D. Powell, H. J. Westerink, H. J. Roberts, A High-Resolution Coupled Riverine Flow, Tide, Wind, Wind Wave, and Storm Surge Model for Southern Louisiana and Mississippi. Part II: Synoptic Description and Analysis of Hurricanes Katrina and Rita, Monthly Weather Review, Vol. 138, No. 2, 378–404, 2010.

Dietrich, J. C., M. Zijlema, J. J. Westerink, L. H. Holthuijsen, C. N. Dawson, R. A. Luettich Jr, R. E. Jensen, J. M. Smith, G. S. Stelling, G. W. Stone. Modeling Hurricane Waves and Storm Surge using Integrally-Coupled, Scalable Computations, Coastal Engineering, Vol. 58, No. 45-65, 2011a.

Dietrich, J. C., S. Tanaka, J J. Westerink, C. N. Dawson, R. A. Luettich Jr, M. Zijlema, L. H. Holthuijsen, J. M. Smith, L. G. Westerink, H. J. Westerink. Performance of the Unstructured-Mesh, SWAN+ADCIRC Model in Computing Hurricane Waves and Surge. Journal of Scientific Computing, in press, 2011b.

Dietrich, J. C., J. J. Westerink, A. B. Kennedy, J. M. Smith, R. E. Jensen, M. Zijlema, L. H. Holthuijsen, C. Dawson, R. A. Luettich Jr., M. D. Powell, V. J. Cardone, A. T. Cox, G. W. Stone, H. Pourtaheri, M. E. Hope, S. Tanaka, L. G. Westerink, H. J. Westerink, and Z. Cobell, Hurricane Gustav (2008) Waves and Storm Surge: Hindcast, Synoptic Analysis, and Validation in Southern Louisiana, Monthly Weather Review, Vol. 139, 2488 – 2522, 2011c.

Dresback. K. M., R. L. Kolar, C. A. Blain, C. M. Szpilka, A. M. Szpilka, R. A. Luettich, and T. Shay, Development and Application of the Coupled HYCOM and ADCIRC System, Proceedings of the Eleventh International Conference on Estuarine and Coastal Modeling, 2010.

Douglass, S. L., S. A. Hughes, S. Rogers, and Q. Chen, The Impact of Hurricane Ivan on the Coastal Roads of Florida and Alabama: A Preliminary Report, 2004.

Ebersole, B.A., J.J. Westerink, S. Bunya, J.C. Dietrich, M.A. Cialone, Development of Storm Surge Which Led to Flooding in St. Bernard Polder during Hurricane Katrina, Ocean Engineering, 37, 91-103, 2010.

FEMA, Wave Height Analysis for Flood Insurance Studies (WHAFIS), Technical Documentation, Version 3.0, September 1988.

FEMA, Atlantic Ocean and Gulf of Mexico Coastal Guidelines Update, February 2007.

FEMA, Mississippi Coastal Flood Hazard Project, Calibration and Validation of Model Report, November 19, 2007b.

Fitzpatrick, P. J., N. Tran, Y. Li, Y. Lau, and C. M. Hill, A Proposed New Storm Surge Scale, Geosystems Research Institute, Mississippi State University, BLDG 1103, Room 108, Stennis Space Center, MS 39529 USA. June 2010. http://www.drfitz.net/uploads/fitz_ocean_surge_scale_ieee_certified.pdf

Forbes, C., R. A. Luettich Jr., C. A. Mattocks, J. J. Westerink, A Retrospective Evaluation of the Storm Surge Produced by Hurricane Gustav (2008): Forecast and Hindcast Results, Weather and Forecasting Vol. 25, No. 6, pages 1577-1602, 2010.

Glahn, B., A. Taylor, N. Kurkowski, and W. A. Shaffer, The Role of the SLOSH Model in National Weather Service Storm Surge Forecasting. National Weather Digest, Vol. 33, No. 1. August 2009.

Gulf of Mexico Alliance, Summary of the Special Session “Management Strategies for Sea-Level Rise in the Gulf Region” at the Harte Research Institute’s International Conference on Sea-Level Rise in the Gulf of Mexico, March 2010, Report Completed January 25, 2011.

Lonnie G. Harper and Associates, Cameron Parish Flood Insurance Study Appeal. 2009.

Interagency Performance Evaluation Task Force (IPET), Performance Evaluation of the New Orleans and Southeast Louisiana Hurricane Protection System, Volumes IV, The Storm, U.S. Army Corps of Engineers, June 2006.

Irish, J. L., D. T. Resio, J. J. Ratcliff, The Influence of Storm Size on Hurricane Surge, Journal of Physical Oceanography, Vol. 38, p. 2003, September 2008.

Jacobsen, R. W. and J. N. Suhayda, The Direct Impact of the MRGO on Hurricane Storm Surge, for the Louisiana Department of Natural Resources, URS Corporation, February 2006.

Jacobsen, R. W. and N. Dill, Assessing Baseline and Modified Astronomical Tide Propagation in the Pontchartrain Basin Using ADCIRC, for the USACE Louisiana Coastal Protection and Restoration Study, URS Corporation, July 2007.

Jacobsen, R. W., W. Miller, A. Naimaster, and C. B. Bender, BakerAECOM, ADCIRC Model Mesh Requirements Final Report, BakerAECOM, prepared for FEMA Region IV RiskMAP Support Services, Surge Study Needs Analysis — Florida and Georgia, December 2010.

Kennedy, A. B., Q. Chen, J. T. Kirby, and R. A. Dalrymple, Boussinesq Modeling of Wave Transformation, Breaking, and Runup. Part I: 1D, Journal of Waterway, Port, Coastal, Ocean Engineering. Vol, 126, No. 1, 2000.

Kennedy, A. B, U. Gravois, and B. Zachry, Observations of Landfalling Wave Spectra during Hurricane Ike, Journal of Waterway, Port, Coastal, and Ocean Engineering, Vol. Volume 137, Issue 3, 2010.

Kennedy, A. B., U. Gravois, B. C. Zachry, J. J. Westerink, M. E. Hope, J. C. Dietrich, M. D. Powell, A. T. Cox, R. A. Luettich Jr., and R. G. Dean, Origin of the Hurricane Ike Forerunner Surge, Geophysical Research Letters, Vol. 38, 2011.

Kubatko, E.J., S. Bunya, C. Dawson, J.J. Westerink, C. Mirabito, A Performance Comparison of Continuous and Discontinuous Finite Element Shallow Water Models, Journal of Scientific Computing, 30, 315-339, 2009a.

Kurian, N. P., N. Nirupama, M. Baba, and K. V. Thomas, Coastal Flooding Due to Synoptic Scale, Meso-Scale and Remote Forcings. Natural Hazards, 48, 259-273, 2009.

Loder, N. M., An Evaluation of the Potential of Coastal Wetlands for Hurricane Surge and Wave Energy Reduction, Thesis, Texas A&M University, 2008.

Lopez, J. Comprehensive Recommendations Supporting the Use of the Multiple Lines of Defense Strategy to Sustain Coastal Louisiana (Version I), MLDS.org, 2008.

Louisiana Coastal Protection and Restoration Authority (Louisiana CPRA), Louisiana's Comprehensive Master Plan for a Sustainable Coast, 2012.

Luettich, R., and J. Westerink, Formulation and Numerical Implementation of the 2D/3D ADCIRC Finite Element Model Version 44.XX, 2004. http://www.adcirc.org

Luettich, R., and J. Westerink, ADCIRC: A (Parallel) Advanced Circulation Model for Ocean, Coastal and Estuarine Waters; Model Documentation, 2005. http://www.adcirc.org

Lynett, P. J., J. A. Melby, and D. Kim, An Application of Boussinesq Modeling to Hurricane Wave Overtopping and Inundation, Ocean Engineering, Vol. 37, p. 135, 2010.

Massey, C. and C. A. Blain, Performance Analysis for the 2D Wetting and Drying Scheme Used in the Continuous Galerkin Formulation of ADCIRC, 2008.

Massey, W. G., J. W. Gangai, E. Drei-Horgan, and K. J. Slover, History of Coastal Inundation Models, Marine Technology Society Journal, Vol. 41, No. 1, 7–17, 2007.

McCorquodale, J. A., I. Georgiou , A. G. Retana, D. Barbe, M. J. Guillot, Hydrodynamic modeling of the Tidal Prism in the Pontchartrain Basin, Final Report, for the USACE Louisiana Coastal Protection and Restoration Study, June 2007.

National Oceanic and Atmospheric Administration (NOAA), Tidal and Geodetic Datums: Tidal and Geodetic Relationships, http://www.laseagrant.org/pdfs/NOAA_TidalGeodeticRelationships.pdf

NOAA, Center for Operational Oceanographic Products and Services, Tides and Currents, December 2011, http://tidesandcurrents.noaa.gov/geo.shtml?location=8761724

NOAA, http://www.vos.noaa.gov/MWL/aug_05/nws.shtml

NOAA, http://tidesandcurrents.noaa.gov/data_menu.shtml?stn=8761305 Shell Beach, LA&type=Harmonic Constituents

Powell, M.D., P.J. Vickery, and T.A. Reinhold, Reduced Drag Coefficient for High Wind Speeds in Tropical Cyclones" Nature, Vol. 422, March 20. pp. 279-283, 2003.

Rego, J. L. and C. Li, On the Receding of Storm Surge along Louisiana's Low-Lying Coast, Journal of Coastal Research, Special Issue 56, p. 1045-1049, 2009.

Resio, D. T. and J. J. Westerink, Modeling the Physics of Storm Surges, Physics Today, Vol. 61, Iissue 9, p. 33, September 2008.

Resio, D. T., S. J. Boc, L. Borgman, V. J. Cardone, A. Cox, W. R. Dally, R. G. Dean, D. Divoky, E. Hirsh, J. L. Irish, D. Levinson, A. Niederoda, M. D. Powell, J. J. Ratcliff, V. Stutts, J. Suhada, G. R. Toro, and P. J. Vickery, White Paper on Estimating Hurricane Inundation Probabilities, U.S. Army Corps of Engineers, ERDC-CHL, 2007.

Sheng, Y. P., Y. Zhang, V. A. Paramygin, Simulation of Storm Surge, Wave, and Coastal Inundation in the Northeastern Gulf of Mexico Region during Hurricane Ivan in 2004, Ocean Modelling, Volume 35, Issue 4, Pages 314–331, 2010.

Smith, J. M., Modeling Nearshore Waves for Hurricane Katrina, USACE Engineer Research and Development Center, Coastal and Hydraulics Laboratory, August 2007. http://chl.erdc.usace.army.mil/Media/9/3/7/tnswwrp-07-6.pdf

Suhayda J. N., and R. W. Jacobsen, Interaction of Hurricane and Coastal Landscape Features: A Literature Review, for the U.S. Army Corps of Engineers (USACE), URS Corporation, August 2007.

URS Group Inc., for Federal Emergency Management Agency, High Water Mark Collection for Hurricane Katrina in Louisiana (Final), FEMA-1603-DR-LA, Task Orders 412 and 419, March 30, 2006.

USACE, Southeast Louisiana Joint Surge Study, Independent Technical Review, Final Report, for FEMA, October 15, 2007.

USACE, Flood Insurance Study, Southeast Parishes of Louisiana, Intermediate Submission 2: Offshore Water Levels and Waves, for FEMA, July 2008.

USACE, Incorporating Sea-Level Change Considerations in Civil Works Programs, Engineering Circular No. 1165-2-211 1, July 2009.

USACE, http://www.mvn.usace.army.mil/prj/mtog/feasibility_study_documents/mtog_index.htm.

USACE (New Orleans District), Hurricane and Storm Damage Risk Reduction System, Design Elevation Report, Draft Report Version 4.0, August 18, 2010.

Wamsley, T. V., M. A. Cialone, J. Westerink, and J, M. Smith, Influence of Marsh Restoration and Degradation on Storm Surge and Waves, USACE, ERDC/CHL CHETN-I-77, July 2009.

Wang, D. W., D. A. Mitchell, W. J. Teague, E. Jarosz. and M. S. Hulbert. Extreme Waves Under Hurricane Ivan. Science 5 Vol. 309, No. 5736, p. 896, August 2005.

Weaver R. J. and R. A. Luettich, Jr., 2D vs. 3D Storm Surge Sensitivity in ADCIRC: Case Study of Hurricane Isabel, Proceedings of the Eleventh International Conference on Estuarine and Coastal Modeling, 2010.

Weisberg, R. H. and L. Zheng, Hurricane Storm Surge Simulations Comparing Three-Dimensional with Two-Dimensional Formulations Based on an Ivan-like Storm over the Tampa Bay, Florida Region, Journal of Geophysical Research – Oceans, Vol. 113, 2008.

Weaver R. J. and R. A. Luettich, Jr., 2D vs. 3D Storm Surge Sensitivity in ADCIRC: Case Study of Hurricane Isabel, Proceedings of the Eleventh International Conference on Estuarine and Coastal Modeling, 2010.

Westerink, J. J., J. C. Feyen, J. H. Atkinson, R. A. Luettich, C. N. Dawson, M. D. Powell, J. P. Dunion, H. J. Roberts, E. J. Kubatko, and H. Pourtaheri, A New Generation Hurricane Storm Surge Model for Southern Louisiana, 2004. http://nd.edu/~adcirc/pubs/westerinketal_bams_ref1935b.pdf

Part III.

Hurricane Surge Hazard Analysis

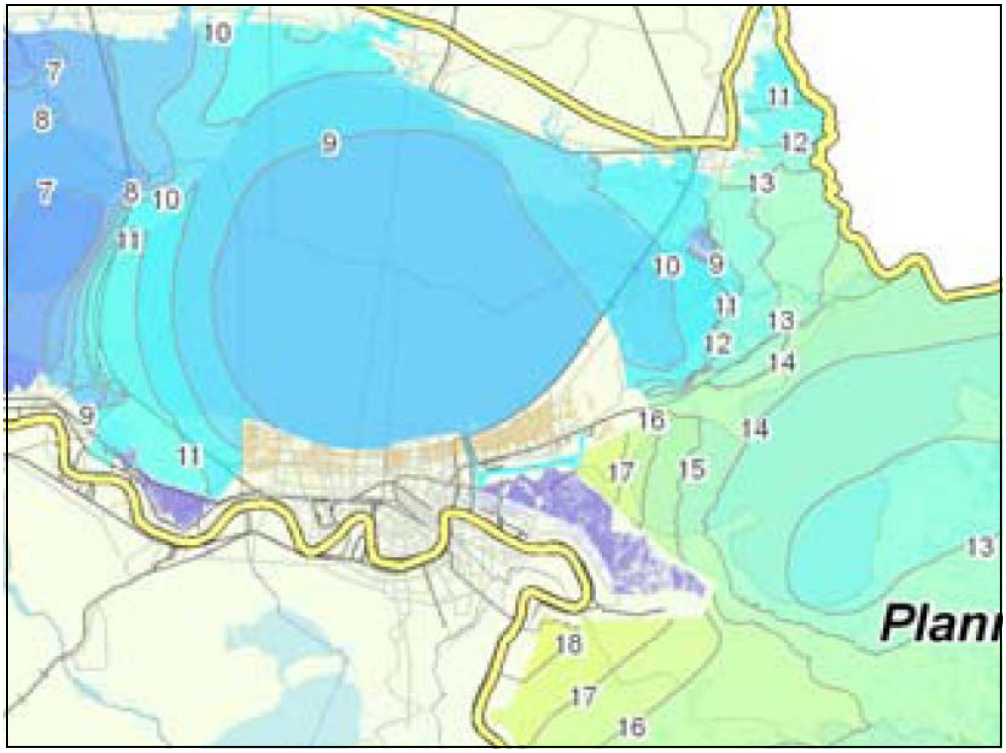

USACE 2009

As discussed in the Introduction, the full range of hurricane surge risk management programs—perimeter structures, evacuation, property flood damage insurance, building codes, coastal restoration, etc.—requires good surge hazard information. Hydrologists describe surge and other flood hazards using a return frequency analysis (see GTN-1) to quantify the recurrence probability of surge by magnitude. The estimated surge hazard varies across a region in accordance with hurricane joint probability characteristics (see Part I) and the physics of surge interaction with local coastal landscape features (see Part II).

Return frequency analysis relies on sophisticated mathematical techniques to provide seemingly exact hazard estimates—such as surge SWL elevations and wave height to the nearest 0.1 ft for the 100- and 500-year return period. However, the apparent accuracy of these probability estimates is belied by major uncertainties in critical inputs regarding hurricane climatology and the modeling of surge physics (see Parts 1 and II). A significant limitation is the short duration of records on which inputs are based. Despite these uncertainties, the advantages of probabilistic surge elevation estimates include:

- The estimates can be used to further support detailed quantitative risk assessment and cost-benefit analysis for risk management alternatives (e.g., optimal perimeter structure height).
- Estimates for different locations that are developed with the same methodology can be compared and the relative differences can be used to establish regional risk management priorities.
- A variety of useful probabilities can be calculated—such as the probability of a 100-year surge occurring at a particular location over the term of a typical mortgage; or the probability of a 500-year surge occurring across a wide region over an agency's planning horizon.

This Part III reviews the state of the practice in hurricane surge SWL and wave return frequency analysis, including the following subjects:

Section 12., the direct approach involving analysis of data records from tide gauge stations and other observations to estimate local surge SWL and wave hazards. If sufficiently long and reliable records are available, a direct analysis provides the best estimate of local surge hazard;

Section 13., the JPA approach to combining the results of hurricane JPA and deterministic surge modeling. As tide gauge records are not widely available, this technique is usually employed—in a way similar to that used in characterizing riverine flood hazards; and

Section 14., recent applications of the JPA approach, including the surge hazard analysis performed by the USACE for the southeast Louisiana.

Sections 12 and 13 examine the established literature and ongoing research, including methods, assumptions, and limitations. Section 14 addresses the published information on surge analyses performed as part of FISs. Afterwards, findings and conclusions are presented, together with recommendations for improving future hurricane surge hazard analyses.

The ensuing Part IV discusses hazard analyses for interior polder inundation associated with surge overtopping and breaching of perimeter protection. The USACE has employed analysis of perimeter overtopping and breaching in designing post-Katrina upgrades to the New Orleans regional hurricane protection systems. Part V examines additional technical approaches to evaluating hurricane surge hazard for future conditions and surge estimates for selected storm-scenarios.

Section 12. Analysis of Surge Records

12.1 Analysis of Tide and HWM Data

As with riverine flood hazard analysis, surge SWL return frequencies can be evaluated using long term gauge station records (FEMA February 2007). Gauge stations which provide daily maximum water levels are maintained by NOAA, USGS, and USACE in coastal sounds, bays, lakes, and rivers and near important coastal works. NOAA has four CN-GoM tide stations with records dating back many decades at Pensacola FL (80+ years), Dauphin Island AL (40+ years), Grand Isle LA (60+ years), and Sabine Pass TX (50+ years). The USGS gauge record for Biloxi MS covers over 100 years.

Important limitations in the direct analysis of tide gauge data include the following:

- The record may not be sufficiently long to reasonably estimate a particular return period event. As discussed in GTN-1, the probability of a 100-yr (or greater) surge occurring during a given 100-yr tide record is 63%. The probabilities do not exceed 95% and 99% for at least one occurrence until the record approaches 300 and 500 years. Note that this limitation is not unique to tide records. The records used to establish joint probability characteristics for regional hurricane climatology are also subject to length limitations.
- The uncertainties associated with extrapolating extreme events—with return periods many times longer than the record length—can be very large.
- Tide stations often fail during major surge events. Peak SWL values for recent events can sometimes be estimated using nearby SWL HWM data. However, for many events HWM data may not be available in close proximity to the station or, if available, may not be reliable.
- Tide data must be converted to the proper geoid reference (NAVD88 and epoch, see GTN-2). Conversion of older data must account for regional and local sources of coastal subsidence (see Section 18). Long-term tide data are also affected by SLR.
- The analysis only applies to a small geographical area in close proximity to the gauge station—e.g., up to a few miles at most. Coastal landscape features can significantly alter surge magnitude (see Section 7).
- Changes in the coastal landscape over time impact gauge data representativeness and usability. Examples include changing coastal pass bathymetry; construction of levees, roads, and other embankments; subsidence and erosion; loss of coastal barriers and dunes; etc. Coastal hydrologists often study the effect of landscape changes on the tidal exchange and water quality for important estuaries (Jacobsen and Dill 2007, McCorquodale et al 2007).

GTN-1 describes the estimation of return periods from a data series using observed rankings. The observed return frequency (F_R, equal to the inverse of the return period) is typically defined as:

$$F_R = n/\tau \text{ ; or sometimes as } F_R = (n - a) \,/\, (\tau + 1 - 2a)$$

where

n is the observed rank,
τ is the record length, and
a provides a minor adjustment to the observed return period.

To extrapolate recurrence estimates from the observed return frequency (or return period) hydrologists use probability distribution functions. These functions account for normal or log-normal distributions

around a mean, skewness, kurtosis, and other factors typical of recurrence data distribution. Example distributions include

- Log-Normal distribution, takes the logarithm of the return period (log (100) = 2) and uses a normal distribution of the magnitude versus log transformed return period (or return frequency); defined by two parameters, mean and the variance.
- Log Pearson Type III distribution, adds the coefficient of skewness to the Log-Normal Distribution and reduces to the Log-Normal Distribution when coefficient of skewness equals zero.
- Generalized Extreme Value, (GEV) distribution includes three parameters (the mean, variance, and a shape parameter allowing for a higher probability of extreme values, i.e., a "fat tail") which are grouped according to three types: Type I, (Gumbel) distribution; Type II, (Frechet) distribution; and Type III (Weibull) distribution.
- Generalized Pareto distribution, a three parameter power law function.

The selection of a particular function is somewhat arbitrary but can be aided by visual inspection or more rigorous fitting techniques. Figure 12.1 illustrates the use of the GEV distribution function, and a modified function, with data from the NOAA Pensacola tide station, by Xu and Wang (2008). Note that the GEV derived level is nearly three feet less than the observed value for the 82-yr return period.

In addition to extrapolating extreme return period values, the functions can be used to estimate uncertainty bands. Most probability distribution functions for estimating return frequency are skewed distributions and thus the uncertainty bands will also be skewed. Note the authors of Figure 12.1 did not include an uncertainty band but the difference between the two curves is over 5 ft at 500 years.

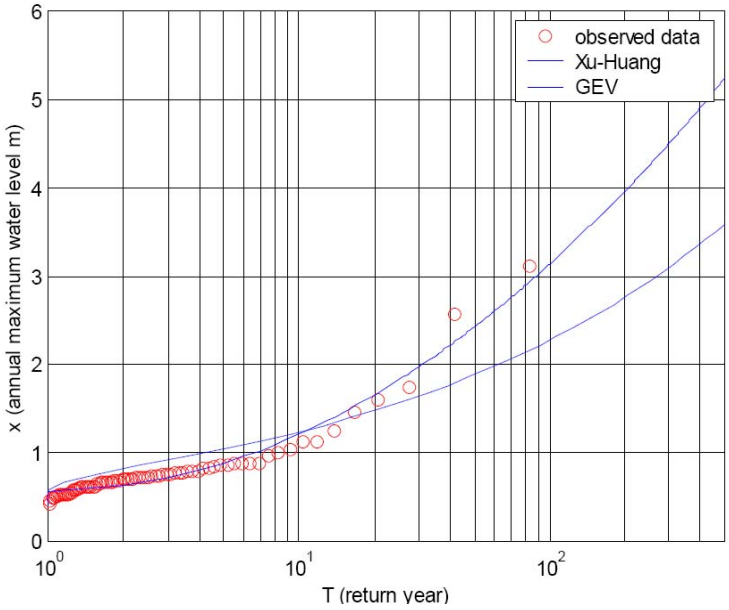

Figure 12.1. Observed Annual Maximums at Pensacola Tide Station with GEV and Modified Distribution Functions

(The GEV curve has the lower water level at the 100-yr return)

Xu and Wang 2008

12.2 Recent Evaluations of Tide Gauge Data

The following is a discussion of two recent return frequency studies encompassing multiple CN-GoM tide stations.

A return frequency analysis of unreferenced tide data was published in 2005 (prior to Hurricane Katrina) by Chris Zervas of NOAA. The objective of this report was to support sea level rise assessment and not to provide a detailed return frequency analysis. Annual high SWLs relative to the gauge Mean Higher High Water (MHHW) in meters were analyzed using the GEV distribution for 117 US tide stations, including five along the CN-GoM. Zervas noted that GoM stations required a positive shape parameter (Type II, Frechet) due to higher probabilities of extreme SWLs associated with hurricane surge, but provided no detailed information about the GEV equation. The report does not present complete return frequency graphs or tabulated results for the various stations. The 1% return frequency magnitudes (in ft above gauge MHHW) are approximately:

- Pensacola, FL 6.5 ft
- Dauphin Island, AL 5.4 ft
- Grand Isle, LA 4.9 ft
- Eugene Island, LA 6.4 ft
- Sabine River, TX 4.5 ft

Grand Isle MHHW is about 0.5 ft above LMSL or 0.7 ft NAVD88-2006.81 (NOAA). Thus, this estimate of the 1% return frequency SWL corresponds to approximately 5.6 ft NAVD88-2006.81.

While Zervas did not focus on assessing local hurricane surge return frequency he noted that

> The GEV exceedance probability curves . . . are best constrained at the more frequent return periods and less well constrained near the 1% annual exceedance probability level . . . . In addition, if the GEV distribution has a positive shape factor (Frechet), the 95% confidence intervals widen considerably for the longer return periods, since they are dependent on the presence or absence of a few rare events in the data series. (Zervas 2005)

Zervas goes on to state that the 1% return frequency SWL for Grand Isle "may have been underestimated." (Zervas 2005)

Shortly after Hurricane Katrina a FEMA contractor was tasked to conduct a return frequency analysis for several regional tide stations in order to provide local governments with advisories on potential changes to NFIP 100- and 500-yr flood elevations. (FEMA issues these advisories in order to expedite rebuilding as the development of detailed FIRMs takes several years.)[1] URS Corporation analyzed data for four NOAA tide stations (Pensacola FL, ,Dauphin Island, AL, Waveland MS, and Grand Isle LA) and two USGS gauges (Pascagoula MS and Biloxi MS). The NOAA tide data were adjusted to gauge MSL and the USGS gauge data were assumed to be equivalent to MSL. No adjustments were made for long-term SLR or station subsidence.

The annual maximum data were plotted using the following formula:

[1] An early draft copy of this report entitled *Preliminary Flood Frequency Analysis for Hurricane Katrina* (URS Corporation 2005) has been obtained. The report appears to have been subsequently revised and is referenced as the *Hurricane Katrina Flood Frequency Analysis* in a later, broader report: *Hurricane Katrina in the Gulf Coast, Mitigation Assessment Team Report*, p. 1-19 (URS Corporation 2006). The later version could not be obtained.

$$F_R = \frac{n - 0.4}{\tau + 0.2}$$

Figure 12.2 illustrates the log-log plot of the annual maximum data for the USGS Biloxi MS gauge. The SWL for Hurricane Katrina is the highest rank value, which for 100 records yielded a plotted return frequency of `0.6%, or a return period of 167 years. The 100-yr return period on the plot corresponds to a SWL of 17.8 ft.

The data for all six stations were analyzed using several probability distribution functions, including the GEV and Log Pearson Type III. The results for the 100-yr return period SWL for these two PDFs—in feet above LMSL—are shown in Table 12.1, along with the results of Zervas' analysis for three of the stations. With the addition of the Hurricane Katrina data, the URS GEV 100-yr SWL estimate for Dauphin Island AL was higher than Zervas' GEV estimate by more than 1 ft. The URS GEV estimate rose slightly for Grand Isle LA (by 0.2 ft) and remained the same for Pensacola FL. The Log Pearson Type III estimates were slightly higher than the GEV estimates for all six locations. URS did not provide an uncertainty analysis for these estimates.

In a separate 2006 report URS provided the following estimates of return period SWL:

- Biloxi MS, 15.7 ft (100-yr) and 28.7 ft (500-yr); Hurricane Katrina HWM of 24 ft (250-yr);
- Pascagoula MS, 11.9 (100-yr); Hurricane Katrina HWM of 13 ft (125-yr);
- Waveland MS, 17.6 ft (100-yr) and 22.8 ft (200-yr); Hurricane Katrina HWM of 23 ft (200-yr);
- Dauphin Island AL, 6 ft (50-yr) and 7.5 ft (100-yr); Hurricane Katrina HWM of 5.8 ft (50-yr); and
- Pensacola FL, 5.8 ft (50-yr) and 7.3 ft (100-yr); Hurricane Katrina HWM of 6.1 ft (50-yr).

Note that the Xu-Wang curve in Figure 12.1 indicates a 100-yr SWL for Pensacola FL of closer to 10.5 ft.

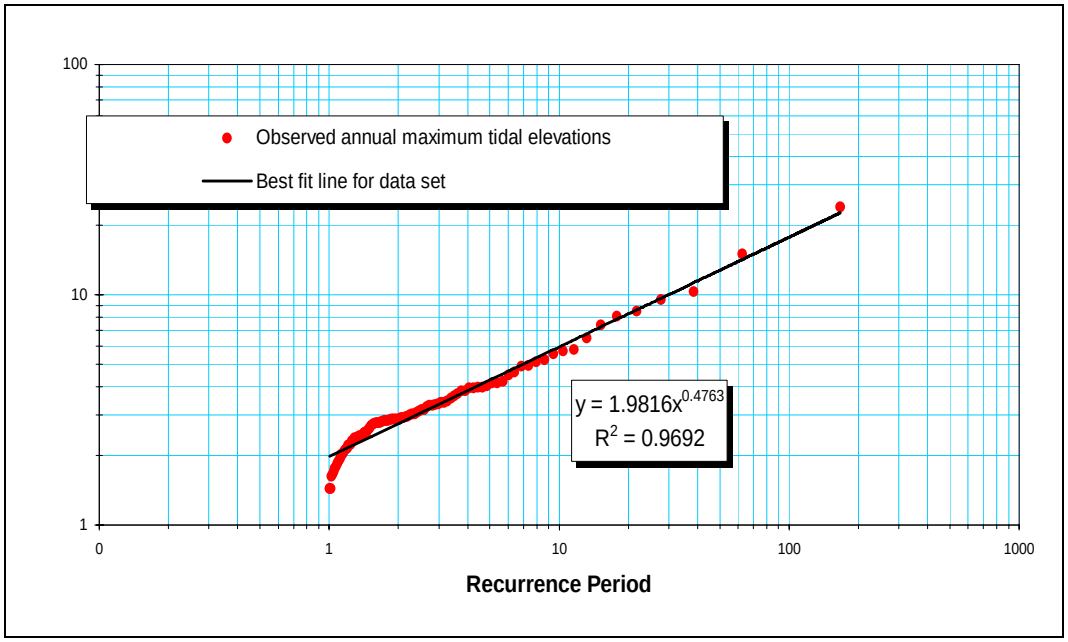

Figure 12.2. Annual Maximum Series for Biloxi MS Tide Gauge
URS Corporation 2005

Table 12.1. Estimates of 100-yr Surge SWL

URS Corporation 2005

Tide Station	URS Post Katrina		Zervas Pre-Katrina
	GEV	Log-Pearson Type III	GEV
Grand Isle, LA	5.6	5.7	5.6
Waveland, MS	23.5	25.8	-
Biloxi, MS	14.8	15.2	-
Pascagoula, MS	11.4	11.6	-
Dauphin Island, AL	7.3	7.5	6.1
Pensacola, FL	7.2	7.3	7.2

NOAA (Tides and Currents, Extreme Water Levels) recently began publishing updated return frequency analyses—employing the GEV distribution— for selected tide gauges on their website. CN-GoM gauges include Pensacola FL, Dauphin Island AL, Grand Isle and Eugene Island LA, and Sabine Pass TX. Figure 12.3 presents the NOAA return period graph for Grand Isle LA, with the water elevation converted to NAVD88-2006.81. The mean, 95%UCL, and LCL levels for the 100-yr return period are 7.1, 11.5,and 5.1 ft. The current mean estimate of 7.1 ft is 1.5 ft higher than the URS value shown in Table 12.1 for the GEV, reflecting NOAAs refinements to the gauge's 60+ years of data—including 2008 observations for Hurricanes Gustav and Ike. This increase indicates the sensitivity of 100-yr return period estimates to record length and quality. Figure 12.3 shows the notable asymmetry of the confidence limits and that the GEV distribution based mean 100-yr level is less than the highest observed value (about 7.5 ft).

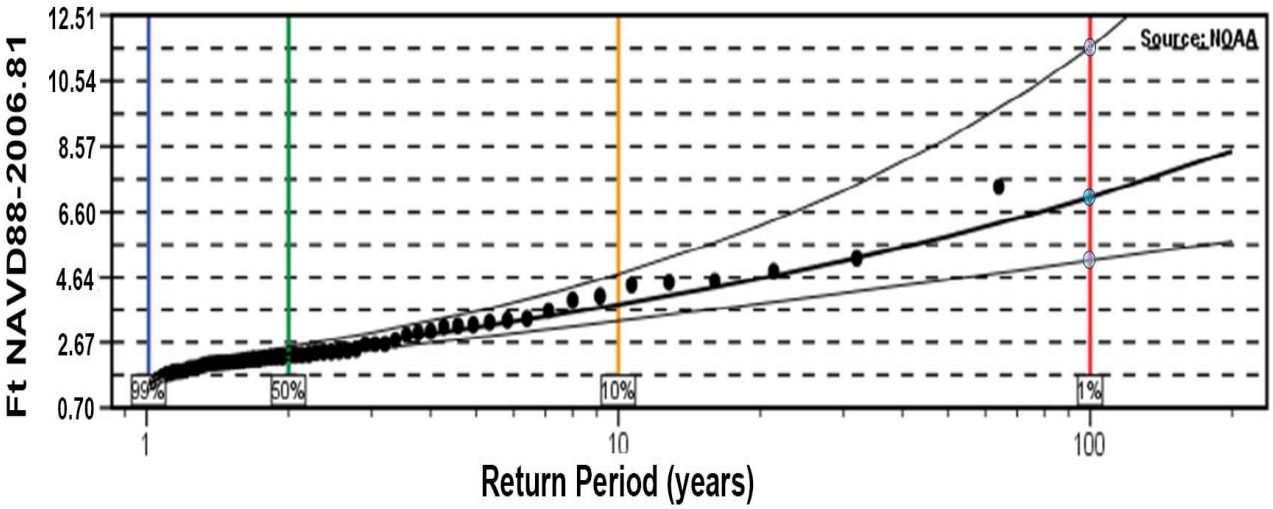

Figure 12.3. Grand Isle LA Tide Station Return Frequency

NOAA (http://tidesandcurrents.noaa.gov/est/est_station.shtml?stnid=8761724)

12.3 Recent Evaluations of HWM Data

In 2010 Needham developed a surge database for the US GoM shoreline covering the 130-yr period of 1880 to 2009. The database

> identifies the maximum surge height and peak surge location for storm surge events. Although this information does not depict the regional extent of specific surges, or a list of all historic surge levels at a particular location, these data are useful for understanding surge height potentials for the entire basin and regions within the basin, identifying locations that observe enhanced or reduced numbers of peak surges, and potentially for understanding the relationship between specific tropical cyclone characteristics and resultant surge heights. (Needham 2010)

Needham's search of tropical cyclone data sets identified a total of 421 storms, with 463 landfalls (42 storms involved double landfalls) which he classified as having at the potential to generate a peak SWL of 4 ft or higher (above LMSL). This equates to a frequency of more than 3.5 US GoM tropical cyclone landfalls per year. By investigating tide gauge records, scientific and technical literature, HWM studies, newspaper reports, and other data sources Needham confirmed 193 peak SWL events of 4 ft or higher. For the CN-GoM, he identified 76 events of 4 ft or higher and 32 of 8 ft or higher (frequencies of 58% and 25%, respectively). Table 12.2 lists the 76 events.

Needham analyzed frequency and magnitude time-series for the 193 surge events for evidence of long-term trends associated with the SO, AMO, and NAO (see Section 2). He noted a period of relatively suppressed surge frequency and magnitude from the 1970s through the 1990s attributable to the cooler AMO phase. He also described statistical correlations of US Gulf-wide surge events with the AMO, SO, and NAO. Needham did not attempt to define an overall cycle for GoM surge events.

Needham also analyzed 181 peak SWL records for the period from 1900 to 2009 to evaluate US Gulf-wide return frequency surge magnitude. Needham analyzed the series using several probability distribution functions, including the Gumbel, Huff-Angel, and Southern Regional Climate Center (SRCC) distributions. (The latter two equations were previously developed for evaluating rainfall frequency.) Table 12.3 presents the results of his analysis, with the estimate of the US Gulf-wide 100-yr surge ranging from 23.8 to 32.8 ft.

Two important limitations with Needham's US Gulf-wide return period analysis include the following.

1. Lumping surge HWM data for different coastal regions ignores the dramatic effects on surge magnitude associated with a) particular hurricane track Loop Current interactions; b) regional continental shelf conditions; and c) local landscape features.
2. The surge HWM data are subject to many error sources, including lack of a true local peak measurement and the quality of LMSL vertical referencing;

Needham did not provide an uncertainty analysis for his Gulf-wide return period estimates. Uncertainty bands are crucial as the probability of a 100-yr event occurring at least once within a particular 100-yr span is only 66.9%.

Table 12.2. List of CN-GoM Surge HWMs

Needham 2010

Storm Name	Year	Peak Surge Location	Peak SWL (ft LMSL)
Katrina	2005	Pass Christian MS	27.8
Camille	1969	Pass Christian MS	24.6
Eloise	1975	Dune Allen Beach	18.2
New Orleans	1917	Southeastern LA, S of New Orleans LA	17.0
Cheniere Caminada	1893	Cheniere Caminada (W of Grand Isle) LA	16.0
Frederic	1979	Gulf State Park	15.3
Betsy	1965	Pointe a la Hache	15.2
Rita	2005	Cameron LA	15.0
Grand Isle	1909	Terrebonne Bay/ Bayou Portage (N of Pass Chris) LA/ MS	15.0
Ivan	2004	Destin, FL to Mobile, AL FL/Al	15.0
Unnamed	1947	Chandeleur Light LA	14.0
Opal	1995	Florida Panhandle FL	14.0
Unnamed	1906	Galt, Santa Rosa County FL	14.0
Audrey	1957	west of Cameron	13.9
Gustav	2008	Southeast LA, near Bay Gardene LA	13.0
Flossy	1956	Ostrica Lock LA	13.0
Terrebonne Parish	1926	Terrebonne Parish 1926 Terrebonne Parish LA	12.5
Lili	2002	Crewboat Channel (Calumet) LA	12.3
Unnamed	1886	Johnson's Bayou LA	12.0
Georges	1998	Fort Morgan AL	11.9
Unnamed	1916	Mobile AL	11.6
Unnamed	1888	Southeastern LA LA	10.9
Unnamed	1896	Fort Walton Beach	10.0
Isidore	2002	Rigolets, LA and Gulfport Harbor, MS MS/LA	8.3
Andrew	1992	Cocodrie LA	8.0
Juan	1985	Cocodrie LA	8.0
Danny	1985	South Central LA Coast LA	8.0
Edith	1971	Vermillion & Cote Blanche Bays LA	8.0
Unnamed	1923	Biloxi MS	8.0
Unnamed	1901	Port Eads and Mobile LA/AL	8.0
Earl	1998	Northwest FL- Big Bend area E of Apalach FL	8.0
Unnamed	1901	Port Eads and Mobile LA/AL	8.0
Hilda	1964	Cocodrie LA	7.8
Ethel	1960	Quarantine Bay LA	7.0
Unnamed	1918	Creole LA	7.0
Erin	1995	just west of Navarre Beach FL	7.0
Ida	2009	Bay Gardene LA	6.5
Danny	1997	HWY 182W, b/t Gulf Shores & Fort Morgan AL	6.5
Unnamed	1931	Frenier LA	6.5
Unnamed	1932	Mobile AL	6.5
Unnamed	1940	Frenier LA	6.4
Bob	1979	Gulfport and Harrison County CD MS	6.3

Table 12.2. List of CN-GoM Surge HWMs, Continued

Needham 2010

Storm Name	Year	Peak Surge Location	Peak SWL (ft LMSL)
Cindy	2005	SE LA, MS, Lakes Borgne & Pont MS/LA	6.0
Florence	1988	Bayou Bienvenue LA	6.0
Chris	1982	Cameron Parish LA	6.0
Carmen	1974	South Central LA Coast LA	6.0
Debbie	1965	Industrial Canal in New Orleans LA	6.0
TS Brenda	1955	Shell Beach LA	6.0
Unnamed	1948	MS Coast MS	6.0
Unnamed	1943	Chef Menteur LA	6.0
Unnamed	1920	Lake Borgne and Mississippi Sound MS/LA	6.0
Unnamed	1897	Sabine Pass TX/ LA	6.0
Unnamed	1936	Fort Walton Beach, Panama City, Valparaiso FL	6.0
Unnamed	1929	Panama City to Apalachicola FL	6.0
Unnamed	1897	Sabine Pass TX/ LA	6.0
Matthew	2004	Frenier LA	5.8
Debra	1978	Atchafalaya Bay to Vermillion Bay LA	5.7
Bill	2003	Bayou Bienvenue MS	5.5
Beryl	1988	Bayou Bienvenue LA	5.5
Baker	1950	Pensacola FL	5.5
Bonnie	1986	Sabine Pass TX	5.2
Hanna	2002	Gulfport Harbor MS	5.1
Claudette	1979	Sabine Coast Guard Station TX	5.0
Babe	1977	Southeastern LA LA	5.0
Esther	1957	MS Coast MS	5.0
Arlene	2005	Walton County FL	5.0
Alberto	1994	Okaloosa Island to Destin FL	5.0
Claudette	1979	Sabine Coast Guard Station TX	5.0
Babe	1977	Southeastern LA LA	5.0
Bertha	1957	west end of Vermillion Bay LA	4.7
TS No.1	1956	Biloxi MS	4.7
Unnamed	1912	Mobile AL	4.4
Ella	1958	Texas and Louisiana Coasts TX/LA	4.0
Unnamed	1938	Cameron and Vermillion Parishes LA	4.0
Ella	1958	Texas and Louisiana Coasts TX/LA	4.0
Unnamed	1916	Mobile AL	4.0

Table 12.3. US Gulf-Wide Surge SWL Return Period Estimates

Needham 2010

Return Period (yr)	Probability Distribution Function		
	Gumbel	Huff-Angel	SRCC
2	9.5	9.1	9.0
5	13.3	12.5	13.2
10	15.9	15.6	16.3
20	18.3	19.6	19.4
25	19.1	21.2	20.5
50	21.5	26.2	23.5
100	23.8	32.8	26.6

12.4 Analysis of Wave Data

Extreme wind waves in the GoM originate with hurricanes. Marine engineers and scientists involved in the design of ocean going vessels and offshore oil and gas exploration and production platforms (such at those at OceanWeather, Inc.) have studied extreme GoM waves. Data on waves off the CN-GoM shore have been collected at regional NOAA buoys since the 1970s. Over the recent decades the network of buoys has expanded to over 100 stations (see NOAA National Data Buoy Center website).

Panchang and Dongcheng (2006) analyzed data from three deep GoM buoys which each had records extending over 25 years. Using a Gumbel distribution, the 100-yr H_s values were found to be between 34.2 and 37.1 ft. The authors noted that the 95% confidence band associated with this 100-yr estimate is on the order of ±3 feet. The $H_{1\%}$ in a wave field is usually estimated at $1.52H_s$; thus, an estimate of the 100-yr $H_{1\%}$ in the deep GoM would exceed 60 ft, allowing for a margin of uncertainty. A major limitation of this analysis, acknowledged by the authors, is the short record duration. Temporary buoys deployed near the transition to the Continental Shelf during Hurricane Ivan recorded H_s up to 58.7 ft. This H_s value is higher than the 100-yr range noted above, but may reflect shallower depth.

Since 1999 the Louisiana State University Coastal Studies Institute has installed seven wave monitoring stations for analyzing the nearshore seasonal wave characteristics and extreme hurricane waves. However, it will likely be many years before a sufficient record is available for direct analysis of extreme nearshore wave conditions.

In the absence of sufficiently long wave records, wave scientists have primarily relied on the stochastic approaches to evaluating extreme GoM waves employing hindcasts of GoM hurricanes dating back over 50 years (e.g., see Jonathan and Ewans February 2011 and May 2011).

Section 13. Surge JPA

13.1 Overview of Surge JPA

The JPA for evaluating hurricane climatology (described in Section 4) can be readily coupled with deterministic high resolution surge hydrodynamic modeling (encompassing wind, SWL, and wave setup components, see Section 9) to estimate the surge hazard at any coastal location of interest (LOI). As described in GTN-1 Sections K and L, JPA of flood return frequency is a common tool in hydrology.

The JPA of surge return frequency can be summarized in a mathematical formulation (from Resio et al 2007 and Toro 2008):

$$\boldsymbol{F}(SWL_i) = \int\int\int\int\int \boldsymbol{p}(CPD, R_{max}, V_f, \theta, X)\, \boldsymbol{H}[\boldsymbol{\Psi}(CPD, R_{max}, V_f, \theta, X) - SWL_i]\, d(CPD)\, d(R_{max})\, d(V_f)\, d(\theta)\, d(X)$$

where

- CPD, R_{max}, V_f, θ, and X are five major hurricane characteristics influencing local surge response, with X being the landfall distance with respect to the LOI (or X and Y for a full areal range). Additional characteristics could be included—such as V_{max} (instead of, or in addition to, CPD), IKE, Holland B, asymmetry, double eye walls, track passage over the Loop Current, intensification and decay dynamics, etc.
- $\boldsymbol{\Psi}$(CPD, R_{max}, V_f, θ, X) is the deterministic *surge response function.* $\boldsymbol{\Psi}$ defines the SWL at the LOI for the range of hurricane characteristics using a high spatial resolution wind/surge/wave-setup model (e.g., PBL plus ADCIRC-STWAVE), incorporating the influence of the regional coastal landscape on surge routing. Mathematically, $\boldsymbol{\Psi}$ is a six dimensional (6D) surface.
- $\boldsymbol{p}$(CPD, R_{max}, V_f, θ, X) is the joint PDF of the five characteristics. Example PDFs for CPD, R_{max}, V_f, and θ were previously shown in Figure 4.2 and 4.3. The joint probability is also a 6D function—of the five attribute probabilities: $\boldsymbol{p}$(CPD), $\boldsymbol{p}$(R_{max}), $\boldsymbol{p}$(V_f), $\boldsymbol{p}$(θ), and $\boldsymbol{p}$(X).
- H[] evaluates if the local SWL determined by $\boldsymbol{\Psi}$ for a particular hurricane is greater than some SWL_i ; if it is, H[]= 1; if not, H[] = 0. The combined term—$\boldsymbol{p}$(CPD, R_{max}, V_f, θ, X) $\boldsymbol{H}$[Ψ(CPD, R_{max}, V_f, θ, X) – SWL_i]—is thus the discrete (mass) probability for the interval [Ψ(CPD, R_{max}, V_f, θ, X) – SWL_i].
- $\boldsymbol{F}(SWL_i)$ is the cumulative probability at SWL_i , integrating $\boldsymbol{p}$(SWL) over the full range of CPD, R_{max}, V_f, θ, and X. Thus, $\boldsymbol{F}(SWL_i)$ provides the surge cumulative distribution function (CDF). The local surge CDF is typically presented as a 2D graph of SWL versus return frequency or period. The return frequency, F_r equal to 1 – $\boldsymbol{F}(SWL_i)$. is the *surge hazard response function*.

Hurricane surge JPA requires a stochastic approach, coupling a good representation of both the probabilistic hurricane climatology for the LOI—$\boldsymbol{p}$(CPD, R_{max}, V_f, θ, X)—with the deterministic model of hurricane driven surge interactions with the local coastal landscape—$\boldsymbol{\Psi}$(CPD, R_{max}, V_f, θ, X). In this approach a synthetic set of hurricanes is typically used to represent the hurricane climatology. As discussed in Section 4, a *full JPM* set approximates the entire range of the 5D (CPD, R_{max}, V_f, θ, X) storms by employing a sufficient combinations of attributes. However, with more values per attribute the number of storm combinations increases drastically. For five values per five attributes 3125 storms would be required to provide the CDF for one location.

An alternative to the full JPM is the *Monte Carlo JPM* which only employs the number of randomly selected storms—drawn from the 5D range—to construct a synthetic record of sufficient length to

confidently contain return frequencies of interest. Thus, for a synthetic 1000-yr record for a LOI that experiences an average landfall of 16 GHMs/century the set would only need to include 160 storms.

With either the Full or Monte Carlo JPM each hurricane in the synthetic set is simulated with the wind/surge/wave-setup model. Each simulation result represents one increment—d(CPD) d(R_{max}) d(V_f) d(θ) d(X)—of the above 5D integrand. Modeling each storm in the set provides all the increments in the integrand, and numerical integration—or quadrature—is then used to compute the surge CDF.

In a regional surge hazard study this entire stochastic analysis must be replicated at a reasonable LOI spacing. The location spacing can be addressed by establishing offsets for each storm such that intermediate points experience nearly the same peak SWL as the nearest landfall point. In theory, conditions along the coast can be represented by replicating each storm in the JPM every $2X_{max}$, where X_{max} is the maximum radial distance at which the peak SWL for that storm is relatively undiminished.[1] X_{max} is not the same for every storm. If the regional study employs a uniform landfall spacing for all storms the landfall spacing should be equal to or less than the shortest $2X_{max}$.

High resolution surge models require the dedication of large HPPC system for hours per storm simulation. Given the time and expense associated with such models further reduction of the synthetic hurricane set size is desirable—provided any increased error is acceptable. Researchers have devised two primary techniques for defining an optimized subset or sample, (OS): the *JPM-OS* and the *Surge Response OS* (Toro et al 2008 and Resio et al 2007).

In addition to SWL, surge return frequency analysis must also consider wave hazards. The return frequency of shoreline and overland (inundated region) surge waves, at a LOI, are typically evaluated by estimating wave field conditions (which encompasses a Rayleigh distribution, see Section 5) associated with the SWL at those return frequencies. The shoreline and overland wave field conditions at any SWL are typically a function of localized, depth-depended wave regeneration, propagation, and transformation processes (see Section 6).

The following sections provide a further explanation of surge JPA using JPM-OS and Surge-Response-OS, the selection of landfall spacing, the treatment of bias and uncertainty in surge JPA, key steps involved in implementing surge JPA, and wave hazard analysis. Approaches to future conditions surge JPA—for examining the influence of potential changes in RSLR, SST, etc. on hazards—are discussed in Part IV.

13.2 JPM-OS

In the JPM-OS approach (Toro 2008) the OS is optimized to represent the hurricane climatology as depicted in the joint probability ***p***(CPD, R_{max}, V_f, θ, X) 6D surface. The targeted error for the JPM-OS relative to ***p*** is reduced by adjusting the number (*n)*, characteristics, and weighting of the JPM-OS hurricanes. The error in the JPM-OS representation of the ***p***() benchmark is mathematically evaluated by comparing their 6D surfaces using numerical integration—also referred to as quadrature (Toro employed the Bayesian quadrature method.) The JPM-OS can be selected to minimize the overall variance or variance within a particular probability range—e.g., around the 100-yr return period. Importantly, the JPM-OS may allow for different relative errors at different return periods.

[1] An assumption is that storms which make landfall farther away can also be represented by the $2X_{max}$ spacing developed from representing the peak SWL. This assumption is generally valid as the SWL slope becomes more gradual with distance from landfall.

Assessing the suitability of a particular JPM-OS to represent ***p*** is analogous to assessing a set of *n* blocks (3D prisms) with varying heights to represent a mathematical 3D surface, as illustrated in Figure 13.1. Increments for each of the 5D independent variables can be refined or coarsened, and thus *n* can be raised or lowered—as shown in Figures 13.1.a and 14.1.b. In addition, varying sized increments can also be employed—as depicted in Figure 13.1.c.—in which case the bases of the 6D prisms are described in terms of their relative—weighted—sizing.

When the JPM-OS is being coupled with a wind model a *wind hazard benchmark* can be used to further optimize the selection. Similarly, when the set is being coupled with a surge model a *surge hazard benchmark* can be employed in refining the optimization. For a surge JPA the surge hazard benchmark has the additional advantage of incorporating interaction between hurricane characteristics and coastal features.

A surge hazard benchmark for a LOI is created by employing a large set of (*N*) storms—e.g., 3,125 storms if five increments were employed for each of the five attributes. This large storm set is coupled with a very *simplified*, much less computationally demanding, surge model. The model is simpler both in terms of the physics and coastal features represented—such as a SLOSH or a low resolution ADCIRC model without wave setup. In some cases, the simplified surge model may use an idealized coastal region, or the analysis may employ the hurricane climatology and a surge model for a similar coastal region. Thus, the surge hazard benchmark serves as a reference only in that it reflects a high resolution of possible storm characteristics. It does <u>not</u> reflect a high resolution of the coastal hydrodynamics. (Depending on the degree of surge model simplification the surge hazard benchmark may not offer much improvement over a wind hazard or basic joint probabilities benchmark).

The surge hazard benchmark at each LOI can be thought of as a "finely discretized" representation of the local 6D CDF described by the *n* storms. For a JPM-OS with a lower *n,* the increments for CPD, R_{max}, V_f, θ, and *X* (i.e., X_{max}) are more coarsely discretized, producing a rougher approximation of the 6D surge CDF. The suitability of any trial JPM-OS, (n_1, n_2, n_3, etc.) can then be evaluated by comparing the associated trial surface to the benchmark surface.

The development of a JPM-OS employing a surge hazard benchmark is illustrated in Figure 13.2.

Potential increments in CPD, R_{max}, V_f, and θ for the JPM-OS can be developed initially based on representing the shape of the surge response—as discussed in the following section. However, the advantage of the JPM-OS is that it is optimized to represent the shape of surge *hazard* response, which may contain critical inflections. Thus increments are adjusted and added in order to best capture the response of SWL at varying hurricane characteristic probabilities—especially combinations that may correspond to hazard levels of interest (e.g., 100- , 500-, 1000-yr etc. levels). As with surge response (see below), an overly simplified surge model's representation of coastal conditions can influence the depiction of surge hazard response. These limitations should be assessed to determine that the benchmark surge model adequately depicts regional hazard response.

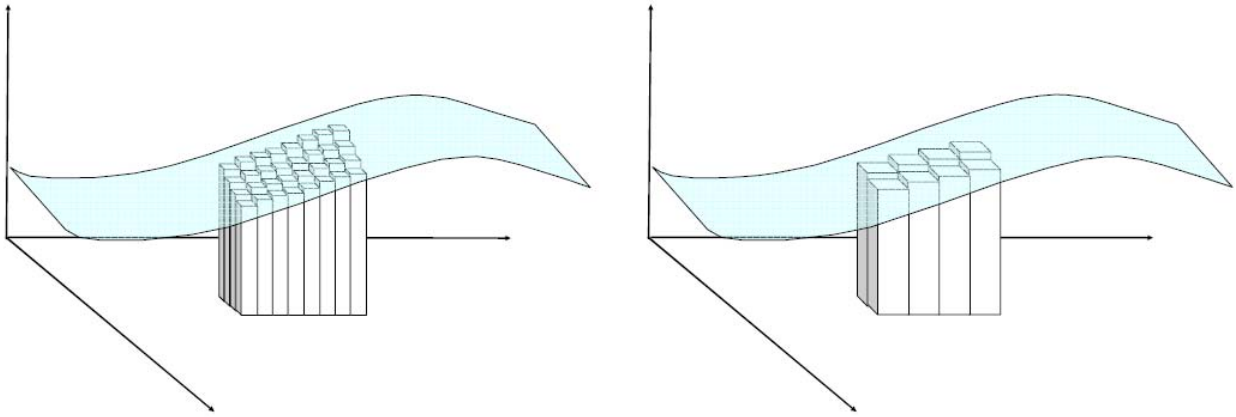

a. Finer Increments (n = 32)

b. Coarser Increments (n = 8)

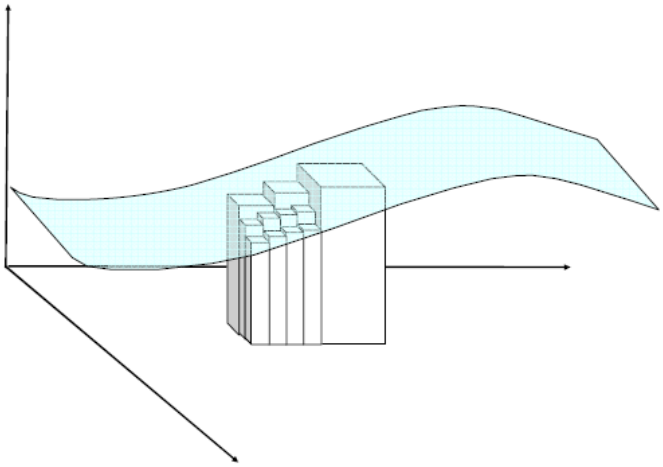

c. Varying Increments (n = 11)

Figure 13.1. Discretization of Volume Under a 3D Surface

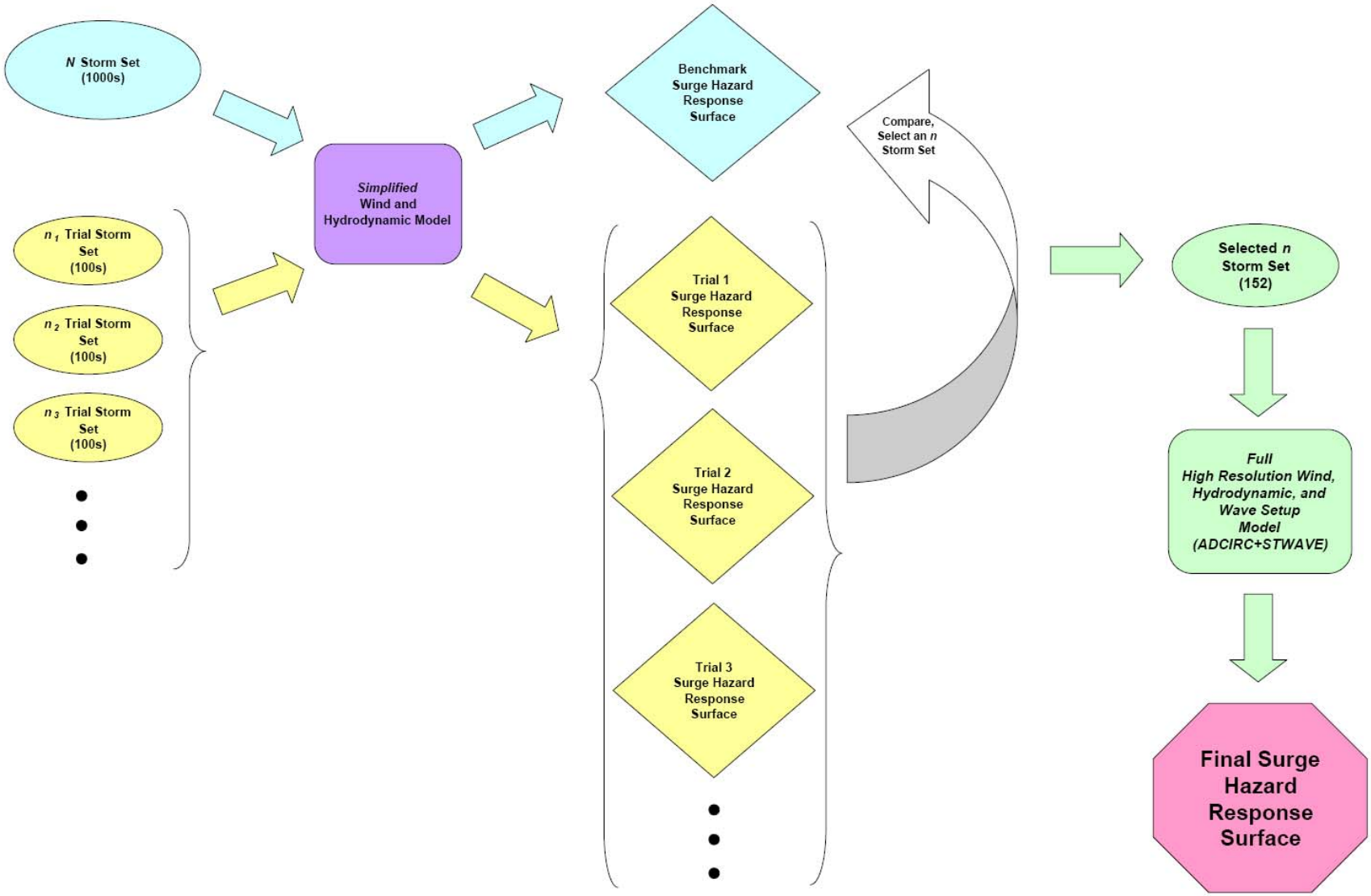

Figure 13.2. Development of JPM-OS Using a Surge Hazard Benchmark

13.3 Surge Response-OS

Another JPM for JPA of hurricane surge is to use an OS of synthetic storms to define the range of the regional surge response $\boldsymbol{\Psi}$ (Resio et al 2007) alone. The approach assumes that a wide range of surge conditions associated with the 5D characteristics can be readily interpolated/extrapolated from limited OS results. In this approach SWL values associated with any combination of storm attributes and their joint probability, as defined by $\boldsymbol{p}$, are obtained from the high spatial resolution Ψ defined with the OS. This OS is more properly considered a part of the deterministic surge hydrodynamic analysis than the joint probability and is referred to in this Report as a *Surge Response-OS*.

This Surge Response OS approach can reduce the size of the storm set when $\boldsymbol{\Psi}$ is considered to have a fairly simple, smooth, response to all five variables—i.e. no abrupt changes in SWL in response with small changes in hurricane characteristics due to regional hurricane-landscape interactions. However, use of a reduced Surge Response-OS also assumes that the interactions of $\boldsymbol{p}$ and $\boldsymbol{\Psi}$ will be fairly smooth. If both of these assumptions are valid, utilizing the Surge Response OS can be an efficient approach.

As noted in Section 1, peak SWLs to the right of landfall increase with increasing CPD, (or V_{max}), R_{max}, V_f, and positive θ (easterly heading with approach to an east-west shoreline). If $\boldsymbol{\Psi}$ is considered to be nearly linear and smooth for all five factors within the region of interest, then an OS can be defined using $\boldsymbol{\Psi}$ alone (i.e., apart from the surge *hazard* response).

Several coastal scientists have recently evaluated the nature and sensitivity of $\boldsymbol{\Psi}$ for the CN-GoM (see Fitzpatrick et al 2010 and Xu 2010), including research supporting JPA OS applications to coastal FISs (Resio et al 2007, Irish et al 2008, URS Corporation 2008, Resio et al 2009, and Irish et al 2009). Major recent findings include:

- CPD—On an idealized coastline, other characteristics being equal, surge SWL increases linearly with increasing CPD (with the V_{max}^2). URS (2008) conducted extensive sensitivity tests using a SLOSH model of the Mississippi coast to evaluate the relationship of CPD and SWL. Using a baseline model with CPD, R_{max}, V_f, and θ values of 70 mb, 30 mi, 12 mph, and 0°, respectively, URS varied CPD between 30 and 110 mb at increments of 10 mb. The SWL results were evaluated at three groups of coastal locations—outer shoreline, inshore river, inland floodplain. Figures 13.3.a, b, and c present results for the three groups of coastal locations. As expected, SWL response to CPD was linear, with steeper slopes further inshore, reflecting the impact of the momentum balance. CPD generally exerts the greatest influence on peak SWL, followed in decreasing order by R_{max}, θ, and finally V_f.
- R_{max}—Irish et al (2008) conducted numerical experiments using a range of idealized shelf slopes to evaluate the affect of R_{max}x on SWL. The simulations employed three R_{max} values (11.5, 23, and 34.5 miles) and six CP values (ranging from 40 to 130 mb). The results, shown in Figure 13.4, also indicate a linear relationship between R_{max} and SWL.
- V_f—URS (2008) used their baseline SLOSH model tested V_f values of 6, 8, 10, 12, 14, 16, and 18 mph. Figure 13.5 illustrates linear response at outer shoreline locations.
- θ—URS (2008) also tested the baseline SLOSH model with headings of -45, -30, -15, 0, +15, +30, and +45 degrees. Figure 13.6 shows that generally SWL increased smoothly, though non-linearly, with more positive θ.
- Holland B—Resio et al (200&) referred to numerical experiments (unpublished) suggesting that modest Holland B variations (e.g., ±20%) are linearly correlated with surge.

a. Outer Shoreline Locations

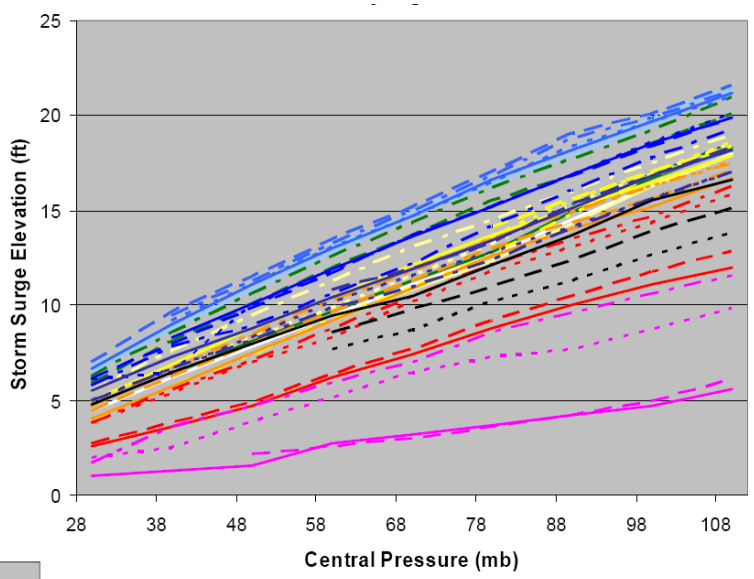

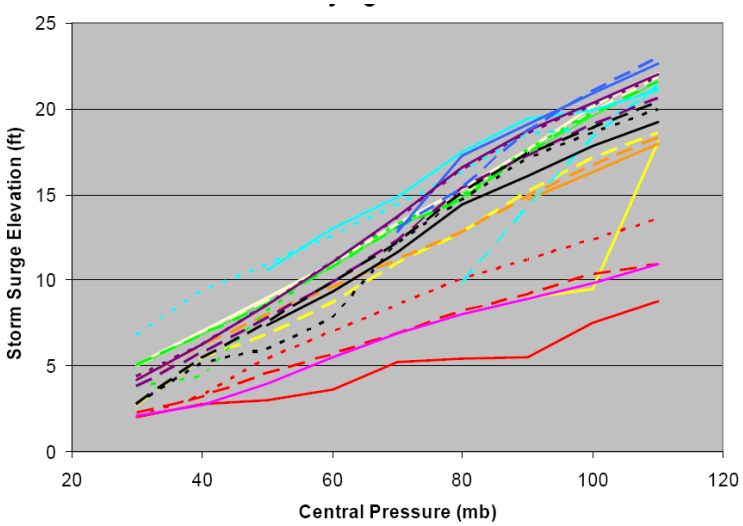

b. Inshore River Locations

c. Inland Floodplain Locations

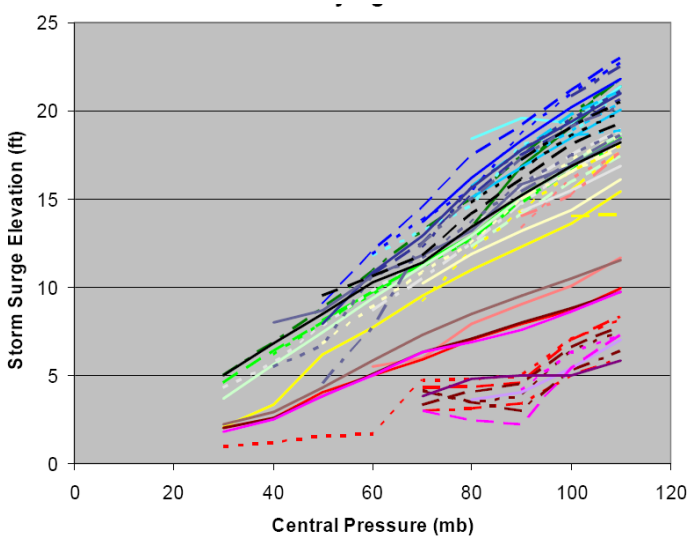

Figure 13.3. Peak SWL versus CPD

(color spectrum blue-red for east-west of landfall)

URS Corporation 2008

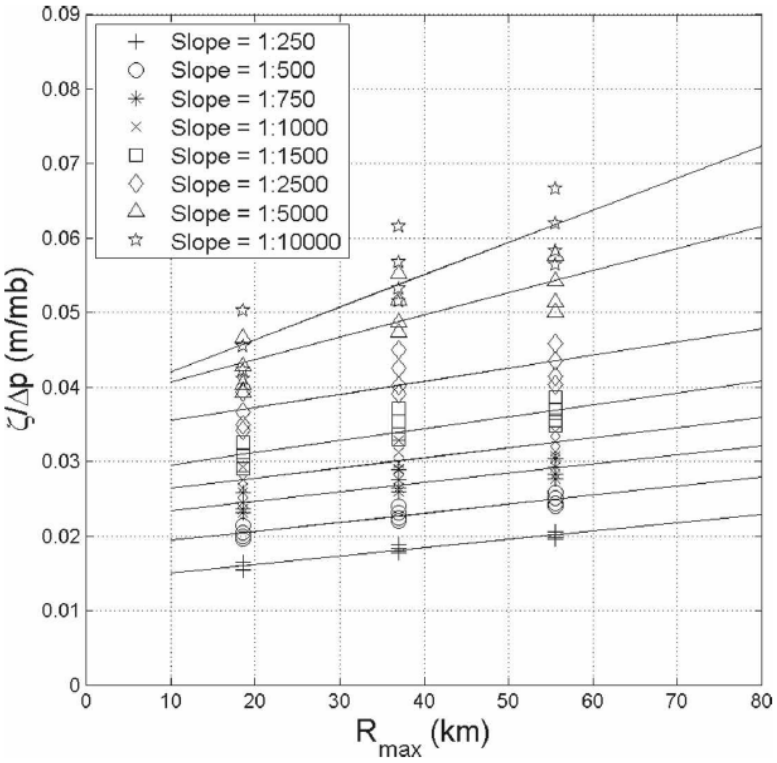

Figure 13.4. Peak SWL versus R_{max} (normalized for CPD)
Irish et al 2008

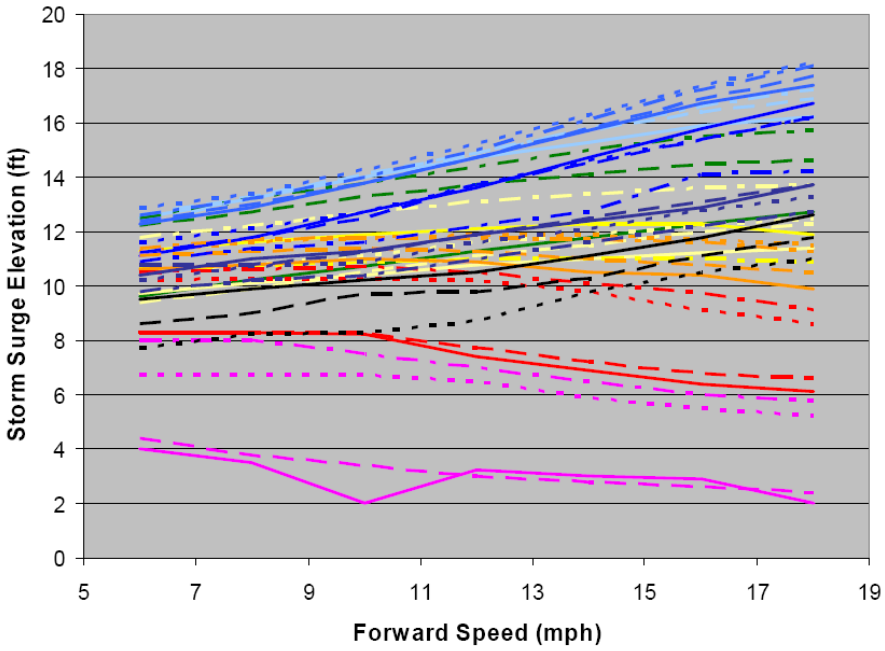

Figure 13.5. Peak SWL versus V_f
URS Corporation 2008

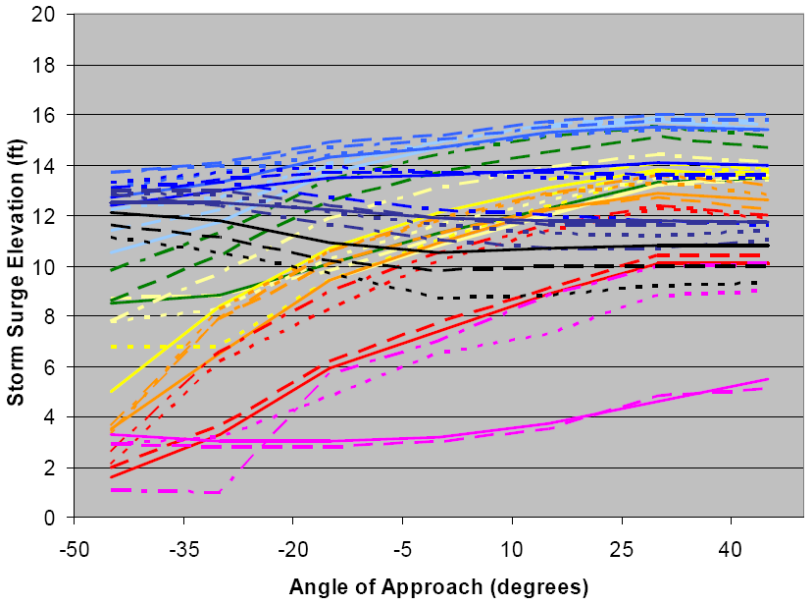

Figure 13.6. Peak SWL versus θ

URS Corporation 2008

However, these indications of smooth response have been based on *very simplified* surge models (e.g., SLOSH). Use of simplified surge models can affect representation of surge response in ways similar to model hindcast performance (see Sections 8, 10, and 11). Seven important simplifications include:

1. Vortex modeling. Simplified vortex models may not reasonably depict wind peaks and durations. The synthetic vortex model simulates the approaching hurricane wind field based on inputs of CPD, R_{max}, V_f, θ, and landfall location, and incorporating correlations on decay, but may not fully account for the observed variability in V_{max} associated with CPD. A major example is Hurricane Katrina, which had a landfall CPD of 100 mb (borderline Category 4/5) but V_{max} winds of 126.5 mph (strong Category 3). In addition, not all vortex models account for storm asymmetry. Finally, vortex models do not describe wind field variability, such as experienced with banding and eye wall replacement.

2. Mesh resolution. Surge hydrodynamic results are sensitive to the terrain fidelity of the model, particularly in the representation of critical coastal landscape features. The simplified models used in OS development may not adequately account for local surge variations that result from the interaction of storm conditions and landscape features. An important example is the local wind setup in sheltered water bodies—such as coastal bays, lakes, and rivers—that is highly sensitive to small variations in storm conditions.

3. Friction. Bottom friction sensitivity to inundation is not addressed in the current SWL models. Thus, it is also not incorporated into simplified models. Furthermore, simplified models may apply uniform friction values across widely differing terrains. The simplification of friction may lead to reducing the number of storms for depicting critical non-linear interactions between surge driving forces and coastal landscape features. The importance of this interaction has been indicated by limited tests on the sensitivity of surge to the presence of coastal marsh (Wamsley et al 2009). Extensive testing of the sensitivity of surge hazard response to friction parameterization, and its interaction with hurricane characteristics, has not be undertaken.

4. Other surge model settings and parameters. Hindcast evaluations of FIS surge models have shown sensitivity to additional settings and parameters, including: numerical method, acceleration terms, time step, eddy viscosity, wind sheltering coefficients, and air-sea drag coefficient. These factors may also influence OS selection.
5. Wave setup. The simplified surge models employed in the development of the OS do not usually include wave radiation stress gradients, and thus do not capture wave setup contribution to SWL, (up to 30%). Furthermore, recent hindcasts of Hurricane Katrina and Rita HWMs indicate that the current wave coupling approach used with the high resolution surge models may not sufficiently depict setup in coastal bays and lakes.
6. Baroclinic forcing. In limited areas, such as near major coastal passes, temperature and salinity gradients can create forces which require 3D analysis. If future studies indicate a significant localized impact, baroclinic forcing may need to be incorporated into the OS selection.
7. LMMSL rise, pre-storm setup, and astronomical tides. The simplified models typically neglect these factors. In the CN-GoM they can combine to contribute over 2 ft to SWL rise, leading to some non-linear interactions with surge.

The URS tests revealed that $\boldsymbol{\Psi}$ becomes more complex as varying coastal features and more complicated momentum exchanges come into play, e.g., Figures 13.3 b) and c). In investigating $\boldsymbol{\Psi}$ for the southwest Texas coast, Irish et al (2009) found that a simplified, nearly linear $\boldsymbol{\Psi}$ is primarily applicable for open coastlines. Sensitivity analyses using high resolution coastal models of very intricate coastlines—such as those with large sheltered water bodies—would likely reveal more irregular interactions. For complex coastlines, a proper Surge Response-OS requires many more storms and may not offer an advantage over the standard JPM-OS approach. Importantly, a Surge Response-OS does not support further JPA of polder inundation hazards (see Section 16).

13.4 Landfall Spacing

In addition to discretizing CPD, R_{max}, V_f, and θ, selecting the number of JPM-OS or Surge Response-OS storms depends on defining increments for landfall spacing. As noted above, each storm is considered to have an appropriate X_{max}—and hence landfall spacing—defined by the SWL gradient near the landfall at peak. URS (2008) summarized sensitivity tests using the simplified SLOSH model of the Mississippi coast; a storm with CPD, R_{max}, V_f, and θ values of 80 mb, 25 mi, 10 mph, and 0°, respectively; and various landfall spacing in fractions of R_{max}. The study found that landfall spacing equivalent to R_{max}—or X_{max} equivalent to $\frac{1}{2}R_{max}$—could be used with minimal effect on estimates of surge hazard across a region. Employing uniform landfall spacing greater than the R_{max} of the smallest storm will thus introduce some error in the OS which must be evaluated as part of the optimization.

Resio et al (2007) reported on a sensitivity analysis conducted with an idealized linear E-W shoreline model of varying shelf slopes and employing three values for R_{max}, 11.5, 23, and 34.5 mi. The results for a modest shelf slope are shown in Figure 13.7. For the 34.5-mi R_{max} storm, as X approaches $\pm\frac{1}{2}R_{max}$ the local peak SWL reduces by about 10% compared to the peak SWL at landfall. The peak fall-off with normalized distance is less for smaller size storms.

Resio et al reported that modification of the idealized E-W shoreline, with part of the shoreline offset southward, induced surge increases, (Figure 13.8). They suggested these increases (due to conveyance effects) would dominate over spacing influences. However, reduced sensitivity to track spacing with this or greater shoreline complexity, or major landscape features, was not specifically analyzed.

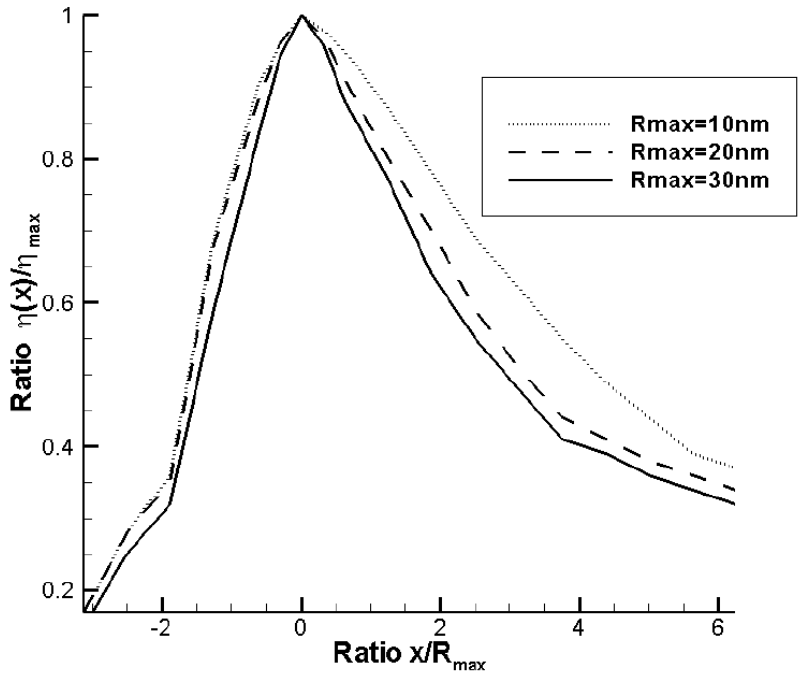

Figure 13.7. Peak SWL versus X

(local peak SWL normalized to landfall peak SWL; X normalized to R_{max})

Resio et al 2007

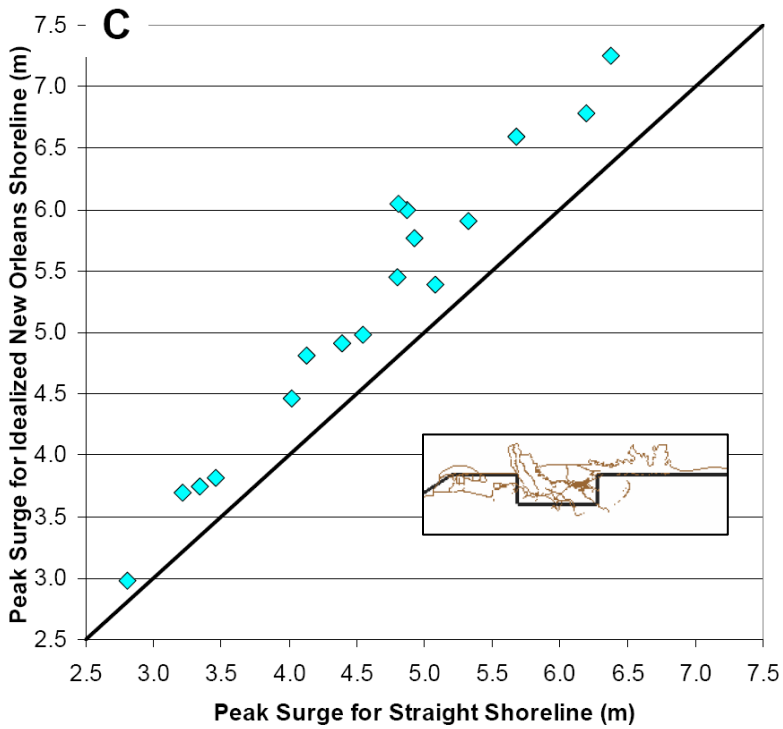

Figure 13.8. Peak SWLs for Modified versus Straight Shoreline

Resio et al 2007

13.5 Bias and Uncertainty in Surge JPA

In employing any methodology scientists typically take steps to identify and correct consistent errors and to define uncertainties. In developing an OS for a surge JPA these steps can include:

- Validation of the benchmark (wind hazard response, surge hazard response, or surge response) with available empirical analysis, such as using a surge return frequency analysis based on the tide records to validate a surge hazard benchmark; development and application of correction factors and uncertainty bands.
- For surge hazard response and surge response benchmarks, validation of the simplified surge model using a hindcast event, and development of associated correction factors and uncertainty bands. Including sufficient number of trials to assess influence of simplified surge model uncertainty on the selection of the OS.
- Assessing the influence of additional storm characteristics on the surge hazard response. Research discussed in Part I suggests it may also be important to account for other variables in hurricane climatology. Fitzpatrick et al (2010) showed that surge is highly correlated with the combined intensity, size, and wind field distribution—i.e., $IKE^{1/2} \cdot V_{max}$. Wind field profile (Holland B), asymmetry, and banding may also be influential.[2] In addition, the role of probabilities associated with certain intensification and decay factors may be important. The FISs to date have tended to regard these parameters as minor and suitable for inclusion in an uncertainty term. In the future, discretization of hurricane characteristics may need to address such parameters directly.
- Expanding trials to assess the influence of discretization of CPD, R_{max}, V_f, θ, and X on the residual error in the selected set's representation of the wind or surge hazard benchmark. Given potential uncertainties, the quality of the JPA results may benefit from enlarging the set to include additional storms that reflect hazards of interest.

An advantage of the JPM-OS is that it can be evaluated versus multiple benchmarks: ***p***, wind hazard, and surge hazard. As the wind model is less computationally demanding, the wind hazard benchmark can be based on a very large storm set.

The biases and uncertainties associated with the selection of an OS will necessarily contribute to biases and uncertainties in the final surge return frequency analysis, together with those associated with the high resolution surge model. Table 13.1 summarizes five major categories of stationary uncertainty, ε, associated with JPA and the use of an OS and how they can be assessed (see Resio et al 2007 and URS Corporation 2008). Importantly, some measured uncertainties encompass more than one ε term.

Research into the nature of uncertainties often distinguishes between uncertainties that are aleatory (inherent in nature and irreducible) versus epistemic (due to reducible limitations on observations and measurements). Distinctions are also often drawn between uncertainties having parametric (system) versus modeling origins (USACE 2009). Methods of quantifying uncertainties, such as model validation, may encompass more than one category.

[2] Irish conducted surge simulations for Texas hurricane landfalls and found that varying Holland B from 0.9 to 1.9 influenced surge SWL by only 15%; but this result may not be applicable to other regions.

Table 13.1. Quantification of Stationary Uncertainties in Surge JPA with OS

Uncertainty In	Distribution	Quantified By	Based On
1. $\varepsilon_{\boldsymbol{p}}$—the hurricane climatology as represented by a function of selected attributes—$\boldsymbol{p}$(CPD ,R_{max}, V_f, θ, X).	Non-Normal (e.g., Gumbel)	CPD return frequency distribution parameters (a_0 and a_1)	Historical data; (note potential discounting of the probability of extremely intense hurricanes, see Figure 3.10)
	Normal	σ_{Rmax}, σ_{Vf}, σ_{ϑ}, σ_X	Historical data.
2. $\varepsilon_{\boldsymbol{W}}$—the hurricane climatology due to attributes not selected—such as CPD-V_{max} variability, asymmetries, spiral banding, eye wall replacement, Holland B ($\varepsilon_{\boldsymbol{B}}$), IKE, etc.	Normal	$\sigma_{\boldsymbol{W}}$ (e.g., $\sigma_{\boldsymbol{B}}$ and $\sigma_{\boldsymbol{PBL}}$)	Validation against a detailed wind hazard benchmark that incorporates more degrees of freedom; or sensitivity tests.
3. ε_{OS}—the coarser discretization of the hurricane climatology relative to the benchmark, i.e. the selected increments in the JPM-OS (not applicable for Surge Response OS); the simplified benchmark; simplified surge response; an example is simplified set of storm tracks	Normal	σ_{OS}	Residual error between two hazard response surfaces; validation against regional tide gauge data or coastal sensitivity tests.
4. ε_{ψ}—the full, coupled high resolution wind/surge/wave-setup model due to imprecision in model physics, setup, geometry, mesh attributes, etc.	Normal	σ_{ψ}	Model validation.
5. ε_T—concurrent contribution of low amplitude tides. (Note this could also include uncertainties in pre-storm meteorological conditions affecting SWL.)	Normal	σ_T	Tide data.

Stationary uncertainty can be normally distributed—mathematically equivalent to a diffusion/spreading term. Such ε terms have an associated RMSE or standard deviation (σ). Multiple, independent ε terms described as normally distributed can be added to provide an overall error term, ε_Σ. When individual σ are in units of SWL the overall σ_Σ can be estimated by summing each individual σ^2 and taking the square root of the sum. Values for σ are not necessarily constant, but can vary with other parameters.

Stationary uncertainty terms can also be non-normally distributed—asymmetric and/or with distorted curves (e.g., fat or pinched tails). In addition to σ these distributions are described with coefficients for skewness, kurtosis, and other shape factors. A major example is uncertainty in the probability distribution for CPD—as CPD is considered the most significant contributor to surge among the hurricane characteristics.. The Louisiana and Mississippi FISs employed Gumbel and Weibull non-normal distributions for CPD. Standard statistical techniques are also available for estimating uncertainties in non-normal distributions (see GTN-1).

Both normal and non-normally distributed uncertainty can be used to construct confidence bands around the estimated the CDF. Furthermore, statistical approaches can be used to also evaluate the influence of combined non-normal and normal distributed uncertainty on the actual CDF (see Resio et al 2012). In addition to evaluating uncertainty, implementation of the JPM-OS approach requires that corrections be applied for any identified bias in the hurricane climatology and/or the high resolution wind/surge/wave-setup model. Non-stationary uncertainty—such as the influence of climate change on hurricane characteristics or RSLR on surge hydrodynamics—must be investigated with separate JPAs by modifying the climatology and wind/surge model (see Part V).

13.6 Preparation of Return Frequency Curves

The simulation of each of the *n* OS storms with the full, high resolution wind/hydrodynamic/wave-setup model produces time-series and peak SWL values at the regional LOIs—mesh nodes as well as intermediate locations with interpolated peak SWL values. Production runs are subject to a series of quality checks to ensure that runs complete successfully—with the specified model setup, parameters, and other input files; that the results over the course of the entire simulation are physically reasonable; and that results do not contain excessive spurious values (non-fatal instabilities that appreciably change the surge SWL peaks). A percentage of runs are usually reviewed in detail, such as by using zoomed animations of surge dynamics near critical coastal areas. Additional quality control procedures are described in FIS documentation (e.g., FEMA February 2007).

Following completion of production runs, the generation of LOI-specific CDF curves involve four steps:

1. CDF integration and smoothing;
2. CDF validation;
3. Adjustments to spatial variations in specific surge hazard levels; and
4. Construction of confidence limits.

STEP 1: CDF Integration and Smoothing

Figure 13.9 illustrates the relative frequencies of surge SWL peaks from a series of JPM-OS storms at a location (URS Corporation 2008). The results have been grouped into 2 cm SWL bins, which are plotted vertically against the joint probability for the storms in the bin. The relative frequency bars depict a very "jagged" distribution and include gaps at many SWL increments. The jaggedness is caused by storms with similar joint probability making landfall at varying X (i.e., at the various landfall spacing). Some minimal smoothing of the PDF can be done to avoid excessive irregularities in integrating the CDF. *However, the smoothing should not significantly distort the CDF and modify the median estimate of surge return frequencies*.

One smoothing approach is to replace each vertical bin bar distribution with a normal distribution—somewhat wider than the vertical bar but having the same area. This spreads out the discrete bin probability over a wider range of SWLs. The value for σ_{Smooth} can be based on some portion of the normally distributed uncertainty described in Section 13.5 above. This spreading of each bin bar in effect incorporates the corresponding portion of ε as an additional dimension of the integrand in the CDF formula (as indicated by Resio et al 2007 and URS Corporation 2008). Figure 13.9 illustrates a smoothed PDF resulting from the use of ε and Figure 13.10 shows the derived CDF.

However, as σ_{Smooth} increases, the PDF and CDF are increasingly modified. Resio et al 2007 (and Resio et al 2012) suggested that this CDF modification could be employed as one way to asses the impact of uncertainty on the 100-yr SWLs—as 100- to 500-yr SWLs were shown to increase notably when σ_{Smooth} was based on both epistemic and aleatory uncertainty. This approach to assessing uncertainty is problematic compared with a traditional approach of computing an undistorted, median, CDF with confidence intervals. In the case of a JPM in which a set of storms is carefully selected, significantly modifying the bin distributions would not seem to support developing a median estimate of the CDF.

Another smoothing approach is to refine the PDF increments. If the Surge Response-OS approach is used the $\boldsymbol{\Psi}$ increments can be refined in the respective dimensions (CPD, R_{max}, V_f, θ, and X) to aid smoothing prior to integration. This is akin to refining the representation in Figure 13.1.c) into the representation in Figure 13.1.a). The intermediate values in surge response are determined through piece-wise interpolations appropriate to each dimension (CPD, R_{max}, V_f, θ, and X). The interpolations in each dimension can use linear or nonlinear fitting techniques—e.g., if a Gumbel distribution is used to characterize the probability of CPD then this function can be used to aid in refining this dimension. Figure 13.11 illustrates the refinement of surge hazard response.

The spreading and refining smoothing techniques can also be used together.

Another technique for developing a smooth CDF would be to employ the results to define values for μ, σ, and coefficients of skewness, kurtosis, etc. These, in turn, would be used to define a surge return frequency curve according to a standard function commonly used in return frequency analysis, such as the Log-Pearson Type III, GEV (e.g., Gumbel, Weibull), etc (see GTN-1).

Comparing the results of different approaches to smoothing and numerical integration can provide a measure of the imprecision associated with this step, which may be crucial for particular surge hazard levels of interest, e.g., 100- and 500-yr SWLs. Importantly, the CDF integration technique itself can be considered to introduce an additional sixth uncertainty, ε_I , beyond the five noted in Table 13.1.

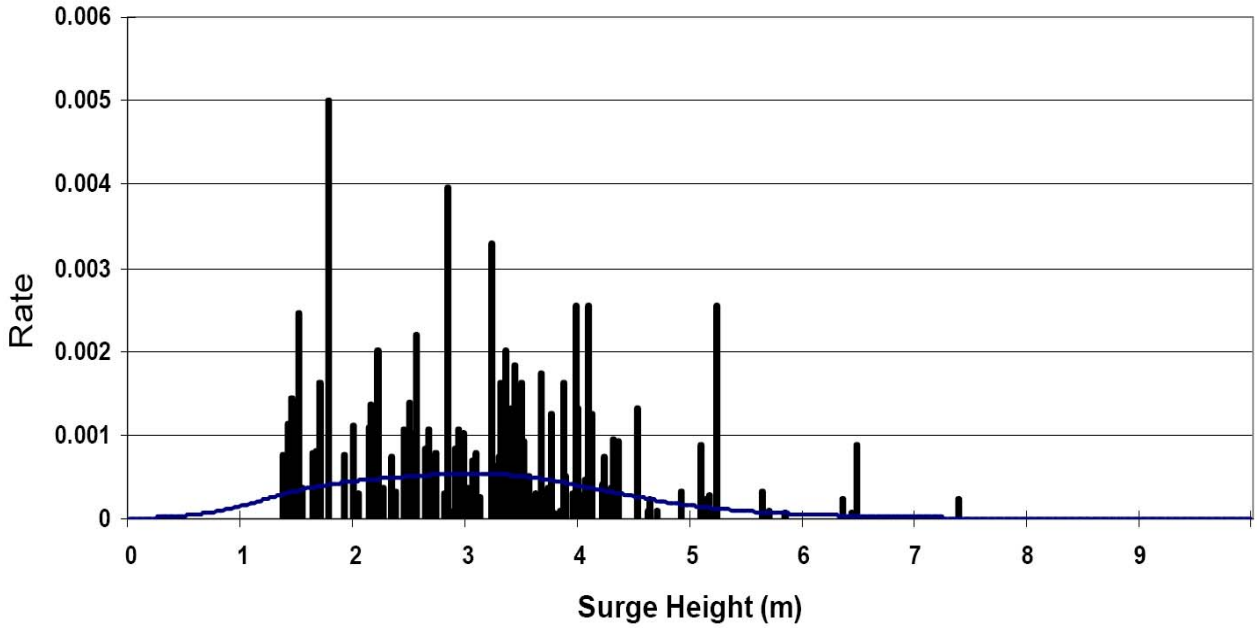

Figure 13.9. Histogram of Relative Frequencies for Peak Surge and Smoothed PDF

black histogram bars = raw SWL values, blue curve = smoothed PDF with uncertainty dampening
URS Corporation 2008

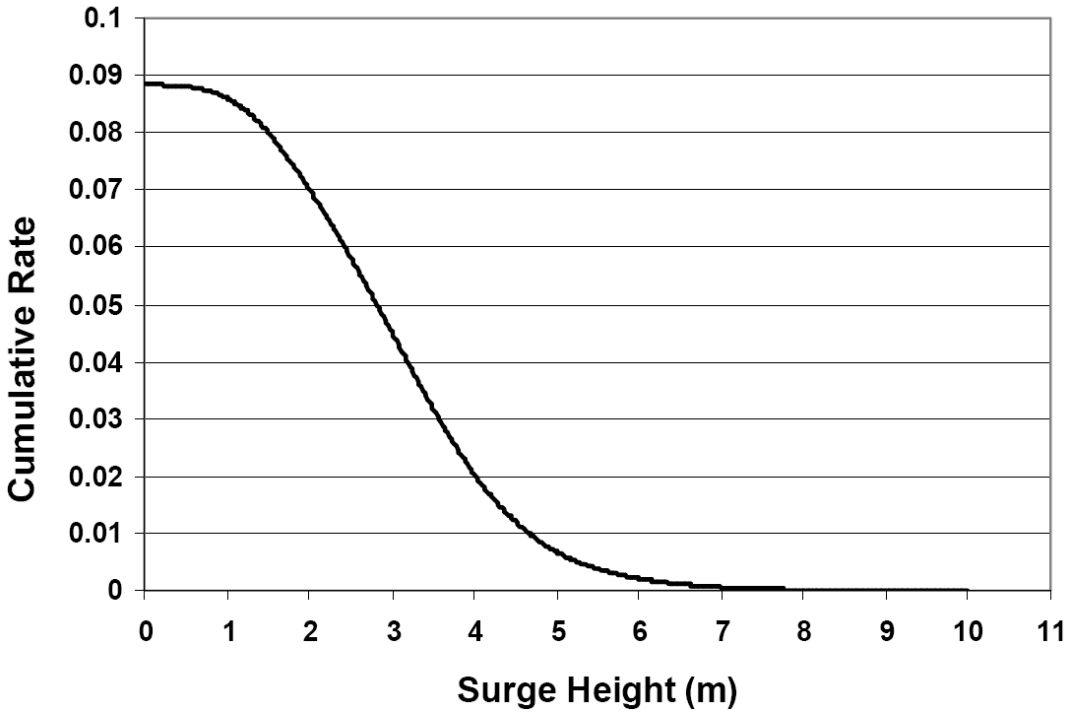

Figure 13.10. Smoothed Surge (Peak SWL) CDF

URS Corporation 2008

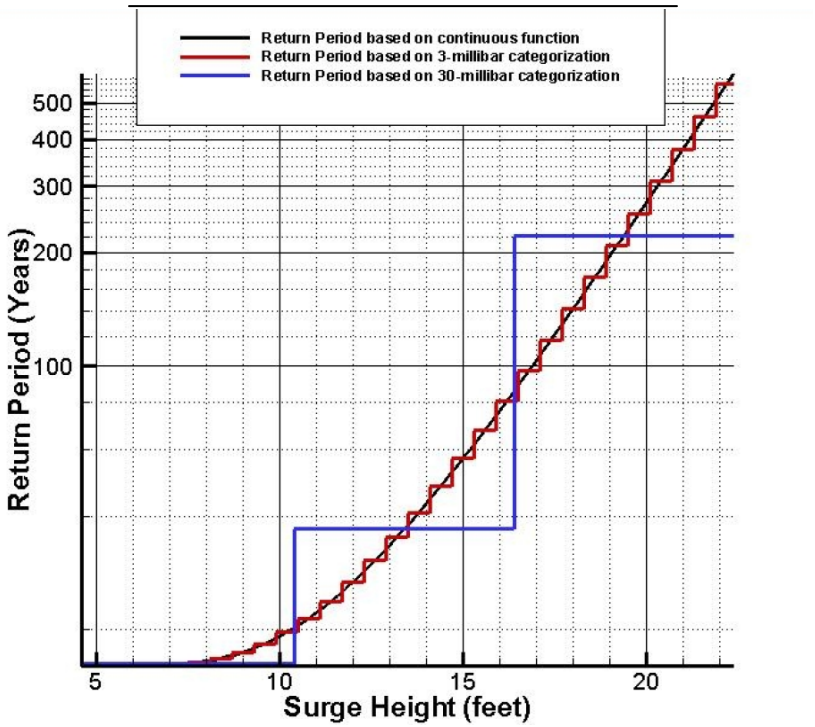

Figure 13.11. Refinement and Interpolation of Surge Hazard Response

Resio et al 2007

STEP 2: CDF Validation

As with any flood return frequency stochastic analysis (see GTN-1), an important post-processing step is comparing the surge hazard CDFs produced in the stochastic analysis against available CDFs derived from gauge return frequency analyses. Comparisons at key locations are used to evaluate residual bias and normally and non-normally distributed uncertainties.

Scientists undertake rigorous investigations of potential bias using

- comparisons of the surge JPA CDF to tide gauge analysis CDF;
- the validation results for the wind/surge/wave-setup model;
- the results of any validations of the OS set; and
- lessons on bias from other studies,

If residual bias is suspected the simulation results for each of the *n* storms must be carefully re-examined, together with the setup and parameterization of models and the selection of the JPM-OS set. If appreciable bias is identified, the source of bias must either be eliminated or appropriate correction factor devised and applied to the surge hazard CDF.

With bias removed or corrected, the magnitude and trends of overall uncertainty can be assessed—e.g., by determining RMSE or σ between the JPA and tide gauge CDFs. The uncertainty may be SWL dependent. If appropriate the smoothing and numerical integration can be revised by incorporating the additional uncertainty. A revision of CDFs to account for bias and uncertainty amounts to a calibration of the JPA CDFs. If JPA CDFs are revised then the estimate of residual uncertainty versus tide gauge CDFs are also updated.

STEP 3. Adjustments to Spatial Variations in Specific Surge Hazard Levels

Following CDF validation the geographic distribution of surge SWL at any return period of interest (e.g., the 100-yr surge SWL) can be depicted as in Figure 13.12. The surge SWL can be overlaid on a variety of regional maps (e.g., topography, land cover, etc.) and aerial imagery and evaluated. The geographic SWL surface is typically examined for irregularities, such as:

a. Lateral misalignments due to resolution limitations in the surge SWL model (e.g., SWL surface incorrectly shown crossing a major topographic crest higher than the SWL); and

b. Sharp gradients not consistent with local topography or land cover.

Identified surge hazard irregularities can be corrected and sharp lateral gradients can be smoothed. These spatial adjustments would, in turn, modify the local CDFs. In theory, rigorous quality control reviews of the individual OS simulations should uncover major problems with surge spatial results prior to this step.

STEP 4: Construction of Confidence Limits

Final residual uncertainty in the JPA CDFs can be evaluated in several ways:

- Assessing the effect of the quantified sources of uncertainty (from Step 2) on the resulting CDF. The linear uncertainty, ε_Σ, can simply be added to (subtracted from) the CDF.
- Comparing CDFs derived with different smoothing/integration techniques.
- Computing a standard curve (e.g., Gumbel distribution) and associated uncertainty bands directly from the stochastic analysis results.
- Comparing JPA and tide gauge CDFs.

These techniques can be employed to construct UCL/LCL bands around a CDF. Bands can be calculated to encompass a range of uncertainty—such as 68.2%, 90%, 95%, 95.4%, 99.6% etc. (equivalent to ± 1σ, 45%, 47.5%, 2σ, 3σ).

As discussed in the Introduction and GTN-1 Section N, FISs are typically based on the median estimated CDF and do not typically employ a CDF with some adjustment for uncertainty or at some confidence limit. The 100-yr flood elevations shown on FEMA maps are not required to reflect allowances for uncertainty. However, the use of confidence limits is more common in other planning and design studies for flood risk management—e.g., the design of flood protection structures. An example of a JPA CDF with confidence limits is shown in Figure 13.13.

Asymmetric uncertainties (associated with skewness, kurtosis, etc.) in the hurricane landfall intensity return frequency (see Figure 3.10) are an important source of asymmetric uncertainty for SWL at higher return periods (e.g., 500-yr). Figure 12.3 illustrates the greater widening of the UCL band relative to the LCL band for Grand Isle LA return frequency at longer return periods. For the 500-yr return period SWL of 11.2 ft, Figure 13.13 shows 95% LCL/UCLs of 8.7 and 14.1 ft. (bands of 2.5 and 2.9 ft, respectively)

In addition to evaluating confidence limits, the quality of a JPA can also be gauged by comparing results in an area common to two adjacent, overlapping, studies, provided they employ reasonably similar rigorous methodologies.

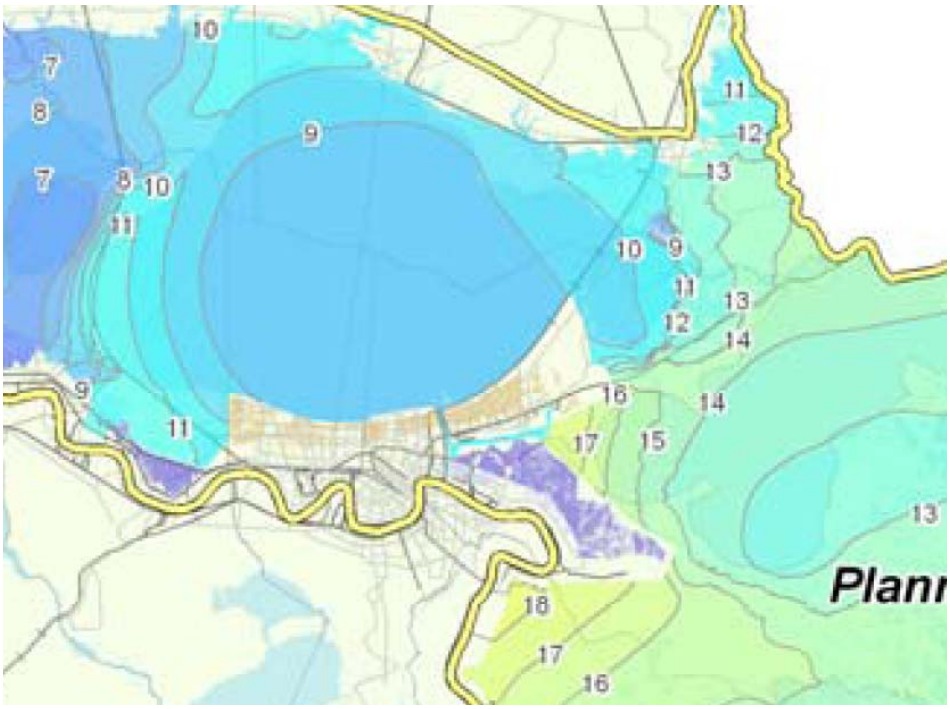

Figure 13.12. Example of Overlay of 100-yr Surge (LACPR Study)
USACE 2009

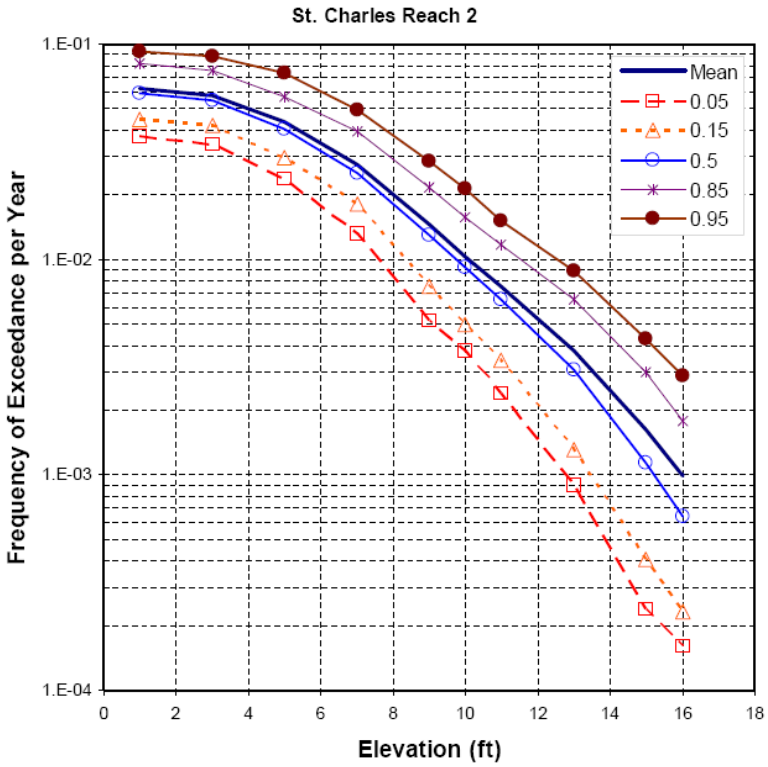

Figure 13.13. Example of Surge CDF with Confidence Limits
(Epistemic Uncertainty Only)
IPET 2009

13.7 Wave Hazard

In overland flood risk applications the wave hazard is considered in terms of the wave height added to the SWL at a particular SWL hazard level, e.g., the 100-year SWL plus associated waves.[3] Currently, wave hazards for most coastal floodplain LOIs are computed under the NFIP, which addresses 1% wave heights using the simple 1D WHAFIS model (see Section 9). This model employs a $H_{1\%}$ depth limitation of 0.78*Depth, and basic assumptions regarding wind speed and direction, boundary conditions, and wave transformation and dampening from friction. If the 100-year SWL can be associated with multiple storm tracks, multiple WHAFIS simulations can be performed to capture wave hazard variations due to differences in wind direction and speed. In this case it would be common practice to employ the "worst-case" wave characteristics—$H_{1\%}$ and T_p— from the multiple simulations.

2D wave models (e.g., STWAVE and SWAN) can also be used to assess H_s, $H_{1\%}$, and other criteria associated with a specific SWL. However, similar assumptions must still be applied. These models can improve the estimation of wave characteristics compared to the 1D WHAFIS model where 2D wave transformations (e.g., refraction and diffraction) are important.

For locales with complicated shorelines or terrain the characteristics of waves during inundation at a particular SWL may be a function of more complex, non-linear, wave physics. In this case Boussinesq models may be employed to assess appropriate values for H_s and T_p (see Section 9).

Important interior water bodies which are enclosed or semi-enclosed—such as long reaches of rivers and canals—but contain significant fetch, may require special analysis to assess the locally generated waves at the SWL of interest. Methods for analyzing these wave conditions include input of assumed wind direction and velocity, fetch, water depth, and duration. By ignoring duration, an estimate can be made of "fully developed" wave fields. Standard methods of analysis, such as developed by Brettschneider, are described in the USACE Coastal Engineering Manual, Part II-2-2 (USACE 2005).

At a specified SWL, depth limitations can cap wave heights where other conditions (boundary, wind speed, fetch, etc.) might otherwise indicate the potential for higher waves. As noted in Section 6 the relationship of H_s to depth is highly variable, with ratios of 0.4 to 0.7 commonly employed.

As discussed in Section 5, coastal scientists and engineers employ the Rayleigh distribution to describe height variability in a wave field. Several relationships dictated by this distribution are:

$H_{avg} = 0.625H_s \approx 5/8\ H_s$;

$H_P = .705H_s\ (-\ln P)^{1/2}$, where P is the Percentile;

$H_{50\%} = 0.59H_s$;

$H_{1\%} = 1.52H_s$; and

$H_{0.1\%} = 1.9H_s$

However, the peak SWL during an extreme surge event typically has a limited duration (e.g., 4 hours or less). Thus, the number of waves occurring during the peak SWL is also limited. For example, during Hurricane Katrina approximately 2,000 waves (with T_p of 7 s , Smith 2007) would have been associated with peak SWL off the south shore of Lake Pontchartrain. For this brief event the Rayleigh distribution may not be representative for ratios of H_s to the top 20 and two wave heights. With a short duration the ratios are likely to be lower.

[3] In offshore applications for vessels and marine structures wave hazards are analyzed apart from SWL variations.

Section 14. Recent Applications of Surge JPA

JPAs of hurricane surge were first undertaken in the 1970s (see Ho and Myers 1975). By the late 1980s researchers on Atlantic Basin and GoM hurricane climatology had provided probabilistic estimates for CP, R_{max}, V_f, and θ, (NOAA-NWS 1987), facilitating wider application of JPM to hurricane surge in combination with the FEMA Surge Model. In 1989 Suhayda completed a surge JPA for Cameron Parish LA using NOAA's latest regional hurricane climatology information, a 685-storm JPM, and the FEMA Surge Model. Interestingly, no surge JPAs were applied to the New Orleans LA region prior to Hurricane Katrina.

In the aftermath of the 2005 hurricane season, JPA with OS has been applied for FISs in Louisiana (in two regions, southeast and southwest) and Mississippi, and is being used in seven ongoing FISs for Texas, North Carolina, South Carolina, Florida—Big Bend, Northeast Florida/Georgia, Northwest Florida/Alabama, and Central Florida—Atlantic. This section describes the application of JPA with OS employed in these and other studies based on available documentation, including OS development, the treatment of bias and uncertainties, and the four post-processing steps.

14.1. Southeast Louisiana FIS

The southeast Louisiana FIS JPA and OS development and post-processing steps are primarily documented in Resio et al 2007.[1] Some supplementary documentation is provided in reports for the four coordinated projects undertaken by the USACE in 2006-09: the FIS (USACE 2008), the HSDRRS design (USACE 2010), the IPET Risk and Reliability Analysis (IPET 2009), and the LaCPR Study of future coastal protection and restoration alternatives (USACE 2009). This section reviews the USACE approach used in the FIS exterior surge SWL and wave hazard analysis—i.e., surge hazards outside the HSDRRS. The subsequent section describes a modified approach used in the IPET Study. The USACE and IPET analyses of wave hazards as modified by the foreshore of HSDRRS structures, HSDRRS overtopping and breaching hazards, and polder inundation hazards, are discussed in Part IV.

OS Development

In their surge JPA for the 151-mile (2½°) segment south of New Orleans Resio et al utilized a Surge Response-OS, as opposed to JPM-OS, (see Section 13). The team conducted numerical experiments of hurricane landfall conditions along an idealized coast line to determine benchmark smooth, SWL response functions for CP, R_{max}, V_f, and θ. The team deferred consideration of the Holland B attribute to the uncertainty term (see below). Full documentation of the simplified surge model and the numerical experiments was not included in the various reports. The authors illustrated an example of a SWL response to CP-R_{max} (see Figure 14.1).

The Resio team discretized the surge response function into 15 CP-R_{max} combinations: three GoM CPs—960, 930, and 900 mb—with six, three, and six R_{max}, variations for each of these three respective CPs. Twelve of the 15 CPD-R_{max} combinations employed one V_f. Two V_f variations were provided for the 20.4 mi storms at 960 and 900 mb, while three were provided at 930 mb. Table 14.1 summarizes the 19 CP-R_{max}-V_f combinations, as well as the 30 CP-R_{max}-V_f-θ combinations, used in the southeast Louisiana study. Resio et al employed a GoM Holland B parameter value of 1.27 for all storms, based on the mean GoM value.

[1] Additional detail is provided in the two part publication: Resio et al 2009 and Irish et al 2009.

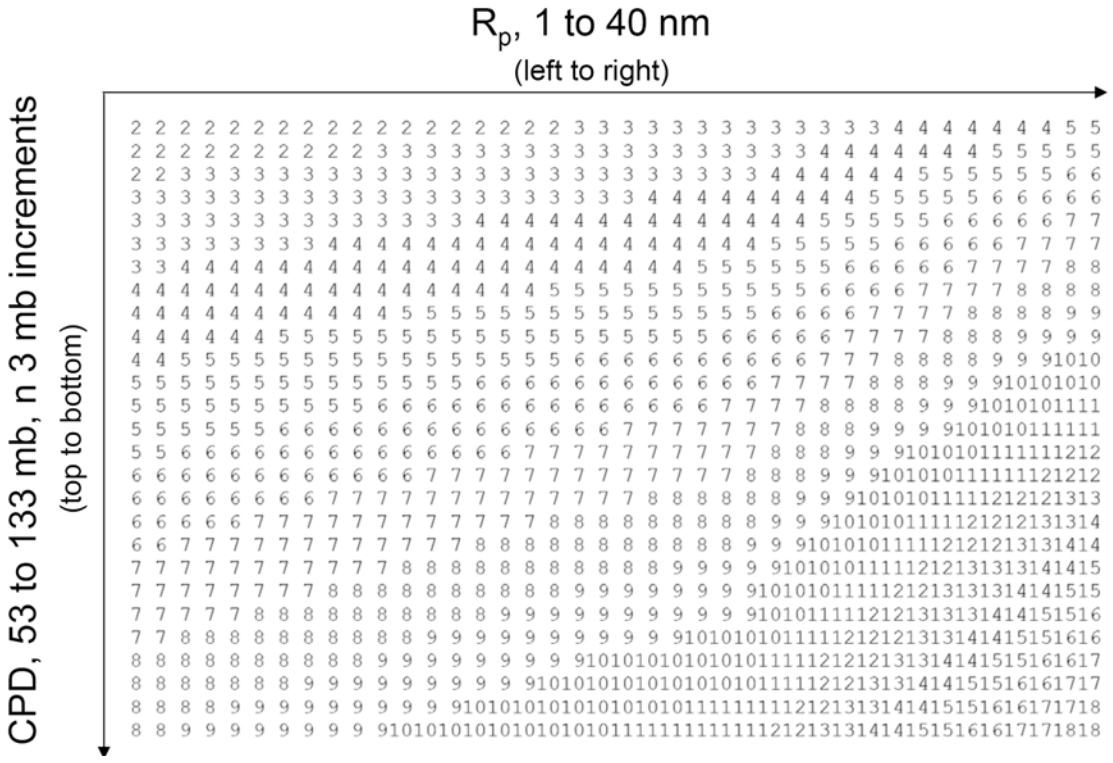

Figure 14.1. Example SWL Response to CPD-R_{max}
Resio et al 2007

To discretize the surge response surface over the study area Resio et al selected five primary landfall locations for the central tracks and four each for the southeast and southwest tracks—with landfall spacing at about 1° longitude, or 30 mi. Intermediate (secondary) landfalls spaced at 15 mi were also used. This arrangement assigned half the storm landfalls within a 1° segment south of New Orleans.

Of the 30 CPD-R_{max}-V_f-θ variations, 24 were employed with primary tracks—12 central, 6 southeast, and 6 southwest, for a total of 108 storms. Thirteen variations were employed with secondary tracks—5 central, 4 southeast, and 4 southwest, for at total of 44 storms. The total combination of attribute variations and tracks provided for 152 storms. The combinations of θ and primary landfall locations are illustrated in Figure 14.2.

Table 14.1 shows that all 152 storms in the Surge Response OS were GMHs, with 50 at Category 3 (960 mb CP, 60 mb CPD), 52 at Category 4 (930 mb CP, 90 mb CPD), and 50 at Category 5 (900 mb CP, 120 mb CPD). Hurricane Katrina's maximum GoM CPD was 118 mb. Of the 50 Category 5 storms, 32 are quite large, with R_{max} above 20 miles. Nine of these large, intense hurricanes are slow moving, with V_f of 6.9 mph. These nine 900 mb CP storms at V_f of 6.9 mph actually have vortex model V_{max} at Category 4.

Resio et al coupled the OS with a vortex model to generate a hurricane wind field. Model winds are provided as 30-minute average winds (in m/s), which can be readily converted to 1-minute winds (in mph). Attachment 1 lists the 152 hurricanes and their GoM and landfall attributes, including the peak GoM and landfall V_{max}, and peak GoM and landfall SSS category (which are assigned on the basis of the 1-minute V_{max}) (USACE 2011). Figure 14.3 illustrates the track of Hurricane No. 26. Figures 14.4 and 14.5 illustrate the GoM winds and at landfall wind field for Hurricane No. 26.

Table 14.1. Southeast Louisiana OS

GoM CP mb	GoM R_{max} miles	Landfall V_f mph	θ direction from	Track Set (Number)
960	40.9	12.7	Central	P (5)
	28.3	12.7	SE	P (4)
			SW	P (4)
	24.2	12.7	Central	P (5)
	20.9	12.7	SE	P (4)
			SW	P (4)
	20.4	12.7	Central	S (4)
			SE	S (3)
			SW	S (3)
		6.9	Central	P (5)
				S (4)
	12.7	12.7	Central	P (5)
930	29.7	12.7	Central	P (5)
	20.4	19.6	Central	P (5)
				S (4)
			SE	P (4)
				S (3)
			SW	P (4)
				S (3)
		12.7	Central	P (5)
		6.9	SE	P (4)
				S (3)
			SW	P (4)
				S (3)
	9.2	12.7	Central	P (5)
900	25.1	12.7	Central	P (5)
	21.2	12.7	SE	P (4)
			SW	P (4)
	20.4	12.7	Central	S (4)
			SE	S (3)
			SW	S (3)
		6.9	Central	P (5)
				S (4)
	17.1	12.7	Central	P (5)
	14.4	12.7	SE	P (4)
			SW	P (4)
	6.9	12.7	Central	P (5)
3 CP	**15 CP-R_{max}**	**19 CP-R_{max}-V_f**	**30 CPD-R_{max}-V_f-θ**	**152 Storms**

Resio et al 2007

P-Primary Track Set; S-Secondary Track Set (Landfall located between Primary Tracks)

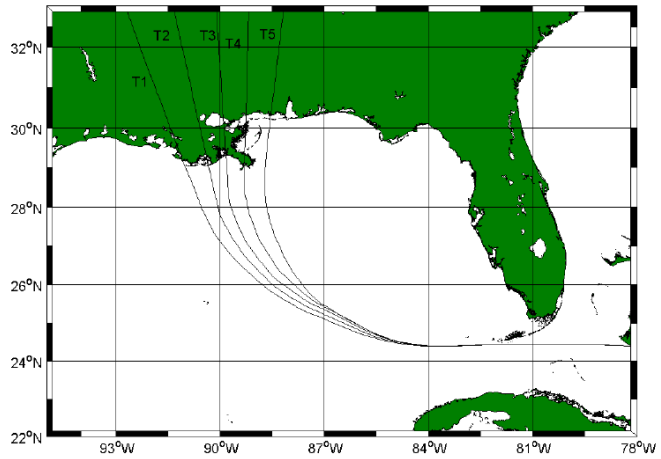

Five Primary Central Tracks (Four Secondary Tracks not shown)

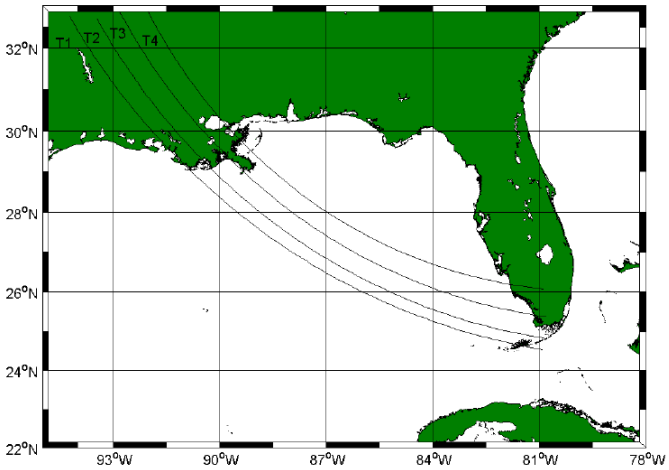

Four Primary Southeast Tracks (Three Secondary Tracks not shown; some origins shifted)

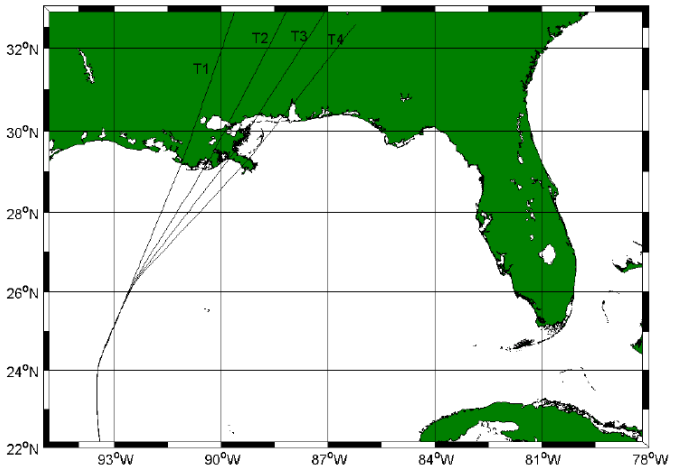

Four Primary Southwest Tracks (Three Secondary Tracks not shown)

Figure 14.2. Hurricane Tracks for Southeast Louisiana JPM-OS

Resio et al 2007

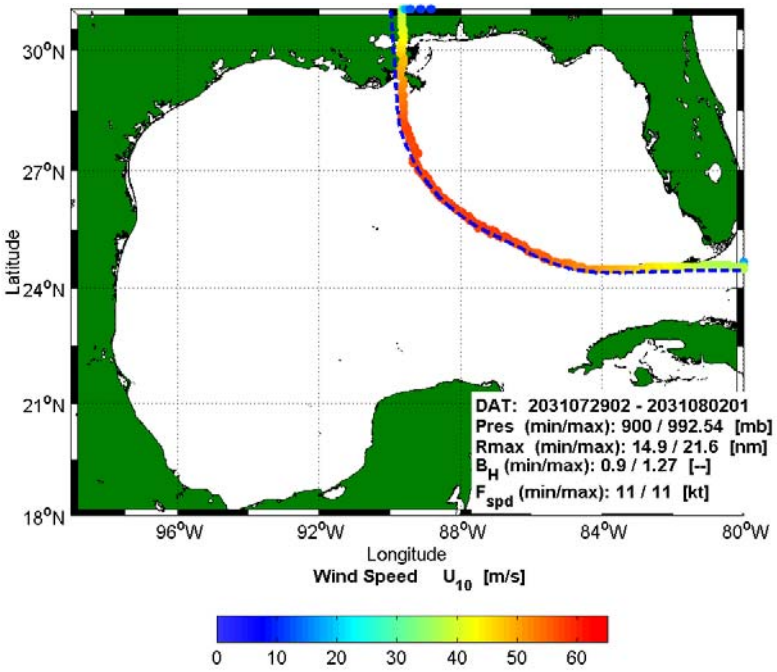

Figure 14.3. Synthetic Hurricane No. 26 Track and V_{max} (30-min winds in m/s)

USACE 2011

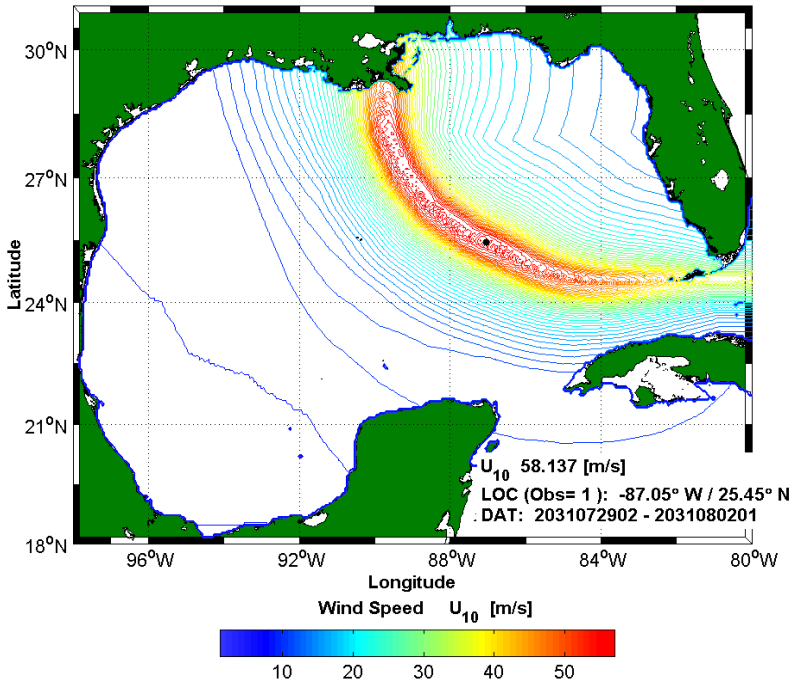

Figure 14.4. Synthetic Hurricane No. 26 Wind Field Along Track

USACE 2011

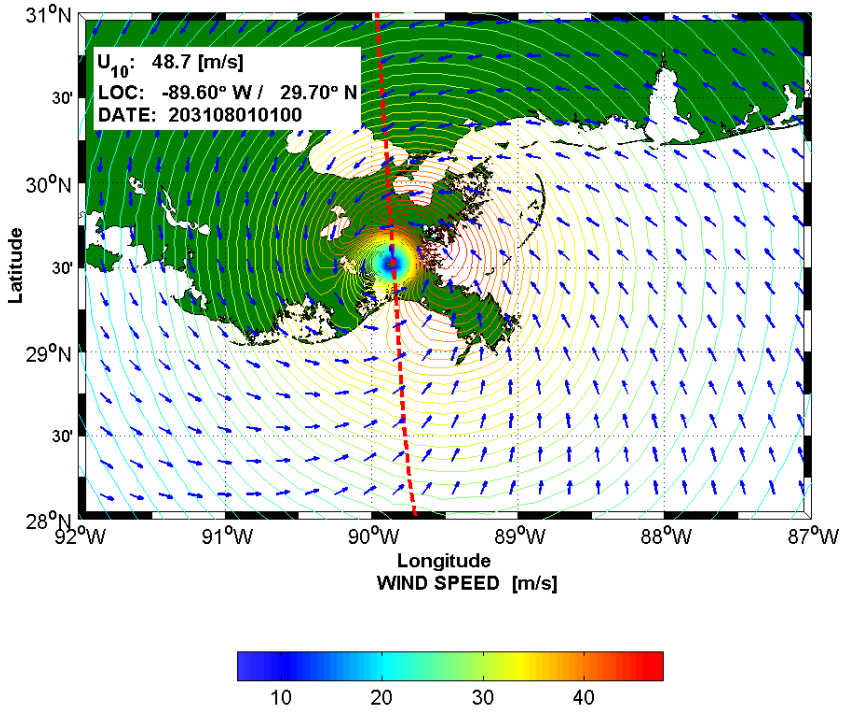

Figure 14.5. Synthetic Hurricane No. 26 Landfall Wind Field

USACE 2011

The vortex model incorporated a linear decay prior to landfall for CP, R_{max} and Holland B. Individual hurricanes decayed by somewhat different amounts according to track and forward speed and thus landfall conditions are more variable than GoM peak conditions. No storm made landfall at Category 5.

Given the set is a Surge Response-OS and not a JPM-OS, Resio et al did not assign joint probabilities to the individual 152 storms.[2] In designing the OS to be representative of a simplistic landfall surge response the authors did not consider special regional surge response characteristics.

Bias and Uncertainty

The reports describe the treatment of the five JPA uncertainties listed in Table 13.1 as follows.

1. ε_P—uncertainty regarding hurricane climatology (joint probability) for selected attributes:
   - Research on GMH CPD, R_{max}, V_f, θ (see Part I, Sections 1 and 3) was utilized to establish the joint probability expression. The ***p***(CPD) is combined with the overall reach hurricane return frequency as a Gumbel distribution with the parameters (a_0 and a_1) varying for 1° longitude increments. Resio et al illustrated the general regional varying values for a_0 and a_1 but did not explicitly provide values for individual increments or the (aleatory) uncertainty bands.

[2] The authors did state that the total of 152 storms GMHs would conservatively represent a record of 853 years, at an average GMH/L-151 return period of 5.6 years. They note this return period is less than taking the GMH/L-60 return period of 16 years and estimating an equivalent GMH/L-151 return period of 16/2.5 or 6.4 years.

- Resio et al did not explicitly provide values for σ_{Rmax} and σ_{Vf}. Resio et al suggested dependency of σ_{Rmax} (epistemic uncertainty) on CPD.

2. ε_W—wind field uncertainties not encompassed in the joint probability:
   - The variability in the CPD-V_{max} relationship (as illustrated by Hurricane Katrina, which made landfall at a borderline Category 4/5 CPD but with strong Category 3 winds), was not explicitly discussed.
   - The team addressed epistemic uncertainty in the Holland B—ε_B—which was estimated to have a linear response in surge, with σ_B equal to about 0.1 to 0.2 * SWL.
   - Other uncertainties contributing to ε_W (e.g., asymmetry, IKE, spiral banding, eye wall replacement,) were addressed to some degree with the PBL representation of hindcast winds (see below).
3. ε_{OS}—epistemic uncertainty associated with the surge response benchmark and the OS:
   - Resio et al selected the OS strictly to represent the surge response—as opposed to a surge hazard or wind hazard response. Simplifications associated with an idealized coastline model, which neglects the influence of complex coastal features (see Section 13.3)—such as the blocking of westward driven surge by the Mississippi River Delta and localized wind setup over large coastal bays, sounds, and lakes—were not addressed with respect to selection of the OS set CPD, R_{max}, and V_f values.. The team did not quantify potential errors/uncertainties associated with limited representation of surge response.
   - The general error of a 1° landfall spacing scheme based on an idealized coastal model was noted as being up to 20%, 9%, and 4% for storms with R_{max}.of 11.5, 23, and 34.5 mi, respectively. However, the potential spatial error associated with the proposed OS—accounting for the distribution of the 30 CPD-R_{max}-V_f-θ combinations and secondary landfalls—was not addressed. For example, with the 152-storm OS some locations along the coast may have a disproportionate share of smaller R_{max} landfalls, and might be subject to greater error. Furthermore, the team's limited investigation of coastal feature influence on spacing did not account for important local conveyance and wind setup effects (see Section 13.4).
   - Resio et al suggested an σ_ϑ based on the influence of track variability on wave setup, with σ_ϑ equivalent to 20% of the wave setup contribution to SWL, or about 0.02 to 0.06 * SWL.
4. ε_ψ—epistemic uncertainty associated with the high resolution surge model:
   - Resio et al defined the portion of σ_ψ associated with ADCIRC-STWAVE as 1.75 to 2.5 ft. This σ_ψ appears to be consistent with the Hurricane Katrina hindcast validation.
   - Resio et al discussed additional relative error associated with the PBL model in contributing to hindcast errors. They suggested that the combined PBL and ADCIRC-STWAVE model σ_ψ was on the order of 2.0 to 3.5 ft.—which equates to a 90% confidence band width of ±3.3 to 5.8 ft.
5. ε_T—epistemic uncertainty associated with tides:
   - The suggested value for σ_T is 0.66 ft (IPET 2009).

The values for $(\sigma_\vartheta^2 + \sigma_B^2)^{0.5}$ and $(\sigma_\psi^2 + \sigma_T^2)^{0.5}$ are therefore about 0.1 to 0.2 * SWL and 2.1 to 3.6 ft, respectively. For a SWL of 10 ft, the overall combined epistemic uncertainty σ_e is $(\sigma_\vartheta^2 + \sigma_B^2 + \sigma_\psi^2 + \sigma_T^2 +)^{0.5}$ and equates to about 2.3 to 4.1 ft—or 90% confidence band widths of ±3.8 to 6.8 ft.

Production and Post-Processing

The production runs included simulation of the 152-storm Surge Response OS with the following:

- Wind and atmospheric pressure forcing conditions throughout the model domain for all 152 storms using the PBL vortex model.
- The ADCIRC-STWAVE model validated for Hurricanes Katrina and Rita, (see Section 11 for a full discussion of the model limitations). The FIS production model included modified acceleration terms, the implicit/explicit numerical method, a constant eddy viscosity value of 50 m^2/s, a time step of 1 s, and node Manning's *n* and wind sheltering coefficients assigned based on land cover data and associated values from technical literature.
- Two modified versions of the 2005 mesh validated for Hurricane Katrina.
  - The current FIS documentation describes a 2007 mesh reflecting post-Katrina improvements to the HSDRRS—e.g., outfall canal gates (vSL15v3_2007_r09). However, the 2007 mesh did not include the most recent HSDRRS improvements, such as further height enhancements and construction of the IHNC and Seabrook Surge Barriers.
  - The project team also developed a 2010 mesh depicting further authorized HSDRRS improvements—including height enhancements and the IHNC Surge Barrier (but **not** the Seabrook Barrier), (USACE 2009 and USACE 2010). Limited documentation for the 2010 mesh runs is provided but the team presumably used the same FIS setup and parameters and implemented similar quality control.

  Minor adjustments to both meshes were also performed for individual storms to mitigate instabilities.
- Omission of tidal boundaries and forcing and instead including tides as a linear uncertainty term (see Section 13).
- A combined LMSL and LMMSL adjustments of 1.1 ft NAVD88-2004.65.
- Boundary inflows for the Mississippi and Atchafalaya Rivers, adjusted for surge wave outflow (with inflows presumably at 195,000 and 58,000 cfs as per the tidal validation); and
- WAM and STWAVE (three of four grids in half plane mode and all without friction, per the Hurricane Katrina hindcast) to compute open ocean and nearshore wave conditions and wave radiation stress gradients. STWAVE was loosely coupled with ADCIRC and radiation stress gradients were updated in the ADCIRC model at 30-minute intervals.

Post-processing quality control steps were discussed in the FIS documentation (USACE 2008). The team used a filtering algorithm to identify and smooth non-fatal instabilities in areas of steep terrain gradients. The team animated 25% of the simulations to facilitate additional checks for unphysical results. The FIS documentation does not itemize individual mesh modifications and the magnitude of non-fatal instabilities.[3]

Resio et al (2007) utilized both the refinement and σ smoothing steps in integrating the CDF at each output location (described in Section 13.6). CDF results of the JPA and Surge Response-OS using the 2007 case ADCIRC mesh were provided by Dr. Jay Ratcliff (USACE 2012). According to Resio et al (2007) the combined epistemic σ_e term (equal to about 2.1 ft plus 0.15 *SWL) was employed to modify the CDF. Resio et al (2007) showed that incorporating ε_e in the CDF integration shifted up the 100- and 500-yr SWLs estimates up. For one location, including ε_e increased the estimated 100-yr SWL of 14.8 ft, by 0.4 ft, and the 500-yr SWL by 1.1 ft. Resio et al (2012) subsequently discussed the effect of also incorporating aleatory ε into the integration—indicating that the total ε would raise the 100-yr SWL by more than 1.5 ft.

The FIS project team did not provide a validation of 2007 JPA versus tide gauge CDFs. Figure 14.6 presents a comparison of NOAA's observed return period SWLs and GEV curve for the Grand Isle tide gauge (see Figure 13.3) versus the 2007 JPA CDF results for several nearby locations. The two sources of return period analysis overlap between 50 and 200 years. The tide gauge is located behind Grand Isle close to Barataria Pass. The JPA results indicate Point 62 is most influenced by the combination of frontal dune sheltering and Barataria Pass. The 100-yr SWL results for Point 62 was 7.8 ft versus 7.1 ft for the gauge CDF. This slight relative over-prediction could be a result of under-prediction of the 100-yr SWL by the GEV curve (the highest return period surge actually matches closely with JPA result).

Figure 14.7 depicts the FIS JPA CDFs around the east-bank HSDRRS for the post-Katrina 2007 case. As noted above, these CDFs have not been corrected for bias (under-prediction) from the Hurricane Katrina hindcast validation for the ADCIRC-STWAVE model. The CDFs are subject to the Resio et al treatment of uncertainty described above. Any errors and uncertainties in the CDFs in Figure 14.7 are likely to be greater at more extreme return periods.

The USACE collected gauge data for Lake Pontchartrain at Frenier and West End beginning in 1931, with observations extending to May 2005 for Frenier and the present for West End. Both sets of observations have significant gaps—September 1965 to January 1969 for Frenier and November 1946 to March 1949 for West End. To date, there has been no published annual series of SWL maximums (in a common vertical datum) for the two gauges. Such a series would require addressing data gaps based on other evidence. Development of annual maximum series for these two gauges could assist in validating the surge CDFs for the south shore of Lake Pontchartrain.

In response to queries from independent technical review (USACE 2007) the project team did employ some available (but very limited) surge data to evaluate the JPA CDFs at four locations—south shore Lake Pontchartrain, IHNC, MRGO near Bayou Bienvenue, and Mississippi Coast just east of the state line. The results showed that the JPA underestimated surge hazard relative to the gauge analysis, which was influenced by the Hurricane Katrina observations. The project team employed the JPA to assess the return period for Hurricane Katrina HWMs and noted that the very long estimated return period of Katrina HWMs—e.g., 660 years for the south shore of Lake Pontchartrain—"are a concern."

[3] The documentation notes that for one synthetic storm, over each time-step (1 s) an average of 6% of the domain area had a relative mass conservation error exceeding ±0.01%. Further breakdown of this error was not provided.

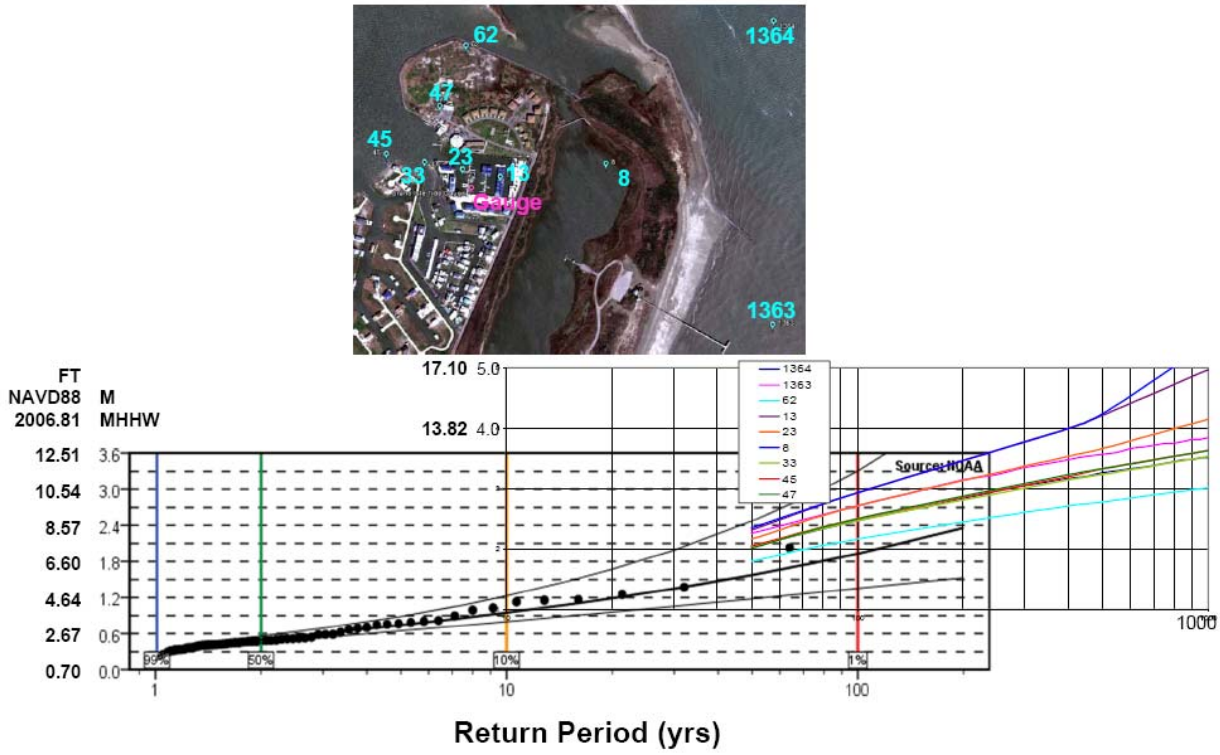

Figure 14.6. JPA versus Tide Gauge Return Frequency Analysis Grand Isle LA
NOAA (http://tidesandcurrents.noaa.gov/est/est_station.shtml?stnid=8761724) and USACE 2012

For comparison purposes Figure 14.8 presents CDF curves developed by the USACE in 1966, following Hurricane Betsy, as part of improving the New Orleans area hurricane protection system (USACE 1966). Surge elevations in Figure 14.8 are given in ft MSL, which must be converted to NAVD88-2006.81. These curves were developed using methods that pre-dated application of JPA. The 1966 estimated 100-yr surge SWL along the south shore of Lake Pontchartrain and along the MRGO near Chalmette in Figure 14.9 are approximately 9.2 and 11.2 ft NAVD88-2006.81, compared to the JPA estimates for the 2007 condition of 8.8 and 17.5 ft NAVD88-2006.81 in Figure 14.7.

In 1988 the USACE developed surge CDFs for the design of levees in east-bank St. Charles Parish (Figure 14.10). For a location east of the Bonnet Carre Spillway Figure 14.9 shows that the 1988 estimated 100-yr surge SWL was 10.8 ft NAVD88-2006.81, compared to 11.4 ft NAVD88-2006.81 in Figure 14.7.

According to FIS documentation, following construction of CDFs at all output locations the team applied only limited spatial smoothing of the return period results. A linear blending algorithm was applied to southeast Louisiana locations near the Mississippi state line due to differences in results between the southeast Louisiana and Mississippi JPAs. (See description of the Mississippi surge JPA methodology below.) The blending region was a few miles wide and modified surge hazard values were determined by interpolating between fully weighted Mississippi and Louisiana study values on the respective sides of the blending region. The differences in 100-yr surge SWL between the two studies were not reported, but may have reached 20 percent, another indication of study uncertainty. Near latitude 30.256 the 100-yr SWL was noted as 13.2 ft west of the Pearl River (USACE 2012) but 16 ft east of the Pearl River (per nearby AE Zone, Hancock Co., Preliminary FIRM Panel 295, FEMA November 2007).

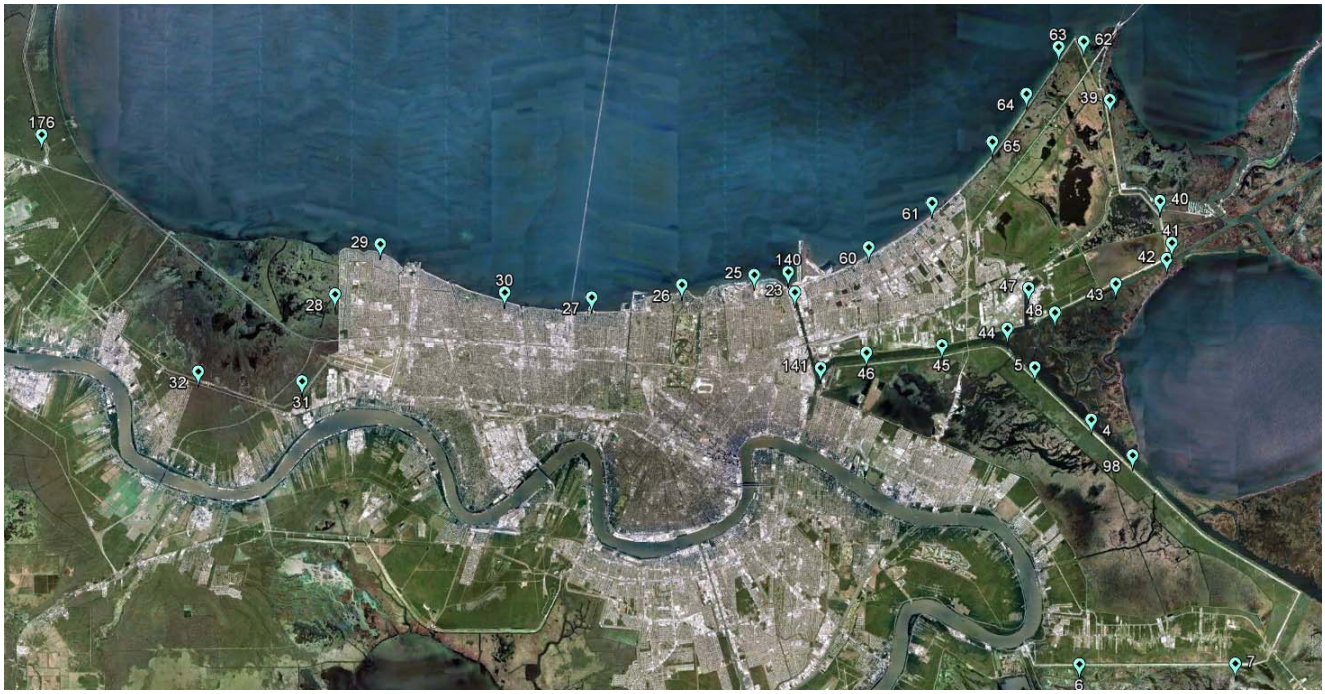

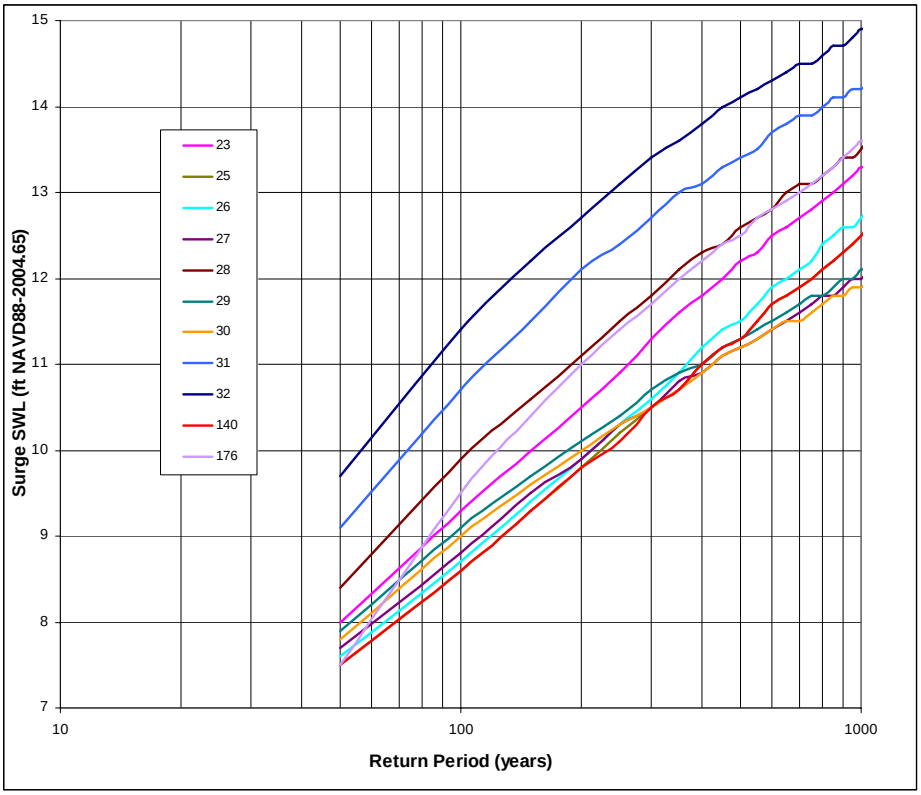

Figure 14.7. Surge SWL CDFs for 2007 FIS, East-Bank New Orleans
USACE 2012

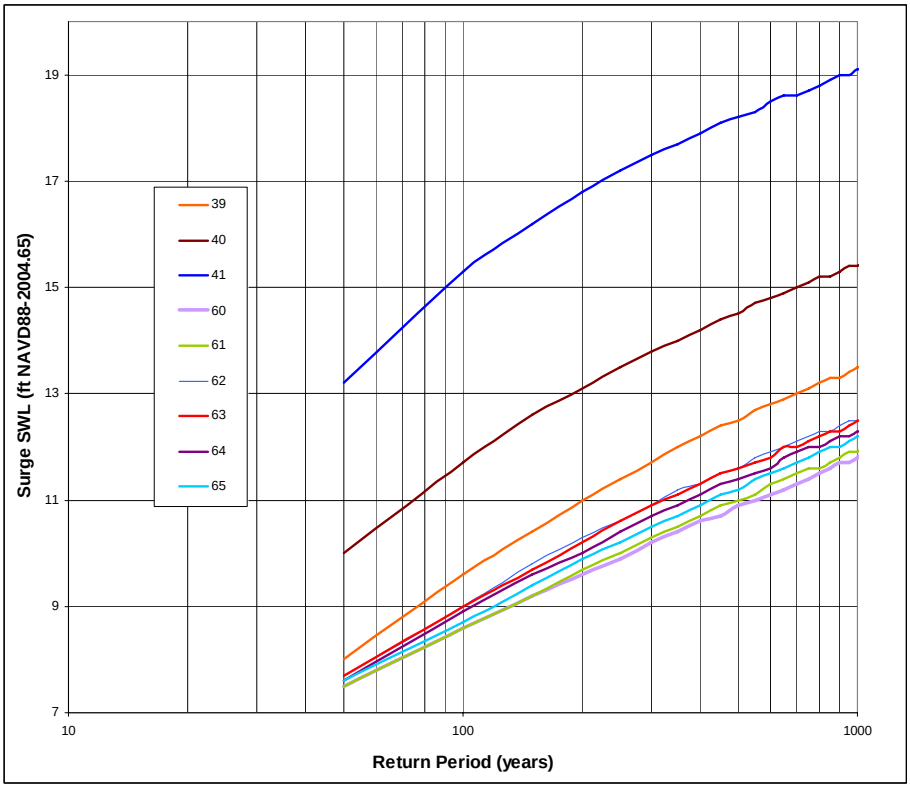

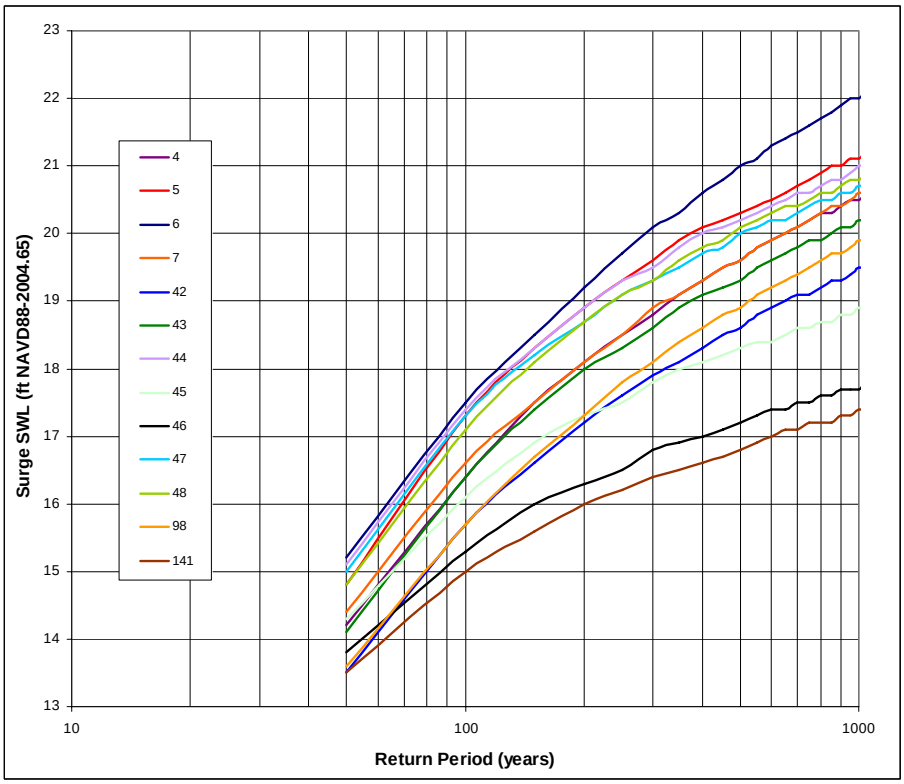

Figure 14.7. Surge SWL CDFs for 2007 FIS, East-Bank New Orleans (continued)

USACE 2012

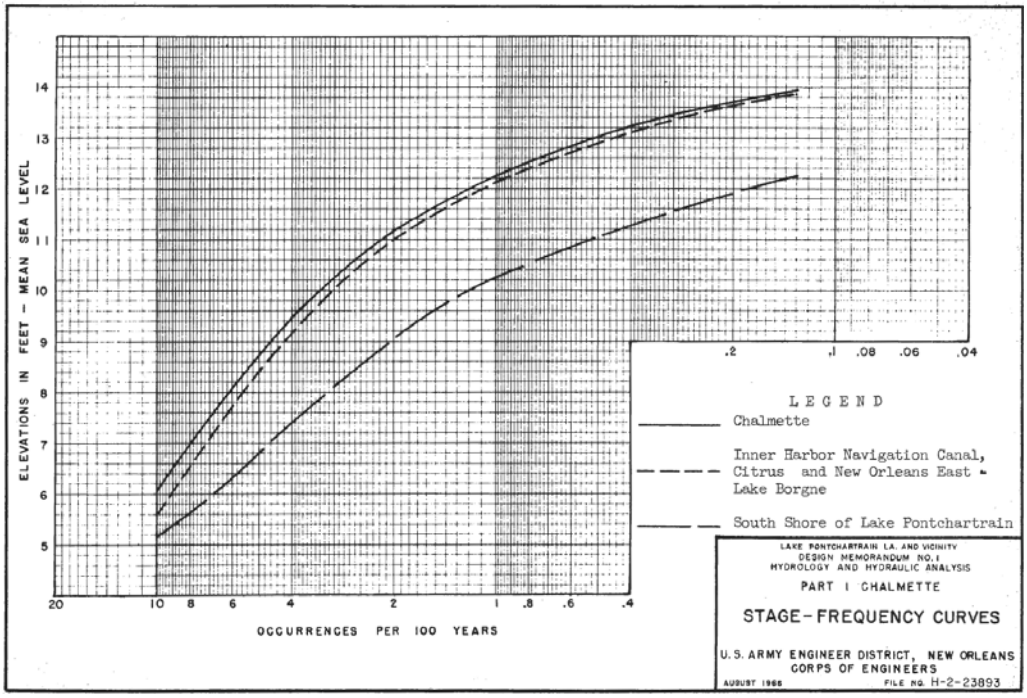

Figure 14.8. 1966 CDFs for East-Bank New Orleans Area

Subtract 1 ft to convert MSL to NAVD88-2006.81

USACE 1966

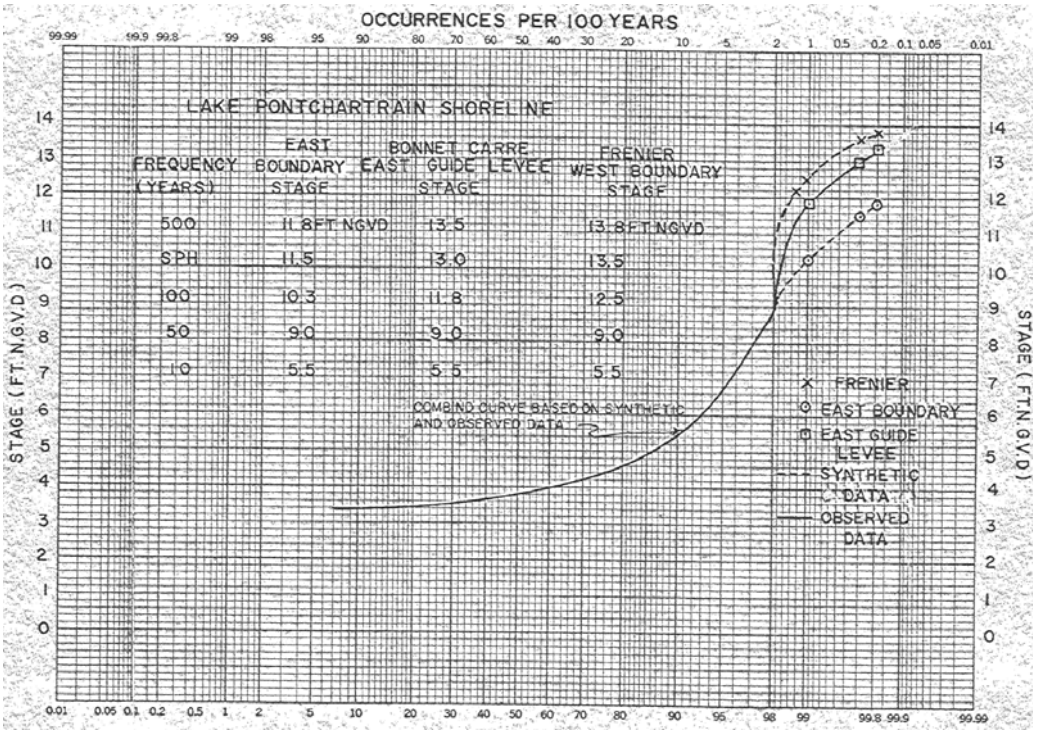

Figure 14.9. 1988 CDFs for East-Bank St. Charles Parish

Subtract 1 ft to convert MSL to NAVD88-2006.81

USACE 1989

As previously discussed (see Section 13.6) confidence limits for CDF curves are not typically prepared as part of the FIS documentation and were not made available for the 2007 CDF results. Resio et al suggested that the Gumbel distribution could be used to represent the surge SWL return frequency at any location, and noted that confidence limits for the resulting Gumbel curve could be computed (Resio et al 2007). However, no Gumbel curves of surge SWL hazard or associated confidence limits were provided.

Wave Hazards

FEMA FIS contractors[4] analyze overland wave hazards associated with the 100-yr SWL hazard using WHAFIS as described in Sections 9.2 and 13.7. In accordance with FIS requirements, special wave hazard zones, termed VE Zones—in which the overland wave height, or the depth of wave runup, associated with the 100-yr SWL exceeds 3 ft—are delineated on the FIRMs (see Figure 14.10). FEMA has completed FIRMs for several coastal southeast Louisiana parishes (Tangipahoa, Livingston, St. James, and St. John the Baptist), and proposed a preliminary FIRM for St. Tammany Parish. FEMA is preparing preliminary FIRMs for those parishes that include some areas enclosed by the HSDRRS (St. Charles, Jefferson, Orleans, St. Bernard, and Plaquemines). For each FIS the 100-yr SWLs will be taken from the foregoing surge JPA.

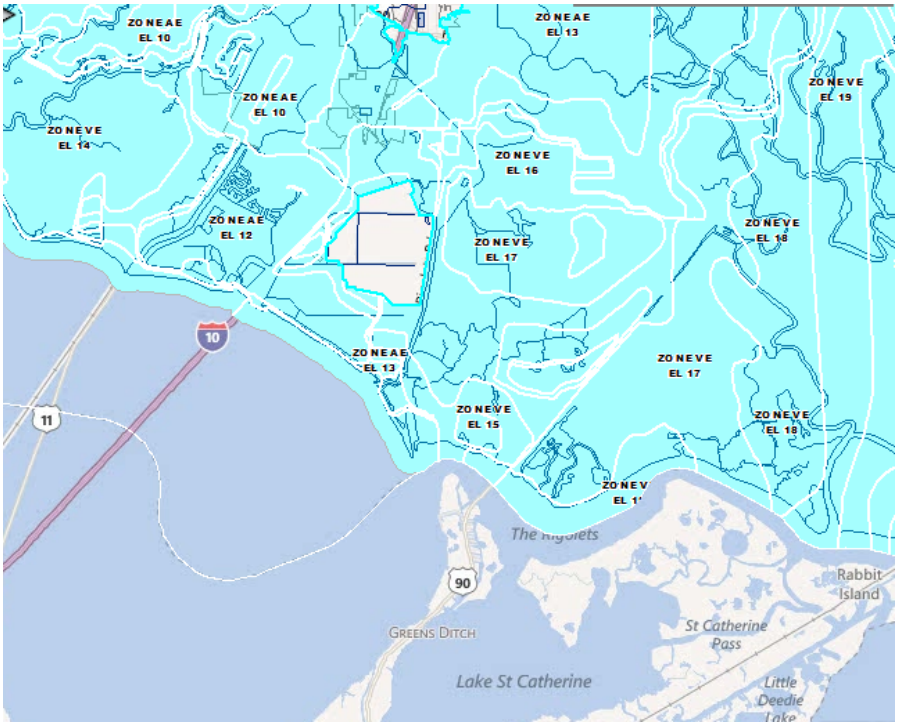

Figure 14.10. Example of Wave Hazard Areas (VE Zones) Shown on FIRM
http://lamp.lsuagcenter.com/?FIPS=22103

[4] The USACE did not perform overland wave analysis for southeast Louisiana coastal FISs. FEMA retained independent engineering firms to perform the analysis and prepare the FIRMs.

A detailed review of the application of WHAFIS in each parish—including inputs regarding 1D transect locations, topography, friction, boundary conditions, etc.—is beyond the scope of this Report. St. Tammany Parish, which include sizeable communities outside of the HSDRRS and exposed to overland wave hazards (e.g., eastern Slidell LA), is currently contesting the accuracy of inputs to the proposed WHAFIS analyses. Local officials contend that VE Zones are smaller than proposed by FEMA.

14.2. IPET Study

The IPET study (IPET 2009, see Volume VIII, Appendix 9) for southeast Louisiana required a separate JPA approach from the FIS. In order to conduct further hazard analysis of HSDRRS overtopping, breaching, and polder inundation (see Section 17) IPET needed an actual JPM-OS, with probabilities assigned to specific storms in the set and their individual associated surge events.

The IPET study took 76 of the 152 Resio et al Surge Response-OS storms affecting the New Orleans metropolitan area—reasonably similar to L-60—and assigned joint probabilities for each storm. Attachment 1 includes the information on the IPET 76-storm set. The overall average return frequency for GMH/L-60 reflected in the IPET set is 0.0745, or an average return period of 13.4 years (reasonably close to 5.6*2.5). No confidence intervals were provided with the joint probabilities but they would likely be greater than those discussed in Section 3 for V_{max} alone.

Figure 14.11 shows the IPET JPM-OS V_{max} return period distribution based on the 76-storm probabilities compared to a) the Gumbel distribution for L-60 based on escalated recent frequencies for GMH activity over the last 60-years, and b) the Resio et al distribution based on the 1941 to 2005 period (both previously given in Figure 3.18). The figure indicates that the 76-storm set overstates V_{max} at return periods below 200 years but understates V_{max} above a 200-year return period, flattening out dramatically between 153 mph (106-year return period) and 155 mph (885-year return period). This range corresponds to the borderline Category 4/5 storm, such as represented by Hurricane Katrina's landfall CP. This flattening out is consistent with the fact that the Resio Surge Response-OS did not contain any Category 5 landfall storms. Figure 14.11 shows that storms below the Category 4/5 are generally over-represented in the IPET JPM-OS, while storms above this intensity are under-represented. Strong Category 3 storms—e.g., Katrina's landfall V_{max} of 126.5-mph—appear to be over-represented, i.e., they have a shorter return period. The IPET Report provided no discussion of whether their JPM-OS was representative of Resio et al's joint probability function, ***p***, applied to L-60.

Surge CDFs were constructed using the results of the 76 storms, presumably without smoothing. The IPET CDF integration code has not been made available.

IPET's improvised 76-storm JPM-OS produced different surge hazard estimates in the vicinity of the HSDRRS than the FIS 152-storm Surge Response-OS. In east-bank St. Charles Parish west of I-310 near the FIS JPA (Point 32 , Figure 14.8) yielded 100- and 500-yr SWL estimates of 11.4 and 14.2 ft, while IPET (see Figure 13.13) produced estimates of 9.7 and 10.7 ft, the latter being 24% lower.

The IPET Study did assess confidence limits for their CDFs. Figure 13.13 illustrates confidence limits for the IPET CDF for St. Charles Parish west of Interstate 310. Note that the figure illustrates confidence limits only for epistemic uncertainties consisting of ε_P, which was not explicitly defined, and ε_ψ, which was defined according to σ_ψ equal to 0.1·SWL. At the 100-yr return period, the estimated surge SWL (50% or median value) is about 9.7 ft, which thus has a σ_ψ of 0.97 ft, or a 90% confidence band (LCL/UCL of 5 to 95%) of ±1.6 ft. The illustrated 90% confidence band is skewed due to the contribution of non-normally distributed ε_P, which spans from about 7.6 to 12.5 ft. (-2.1 to +2.8 ft). The illustrated epistemic uncertainty band thus extends -0.5 and +1.2 ft wider than for ε_ψ alone.

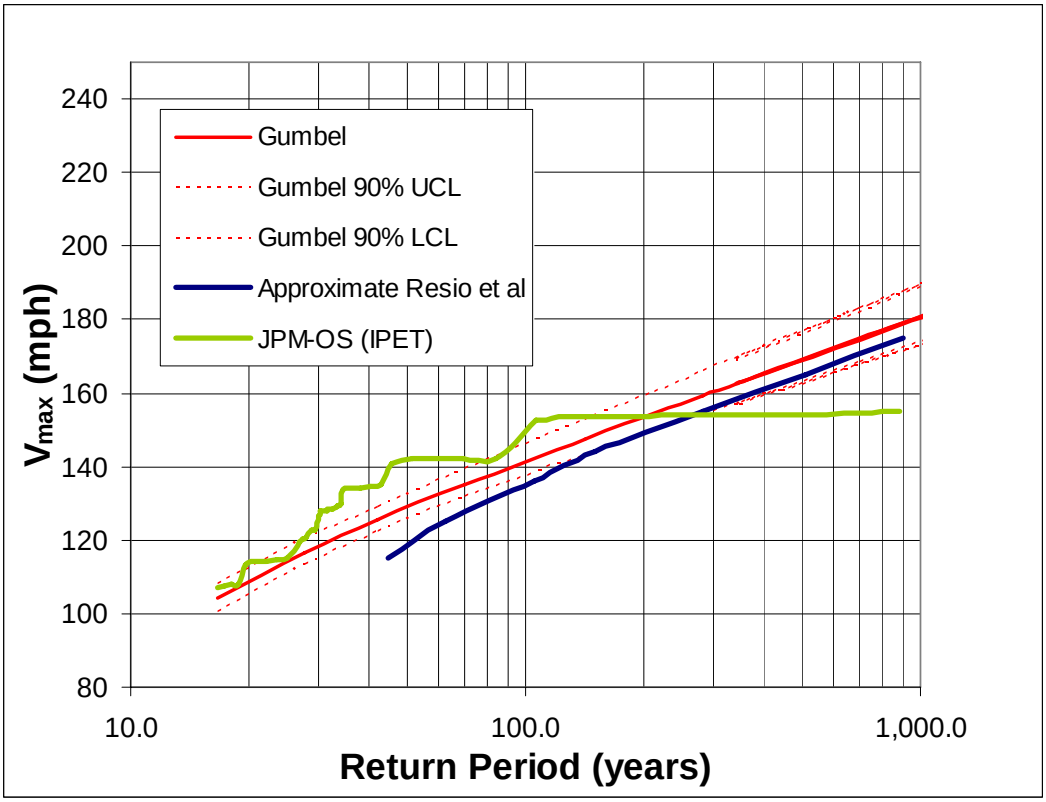

Figure 14.11. Recent Return Period Distribution for L-60 V_{max} versus IPET JPM-OS

IPET defined, but did not illustrate, four sources of normally distributed aleatory uncertainty (σ_B of 0.15·SWL; σ_M parametric of 1.18 ft; σ_M modeling of 0.75 ft; and σ_T of 0.66 ft) which would combine for an additional σ of 2.1 ft at the median estimate of 9.7 ft. Combining the epistemic and aleatory normal distributed uncertainties ONLY yields a total σ_Σ of 2.3 ft, or a 90% confidence band of ±3.8 ft, somewhat less than the lower bound of the total normally distributed σ_Σ associated with the Resio et al approach (noted above). Inclusion of ε_P means the overall magnitude of uncertainty is even higher.

Although the IPET JPA was not representative of the FIS JPA, it—together with the uncertainty information—provided a basis for a preliminary stochastic analysis of residual flood hazards (overtopping, breaching, and polder inundation) and associated risks (see Part IV).

14.3. Southwest Louisiana FIS

The southeast Louisiana project team also a completed surge JPA for southwest Louisiana using the same Surge Response-OS. The southwest study also employed 152 storms distributed among the same 19 combinations of CP-R_{max}-V_f and landfall spacing as in the southeast Louisiana study—but on western tracks. ADCIRC-STWAVE production model, setup and parameters for the southwest study, together with steps for treatment of uncertainty and bias, production, and post-processing steps, were reported to be the same as used in the southeast study. The report does not indicate that any adjustments were made to production SWL results to account for ADCIRC-STWAVE model Hurricane Rita hindcast validation bias (see Section 11).

The southwest Louisiana study report does not present a comparison of stochastic CDF curves versus local tide gauge curves. The NOAA Sabine Pass tide gauge record would seem to provide a reasonable basis for validating the stochastic analysis.

FEMA FIRM mapping contractors for the southwestern Louisiana utilized WHAFIS to identify VE-Zones.[5]

14.4. 2012 Louisiana Master Plan

In 2011 RAND Corporation implemented a highly simplified JPM-OS approach (Louisiana CPRA 2012, Appendix D25) as part of a preliminary investigation into future coastal Louisiana surge hazard. RAND significantly truncated the IPET JPM-OS, which (as noted in Section 14.2) improvised using 76 of the Resio et al Surge Response OS storms for a JPM-OS. RAND first selected 154 storms from the overall 304 Resio et al Surge Response-OS (combined southeast and southwest) to serve as a benchmark. The RAND report stated that they chose the 154 storms to reflect a variety of attributes.

RAND did not introduce any new hurricane climatology information or hurricane JPA. They presumably assigned fractional joint probabilities to each storm based on the Resio et al joint probability expression. RAND then employed the ADCIRC-STWAVE FIS production results for the 154 storms and assigned fraction joint probabilities for each storm to compute benchmark 50-, 100-, and 500-yr return period surges at 449 coastal Louisiana locations. Details on the integration of the CDFs were not presented.

RAND did not provide an evaluation of the 154-storm benchmark's representation of the Louisiana coastal surge hazard. The 154-storm set has inherent limitations as a surge hazard benchmark, given that the original 152 storms for each study (304 combined) were selected by Resio et al to represent surge response and NOT surge hazard. This is especially typified by the absence of any landfalling Category 5 storms.

RAND evaluated a range of subsets from the 154-storm benchmark to select a JPM-OS. RAND ultimately selected a subset of 40 storms, with four storms (combinations of two CPDs and two R_{max}) at 10 coastal landfall points (combined southeast and southwest Louisiana), each at mean V_f and θ. RAND proceeded to employ the 40-storm OS in conjunction with the OCPR2012 model described in Section 11 to evaluate future coastal protection scenarios (see Part V).

Importantly, the 40-storm OS:

- Shares the limitations of the 154-storm benchmark;
- Displays further significant discrepancies in representing the 154-storm benchmark; and
- Is too small to capture important nonlinear surge dynamics and surge hazard response due to the interaction of hurricane attributes and coastal Louisiana features.

The major benefit of the 40-storm JPM-OS was its very small size, which supported its use as an initial tool in assessing alternative future coastal protection scenarios.

[5] As much of the FIS team's focus in 2005-07 was on southeast Louisiana, less attention was apparently paid to mesh details for southwest Louisiana. Following publication of preliminary FIRMs Cameron Parish officials retained a separate team to recommend further improvements to the input for ADCIRC and WHAFIS topography (horizontal alignment and elevation) and hydrodynamic friction (Manning's *n*) for several critical coastal features (e.g., cheniers).

14.5. Mississippi FIS

Concurrent with the southeast Louisiana surge JPA, Toro completed a surge hazard study for coastal Mississippi, (Toro 2008 and URS Corporation 2008). Toro closely coordinated the Mississippi work with Resio et al but choose to develop the Mississippi storm set as a JPM-OS. The Mississippi team evaluated five different JPM-OS in comparison with a benchmark surge hazard using a simplified SLOSH model of the Mississippi coast. The benchmark hazard (referred to in the report as the "Gold Standard") was developed by simulating nearly 3000 storms.

Figure 14.12 compares the benchmark (JPM-Ref) representation of the 100-yr SWL hazard versus the selected JPM-OS (OS6) representation at 147 points along the Mississippi coast. The selected JPM-OS had RMSEs (OS versus benchmark) of 0.47 and 0.59 ft for the 100-yr and 500-yr hazards.

The selected JPM-OS divides the overall probability of a "greater" hurricane (CPD > 48 mb) landfall along the Mississippi coast (estimated at 0.000463 per year per mile or a return period of about 36 years for 1° longitude) into 19 groups, shown in Table 14.2. These 19 groups include five general track θs (see Figure 14.13). Each of the 19 groups contained a number of landfall locations based on tracks offset by R_{max}, for a total set size also of 152 storms.

Six groups have a landfall CPD >100 mb, thus providing for Category 5 landfall storms, unlike the Louisiana Surge Response OS. These 100 mb CPD storms have a total weighted fractional joint probability of 0.091, or an overall return frequency of 0.0000422 per year mile, or an estimated return period of about 395 years for 1° longitude. Figure 14.14 illustrates the JPM-OS joint probabilities for pairs of attributes (which could have been better depicted with contour plots). Toro did not provide information on the uncertainty of these estimated joint probabilities.

The Mississippi project team did not address implications of the simplified SLOSH model limitations in the JPM-OS selection and JPA. While the Mississippi coast is more linear and smoother than the southeast Louisiana coast, it does include several notable irregularities (e.g., St. Louis and Biloxi Bays). Toro did not develop wind return frequency results and validate the Mississippi JPM-OS versus a wind hazard benchmark (e.g., Vickery et al's wind return studies).

The Mississippi production runs employed the calibrated/validated ADCIRC-SWAN (loosely coupled) model (see Section 11). Quality control included automated screening of selected station time-series for large SWL oscillations, as well as screening for abrupt changes in peak SWL between adjacent mesh nodes.

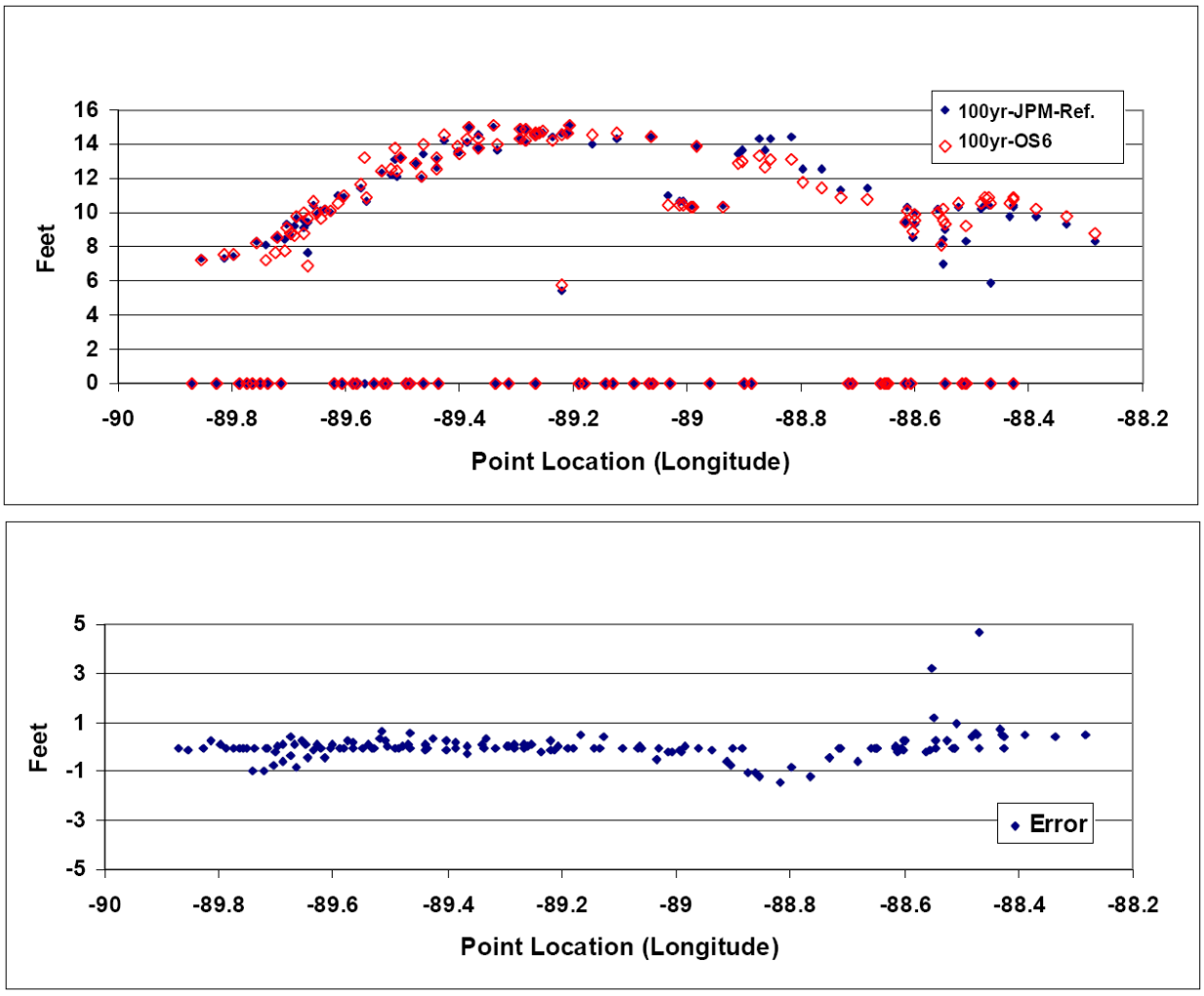

Figure 14.12. Comparison of Benchmark versus JPM-0S 100-yr SWL
URS Corporation 2008

The Mississippi team employed a normally distributed uncertainty term, ε_Σ, consisting of the following components:

1. Uncertainty associated with wind field attributes omitted from the joint probability—ε_W—was defined with a separate σ_B for Holland B of 0.15·SWL ft and σ_{PBL} of 1.17 ft
2. Uncertainty associated with the high resolution ADCIRC-STWAVE surge model—ε_Ψ—was defined with σ_Ψ = 0.77 ft. The combined $\sigma_{PBL\&\Psi}$ = 1.4 ft, much lower than the Resio et al $\sigma_{PBL\&\Psi}$ of 2.0 to 3.5 ft.
3. Uncertainty associated with the tides—ε_T—was defined with σ_T = 0.65ft;
4. Uncertainties regarding hurricane climatology (joint probability) and the JPM-OS—ε_P and $\varepsilon_{JPM\text{-}OS}$—were not defined.

The overall σ_Σ equated to 2.2 ft at a SWL of 10 ft, or a 90% interval of about ±3.4 ft.

Table 14.2. "Greater" Hurricanes for Mississippi JPM-OS

Toro 2008

Landfall CPD mb	GoM R_{max} mile	Landfall V_f mph	Landfall θ	Weighted Fractional Joint Probability
66.69	21.4	13.5	-38.9	0.1330
57.17	45.8	13.5	-12.8 to -13.5	0.1200
49.72	26.4	13.5	-38.9	0.1330
57.17	12.5	13.5	-12.8 to -13.5	0.1200
57.17	23.9	13.5	56.7	0.1080
92.95	16.9	13.3	-12.8 to -13.5	0.0342
78.59	35.4	13.5	-12.8 to -13.5	0.0534
78.59	19.1	9.7	47.3	0.0420
78.59	10.2	13.5	-12.8 to -13.5	0.0534
78.59	19.1	32.5	-12.8 to -13.5	0.0349
70.02	20.7	13.3	-12.8 to -13.5	0.0342
78.59	19.1	9.7	-71.0	0.0420
128.7	13.4	13.3	-12.8 to -13.5	0.0106
103.7	29.1	13.5	-12.8 to -13.5	0.0165
103.7	15.7	9.7	47.3	0.0130
103.7	8.4	13.5	-12.8 to -13.5	0.0165
103.7	15.7	32.5	-12.8 to -13.5	0.0108
94.47	16.7	13.3	-12.8 to -13.5	0.0106
103.7	15.7	9.7	-71.0	0.0130
				Total 0.9991

To post-process the results from the JPM-OS storms run with the ADCIRC-SWAN model the Mississippi team employed a different integration approach from the southeast Louisiana study. The team used the PDF smoothing technique described in Section 13.6, with ε_Σ as a diffusion term (see Figures 13.9 and 13.10). The team did not discuss validation of the JPA CDF versus a CDF that could have been developed from the long-term record at the Biloxi tide gauge. Confidence bands for the JPA CDF were not discussed. The team determined VE Zones associated with the 100-yr SWL hazard using WHAFIS. [6]

[6] Following publication of preliminary FIRMS local Mississippi officials engaged FEMA to improve the input for WHAFIS elevation and wave energy dissipation for several transects.

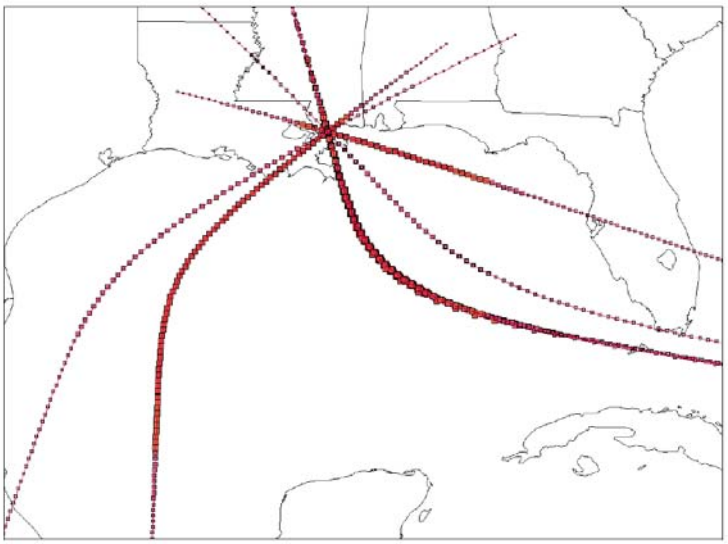

Figure 14.13. "Greater" Hurricane Tracks for Mississippi Coast JPM-OS

Toro 2008

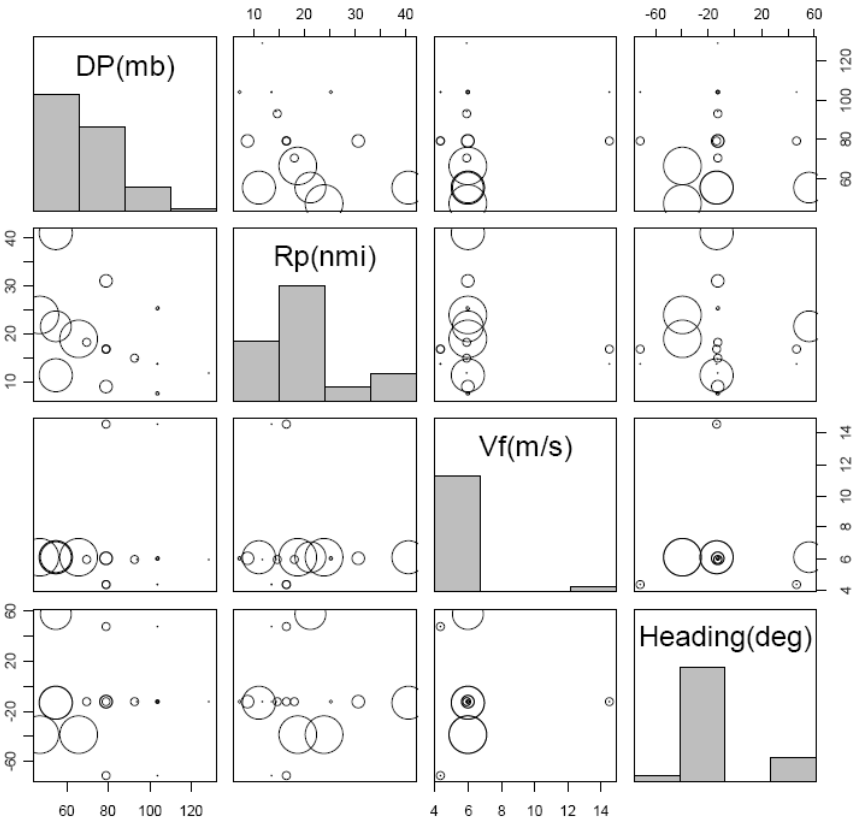

The main diagonal shows the probability distribution of the corresponding quantity (in the form of a histogram). Each off-diagonal scatter diagram shows how each pair of quantities are jointly distributed, with the areas of the circles being proportional to the associated annual rates.

Figure 14.14. JPM-OS Joint Probabilities

Toro 2008

14.6. Other FISs

The Mississippi JPM-OS approach is being employed for two other ongoing GoM coastal FISs, that include key team members from the Mississippi coastal FIS. For the Florida—Big Bend study (less than 100-mi east-west study segment) the surge hazard benchmark was created with 3,263 storms and a regional SLOSH model, resulting in selection of a 159-storm JPM-OS (Northwest Florida Water Management District 2010). A similar approach is being used for Northwest Florida/Alabama by the same team, with the benchmark set and OS reportedly approximating 4,000 and several hundred storms, respectively (Northwest Florida Water Management District 2011).

The North Carolina FIS team is using a 675-storm JPM-OS, with 351 landfalling and 324 bypassing storms. The set reflects combinations of historical tracks with incremental adjustments to storm CDP, R_{max}, Holland B, V_f, , and variations in θ. This set is much larger than the JPM-OS for southeast Louisiana and Mississippi. The North Carolina team compared the return period wind results at five locations for the 675 storm set versus results from Vickery's wind JPA, which employed a much larger Monte Carlo based storm set (see Section 4). Figure 14.15 illustrates the comparison of wind results for one location. The team has indicated that visual comparison of the two wind results supports use of the 675-storm JPM for the hurricane surge return frequency analysis. A measure of the agreement between the two results over the five stations was not included.

The South Carolina and Northeast Florida/Georgia FISs are using JPM-OS. The South Carolina study has a 122-storm JPM-OS, based on comparison with a SLOSH surge hazard benchmark. The number of storms employed in the South Carolina SLOSH benchmark was not available. The Northeast Florida/Georgia study is expected to have on the order 200 to 300 storms. The JPM-OS is being developed in comparison against a lower resolution ADCIRC surge hazard benchmark based on several thousand storms.

The coastal FIS for Texas is being led by the USACE and has utilized the Surge Response-OS used for southeast and southwest Louisiana. Presumably the Texas OS employs the 19 CPD-R_{max}-V_f combinations used for Louisiana. Detailed information on the Texas OS is not currently available. The Texas OS has reportedly included about 360 storms (divided into two 180 storm sets for north and south coastal regions) for a JPA of 100-yr plus return period surge.

Details have not yet been released for these coastal FISs on the treatment of uncertainty, integration procedures, validation against tide gauge CDFs, and result differences at study boundaries.

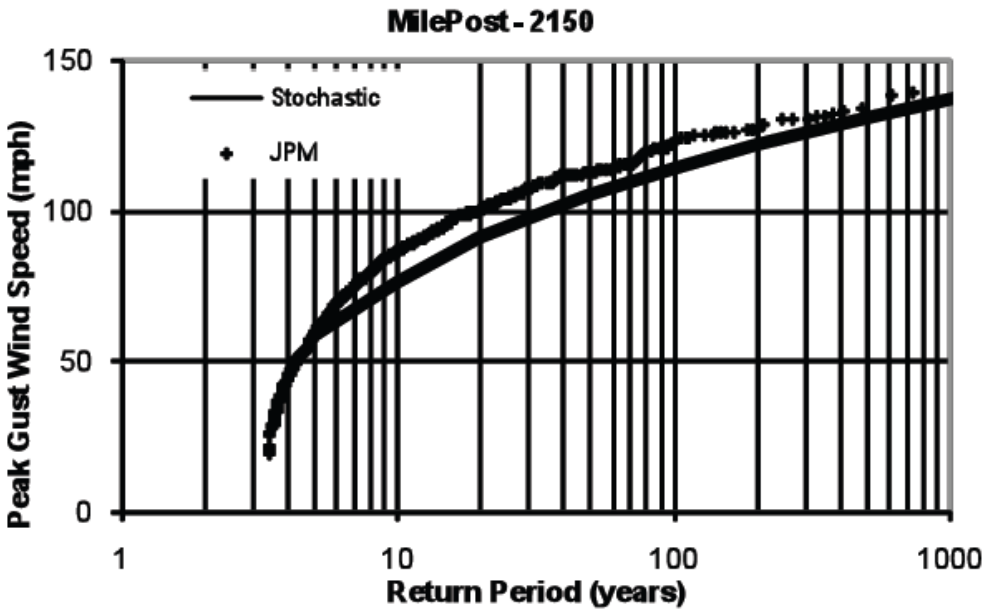

Figure 14.15. Example Comparison of Return Period Wind Gusts from 675-Storm versus Full Monte Carlo JPM

Blanton and Vickery 2008

Part III. Conclusions and Recommendations

Conclusions

Part III has reviewed the state-of-the-practice on hurricane surge return frequency analysis and applications to the CN-GoM. This information supports the following important findings:

1. Surge return frequency analysis can be readily performed with long-term daily tide records using established methods for five CN-GoM gauges (Pensacola, Dauphin Island, Biloxi, Grand Isle, and Sabine Pass). Record lengths, gauge outages, datum issues, local restrictions, the choice of return frequency distribution equations, and extrapolation uncertainties all limit applicability. NOAA's recent analysis of the Grand Isle tide gauge record shows an estimated 100-yr return SWL of 7.1 ft, with 95% confidence intervals of 5.1/11.4 ft. The size of this confidence interval, i.e., -2.0/+4.4 ft (62% for the upper interval), is an important indicator of limitation in surge return estimates.

2. Hurricane JPA (see Part I) can be extended to surge to provide more comprehensive estimates of surge hazard and address some limitations of gauge analysis. Hurricane surge JPA is mathematically expressed in a PDF coupling the analytical joint probability expression, $\boldsymbol{p}$, for hurricane occurrence as a function of hurricane attributes (e.g., CPD, R_{max}, V_f, θ, X) with the high resolution surge response function, $\boldsymbol{\Psi}$, for the same attributes. $\boldsymbol{\Psi}$ must be solved numerically for discrete attribute values using a wind field vortex model (e.g., PBL) coupled with a validated hydrodynamic model (e.g., ADCIRC/STWAVE, described in Part II). Surge PDF results over a wide range of combined attributes are then integrated to provide a surge CDF.

3. There are four established approaches to developing a sufficient number of discrete solutions to the coupled $\boldsymbol{p}$-$\boldsymbol{\Psi}$:

    a. Full-JPM—choose discrete intervals for each attribute to represent $\boldsymbol{p}$ and simulate each storm combination with $\boldsymbol{\Psi}$; joint probabilities based on the combination of attributes are assigned to each storm's surge results; requires a very large number of simulations.

    b. Monte-Carlo-JPM—randomly select storms according to $\boldsymbol{p}$ to construct a reasonably long synthetic record—e.g., 10X the return period of interest—and simulate each storm with $\boldsymbol{\Psi}$; joint probabilities based on the combination of attributes are assigned to each surge result; smaller set than the Full-JPM.

    c. JPM-OS—depending on high resolution $\boldsymbol{\Psi}$ computational requirements, develop a subset from Full/Monte Carlo-JPM to represent $\boldsymbol{p}$ using fractional weightings; further optimize the set to represent a benchmark surge JPA derived with a simplistic $\boldsymbol{\Psi}$ and the Full/Monte Carlo-JPM; the subset is then simulated with the high resolution $\boldsymbol{\Psi}$; weighted joint probabilities of each storm are assigned to each surge result.

    d. Surge Response-OS—as an alternative to JPM-OS, develop a set of storms as needed to depict $\boldsymbol{\Psi}$ only; this set size can be reduced in surge response is assumed to be nearly linear and smooth and interpolation/extrapolation can be used to provide a range of surge response; a large set of discrete $\boldsymbol{p}$-$\boldsymbol{\Psi}$ solutions are provided by combining analytically-derived $\boldsymbol{p}$ with surge values from $\boldsymbol{\Psi}$ defined with the Surge Response-OS; note that the Surge Response-OS and simulation results do not have assigned joint probabilities and cannot be used to support subsequent polder hazard analysis.

4. The use of any of the four surge JPA approaches includes uncertainties which are in addition to uncertainties regarding the hurricane joint probability, $\boldsymbol{p}$ (i.e., the defined hurricane climatology)

and the surge model, $\boldsymbol{\Psi}$. The use of JPM-OS and Surge Response-OS approaches both add significant uncertainties associated with reducing set size. The surge response of certain coastal regions is nonlinear (i.e., the response curve contains notable inflections) and the coupled $\boldsymbol{p}$-$\boldsymbol{\Psi}$ surge hazard may be even more nonlinear. A crucial example is the tilting response of large coastal lakes and bays to local hurricane winds (e.g., Lakes Pontchartrain and Borgne). The OS approaches must contain sufficient storms to represent localized surge response and surge hazard conditions.

5. Altogether there are five major categories of stationary uncertainty in surge JPA:

   i. $\varepsilon_{\boldsymbol{p}}$—aleatory uncertainty in hurricane climatology as defined in $\boldsymbol{p}$, such as uncertainty in return frequency of CPD, and frequency of R_{max}, V_f, and θ;

   ii. $\varepsilon_{\boldsymbol{W}}$—epistemic uncertainty associated with additional hurricane wind field factors excluded from $\boldsymbol{p}$; uncertainty with Holland B (ε_B) is one component; others include intensification and decay;

   iii. ε_{Ψ}—epistemic uncertainty associated with the high resolution surge response model $\boldsymbol{\Psi}$; including winds (PBL), surge (ADCIRC) and waves (STWAVE);

   iv. ε_{OS}—epistemic uncertainties associated with the JPA method (see No. 4 above); uncertainty with the limited number of tracks (ε_{ϑ}) is one component ; and

   v. ε_{T}—tides and pre-storm meteorological conditions affecting the SWL.

   Most sources of uncertainty, with the exception of CPD return frequency, have been treated as normally distributed with an associated $\boldsymbol{\sigma}$, which can be combined into an overall $\boldsymbol{\sigma}_{\Sigma}$. CPD uncertainty is typically skewed and can be assessed using the assigned distribution equation (e.g., Gumbel). Non-stationary uncertainties, such as RSLR, coastal erosion, and subsidence affect future surge return frequency.

6. Numerical integration of the discrete p-Ψ results can include smoothing the PDF and CDF. A σ value can be used; however, a large σ value can distort the CDF. Techniques for refining the discrete results can also aid in smoothing. .

7. Potential bias in a surge JPAs is investigated by comparing the surge JPA CDF versus one derived from a sufficiently long local gauge record (No. 1 above); bias can be further assessed by addressing validation results for key components (such as the high resolution $\boldsymbol{\Psi}$, surge benchmark, and simplified $\boldsymbol{\Psi}$, where used) and lessons from other JPAs.

8. Uncertainty in surge CDFs are evaluated by comparing the computed median curve with confidence intervals accounting for all normally and non-normally distributed sources of uncertainty. FISs do not typically introduce adjustments for uncertainty into final estimates of surge hazard. However, such adjustments are commonly applied in planning and design studies. The final residual uncertainty can be evaluated by comparing the JPA CDF versus local gauge CDF.

9. General inland wave hazards associated with extreme surges are evaluated with simple 1D wave models (e.g., WHAFIS, see Part II). Locations subject to sensitive wind-wave generation conditions, or to complex wave transformations, require more sophisticated 2D and higher-order wave models.

10. The Rayleigh Distribution may over-predict nearshore extreme waves associated with surge SWL peaks lasting only a few hours.

11. Application of hurricane surge JPA to the CN-GoM began in the 1980s. However, hurricane surge JPA was not employed for southeast Louisiana prior to Hurricane Katrina.

12. The FIS surge JPA project team (Resio et al) employed a 152-storm Surge Response-OS for the 151-mi (2.5°) segment for southeast Louisiana. The team developed the storm set with a idealized coastal surge response model. The set included 3 different CPDs, 15 different CPD-R_{max} combinations, and 19 different CP-R_{max}-V_f variations. The set used 9, 7, and 7 landfall locations within the 151-mi range, for three basic variations in θ—central, northeast, and northwest headings. Selected CP-R_{max}-V_f combinations from the 19 variations were used with each of the 23 tracks. The spatial distribution of landfalls within the 151-mi range was adjusted to provide a higher landfall rate in the 60-mi (2.5°) centermost segment—generally in accordance with the Resio et al hurricane intensity-frequency relationship (see Part I).

13. All 152 storms in the Surge Response-OS set were Category 3 or higher in the GoM, including 50 at Category 5. However, none made landfall at Category 5.

14. In designing the Surge Response-OS to be representative of a simplistic regional coastal landfall surge response the authors did not address special nonlinear surge response issues, such as those associated with extreme local winds over Lakes Pontchartrain and Borgne.

15. The southeast Louisiana FIS JPA defined sources of normally distributed uncertainty with total epistemic uncertainty σ_e totaling 2.1 to 3.6 plus 0.1 to 0.2 * SWL. For a 10 ft SWL this equates to a 90% confidence interval of ±3.8 to 6.8 ft. This level uncertainty is generally consistent with that seen in the Grand Isle gauge data (No. 1 above). This σ_e was based on epistemic uncertainties in θ, Holland B, the PBL/ADCIRC/STWAVE model, and tides. Uncertainties associated with other hurricane climatological attributes, and the Surge Response-OS itself were not provided. 2.0 to 3.5 ft. The report does not indicate that any explicit adjustments were made to production SWL results to account for ADCIRC-STWAVE model Hurricane Katrina hindcast validation bias along the south shore of Lake Pontchartrain (>1.5 ft, see Section 11).

16. The current FIS documentation states that production runs for the 152-storm Surge Response-OS were completed with the validated Hurricane Katrina ADCIRC-STWAVE model (including various settings and parameters, see Section 11). The current FIS documentation reflects 2007 mesh updates, but not the IHNC or Seabrook Surge Barrier. The LaCPR Study and HSDRRS design employed the 152-storm Surge Response-OS with a 2010 mesh version which included the IHNC Surge Barrier (but not the Seabrook Barrier) and presumably the same model settings and parameters (see Part IV for a discussion of the 2010 surge JPA results).

17. The southeast Louisiana FIS CDF numerical integration reportedly included both refining and smoothing. The refining utilized piece-wise linear interpolation of the surge response function. Smoothing was applied the discrete values of the integrand and employed the σ_e, which increased the estimated 100- and 500-yr SWLs for one location by 0.4 and 1.1 ft, respectively.

18. The FIS documentation does not contain any validation of the JPA CDFs. This Report provides a comparison of the FIS JPA and NOAA tide gauge CDFs for Grand Isle—which is along the *open coast*—and shows reasonable agreement.

19. In a separate documentation of independent technical review comments and responses, the project team compared JPA results with a limited analysis of regional *interior (sheltered) coast* gauge data (e.g., Lake Pontchartrain, MRGO). The JPA consistently underestimated surge hazard relative to the gauge analysis, primarily due to the extreme surge observations for Hurricane

Katrina. The project team noted that the very long return period estimates for Hurricane Katrina observations—e.g., 660-yrs for the south shore of Lake Pontchartrain—"are a concern."

20. The apparent underestimation of sheltered coast surge hazard versus more reasonable estimation of open coast surge hazard may reflect:

    a. Some underestimation of the recurrence of extreme hurricanes—such as the return period of Hurricane Katrina (see the conclusion of Part I);

    b. The ADCIRC-STWAVE model under-prediction bias in some sheltered areas (see conclusions of Part II); and/or

    c. Limitations of the Surge-Response OS in representing important local nonlinear surge response of sheltered areas.

21. USACE 1966 100-yr surge SWL estimates for south shore Lake Pontchartrain and the MRGO near Chalmette—which pre-dated JPA—were 9.2 ft and 11.2 ft, compared to 8.8 and 17.5 ft for the 2007 JPA. A USACE 1988 100-yr surge SWL estimate for St. Charles Parish west of I-310—based on an extension of the 1966 analysis—was 10.8 ft compared to 11.4 ft for the 2007 JPA.

22. For those parishes with published preliminary FIRMs (at the Part was prepared) the FIS contractor (not the USACE) employed the 1D WHAFIS model to define general inland 100-yr wave hazards (VE Zones) associated with the 2007 JPA 100-yr SWL results. St. Tammany Parish is appealing preliminary FIRMs on the basis of inaccurate 1D transect information and wave transformation parameters.

23. The southeast Louisiana FIS project team also undertook a JPA using the Surge Response-OS approach for southwest Louisiana. The southwest Louisiana FIS employed the same 19 CP-R_{max}-V_f variations and number and variations of tracks, together with the same validated ADCIRC/STWAVE model and 2007 mesh. Following publication of preliminary FIRMs Cameron Parish retained a team to recommend improvements in the local surge and wave JPA results, including modifying model inputs for topography and Manning's *n*.

24. To date there have been two very limited applications of the JPM-OS approach for southeast Louisiana. Both applications supported a JPA used in a "planning level" relative comparison of residual hazards associated with selected protection alternatives (e.g., polder inundation hazards associated with overtopping and breaching). These JPM-OS were not sufficiently developed to provide reasonable estimates of the actual surge or inundation hazard.

    i. IPET improvised use of 76 of the southeast Louisiana Surge Response-OS 152 storms for a JPM-OS. IPET assigned fractional probabilities to individual storms and their surge results, although the set was not developed to include storms with a suitable probability range (i.e., the set was developed as a Surge Response OS and did not include any landfalling Category 5 hurricanes). The IPET 76-storm JPM-OS was not representative of hurricane intensity above the 200-yr return period. IPET's 500-yr surge SWL for St. Charles Parish west of I-310 was 24% lower than the 2007 FIS JPA value. The 76-storm set also has other limitations associated with its small size and not being optimized to represent regional surge hazard.

    The IPET Study defined epistemic and aleatory uncertainty sources totaling to a σ_{Σ} of about 2.6 ft at a 10 ft SWL, or a 90% interval of ±4.3 ft, smaller than identified by the FIS JPA. The IPET study employed only the epistemic portion of the uncertainty—σ of about 1 ft at a 10 ft SWL plus skewed uncertainty associated with ε_{CP}—in the final development of confidence intervals around the JPA.

ii. The 2012 State of Louisiana Master Plan team employed a truncated version of the IPET JPM-OS approach. The Master Plan JPM-OS assigned fractional joint probabilities to 40 of the 152 storms—which included four CP-R_{max} combinations, each applied to 10 basic tracks spaced across the full Louisiana coast (one heading for 10 landfall locations). Given the characteristics of the 152-storm Surge Response-OS, the 40-storm set (like the IPET 76-storm set) was not suitable for representing hurricane intensities above the 200-yr return period. Even more than the IPET set, the 40-storm set has limitations associated with small size and not being representative of the regional and local surge hazards.

25. Since the application of the Surge Response-OS to the Louisiana coastal FIS, ensuing coastal FISs have primarily adopted the JPM-OS approach. Some recent surge JPAs are also expanding the hurricane attributes.

i. One other FIS—for Texas, which is being performed by the same team that undertook the Louisiana FIS—has employed the Surge Response-OS approach. The Texas Surge Response-OS reportedly includes about 360 storms—two 180 storm sets for north and south coastal regions.

ii. The Mississippi FIS used a JPM-OS approach, with a 152-storm set optimized versus hurricane joint probability and further refined to represent a benchmark surge hazard. The team employed the same hurricane attributes used in the Louisiana FIS. The team produced a benchmark surge hazard using a simplified SLOSH model of the Mississippi coast and close to 3,000 storms. The integration approach for the Mississippi project included smoothing using a σ_{Σ} of 2.2 ft at a SWL of 10 ft, equivalent to a 90% interval of about ±3.4 ft. The team determined VE Zones associated with the 100-yr SWL hazard using WHAFIS.

iii. In the GoM, the JPM-OS approach is being employed for the Florida—Big Bend and Northwest Florida/Alabama FISs. In the former study the surge hazard benchmark was created with 3,263 storms and a regional SLOSH model, resulting in selection of a 159-storm JPM-OS. For the latter study, the benchmark set and OS reportedly approximating 4,000 and several hundred storms, respectively.

iv. The North Carolina FIS team is using a 675-storm JPM-OS, reflecting combinations of historical tracks with incremental adjustments to storm CDP, R_{max}, Holland B, V_f, , and variations in θ. The North Carolina team compared the return period wind results at five locations for the 675 storm JPM-OS versus results from Vickery's wind JPA, which employed a much larger Monte Carlo based storm set.

v. The South Carolina and Northeast Florida/Georgia FISs are also using JPM-OS. The former with a 122-storm JPM-OS, based on comparison with a SLOSH surge hazard benchmark. The latter study is expected to have a JPM-OS on the order 200 to 300 storm and is being developed in comparison against a lower resolution ADCIRC surge hazard benchmark employing several thousand storms.

vi. The JPM-OS approach is expected to be employed in upcoming FISs for the Central Atlantic and the West GoM Florida Coasts.

Recommendations

The above conclusions indicate that the JPA approach employed in southeast Louisiana surge hazard analysis is outdated, particularly given advances in other FISs over recent years. They also provide the basis for recommendations to improve hurricane surge hazard analysis for southeast Louisiana. Four specific recommendations to update the surge hazard analysis include:

1. Employ a true JPM-OS approach with a much expanded set size (e.g., hundreds of storms) in the surge JPA. The JPM-OS should be determined using appropriate regional wind and surge benchmarks. The surge benchmark should sufficiently capture critical nonlinear responses and surge hazard conditions—particularly around large sheltered water bodies. Sensitivity tests should be used to examine the scope of regional nonlinear surge response and surge hazard conditions. Alternatively, the revised surge JPA can employ a Monte Carlo JPM or an expanded Surge Response-OS—with sufficient storms addressing nonlinear surge response.
2. Rigorously validate the surge JPA versus tide gauge-based return frequency analyses to evaluate potential bias in JPA results.
3. Employ an integration method which provides the median estimated CDF.. Sensitivity tests should be conducted on possible variations to the integration method to identify the best approach.
4. Define and quantify all sources of normally and non-normally distributed uncertainty contributing to the overall uncertainty in the surge hazard analysis, including uncertainties in the hurricane climatology, wind/surge/wave model, the selected surge JPA method, and set size. Prepare uncertainty intervals for the estimated CDF based on all sources of uncertainty.

The Louisiana CPRA, together with federal partners, should fund critical research to improve surge hazard analysis, including:

1. Expand the number of high quality long-term regional gauge records. Long-term records for several regional USGS and USACE gauges can be enhanced by addressing datum and gap issues.
2. Further evaluate appropriate return frequency distribution equations for the analysis of tide gauge records. In particular, equations should provide reasonable treatment of extreme historical observations.
3. Examine nonlinear surge response and surge hazard conditions for complex coastlines, including sheltered water bodies, particularly for southeast Louisiana.
4. Assess JPM approaches and set size optimization, CDF integration techniques, and the estimation and treatment of hazard uncertainty.
5. Study JPM wind field (10-min average) representation of surge forcing conditions
6. Investigate methods for wave hazard analysis. Such as the appropriate application of 1D overland wave modeling (WHAFIS transect selection and attribution, local wind-wave boundary conditions, wave transformation parameters, etc.) and determining those locations and conditions where more advanced modeling (2D, Boussinesq, etc.) should be applied.

The above recommendations can mitigate systemic and localized bias in estimates of surge hazard. Notably, localized bias is typically of less import to the NFIP than to the community, which must deal with the consequences of over- or under-estimating flood hazards.

However, it is important to recognize the large uncertainty that remains in estimated surge hazard based on either gauge records or JPA—i.e., 50%-plus for the 100-yr return at the 90% confidence level and much higher at the 500-yr return. Much of this uncertainty is associated with limitations inherent in hurricane climatological and surge records. In the near-term, methodological improvements and research are not likely to yield major reductions in uncertainty.

Part III. References

Blanton, B. O., P. J. Vickery, North Carolina Coastal Flood Analysis System: Hurricane Parameter Development, A Draft Report for the State of North Carolina, Floodplain Mapping Project, Technical Report TR-08-06 September 12, 2008.

FEMA, Atlantic Ocean and Gulf of Mexico Coastal Guidelines Update, February 2007.

FEMA, Hancock Co. Preliminary FIRM, Panel 295, November 2007, http://geology.deq.ms.gov/floodmaps/Projects/MapMOD/panels/28045C0295.pdf

Fitzpatrick, P. J., N. Tran, Y. Li, Y. Lau, and C. M. Hill, A Proposed New Storm Surge Scale, Geosystems Research Institute, Mississippi State University, BLDG 1103, Room 108, Stennis Space Center, MS 39529 USA. June 2010. http://www.drfitz.net/uploads/fitz_ocean_surge_scale_ieee_certified.pdf

Ho, F.P and V.A. Myers, Joint Probability Method of Tide Frequency Analysis Applied to Apalachicola Bay and St. George Sound, Florida, NOAA Tech. Rep. NWS 18, 1975.

Interagency Performance Evaluation Task Force (IPET), Performance Evaluation of the New Orleans and Southeast Louisiana Hurricane Protection System, Volumes VIII, Engineering and Operational Risk and Reliability Analysis, U.S. Army Corps of Engineers, June 2009.

Irish, J. L., D. T. Resio and M. A. Cialone, A surge response function approach to coastal hazard assessment. Part 2: Quantification of spatial attributes of response functions, Natural Hazards, Vol. 51, No. 1, 2009

Jonathan, P. and K. Ewans, ,A Spatiodirectional Model for Extreme Waves in the Gulf of Mexico, Journal of Offshore Mechanics and Arctic Engineering, Vo. 133, February 2011.

Jonathan, P. and K. Ewans, Modeling the Seasonality of Extreme Waves in the Gulf of Mexico, Journal of Offshore Mechanics and Arctic Engineering, Vo. 133, May 2011.

Jacobsen, R. W. and N. Dill, Assessing Baseline and Modified Astronomical Tide Propagation in the Pontchartrain Basin Using ADCIRC, for the USACE Louisiana Coastal Protection and Restoration Study, URS Corporation, July 2007.

Louisiana Coastal Protection and Restoration Authority (Louisiana CPRA), Louisiana's Comprehensive Master Plan for a Sustainable Coast, 2012.

McCorquodale, J. A., I. Georgiou , A. G. Retana, D. Barbe, M. J. Guillot, Hydrodynamic modeling of the Tidal Prism in the Pontchartrain Basin, Final Report, for the USACE Louisiana Coastal Protection and Restoration Study, June 2007.

National Research Council of the National Academies, Mapping the Zone: Improving Flood Map Accuracy, Committee on FEMA Flood Maps, Board on Earth Sciences and Resources/Mapping Science Committee, Water Science and Technology Board, The National Academies Press, Washington D. C., 2009.

Needham, H., Identifying Historic Storm Surges and Calculating Storm Surge Return Periods for the Gulf of Mexico Coast, Master's Thesis, Louisiana State University, Department of Geography and Anthropology, May 2010.

NOAA, Tidal and Geodetic Datums: Tidal and Geodetic Relationships, (no date) http://www.laseagrant.org/pdfs/NOAA_TidalGeodeticRelationships.pdf

NOAA, Tides an Currents, Extreme Water Levels, Website. http://tidesandcurrents.noaa.gov/est/

NOAA-NDBC, Website. http://www.ndbc.noaa.gov/

NOAA-NWS, (Ho, F. P., J. C. Su, K. L. Hanevich, R. J. Smith, and F. P. Richards) Hurricane Climatology for the Atlantic and Gulf Coasts of the United States, NOAA Technical Report NWS 38, April 1987.

Northwest Florida Water Management District, Scoping Report for the Coastal Remapping Study of Northwest Florida, Revised December 22, 2010, http://www.nwfwmdfloodmaps.com/pdf/Coastal_Remapping_Study_FinalReport.pdf

Northwest Florida Water Management District, Coastal Modeling and DFIRM Production Technical Approach Report for Coastal Northwest Florida, Revised October 3, 2011, http://www.nwfwmdfloodmaps.com/documents/TechnicalApproachReport10311.pdf

Panchang, V. G. and L Dongcheng, Large Waves in the Gulf of Mexico Caused by Hurricane Ivan, Bulletin of the American Meteorological Society, April 2006.

Resio, D. T., S. J. Boc, L. Borgman, V. J. Cardone, A. Cox, W. R. Dally, R. G. Dean, D. Divoky, E. Hirsh, J. L. Irish, D. Levinson, A. Niederoda, M. D. Powell, J. J. Ratcliff, V. Stutts, J. Suhada, G. R. Toro, and P. J. Vickery, White Paper on Estimating Hurricane Inundation Probabilities, U.S. Army Corps of Engineers, ERDC-CHL, 2007.

Resio, D. T., J. L., and M. A. Cialone, A surge response function approach to coastal hazard assessment. Part 1: Basic concepts, Natural Hazards, Vol. 51, No. 1, 2009.

Resio, D. T., J. L. Irish, J. J. Westerink, N. J. Powell, The Effect of Uncertainty on Estimates of Hurricane Surge Hazards, Natural Hazards, October 2012.

Smith, J. M., Modeling Nearshore Waves for Hurricane Katrina, USACE Engineer Research and Development Center, Coastal and Hydraulics Laboratory, August 2007. http://chl.erdc.usace.army.mil/Media/9/3/7/tnswwrp-07-6.pdf

Suhayda, J. N., Flood Insurance Rate Map Revision Request for Cameron Parish, Vol. I, Cameron Parish Police Jury, 1989.

Toro, G. R., Joint Probability Analysis of Hurricane Flood Hazard for Mississippi, Final Report, Revision 1. Prepared for URS Group, Tallahassee, FL, in support of the FEMA-HMTAP, Flood Study of the State of Mississippi, Risk Engineering, Inc. 4155 Darley Avenue, Suite A Boulder, CO 80305. June 23, 2008.

URS Corporation, Preliminary Flood Frequency Analysis for Hurricane Katrina, for FEMA, 2005

URS Corporation, Mitigation Assessment Team Report, Hurricane Katrina in the Gulf Coast, for FEMA, 2006. http://www.fema.gov/library/viewRecord.do?id=1857

URS Corporation, Mississippi Coastal Analysis Project, Coastal Documentation and Main Engineering Report, Final Report: HMTAP Task Order 18, for Federal Emergency Management Agency, June 17, 2008.

USACE, Lake Pontchartrain, Louisiana and Vicinity, Design Memorandum No. 1, Hydrology and Hydraulic Analysis, Part I Chalmette, August 1966.

USACE, Lake Pontchartrain, Louisiana and Vicinity, Lake Pontchartrain High Level Plan, Design Memorandum No. 18, General Design, St. Charles Parish North of Airline Highway, February 1989.

USACE, Coastal Engineering Manual, EM1110-2-1100, April 2005.

USACE, Southeast Louisiana Joint Surge Study, Independent Technical Review, Final Report, for FEMA, October 15, 2007.

USACE, Flood Insurance Study, Southeast Parishes of Louisiana, Intermediate Submission 2: Offshore Water Levels and Waves, for FEMA, July 2008.

USACE, Louisiana Coastal Protection and Restoration, Final Technical Report, June 2009.

USACE (New Orleans District), Hurricane and Storm Damage Risk Reduction System, Design Elevation Report, Draft Report Version 4.0, August 18, 2010.

USACE, Supporting Information for Southeast Louisiana JPM-OS on 152 Hurricanes Provided by Nancy Powell, 2011.

USACE, Supporting Information for Southeast Louisiana JPM-OS, Results for 2007 Condition, Provided by Dr. Jay Ratcliff together with personal communication on JPM-OS methodology, May 2012

Wamsley, T. V., M. A. Cialone, J. Westerink, and J, M. Smith, Influence of Marsh Restoration and Degradation on Storm Surge and Waves, USACE, ERDC/CHL CHETN-I-77, July 2009.

Xu, L. A Simple Coastline Storm Surge Model Based on Pre-Run SLOSH Outputs, 29th Conference on Hurricanes and Tropical Meteorology, May 2010.

Xu, S. and W. Huang, Integrated Hydrodynamic Modeling and Frequency Analysis for Predicting 1% Storm Surge, Journal of Coastal Research, No. 10052, Pages 253-260. 2008.

Zervas, C. E., Response of Extreme Storm Tide Levels to Long-term Sea Level Change, in Oceans 2005, IEEE, 2005, http://tidesandcurrents.noaa.gov/est/050415-53.pdf

Attachment 1

Attributes for 152 Hurricanes for Southeast Louisiana Hurricane JPA

Sources:

Interagency Performance Evaluation Task Force (IPET), Performance Evaluation of the New Orleans and Southeast Louisiana Hurricane Protection System, Volumes VIII, Engineering and Operational Risk and Reliability Analysis, Appendix 9 Risk Methodology, U.S. Army Corps of Engineers, June 2009.

Resio, D. T., S. J. Boc, L. Borgman, V. J. Cardone, A. Cox, W. R. Dally, R. G. Dean, D. Divoky, E. Hirsh, J. L. Irish, D. Levinson, A. Niederoda, M. D. Powell, J. J. Ratcliff, V. Stutts, J. Suhada, G. R. Toro, and P. J. Vickery, White Paper on Estimating Hurricane Inundation Probabilities, U.S. Army Corps of Engineers, ERDC-CHL, 2007.

USACE, Flood Insurance Study, Southeast Parishes of Louisiana, Intermediate Submission 2: Offshore Water Levels and Waves, July 2008.

Southeast Louisiana JPM-OS Hurricanes

FIS Documentation

No.	GoM CP mb	Peak GoM Winds 30 min (m/s)	(mph)	1-min (mph)	Rmax nm	mile	Vf kn	mph	Track	P or S	θ	Landfall CP mb	Peak Landfall Winds 30 min (m/s)	(mph)	1-min (mph)	SS Category GoM	Landfall
1	960	45	100.7	124.8	11.0	12.7	11	12.7	Central 1	P	0	960	43.1	96.4	119.6	3	3
2	960	43.9	98.2	121.8	21.0	24.2	11	12.7	Central 1	P	0	977	31.5	70.5	87.4	3	2
3	960	42.2	94.4	117.1	35.6	40.9	11	12.7	Central 1	P	0	981	28.9	64.6	80.2	3	2
4	930	52.8	118.1	146.5	8.0	9.2	11	12.7	Central 1	P	0	930	51.2	114.5	142.0	4	4
5	930	52.5	117.4	145.6	17.7	20.4	11	12.7	Central 1	P	0	943	41.2	92.2	114.3	4	3
6	930	51.8	115.9	143.7	25.8	29.7	11	12.7	Central 1	P	0	951	38.8	86.8	107.6	4	3
7	900	57.2	128.0	158.7	6.0	6.9	11	12.7	Central 1	P	0	900	55.3	123.7	153.4	5	4
8	900	58.4	130.6	162.0	14.9	17.1	11	12.7	Central 1	P	0	910	48.4	108.3	134.3	5	4
9	900	57.9	129.5	160.6	21.8	25.1	11	12.7	Central 1	P	0	918	46.6	104.2	129.3	5	3
10	960	45.1	100.9	125.1	11.0	12.7	11	12.7	Central 2	P	0	960	44.2	98.9	122.6	3	3
11	960	43.9	98.2	121.8	21.0	24.2	11	12.7	Central 2	P	0	977	31.7	70.9	87.9	3	2
12	960	42.1	94.2	116.8	35.6	40.9	11	12.7	Central 2	P	0	981	29.0	64.9	80.4	3	2
13	930	52.8	118.1	146.5	8.0	9.2	11	12.7	Central 2	P	0	930	51.3	114.8	142.3	4	4
14	930	52.4	117.2	145.3	17.7	20.4	11	12.7	Central 2	P	0	943	41.3	92.4	114.6	4	3
15	930	51.7	115.6	143.4	25.8	29.7	11	12.7	Central 2	P	0	951	38.9	87.0	107.9	4	3
16	900	57.2	128.0	158.7	6.0	6.9	11	12.7	Central 2	P	0	900	55.4	123.9	153.7	5	4
17	900	58.3	130.4	161.7	14.9	17.1	11	12.7	Central 2	P	0	910	48.5	108.5	134.5	5	4
18	900	57.8	129.3	160.3	21.8	25.1	11	12.7	Central 2	P	0	918	46.7	104.5	129.5	5	3
19	960	45	100.7	124.8	11.0	12.7	11	12.7	Central 3	P	0	960	44.2	98.9	122.6	3	3
20	960	43.7	97.8	121.2	21.0	24.2	11	12.7	Central 3	P	0	977	31.7	70.9	87.9	3	2
21	960	42.2	94.4	117.1	35.6	40.9	11	12.7	Central 3	P	0	981	29.1	65.1	80.7	3	2
22	930	52.8	118.1	146.5	8.0	9.2	11	12.7	Central 3	P	0	930	51.2	114.5	142.0	4	4
23	930	52.3	117.0	145.1	17.7	20.4	11	12.7	Central 3	P	0	943	41.5	92.8	115.1	4	3
24	930	51.7	115.6	143.4	25.8	29.7	11	12.7	Central 3	P	0	951	38.9	87.0	107.9	4	3
25	900	57.2	128.0	158.7	6.0	6.9	11	12.7	Central 3	P	0	900	55.9	125.0	155.1	5	4
26	900	58.1	130.0	161.2	14.9	17.1	11	12.7	Central 3	P	0	910	48.7	108.9	135.1	5	4
27	900	57.7	129.1	160.0	21.8	25.1	11	12.7	Central 3	P	0	918	46.8	104.7	129.8	5	3
28	960	44.9	100.4	124.5	11.0	12.7	11	12.7	Central 4	P	0	960	43.5	97.3	120.7	3	3
29	960	43.8	98.0	121.5	21.0	24.2	11	12.7	Central 4	P	0	977	31.2	69.8	86.5	3	2
30	960	42.1	94.2	116.8	35.6	40.9	11	12.7	Central 4	P	0	981	28.8	64.4	79.9	3	2
31	930	52.6	117.7	145.9	8.0	9.2	11	12.7	Central 4	P	0	930	51.2	114.5	142.0	4	4
32	930	52.6	117.7	145.9	17.7	20.4	11	12.7	Central 4	P	0	943	41.1	91.9	114.0	4	3
33	930	51.7	115.6	143.4	25.8	29.7	11	12.7	Central 4	P	0	951	38.6	86.3	107.1	4	3
34	900	57.3	128.2	158.9	6.0	6.9	11	12.7	Central 4	P	0	900	55.1	123.3	152.8	5	4
35	900	58.1	130.0	161.2	14.9	17.1	11	12.7	Central 4	P	0	910	48.3	108.0	134.0	5	4
36	900	57.8	129.3	160.3	21.8	25.1	11	12.7	Central 4	P	0	918	46.5	104.0	129.0	5	3
37	960	44.9	100.4	124.5	11.0	12.7	11	12.7	Central 5	P	0	960	43.4	97.1	120.4	3	3
38	960	43.7	97.8	121.2	21.0	24.2	11	12.7	Central 5	P	0	977	31.0	69.3	86.0	3	2
39	960	42.2	94.4	117.1	35.6	40.9	11	12.7	Central 5	P	0	981	28.7	64.2	79.6	3	2
40	930	52.7	117.9	146.2	8.0	9.2	11	12.7	Central 5	P	0	930	50.7	113.4	140.6	4	4
41	930	52.3	117.0	145.1	17.7	20.4	11	12.7	Central 5	P	0	943	40.9	91.5	113.4	4	3
42	930	51.8	115.9	143.7	25.8	29.7	11	12.7	Central 5	P	0	951	38.3	85.7	106.2	4	3
43	900	57.2	128.0	158.7	6.0	6.9	11	12.7	Central 5	P	0	900	55.5	124.1	153.9	5	4
44	900	58	129.7	160.9	14.9	17.1	11	12.7	Central 5	P	0	910	48.2	107.8	133.7	5	4
45	900	57.6	128.8	159.8	21.8	25.1	11	12.7	Central 5	P	0	918	46.1	103.1	127.9	5	3
46	960	44.3	99.1	122.9	18.2	20.9	11	12.7	SE 1	P	-45	974	33.0	73.8	91.5	3	2
47	960	43.5	97.3	120.7	24.6	28.3	11	12.7	SE 1	P	-45	980	30.5	68.2	84.6	3	2
48	900	58.3	130.4	161.7	12.5	14.4	11	12.7	SE 1	P	-45	909	55.6	124.4	154.2	5	4
49	900	58.1	130.0	161.2	18.4	21.2	11	12.7	SE 1	P	-45	920	46.3	103.6	128.4	5	3
50	960	44.2	98.9	122.6	18.2	20.9	11	12.7	SE 2	P	-45	974	33.2	74.3	92.1	3	2
51	960	43.3	96.9	120.1	24.6	28.3	11	12.7	SE 2	P	-45	980	30.5	68.2	84.6	3	2
52	900	58.2	130.2	161.4	12.5	14.4	11	12.7	SE 2	P	-45	909	55.4	123.9	153.7	5	4
53	900	58	129.7	160.9	18.4	21.2	11	12.7	SE 2	P	-45	920	46.2	103.3	128.1	5	3
54	960	43.8	98.0	121.5	18.2	20.9	11	12.7	SE 3	P	-45	974	33.0	73.8	91.5	3	2
55	960	43.1	96.4	119.6	24.6	28.3	11	12.7	SE 3	P	-45	980	30.5	68.2	84.6	3	2
56	900	58	129.7	160.9	12.5	14.4	11	12.7	SE 3	P	-45	909	55.5	124.1	153.9	5	4
57	900	57.5	128.6	159.5	18.4	21.2	11	12.7	SE 3	P	-45	920	46.2	103.3	128.1	5	3
58	960	43.6	97.5	120.9	18.2	20.9	11	12.7	SE 4	P	-45	974	32.9	73.6	91.3	3	2

IPET Documentation

No.	Storm Frequency per yr	GoM CP mb	Rmax nm	Vf kn	Holland's B	Track angle at landfall	Track Identifer
1	7.90E-04	960	11	11	1.27	0	1
2	9.19E-04	960	21	11	1.27	0	1
3	4.92E-04	960	35.6	11	1.27	0	1
4	2.50E-03	930	8	11	1.27	0	1
5	2.73E-03	930	17.7	11	1.27	0	1
6	2.30E-03	930	25.8	11	1.27	0	1
7	1.13E-03	900	6	11	1.27	0	1
8	1.39E-03	900	14.9	11	1.27	0	1
9	3.46E-04	900	21.8	11	1.27	0	1
10	7.90E-04	960	11	11	1.27	0	2
11	9.19E-04	960	21	11	1.27	0	2
12	4.92E-04	960	35.6	11	1.27	0	2
13	2.50E-03	930	8	11	1.27	0	2
14	2.73E-03	930	17.7	11	1.27	0	2
15	2.30E-03	930	25.8	11	1.27	0	2
16	1.13E-03	900	6	11	1.27	0	2
17	1.39E-03	900	14.9	11	1.27	0	2
18	3.46E-04	900	21.8	11	1.27	0	2
19	7.90E-04	960	11	11	1.27	0	3
20	9.19E-04	960	21	11	1.27	0	3
21	4.92E-04	960	35.6	11	1.27	0	3
22	2.50E-03	930	8	11	1.27	0	3
23	2.73E-03	930	17.7	11	1.27	0	3
24	2.30E-03	930	25.8	11	1.27	0	3
25	1.13E-03	900	6	11	1.27	0	3
26	1.39E-03	900	14.9	11	1.27	0	3
27	3.46E-04	900	21.8	11	1.27	0	3
28	7.90E-04	960	11	11	1.27	0	4
29	9.19E-04	960	21	11	1.27	0	4
30	4.92E-04	960	35.6	11	1.27	0	4
31	2.50E-03	930	8	11	1.27	0	4
32	2.73E-03	930	17.7	11	1.27	0	4
33	2.30E-03	930	25.8	11	1.27	0	4
34	1.13E-03	900	6	11	1.27	0	4
35	1.39E-03	900	14.9	11	1.27	0	4
36	3.46E-04	900	21.8	11	1.27	0	4
37	7.90E-04	960	11	11	1.27	0	5
38	9.19E-04	960	21	11	1.27	0	5
39	4.92E-04	960	35.6	11	1.27	0	5
40	2.50E-03	930	8	11	1.27	0	5
41	2.73E-03	930	17.7	11	1.27	0	5
42	2.30E-03	930	25.8	11	1.27	0	5
43	1.13E-03	900	6	11	1.27	0	5
44	1.39E-03	900	14.9	11	1.27	0	5
45	3.46E-04	900	21.8	11	1.27	0	5
46	3.50E-04	960	18.2	11	1.27	-45	1
47	3.90E-04	960	24.6	11	1.27	-45	1
48	7.16E-04	900	12.5	11	1.27	-45	1
49	5.48E-04	900	18.4	11	1.27	-45	1
50	3.50E-04	960	18.2	11	1.27	-45	2
51	3.90E-04	960	24.6	11	1.27	-45	2
52	7.16E-04	900	12.5	11	1.27	-45	2
53	5.48E-04	900	18.4	11	1.27	-45	2
54	3.50E-04	960	18.2	11	1.27	-45	3
55	3.90E-04	960	24.6	11	1.27	-45	3
56	7.16E-04	900	12.5	11	1.27	-45	3
57	5.48E-04	900	18.4	11	1.27	-45	3
58	3.50E-04	960	18.2	11	1.27	-45	4.1

Southeast Louisiana JPM-OS Hurricanes

FIS Documentation

No.	GoM CP mb	Peak GoM Winds 30 min (m/s)	30 min (mph)	1-min (mph)	Rmax nm	Rmax mile	Vf kn	Vf mph	Track	P or S	θ	Landfall CP mb	Peak Landfall Winds 30 min (m/s)	30 min (mph)	1-min (mph)	SS Category GoM	SS Category Landfall
59	960	42.9	96.0	119.0	24.6	28.3	11	12.7	SE 4	P	-45	980	30.4	68.0	84.3	3	2
60	900	57.8	129.3	160.3	12.5	14.4	11	12.7	SE 4	P	-45	909	55.3	123.7	153.4	5	4
61	900	57.6	128.8	159.8	18.4	21.2	11	12.7	SE 4	P	-45	920	46.3	103.6	128.4	5	3
66	960	44.4	99.3	123.2	18.2	20.9	11	12.7	SW 1	P	45	974	32.7	73.1	90.7	3	2
67	960	42.9	96.0	119.0	24.6	28.3	11	12.7	SW 1	P	45	980	30.1	67.3	83.5	3	2
68	900	58.8	131.5	163.1	12.5	14.4	11	12.7	SW 1	P	45	909	55.7	124.6	154.5	5	4
69	900	58.3	130.4	161.7	18.4	21.2	11	12.7	SW 1	P	45	920	46.1	103.1	127.9	5	3
70	960	44.2	98.9	122.6	18.2	20.9	11	12.7	SW 2	P	45	974	32.7	73.1	90.7	3	2
71	960	43.6	97.5	120.9	24.6	28.3	11	12.7	SW 2	P	45	980	30.1	67.3	83.5	3	2
72	900	58.6	131.1	162.5	12.5	14.4	11	12.7	SW 2	P	45	909	55.4	123.9	153.7	5	4
73	900	58.2	130.2	161.4	18.4	21.2	11	12.7	SW 2	P	45	920	45.8	102.5	127.0	5	3
74	960	44.1	98.6	122.3	18.2	20.9	11	12.7	SW 3	P	45	974	32.5	72.7	90.1	3	2
75	960	43.6	97.5	120.9	24.6	28.3	11	12.7	SW 3	P	45	980	29.9	66.9	82.9	3	2
76	900	58.6	131.1	162.5	12.5	14.4	11	12.7	SW 3	P	45	909	55.1	123.3	152.8	5	4
77	900	58.2	130.2	161.4	18.4	21.2	11	12.7	SW 3	P	45	920	45.6	102.0	126.5	5	3
Total																	
78	960	44.1	98.6	122.3	18.2	20.9	11	12.7	SW 4	P	45	974	32.6	72.9	90.4	3	2
79	960	43.6	97.5	120.9	24.6	28.3	11	12.7	SW 4	P	45	980	30.0	67.1	83.2	3	2
80	900	58.6	131.1	162.5	12.5	14.4	11	12.7	SW 4	P	45	909	54.9	122.8	152.3	5	4
81	900	58.2	130.2	161.4	18.4	21.2	11	12.7	SW 4	P	45	920	45.7	102.2	126.8	5	3
82	960	40.4	90.4	112.1	17.7	20.4	6	6.9	Central 1	P	0	973	30.5	68.2	84.6	3	2
83	900	55.6	124.4	154.2	17.7	20.4	6	6.9	Central 1	P	0	913	45.5	101.8	126.2	4	3
84	960	40.5	90.6	112.3	17.7	20.4	6	6.9	Central 2	P	0	973	30.5	68.2	84.6	3	2
85	900	55.7	124.6	154.5	17.7	20.4	6	6.9	Central 2	P	0	913	45.5	101.8	126.2	4	3
86	960	40.3	90.1	111.8	17.7	20.4	6	6.9	Central 3	P	0	973	30.3	67.8	84.0	3	2
87	900	55.5	124.1	153.9	17.7	20.4	6	6.9	Central 3	P	0	913	45.2	101.1	125.4	4	3
88	960	40.5	90.6	112.3	17.7	20.4	6	6.9	Central 4	P	0	973	30.2	67.6	83.8	3	2
89	900	55.8	124.8	154.8	17.7	20.4	6	6.9	Central 4	P	0	913	45.3	101.3	125.7	4	3
90	960	40.4	90.4	112.1	17.7	20.4	6	6.9	Central 5	P	0	973	30.0	67.1	83.2	3	2
91	900	55.5	124.1	153.9	17.7	20.4	6	6.9	Central 5	P	0	913	45.1	100.9	125.1	4	3
92	930	48.8	109.2	135.4	17.7	20.4	6	6.9	SE 1	P	-45	946	37.6	84.1	104.3	4	3
93	930	48.9	109.4	135.6	17.7	20.4	6	6.9	SE 2	P	-45	946	37.6	84.1	104.3	4	3
94	930	48.8	109.2	135.4	17.7	20.4	6	6.9	SE 3	P	-45	946	37.5	83.9	104.0	4	3
95	930	48.7	108.9	135.1	17.7	20.4	6	6.9	SE 4	P	-45	946	37.6	84.1	104.3	4	3
97	930	49.3	110.3	136.7	17.7	20.4	6	6.9	SW 1	P	45	946	37.3	83.4	103.5	4	3
98	930	49.2	110.1	136.5	17.7	20.4	6	6.9	SW 2	P	45	946	37.3	83.4	103.5	4	3
99	930	49.3	110.3	136.7	17.7	20.4	6	6.9	SW 3	P	45	946	37.3	83.4	103.5	4	3
100	930	49.3	110.3	136.7	17.7	20.4	6	6.9	SW 4	P	45	946	37.2	83.2	103.2	4	3
101	930	55.9	125.0	155.1	17.7	20.4	17	19.6	Central 1	P	0	944	45.0	100.7	124.8	4	3
102	930	55.8	124.8	154.8	17.7	20.4	17	19.6	Central 2	P	0	944	44.8	100.2	124.3	4	3
103	930	56	125.3	155.3	17.7	20.4	17	19.6	Central 3	P	0	944	44.9	100.4	124.5	4	3
104	930	56	125.3	155.3	17.7	20.4	17	19.6	Central 4	P	0	944	44.5	99.5	123.4	4	3
105	930	56	125.3	155.3	17.7	20.4	17	19.6	Central 5	P	0	944	44.2	98.9	122.6	4	3
106	930	55.9	125.0	155.1	17.7	20.4	17	19.6	SE 1	P	-45	946	44.1	98.6	122.3	4	3
107	930	55.7	124.6	154.5	17.7	20.4	17	19.6	SE 2	P	-45	946	44.3	99.1	122.9	4	3
108	930	55.8	124.8	154.8	17.7	20.4	17	19.6	SE 3	P	-45	946	44.2	98.9	122.6	4	3
109	930	55.4	123.9	153.7	17.7	20.4	17	19.6	SE 4	P	-45	946	44.0	98.4	122.0	4	3

IPET Documentation

No.	Storm Frequency per yr	GoM CP mb	Rmax nm	Vf kn	Holland's B	Track angle at landfall	Track Identifer
59	3.90E-04	960	24.6	11	1.27	-45	4.1
60	7.16E-04	900	12.5	11	1.27	-45	4.1
61	5.48E-04	900	18.4	11	1.27	-45	4.1
63	2.50E-04	960	24.6	11	1.27	45	1
64	3.02E-04	900	12.5	11	1.27	45	1
65	2.01E-04	900	18.4	11	1.27	45	1
66	1.54E-04	960	18.2	11	1.27	45	2
67	2.50E-04	960	24.6	11	1.27	45	2
68	3.02E-04	900	12.5	11	1.27	45	2
69	2.01E-04	900	18.4	11	1.27	45	2
70	1.54E-04	960	18.2	11	1.27	45	3
71	2.50E-04	960	24.6	11	1.27	45	3
72	3.02E-04	900	12.5	11	1.27	45	3
73	2.01E-04	900	18.4	11	1.27	45	3
74	1.54E-04	960	18.2	11	1.27	45	4
75	2.50E-04	960	24.6	11	1.27	45	4
76	3.02E-04	900	12.5	11	1.27	45	4
77	2.01E-04	900	18.4	11	1.27	45	4
76	**7.45E-02**						
62	Not Provided	960	18.2	11	1.27	45	1

IPET 63, 64, 65 appear to be FIS 79, 80, 81

No.	Storm Frequency per yr	GoM CP mb	Rmax nm	Vf kn	Holland's B	Track angle at landfall	Track Identifer
78	Not Provided	960	17.7	6	1.27	0	1
79	Not Provided	900	17.7	6	1.27	0	1
80	Not Provided	960	17.7	6	1.27	0	2
81	Not Provided	900	17.7	6	1.27	0	2
82	Not Provided	960	17.7	6	1.27	0	3
83	Not Provided	900	17.7	6	1.27	0	3
84	Not Provided	960	17.7	6	1.27	0	4
85	Not Provided	900	17.7	6	1.27	0	4
86	Not Provided	960	17.7	6	1.27	0	5
87	Not Provided	900	17.7	6	1.27	0	5
88	Not Provided	930	17.7	6	1.27	-45	1
89	Not Provided	930	17.7	6	1.27	-45	2
90	Not Provided	930	17.7	6	1.27	-45	3
91	Not Provided	930	17.7	6	1.27	-45	4.1
92	Not Provided	930	17.7	6	1.27	45	1
93	Not Provided	930	17.7	6	1.27	45	2
94	Not Provided	930	17.7	6	1.27	45	3
95	Not Provided	930	17.7	6	1.27	45	4
96	Not Provided	930	17.7	17	1.27	0	1
97	Not Provided	930	17.7	17	1.27	0	2
98	Not Provided	930	17.7	17	1.27	0	3
99	Not Provided	930	17.7	17	1.27	0	4
100	Not Provided	930	17.7	17	1.27	0	5
101	Not Provided	930	17.7	17	1.27	-45	1
102	Not Provided	930	17.7	17	1.27	-45	2
103	Not Provided	930	17.7	17	1.27	-45	3
104	Not Provided	930	17.7	17	1.27	-45	4.1

Southeast Louisiana JPM-OS Hurricanes

FIS Documentation

No.	GoM CP mb	Peak GoM Winds 30 min (m/s)	30 min (mph)	1-min (mph)	Rmax nm	Rmax mile	Vf kn	Vf mph	Track	P or S	θ	Landfall CP mb	Peak Landfall Winds 30 min (m/s)	30 min (mph)	1-min (mph)	SS Category GoM	SS Category Landfall
111	930	56.2	125.7	155.9	17.7	20.4	17	19.6	SW 1	P	45	946	43.7	97.8	121.2	4	3
112	930	56	125.3	155.3	17.7	20.4	17	19.6	SW 2	P	45	946	43.4	97.1	120.4	4	3
113	930	56.1	125.5	155.6	17.7	20.4	17	19.6	SW 3	P	45	946	43.3	96.9	120.1	4	3
114	930	56	125.3	155.3	17.7	20.4	17	19.6	SW 4	P	45	946	43.6	97.5	120.9	4	3
115	960	44.2	98.9	122.6	17.7	20.4	11	12.7	Central 1b	S	0	973	33.0	73.8	91.5	3	2
116	900	58.2	130.2	161.4	17.7	20.4	11	12.7	Central 1b	S	0	913	47.6	106.5	132.0	5	4
117	960	44.2	98.9	122.6	17.7	20.4	11	12.7	Central 2b	S	0	973	33.1	74.0	91.8	3	2
118	900	58	129.7	160.9	17.7	20.4	11	12.7	Central 2b	S	0	913	47.8	106.9	132.6	5	4
119	960	44.2	98.9	122.6	17.7	20.4	11	12.7	Central 3b	S	0	973	33.3	74.5	92.4	3	2
120	900	58	129.7	160.9	17.7	20.4	11	12.7	Central 3b	S	0	913	48.0	107.4	133.1	5	4
121	960	44.1	98.6	122.3	17.7	20.4	11	12.7	Central 4b	S	0	973	33.1	74.0	91.8	3	2
122	900	58	129.7	160.9	17.7	20.4	11	12.7	Central 4b	S	0	913	47.7	106.7	132.3	5	4
123	960	44.1	98.6	122.3	17.7	20.4	11	12.7	SE 1b	S	-45	974	33.3	74.5	92.4	3	2
124	960	43.8	98.0	121.5	17.7	20.4	11	12.7	SE 2b	S	-45	974	33.1	74.0	91.8	3	2
125	960	43.7	97.8	121.2	17.7	20.4	11	12.7	SE 3b	S	-45	974	32.7	73.1	90.7	3	2
126	900	58	129.7	160.9	17.7	20.4	11	12.7	SE 1b	S	-45	919	46.4	103.8	128.7	5	3
127	900	57.9	129.5	160.6	17.7	20.4	11	12.7	SE 2b	S	-45	919	46.5	104.0	129.0	5	3
128	900	57.8	129.3	160.3	17.7	20.4	11	12.7	SE 3b	S	-45	919	45.8	102.5	127.0	5	3
131	960	44.2	98.9	122.6	17.7	20.4	11	12.7	SW 1b	S	45	974	32.9	73.6	91.3	3	2
132	900	58.3	130.4	161.7	17.7	20.4	11	12.7	SW 1b	S	45	919	46.0	102.9	127.6	5	3
133	960	44.2	98.9	122.6	17.7	20.4	11	12.7	SW 2b	S	45	974	32.8	73.4	91.0	3	2
134	900	58.3	130.4	161.7	17.7	20.4	11	12.7	SW 2b	S	45	919	45.8	102.5	127.0	5	3
135	960	44.2	98.9	122.6	17.7	20.4	11	12.7	SW 3b	S	45	974	32.9	73.6	91.3	3	2
136	900	58.3	130.4	161.7	17.7	20.4	11	12.7	SW 3b	S	45	919	45.8	102.5	127.0	5	3
137	960	40.5	90.6	112.3	17.7	20.4	6	6.9	Central 1b	S	0	973	30.1	67.3	83.5	3	2
138	900	55.6	124.4	154.2	17.7	20.4	6	6.9	Central 1b	S	0	913	45.1	100.9	125.1	4	3
139	960	40.4	90.4	112.1	17.7	20.4	6	6.9	Central 2b	S	0	973	30.0	67.1	83.2	3	2
140	900	55.7	124.6	154.5	17.7	20.4	6	6.9	Central 2b	S	0	913	45.1	100.9	125.1	4	3
141	960	40.3	90.1	111.8	17.7	20.4	6	6.9	Central 3b	S	0	973	30.2	67.6	83.8	3	2
142	900	55.6	124.4	154.2	17.7	20.4	6	6.9	Central 3b	S	0	913	45.3	101.3	125.7	4	3
143	960	40.6	90.8	112.6	17.7	20.4	6	6.9	Central 4b	S	0	973	29.9	66.9	82.9	3	2
144	900	55.8	124.8	154.8	17.7	20.4	6	6.9	Central 4b	S	0	913	45.0	100.7	124.8	4	3
145	930	48.8	109.2	135.4	17.7	20.4	6	6.9	SE 1b	S	-45	946	37.5	83.9	104.0	4	3
146	930	48.9	109.4	135.6	17.7	20.4	6	6.9	SE 2b	S	-45	946	37.6	84.1	104.3	4	3
147	930	48.8	109.2	135.4	17.7	20.4	6	6.9	SE 3b	S	-45	946	37.2	83.2	103.2	4	3
149	930	49.3	110.3	136.7	17.7	20.4	6	6.9	SW 1b	S	45	946	37.3	83.4	103.5	4	3
150	930	49.4	110.5	137.0	17.7	20.4	6	6.9	SW 2b	S	45	946	37.0	82.8	102.6	4	3
151	930	49.4	110.5	137.0	17.7	20.4	6	6.9	SW 3b	S	45	946	37.5	83.9	104.0	4	3
152	930	55.8	124.8	154.8	17.7	20.4	17	19.6	Central 1b	S	0	944	44.7	100.0	124.0	4	3
153	930	55.8	124.8	154.8	17.7	20.4	17	19.6	Central 2b	S	0	944	44.5	99.5	123.4	4	3
154	930	55.9	125.0	155.1	17.7	20.4	17	19.6	Central 3b	S	0	944	44.8	100.2	124.3	4	3
155	930	56	125.3	155.3	17.7	20.4	17	19.6	Central 4b	S	0	944	44.6	99.8	123.7	4	3
156	930	55.9	125.0	155.1	17.7	20.4	17	19.6	SE 1b	S	-45	946	44.3	99.1	122.9	4	3
157	930	55.6	124.4	154.2	17.7	20.4	17	19.6	SE 2b	S	-45	946	44.1	98.6	122.3	4	3
158	930	55.3	123.7	153.4	17.7	20.4	17	19.6	SE 3b	S	-45	950	42.9	96.0	119.0	4	3
160	930	56	125.3	155.3	17.7	20.4	17	19.6	SW 1b	S	45	946	43.6	97.5	120.9	4	3
161	930	56.2	125.7	155.9	17.7	20.4	17	19.6	SW 2b	S	45	946	43.6	97.5	120.9	4	3
162	930	55.9	125.0	155.1	17.7	20.4	17	19.6	SW 3b	S	45	946	43.9	98.2	121.8	4	3
Total	**152**																

	in GoM	at Landfall
Number of Category 1	**0**	**0**
Number of Category 2	**0**	**45**
Number of Category 3	**50**	**80**
Number of Category 4	**61**	**27**
Number of Category 5	**41**	**0**

IPET Documentation

No.	Storm Frequency per yr	GoM CP mb	Rmax nm	Vf kn	Holland's B	Track angle at landfall	Track Identifer
105	Not Provided	930	17.7	17	1.27	45	1
106	Not Provided	930	17.7	17	1.27	45	2
107	Not Provided	930	17.7	17	1.27	45	3
108	Not Provided	930	17.7	17	1.27	45	4
109	Not Provided	960	17.7	11	1.27	0	1.5
110	Not Provided	900	17.7	11	1.27	0	1.5
111	Not Provided	960	17.7	11	1.27	0	2.5
112	Not Provided	900	17.7	11	1.27	0	2.5
113	Not Provided	960	17.7	11	1.27	0	3.5
114	Not Provided	900	17.7	11	1.27	0	3.5
115	Not Provided	960	17.7	11	1.27	0	4.5
116	Not Provided	900	17.7	11	1.27	0	4.5
117	Not Provided	960	17.7	11	1.27	-45	1.5
118	Not Provided	960	17.7	11	1.27	-45	1.5
119	Not Provided	960	17.7	11	1.27	-45	2.5
120	Not Provided	900	17.7	11	1.27	-45	2.5
121	Not Provided	900	17.7	11	1.27	-45	3.5
122	Not Provided	900	17.7	11	1.27	-45	3.5
123	Not Provided	960	17.7	11	1.27	45	1.5
124	Not Provided	900	17.7	11	1.27	45	1.5
125	Not Provided	960	17.7	11	1.27	45	2.5
126	Not Provided	900	17.7	11	1.27	45	2.5
127	Not Provided	960	17.7	11	1.27	45	3.5
128	Not Provided	900	17.7	11	1.27	45	3.5
129	Not Provided	960	17.7	6	1.27	0	1.5
130	Not Provided	900	17.7	6	1.27	0	1.5
131	Not Provided	960	17.7	6	1.27	0	2.5
132	Not Provided	900	17.7	6	1.27	0	2.5
133	Not Provided	960	17.7	6	1.27	0	3.5
134	Not Provided	900	17.7	6	1.27	0	3.5
135	Not Provided	960	17.7	6	1.27	0	4.5
136	Not Provided	900	17.7	6	1.27	0	4.5
137	Not Provided	930	17.7	6	1.27	-45	1.5
138	Not Provided	930	17.7	6	1.27	-45	2.5
139	Not Provided	930	17.7	6	1.27	-45	3.5
140	Not Provided	930	17.7	6	1.27	45	1.5
141	Not Provided	930	17.7	6	1.27	45	2.5
142	Not Provided	930	17.7	6	1.27	45	3.5
143	Not Provided	930	17.7	17	1.27	0	1.5
144	Not Provided	930	17.7	17	1.27	0	2.5
145	Not Provided	930	17.7	17	1.27	0	3.5
146	Not Provided	930	17.7	17	1.27	0	4.5
147	Not Provided	930	17.7	17	1.27	-45	1.5
148	Not Provided	930	17.7	17	1.27	-45	2.5
149	Not Provided	930	17.7	17	1.27	-45	3.5
150	Not Provided	930	17.7	17	1.27	45	1.5
151	Not Provided	930	17.7	17	1.27	45	2.5
152	Not Provided	930	17.7	17	1.27	45	3.5

Part IV.

Hurricane Surge Hazard Analysis for Polders

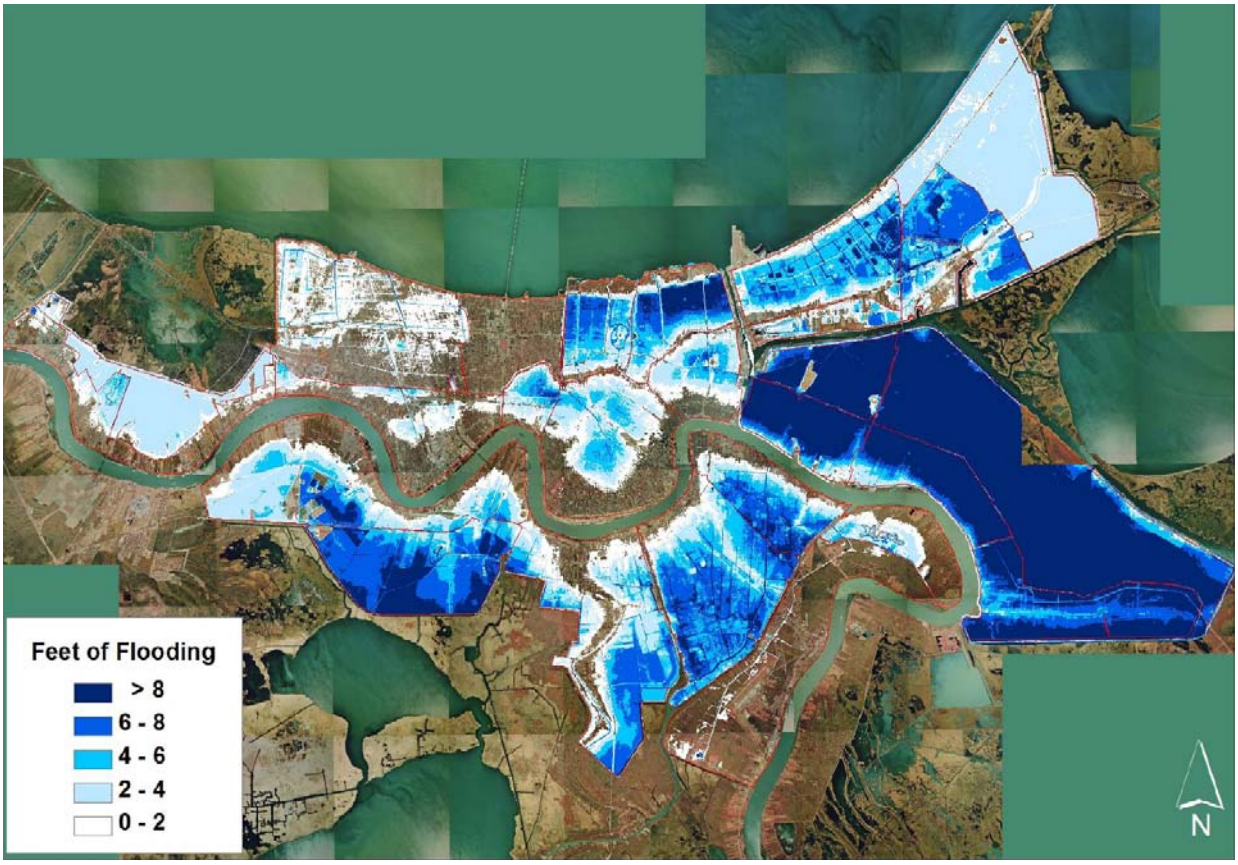

IPET 2009a

Critical urban portions of the New Orleans Metropolitan Area in southeast Louisiana are surrounded by federally or locally sponsored hurricane surge protection systems (see Figure 15.1). Such perimeter systems can have lengths approaching one hundred miles, enclosing large polders[1] encompassing many tens of thousands of acres. Inundation hazards for these polders are exacerbated by interior drainage and reduced water tables, which lead to oxidation and consolidation/compression of the organic deltaic soils, causing the internal topography to subside well below LMSL.

Each perimeter system is comprised of numerous reaches, with various structures—e.g., earthen levees, floodwalls, and gates. The individual reaches within polder systems can be exposed to markedly different storm surge hazards. Eastern portions of the New Orleans regional system are oriented towards Breton Sound, Lake Borgne, and the "funnel" described in Section 7. Northern parts of the system face the massive Lake Pontchartrain, with Jefferson and Orleans Parish reaches located along the open lake but St. Charles Parish segments fronted by miles of degrading cypress swamps. Southern reaches on the west-bank are sheltered by the expansive but eroding coastal marshes of Barataria Bay. Furthermore, the entire system is bifurcated by Mississippi River levees.

As discussed in Part II, Subpart A, the surge dynamics of individual hurricane can produce highly variable SWL and wave conditions around polder perimeters. Importantly, the particular surge hazard level posed by an individual storm can vary dramatically along the system. For example, for east-bank New Orleans Hurricane Katrina produced an extreme surge hazard near the "funnel"—possibly exceeding a 500-yr event, a 100-yr surge along the central Lake Pontchartrain south shore, but well under a 100-yr surge event at the western end of the Lake Pontchartrain south shore. Part III discussed the technical approaches to evaluating the variable surge hazard outside of polders.

The assessment of polder interior surge inundation hazards—i.e. the return frequency of particular surge-induced flood levels at any location inside the perimeter system—is further complicated by additional hydrologic/hydraulic processes associated with storm-specific perimeter inflows, rainfall, forced drainage performance, internal flood routing, and interior wind setup and wave . Critical polder inundation processes—especially breach inflow but also rainfall and pumping—are also conditioned on probabilities, requiring a sophisticated expanded JPA to determine interior inundation hazards.

This Part IV reviews the current state of the practice in hurricane surge polder inundation hazard analysis, including the following subjects:

> Section 15., deterministic and probabilistic methods for examining polder hydrologic/hydraulic processes;
>
> Section 16., expanding the JPA to combine the exterior hurricane surge hazard with the additional polder inundation processes and probabilities; and
>
> Section 17., recent applications of the hurricane surge polder inundation hazard analysis, including IPET's 2009 post-Katrina risk and reliability study, the USACE's 2009 CPR Study, and the USACE's HSDRRS 100-yr and resiliency design and residual risk assessment.

In addition to examining the approaches established in the current literature, these sections expand on methodology requirements, assumptions, and limitations based on sound scientific and engineering practice. Afterwards, a list of conclusions is presented, together with recommendations for improving hurricane surge polder inundation analyses. Part V addresses technical approaches to evaluating hurricane surge hazard for future conditions and surge estimates for selected storm-scenarios.

---

[1] *Polder* is a Dutch word for low-lying area protected from coastal flooding by an encircling barrier.

Section 15. Additional Hydrologic and Hydraulic Analysis

Figure 15.1 depicts the four main New Orleans area federally sponsored HSDRRS polders—Metro New Orleans, New Orleans East, Lower 9th Ward/St. Bernard Polder, and West Bank. Flooding of polders during a hurricane surge event occurs through eight hydrologic/hydraulic processes:

1. The storm surge dynamics producing the exterior surge SWL and wave conditions;
2. Seepage perimeter inflows;
3. Overtopping perimeter inflows;
4. Breach perimeter inflows;
5. Rainfall accumulation;
6. Drainage pumping outflows;
7. Internal routing of the time-varying and location-specific perimeter inflows, rainfall, and pumping outflows; and
8. Local wind-induced interior setup and waves.

The following sections describe additional analyses for quantifying these eight processes, including limitations and uncertainties associated with each analysis.

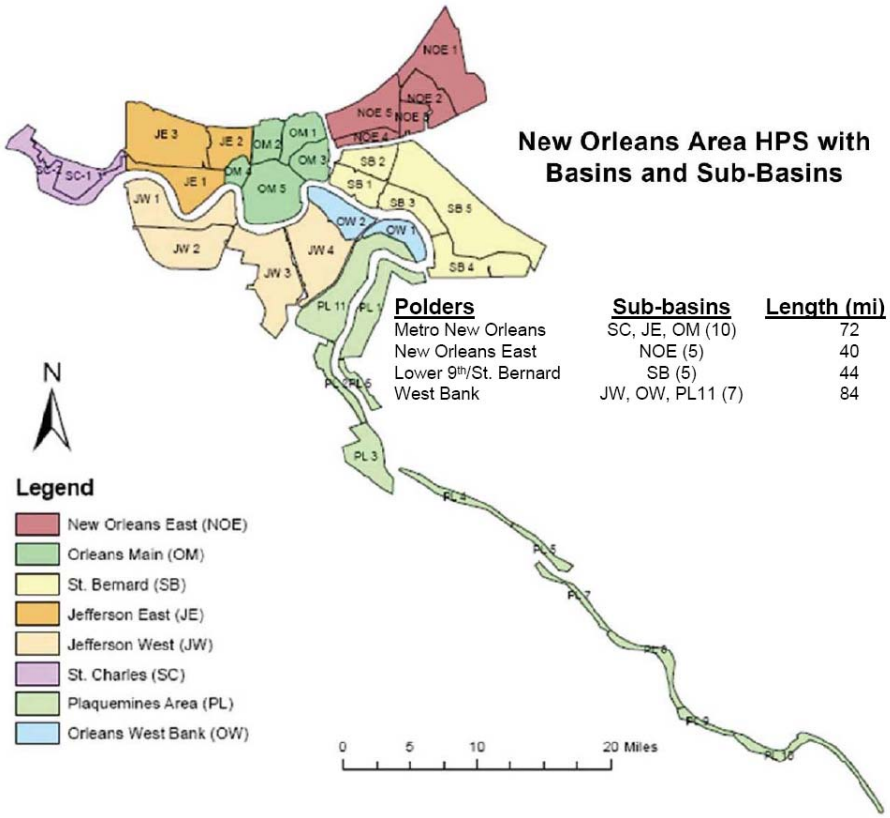

Figure 15.1. New Orleans Area Polders and Sub-Basins

IPET 2009a

15.1 Perimeter Surge SWL and Wave Conditions

The three polder perimeter inflows—seepage, overtopping, and breaching—are dependent on the exterior surge SWL. The physics of surge SWL are described Part II, Subpart A. Time-varying physics for hindcast and synthetic storms (e.g., for a surge JPA) are evaluated with a high resolution 2D hydrodynamic model as described in Subpart B. The rise, peak, and fall in surge SWL (i.e., hydrograph) is often compared to the barrier crown elevation in terms of the *freeboard* (equal to the crown elevation minus SWL)—the value is positive when SWL is below the structure crown and negative when SWL is above the crown.

Detailed time-series results from the high resolution 2D surge model are expensive to output and retain. Thus, model output is often limited to peak SWL at all mesh nodes, with time-series at selected locations. To construct a hydrograph for additional perimeter locations a curve shape can be assumed and curve coefficients obtained from those model hydrographs retained. For example, a Normal Distribution type curve can be used, with separate σ_R and σ_F values for the rising and falling hydrograph limb (IPET 2009). If a Surge-Response relationship is being used to evaluate a range of hurricane conditions, the values of σ_R and σ_F can also be developed as functions of the perimeter location and storm parameters.

Overtopping and breaching inflows are also dependent on the local wave conditions (H_S, T_P, and direction). As discussed in Section 5.1, storm surge wave fields are irregular, with a Rayleigh Distribution typically used to describe the relative statistical frequency of different wave heights (e.g., $H_{50\%}$, H_s, $H_{1\%}$, and $H_{0.1\%}$). This distribution is appropriate for a long-term steady wave field, such as for slow-moving weak storms, which can sustain intensity while stalled over many hours. However, more intense storms tend to decay and only sustain local peak conditions for a few hours. In the latter case, the Rayleigh Distribution may not describe the relationship between various wave heights—i.e., the ratio of $H_{1\%}$:H_S may be somewhat lower. The assumption of a Rayleigh Distribution for extreme storms would likely therefore be conservative. To date there have been no studies suggesting alternative distributions for hurricane surge wave fields.

Wave characteristics undergo successive transformations as they pass through different zones, illustrated in Figure 15.2:

A. Open water—including the GoM and large, open coastal sounds, bays, and lakes. The high resolution 2D surge model, coupled with a linear wave model, provides a reasonable analysis of transformations in H_S, T_P, and θ in Zone A (see Section 10.2).

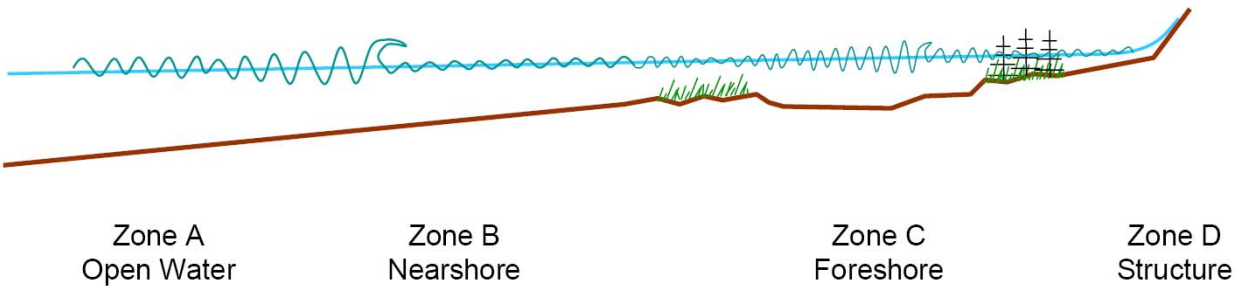

Figure 15.2. Transformation of Waves Approaching a Perimeter Barrier
(Not to scale)

B. Nearshore—this zone includes bathymetry-driven shoaling, breaking, refraction, and diffraction of the open water waves, modifying H_S, T_P, θ, and associated radiation stress. The wave models coupled with the high resolution surge model are intended to capture most of these processes. However, as noted in Section-6.2, little surge wave data exists for evaluating these models.

C. Inundated foreshore zone between the water body and the barrier. This zone can extend just a few hundred feet, (e.g., along the Lake Pontchartrain south shore) or many miles (e.g., east-bank St. Charles Parish and West Bank). Foreshore regions can include a wide variety of landscapes at a range of distances: open interior water; marsh at various states of integrity and inundation; forested wetlands/swamps, some with modestly elevated ridges; coastal communities; etc. The landscape friction applies varying amounts of energy dampening to the wave fields. The greatest perimeter wave heights generally occur at those barriers that are within a short distance of deeper open water, and where the foreshore provides for little or no shoaling/breaking at the peak SWL. However, as surge SWL rises higher waves can pass into the foreshore region. Given sufficient local winds, inundation, and open fetch, the foreshore wave field can regenerate to H_S of several feet. Importantly, as waves move through Zones B and C they become increasingly asymmetric—with disproportionate crests/troughs (amplitude above SWL > amplitude below SWL) and profiles.

D. The Structure, from the outside toe to the structure crest. The zone usually includes a compound sloping embankment, with 100 ft or more of gentle sloping outer embankment (e.g., 10:1 to 20:1) followed by a steeper main embankment (e.g., 4:1 for the actually levee or floodwall support). The outer embankment may include shoreline armoring which can aid in wave breaking, berms, and other features. During inundation of this zone wave heights are typically reduced at the transition from the foreshore to the outer slope, and again at the transition from the outer to the main embankment, by the rapid changes in surge depth.

The wave conditions across and along perimeter Zones C/D are not covered by the high resolution surge SWL-wave coupled model for either hindcast or synthetic storms. While values for Zones C/D wave T_P and θ[1] are generally regarded as consistent from Zone A/B, wave heights can change significantly. Therefore, reach-specific, storm-specific wave height analysis is required for Zones C/D. Four approaches are:

1. Employ a ceiling criteria—termed breaker parameter (or index)—limiting the ratio of H_S to the surge depth. Values ranging from 40 to 70% may be considered. As noted in Section 6.2, Kennedy found a ratio of 50% for observed nearshore waves along the Texas coast during Hurricane Ike. However, there is very little published data on appropriate limiting ratios for the highly asymmetric wave conditions in Zones C/D. Importantly, a ceiling ratio may over- or under-estimate H_S. depending on actual local storm wind conditions.
2. Use WHAFIS where simple 1D, steady-state analysis of wave transformations is adequate.

[1] Wave periods can also be assumed based on literature values. For a worst case analysis a perpendicular wave direction (to the perimeter structure) is usually assumed, although this may not be consistent with the orientation of the nearby water body fetch.

3. Model foreshore waves with STWAVE or SWAN for more complex cases requiring analysis of unsteady 2D processes, but still assuming linear (symmetric) wave processes.
4. For non-linear wave processes utilize higher-order Boussinesq model.

There is currently no technical literature providing a thorough validation of WHAFIS, STWAVE, SWAN, or Boussinesq models for Zones C/D during hurricane surge events.

Use of WHAFIS, STWAVE, SWAN, or Boussinesq models for Zones C/D wave analysis can be facilitated by programming one-way loose coupling of foreshore models with the high resolution Zone A/B surge-wave model (to automate input of SWLs, currents, and wave boundary conditions at suitable time steps). If the local Zones C/D wave conditions imply significant modification of local radiation stress gradients, and influence on local SWL setdowns and setups, further two-way loose coupling with the high resolution 2D surge model may be required. To date there have been no publications addressing such two-way coupling Zones A/B modeling with Zones C/D wave analysis and it is considered beyond the current state-of the-practice.

15.2 Seepage

Perimeter seepage can occur along reaches which are penetrated by highly permeable subterranean flow paths. The most significant type of flow path is a broad, naturally occurring sand layer beneath the local area. The shallow subsurface geology of southeastern Louisiana is known to include such sand layers. A major example is the Pine Island buried beach complex in the New Orleans area near Lake Pontchartrain, shown in Figure 15.3.

Water pressure in the subsurface sand layer will naturally build as the SWL rises on the exterior-side of the barrier. The pressure difference between the flood and interior sides within the sand layer will then induce sand layer groundwater to flow underneath the barrier toward the interior. The high porosity, and hence permeability, of the sand layer will cause the subsurface pressure to rapidly rise at the protected side. Such a rapid transmission of the external subsurface pore-water pressure to the internal side does not occur in areas where the barrier is underlain by low permeability soils (e.g., clay).

The high interior-side pressure in the sand layer will induce the groundwater to seek flow paths to the surface. Natural variations in the overlying interior strata can lead to a “piping” type flow to the surface. Rising flow rates along a higher permeability conduit to the surface can “flush the pipe,” widening it, and accelerating seepage flow to the surface. At points where the sand is only a few feet below the surface, the pressure may be sufficient to push the sand through the overlying soil. This phenomenon, often described as a “sand boil,” is common along the Mississippi River levee during high river stages[2]. “Piping” and “sand boil” flows to the surface can initiate in locations where the interior ground surface is very low and can be enhanced by man-made penetrations—such as sand-filled (or poorly-filled) excavations (e.g., building foundations and infrastructure trenches).

[2] Over the course of many decades of experience with high Mississippi River stages, the USACE and local officials have identified most “sand boil” locations and therefore closely monitor them during river floods. They also employ precautionary measures to relieve the interior-side sand layer pressure, which prevents the sand boils from expanding and possibly leading to a river levee failure.

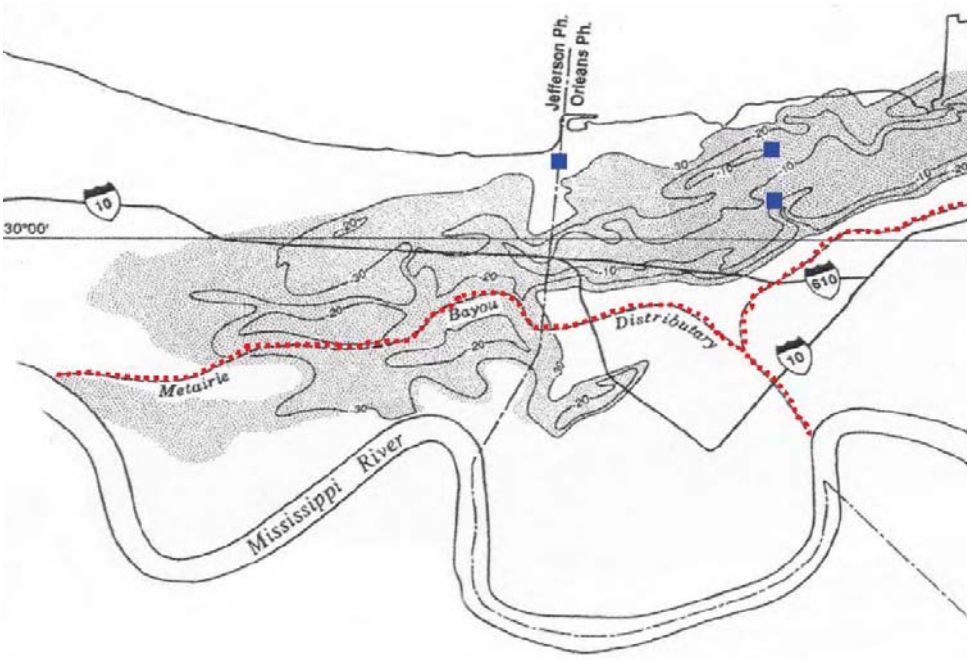

Figure 15.3. Pine Island Buried Beach Complex in the New Orleans Area

Contours are Depth Below Surface, ft; points show Hurricane Katrina Breaches
IPET 2006

In addition to seepage facilitated by natural sand layers, inflow can also occur along man-made preferential pathways underneath and within the barrier itself. Examples include:

- Legacy excavations underlying the barrier that pre-date barrier construction;
- The annular space around subsurface pipelines crossing underneath the barrier;
- Interconnected exterior and interior excavations in close proximity to the barrier—e.g., by natural subsurface "piping" pathways; and
- Material used in older levee embankments which over time allows for the formation of significant voids; such as non-cohesive soils which settle differentially within the embankment; degradable organic matter; and debris.[3]

During Hurricane Katrina a major "sand boil" occurred at the north and south ends of the London Avenue Canal. High surge entered the outfall canal from Lake Pontchartrain and induced flow in the Pine Island sand layer underneath the canal floodwall. The locations are noted on Figure 15.3, and Figure 15.4 presents a schematic of the northern sand boil. During Hurricane Katrina seepage was also suspected along the IHNC (ILIT 2006)

Researchers are investigating the use of remote geophysical sensing techniques to identify potentially significant natural and man-made seepage pathways, as well as the integrity of sheet pile "cut-off" walls used to reduce seepage. Important techniques include the use of ground

[3] Current design and construction practices attempt to greatly minimize the presence of potential void-forming materials (USACE 2008b).

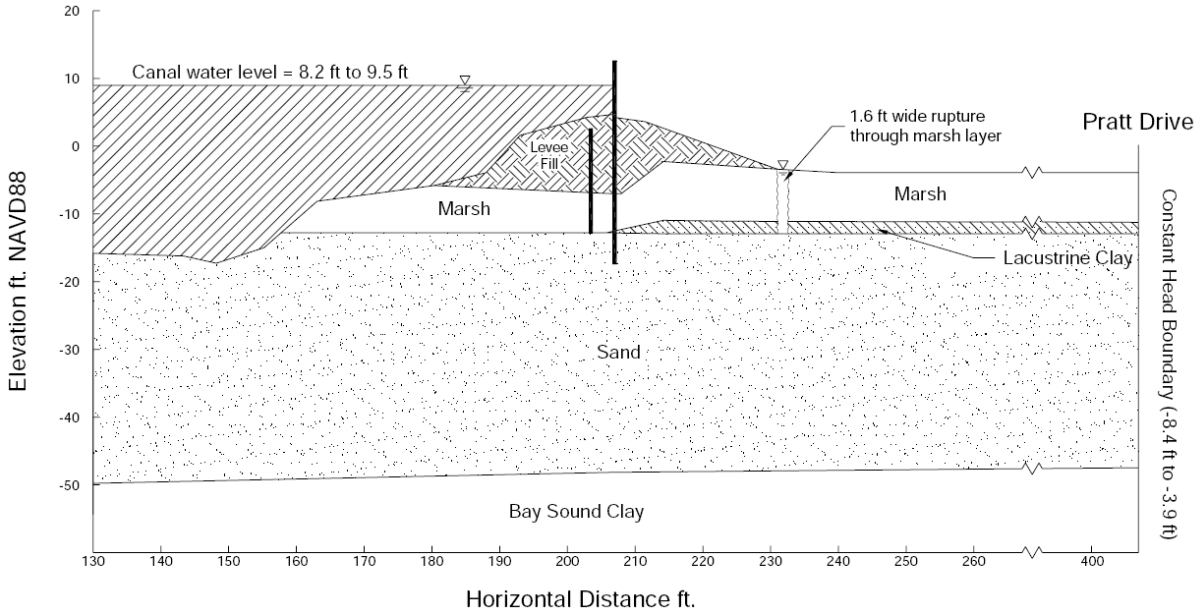

Figure 15.4. Cross Section at London Avenue North Floodwall Seepage Location
IPET 2006

penetrating radar,[4] soil electro-magnetic conductivity surveys, and shallow seismic profiling.[5] To date, techniques for identifying seepage paths have not been standardized, and a comprehensive data base of significant paths has not been compiled for southeastern Louisiana polder perimeter systems.

Techniques are available for estimating seepage discharge—which is proportional to the head loss and porosity along the flow path—given geologic and other data or assumptions. The techniques include analysis with flow nets and computer groundwater flow models. The interior discharge associated with a major seepage inflow can potentially exceed 0.1 acre-ft/hr (1.2 cfs) for several hours.[6]

While seepage inflow can contribute to localized interior inundation the cumulative volumes are much less than those associated with overtopping or breaching and generally do not pose a polder-wide inundation hazard. The more significant hazard from seepage is the potential contribution to a barrier breach, which is discussed below. Investigations have yet to be undertaken of potential seepage rates associated with hurricane surge for southeastern Louisiana polders and a detailed review of the techniques for quantifying seepage inflows alone is beyond the scope of this report.

---

[4] See the website for the Center for Nondestructive Evaluation, http://www.cnde.iastate.edu/research-areas/ground-penetrating-radar

[5] See the website for the LSU-UNO Levee Monitoring Group, http://lmg.uno.edu/

[6] Time-varying perimeter inflow rates (or discharges)—for seepage, overtopping, and breaching—are typically evaluated as volumetric rates per unit length along a particular reach (in units such as cubic feet per second, cfs, per linear foot, cfs/ft). An inflow rate of 1 cfs/ft over a length of 1 mile (or 5,280 cfs), over a period of 1 hour, accumulates to 436.4 acre-ft of water (1 foot of inundation over an area of 436 acres). At any point during a particular storm the inflow rate—and the cumulative inflow--will vary greatly by reach.

15.3 Overtopping

Figure 15.5, illustrates five phases of overtopping, with dramatically increasing overflow rates in succeeding phases:

1. The SWL and all Zone D wave crests are below the barrier crown (positive freeboard) but the elevation of wave runup for the more extreme waves (e.g., runup associated with Zone D wave heights ≥ H_S) on the barrier's exterior-side slope exceeds the barrier crown. Since waves arrive intermittently, runup overtopping may occur only a couple of times per minute. As the SWL rises and/or wave heights increase, the overtopping frequency and overflow increases.
2. The SWL is still below the barrier crown (positive freeboard) but some Zone D wave crests now exceed the crown. This second phase includes runup overtopping from a large percentage of waves plus direct overtopping from the higher Zone D waves. Figure 15.6 illustrates intermittent overtopping against the vertical floodwalls of the Inner Harbor Navigation Canal during Hurricane Gustav that appears to be in Phase 2. As the SWL rises and/or Zone D wave heights increase, more waves will directly overtop the barrier.
3. The surge SWL reaches the crown (zero freeboard) and all Zone D waves directly overtop the barrier. However, the overflow is still associated with the wave volume and overtopping briefly ceases when wave troughs reach the crown. As the SWL rises more wave troughs are above the crown and the overflow eventually becomes continuous.
4. The surge SWL is sufficiently above the crown (negative freeboard) for all Zone D wave troughs to exceed the crown. The overflow is now continuous but still has significant "pulsing."

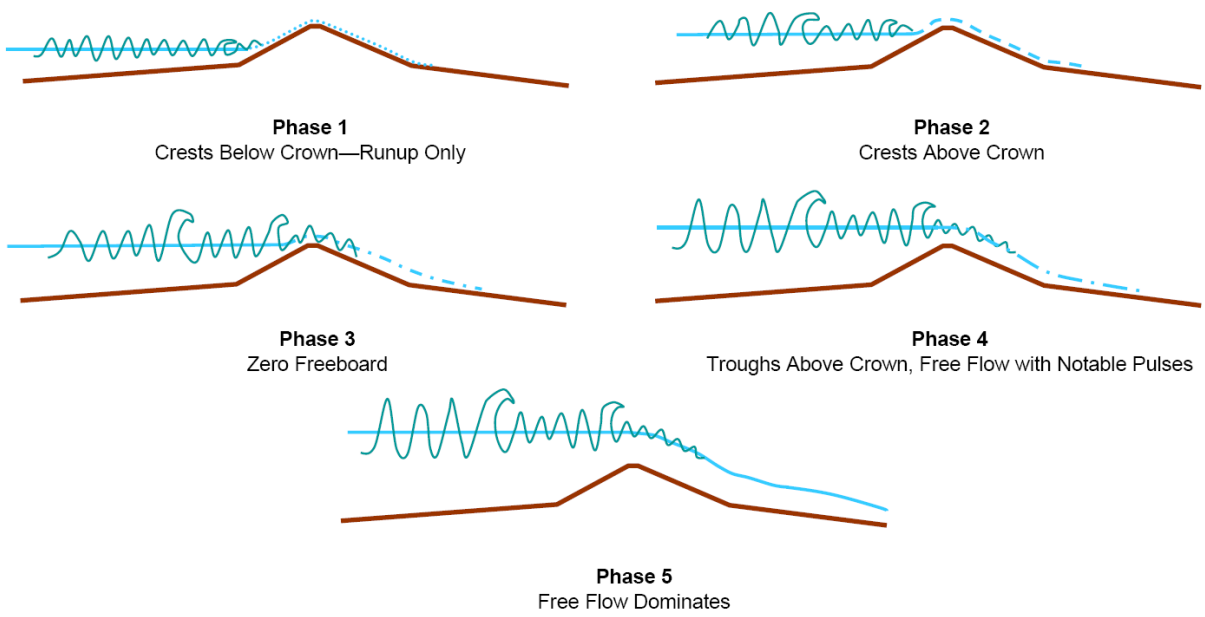

Figure 15.5. Five Phases of Barrier Overtopping
(Not to scale)

Figure 15.6. Phase 2 Overtopping of the IHNC Floodwall During Hurricane Gustav

Eliot Kamenitzd Times Picayune

5. As SWL continues to rise (as the freeboard becomes more negative) the overflow becomes more and more dominated by near-steady "weir flow," which dwarfs the variation from the Zone D waves.

When the surge peak passes, the overtopping phases are reversed.

Zone D waves at a highly sheltered barrier may exhibit very small amplitude (e.g., H_S<1 ft). In this case the SWL may need to rise very close to the barrier crown before any overflow occurs. A reach experiencing small waves and rapidly rising SWL, may see very limited Phases 1 through 4 overtopping, with overtopping transitioning quickly from zero to a near-steady discharge. Conversely, a reach experiencing larger waves with a slow decline in freeboard can experience more prolonged pulsing overflow associated with Phases 1 through 4.

The technical literature provides empirical expressions for quantifying an average overflow for the various phases—ignoring pulsing. To assess wave-only overtopping—Phase 1 through 3—researchers have conducted controlled wave runup and overtopping experiments with irregular wave fields. The USACE Coastal Engineering Manual (CEM) Part VI (USACE 2005), Chapter 5, Table VI-5-7 summarizes overtopping research for various barrier structures, including simple trapezoidal shaped levees with smooth impermeable surfaces, permeable rock structures, and floodwalls. An expression proposed by Van der Meer, described in the CEM Table VI-5-11, is typically used for wave-only overtopping of levees. CEM Tables VI-5-7 and VI-5-11 are reproduced as Tables 15.1 and 15.2.

Table 15.1. Empirical Overtopping Equations for Various Barriers

USACE 2005

Table VI-5-7
Models for Average Overtopping Discharge Formulae

Authors	Structures	Overtopping model	Dimensionless discharge Q	Dimensionless freeboard R
Owen (1980,1982)	Impermeable smooth, rough, straight and bermed slopes	$Q = a\ exp(-b\,R)$	$\frac{q}{g\,H_s\,T_{om}}$	$\frac{R_c}{H_s}\left(\frac{s_{om}}{2\,\pi}\right)^{0.5}\frac{1}{\gamma}$
Bradbury and Allsop (1988)	Rock armored impermeable slopes with crown walls	$Q = a\,R^{-b}$	$\frac{q}{g\,H_s\,T_{om}}$	$\left(\frac{R_c}{H_s}\right)^2\left(\frac{s_{om}}{2\,\pi}\right)^{0.5}$
Aminti and Franco (1988)	Rock, cube, and Tetrapod double layer armor on rather impermeable slopes with crown walls, (single sea state)	$Q = a\,R^{-b}$	$\frac{q}{g\,H_s\,T_{om}}$	$\left(\frac{R_c}{H_s}\right)^2\left(\frac{s_{om}}{2\,\pi}\right)^{0.5}$
Ahrens and Heimbaugh (1988b)	7 different seawall/revetment designs	$Q = a\,exp(-b\,R)$	$\frac{q}{\sqrt{g\,H_s^3}}$	$\frac{R_c}{(H_s^2\,L_{op})^{1/3}}$
Pedersen and Burcharth (1992)	Rock armored rather impermeable slopes with crown walls	$Q = a\,R$	$\frac{q\,T_{om}}{L_{om}^2}$	$\frac{H_s}{R_c}$
van der Meer and Janssen (1995)	Impermeable smooth, rough straight and bermed slopes	$Q = a\,exp(-b\,R)$	$\frac{q}{\sqrt{g\,H_s^3}}\sqrt{\frac{s_{op}}{\tan\alpha}}$ for $\xi_{op} < 2$ $\frac{q}{\sqrt{g\,H_s^3}}$ for $\xi_{op} > 2$	$\frac{R_c}{H_s}\frac{\sqrt{s_{op}}}{\tan\alpha}\frac{1}{\gamma}$ for $\xi_{op} < 2$ $\frac{R_c}{H_s}\frac{1}{\gamma}$ for $\xi_{op} > 2$
Franco et al. (1994)	Vertical wall breakwater with and without perforated front	$Q = a\,exp(-b\,R)$	$\frac{q}{\sqrt{g\,H_s^3}}$	$\frac{R_c}{H_s}\frac{1}{\gamma}$
Pedersen (1996)	Rock armored permeable slopes with crown walls	$Q = R$	$\frac{q\,T_{om}}{L_{om}^2}$	$3.2\cdot 10^{-5}\frac{H_s^5\,\tan\alpha}{R_c^3\,A_c\cdot B}$

Table 15.2. Van der Meer Empirical Overtopping Equation for Levees

USACE 2005

Table VI-5-11
Overtopping Formula by van der Meer and Janssen (1995)

Straight and bermed impermeable slopes including influence of surface roughness, shallow foreshore, oblique, and short-crested waves, Figures VI-5-14a and VI-5-14b.

$\xi_{op} < 2$

$$\frac{q}{\sqrt{g\,H_s^3}}\sqrt{\frac{s_{op}}{\tan\alpha}} = 0.06\,exp\left(-5.2\,\frac{R_c}{H_s}\,\frac{\sqrt{s_{op}}}{\tan\alpha}\,\frac{1}{\gamma_r\,\gamma_b\,\gamma_h\,\gamma_\beta}\right) \qquad \text{(VI−5−24)}$$

application range: $0.3 < \dfrac{R_c}{H_s}\,\dfrac{\sqrt{s_{op}}}{\tan\alpha}\,\dfrac{1}{\gamma_r\,\gamma_b\,\gamma_h\,\gamma_\beta} < 2$

Uncertainty: Standard deviation of factor 5.2 is $\sigma = 0.55$ (See Figure VI-5-15).

$\xi_{op} > 2$

$$\frac{q}{\sqrt{g\,H_s^3}} = 0.2\,exp\left(-2.6\,\frac{R_c}{H_s}\,\frac{1}{\gamma_r\,\gamma_b\,\gamma_h\,\gamma_\beta}\right) \qquad \text{(VI−5−25)}$$

Uncertainty: Standard deviation of factor 2.6 is $\sigma = 0.35$ (See Figure VI-5-15).

The reduction factors references are

γ_r Table VI-5-3

γ_b Eq VI-5-8

γ_h Eq VI-5-10

Short-crested waves

$\gamma_\beta = 1 - 0.0033\,\beta$

Long-crested waves (swell)

$$\gamma_\beta = \begin{cases} 1.0 & \text{for } 0° \le \beta \le 10° \\ \cos^2(\beta - 10°) & \text{for } 10° < \beta \le 50° \\ 0.6 & \text{for } \beta > 50° \end{cases} \qquad \text{(VI−5−26)}$$

The minimum value of any combination of the γ-factors is 0.5.

In the Van der Meer equation the average discharge per unit barrier length, q, is a function of

- The Zone D wave height, H_S ;
- Freeboard, R_c (R_c/H_S is termed the relative freeboard);
- Slope of the levee floodside bank, tan α;
- Peak open water (deepwater, pre-shoaling) wave steepness, S_{op} (equal H_S divided by wave length L_o); the ratio of the levee slope to wave steepness, tan α/S_{op}, is termed the surf similarity parameter, ξ_{op}; slightly different equations are used for $\xi_{op}<2$ and $\xi_{op}>2$; and
- Reduction factors (or transmission coefficients) to account for slope roughness, fronting berm, shallow Zone D, and wave incident angle, γ_r, γ_b, γ_h, γ_β . (The combined factor is typically not less than 0.5).

As R_c declines toward 0, the exp term in Table 15.2 converges to 1 and

$$q = C_{wave}\sqrt{H_s^{\,3}}$$

C_{wave} is a lumped transmission coefficient for wave overtopping. For large ξ_{op} (steeper levee slope relative to wave face) C_{wave} approaches 1.1. For smaller ξ_{op} C_{wave} is much less than 1.

The technical literature suggests that these empirical equations for average wave overtopping while useful have significant uncertainty. Figure 15.7 illustrates the uncertainty for the Van Der Meer equation. Note that the overflow on the y-axis is presented on a logarithmic scale. Importantly, there are no data, and thus no empirical studies, for wave-only overtopping during brief, intense hurricane surge events. This implies considerable uncertainties *in addition to* the kind illustrated in Figure 15.7. For example, overtopping estimates are highly sensitive to the assumed breaker parameter. In the Van der Meer equation a 20% increase in H_S. from 5 to 6 ft with R_c of 1 ft and ξ_{op} of 2, with all γ at 1, translates into a 46% increase in overtopping discharge. Another source of uncertainty is the assumption of a Rayleigh Distribution, which may tend to over-estimate extreme wave frequency and associated overtopping.

For negative freeboard and negligible waves the average barrier overflow, q, is typically given using a version of the standard equation for steady supercritical flow over a broad-crested weir:

$$q = C\sqrt{|R_c|^3}$$

where the absolute value of the negative freeboard is the height in ft of the SWL above the barrier crest. Typical values of the weir transmission coefficient, C, range from 1 to 3.1 ($ft^{½}/s$).[7] Thus, for Phase 3 at a large ξ_{op} the average wave overflow for a levee is equivalent a simple broad-crested weir overflow at a low transmission factor, using $|R_c|$ equal to H_S.

[7] Another version of the broad crested weir equation derived directly from basic hydraulics is $q = \frac{2}{3}C^*\sqrt{2g|Rc|^3}$,

thus $C = \frac{2}{3}C^*\sqrt{2g}$

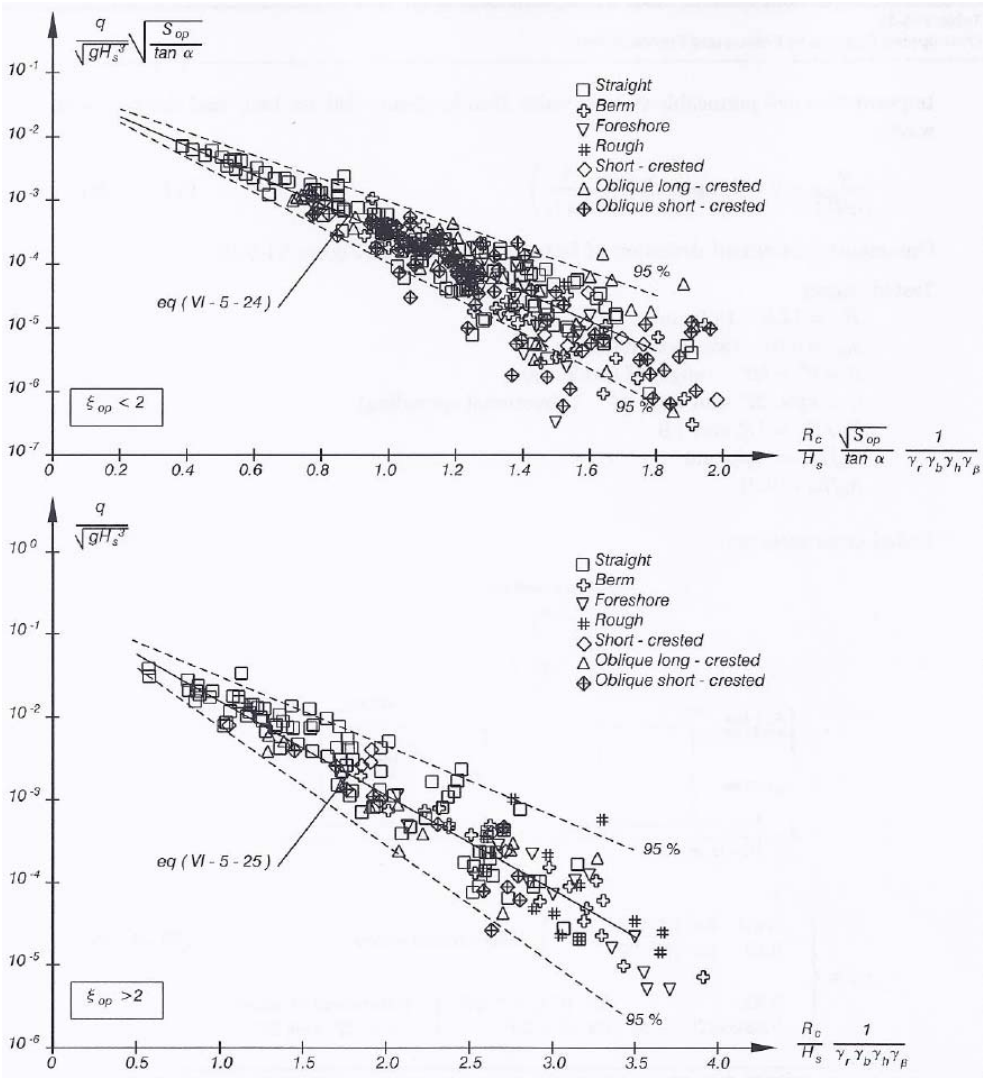

Figure 15.7. Van der Meer Empirical Wave Overtopping Equation for Levees with Confidence Bands

Van der Meer and Jannssen, 1995 in USACE 2005

For Phases 4 and 5, levee overflow can be estimated using the sum of two broad crested weir formulas, one with H_S and the other with $|R_c|$ for $R_c<0$, and each with their respective transmission factors:

$$q = C_w \sqrt{H_s^{\,3}} + C\sqrt{|R_c|^3}$$

Thus, as SWL rises and $|R_c|>H_S$, the second equation will dominate the estimate of overflow. The broad-crested weir equation is typically used throughout rising/falling SWL during Phase 5 by modifying $|R_c|$. The steady overtopping flow using the broad-crested weir equation is been widely applied, but defining appropriate values for C for a wide variety of overtopped surge barriers has not been studied. The uncertainties in steady Phase 5 overtopping are not as high as for Phase 1 and 2 wave-only overtopping. A range of ±25% in the value of C translates to a ±25% range in the discharge rate.

In 2010 Lynette et al employed Boussinesq modeling to aid in simulating the initial average wave overtopping along the MRGO during Hurricane Katrina. Noting that Hurricane Katrina wave heights along the MRGO generally correlated to freeboard, they provided a simple empirical equation for the average overflow as a function of R_c encompassing all five phases:

$$q \approx 0 \ for \ R_c > 0.75m$$
$$q = 0.17(R_c) + 0.13 \ for \ 0.75m > R_c \geq 0$$
$$q = 0.48\sqrt{g|R_c|^3} + 0.13 \ for \ R_c < 0$$

Figure 15.8 compares the above equation to the MRGO Boussinesq model output. Figure 15.9 presents the average overflow on a log-scale and more clearly illustrates the overflow by phase. Dashed lines have been included on Figure 15.9 to depict overflow associated with smaller waves.

As shown in Figure 15.9, overtopping can begin to contribute significantly to polder inundation when freeboard turn negative, with accumulations reaching 610 acre-ft/hour per mile (equivalent to 1.4 cfs/ft) at zero freeboard. During Hurricane Katrina the New Orleans East Polder was inundated largely due to overtopping inflow (IPET 2009). High overtopping rates have also been associated with the interior-side embankment scour and the additional hazard of barrier breaching, discussed further below.

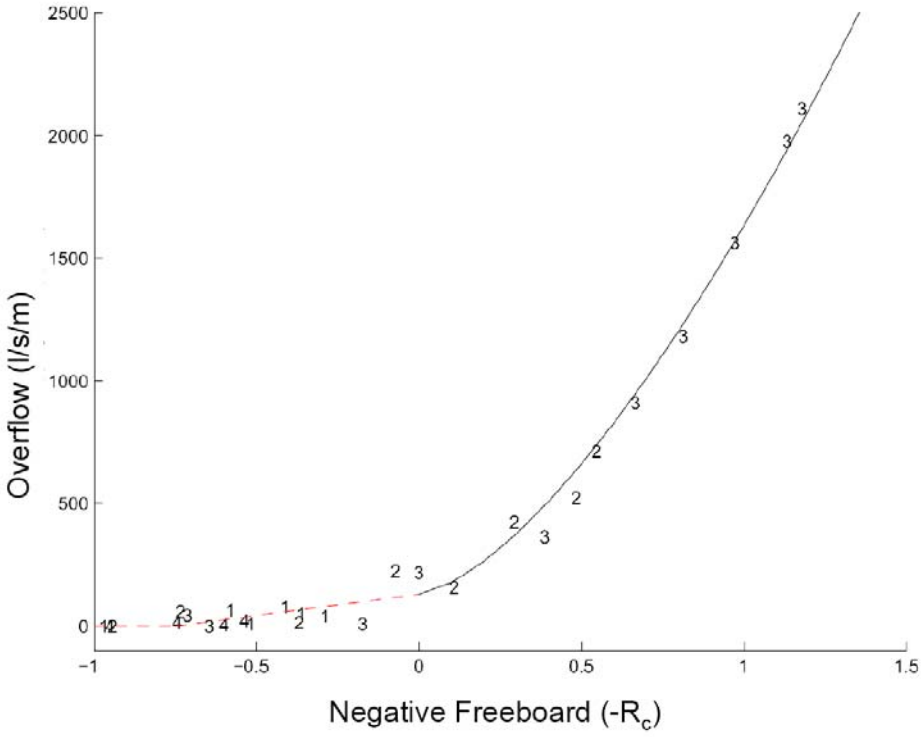

Figure 15.8. Modelled MRGO Levee Overtopping versus Simple Equation
Lynett et al 2010

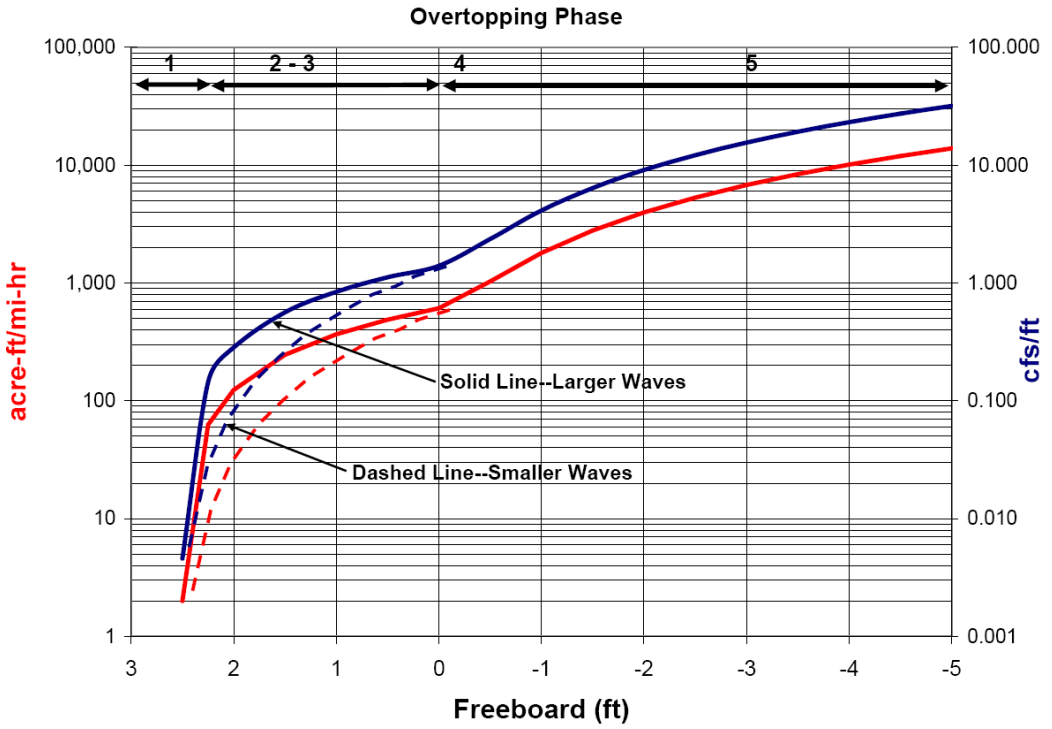

Figure 15.9. Simple Overtopping by Phase

based on Lynett et al 2010

As noted above, when wave contributions to overtopping are significant the overflow is not steady but pulsates. The variability in the instantaneous overflow discharge can be extreme, with peak rates more than 100 times the average (USACE CEM p., VI-5-19), exacerbating potential protected-side scour and breach hazards. In 2008 Hughes reviewed the empirical equations for wave-only overtopping and provided additional equations for determining overflow depth and velocity exceedance levels along the interior slope. In one example Hughes showed that an average overtopping discharge of 0.1 cfs/ft could include a 50% exceedance velocity (the velocity exceeded by an average of 5 out of every 10 waves) of over 17 ft/s at a distance of 20 ft down the inside levee slope.

15.4 Breaching

Breaching dynamics are often quite complex and experts often disagree on the exact sequence and relative importance of various contributing mechanisms.[8] While a detailed discussion of breach processes is beyond scope of this report, a brief overview is warranted.

Breaching is a failure to some degree in the integrity of a polder perimeter barrier which allows a significant increase in surge inflow that would not have otherwise occurred during seepage or overtopping. Two important broad categories of breaches are those *with erosion and those without erosion, i.e., a pure collapse*. A third category includes unsecured openings, such as gates left open and

[8] For a further detailed assessment of Hurricane Katrina breaches see IPET 2006, ILIT 2006, and Team Louisiana 2006.

temporary barriers insufficient to withstanding exterior conditions. A variety of breach processes that occurred in Hurricane Katrina along New Orleans area perimeter system are shown in Figure 15.10.

Exterior- and interior-side erosion of soil on barrier embankment surfaces can lead directly to barrier breaching. Exterior-side erosion can occur with extremely high currents or current eddies (with velocities of several ft/s) acting along the embankment—in a manner similar to river bank erosion. Waves breaking and running up the exterior-side of an embankment can also cause erosion—in a manner similar to shoreline beach erosion (Figure 15.10.a). On the protected side, free-falling water over steep walls or crowns and accelerating down-slope overflows can quickly erode soils (Figures 15.10.b, c, d, e, and f).

Both exterior- and interior-side erosion can be exacerbated by the presence of weak, non-cohesive soils; exposed soil surfaces (e.g., due to absence of well-rooted vegetated cover or armoring); and transitions. Transitions—such as embankment slope changes (e.g., at the toe of the interior slope) and interfaces between soil embankments and other structures (e.g., exposed concrete or steel walls, aprons, pads, footings, piers, pipes, etc.)—create localized horizontal and vertical turbulence zones containing much higher velocities easily capable of initiating erosion; (Figure 15.10.e; the presence of the pipe rack and vehicle traffic over the levee were also hypothesized as pre-storm subsidence and erosion of the local crown, making this point vulnerable to overtopping).

Wherever the velocities of exterior currents and waves or interior overflow exceed erosion thresholds soil scour can begin. Once surface scour starts, the underlying soils are exposed to rapid erosion (e.g., from high velocity in the scour scar) and the initial opening can be quickly expanded. At critical weak points, both exterior- and interior-side erosion breaches can easily proceed from initial scour to a major crown breach in less than an hour.

If local conditions focus intense wave energy at a location, exterior-side erosion can lead to crown sloughing, creating a breach to rising surge. This type of failure has been hypothesized for portions of the MRGO levee during Hurricane Katrina (see Figure 15.10.a), ILIT 2006). During levee overtopping, interior-side erosion (which often starts at the slope transition at the toe of the slope) can rapidly scour upslope—referred to as “head cutting”—until it reaches the crown, where the erosion can then widen and deepen a breach (Figure 15.10.b). The USACE hypothesized that interior-side erosion led to most of the MRGO levee breaches (IPET 2006).

During pulsing overflow the high velocities associated with peaks can induce erosion (Figure 15.10.c and d). Along with the pulsating overflow rate, the depth and velocities of the overtopping vary widely on the barrier protected-side slope. Rapid depth and velocity changes can also produce sudden pressure changes on the wetted surface—including cavitation effects that can initiate erosion in soils with weak cohesive strength.

Breaches can also occur in the absence of erosion due to component movement and collapse. The component may be a floodwall, a supporting foundation structure (e.g., footing, pile member, etc.), a soil embankment, or even the natural underlying or adjacent soil. A crucial cause of movement is the differential static water pressure acting on the exterior and interior sides of the component, which at some magnitude can exceed the strength of the component and its related support to resist movement. When beyond strength tolerances, the magnitude of the differential pressure and associated movement can proceed in accelerating, exacerbating, increments. In the case of a vertical floodwall with a vertical sheet-pile support (termed an “I-wall”) when exterior-side SWLs exceed tolerances the wall can start to deflect, causing a further increase in stress, and then a further deflection and so on rapidly leading to a critical point of sudden and catastrophic collapse (Figure 15.10.g and h). The USACE considered this the primary contributing factor in the 17th St. Canal floodwall failure.(IPET 2006).

a. MRGO South Levee Erosion from Waves (ILIT 2006)

b. Overtopping Scar and Breach Initiation at New Orleans East Lakefront (Suhayda and Jacobsen 2005)

Figure 15.10. Breach Processes Illustrated During Hurricane Katrina

c. Pulsing Overtopping Flow at GIWW North Levee (IPET 2006)

d. Same Location Showing Erosion, No Breach (IPET 2006)

Figure 15.10. Breach Processes Illustrated During Hurricane Katrina (Continued)

e. Scour of Mississippi River West Bank at BP Refinery Pipe Rack (Jacobsen 2006)

f. Interior-Side Scour from Overtopped I-Wall, with Deflection, IHNC East (IPET 2006)

Figure 15.10. Breach Processes Illustrated During Hurricane Katrina (Continued)

g. I-Wall Deflection on London Ave Canal, No Overtopping (IPET 2006)

h. Translation of 17th St. Canal East I-Wall (IPET 2006)

Figure 15.10. Breach Processes Illustrated During Hurricane Katrina (Continued)

Barrier soil components—the barrier's underlying foundation, the barrier itself (in the case of an embankment), and the earth at the barrier's interior toe—are important supports to motion resistance. Reductions in either soil density or internal cohesion can weaken resistance to uplift (or "heaving") and lateral sliding. The sand boils at the London Avenue Canal floodwall breaches are an example of this failure mode.

Levee interior-side scour can remove significant mass to the point that slopes or interior toe foundations fail before crown erosion occurs. Similarly, floodwall interior-side scour from free-fall overtopping can weaken the interior soil's support of the wall, precipitating or exacerbating deflection and collapse. The USACE suggested that interior erosion was a major factor in a floodwall collapse along the eastern IHNC floodwall just north of the Claiborne Avenue bridge.

Natural and man-made seepage pathways can allow the rapid transmission of exterior-side water pressures through the groundwater, creating higher pore-water pressures in protected-side foundation soils, and causing them to expand and weaken. A separate floodwall breach on the eastern IHNC near Florida Avenue, which occurred during Hurricane Katrina hours before SWL reached overtopping levels, was found to be associated with seepage induced interior soil movement (IPET 2006).

Engineers employ "failure rules" for basic breaching mechanisms that can be applied to individual reaches/transitions. These failure rules describe the conditions—i.e., breach invert and length (I-L)—that would result at reach due to the various location-specific factors in combination with the time-varying exterior SWL. The location-specific factors can be summarized as:

a. Type—levee, I-wall, T-wall, gate, levee-floodwall transition, etc.;

b. Critical Design Features—elevation, embankment soil type (e.g., clay versus hydraulic fill), slopes, pile depths, etc.; and

c. Reach Geology—depth and permeability of seepage zones; depth, density, and cohesive strength of overlying soils; presence of seepage pathways; etc.

A failure rule for seepage induced breaching could specify I-L as a function of estimated soil pore water pressures at the interior barrier toe. These pressures would be estimated using the reach-specific geology information and the exterior and interior SWLs. A failure rule for erosion or collapse breaching at reach with given location-specific factors might specify breach I-L as a "step function" of R_c—with a lower I resulting from increasingly negative freeboard to some limit. A very simple breach failure rule would be to specify only a single step—e.g., a single I-L for each reach based on the peak exterior SWL.

Rather than specifying an absolute I-L step or steps, the failure rules can be written to account for uncertainty in each step. For example, the probability of a particular I-L step can start at 0 and become 1.0 as the negative freeboard worsens beyond the step threshold R_c. (For each exterior SWL the sum of all failure condition probabilities, including the no failure condition, must equal 1.0). The relationship between the probability of failure and the negative freeboard can be depicted in a "fragility curve" (or set of tabulated values). Figure 15.11 illustrates the concept of a fragility curve. Failure conditions and fragility curves can also be expanded to incorporate wave conditions and interior SWL.

At this time there is very limited empirical research for quantifying failure rules and probabilities (fragility expressions). As a result, polder inundation hazard analyses relying on these techniques primarily qualify as planning (or "what if") exercises.

For a polder-wide inundation analysis breach discharge can be estimated with stepped changes in the broad-crested weir equation. Most significant breach flow can be regarded as Phase 5 overflow (negative $\boldsymbol{R_c}$) and evaluated using the steady supercritical flow equation. The value of $|\boldsymbol{R_c}|$ will be

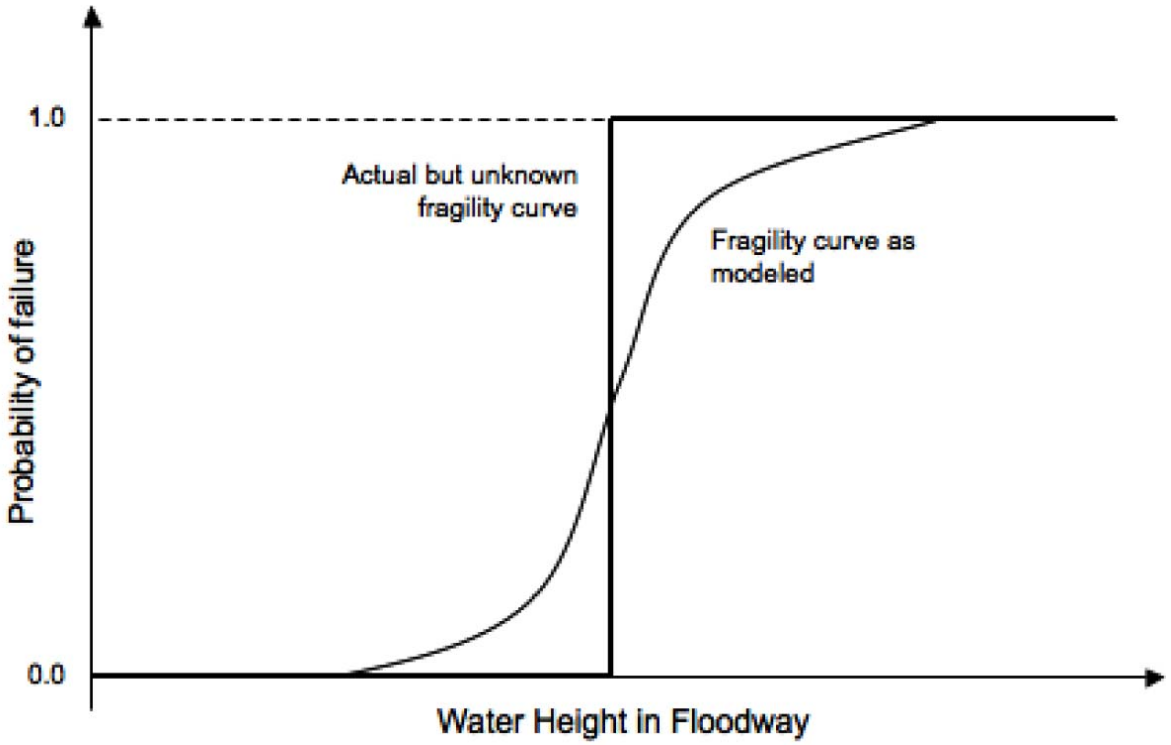

Figure 15.11. Concept of Fragility Curve For Breach Failure
IPET 2009

determined by the SWL and average breach invert. If the breach invert deepens over time (or as the exterior SWL changes), the value of $|R_c|$ can be adjusted accordingly.

As the interior SWL rises at some point the breach invert may be submerged (or "drowned"), in which case the inflow discharge will be affected by the interior tailwater elevation. A steady submerged flow equation for a broad-crested weir can be applied that takes into account both the exterior and interior SWL height above the breach invert—i.e., $|R_{c\text{-Exterior}}|$ and $|R_{c\text{-Interior}}|$ at the breach. The Villemonte equation for submerged flow equation multiplies the supercritical equation by a second transmission factor, C':

$$C' = \left[1 - \left(\frac{R_{c-Interio\ r}}{R_{c-Exterior}}\right)^{1.5}\right]^{0.385}$$

Another version of the submerged weir flow equation is

$$q = C_{sub}\,|R_{c\text{-Interior}}|\sqrt{2g\left(\left|R_{c-Exterior}\right| - \left|R_{c-Interior}\right|\right)}$$

which is used for $|R_{c\text{-Interior}}| > 0.667|R_{c\text{-Exterior}}|$.(ADCIRC Development Group, http://www.adcirc.org). This equation uses a separate submerged transmission coefficient, C_{sub}:

Submerged and supercritical broad-crested weir equations can also be used to analyze breach outflows, which occurs when the exterior surge SWL falls below the internal SWL (i.e., $|R_{c\text{-Interior}}| > |R_{c\text{-Exterior}}|$).

The equations for supercritical and submerged breach discharge are highly sensitive to the choice of transmission coefficients. Appropriate values for levee or floodwall breach discharges have not been studied. Laboratory and field scale experimental data are needed to assess the fit of the broad-crested weir equations. In practice, lower transmission coefficients are applicable for breaches than for overtopping of a pre-breach barrier due to much rougher openings.

The above methods for analyzing polder-wide inundation are not applicable to interior conditions in the vicinity of the breach, especially in the moments following a sudden collapse. Detailed hydraulic studies of these conditions—including shock waves—require specialized "dam break" type analysis.

A very simple failure rule is specifying an invert that remains continuously submerged, i.e., below the final exterior SWL. In this case the polder interior SWL eventually equalizes with the exterior SWL. This occurred in Orleans Parish portion of the Metro New Orleans Polder the day after Hurricane Katrina landfall due to the low breach inverts along the 17th Street and London Avenue canals. The interior sub-basins connected to these breaches equalized with Lake Pontchartrain at between 2.5 and 3.0 ft NAVD88. For a polder hazard analysis this simplification makes level-pool routing easy—i.e., it is not necessary to calculate inflow rates. However, this simplified rule cannot account for massive breaches with interior levels peaking at higher, earlier SWLs, such as with the Lower 9th Ward/St. Bernard polder which reached interior SWLs above 10 ft NAVD88 in many areas during Hurricane Katrina.

15.5 Rainfall Accumulation

Throughout the CN-GoM, major rainfall events have often been associated with tropical cyclones. Under weak meteorological steering conditions, the forward motion of lower intensity tropical cyclones may become very slow and erratic, leading to prolonged rainfall, as exemplified by Category 1 Hurricane Juan (1985), Tropical Storm Allison (2001), and Hurricane Isaac (2012) compared to Category 3 Hurricane Katrina (2005), shown in Figure 15.12. Tropical cyclone precipitation can vary widely over short distances, as illustrated by the rainfall totals in Figure 15.12. A major reason is the "training" of intense rainfall cells within bands circulating the storm core. In slow moving storms a band may continue to pass over a location for many hours, subjecting it to repeated downpours from passing cells, while sites less than 10 miles receive a fraction of the heaviest rainfall.

Precipitation amounts for actual storms are estimated by the National Weather Service using meteorological rainfall gauge stations and radar reflectivity data. Due to rainfall spatial variation and the scarcity of gauge stations, radar reflectivity often provides a better estimate of precipitation on a sub-basin scale.

Low-lying, poorly-drained coastal areas can experience large rainfall amounts in addition to surge. For areas outside of polders, rainfall accumulations need to be added to the surge routing model to determine the total SWL. High resolution 2D models—such as the ADCIRC model—are expected to include rainfall in the near future (see Section 10.1) [9]

[9] Rainfall from tropical cyclones further inland can produce major river flooding. In the floodplains surrounding a coastal river outlet the inundation levels may be influenced by three hydraulic processes: a) residual surge that has yet to fully recede; b) direct rainfall in the locale; and c) river discharge. This type of combined flooding recently occurred in lower Livingston, Ascension, and St. James parishes at the mouth of the Amite and Blind Rivers in Lake Maurepas following Hurricane Isaac (2102). High resolution 2D surge modeling capabilities for these complicated flood events are also being developed.

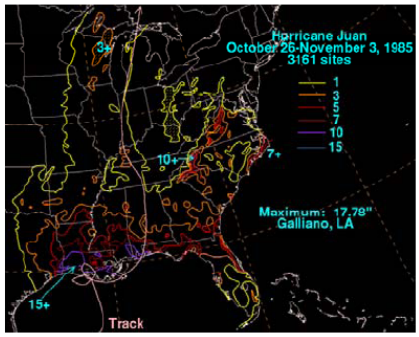

Hurricane Juan (1985)

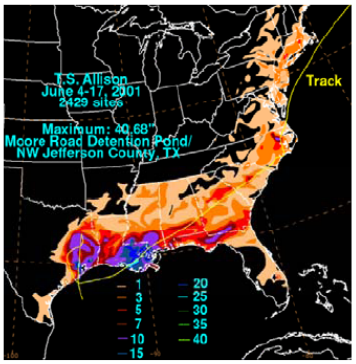

Tropical Storm Allison (2001)

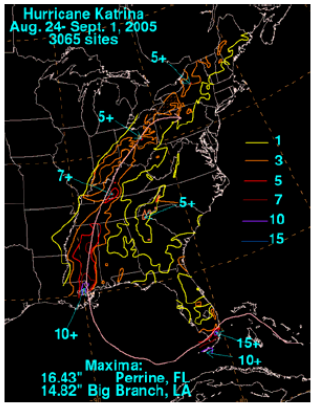

Hurricane Katrina (2005)

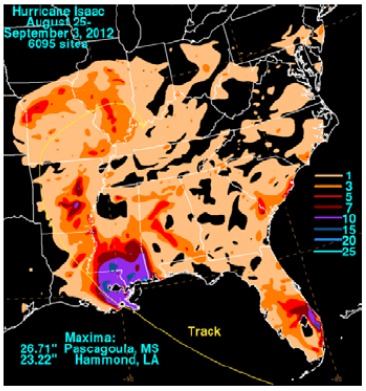

Hurricane Isaac (2012)

Figure 15.12. Example CN-GoM Tropical Rainfall Totals

http://www.hpc.ncep.noaa.gov/tropical/rain/

For surge events that threaten to flood a polder, the interior rainfall must be added to the perimeter inflows. The polder rainfall accumulations are usually considered according to internal "sub-basins," such as those depicted in Figure 15.1, which are delineated according to respective forced-drainage systems (i.e., conveyance network and pumping).

A small portion of precipitation which would otherwise contribute to inundation can be lost to:

- Interception of moisture above the ground (e.g., by tree leaves, rooftops, etc.);
- Evaporation near the ground surface; and
- Infiltration into the shallow soil, which is restricted by antecedent soil moisture and soil permeability.

In low-lying areas of southeast Louisiana such losses during tropical cyclone rainfalls probably equate to less than 0.1 ft of precipitation.

Meteorologists have evaluated generalized correlations of large scale rainfall precipitation with hurricane parameters, including intensity, size, and forward speed and some accounting for asymmetries (see, Lonfat et al 2004, Lonfat et al 2007, and Langousis and Veneziano 2008). However, generalized models have not been produced which describe highly localized rainfall variations.

15.6 Drainage Pumping

Polders require forced drainage systems to accommodate residual rainfall flood hazards and to operate during surge events (subject to limitations) to remove inundation water. The forced drainage systems typically have four components:

1. Local gravity collection systems, comprised of subsurface pipelines ranging up to several feet in diameter;
2. The major gravity channel network, which encompasses large open as well as covered canals (often concrete lined);
3. Local lift stations, which aid in transferring storm water from particularly low areas within the polder to the major gravity channel network; and
4. Perimeter pump stations which remove water at terminal points in the major gravity channel network and discharge into exterior water bodies.

The various components of the interior forced drainage systems typically have limited design capacities.[10]

The overall discharge rate at each perimeter pump station is controlled by the pump mechanical capacity, which is subject to the difference between exterior and interior SWL conditions. As the exterior to interior differential rises, the pump has to do more work and the discharge rate declines. Similarly, as the differential falls, discharge rates increase. The changing pump discharge with SWL differential is not linear and is specified by the manufacturer with an associated uncertainty. A pump station usually include many pumps—with varying capacities designed to come online in stages to accommodate the gravity channel inflow. Overall pump tables relating discharge to the SWL differential, with uncertainty, can be prepared for each station as a whole.

During polder inundation, pump stations may be subject to outages due to:

- Loss of power, including back-up power (e.g., flooding of generators, exhaustion of back-up generator fuel);
- Submergence of electrical or mechanical components;
- Shutdowns or start-up failures by automated control systems (e.g., due to loss of cooling liquid and trigger of temperature limits); and
- Absence of manual control (operators may have been removed or they may be unable to access controls).

Table 15.3 summarizes pump station operating capacity in the various New Orleans regional polders during Hurricane Katrina inundation. For the Metro New Orleans polder less than 10% of the rated capacity was operational. In general. for planning purposes IPET and the USACE have used overall pumping capacity alternatives of 0, 50, and 100% (IPET 2009). However, they have not assessed the probabilities of these alternatives.

---

[10] Many urban drainage conveyance/pumping systems are designed to only accommodate a 10-year return frequency rainfall event and accept that low polder areas will experience occasional "flash flooding." (see http://tg.jeffparish.net/index.cfm?DocID=1162)

Table 15.3. New Orleans Area Pump Station Hurricane Katrina Outages

IPET 2006 (Volume VI)

	Rated Capacity (cfs)	Pumped During Katrina?
I) Orleans Parish		
A) East Bank (E-3)		
1) OP 1 – PS 1	6825 cfs	No
2) OP 2 – PS 2	3150 cfs	No
3) OP 3 – PS 3	4260 cfs	No
4) OP 4 – PS 4	3720 cfs	No
5) OP 5 – PS 5	2260 cfs	No
6) OP 6 – PS 6	9480 cfs	No
7) OP 7 – PS 7	2690 cfs	No
8) OP 12 – PS 12	1000 cfs	No
9) OP 19 – PS 19	3650 cfs	Yes
10) OP I 10 – PS I 10	860 cfs	Yes
11) OP 17 – PS 17	625 cfs	No
12) Whitney-Barataria	3750 cfs	No
13) Pric – Prichard	253 cfs	No
14) Mont – Monticello	99 cfs	No
B) East Bank (E-4a)		
1) OP 10 – PS 10 Citrus	1000 cfs	No
2) OP 14 – PS 14 Jahncke	1200 cfs	No
3) OP 16 – PS 16 St Charles	1000 cfs	Yes
4) OP 18 – PS 18 Maxent	60 cfs	No
5) OP 20 – PS 20 Amid	500 cfs	No
6) DR – Dwyer Rd	120 cfs	No
7) GS – Grant	192 cfs	No
8) Elai – Elaine St	90 cfs	No
9) OP 15 – PS 15	750 cfs	No
C) West Bank (W-3b & W-4b)		
1) OP 13 – PS 13 (W-3b)	4650 cfs	No
2) OP 11 – PS 11 (W-4b)	1670 cfs	Yes
II) Jefferson Parish		
A) East Bank (E-2)		
1) PS 1 – Bonnabel	3750 cfs	Yes
2) PS 2 – Suburban	5440 cfs	No
3) PS 3 – Elmwood	5700 cfs	No
4) PS 4 – Duncan	4800 cfs	No
5) PS 5 – Parish Line	900 cfs	No
6) Canal Street	160 cfs	Yes
B) West Bank (W-1)		
1) LC1-PS – Lake Cataouatche 1	500 cfs	No
2) LC2-PS – Lake Cataouatche 2	600 cfs	No
3) BS-PS – Bayou Segnette	936 cfs	No
4) H90-PS – Highway 90	90 cfs	
C) West Bank (W-2)		
5) A-PS – Ames	1930 cfs	No
6) W-PS – Westminster	1200 cfs	No
7) C2-PS – Cousins 2	2300 cfs	No
8) E2-PS – Estelle 2	1140 cfs	No
9) C1-PS – Cousins 1	960 cfs	No
10) Harv-PS – Harvey	960 cfs	Yes
11) W2-PS – Westwego 2	936 cfs	No
12) EST1 – Estelle 1	550 cfs	No
13) WEG1 –Westwego 1	300 cfs	Unk
14) MTKN – Mt Kennedy	274 cfs	Unk
D) West Bank (W-3)		
15) Hero-PS – Hero	3902 cfs	No
16) P-PS – Planters	2360 cfs	No
III) St Bernard Parish		
A) East Bank (E-5a)		
1) F-1 – PS 1 Fortification	1245 cfs	No
2) M-4 – PS 4 Meraux	1245 cfs	No
3) JL-6 – PS 6 Jean Lafitte	1000 cfs	No
4) BD-7 – PS 7 Bayou Ducros	1017 cfs	No
5) SM-8 – PS 8 St Mary	834 cfs	No
6) BV-3 – PS 3 Bayou Villere	500 cfs	No
7) G-2 – PS 2 Guichard	350 cfs	No
8) EJG-5 – PS 5 E.J. Gore	660 cfs	No

15.7 Internal Routing

The spatial patterns of surge inundation and circulation over exposed coastal urban areas are controlled by the 2D depth-averaged physics described in Section 6.1. Open coast urban surge inundation can therefore be evaluated with the 2D depth-averaged hydrodynamic model codes employed in surge analysis (see Section 8)[11]—which has been done for many decades under coastal FISs. In recent years, high resolution FIS 2D ADCIRC surge models have addressed the inundation of low-lying coastal urban

[11] Hydrologists have applied 2D dynamic routing models (e.g., RMA2, MIKE21, SOBEK, TUFLOW, see Néelz and Pender 2009) to the inundation of urban areas in complex river floodplains for more than a decade. 1D dynamic river floodplain models—e.g., HEC-RAS, OTHER FEMA/DOT MODEL, MIKE 11—have been used since at least the mid-1990s (see USACE 1997). Use of steady-state flood models for river urban areas has an even longer history.

areas such as Gulfport/Biloxi in Mississippi (Hurricane Katrina) and Galveston/Houston/Port Arthur Texas (Hurricane Ike). No special modifications to the surge modeling applications described in Section 11 were required for these areas.

Polder inundation routing, however, must address the local, time-varying seepage, overtopping, breaching, rainfall, and pumping (SOBRP) processes occurring around and within the polder, as well as internal conditions:

- Detailed interior topography—including gradients toward low areas within the polder;
- Major internal gravity drainage features—such as canals which collect and convey stormwater to the major pump stations;
- Natural and man-made internal barriers—such as topographic ridges and elevated railroad and road embankments, which can modify internal circulation; and
- Major openings in the internal barriers—such as canal crossings (bridges and large culverts).

Figure 15.13 illustrates the internal features for the New Orleans East Polder in southeast Louisiana.

Internal topography is generally developed from high resolution DEMs (see GTN-2). In the case of southeast Louisiana, such models may include errors in excess of 1 ft due to vertical control issues, as well as inherent uncertainty on the order of 0.5 ft.

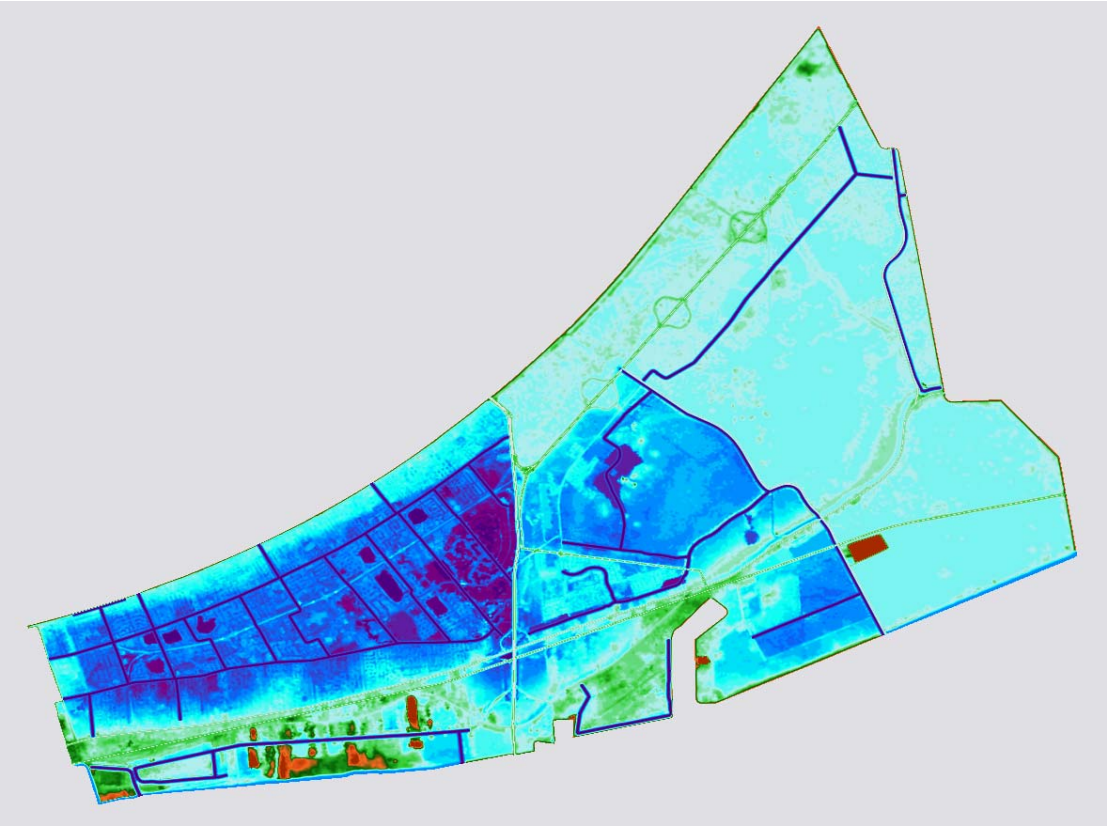

Figure 15.13. Features of New Orleans East Polder

Modified from LIDAR DEM to include channels

The unstructured meshes of high resolution 2D surge models, such as ADCIRC, can be refined to represent many of these conditions, subject to the general modeling limitations discussed in Sections 8 and 10 , including:

- Choice of numerical method (finite difference/element/volume, explicit/implicit, etc.) and associated settings and grid versus unstructured mesh;
- Model time-step requirements (e.g., for Courant stability condition);
- Treatment of acceleration terms; note that momentum terms for tide, Coriolis, and wave radiation stress gradients can typically be ignored for internal polder routing;
- Wetting and drying subroutines (e.g., control of gradients and oscillations);
- Resolution of the grid/mesh to depict topographic and bathymetric features and interior landscape conditions;
- Accuracy of the source topographic, bathymetric, and landscape data.
- Assignment of bottom friction coefficient values for land covers ranging from dense underbrush to open pavement to congested urban development; and
- Choice of eddy viscosity value.

Greater refinement of polder meshes allows a "high definition" depiction of spatial patterns of inundation associated with particular inputs and internal features.

The high resolution 2D surge models can have limitations when applied to polder routing, such as:

- Mesh refinement cannot capture sub-mesh scale interior drainage conveyances (e.g., storm sewers);
- The model may not address important interior mechanical structures—e.g., timed gates and lift stations;
- Some codes (e.g., ADCIRC) do not currently provide for sub-basin scale rainfall inputs;
- The code may not support assessment of interior near-breach inundation conditions. The initial inundation just inside the breach can experience supercritical (e.g., very steep) flow and shock waves. Simulating these conditions requires modeling of complex depth/velocity dynamics, as well as hydraulic jumps, similar to those associated with dam break scenarios. General 2D inundation models, such as ADCIRC, do not address these dynamics just inside the breach.

Code developers (e.g., ADCIRC Development Group) are currently researching ways to provide these capabilities.

The magnitude of high resolution 2D routing uncertainties—apart from uncertainties regarding inflows, outflows, and internal conditions—has not been thoroughly evaluated in the technical literature. Detailed sensitivity studies and hindcast validations for urban floodplain routing are not currently available.[12]

[12] The southeast Louisiana FIS Hurricane Katrina hindcast model provided some representation of the polders within the overall domain in order capture effects on regional exterior surge routing. However this model was not validated for the interior polder flooding.

Under some scenarios inundation can be nearly uniform polder-wide, with little spatial and temporal variation in interior SWL.[13] If these cases the hydrologist can employ a basic stage-storage relationship, which dictates the volume of water associated with a level pool at any given increment of SWL. In level-pool routing the net cumulative input volume at any time—cumulative rainfall and perimeter inflows minus cumulative pumping discharge—will equate to a specific polder-wide internal SWL. This simple level-pool routing method is often used for reservoirs and its accuracy and precision depend on the quality of inflow, outflow, and terrain information.

The level-pool routing method may be refined by dividing the inundation analysis according to several individual polder sub-basins, and providing for stage dependent exchange relationships between sub-basins—such as a broad-crested weir equation. As the number of sub-basins increases and interconnections become too complex for simple exchange relationships, 2D routing becomes a more effective tool for simulating spatially varying inundation. Sensitivity tests can be used to assess the degree of routing improvement with sub-basin refinements, as well as 2D routing.

To analyze inundation for any particular surge hindcast or scenario the interior routing model is coupled with a SOBRP model, which incorporates the methods described in Section 15.2 through 15.6:

- Seepage—simple SWL-dependent groundwater flow equations, parameterized to reflect local geology and infrastructure information, are used for those scenarios and reaches which may have non-negligible seepage inflow.
- Overtopping—reach-specific deterministic equations are employed to estimate inflows as a function of storm SWL (R_c) and waves. Reach-specific equations incorporate wave transmission coefficients (γ_r, γ_b, γ_h, γ_β) and weir coefficients (C_w, C, and C_{SUB}).
- Breaching—failure rules are used to describe potential breach dynamics—i.e., I-L at each reach/transition over time. Inflow rates are estimated using a broad-crested weir equation, which is a function of exterior and interior SWL, the breach I-L, and location-specific C or C'. (A simple failure rule for a deep I or long L could specify exterior-interior equalizing SWLs—e.g., at some time following peak exterior SWL—an eliminate the need for internal routing to assess peak interior inundation.)
- Rainfall—sub-basin accumulations are expressed as assumed quantities (e.g., a 24-hr/100-yr volume) or a hypothesized function of hurricane attributes, providing higher rainfall rates for slower moving storms.
- Pumping—withdrawal rates at each station are expressed as a tabulated function of local exterior and interior SWL.

The SOBRP model is *two-way* coupled with the interior routing model—the SOBRP output drives the routing model and the routing model output contributes to flow computations for pumping and submerged breaches. The SOBRP model in turn is *one-way* coupled with the exterior surge model and local wave model—the exterior surge and local wave model outputs drive the seepage, overtopping, and breaching inflow computations. Two way coupling of the exterior surge and SOBRP models would be required to consider the effect of perimeter inflows (primarily breaching) on drawing down exterior

[13] The Hurricane Katrina inundation in the New Orleans Metro Polder reached a peak of about 2.5 ft NAVD88 fairly uniformly as interior water levels gradually equalized with Lake Pontchartrain for over 24 hours after the storm. On the other hand, massive breaches in St. Bernard Parish and along the eastern IHNC floodwall caused peak inundation in the Lower 9th Ward/St. Bernard Polder to occurr near noon on the day of the storm.

SWL and the further impact on regional surge. The SOBRP and internal routing models require time stepping on the order of a few minutes. No commercial or research software programs are currently available to address SOBRP modeling and the associated coupling.[14] However, as the individual process calculations are relatively straightforward, FORTRAN, MS-EXCEL, or MATLAB etc. can be readily used for simulating SOBRP and to accommodate the necessary file actions.

The influence of variability/uncertainty in SOBRP process inputs and parameters on the flow rates and cumulative volumes for a selected storm can be studied with sensitivity tests. If the tests are focused only on the SOBRP process at individual locations, coupling with the exterior surge and wave model, as well as the routing model, can usually be ignored. Sensitivity tests of a SOBRP factor can be performed for specific scenarios (e.g., ± 50% of some base value), or a range of values to reflect normally or non-normally distributed probability. Sensitivity tests can address a single factor in a single SOBRP process at a location or can be expanded to cover multiple factors in combined SOBRP processes at a location. A Monte Carlo technique can be employed to examine the influence of multiple uncertainties (see GTN-1, Part J). An example is assessing the sensitivity of the overtopping rate at a particular segment of given crest elevation to combined uncertainties in exterior SWL, H_S, and T_P.

It is important to note that the limited observations of SOBRP and interior HWMs—such as for Hurricane Katrina—have not enabled validation of polder inundation modeling.

15.8 Interior Wind Setup and Waves

If an inundated polder includes areas oriented with a long, open fetch—such as canals (e.g., the GIWW and IHNC sub-basin) or submerged roads and greenways—the hydrologist can also examine the influence of interior wind setup (on SWL and routing) and waves. Most 2D hydrodynamic models—and surge models specifically—can address the effects of local wind stress, including changing wind fields, on polder inundation patterns. Level-pool routing does not address interior wind setup but can be supplemented with simple wind setup analyses.

The wind setup, h, across a confined body of water (e.g., an inundated polder) is a function of:

- The wind speed, U, typically estimated measured at 10 m above the surface;
- The fetch length, L;
- The water depth (SWL minus bathymetric elevation), d;
- An air-water drag coefficient, $C_{Dair\text{-}water}$; $C_{Dair\text{-}water}$ can be adjusted for local air-water interface factors (e.g., waves) and canopy conditions—such as the presence of dense trees and buildings. and
- The specific gravity of air and water, ρ_{air} and ρ_{water}.

Wind stress on the water, τ_W, is given by

$$\tau_W = C_{D\,air-water}\,\rho_{air}\,U^2$$

[14] Dynamic breaching has been recently included in ADCIRC surge modeling and, as noted in Section 15.7, ADCIRC can be used for internal routing. However, ADCIRC cannot provide complete SOBRP modeling as it does not currently address seepage, Zone C/D waves, wave-related overtopping, and rainfall. Thus, integrated modeling of surge and SOBRP processes within ADCIRC is beyond the current state-of-the practice.

A simple 1D approximation for a steady-state wind setup is given from a balance of the wind stress and hydrostatic forces (ignoring bottom friction and other forces):

$$h = C_{D\,air-water}\frac{\rho_{air}}{\rho_{water}}\frac{LU^2}{g\,d} \text{ with } C_{D\,air-water}\frac{\rho_{air}}{\rho_{water}} \approx 2.0\,x\,10^{-6}$$

Thus, a sustained 60 mph (88 ft/s) wind over an open 5 mile (26,400 ft) fetch with an inundation depth of 10 ft can contribute approximately 1.3 ft of setup. For a deeper water body—e.g., 30 ft—the setup would be 0.4 ft. To date there have been no empirical studies or hindcasts of localized wind setup acting within inundated polders to assist in addressing appropriate values for $\boldsymbol{C_{D\ air\text{-}water}}$ or canopy-induced wind stress reduction.[15]

Local winds acting on long open fetches also generate interior waves. Such waves can expose property that is above the SWL to flood damage. If interior wave heights reach several feet they can also influence polder SWL patterns through wave setup (see Section 6.2). However, for smaller wave heights interior wave setup can usually be ignored in a 2D routing analysis.

The wave field in a confined area at particular local wind speed is likely to be limited by depth, and breaker parameters can be used to provide a ceiling for interior, downwind H_S or $H_{1\%}$.[16] Wave heights can be further limited below the depth controlled ceiling, by:

- Insufficient fetch;
- The short duration of sustained peak winds along a particular fetch orientation;
- Bottom friction effects; and
- The fetch width, with narrower fetches introducing dampening;

For polders the actual applied winds at the water surface must also be reduced to account for canopy conditions. To estimate upper bounds on wave field $\boldsymbol{H_S}$ and T_p[17] in an open, confined water body, simple methods for wind wave generation normally consider only fetch and duration limitations and ignore possible limitations due to depth, bottom friction, and fetch width. Several simplified methods include:

- Sverdrup-Munk-Bretschneider (SMB, Bretschneider 1970),
- Wilson (1965),
- Donelan (1980),
- Joint North Sea Wave Project (JONSWAP, Hasselman et al 1973), and
- CEM (USACE 2006)

Figure 15.14.a and b illustrate estimated $\boldsymbol{H_S}$ and T_p for fetch-only limited conditions using the CEM method. A sustained 60 mph (27 m/s) wind over a 5 mile (8 km) fetch can induce $\boldsymbol{H_S}$ on the order of 4 ft.

[15] The Hurricane Katrina interior HWMs were of widely varying quality and—combined with wind and other data limitations—have made such a detailed hindcast of polder routing difficult.

[16] As noted in Section 10, the NFIP employs the 1% wave a breaker parameter of 0.78

[17] Wind wave $\boldsymbol{H_S}$ is often also assumed to reflect a JONSWAP distribution for the wave energy spectrum.

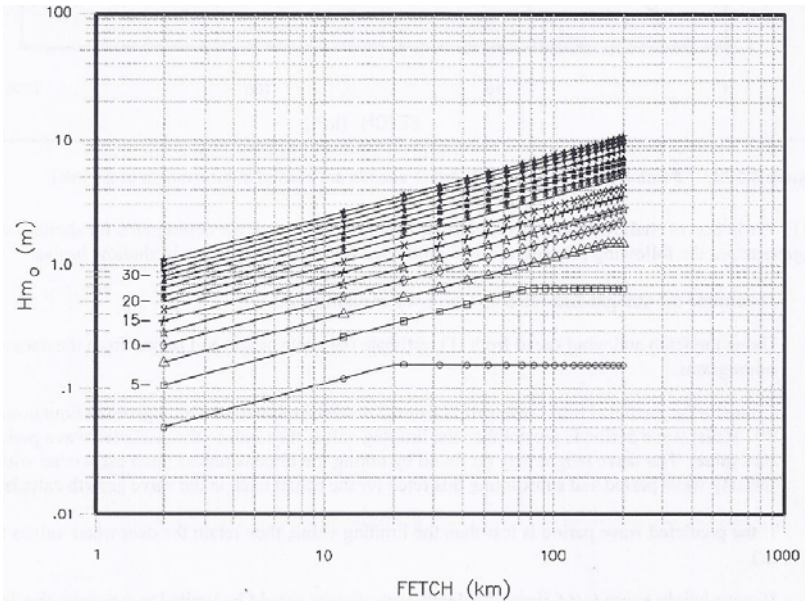

a. Wave Height

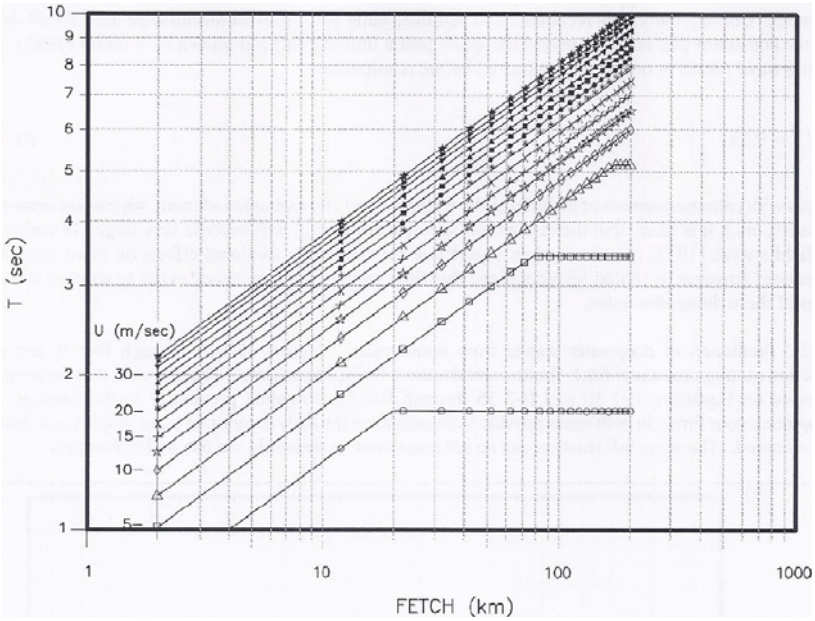

b. Wave Period

Figure 15.14. Fetch Limited Wave Heights and Periods (Winds in 2.5 m/s increments)
USACE 2006

In 2009 Etemad-Shahidi et al published a comparison of the SMB, Wilson, and CEM methods for predicting waves in fetch-only and fetch+duration limited conditions using wave data from Lake Ontario. Under fetch-only limiting conditions they found that all three methods exhibited slight height over-prediction bias, with the CEM method having the lowest bias. All three methods had similar scatter index values of about 25 to 28%. However, under fetch+duration limited conditions the methods

exhibited more notable under-prediction bias, as well as much higher SI values. The CEM method performed the worst in the fetch+duration limited condition.

FEMA FIS guidance (FEMA 2008) provides for use of these simplified methods in sheltered water bodies, and 1D wind-wave modeling codes (e.g., WHAFIS) and 2D codes (e.g., STWAVE or SWAN, see Section 9) for complex interior coastal regions.

While wind waves in shallow estuaries, bays, lakes, and harbors have been studied, no literature has been identified for channels or inundated polders.

Section 16. Polder Inundation JPA

16.1 Polder Inundation Hazards

Analysis of polder inundation hazards associated with hurricane surge events as described in Section 15 does **not** address three separate, independent and additional probabilities of polder flooding from:

a. Severe tropical rainfall only, i.e., without surge-driven inundation. Rainfall only accumulations with tropical cyclones can easily exceed the commonly referenced 25-year return period, 24 hour duration magnitudes—on the order of 9 to 11 in for southeast Louisiana (Faiers et al 1997). During Tropical Storm Allison (2001) over 15 in of rainfall fell in one 24-hr period, and nearly 30 in over the course of the storm, at Thibodaux Louisiana (NOAA NWS 2001).

b. Severe non-tropical rainfall events. On May 7-8, 1995 a non-tropical storm in southeast Louisiana produced up to 20 inches of rainfall, inundating some low areas inside the Metro New Orleans Polder by several feet (NOAA NWS 2005).

c. Non-surge perimeter failures. For example, portions of the New Orleans polder barriers fronting the Mississippi River protect the region from extreme river floods.

Within southeast Louisiana polders, some locations can experience significant flooding even during modest rainfall events. Internal topography—e.g., lower areas within the polder and the presence of sub-basin compartmentalization features—can cause localized ponding and higher hazard levels. Figure 16.1 illustrates the "bowl" characteristics of the Metro New Orleans polder. The performance of drainage pump stations and conveyance systems (which are typically designed only for 10-yr return rainfall events) can also influence localized inundation hazards. For large portions of the New Orleans regional polders, the rainfall-only 100-yr inundation depth is more than a foot.

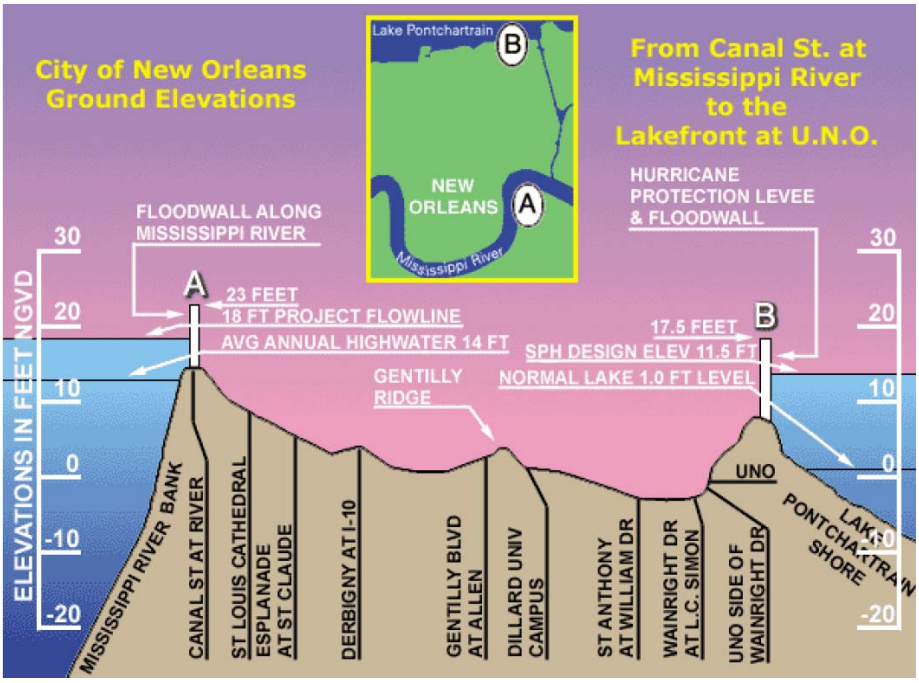

Figure 16.1. Metro New Orleans "Bowl"

(Note the Vertical Datum is outdated)

http://www.nola.com/weather/elevationsmap.html

A levee failure during an extreme Mississippi River flood (>800-yr return) has the potential to inundate the Metro New Orleans Polder to SWLs exceeding 15 ft—much higher than the equivalent >800-yr surge hazard. The technical approach to a combined assessment of all four inundation hazards—surge, tropical rainfall-only, non-tropical rainfall, and river flood—is beyond the scope of this report.

The sources of surge-related polder flooding described in Section 15 themselves pose different inundation hazards. Individual seepage locations alone (i.e., without breaching) pose the lowest hazard, with inflow discharges typically at much less than 0.1 cfs/ft (43.6 acre-ft/mi-hr). Minor-to-moderate overtopping at a reach can produce rates between 0.1 cfs/ft for positive freeboard with small waves to 4 cfs/ft (1,745 acre-ft/mi-hr) for a negative freeboard of 1 ft. The highest hazard is posed by major overtopping and breaching, with inflow rates capable of exceeding 20 cfs/ft (8,727 acre-ft/mi-hr) when SWL rises several feet above the barrier.

The equivalent volumes for five very simplified, steady inflow scenarios with six hour duration are:

Multiple Seepage/Small Wave Overtopping at 0.1 cfs/ft and 3 mi	785 acre-ft
Moderate Wave-Only Overtopping at 0.5 cfs/ft and 3 mi	3,924 acre-ft
Overtopping at 1 cfs/ft (<1 ft freeboard) and 3 mi	7,855 acre-ft
Major Breach at 20 cfs/ft and 2,000 ft	19,835 acre-ft[1]
Multiple Major Breaches at 20 cfs/ft and 10,000 ft	99,174 acre-ft

To put these inflow volumes in perspective Table 16.1 provides rainfall accumulation rates and volumes for the 6-hr/10-yr, 6-hr/100-yr, and 24-hr/100-yr hazards for the New Orleans area sub-basins (see Figure 15.1). The rainfall accumulation rate hazard is very localized, but for a point of reference volumes are summed using these rates across entire sub-basin areas. Inflow volumes for the first two scenarios are much less than the equivalent 6-hr/10-yr precipitation volumes for all five urban areas. The volume for the third scenario, <1 ft SWL overtopping, exceeds the 6-hr/10-yr precipitation volume for St. Charles parish urban area, but is well under the 6-hr/10-yr volumes for the other areas. The volume for the fourth scenario, a single breach, is less than the 24-hr/100-yr precipitation volume for three of the five parish urban areas. Only the volume for a multiple breach scenario far outstrips the 24-hr/100-yr precipitation hazard for all five areas.

For further context, Table 16.2 presents the observed inundation volumes for the New Orleans area urban sub-basins resulting from the extreme Hurricane Katrina exterior surge on the morning of August 29, 2005 (see Figure 5.5). The range of polder conditions demonstrates that for a single storm adjacent polders can experience drastically different SWL inundation hazards. (Importantly, variations in interior polder topography—major portions of each polder are well below 0 NAVD88—meant that the lower lying neighborhoods experienced more severe flood *depth* hazards.)

The particular exterior SWL exposure of each polder and the length and invert of breaches influenced the magnitude and timing of peak interior SWL. The Lower 9th Ward/St. Bernard Polder experienced massive erosion of levees along the MRGO and "the Funnel" in the face of 20+ ft exterior SWLs, together with the failure of floodwalls along the IHNC, which produced very high interior peak SWLs nearly within a short time following the peak exterior surge. The relatively shorter breaches (in length) for the Metro New Orleans system facing Lake Pontchartrain delayed peak SWLs (associated with equalization of the polder and lake) until over 24 hours after the peak exterior surge. An important reason for the lower inflows for the New Orleans East Polder was the relatively minor contribution of breaching.

[1] In these breach inflow scenarios the polder SWL does not equalize with the exterior SWL.

Table 16.1. Equivalent Volume for Precipitation

Acre-Ft of Accumulation Excluding Losses (Faiers et al 1997)

Polder	Sub-Basin	Area Acres	6-hr Duration		24-hr Duration
			10-yr 6.5 In	100-yr 10 In	100-yr 13 In
New Orleans East	NOE1 Maxent Lagoon	14,233	7,710	11,861	15,419
	NOE2 Maxent Wetland	5,683	3,078	4,736	6,157
	NOE3	2,866	1,552	2,388	3,105
	NOE4	2,338	1,266	1,948	2,533
	NOE5	9,588	5,194	7,990	10,387
	NOE3, 4, 5*	***14,792***	***8,012***	***12,327***	***16,025***
	Total Polder*	***34,708***	***18,800***	***28,923***	***37,600***
Lower 9th Ward/ St. Bernard	SB2 Central Wetland	5,066	2,744	4,222	5,488
	SB5 Central Wetland	24,340	13,184	20,283	26,368
	SB1	5,115	2,771	4,263	5,541
	SB3	5,485	2,971	4,571	5,942
	SB4	9,415	5,100	7,846	10,200
	SB1, 3, 4*	***20,015***	***10,841***	***16,679***	***21,683***
	Total Polder*	***49,421***	***26,770***	***41,184***	***53,539***
Metro New Orleans	SC1 (mostly swamp)	5,906	3,199	4,922	6,398
	SC2	7,364	3,989	6,137	7,978
	SC1 & 2*	***13,270***	***7,188***	***11,058***	***14,376***
	JE1	7,784	4,216	6,487	8,433
	JE2	5,510	2,985	4,592	5,969
	JE3	15,395	8,339	12,829	16,678
	JE1, 2, 3*	***28,689***	***15,540***	***23,908***	***31,080***
	OM1	5,041	2,731	4,201	5,461
	OM2	4,176	2,262	3,480	4,524
	OM3	4,720	2,557	3,933	5,113
	OM4	2,063	1,117	1,719	2,235
	OM5	11,268	6,104	9,390	12,207
	OM 1, 2, 3, 4, 5*	***27,268***	***14,770***	***22,723***	***29,540***
	Total Polder*	***69,227***	***37,498***	***57,689***	***74,996***

Table 16.2. Hurricane Katrina Inundation of New Orleans Regional Polders

IPET 2009, Volume VI Tables 7 and 8, and FEMA 2006[2]

Polder	Sub-Basins	Inundation Peak			Source of Inflow %		
		Time	SWL Ft NAVD88	Volume Acre-Ft	Breaching	Overtopping	Rainfall
Metro New Orleans	OM1, 2, 3, 4 &5	Late Afternoon 8/30	2.5 to 3	88,000 to 99,000	66	13	21
Lower 9th Ward/St. Bernard	SB1, 3, &4	Before Noon 8/29	10 to 12	153,000 to 192,000	63	29	8
New Orleans East	NOE3	High Water Marks Not Available					
	NOE4	Before Noon 8/29	2 to 2.5	4,000 to 5,000	17	70	13
	NOE5	Before Noon 8/29	-1.5 to -1	42,000 to 46,000			

16.2 Overview of Hurricane Surge Polder Inundation JPA

Quantifying polder inundation probabilities associated with hurricane surge events requires expanding the JPA for exterior surge approach described in Section 13. The equation for $\boldsymbol{F}(SWL_i)$—the cumulative probability of any surge SWL at an exterior LOI, (see Section 13.1)—is changed to $\boldsymbol{F^*}(SWL_i)$—for the cumulative probability of any surge related SWL at a polder interior LOI—as follows:

$$\boldsymbol{F^*}(SWL_i) = \int\int\int\int\int\int\int \boldsymbol{p^*}(CPD, R_{max}, V_f, \theta, X, I, L, R, t)\, \boldsymbol{H}[\boldsymbol{\psi_P}(\boldsymbol{\psi}, \boldsymbol{\psi_W}, \boldsymbol{\psi_{SOBRP}}) - SWL_i]\, d(CPD)\, d(R_{max})\, d(V_f)\, d(\theta)\, d(X)\, d(I)\, d(L)\, d(N_R,)$$

where

$\boldsymbol{p^*}$ is the joint probability expression modified to encompass additional probabilities (dimensions) for breach I and L (invert and length, see Section 15.4) at each individual reach/transition, N_R. Probability dimensions could be also be added for seepage, rainfall, and pumping.

$\boldsymbol{\psi_P}$ is the internal polder routing (level-pool or 2D as appropriate), which, in turn, is a function of

- $\boldsymbol{\psi}$, the high-resolution 2D surge SWL-wave model, which is a function of the hurricane variables CPD, R_{max}, V_f, θ, and X, as well as the mesh and other settings and parameters.
- $\boldsymbol{\psi_W}$,, the local Zone D wave conditions, which is in turn a function of $\boldsymbol{\psi}$, as well as local perimeter wind and bathymetric conditions.

[2] IPET stage-storage data for the sub-basins was not available and therefore volumes were computed using the regional LIDAR DEM (see GTN-2). Slight differences may occur due to sub-basin delineation

- $\boldsymbol{\psi_{SOBRP}}$, the inflow function for SOBRP. $\boldsymbol{\psi_{SOBRP}}$ is a function of both interior and exterior SWLs—i.e., $\boldsymbol{\psi}$ and $\boldsymbol{\psi_P}$—as well as perimeter crowns and other conditions.

$\boldsymbol{\psi_P}$ could also include the effect of interior wind setup.

Given the relative hazards of the inflows noted above, a JPA for more extreme surge-related polder inundation hazards may choose to ignore seepage-only inflow, and possibly wave-only overtopping inflow as well.

An expanded JPA approach is needed because the polder inundation hazard cannot be evaluated by simply routing the exterior surge hazard—e.g., routing the perimeter 500-yr SWLs to determine an internal 500-yr inundation hazard. While this analysis may be useful for some planning purpose (e.g., to roughly compare results for different polders, or results for different exterior surge hazards for the same polder), it does not provide an estimate of the polder 500-yr inundation hazard. In reality, a single storm is highly unlikely to produce a consistent 500-yr surge level along the entire perimeter system.

Furthermore, large perimeter systems have reaches with some independent exposure. *It follows that a surge overtopping event along a segment produces a volume that actually has a **MUCH LOWER** internal than reach-specific return period.*[3]

Given the range of independent factors contributing to the surge-related polder inundation hazard, an expanded JPM approach[4] is required to evaluate ***F****. This approach employs three steps:

1. Prepare a JPM set of exterior *whole-perimeter* surge events representative of the regional hurricane climatology joint probability, $\boldsymbol{p}$; each event encompasses i) the local surge SWL peaks and hydrographs—specified along the polder perimeter—which are a function, $\boldsymbol{\psi}$, of storm characteristics, and ii) the local exterior wave conditions associated with each SWL hydrograph, $\boldsymbol{\psi_W}$.
2. Define a range of scenarios to reflect SOBRP probabilities for each whole-perimeter surge event. For example, for breach probabilities include joint probabilities for combinations of N_R, I, and L (and rainfall and pumping if also considered probabilistically). For each scenario compute SOBRP flows as functions of $\boldsymbol{\psi}$, $\boldsymbol{\psi_W}$ and $\boldsymbol{\psi_P}$ and conduct the internal routing simulations, $\boldsymbol{\psi_P}$, (using level-pool or 2D, with or without wind setup, as appropriate).
3. Numerically integrate the resulting PDF to produce the CDF curve, with appropriate smoothing and treatment of potential bias and uncertainty.

In addition to employing the same 2D SWL routing model program described in Parts II and III (e.g., ADCIRC/STWAVE or SWAN+ADCIRC), the JPM approach to surge polder inundation requires three more hydraulic models: a local storm-specific wave model; polder SOBRP inflow modeling; and internal routing. The following five sections discuss the five JPM steps and associated models for evaluating ***F****. Afterwards, a sixth section describes the approach to analyzing potential interior wave hazards.

---

[3] Suppose a perimeter system has been designed with elevations that allows for a minor amount of wave-only overtopping when the exterior SWL at any reach is at the 100-yr level. If the 100-yr exterior surge hazard for this system actually reflects several totally independent exposures (e.g., storms passing along several widely different tracks), surge-related inflow into the polder at this minor overtopping rate (i.e., from ***anywhere*** along the overall perimeter) is in fact a much higher probability—e.g., close to a 33-yr hazard for three independent exposures. The South Lafourche Polder clearly illustrates an example of two independent exposures—east versus west side.

[4] For more background on JPA and the JPM approaches see GTN-1, Part J, as well as Section 4.1, and 14.1.

16.3 JPM Set of Perimeter Surge Events

A JPM approach to polder inundation hazard analysis requires a set of perimeter SWL events (SWL peaks and associated hydrographs) that reflects the regional hurricane climatology. Studies of extensive polder systems—with long and complex perimeters—examining a wide range of inundation probabilities—e.g., from 100-yr to >1,000-yr—necessitate a large set composed of a sufficient number of extreme exterior SWL events.

The set of SWL events is generated using a Full-JPM, Monte Carlo-JPM, or JPM-OS storm set (see GTN-1, Section J, and Sections 4.1 and 13.1)—with set size and composition appropriate for the range of polder inundation scenarios under consideration. Each storm is simulated with the high resolution 2D wind/surge/wave SWL routing model. Each storm event—composed of SWL peaks along the entire perimeter and hydrographs determined as described in Section 15.1—has the fractional joint probability associated with that storm. The set of perimeter results for all the storms then statistically represents the probability of perimeter surge SWL (peak and hydrograph) events.

For inundation studies of polders located near complex coastlines and sheltered water bodies it may be necessary to expand the set of storms to adequately portray the surge-response of these areas. For a JPM-OS storm set, the size and composition of the set can be tailored to better capture complex local surge-response through careful attention to the benchmark procedure described in Section 13.2.

The Surge Response-OS approach cannot be employed in analyzing polder inundation joint probabilities.[5] The Surge Response-OS approach is not developed to capture the combined probabilities of various exterior surge conditions at various reaches, i.e., to provide a set of *whole-perimeter surge events* effectively representing the full *whole-perimeter surge hazard*.

As seen in Section 15, seepage, overtopping, and breach inflows are highly sensitive to the estimates of exterior SWL. A polder inundation analysis requires that the high resolution 2D SWL model (described in Sections 8 through 11) be carefully reviewed for identifying/correcting residual bias and defining/minimizing uncertainty at perimeter system LOIs. To better capture the exterior surge response near perimeter LOIs it may be necessary to refine the surge model mesh and to improve nodal attributes (e.g., topography/bathymetry, Manning's n).

Results near LOIs for all JPM storm simulations can be examined for possible instabilities. The mesh near LOIs may require refinement and smoothing if numerical instabilities affect the results. The choice of model settings and other parameters (e.g., acceleration terms, eddy viscosity) may also need adjustment to improve the representation of local surge SWL conditions.

Polder hazard analysis—particularly consideration of wave-only overtopping—also requires information about the local exterior wave conditions for each perimeter surge event in the JPM. Zones C/D wave conditions must therefore be modeled at each reach for each JPM storm using one of the techniques described in Section 15.1. Assessment of overall SOBRP volume sensitivity to wave conditions, especially H_s, (see below) can support the selection of a wave modeling approach. For low sensitivities, use of simple breaker parameter limited H_s would be sufficient.

[5] As discussed in Section 14.3, a Surge Response-OS set is used in conjunction with a high resolution 2D routing model ONLY to define the SWL surge response, $\boldsymbol{\psi}$. The surge response, $\boldsymbol{\psi}$, is subsequently combined with the mathematical expression for $\boldsymbol{p}$, as a valid approach to defining *local, exterior surge hazards*. Under the assumption of smooth surge-response, the Surge Response-OS set can be much smaller than a JPM-OS set.

16.4 SOBRP Probability Scenarios

In an inundation JPA the time-varying inflows from seepage, overtopping, and breaching, together with rainfall accumulations and pumping withdrawals are estimated over the course of each JPM storm. As discussed in Section 15, these SOBRP flows are a function of changing exterior SWL and wave conditions, changing interior SWLs, and transmission coefficients. The inundation JPA must consider variability/ uncertainty for these conditions and coefficients when the magnitude of variability/uncertainty is significant to the interior inundation hazard. For example, in JPAs dominated by overtopping—or even more so by breaching—seepage, seepage uncertainty, and rainfall uncertainty are typically neglected. When breaching is not included in the inundation analysis rainfall uncertainty becomes more significant. Sensitivity tests can be used to assess the influence of input uncertainties.

Probabilistic variability/uncertainty in a SOBRP factor can be incorporated into the JPA in one of two ways, depending on whether the factor's influence on the interior volume is linear or nonlinear. Uncertainties in rainfall, pumping, general terrain DEMs, and overtopping and breach lengths and coefficients are examples of linear factors. For convenience, all linear factors can be considered to have a normal distribution. A combined overall σ_P can then be used directly during post-processing to assess the influence on peak inundation volume probability (see Section 16.5 below).

For SOBRP attributes with nonlinear influence—such as the effect of exterior SWL (i.e., R_C) on the likelihood of a breach failure condition, I-L, at any reach, as well as the effect of H_s/breaker parameter and R_C on the overtopping and breach volumes—examining this influence requires expanding the JPM methodology. The expanded JPM must include a *subset* of whole-polder SOBRP scenarios for each storm, and each storm's subset must represent the full range of perimeter inflow joint probabilities for that storm. For each JPM storm—with climatological joint-probability $\boldsymbol{p}$—the whole-polder SOBRP subset can be composed of either:

- Predefined whole-polder SOBRP scenarios to represent a broad combinations of attributes. The range of each attribute is discretized into a few alternative values. Each scenario is then assigned a fraction of $\boldsymbol{p}$ based on the scenario's $\boldsymbol{p^*}$). The total probability of all scenarios for any storm thus equals $\boldsymbol{p}$. This Full-JPM approach to constructing the subsets and is preferable when there are only one or two attributes.
- A sufficiently large number of randomly selected whole-polder SOBRP scenarios with their respective $\boldsymbol{p^*}$, This Monte Carlo-JPM approach to constructing the subsets with randomly selected scenarios is appropriate for multiple factors.

Depending on the complexity of model coupling and the resources required for additional SOBRP scenarios, the expanded JPM may be limited to only those factors which have a large impact on the inundation hazard. Given the large order of magnitude of the influence of breach fragility on inundation hazard, the above expression for $\boldsymbol{p^*}$ only incorporates probabilities for I-L at each reach (N_R). The numerical solution to $\boldsymbol{p^*}$ thus requires $\boldsymbol{\psi_{SOBRP}}$ solutions for a wide range of whole-polder scenarios—encompassing a number of combined breach I-L conditions encompassing every N_R—for each JPM storm. This expansion of the JPM can necessitate thousands of $\boldsymbol{\psi_{SOBRP}}$-$\boldsymbol{\psi_P}$ solutions per JPM storm, with more scenarios for the more extreme storms. The associated computational demands for thousands of scenarios can therefore dictate simplified internal level-pool routing—which allows the use of a combined $\boldsymbol{\psi_{SOBRP}}$-$\boldsymbol{\psi_P}$ model prepared in EXCEL, MATLAB, or FORTRAN (see Section 15.7).

For major overtopping and breaching hazard analyses the nonlinear influences of uncertainties in SWL, H_s, and pumping can also be meaningful, requiring more probability dimensions for $\boldsymbol{p^*}$. In the case of

SWL, the overall uncertainty factor σ_Σ discussed in Section 13.5 can be used to develop the SOBRP subsets.

During the simulation of some individual exterior-SOBRP scenarios it may be important to consider the effect of interior wind stress—e.g., where inundation is occurring simultaneously with presence of strong winds over long open fetches. Addressing the influence of time- and spatially-varying wind stress during inundation requires a 2D $\boldsymbol{\psi_P}$ model program (such as ADCIRC). If the peak inundation scenarios entail limited wind setup conditions, the level-pool routing results can be combined with a supplementary wind setup calculation. The results of the wind setup calculation can then be used to finalize sub-basin peak level-pool SWLs. As noted in Section 16.3, for polders with potential exposure to interior wind setup hazards it is crucial to include an appropriate number of storms in the JPM set reflecting attributes—such as tracks—that contribute to the wind setup hazard.

16.5 Preparation of Return Frequency Curves

Production runs for each JPM-storm/SOBRP-scenario combination—employing $\boldsymbol{\psi}$, $\boldsymbol{\psi_W}$, $\boldsymbol{\psi_{SOBRP}}$, and $\boldsymbol{\psi_P}$ models (and interior wind setup as needed)—must be reviewed and checked for completeness and quality. Quality control for surge modeling has been addressed in Section 13.6. Selected outputs from individual Zones C/D wave, SOBRP, and interior routing model runs are similarly prepared in graphical and map overlay formats to facilitate inspection. Output values can be screened to flag simulations that produce physically unrealistic results or results inconsistent with general trends. Nonconforming results may indicate that a model program has been inappropriately setup or the wrong input has been used. A final file of peak SWL results from the $\boldsymbol{\psi_P}$ model—for each of the thousands of scenarios at each polder sub-basin or mesh node—is then produced.

For each location (e.g., sub-basin or node), these thousands of peak interior SWL results are used to finalize surge-related flood return frequency curves, in four steps similar to those employed for exterior SWL (Section 13.6):

a. CDF integration;

b. CDF validation;

c. Adjustments to spatial variations in specific surge hazard levels; and

d. Construction of confidence limits.

The interior PDF can be numerically integrated to produce the cumulative probability at each incremental SWL. The integration step can include smoothing of the individual results using an overall σ_P. As discussed in the preceding sections the σ_P encompasses uncertainties which are regarded as normally distributed and related linearly to polder inundation volume. Example uncertainties include:

- The exterior SWL (computed with $\boldsymbol{\psi}$) as it affects seepage rates; if seepage flows are very small relative to the inundation hazards being assessed, this term can be ignored;
- The length of overtopping and breaching;
- Weir coefficients for overtopping and breaching;
- Rainfall rates;
- Pumping rates; and
- General terrain DEM.

These linear uncertainties, and thus $\sigma_{\boldsymbol{P}}$, are expressed in units of inundation volume. For smoothing the peak interior SWL results, $\sigma_{\boldsymbol{P}}$ would need to be converted to units of inundation elevation, either a single sub-basin wide $\sigma_{\boldsymbol{P}}$ for level-pool routing or spatially varying $\sigma_{\boldsymbol{P}}$ for 2D routing. The difficulty, however, with using $\sigma_{\boldsymbol{P}}$ is often a lack of data and empirical research for defining the component $\sigma_{\boldsymbol{P}}$ values, resulting in the use of educated guesses.

An alternative to numerical integration is to select an established PDF curve type (e.g., Gumbel, Weibull, etc., see GTN-1 Part H) and assign coefficients using the results. The CDF is then simply the standard integral of that PDF.

Unlike exterior surge CDFs, observations from a sufficient number of surge-driven polder inundation events are not available to validate interior CDFs. Sub-basin surge-related CDFs, however, can be evaluated for physical reasonableness by comparing them with

a. Each other—for example, assessing differences in the SWL at key hazard levels and whether such differences make physical sense. For a 1,000-yr return period, a sub-basin protected by compartmentalization features might be expected to have a lower inundation level relative to sub-basins in close proximity to potential breach locations.

b. CDFs for other polder flood hazards, such as tropical storm rainfall-only and non-tropical rainfall. Low-lying sub-basins might be expected to have higher inundation levels in all cases.

The sub-basin (or node) CDFs are used to construct maps illustrating the polder-wide surge inundation hazards—e.g., 100- and 500-yr return period etc.—such as those shown in Figure 16.2 Flood hazard overlays are then compared against more accurate maps and aerial images. Adjustments can then be made to sub-basin flood level boundary alignments, and to smooth boundary differences.

The fourth step addresses residual uncertainty in the interior CDFs. Sources of potential bias in the various inputs, parameters, and assumptions for all of the model components in $\boldsymbol{\psi_P}$ are first identified and evaluated. If there is reasonable evidence of bias or error—e.g., from a CDF comparison—then the source of the bias is corrected and the CDFs are redeveloped.

The influence of the linear, normally fistributed uncertainties can be readily evaluated by using $\sigma_{\boldsymbol{P}}$ to construct corresponding LCL/UCLs for the local CDF (e.g., 90%). These LCL/UCLs are subject to the limitation regarding the estimate of $\sigma_{\boldsymbol{P}}$.

Two important non-linear uncertainties include:

- The exterior SWL (computed with $\boldsymbol{\psi}$) as it affects overtopping and breaching rates; (exterior SWL uncertainty is discussed in Sections 13. 5 and 13.6); and
- Breach fragility response to exterior SWL.

As discussed above, the influence of these two uncertainties on the polder inundation hazard can be assessed with sensitivity tests. The sensitivity tests can provide a basis for a professional judgment to modify the LCL/UCLs. If significant expansions in the number of scenarios for $\boldsymbol{\psi_{SOBR}}$ and $\boldsymbol{\psi_P}$ modeling can be accommodated, it may be practical to add these uncertainties into the JPA—i.e., expanding $\boldsymbol{p^*}$. (The additional scenarios would be selected using the Monte Carlo technique). The resulting effect of these uncertainties can then be computed and used to adjust the LCL/UCLs.

If a standard PDF curve (e.g., Gumbel, Weibull, etc.) has been fitted to the inundation modeling results, the LCL/UCLs regarding this fit (apart from the uncertainties above) can also be provided.

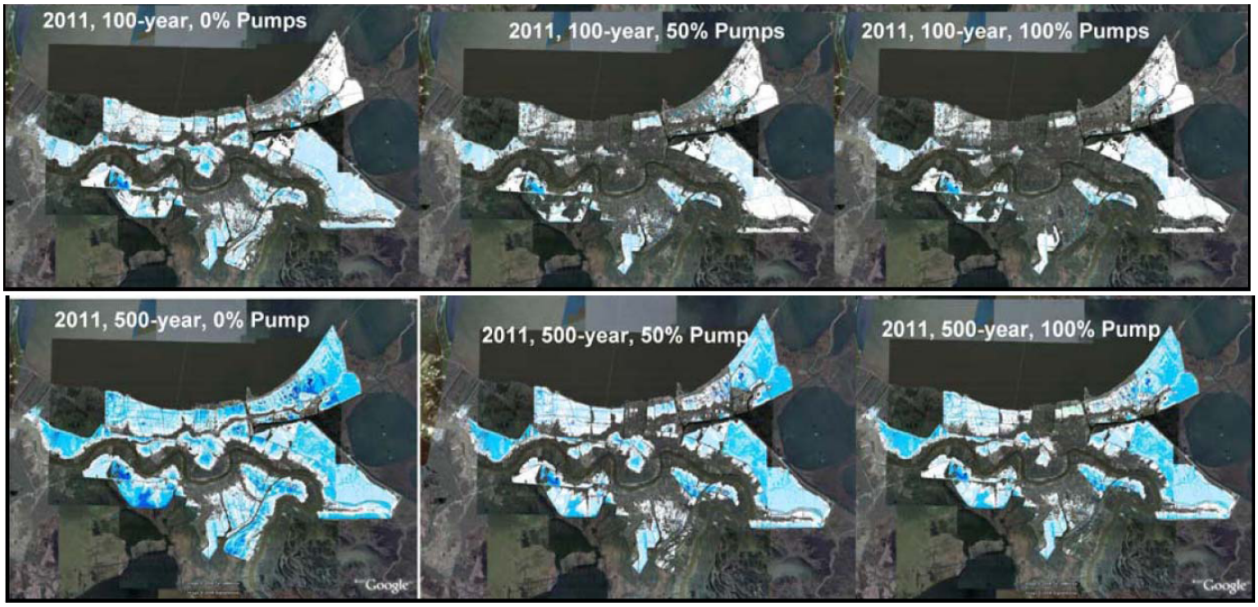

Figure 16.2. Example of Polder Inundation Hazard Maps

IPET 2009b

16.6 Interior Wave Hazard

As with exterior surge wave hazards (see Section 13.7) interest in polder wave hazards is limited primarily to wave conditions that occur at the reference SWL hazard level. These wave conditions can be analyzed using techniques reviewed in Section 15.8, including the breaker parameter. For longer, deeper interior fetches—e.g., wide channels—wave heights at a referenced SWL hazard can be computed for several appropriate hurricane scenarios (storm intensity, size, wind-field, forward speed, track, etc.) and their associated local wind speed, direction, and duration. The wave heights are computed using the simple 1D equations, or models for more elaborate conditions. The maximum wave height—derived from the breaker parameter, equation, or model—can be used for the wave hazard at the referenced SWL hazard. It follows that the wave hazard at a particular SWL hazard can differ widely across a polder due to differences in topography, proximity to wind sheltering features located in the predominant upwind wind direction, and/or the presence of heavy canopy.

Section 17. Recent Applications of Polder Hazard Analysis

The additional hydraulic methods and JPA for polder inundation hazard discussed in Sections 15 and 16 have recently been applied to planning and engineering for the New Orleans regional HSDRRS illustrated in Figure 17.1. The applications include four major efforts:

1. The IPET Performance Evaluation of the New Orleans and Southeast Louisiana Hurricane Protection System (Volume VIII, Risk and Reliability IPET 2009a and 2009b);
2. The USACE LaCPR Study, (Final Technical Report USACE 2009);
3. The USACE HSDRRS Design—(Interim Guidelines and Draft Elevation Report, USACE 2008b and 2010); and
4. The USACE Armoring Alternative Evaluation Process, (Summary Report, USACE 2011).

The following sections discusses these efforts and important limitations. The LaCPR Study and HSDRRS Design, as well as the Louisiana CPRA's 2012 Master Plan, also employed polder inundation hazard analysis to evaluate future conditions—which are covered in Part V.

Figure 17.1. New Orleans HSDRRS

Swenson, D. (Times-Picayune) 2012

17.1 IPET Risk and Reliability Study

In 2009, nearly four years after devastating flooding caused by Hurricane Katrina's surge, IPET published results from a JPA for surge-driven inundation hazard for the New Orleans regional east- and west-bank polders shown in Figure 16.1. IPET employed inundation JPA to compare pre-Katrina HSDRRS risk and reliability versus the 2007 post-Katrina reconstructed HSDRRS and planned 2010 HSDRRS (also referred to as 2011 in IPET 2009b). The IPET 2010 HSDRRS alternative did not include the IHNC/GIWW or Seabrook Barriers or the higher replacement West Return Wall. (Note: a final summary report, IPET 2009b, acknowledges these barriers as having been added to the 2011 HSDRRS design.) The following paragraphs summarize key aspects of the IPET approach together with the results.

As noted in Section 16.1, a Surge Response-OS cannot be used for polder inundation hazard analysis as it does not provide a set of *whole-perimeter* surge events representative of the regional hurricane climatology. The IPET study, as discussed in Section 14.2, therefore improvised a JPM-OS set of perimeter events, utilizing 76 of the 152-storm FIS Surge Response-OS and assigned a value for ***p*** to each storm (see Part III, Attachment 1). However, the 76-storm Surge Response-OS does not include storm intensity above the 200-yr return period, such as a landfalling Category 5 storm. As also described in Section 14.2, IPET 100- and 500-yr exterior surge hazards were notably different from those found in the FIS—24% lower for the 500-yr hazard at an east-bank St. Charles Parish location.

The IPET study utilized the FIS validated ADCIRC-STWAVE model for the pre-Katrina alternative, which was validated in southeast Louisiana (see Section 11.2). For the 2007 alternative IPET employed the FIS 2007 mesh to assess exterior SWL return frequencies. IPET did not address the bias in the validation of the ADCIRC-STWAVE model with respect to the south shore of Lake Pontchartrain and did not provide a bias correction.

IPET (2009a Appendix 8) indicated that a 2010 mesh version was employed for the improved HSDRRS alternative. As the IPET 2010 HSDRRS alternative did not include the IHNC or Seabrook Barriers (as indicated by overtopping and breaching scenarios along the IHNC/GIWW) it is assumed that the 2010 mesh version likewise did not include these structures.

The ADCIRC-STWAVE model provided SWL time series at selected regional locations. Additional hydrographs at about 260 locations were generated around the perimeter for each of the 76 events, for each of the three barrier alternatives (equating to abut 20,000 perimeter SWL hydrographs per alternative). For these additional hydrographs the model result for the peak SWL was taken from the nearest node and the hydrograph shape was then derived from the closest time-series.[1]

IPET applied a breaker parameter of 0.43 to each local SWL hydrograph to estimate the time-varying Zone D H_s condition. As discussed in Section 6.2, there is a critical need for more data on foreshore waves, including the application of breaker parameters. For local wave periods (mean) during each event IPET used the value from the nearest STWAVE grid point.

IPET employed the expanded the JPA discussed in Section 16.2 to address whole-polder SOBRP scenarios for each of the 76 exterior surge/wave events. The whole-polder SOBRP subset for each storm included one potential breach failure I-L case per reach (including transitions and gates):

1. Breach occurrence was conditioned first on the local exterior peak SWL and associated freeboard R_c (crest elevation minus peak SWL). If R_c remained greater than the a defined minimum threshold then no breach occurred at the reach.

[1] The IPET description of this methodology is not fully explained.

2. For R_c less than the threshold, IPET defined a simple one-step location-specific breach I-L case.[2] This case was based on whether:
   - R_c at the peak SWL was positive (peak SWL below the reach crown elevation, i.e., no overtopping) or negative (peak SWL above the crown, i.e., overtopping); and
   - Structure type—levee (hydraulic fill/clay/unknown soil), floodwall, gate, or transition.

   Figure 17.2 presents the IPET breach cases.
3. If R_c was reduced to less than the threshold, then the occurrence of the breach case as defined above was then further conditioned using a fragility expression, as depicted in Figure 17.3, to assign a probability for erosion and collapse breaching:
   - Distinct collapse and erosion fragility relationships were assigned for each structure type. Levee type included hydraulic fill/clay/unknown soil composition subtypes.
   - If the minimum R_c at a reach during a storm resulted in no overtopping (peak SWL remained below the structure crest) collapse fragility was used to estimate the probability of the breach case occurring. The collapse fragility incorporated categories of local subsurface conditions which might lead to soil failures, including seepage mechanisms.
   - If the minimum R_c at a reach during a storm resulted in overtopping, erosion fragility was used to estimate the probability of the breach case occurring. Erosion fragility incorporated the magnitude of negative R_c.
   - In addition to erosion and collapse breaching, IPET considered probabilities for gate closure and transition failures.
4. For peak SWL above the threshold, the no breach probability equals one minus the breach probability.

For each surge event, N reaches (including gates and transitions) implies a maximum of 2N individual breach conditions. Treating each reach breach independently yields 2^N possible combined scenarios. However, the defined threshold R_c for the first condition meant that the vast majority of reaches for the vast majority of storms had the "no breach" condition. Thus, the number of breach scenarios per storm was much less 2^N, but still totaled hundreds per surge event; and many thousands of whole-polder scenarios for the overall 76-storm set. For each storm, with joint probability ***p***, each of the hundreds of whole-polder scenarios was assigned its relative fraction of ***p***—based on the joint probability of the condition at each independent reach.

[2] A breach condition consists of a single combination of breach *depth* (crest minus breach invert) and length. The IPET breach condition therefore does not provide for a dynamic breach with rising SWL.

Reaches						
Levee/Floodwall Breach Model Given Overtopping (erosion breach)						
		0 to 1ft		1ft to 3ft		
Material	**Symbol**	**Depth (ft)**	**Breach Width (w), Reach Length <1000ft**	**Depth (ft)**	**Breach Width (w) (ft), Reach Length <1000ft**	**Depth (ft)**
Hydraulic Fill	H	0	0	9	0.50*L to max 400	18
Clay	C	0	0	3	0.50*L to max 135	13
Unknown (Average)	U	0	0	6	0.50*L to max 290	17
Wall	W	0	0	0	0	17
		Length Modifiers Reach L>1000 ft				
		Overtopping Depth (ft)				
Material	**Symbol**	**0 to 1ft**		**1ft to 3ft**		**>3 ft**
Hydraulic Fill	H	0.0		400 < w < 0.40*L		430 < w < 0.40*L
Clay	C	0.0		135 < w < 0.10*L		135 < w < 0.10*L
Unknown (Average)	U	0.0		290 < w < 0.30*L		315 < w < 0.30*L
Wall	W	0.0		0.0		315 < w < 0.10*L
Levee/Floodwall Breach Model Given No Overtopping						
			Breach Width (w), (ft)			
Material	**Symbol**	**Depth (ft)**	**L ≤ 1000 ft**	**1000 < L≤ 10,000 ft**	**L>10,000 ft**	**Notes**
Hydraulic Fill	H	18	0.50*L to max 500	500 < w ≤ 0.15*L	0.15*L	3 Breaches / 10,000 reach
Clay	C	13	0.50*L to max 500	500 < w ≤ 0.10*L	0.10*L	2 Breaches / 10,000 reach
Unknown (Average)	U	17	0.50*L to max 500	500 < w ≤ 0.125*L	0.125*L	2.5 Breaches / 10,000 reach
Wall	W	17	0.50*L to max 500	500 < w ≤ 0.075*L	0.075*L	1.5 Breaches / 10,000 reach
Transitions						
Transitions Breach Model Given Overtopping						
		Breach size (ft)				
Transition Type	**Symbol**	**width**	**Depth**			
Ramps	R	25	3			
Floodwall-Levee	T	50	3			
Drainage Structures	D	65	5.5			
Pump Stations	P	100	5			
Gates	G	25	5			
Unprotected sections	U	N/A	N/A			
Transitions Breach Model Given No Overtopping						
		Breach size (ft)				
Transition Type	**Symbol**	**width**	**Depth**			
Ramps	R	-	-	Treated as opened or closed (sand bagged)		
Floodwall-Levee	T	-	-	No breaching until OT		
Drainage Structures	D	-	-	No breaching until OT		
Pump Stations	P	-	-	No breaching until OT		
Gates	G	-	-	Treat as opened or closed		
Unprotected sections	U	N/A	N/A			

Figure 17.2. IPET Breach Failure Conditions

IPET 2009a, Volume VIII Appendix 9

IPET computed and routed inflow volumes for each whole-polder scenario using an integrated series of EXCEL spreadsheets. IPET named the spreadsheet program FoRTE for Flood Risk Analysis for Tropical Storm Environments. IPET's FoRTE program included the following steps:

1. Seepage contribution to the polder inundation was ignored.
2. For scenarios with one or more continuously submerged inverts (i.e., remaining below the final local exterior SWL) the entire polder was assumed to equalize with the highest local final exterior SWL from among those submerged inverts. In this case inundation volume additions from overtopping and rainfall, and removal by pumping were ignored.
3. For scenarios with all breach inverts above the final exterior SWL, each cumulative breach inflow to the adjacent sub-basin was calculated using the SWL hydrograph, presumably using the broad crested weir equation. (IPET did not provide breach weir coefficients.)
4. Overtopping for non-breaching perimeter reaches addressed all five phases and used the local exterior SWL hydrograph and wave information. Wave-only contributions were reportedly analyzed using standard runup and overtopping methods (see Section 15.3) but were performed outside of FoRTE spreadsheets and added afterwards. For Phase 5 overtopping the FoRTE spreadsheets employed the standard broad-crested weir equation with C values ($ft^{½}/s$) of 3.0 for floodwalls, 2.6 for levees, and 2.0 for gates.

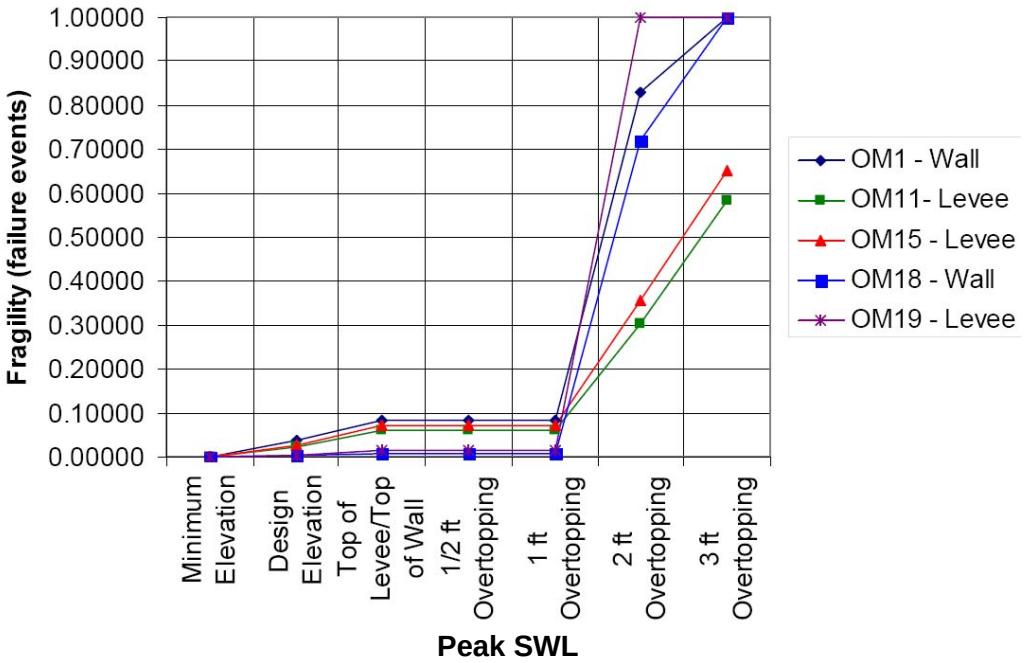

Figure 17.3. Example of IPET Breach Fragility
Selected Metro New Orleans Reaches
IPET 2009b[3]

[3] Other IPET documentation (Link et al Undated) suggests that levee and floodwall overtopping fragility was simplified into a few generalized incremental probabilities.

5. A generalized storm cumulative rainfall by sub-basin was estimated based on storm intensity and distance to the storm center according to Lonfat et al 2004, and a multiplier of 1.5 was applied for rainfall to the right of the hurricane heading.
6. The rainfall cumulative volumes were further adjusted according to three pumping cases:
   - No reduction of volume for a no pumping case;
   - Reduction of volume in accordance with cumulative pumping at 50% capacity; and
   - Reduction of volume in accordance with cumulative pumping at 100% capacity.
7. For scenarios without submerged breaches (without Step 1) level-pool routing with exchanges between sub-basins was used to determine final interior peak SWL for each sub-basin, for each fractional ***p*** scenario, broken down into the three pumping cases.
8. The IPET polder routing did not include interior wind setup and the polder hazard analysis did not consider interior waves.
9. The routing results in each sub-basin for each whole-polder scenario for each storm were assigned the fraction of ***p***.
10. Sub-basin peak SWL CDFs were calculated using the results for the thousands of scenarios. The CDFS were calculated separately for the three different pumping cases.

IPET used the sub-basin inundation SWL CDFs to determine inundation at the 50-, 100- and 500-yr hazard level for the three pumping-cases. Table 17.1 presents the results for the 2010 (2011) HSDRRS. Table 17.1 shows that with the 100% pumping case SWL increased in 13 of 27 sub-basins for the 100-yr versus the 50-yr hazard. Of these, three east-bank sub-basins and one west-bank sub-basin SWLs increased by more than 2 ft: OM1 (6 ft); OM4 (3 ft); Jefferson, JE3 (5 ft); and JW4 (8 ft).

For the 500-yr versus the 50-yr hazard, with the 100% pumping case, SWLs increased in 25 of 27 sub-basins—17 by 3 ft or more, and 10 by 5 ft or more. The IPET report did not discuss the source of these increases, such as the contribution from rainfall. As the IPET 2010 HSDRRS did not include the IHNC and Seabrook Barriers, increased SWLs may also reflect inflow along the IHNC. Figure 17.4. depicts the 50-, 100-, and 500-yr flood depths for 2010 (2011) HSDRRS for the 100% pumping case.

Table 17.2 presents the volumes for 2010 (2011) HSDRRS for the 100% pumping case that correspond to the 100- and 500-yr inundation hazard elevations in each sub-basin. Totals are also included for five combined master drainage areas and the overall polders. Total volumes are provided for reference but as with rainfall-only hazard (Table 16.1), these summed volumes are **not** the associated hazard for these larger areas. IPET did not provide hazard volumes for the master drainage areas or whole-polders.

For comparison Table 17.2 shows the 6-hr/100-yr rainfall (from Table 17.1) minus 6-hr pumping for five combined master drainage areas. *Notably the Orleans master drainage area has a **lower** volume for the 500-yr surge inundation hazard than for the 6-hr/100-yr net rainfall*. However, within the Metro Polder the 500-yr surge inundation volume is a factor of 2.5 times higher than the 6-hr/100-yr net rainfall volume for both East Jefferson and St. Charles. For the Lower 9th Ward/St. Bernard master drainage area the difference is the most, at a factor of 4.3 higher. For New Orleans East the difference is much lower, at 40% higher. Again, these reflect the IPET analysis without the IHNC/GIWW and Seabrook Surge Barriers, and higher West Return Wall.

Table 17.1. IPET Inundation Hazard for the 2010 (2011) HSDRRS

Elevation ft NAVD88-2004.65

Sub-Basin	50-Yr Inundation Hazard			100-Yr Inundation Hazard			500-Yr Inundation Hazard		
	Pumping			Pumping			Pumping		
	0%	50%	100%	0%	50%	100%	0%	50%	100%
OW1	-1	-1	-1	0	-1	-1	1	1	1
OW2	-3	-3	-3	-2	-2	-2	0	0	0
NOE1	0	0	0	0	0	0	3	3	3
NOE2	-4	-5	-5	-3	-4	-4	0	-2	-2
NOE3	-4	-5	-5	-3	-4	-4	-2	-3	-3
NOE4	-1	-2	-3	0	-1	-1	2	0	0
NOE5	-8	-9	-11	-7	-8	-9	-4	-6	-6
OM1	-5	-7	-12	-4	-5	-6	-2	-4	-5
OM2	-5	-12	-12	-4	-12	-12	-2	-7	-12
OM3	-1	-6	-12	-1	-6	-12	1	-2	-12
OM4	-1	-5	-5	-1	-2	-2	1	1	1
OM5	-1	-4	-12	0	-4	-12	1	0	-2
SB1	-1	-5	-12	0	-2	-12	2	1	0
SB2	1	1	1	2	2	2	3	3	3
SB3	0	-1	-3	1	-1	-3	2	0	-1
SB4	2	1	1	3	1	1	5	4	4
SB5	3	3	3	4	3	3	5	5	5
JE1	3	2	2	4	2	2	5	4	4
JE2	-4	-12	-12	-3	-12	-12	-2	-3	-4
JE3	-5	-6	-10	-4	-5	-5	-2	-3	-3
JW1	0	0	0	2	1	1	3	2	2
JW2	-4	-5	-5	-3	-5	-5	0	-2	-2
JW3	-2	-5	-12	0	-1	-2	0	0	0
JW4	-5	-12	-12	-3	-4	-6	-1	-3	-4
PL11	-2	-12	-12	-2	-12	-12	1	-4	-5
SC1	2	2	2	3	3	3	5	5	5
SC2	4	4	3	4	4	3	6	5	5

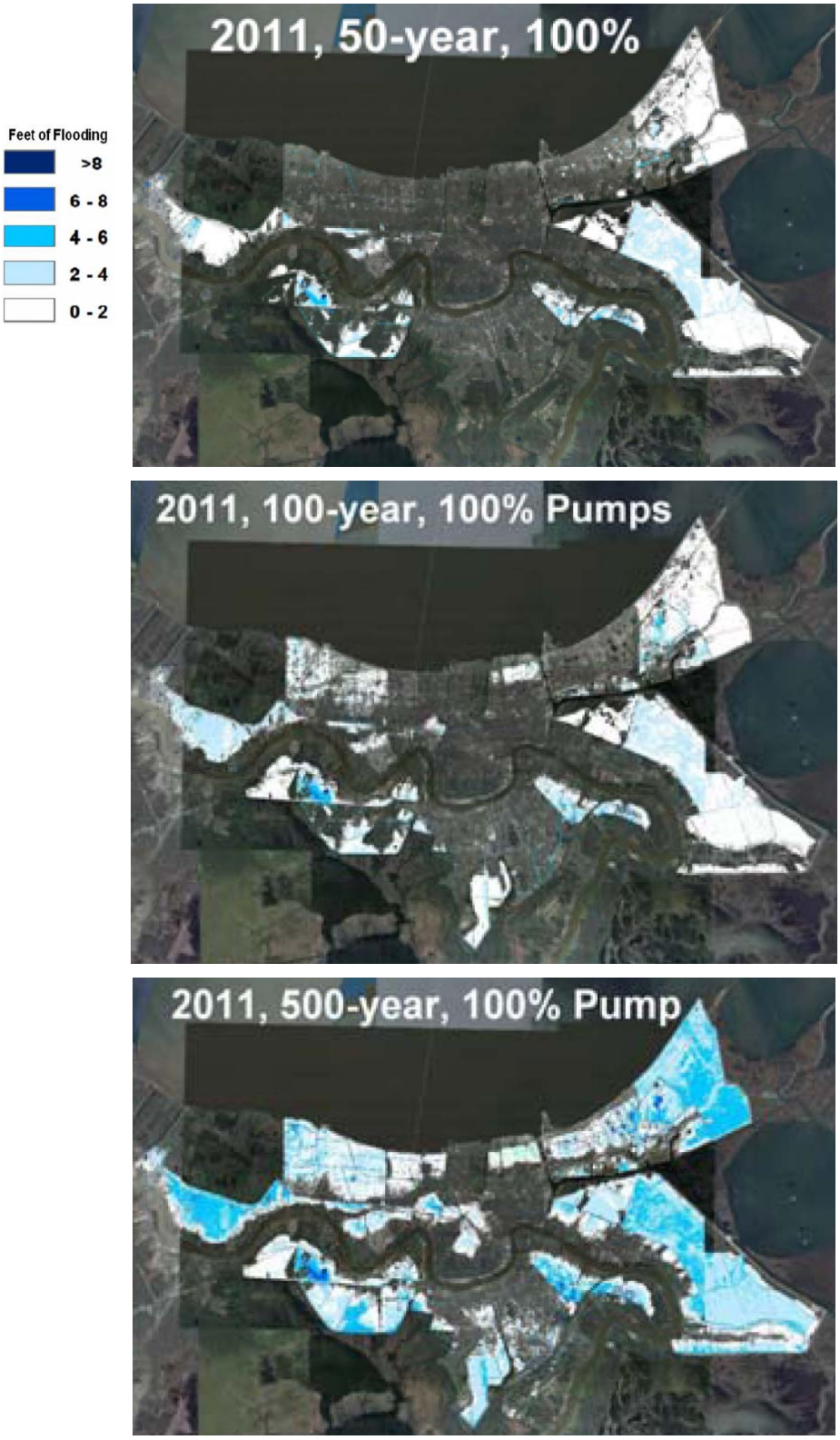

Figure 17.4. IPET Inundation Hazard for the 2010 (2011) HSDRRS
100% Pumping
IPET 2009b

Table 17.2. IPET Inundation Hazard Volume for the 2010 (2011) HSDRRS[4]

100% Pumping

Polder	Sub-Basin	Acres	100-Yr Inundation Hazard		500-Yr Inundation Hazard		6-hr/100-yr Rainfall Minus 6-hr Pumping Acre-ft
			Elev	Vol Acre-ft	Elev	Vol Acre-ft	
New Orleans East	NOE1 Maxent Lagoon	14,233	0	7,975	3	47,635	
	NOE2 Maxent Wetland	5,683	-4	6,206	-2	14,718	
	NOE3	2,866	-4	1,244	-3	2,104	
	NOE4	2,338	-1	1,058	0	1,756	
	NOE5	9,588	-9	2,625	-6	10,598	
	NOE3, 4, 5* (within Maxent Levee)	***14,792***		***4,927***		***14,458***	***12,327 - 1,930 = 10,397***
Lower 9th Ward/ St. Bernard	SB2 Central Wetland	5,066	2	2,475	3	5,462	
	SB5 Central Wetland	24,340	3	21,764	5	62,814	
	SB1	5,115	-12	0	0	35,397	
	SB3	5,485	-3	593	-1	1,706	
	SB4	9,415	1	1,480	4	14,639	
	SB1, 3, 4* within 40 Arpent Levee	***20,015***		***2,073***		***51,742***	***16,679 – 4,518 = 12,161***
Metro New Orleans	SC1 (mostly swamp)	5,906	3	8,057	5	18,654	
	SC2	7,364	3	2,175	5	6,041	
	SC1 & 2*	***13,270***		***10,232***		***24,695***	***11,058 - 1,017) = 10,041***
	JE1	7,784	2	1,995	4	6,366	
	JE2	5,510	-12	45	-4	3,185	
	JE3	15,395	-5	6,721	-3	25,322	
	JE1, 2, 3*	***28,689***		***8,761***		***34,873***	***23,908 – 10,289 = 13,619***
	OM1	5,041	-6	964	-5	2,276	
	OM2	4,176	-12	14	-12	14	
	OM3	4,720	-12	1	-12	1	
	OM4	2,063	-2	468	1	2,361	
	OM5	11,268	-12	16	-2	2,638	
	OM 1, 2, 3, 4, 5*	***27,268***		***1,463***		***7,290***	***22,723 – 12,724 = 9,999***

* Sub-Totals and Totals do NOT represent multi-sub-basin hazard volumes.

[4] IPET's own stage-storage data for the sub-basins were not available and therefore volumes were independently computed using the regional LIDAR DEM.

As discussed in Section 14.2 IPET addressed both epistemic and aleatory uncertainties (see Section 14.5) in exterior surge hazards based on their 76-storm JPM-OS. In the case of one location an asymmetric epistemic uncertainty in the 100-yr SWL (9.7 ft) was illustrated with 90% LCL/UCLs bands at -2.1 and +2.8 ft. This uncertainty included σ_ψ at 10% of SWL (, 0.97 ft, or 90% LCL/UCL bands of about ±1.6 ft) and an asymmetric ε_P, which added more than 1 ft to the ε_ψ 90% UCL band. Components of the aleatory uncertainty were thought to contribute σ_A of 2.1 ft to the 100-yr hazard at the location, indicating an overall σ of 2.3 ft, or a 90% LCL/UCL for normally distributed uncertainty alone of ±3.8 ft. Inclusion of ε_P means the overall magnitude of uncertainty is even higher. However, IPET did NOT address these significant exterior SWLs uncertainties in the analysis of polder inundation hazard. The influence of non-linear contributions was not assessed and confidence limits in the inundation hazard were not identified

17.2 USACE LaCPR Study

The 2009 USACE LaCPR Study examined both exterior surge SWL hazard and surge-related polder inundation under several large-scale planning alternatives. The Study included a current condition alternative reflecting the authorized HSDRRS design—referred to as the 2010 Base Alternative—as well as several future condition alternatives with enhanced surge protection and coastal restoration projects. The USACE's analysis of future alternatives is discussed in Part V, Section 20.1.

The LaCPR Study 2010 Base Alternative version of the authorized HSDRRS used an ADCIRC mesh incorporating the IHNC Surge Barrier (but not the Seabrook Barrier). The Study assessed exterior surge hazards at the 100-, 400-, 1000-, and 2000-yr return periods. The 400-yr hazard was stipulated in the study objectives for evaluating a Katrina-level event. The 400-yr hazard was based on the Resio et al work which estimated Hurricane Katrina's landfall return period for southeast Louisiana at 398 years (see Section 4.2).

The LaCPR Study for the 2010 Base Alternative employed the Surge Response-OS approach used in the FIS JPA of exterior SWL hazards (see Section 14.1). However only 48 of the 152 storms were simulated with the revised mesh (presumably due to limited computational resources). For the 104 storms not rerun, 2010 peak SWLs were instead estimated by applying an adjustment to the 2007 SWLs derived with an algorithm. The algorithm was a quadratic equation specifying the adjustment equal to $A*SWL_{2007} + B*SWL_{2007}^2$. Values for A and B were derived for each output location by fitting this equation to 2007 and 2010 results for the 48 storms that were run. Figure 17.5 illustrates the fitting of the algorithm for two locations. The LaCPR Study report (Hydrology and Hydraulics Appendix) acknowledged that at some locations the quality of fit could be poor.

For the Study, 2010 surge CDFs were computed at each of several hundred locations throughout coastal Louisiana using the 152 local 2010 SWL values (the 48 simulation results plus the 104 estimated values), presumably post-processing similar to the FIS (see Section 14.1). The Study report did not discuss the SWL bias previously noted in the FIS analysis (Section 11.2). The Study report indicated that uncertainty bands were computed for the 2010 SWL hazard levels. However details on how they were developed (including increased uncertainty due to not rerunning all 152 storms), as well as the bands themselves, were not provided.

Zone B Wave H_S and T_P for the 2010 Base Alternative were also developed using a combination of the 48-storm results and the application of fitting algorithms.

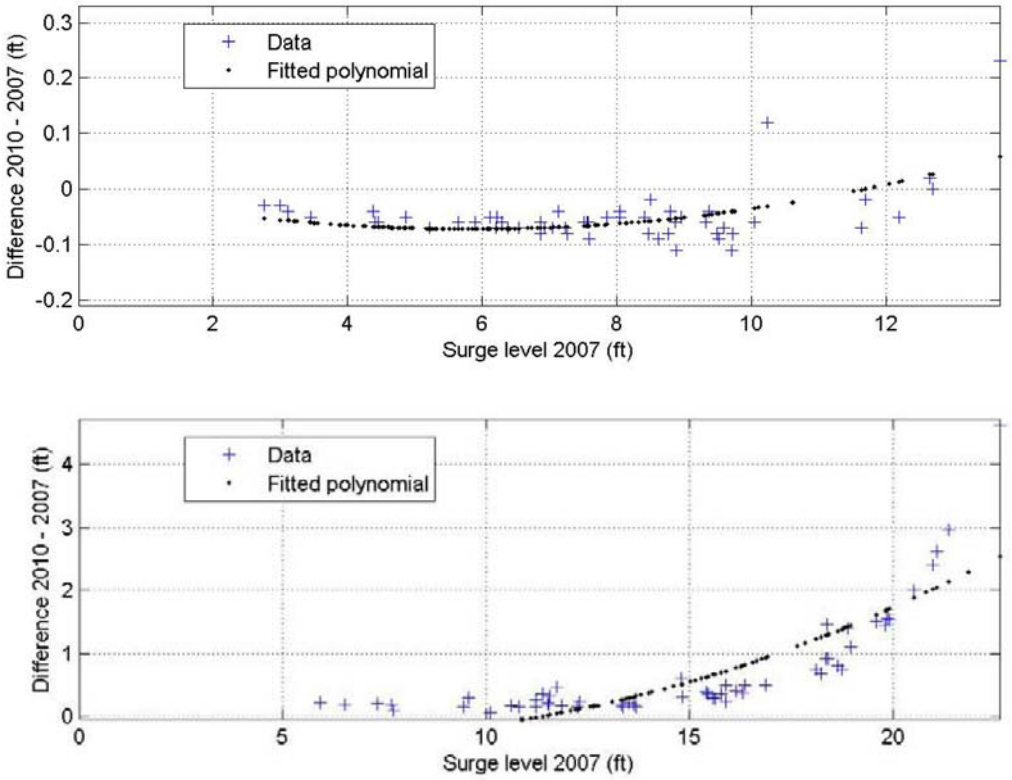

Figure 17.5. Example of 2007-2010 Adjustment Algorithm at Two Locations
USACE 2009

The LaCPR Study did not perform a return frequency for polder inundation or evaluate the cumulative probability of interior SWLs. Unlike the IPET Risk and Reliability Study described above, the LaCPR Study did not assess the joint probability of various inflows associated with probabilistic whole-perimeter surge events. Instead, for this study the USACE simply chose to use the entire set of SWLs around a polder perimeter at the various hazard levels as a "pseudo" surge event. As previously noted, a single storm exceeding the 100-yr (for example) exterior SWL along an entire polder perimeter can have a much greater return period than 100 years. While the study's approach expedited relative comparisons of many alternatives (e.g., future conditions), it cannot be relied upon for estimates of polder inundation hazards. The polder inundation associated with using these "pseudo" surge events are thus better termed *cases*, as in Perimeter Surge Case 100, 400, 1000, and 2000, leaving off any reference to return period to eliminate confusion.

The interior SWLs for the four cases were computed as follows:

- SWL hydrographs were developed at each polder perimeter reach for the three cases using normal distribution curves and values for σ_R and σ_F, obtained by assessing peak SWL versus σ_R and σ_F for the output hydrographs.
- Zone D a wave breaker parameter of 0.4 was applied to the surge depth at the forward embankment toe. and wave T_P was obtained from the STWAVE output. Standard deviations of 10% and 20% were assumed for the Zone D H_S and T_P. Wave θ was assumed to be perpendicular (worst case for overtopping).

- Overtopping hydrographs were computed for each reach (using the structure design elevation) with a combination of the Van der Meer and broad crested weir equations. The Study used C_W and C values of 0.13 and 3.1 $ft^{½}/s$.
- The overtopping estimate included both a 50% (median) and 10% Probability of Exceedance Levels (the same as a 90% Probability of Non-Exceedance and equivalent to the UCL for an 80% Confidence Interval). The overtopping rates at these confidence levels were obtained using the Monte Carlo technique (see GTN-1 Part J) that incorporated uncertainty in the SWL, wave height, wave period, and overtopping coefficients. Figure 17.6 shows an example of a 10%, 50%, and 90% Confidence Level hydrograph at one location, for Perimeter Surge Cases 100, 400, 1000, and 2000
- The LaCPR Study did **NOT** include breaching scenarios.
- Rainfall accumulation was set at 6.5 inches, using the 10-yr 6-hr duration event, with an assumed sinusoidal temporal distribution.
- Pumping volumes were used for each sub-basin based on assumed pump station capacities (not provided in the report).
- Sub-basin peak SWLs were then calculated for the four cases using level-pool routing. Confidence intervals for SWL were based on the overtopping confidence intervals.

Figure 17.7 illustrates the polder inundation results for the 2010 Perimeter Surge Case 1000. (The figure presumably is for the 50% Confidence Level but this information was not clearly stated.)

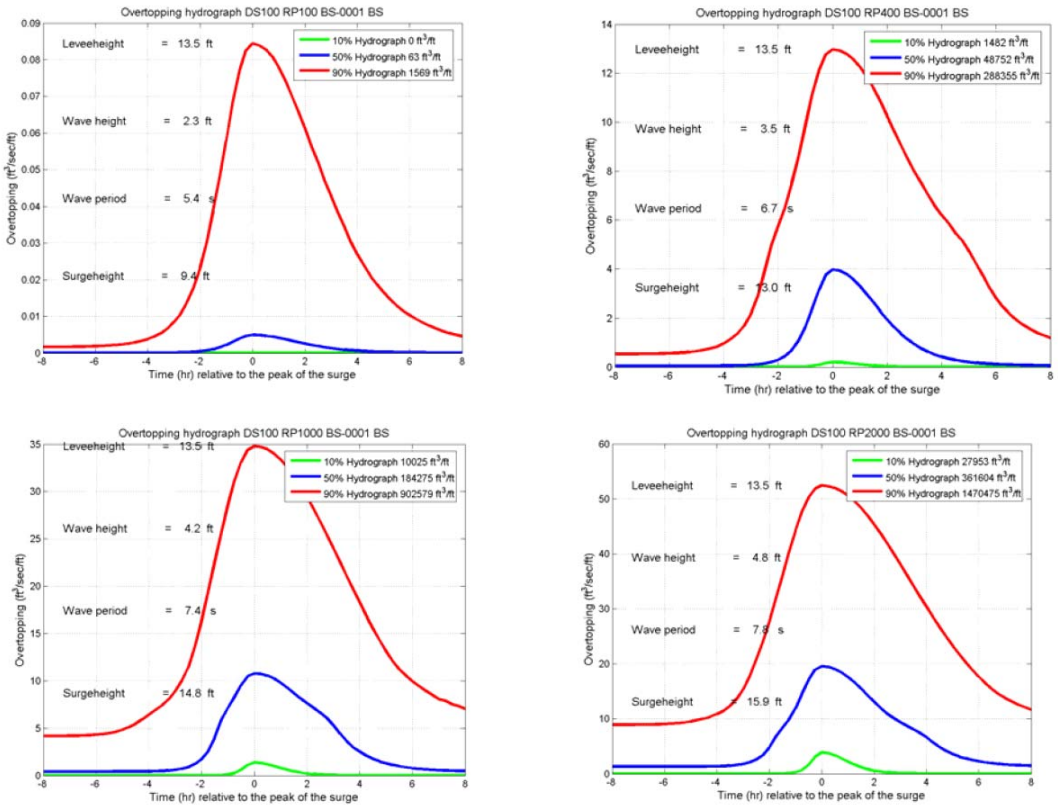

Figure 17.6. Example of Overtopping Hydrographs for Four Cases

USACE 2009

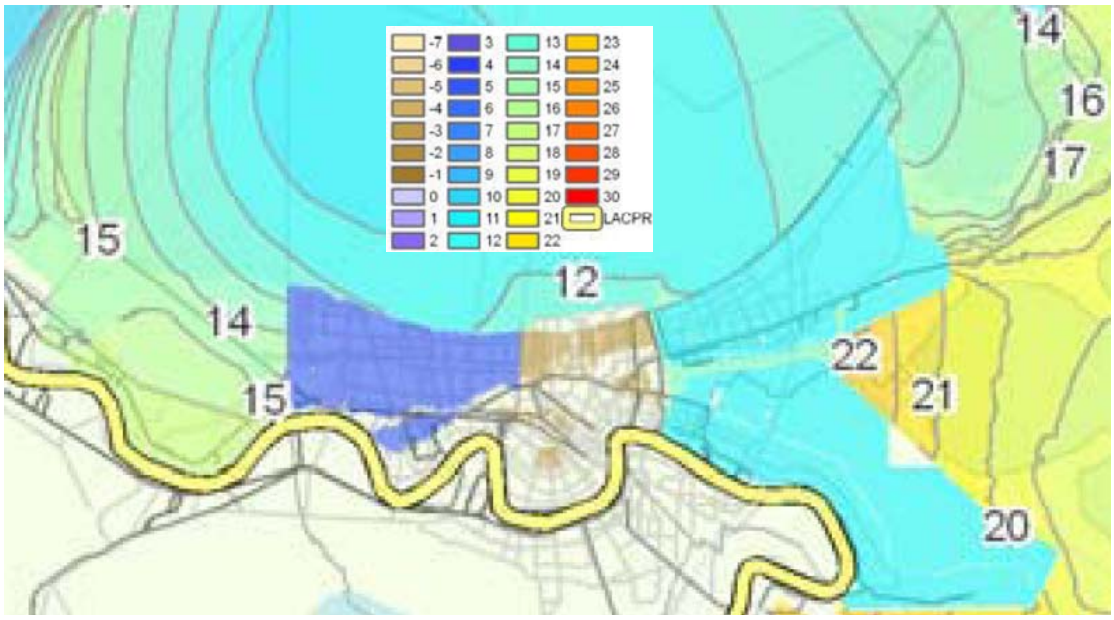

Figure 17.7. Polder Inundation SWLs Associated with Perimeter SWL Case 1000

USACE 2009

(Note the LaCPR Study terrain data mistakenly included a continuous barrier along the St. Charles-Jefferson Parish Line that prevented the 15 ft. high SWL in St. Charles Parish from inundating Jefferson Parish.)

17.3 USACE HSDRRS 100-yr Design

In the wake of Hurricane Katrina Congress authorized the USACE to reconstruct and enhance the New Orleans regional HSDRRS to protect polders from the 100-yr surge hazard.[5] Given that the polders are exposed to substantial 100-yr rainfall flood hazards—even with elaborate drainage systems—the HSDRRS does not eliminate the interior 100-yr flood hazard.[6] The HSDRRS actual design objective therefore is to reduce surge overtopping contributions to the interior 100-yr hazard to a negligible amount (but not zero). T

In accordance with this objective the USACE HSDRRS design provided positive SWL freeboard at the 100-yr SWL—meeting or exceeding NFIP coastal SWL freeboard requirement. (Per 44 CFR 65.10 at least 2 ft of freeboard is required above the 100-yr SWL.) The NFIP also requires 1 ft of clearance above the maximum wave runup for the 100-yr SWL condition unless a lower elevation is supported by appropriate wave overtopping analysis. Given the interior rainfall flood hazard, the USACE proposed HSDRRS design elevations that allowed some *minor* wave-only overtopping at the 100-yr surge hazard. To enhance the design for *minor* wave-only overtopping the USACE addressed some uncertainty in the

[5] As discussed in the Introduction, the 100-yr hazard derives from the NFIP—for which it is a statutorily required (and convenient but somewhat arbitrary) nation-wide benchmark for managing property flood damage risks. However, the 100-yr hazard is widely regarded as an inadequate criteria for comprehensive management of flood risks for a major metropolitan area (see ASCE Louisiana Section 2012).

[6] FEMA and the USACE are currently finalizing FISs for the New Orleans regional polders based on rainfall flood hazards. Some technical documentation is found in FEMA 2012.

overtopping rate estimate. Notably, the NFIP does not require establishing flood hazard elevations with any uncertainty allowance.

The USACE described their approach to specifying 100-yr elevations for each HSDRRS reach in two critical guidance documents (USACE 2008b and 2010). The approach consisted of five steps to account for current (2010) conditions, each with important limitations: (An additional step was also included to address future, 2057, conditions, see Section 20.2).

1. Current 100-yr exterior surge SWL hazards. The USACE 2010 Elevation Report stated that exterior SWL hazards were developed using the 2007 FIS and 2010 ADCIRC meshes (presumably the same one used in the LaCPR Study without the Seabrook Barrier) and the 152-storm Surge Response-OS approach. The design used a combination of 106 storm simulations from the 2007 FIS mesh with 56 storms run on the 2010 mesh (6 more than the 48 used for the LaCPR Study). The 106 2007 SWLs were then adjusted to 2010 conditions, presumably in a manner similar to that described above for the LaCPR Study. The design therefore reflects important limitations in:

   - The treatment of regional hurricane climatology—i.e., joint probability (see Section 4.2);
   - The ADCIRC mesh—as validated for Hurricane Katrina (see Section 11.2), including bias on the south shore of Lake Pontchartrain—lacking the Seabrook Barrier;
   - The Surge Response-OS approach in general (see Section 13.3);
   - The particular Surge Response-OS set used for the southeast Louisiana (see Sections 14.1 and 14.2);
   - The approach to updating the 2010 CDFs (as discussed above in Section 17.2).

   As discussed in Section 15.1, the CDF integration method included smoothing with σ_e , which results in a modest increase in the estimated 100-yr surge hazard.

   Figure 17.8 depicts the 100-yr SWLs used in the east-bank HSDRRS design. Comparing Figure 17.8 HSDRRS 100-yr SWLs with the Figure 14.7 100-yr 2007 SWLs shows little to no difference along Lake Pontchartrain but significant increases along the IHNC, GIWW, and MRGO, due to the inclusion of the IHNC/GIWW Barrier.

2. Current 100-yr exterior surge H_S and T_P hazards. As in the LaCPR Study the USACE established Zone B 100-yr wave conditions based on the 2010 CDFs and adjusted local Zone D wave H_S as necessary with 0.4 breaker parameter. As discussed in Section 6.2, more data are needed on appropriate local breaker parameters. Wave T_P was obtained from the STWAVE output. Wave θ was assumed to be perpendicular (worst case for overtopping).

3. Wave H_S, and T_P within the IHNC/GIWW sub-basin. The USACE estimated wave conditions in the channel confined by the closed IHNC and Seabrook barriers using the Bretschneider Equation (see Section 15.8) and a 1% wind speed of 77 mph. For most reaches a fetch of 0.5 mi was used, providing H_S, and T_P of 3 ft and 3.5 s, respectively. For northern and southern reaches along the IHNC a 0.25 mi fetch was utilized, yielding H_S, and T_P of 2.3 ft and 3.1 s, respectively. Wind setup, as well as more extreme wave conditions, produced along the 6+ mi GIWW fetch—similar to what was observed with Hurricane Gustav, but with the barriers closed—was not considered.

Figure 17.8. 100-yr SWLs for HSDRRS Design

USACE 2010

4. 100-yr SWL and waves in the Mississippi River. The USACE estimated these conditions using a supplementary JPM Surge Response-OS analysis, which has not been finalized:

   - Revised the JPA expression, $\boldsymbol{p}$, to incorporate a probability for the river discharge by month, together with the hurricane landfall frequency by month.
   - Modified the Surge-Response function, $\boldsymbol{\psi}$, to also be a function of Mississippi River discharge. A total of 17 out of the 152-storm set were remodeled using two different Mississippi River discharges (167,000 and 400,000 cfs)
   - Used an improved ADCIRC-STWAVE mesh with greater river details.[7]
   - Recomputed CDFs for points along the river using the revised $\boldsymbol{p}$ and $\boldsymbol{\psi}$.
   - Reran the analysis for sea-level rise of 1 ft (as well as 2, and 3 ft).
   - Estimated the 100-yr $\boldsymbol{H_{1\%}}$, and $\boldsymbol{T_P}$ along the river levees by applying the Bretschneider Equation, along with the location-specific wind speed/direction/fetch conditions at peak SWL for each storm in a subset of the 152 storm set. The subset was similar to the IPET JPM-OS subset and each storm had an assigned probability. For each location, the set of results for $\boldsymbol{H_{1\%}}$, and $\boldsymbol{T_P}$, with their corresponding probabilities, were used to fit a Weibull distribution, which then provided the 100-yr $\boldsymbol{H_{1\%}}$, and $\boldsymbol{T_P}$. The breaking parameter was used to reduce $\boldsymbol{H_{1\%}}$ as appropriate, depending on the local surge depth over the foreshore (batture) at peak SWL.

   The small set size of the southeast Louisiana Surge Response-OS approach may not sufficiently capture critical wind setup variations in the Mississippi River associated with changes in storm V_f and θ. Furthermore, as noted in Sections 14.2 and 17.1 a subset of the southeast Louisiana Surge Response-OS is not likely to provide a JPM-OS representative of more extreme hazards.

5. 100-yr design elevation for 2010 conditions at each reach. The USACE then determined design elevations using the estimates of 100-yr SWL, H_S, and T_P, together with assigned normally distributed uncertainty factors, σ, for each value. Crown design elevations were required to be at least 2 ft above the median (50% Exceedance Level) estimated 100-yr SWL.

   Median estimates of average overtopping rates were then computed with the Van der Meer and Franco equations and crown elevations were raised as necessary to limit the local 100-yr overtopping rate for levees and floodwalls at 0.01 and 0.03 cfs/ft, respectively.

   Next the uncertainty factors were employed with a Monte Carlo technique—using the same overtopping equations—to determine local average overtopping rates at the 10% Exceedance Level. Reach crown elevations were raised as necessary to limit the local 100-yr 10% Exceedance average overtopping rate for levees and floodwalls at 0.1 cfs/ft. Figure 17.9 illustrates the average overtopping rate versus exceedance level for one reach design.

   The USACE guidance (USACE 2010 Appendix E) stated that the technical basis for the average overtopping limits was preventing interior-side scour of embankments and erosion

[7] The USACE stated that the improved ADCIRC mesh was validated for both steady stage-discharge curves at several river locations. However, details of the mesh changes and these validations were not provided in the guidance. The guidance did provide a validation of the ADCIRC model river stages for Hurricanes Katrina, Betsy, and Camille.

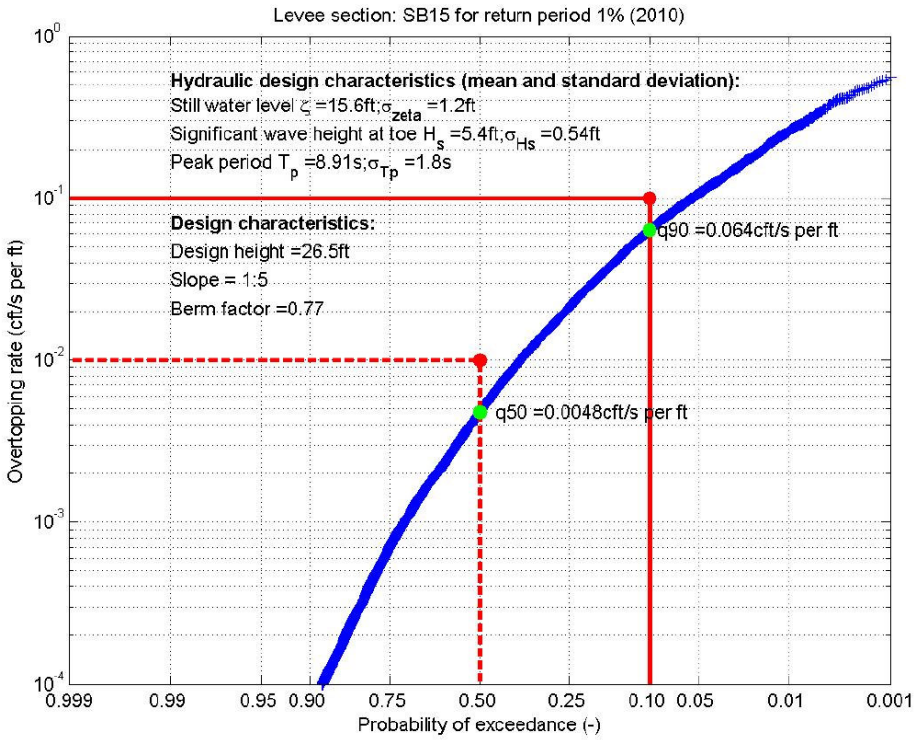

Figure 17.9. Example of Overtopping Rate vs Exceedance Level
USACE 2010

breaching caused by overtopping of extreme waves during brief hurricane surge peaks. On the one hand, concerns regarding overtopping limits may be mitigated to the extent that average overtopping equations can over-predict extreme wave recurrence over short durations, and thus overtopping rates (see Sections 15.1 and 15.3). On the other, however, little experimental data, as well as observations for actual levee and floodwall overtopping under surge type conditions, are available to support development of average overtopping limits. As discussed in Section 15.3, at an average overtopping rate of 0.1 cfs/ft, individual extreme wave overtopping may produce instantaneous velocities of 17 ft/s down the interior-facing slope, as well as cavitation effects on surface soils. A complete discussion of the subject of erosion-based wave overtopping criteria is beyond the scope of this Report.

The USACE an overtopping uncertainty analysis in order to provide some conservativism in the design.[8] Importantly though, the USACE did not utilize the full SWL hazard uncertainty previously determined for the FIS or IPET. Using the information in the FIS documentation, (see Section 14.1) the 100-yr epistemic σ is about $[(2.1)^2 + (0.15*SWL)^2]^{0.5}$—or 18% and 26% at SWLs of 20 and 10 ft, respectively. The HSDRRS design did not employ this σ value in the Monte Carlo analysis, but instead employed values which were below 10%.[9]

[8] The USACE design guidance made frequent use of the word "conservative" but did not explain the use of the 10% Exceedance Level—i.e., 80% Confidence Interval. Goldman 2003 cited the use of a 90% Confidence Interval—i.e., a 5% Exceedance Level—for the design of levees along the Upper Mississippi River.

[9] The Monte Carlo analysis also did not adjust the base value for H_s for draws of higher SWL and depth.

Figures 17.10.a and b illustrate the sensitivity of the wave overtopping rate and levee design elevation to the choice of SWL σ using the Monte Carlo technique. For a SWL of 12 ft an increase of σ from 10% to 20% (1.2 to 2.4) quadruples the 10% Exceedance overtopping and raises the design height by about one foot. An increase to 30% (3.6 ft) raises the 10% Exceedance overtopping by a factor of 10 and raises the design height by two feet.

The design did not discuss the issue of SWL bias associated with the ADCIRC Hurricane Katrina validation (see Section 11.2) and did not introduce bias correction. Figure 17.10.c and d depict the influence of SWL bias on the median (50% Exceedance) overtopping rate and design elevation (ignoring any influence on wave height). A 1.5 ft under-prediction of SWL (13.5 ft versus 12 ft) increases the median overtopping by a factor of three, and requires raising the design by close to 1.5 ft.

Figures 17.11.a, b, c, and d illustrate sensitivities for H_S uncertainty and bias. Overtopping and design elevation are relatively insensitive to H_S uncertainty. However, H_S bias—e.g., if the 0.4 breaking parameter is too low—has a notable influence on overtopping and levee crest height. In the case depicted, a 1 ft H_S under-prediction (3.2 versus 4.2 ft) increases the median overtopping by a factor of five, and requires raising the design by over two feet.

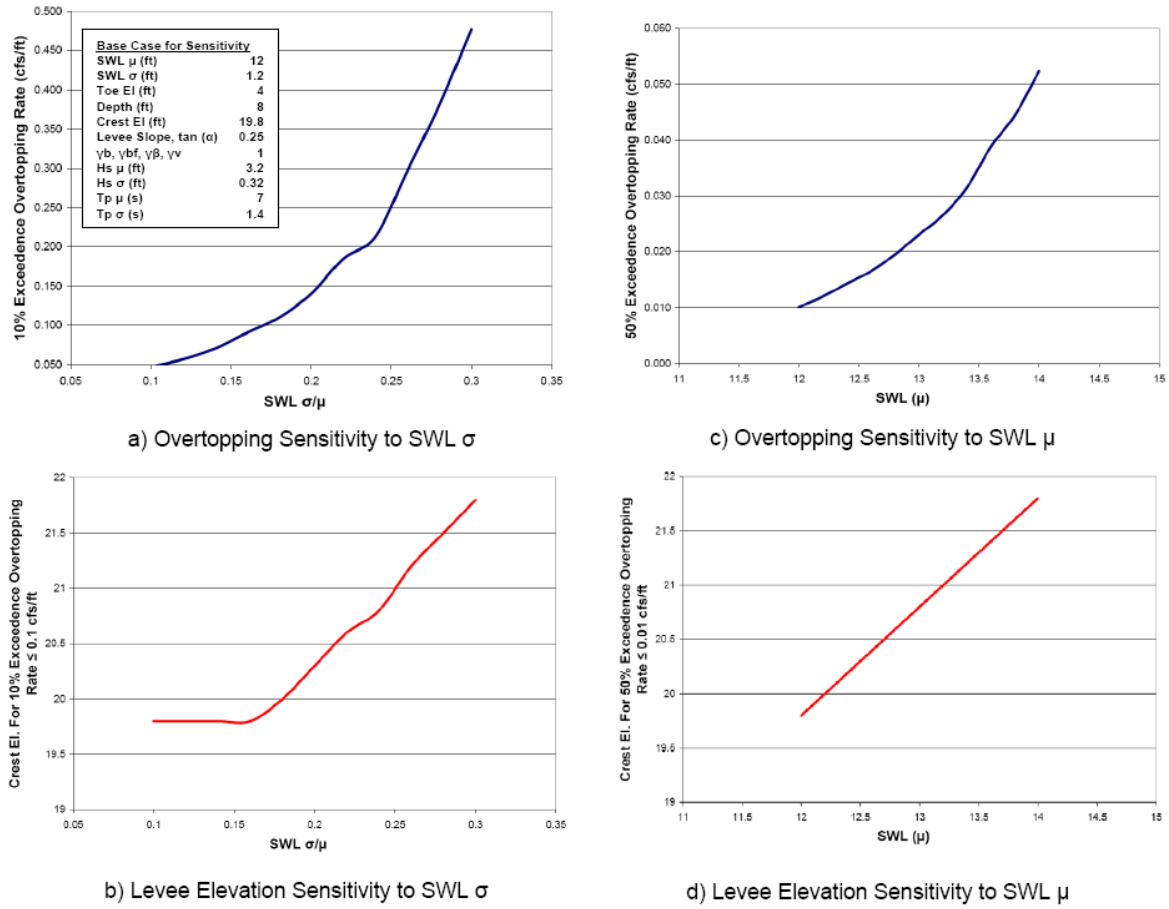

a) Overtopping Sensitivity to SWL σ

c) Overtopping Sensitivity to SWL μ

b) Levee Elevation Sensitivity to SWL σ

d) Levee Elevation Sensitivity to SWL μ

Figure 17.10. Sensitivity of Overtopping Rate and Design Elevation to SWL σ and μ

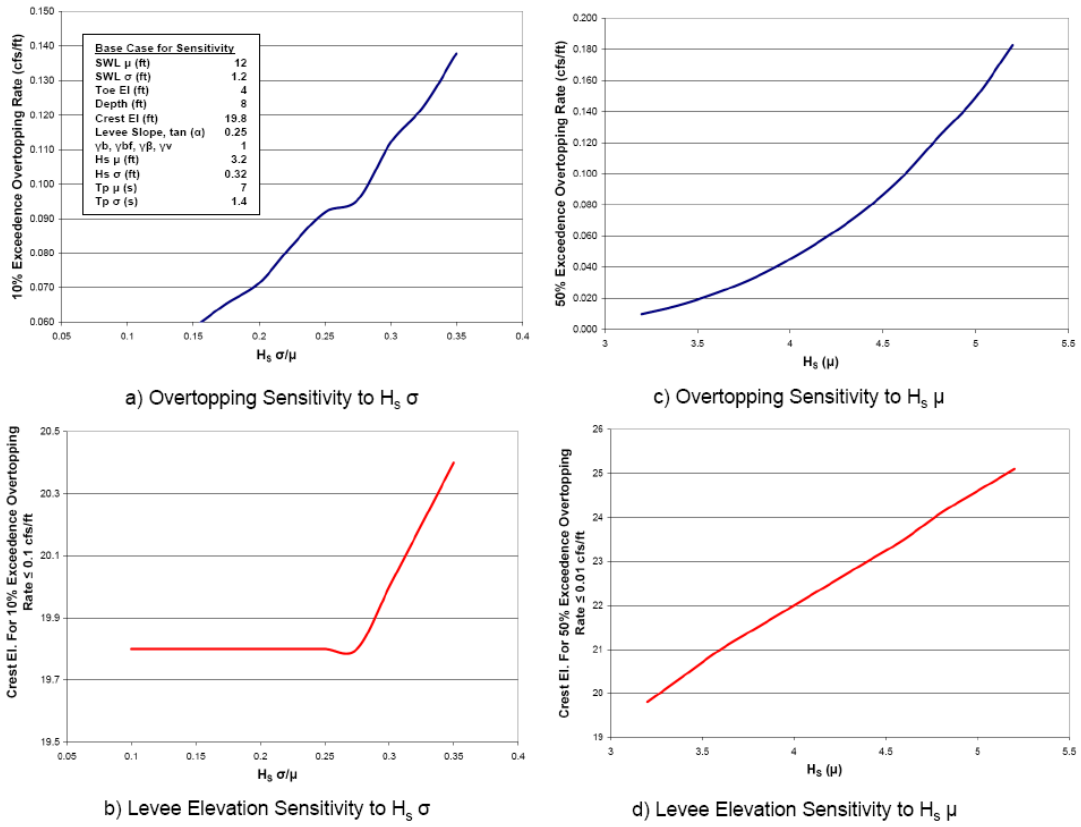

Figure 17.11. Sensitivity of Overtopping Rate and Design Elevation to H_s σ and μ

Attachment 1 provides the current, 2010, 100-yr SWL, H_S, and T_P for each reach, with the respective σ values, together with the 2010 design elevations and overtopping rates derived in Step 5. Final hydraulic design elevations for floodwalls, but not levees, were modified in accordance with future conditions (see Section 20.2). It should be noted that while USACE 2008b required final hydraulic design elevations in accordance with the 10% Exceedance for overtopping in Step 5, it did not specify that all structural components address all hydraulic loads associated with the 10% Exceedance condition. Final plan elevations were adjusted upward in some cases due to geometric design considerations and allowances for post-construction settlement.

The USACE 100-yr elevation design criteria provided for an equal 100-yr overtopping hazard at all reaches (based on levee or floodwall type). However, a consequence of the equivalent 100-yr overtopping criteria was that they necessarily translated into *widely varying 100-yr freeboards.* Figure 17.12 illustrates the range in median 100-yr freeboard for selected HSDRRS levee reaches. Reaches fronted by vast foreshore wetlands generally required less freeboard to minimize wave overtopping. On the other hand, reaches immediately fronted by a large water body necessitated more freeboard to minimize wave overtopping.

The 10% Exceedance average overtopping rate of 0.1 cfs/ft—for a simple case of 3 miles over 6 hours—corresponds to 785 acre-ft. Increasing the length to 10 miles equates to 2,617 acre-ft. At the median overtopping rate of 0.01 cfs/ft the volume for 10 miles of overtopping over 6 hours is 262 acre-ft. Wave-only overtopping volume is not trivial, but is markedly less than the 100-yr 24-hr rainfall for most of the urban sub-basins shown in Table 17.2.

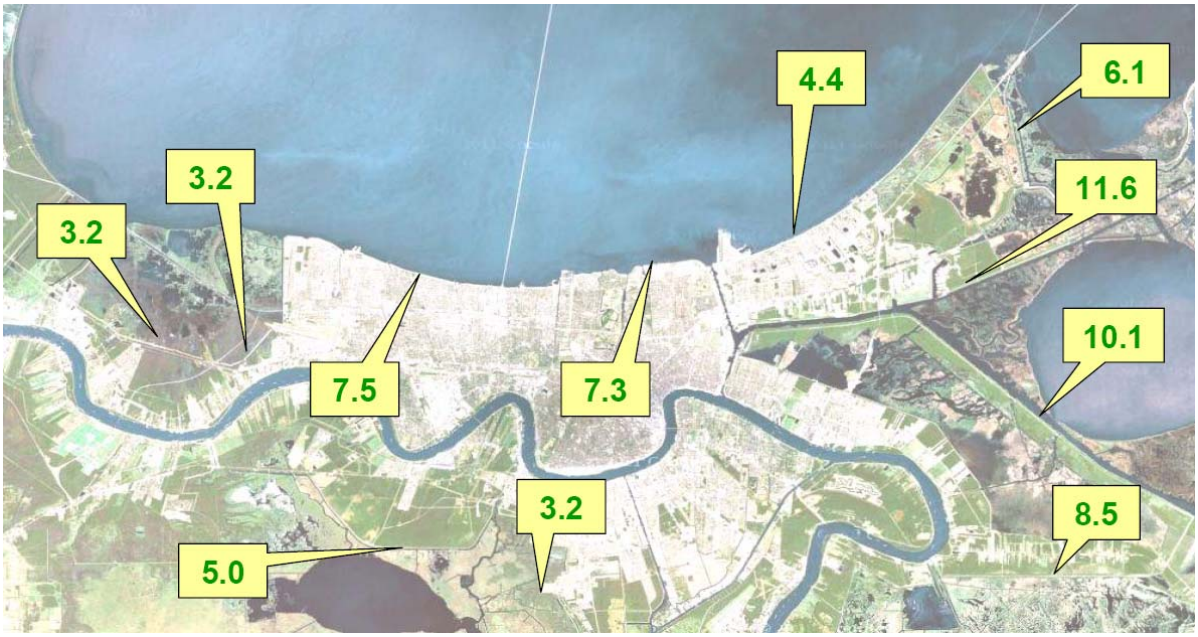

Figure 17.12. Median 100-yr Freeboard at Selected HSDRRS Levee Reaches

A critical design limitation is that—as previously discussed in Section 16.2—local 100-yr overtopping rates, and thus volumes, can correspond to a more frequent equivalent whole-polder inundation volume—due to possible multiple independent reach exposures. For a polder with two independent exposures the 100-yr overtopping hazard associated with either exposure equates to nearly a 50-yr polder volume; and a 100-yr whole-polder- inundation volume is equivalent to nearly a 200-yr overtopping volume at one exposure.

To date, the USACE has not updated the JPA for the 100-yr surge polder inundation hazard associated with the final HSDRRS design. (The IPET analysis described above does not include the IHNC/GIWW and Seabrook Barriers or the upgraded West Return Wall.) The polder FISs do not include an updated JPA of surge inundation hazard (FEMA 2012).

17.4 USACE HSDRRS Resiliency Design

In addition to protecting against the 100-yr surge hazard, Congress authorized HSDRRS resiliency. The USACE has equated resiliency with the secondary objective of reducing the threat of erosion breaching caused by overtopping.[10] To meet this objective the USACE is currently evaluating structural enhancements to reduce embankment interior-side scour. In accordance with guidance the USACE is following two steps (USACE 2008b). Step 1 has been competed while Step 2 is still in progress.

[10] To date, the USACE has determined that other measures are not a subject of their resiliency authorization, including raising reach elevations to provide greater freeboard; protection of the exterior-side from erosion due to waves and long-shore currents associated with non-overtopping surges; and reducing other sources of fragility that could lead to breaching without overtopping. The USACE considers itself prohibited from using resiliency appropriations for such measures even where they achieve greater effective overall risk-reduction.

1. 500-yr SWL overtopping rate for 2010 conditions at each reach. The USACE determined current 500-yr SWL, H_S, and T_P for each reach from the 2010 CDFs, with modifications of H_S in accordance with the breaking parameter of 0.4. Uncertainty factors were also assigned for SWL, H_S, and T_P. The median (50% Probability of Exceedance) and 10% Probability of Exceedance overtopping rates for the current 500-yr conditions were then estimated using the same methods applied to the 100-yr overtopping rate. Attachment 1 includes the current median estimate for the 500-yr SWL and overtopping results for each reach.

   Three important concerns with this first resiliency step are:

   - The USACE JPA is likely to underestimate the 500-yr exterior surge SWL hazard, as noted above in Section 17.2. The USACE design guidance did not address this limitation, nor did it discuss factoring in SWL uncertainty and using a UCL instead of the median estimate for the current 500-yr SWL.
   - The USACE did not provide a minimum freeboard criteria for the 500-yr condition. The general design guidance (USACE 2008b p. I-25) stated that the design elevation is to prevent free flow for the 500-yr condition; the exceedance level is not specified.[11] However, the guidance on HSDRRS elevation (USACE 2010) did not provide for raising reach elevations based on the evaluation of the 500-yr condition. As a result, the current median 500-yr freeboards for eight levee reaches were less than 1 ft, with three being negative:

East-bank St. Charles Parish levee reach east of I-310	0.5 ft
Mississippi River to US 90	0.1 ft
Orleans Village to Ames Pump Station	0.1 ft
Highway 3134 to Old Estelle Pump Station	0.1 ft
Transition Point to Hero Canal	0.1 ft
Robinson Point to Harvey Canal	-0.4 ft
Hero Pump Station to Algiers Canal	-0.4 ft
Hero Canal Area behind Landfill Berm	-1.4 ft

   - At the 500-yr condition, unlike the 100-yr condition, reaches will experience significantly different overtopping rates. Reaches with minimal 500-yr freeboard face the most significant exposure. Figure 17.13 shows that the 2010 10% Exceedance 500-yr overtopping rate can vary by a factor of five.

2. Appropriate interior-side armoring measures to reduce the threat of overtopping induced erosion breaching. Varying overtopping rates above the 100-yr hazard around the HSDRRS—as depicted by Figure 17.13 for the 500-yr hazard—imply that different reaches have significantly different erosion breach probabilities at hazards above the 100-yr level. The USACE is presently evaluating alternative armoring technologies (enhanced turf, turf reinforcement mats, concrete mats, armor stone, etc.) for different overtopping conditions. As part of the evaluation the USACE has conducted initial wave erosion testing at Colorado State University (Thornton et al 2012).

[11] USACE 2008b did not require that structural components address anticipated loads under the 500-yr conditions.

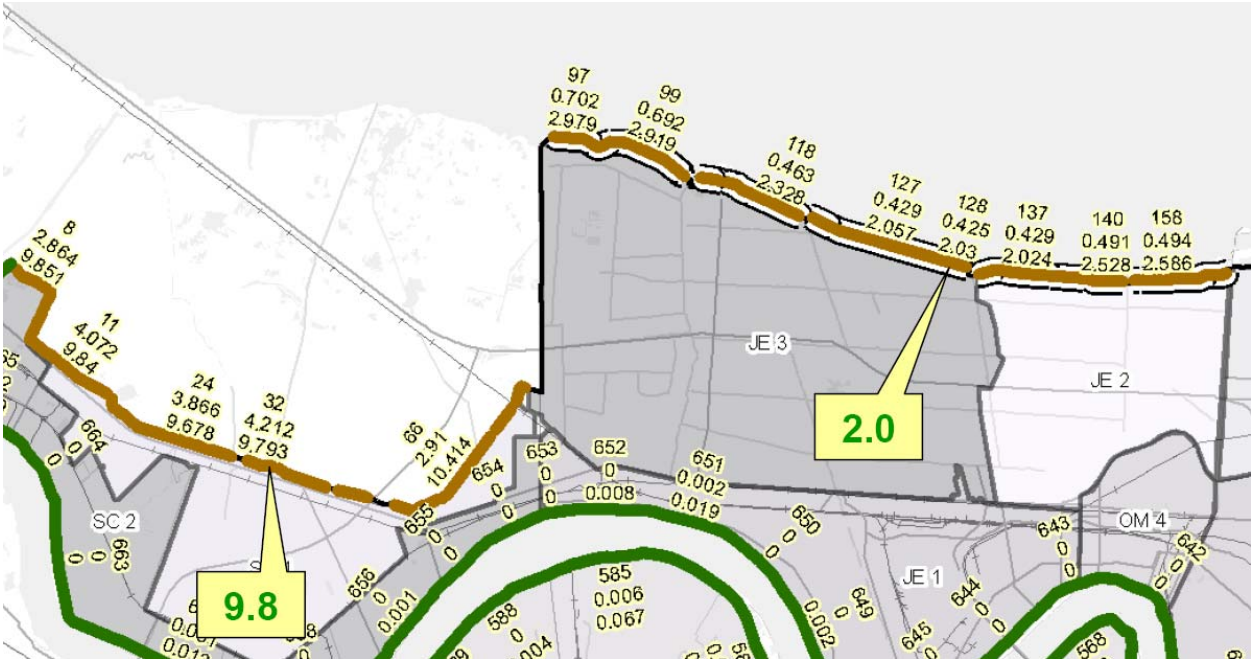

Figure 17.13. 10% Exceedance 500-yr Overtopping at Selected HSDRRS Levee Reaches (cfs/ft)

USACE 2011

To support the selection of cost-effective, reach-specific measures the USACE has indicated it will employ the IPET JPA approach described in Section 17.1. The approach incorporates erosion breach probability (fragility) analysis and uses the FoRTE spreadsheet program to compare polder inundation CDFs under different armoring scenarios. At this time this analysis has not been finalized and documentation for the treatment of breach failure conditions and fragility, as well as uncertainties, has not been released. Figure 17.14 illustrates how hazard comparisons can be compared under different armoring/failure scenarios.

The USACE has indicated that the selection of reach-specific armoring measures are likely to be based primarily on the estimate of the *median* 500-yr overtopping rate, together with information on the degree of hazard reduction, constructability, maintenance issues, and cost (USACE 2011)

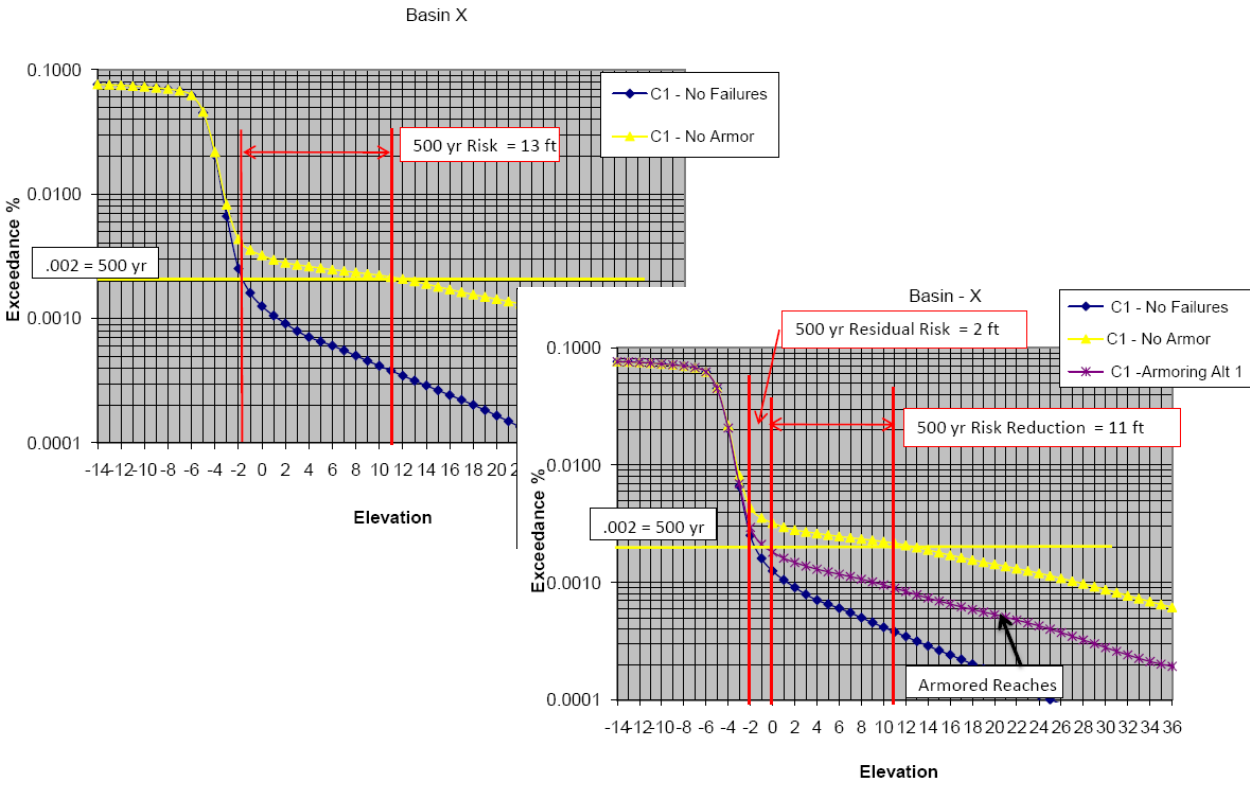

Figure 17.14. Example of Polder Inundation Hazard Comparisons for Armoring Alternatives

USACE 2011

Part IV. Conclusions and Recommendations

Conclusions

Part IV has reviewed methodologies for analyzing polder inundation hazards associated with hurricane surge and recent applications to the New Orleans regional polders. This information supports the following important findings:

1. Eight hydrologic/hydraulic processes control surge inundation of polders. Methodologies are available to quantify these processes but many lack extensive empirical grounding:

    a. The storm surge dynamics. Parts I, II, and III described the approach to estimating exterior surge SWL and wave conditions, with associated limitations and uncertainties. Evaluating polder inundation hazard requires additional attention to local conditions producing SWL variations and wave nearshore and foreshore transformations.

    b. Seepage perimeter inflows. Estimates are limited by data on shallow geology, preferential flow paths, and representative surge-driven seepage rates.

    c. Overtopping perimeter inflows. Analysis usually relies on simple assumptions about wave transformations in the foreshore region—e.g., employing breaker parameters to estimate H_s as a function of depth. However, there are few observations of storm surge foreshore waves. Rayleigh Distribution, which is used to relate the relative frequency of H_s to more extreme waves, may overestimate extreme wave recurrence for surge events. Empirical equations for average wave overtopping—as well as supercritical and submerged weir flow—are subject to limited field observations for defining coefficients. In addition, such overflow estimates have nonlinear sensitivities to estimates of H_s and SWL.

    d. Breach perimeter inflows. Estimates use supercritical and submerged broad-crested weir formulations—but again with limited field observations to define coefficients—and specific breach invert and length (I-L) scenarios for exterior SWL and structure type. Breach occurrence can be conditional, with probability (fragility) also a function of both exterior SWL and structure type. Breach I-L and fragility relationships to exterior SWL and structure type are often restricted to just a few "steps." At this time, the relationships and the steps are highly subjective.

    e. Rainfall accumulation. Estimates typically apply a standard rainfall return event (e.g., 6-hr/10-yr) to the whole-polder. Alternatively, a relationship has been suggested between rainfall accumulation and hurricane intensity, size, forward speed, and track (distance and direction) with respect to polder location. However, such a relationship has not been documented to date.

    f. Drainage pumping outflows. Estimates are based on some percentage of pump station rated capacity. No research has been published to suggest a method for estimating the percentage, or the probability of such performance.

    g. Internal routing of the time-varying and location-specific perimeter inflows, rainfall, and pumping outflows. Evaluating near uniform inundation for whole-polders or sub-basins can be accomplished with a simple level-pool (stage-storage) approach. 2D routing models can describe inundation variability controlled by localized perimeter inflows, interior topographic features, and drainage. Modeling near-field breach dynamics requires special capabilities to examine supercritical flow and shock waves.

h. Local wind-induced interior setup and waves. 2D routing models can include local wind setup. For level-pool routing results can be adjusted using simple 1D wind setup equations accounting for sustained wind speed, fetch, and water depth. For inundated areas with long fetch interior the peak down-wind wave heights can be estimated with breaker parameters. If inundation depths warrant, the Bretschneider, CEM, or other basic equations, or even 1D WHAFIS and 2D STWAVE/SWAN models, can be used to estimate wave conditions(see Part III). These equations are again limited by suitable observations.

2. Evaluation of polder inundation requires a deterministic model of seepage, overtopping, breaching, rainfall, and pumping (SOBRP), that addresses the standard methodologies for quantifying the respective processes. Basic SOBRP modeling, together with level-pool interior routing, can be accomplished with spreadsheets (or programmed with MATLAB or FORTRAN) and coupled (one-way) with the exterior surge and wave model output. Analysis of submerged weir flow and pumping also requires input from the interior routing. Tight coupling of all four models—the high resolution 2D exterior surge and wave model (e.g., ADCIRC-STWAVE or SWAN+ADCIRC), the local wave model, the SOBRP model, and polder routing (with internal wind setup as needed)—has not yet been developed. Furthermore, the limited observations of SOBRP and interior HWMs—such as for Hurricane Katrina—have not enabled detailed validation of four-part polder inundation modeling.

3. Sensitivity tests using the SOBRP model alone, or in combination with the other models, can be used to assess the influence of variability and/or uncertainty in input conditions and process parameters.

4. Polders face other inundation risks apart from surge-driven inundation. The New Orleans regional "bowls" are exposed to notable rainfall-only flood hazards—with some low-lying locations at significant risk from 10-yr rainfall events. Large portions of the Metro New Orleans Polder face a higher SWL for a levee breach during a Mississippi River flood than for an equivalent hurricane surge hazard level.

5. In general, seepage and wave-only overtopping pose a minor inundation hazard, with quantities much less than 6-hr/10-yr rainfall hazards. Wave-only and shallow free-flow overtopping (e.g., SWL less than 1 ft above the crown), over perimeter distances of several miles, produces volumes that are less than the 6-hr/100-yr rainfall hazard. Deeper overtopping and breaching inflows pose the major hazard, exceeding 24-hr/100-yr rainfall quantities.

6. Defining polder inundation hazards from surge requires extending hurricane surge JPA to incorporate those notable SOBRP uncertainties/variabilities with nonlinear influence on inundation volume—such as breach fragility, SWL, H_s/breaker parameter, and crown elevation. JPA is crucial to account for independent reach exposures and to assess the influence of independent SOBRP conditional variables. The inundation JPA requires a JPM set of probability-weighted "whole-polder" surge events to represent the exterior hazard. The exterior surges for each storm in a JPM-OS (or a Full-or Monte Carlo-JPM set) can be used, but not those for a Surge Response-OS as this type of set is not designed to represent the exterior hurricane hazard.

7. A subset of whole-polder scenarios is then employed to represent the range of SOBRP joint probabilities for each JPM-OS storm; a separate subset is required for each JPM-OS storm. The range of scenarios within each subset must reflect the various probabilistic combinations for each independent SOBRP variables at each reach. Computational restrictions can limit the JPA to considering only breach fragility (which may be reasonable as breach volumes can overwhelm the other SOBRP flows) and just a small number of breach I-L steps and/or fragility steps.

8. SWL CDFs throughout the polder interior are computed with the results of the inundation JPA using techniques similar to those described for exterior SWLs (see Part III). Uncertainties/variabilities with a linear influence on inundation volume (e.g., interior terrain data) can be treated as normally distributed and lumped into an overall σ, which can then be used to construct uncertainty bands for the inundation CDF.

9. Interior wind wave hazards at a referenced SWL hazard can be assessed as they are for exterior locations—using breaker parameters. Wave equations and models (e.g., WHAFIS) can be employed to characterize the wave hazards for deeper, longer fetches.

10. IPET employed surge inundation JPA for the New Orleans area polders as part of comparing pre- and post-Katrina HSDRRS risk and reliability.

    - As discussed in Part III, IPET improvised 76 whole-polder exterior events by assigning probabilities to 76 storms from the 152-storm FIS Surge Response-OS. However, the Surge Response-OS was not intended as a JPM-OS and does not adequately represent extreme, >200-yr return, hurricane hazards.
    - The inundation JPA did not address ADCIRC bias on the south shore of Lake Pontchartrain.
    - The improvised 76-storm JPM-OS resulted in notably different estimates of exterior surge hazard than those derived for the FIS.
    - Exterior local wave H_S were set primarily using a breaker parameter of 0.43.
    - The SOBRP scenario subset only addressed breach fragility. The scenarios included independent breach probabilities for each reach. Two breach I-L conditions were identified for each reach—one for overtopping erosion breach and one for non-overtopping breach—each conditioned first on a threshold local SWL. The two breach cases were further conditioned using a few increments of fragility—specified according to structure type and the degree to which peak SWL exceeded the local threshold.
    - The inundation volumes for each of the hundreds of scenarios per storm included the breaching inflow plus any local reach overtopping, rainfall, and pumping at three alternatives (0, 50, and 100% of capacity). IPET performed level-pool routing for each scenario, subdividing each polder into several sub-basins, and computed 50-, 100-, and 500-yr interior hazards using the results.
    - The 500-yr interior surge volume for a 2010 HSDRRS case (without the IHNC/GIWW and Seabrook Surge Barriers and higher West Return Wall) was 25% less than the volume for a 6-hr/100-yr rainfall (less 6-hr pumping) for the Orleans Parish area within the Metro Polder. For the Jefferson and St. Charles Parish areas within the Metro Polder the 500-yr interior surge volume was more than 2.5 times the 6-hr/100-yr rainfall-only volume (less 6-hr pumping). For New Orleans East the 500-yr surge volume was 40% higher.

    While IPET's polder inundation JPA facilitated a comparison of risks for the different HSDRRS cases, the limited empirical basis for breach fragility and breach scenarios meant that the estimates of actual inundation hazard were highly speculative.

11. The USACE's 2009 Louisiana CPR Study used some polder inundation analysis methods, but not an inundation JPA, in order to support planning-level comparisons of potential regional coastal protection and restoration programs. (Additional approaches used to examine future conditions are discussed in Part IV).

- The Study re-evaluated exterior surge hazards for the base (2010) case by modifying the FIS ADCIRC mesh for selected Surge-Response simulations, combined with algorithm-based adjustments for other simulations, and then recomputing the exterior CDFs. As discussed in Part III, the Surge Response-OS does not adequately represent extreme hurricane hazards.
- Exterior local wave H_S were set primarily using a breaker parameter of 0.4.
- Instead of an inundation JPA the study simply used the estimated 100-, 400-, 1000-, and 2000-yr surge hazards around the perimeter as four "pseudo" surge events. Due to the independence of reach exposures around each polder, using the perimeter hazard SWLs as a "pseudo" event equates to a much more extreme whole-polder hazard level—i.e., an event with all reaches attaining the 400-yr SWL is much rarer than a 400-yr event.
- The Study then routed overtopping associated with these "pseudo" events, together with rainfall, but with no breaching, and using a more simplified internal topography than IPET.
- Uncertainties in exterior SWL hazard levels were used to compute UCL/LCLs for overtopping.

While suitable for "what if"-planning-level assessments, the CPR Study approach to inundation analysis is more speculative than that of IPET and cannot be used for estimates of actual inundation hazard.

12. The USACE utilized a simple analysis of local 100-yr overtopping hazard—but not a complete inundation JPA—to design the New Orleans regional HSDRRS for current, 2007, LMSL. (Designs based on future, 2057, LMSL are discussed in Part IV. For some reaches final design elevations were increased to account for construction issues and post-construction settlement.)
    - Exterior 100-yr surge and wave conditions were established in a manner similar to the Louisiana CPR Study. Additional analysis was conducted for 100-yr surge and wave conditions in the IHNC/GIWW sub-basin and Mississippi River.
    - The USACE set crown elevation with at least 2 ft of freeboard for the median estimate of the 100-yr SWL and minimizing local 100-yr wave overtopping to a level intended to prevent interior-side erosion breaching. Minimizing 100-yr wave overtopping produced much higher 100-yr freeboards for reaches with direct open water exposure—e.g., greater than 10 ft for some reaches facing Lake Borgne. A minimal, non-zero local overtopping was apparently adopted given significant residual interior 100-yr flood hazards and as consistent with NFIP requirements.
    - To provide some conservativeness in the overtopping estimate, the design incorporated a sensitivity analysis of the 100-yr overtopping rate as a function of uncertainties in exterior 100-yr SWL, H_S, and T_P (using a Monte Carlo technique). The USACE then specified crown elevations at all levee and floodwall reaches to prevent *average* overtopping from exceeding median criteria (i.e., 50% Exceedance Level) of 0.01 and 0.03 cfs/ft, respectively, and an 80% UCL criteria (i.e., 10% Exceedance Levels) of 0.1 cfs/ft.
    - The elevation design approach would have been more conservative had it employed the more typical 90% UCL/LCLs instead of the 80% UCL/LCLs.
    - Five critical elements of the design were counter to a conservative approach:
        - The ADCIRC model has a noted under-prediction bias along the south shore of Lake Pontchartrain, which was not addressed.

- The assumed breaker parameter value is on the low end of the generally accepted range.
- The design uses a much lower SWL σ in the sensitivity analysis than indicated by the FIS and IPET. At a 100-yr SWL of 12 ft, a more appropriate σ raises the crown design by 1.7 ft. Furthermore, the indicated 10% Exceedance Level is not an actual statistical value.
- The wave height, which is assumed to vary with surge depth, is not a function of surge depth in the sensitivity analysis.
- Criteria for average overtopping rates need to more clearly allow for the dramatically higher instantaneous scour velocities associated with extreme waves, as well as uncertainties in interior-side erosion breach initiation and development.

- One additional factor is likely to contribute additional conservatism in the design. Extreme wave recurrence during short-term wave events, and hence overtopping, is probably over-estimated by empirical equations derived from long duration wave events.

13. The USACE is in the process of additional HSDRRS resiliency design, intended to reduce the threat of interior-side erosion breaching from more extreme surge events. (Structural enhancements to reduce exterior-side wave erosion, improve strength against collapse breaching, or increase freeboard are not addressed in the resiliency design.)
    - The resiliency design has used the Louisiana CPR exterior CDFs—which as noted above do not adequately represent extreme, >200-yr, hurricane hazards. The resiliency design has also assumed a wave breaker parameter of 0.4 to establish exterior 500-yr H_S.
    - The 100-yr overtopping design produced widely varying 500-yr freeboard and overtopping conditions around the polders. Using the median 500-yr SWL, the designs for eight regional New Orleans reaches have 500-yr freeboard of less than 1 ft, with three reaches at negative 500-yr freeboard.
    - Reaches with minimal 500-yr freeboard face the most significant overtopping exposure. At the 10% Exceedance Level, the 500-yr *average* overtopping rate can vary by a factor of five, with some reaches nearing 10 cfs/ft.
    - The USACE is presently evaluating alternative armoring technologies (enhanced turf, turf reinforcement mats, concrete mats, armor stone, etc.) for different overtopping conditions. As part of the evaluation the USACE has conducted initial wave erosion testing.
14. The USACE has initiated but not completed an inundation JPA for the 100-yr design and the resiliency options to facilitate a comparison of alternatives. The JPA follows the IPET approach. Thus, for the reasons noted above, the JPA may not provide a realistic estimate of actual extreme inundation hazard.

Recommendations

The above conclusions indicate that the recent USACE analysis of polder inundation hazard is outdated. They also provide the basis for seven recommendations to improve the New Orleans metropolitan polder inundation hazard analysis:

1. Provide a JPA of the polder inundation hazard, expanding on the IPET approach, and estimate the residual 100-, 500-, and 1000-yr inundation hazards.
2. Base the polder inundation JPA on the larger JPM-OS set of storms as identified in the Part III recommendations.
3. Include a realistic quantification of the range of breach I-L cases and associated fragility conditions for each storm.
4. Estimate local wave conditions and HSDRRS wave overtopping with the state-of-the-practice methods that better account for local peak wave conditions during hurricane peak surge.
5. Further expand the inundation JPA to encompass the nonlinear influence of additional key probabilistics—such as exterior SWL and H_S—on inundation volume.
6. Examine the full influence of uncertainties—associated with the hurricane climatology, the exterior hurricane surge and local wave model, seepage, overtopping, breaching, rainfall, pumping, internal routing, and particular JPMs—on the inundation hazard estimate. Such treatment should be developed to allow estimating a range of confidence intervals—e.g., 80, 90, 95%.
7. Update estimates of the wave overtopping hazard for the HSDRRS design at each reach in accordance with No. 4, and update confidence intervals using full uncertainties for surge and wave conditions.

The Louisiana CPRA, together with federal partners, should fund critical research to improve polder inundation hazard analysis, including:

1. Further research on local wave, SOBRP, and interior routing processes, including laboratory and field studies to evaluate empirical formulations and coefficients. High priority issues are:
    - Appropriate wave height distributions for short duration surge peaks.
    - Appropriate breaker parameters or wave transformation models that can be applied to HSDRRS foreshore regions.
    - The role of preferential seepage pathways in initiating collapse breaching and field investigations to locate and characterize such pathways.
    - The wave and direct (weir) overflow expressions and coefficients for all phases of hurricane surge overtopping and breaching, for a variety of structures and conditions, including both average and instantaneous rates.
    - Exterior- and interior-side wave-induced, and free-flow induced, scour and breach initiation and development.
    - Wind setup and wave equations/models applicable to sheltered southeast Louisiana water bodies (e.g., Lake Borgne and Pontchartrain, Breton Sound, Barataria Bay, Mississippi River, etc.) and inundated polders and sub-basins (e.g., IHNC/GIWW and outfall canals).

2. More efficient coupling of exterior surge, local wave, SOBRP, and internal routing models.
3. Further expansion and enhancement of the inundation JPA to make it less speculative.
4. Better analyses of non-surge polder flood hazards—such as rainfall-only events and overtopping/breaching during a Mississippi River flood—which are critical to evaluating the risk implications of surge inundation hazards.

The above recommendations can mitigate systemic and localized bias in estimates of inundation hazard. Notably, localized bias is typically of less import to the NFIP than to the community, which must deal with the consequences of over- or under-estimating flood hazards.

However, it is important to recognize the large uncertainty that remains in estimating inundation hazards based on JPA. This uncertainty in the inundation hazard for polders is greater than that for exterior surge hazards, which as noted in the Part III is quite considerable. In the near-term, methodological improvements and research are not likely to yield major reductions in uncertainty.

Part IV. References

Aalberts, M. L., The Cost Effectiveness of Compartmentation of the Orleans Metro Bowl, Master Thesis, June 2008.

ADCIRC Development Group, http://www.adcirc.org

ASCE Louisiana Section, 2012 Report Card for Louisiana's Infrastructure, 2012.

Bretschneider, C. L., Wave Forecasting Relations for Wave Generation, Look Lab, Hawaii, 1970.

Donelan, M. A., Similarity Theory Applied to the Forecasting of Wave Heights, Periods, and Directions, Proceedings of the Canadian Coastal Conference, National Research Council of Canada, pp. 47 – 61, 1980.

Etemad-Shahidi, A., M.H. Kazeminezhad, and S.J. Mousavi, On The Prediction of Wave Parameters Using Simplified Methods, Journal of Coastal Research, SI 56, pp 505-509, 2009.

Faiers, G. E., B. D. Keim, R. A. Muller, Rainfall Frequency/Magnitude Atlas for the SouthCentral United States, Southern Regional Climate Center, Louisiana State University, 1997.

FEMA, High Water Mark Collection for Hurricane Katrina in Louisiana, FEMA-1603-DR-LA, Task Orders 412 and 419, March 30, 2006.

FEMA, Guidance for Coastal Flood Hazard Analyses and Mapping in Sheltered Waters, February 2008 http://www.mmrs.fema.gov/library/viewRecord.do?id=3252

FEMA, Hydrologic Analysis Technical Support Data Notebook and Hydraulic Analysis Technical Support for the Hurricane Storm Damage Risk Reduction System (HSDRRS), Louisiana. July 16, 2012

Hasselmann, K., T. P. Barnett, E. Bouws, H. Carlson, D. E. Cartwright, K. Enke, J. A. Weing, H. Gienapp, D. E. Hasselmann, P. Kruseman, A. Meerburg, P. Muller, K. J. Olbers, K. Richter, W. Sell, and W. H. Walden, Measurment of Wind-Wave Growth and Swell Decay During the Joint North Sea Wave Project (JONSWAP), Deutsche Hydrograph, Zeit., 1973.

Hughes,S.A., Estimation of Overtopping Flow Velocities on Earthen Levees Due to Irregular Waves, USACE, Coastal and Hydraulics Laboratory, January 2008.

Hughes,S.A. , N.C. Nadal, "Laboratory study of combined wave overtopping and storm surge overflow of a levee", Coastal Engineering, Volume 56, Issue 3, pp. 244-259, March 2009.

Hughes,S.A., Flood-Side Wave Erosion of Earthen Levees: Present State of Knowledge and Assessment of Armoring Necessity, USACE, Coastal and Hydraulics Laboratory, August 2010.

Independent Levee Investigation Team (ILIT), Investigation of the Performance of the New Orleans Flood Protection Systems in Hurricane Katrina on August 29, 2005, Final Report, July 31, 2006

IPET, Performance Evaluation of the New Orleans and Southeast Louisiana Hurricane Protection System Draft Final Report, Volume V– The Performance—Levees and Floodwalls, June 2006

IPET, Performance Evaluation of the New Orleans and Southeast Louisiana Hurricane Protection System Final Report, Volume VIII– Engineering and Operational Risk and Reliability Analysis, June 2009a

IPET, A General Description of Vulnerability to Flooding and Risk for New Orleans and Vicinity: Past, Present, and Future, June 2009b.

Jonkman, S. N. B Maaskant, E. Boyd, and M. L. Levitan, Loss of Life Caused by the Flooding of New Orleans After Hurricane Katrina: Analysis of the Relationship Between Flood Characteristics and Mortality, Risk Analysis, Vol. 29, No. 5, 2009

Link, E., R. Patev, G. Baecher, M. McCann, T. McAllister, J. Foster, IPET, Engineering and Operational Risk and Reliability Analysis, Presentation, Undated.
http://www.samehuntington.com/shared/content/Presentations/TA_S3_Link.pdf

Lonfat, M., F. D. Marks, Jr., S. S. Chen, Precipitation Distribution in Tropical Cyclones Using the Tropical Rainfall Measuring Mission (TRMM) Microwave Imager: A Global Perspective, Monthly Weather Review, Vol. 132, 1645 – 1660, July 2004.

Lonfat, M., R. Rogers, T. Marchok, F. D. Marks, Jr., A Parametric Model for Predicting Hurricane Rainfall, Monthly Weather Review, Vol. 135, 3086 – 3097, September 2007.

Langousis, A., and D. Veneziano Theoretical Model of Rainfall in Tropical Cyclones for the Assessment of Long-Term Risk, Journal of Geophysical Research, Vol. 114, January 2009.

Louisiana CPRA, Louisiana's Comprehensive Master Plan for a Sustainable Coast, 2012

Lynett, P. J., J. A. Melby, D-H Kim, An Application of Boussinesq Modeling to Hurricane Wave Overtopping and Inundation, Ocean Engineering, Vol. 37, No. 1, p. 135-153, January, 2010.

Néelz S, and G, Pender, Desktop Review of 2D Hydraulic Modelling Packages, Science Report: SC080035, Environment Agency, July 2009.

NOAA, National Weather Service, Service Assessment: Tropical Storm Allison, Heavy Rains and Floods, Texas and Louisiana, June 2001, September 2001

NOAA, National Weather Service, The Historical Flood of May 8 – 10, 1995 Ten Years Later, 2005.

Rand Corporation, Coastal Louisiana Risk Assessment (CLARA) Model, Appendix D-25, Risk Assessment (CLARA) Model Technical Support, Louisiana's Comprehensive Master Plan for a Sustainable Coast, Louisiana CPRA, 2012.

Reeve, D.E., A. Soliman and P.Z. Lin, Numerical study of combined overflow and wave overtopping over a smooth impermeable seawall, Coastal Engineer- ing vol. 55, Elsevier (2008), pp. 155166.

Resio, D. T., J. L. Irish, J. J. Westerink, N. J. Powell, The Effect of Uncertainty on Estimates of Hurricane Surge Hazards, Natural Hazards, October 2012.

Schüttrumpf, H., and H. Oumeraci. 2005. Layer thicknesses and velocities of wave overtopping flow at seadikes. Coastal Engineering 52:473–95.

Schüttrumpf, H., and M. R. van Gent. 2003. Wave overtopping at seadikes. In Proceedings, Coastal Structures, '03, 431–443. Washington, DC: American Society of Civil Engineers.

Schüttrumpf, H., J. Möller, and H. Oumeraci. 2002. Overtopping flow parameters on the inner slope of seadikes. In Proceedings, 28th International Coastal Engineering Conference, 2: 2,116–2,127. World Scientific.

Royal Haskoning, Polder Modeling Orleans Metro Effects of Compartments on Flooding Extent, prepared for the Flood Protection Alliance, March 2009.

Swenson, D. (Times-Picayune) 2012.
http://www.nola.com/hurricane/index.ssf/2012/08/graphic_shows_new_orleans_area.html

Team Louisiana, The Failure of the New Orleans Levee System During Hurricane Katrina, A Report Prepared for Louisiana Department of Transportation and Development, Baton Rouge, Louisiana, December 18, 2006.

Thornton, C., B. Scholl, S. Hughes, and S. Abt, Full-Scale Testing of Levee Resiliency During Wave Overtopping, US Society on Dams Annual Conference Proceedings, 2012.
http://ussdams.com/proceedings/2012Proc/721.pdf

USACE, Coastal Engineering Manual, Part VI, EM1110-2-1100, February 2005.

USACE, Unsteady Flood Model for Forecasting the Mississippi and Missouri Rivers, February 1997, http://www.hec.usace.army.mil/publications/TechnicalPapers/TP-157.pdfUSACE, Coastal Engineering Manual (CEM) Volume II, Chapter 2: Meteorology and Wave Climate, 2006.

USACE, Flood Insurance Study, Southeast Parishes of Louisiana, Intermediate Submission 2: Offshore Water Levels and Waves, for FEMA, July 2008a.

USACE (New Orleans District), Hurricane and Storm Damage Reduction System Design Guidelines INTERIM, October 2007, Revised June 12, 2008b.

USACE, Louisiana Coastal Protection and Restoration, Final Technical Report, June 2009.

USACE (New Orleans District), Hurricane and Storm Damage Risk Reduction System, Design Elevation Report, Draft Report Version 4.0, August 18, 2010.

USACE, Summary Report for the Armoring Alternative Evaluation Process (Draft, and related communications from Reuben Mabry), June 2011

Van der Meer, J., Wave Run-up and Overtopping, in Dikes and Revetments: Design, Maintenance and Safety Assessment, K. W. Pilarczyk, Editor, 1998.

Van Gent, M. R,. Wave overtopping events at dikes. In Proceedings, 28th International Coastal Engineering Conference, 2:2203–2215, World Scientific, 2002.

Powell, N. and M and van Ledden, Hydraulic Assessment at the New Orleans District, Presentation, September 10, 2009.

Wilson, B. W., Numerical Prediction of Ocean Waves in the North Atlantic for December 1959, Deutsche Hydrograph Zeit., Vol. 18, No. 3, 1965.

Attachment 1

HSDRRS 100-yr Surge Conditions and Design Elevations and 500-yr Surge Conditions

Source:

USACE (New Orleans District), Hurricane and Storm Damage Risk Reduction System, Design Elevation Report, Draft Report Version 4.0, August 18, 2010.

St. Charles Parish East Bank Reaches

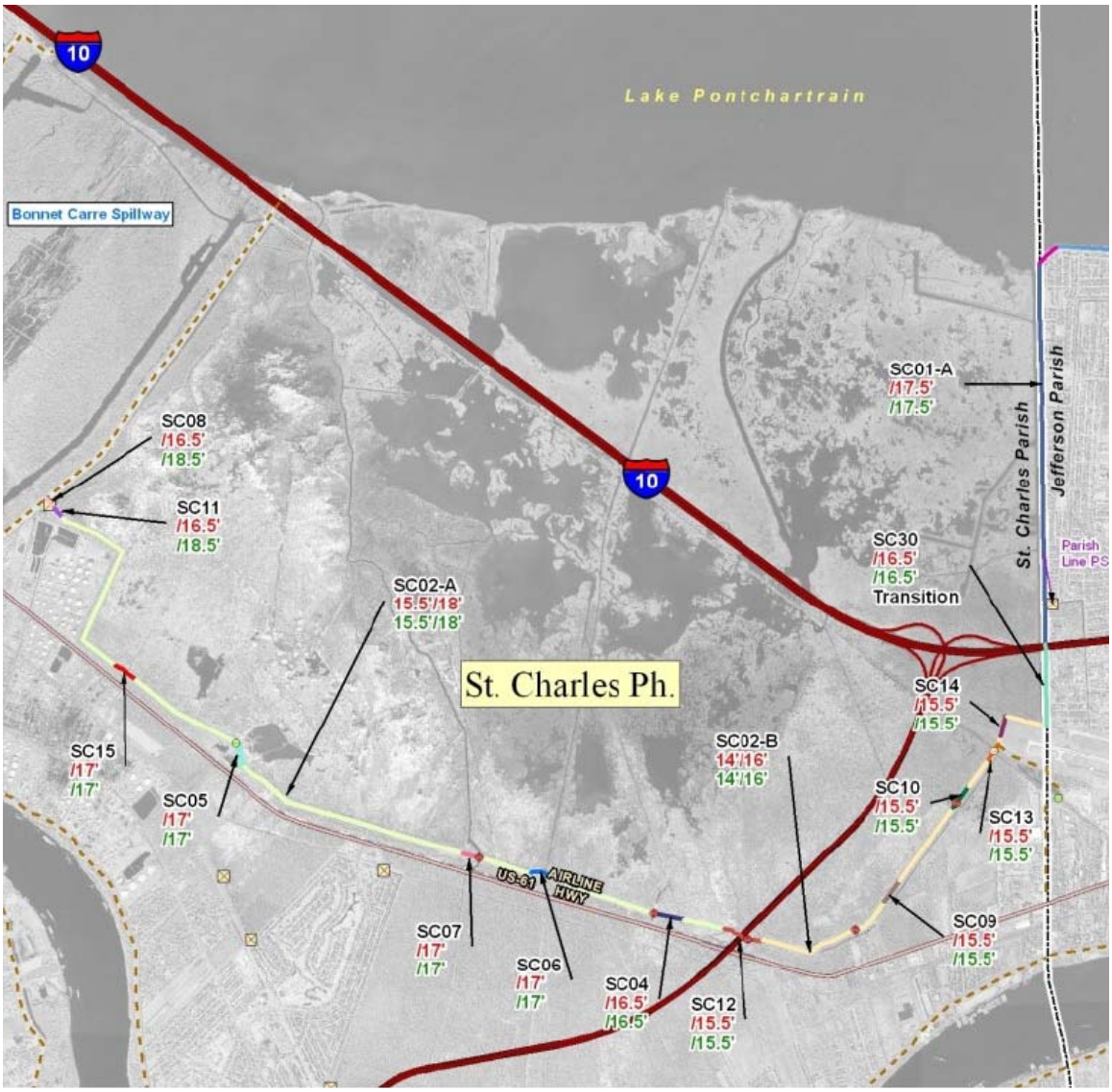

St Charles Parish Sections 1% Hydraulic boundary conditions									
				Surge level (ft)		Significant wave height (ft)		Peak period (s)	
Segment	Name	Type	Condition	Mean	Std	Mean	Std	Mean	Std
SC08	Bayou Trepagnier Pump Station	Structure/Wall	Future	12.8	0.7	2.7	0.2	4.0	0.7
SC11	Bonnet Carre Tie-in Floodwall	Structure/Wall	Future	12.8	0.7	2.7	0.2	4.0	0.7
SC05	Good Hope Floodwall	Structure/Wall	Future	12.9	0.8	3.1	0.2	4.7	0.8
SC02-A	St.Charles Parish Levee west of I-310	Levee	Existing	11.3	0.8	2.3	0.2	4.2	0.8
SC02-A	St.Charles Parish Levee west of I-310	Levee	Future	12.8	0.8	3.1	0.2	4.8	0.8
SC07	Cross Bayou Canal T-Wall	Structure/Wall	Future	12.9	0.8	3.1	0.2	4.7	0.8
SC06	Gulf South Pipeline T-Wall	Structure/Wall	Future	12.9	0.8	3.1	0.2	4.8	0.8
SC04	St. Rose Canal Drainage Structure T-Wall	Structure/Wall	Future	12.6	1.0	2.7	0.2	4.5	0.8
SC12	I-310 Floodwall	Structure/Wall	Future	12.3	0.8	2.3	0.2	3.9	0.6
SC02-B	St.Charles Parish Levee east of I-310	Levee	Existing	10.8	0.8	1.6	0.2	3.2	0.6
SC02-B	St.Charles Parish Levee east of I-310	Levee	Future	12.3	0.8	2.4	0.2	3.9	0.6
SC09	Almedia Drainage Structure	Structure/Wall	Future	12.3	0.8	2.4	0.2	3.9	0.6
SC10	Walker Drainage Structure	Structure/Wall	Future	12.2	0.8	2.5	0.2	3.8	0.6
SC13	Armstrong Airport Floodwall	Structure/Wall	Future	12.1	0.8	2.4	0.2	4.0	0.7
SC14	ICRR Floodgate	Structure/Wall	Future	12.1	0.8	2.4	0.2	4.1	0.7
SC30	Transition	Structure/Wall	Future	11.9	0.8	2.9	0.2	5.0	0.9
SC01-A	St. Charles Return Levee/Wall	Structure/Wall	Future	11.1	0.7	4.1	0.3	6.1	1.1
SC15	Shell Pipeline Floodwall	Structure/Wall	Future	12.9	0.8	3.1	0.2	4.7	0.8

St Charles Parish Sections 1% Design heights							
						Overtopping rate	
Segment	Name	Type	Condition	Depth at toe (ft)	Height (ft)	q50 (cft/s per ft)	q90 (cft/s per ft)
SC08	Bayou Trepagnier Pump Station	Structure/Wall	Future	12.8	18.5	0.001	0.004
SC11	Bonnet Carre Tie-in Floodwall	Structure/Wall	Future	12.8	18.5	0.001	0.004
SC05	Good Hope Floodwall	Structure/Wall	Future	12.9	17.0	0.020	0.078
SC02-A	St.Charles Parish Levee west of I-310	Levee	Existing	11.3	15.5	0.009	0.079
SC02-A	St.Charles Parish Levee west of I-310	Levee	Future	12.8	18.0	0.008	0.071
SC07	Cross Bayou Canal T-Wall	Structure/Wall	Future	12.9	17.0	0.019	0.078
SC06	Gulf South Pipeline T-Wall	Structure/Wall	Future	12.9	17.0	0.020	0.077
SC04	St. Rose Canal Drainage Structure T-Wall	Structure/Wall	Future	12.6	16.5	0.011	0.067
SC12	I-310 Floodwall	Structure/Wall	Future	12.3	15.5	0.009	0.054
SC02-B	St.Charles Parish Levee east of I-310	Levee	Existing	10.8	14.0	0.007	0.064
SC02-B	St.Charles Parish Levee east of I-310	Levee	Future	12.3	16.0	0.008	0.072
SC09	Almedia Drainage Structure	Structure/Wall	Future	12.3	15.5	0.012	0.066
SC10	Walker Drainage Structure	Structure/Wall	Future	12.2	15.5	0.015	0.071
SC13	Armstrong Airport Floodwall	Structure/Wall	Future	12.1	15.5	0.009	0.050
SC14	ICRR Floodgate	Structure/Wall	Future	12.1	15.5	0.009	0.049
SC30	Transition	Structure/Wall	Future	11.9	16.5	0.007	0.031
SC01-A	St. Charles Return Levee/Wall	Structure/Wall	Future	11.1	17.5	0.012	0.041
SC15	Shell Pipeline Floodwall	Structure/Wall	Future	12.9	17.0	0.020	0.075

St Charles Parish Sections Resiliency analysis (0.2% event)						
					Best estimates during 0.2% event	
Segment	Name	Type	Condition	Height (ft)	Surge level (ft)	Overtopping rate (cft/s per ft)
SC08	Bayou Trepagnier Pump Station	Structure/Wall	Future	18.5	15.4	0.156
SC11	Bonnet Carre Tie-in Floodwall	Structure/Wall	Future	18.5	15.4	0.155
SC05	Good Hope Floodwall	Structure/Wall	Future	17.0	15.6	1.242
SC02-A	St.Charles Parish Levee west of I-310	Levee	Existing	15.5	14.0	1.672
SC02-A	St.Charles Parish Levee west of I-310	Levee	Future	18.0	15.5	1.167
SC07	Cross Bayou Canal T-Wall	Structure/Wall	Future	17.0	15.6	1.256
SC06	Gulf South Pipeline T-Wall	Structure/Wall	Future	17.0	15.7	1.277
SC04	St. Rose Canal Drainage Structure T-Wall	Structure/Wall	Future	16.5	16.0	1.531
SC12	I-310 Floodwall	Structure/Wall	Future	15.5	15.1	1.408
SC02-B	St.Charles Parish Levee east of I-310	Levee	Existing	14.0	13.5	1.889
SC02-B	St.Charles Parish Levee east of I-310	Levee	Future	16.0	15.0	1.498
SC09	Almedia Drainage Structure	Structure/Wall	Future	15.5	15.0	1.375
SC10	Walker Drainage Structure	Structure/Wall	Future	15.5	14.9	1.348
SC13	Armstrong Airport Floodwall	Structure/Wall	Future	15.5	14.8	1.204
SC14	ICRR Floodgate	Structure/Wall	Future	15.5	14.8	1.188
SC30	Transition	Structure/Wall	Future	16.5	14.7	0.847
SC01-A	St. Charles Return Levee/Wall	Structure/Wall	Future	17.5	13.7	0.413
SC15	Shell Pipeline Floodwall	Structure/Wall	Future	17.0	15.6	1.248

Jefferson Parish East Bank Reaches

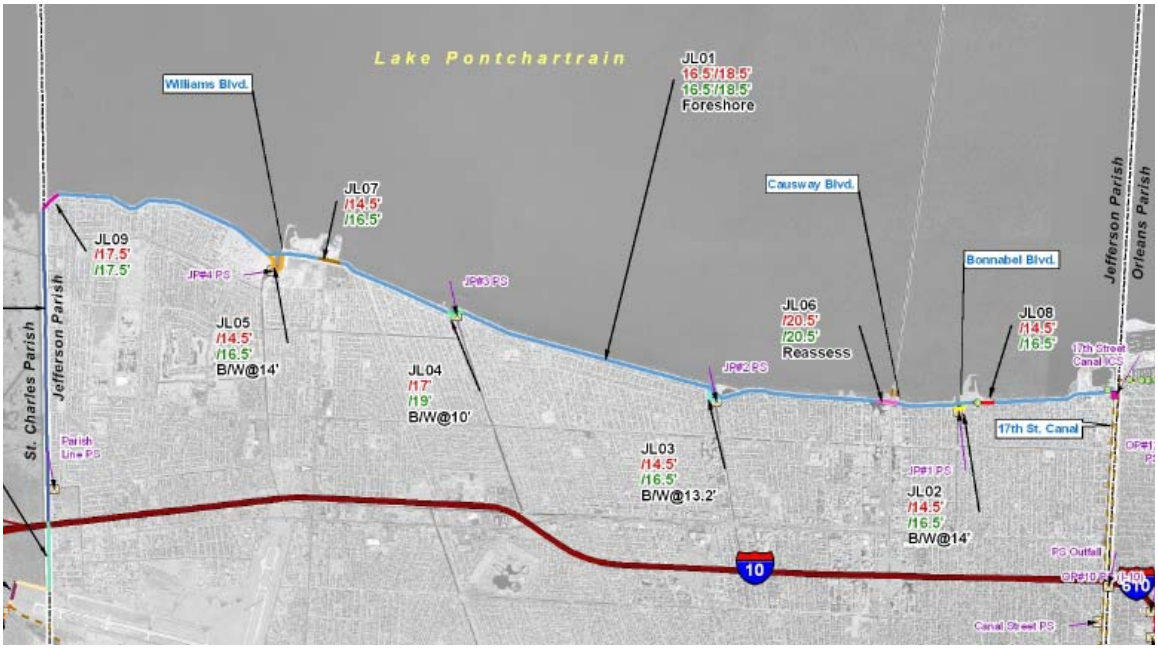

Jefferson Parish Sections 1% Hydraulic boundary conditions									
				Surge level (ft)		Significant wave height (ft)		Peak period (s)	
Segment	Name	Type	Condition	Mean	Std	Mean	Std	Mean	Std
JL01	Lakefront levee	Levee	Existing	9.0	0.6	3.6	0.4	7.7	1.5
JL01	Lakefront levee	Levee	Future	10.5	0.6	4.2	0.4	8.3	1.5
JL02	Pump station 1 with breakwater at 14ft	Structure/Wall	Future	10.3	0.7	2.5	0.3	8.1	1.6
JL03	Pump station 2 with breakwater at 13.2ft	Structure/Wall	Future	10.4	0.7	2.8	0.3	8.1	1.6
JL04	Pump station 3 with breakwater at 10ft	Structure/Wall	Future	10.5	0.6	4.2	0.4	8.1	1.6
JL05	Pump station 4 with breakwater at 14ft	Structure/Wall	Future	10.5	0.7	2.5	0.3	8.1	1.6
JL06	Causeway Crib wall	Structure/Wall	Future	10.3	0.7	6.5	0.6	7.8	1.5
JL07	Williams Blvd Floodgate	Structure/Wall	Future	10.4	0.6	2.8	0.2	8.5	1.5
JL08	Bonnabel Boat Launch Floodgate	Structure/Wall	Future	10.3	0.7	2.7	0.2	8.3	1.5
JL09	Return wall	Structure/Wall	Future	10.8	0.7	4.9	0.4	8.3	1.6

Jefferson Parish Sections 1% Design heights							
						Overtopping rate	
Segment	Name	Type	Condition	Depth at toe (ft)	Height (ft)	q50 (cft/s per ft)	q90 (cft/s per ft)
JL01	Lakefront levee	Levee	Existing	9.0	16.5	0.001	0.015
JL01	Lakefront levee	Levee	Future	10.5	18.5	0.002	0.024
JL02	Pump station 1 with breakwater at 14ft	Structure/Wall	Future	15.3	16.5	0.000	0.002
JL03	Pump station 2 with breakwater at 13.2ft	Structure/Wall	Future	15.4	16.5	0.001	0.005
JL04	Pump station 3 with breakwater at 10ft	Structure/Wall	Future	15.5	19.0	0.003	0.011
JL05	Pump station 4 with breakwater at 14ft	Structure/Wall	Future	15.5	16.5	0.000	0.002
JL06	Causeway Crib wall	Structure/Wall	Future	16.3	20.5	0.021	0.058
JL07	Williams Blvd Floodgate	Structure/Wall	Future	6.9	16.5	0.000	0.003
JL08	Bonnabel Boat Launch Floodgate	Structure/Wall	Future	6.8	16.5	0.000	0.003
JL09	Return wall	Structure/Wall	Future	12.3	17.5	0.029	0.087

Jefferson Parish Sections Resiliency analysis (0.2% event)						
					Best estimates during 0.2% event	
Segment	Name	Type	Condition	Height (ft)	Surge level (ft)	Overtopping rate (cft/s per ft)
JL01	Lakefront levee	Levee	Existing	16.5	11.2	0.088
JL01	Lakefront levee	Levee	Future	18.5	12.7	0.096
JL02	Pump station 1 with breakwater at 14ft	Structure/Wall	Future	16.5	12.7	0.008
JL03	Pump station 2 with breakwater at 13.2ft	Structure/Wall	Future	16.5	12.7	0.018
JL04	Pump station 3 with breakwater at 10ft	Structure/Wall	Future	19.0	12.7	0.019
JL05	Pump station 4 with breakwater at 14ft	Structure/Wall	Future	16.5	12.8	0.010
JL06	Causeway Crib wall	Structure/Wall	Future	20.5	12.7	0.174
JL07	Williams Blvd Floodgate	Structure/Wall	Future	16.5	12.6	0.056
JL08	Bonnabel Boat Launch Floodgate	Structure/Wall	Future	16.5	12.7	0.064
JL09	Return wall	Structure/Wall	Future	17.5	13.1	0.362

Orleans Parish East Bank Metro Reaches

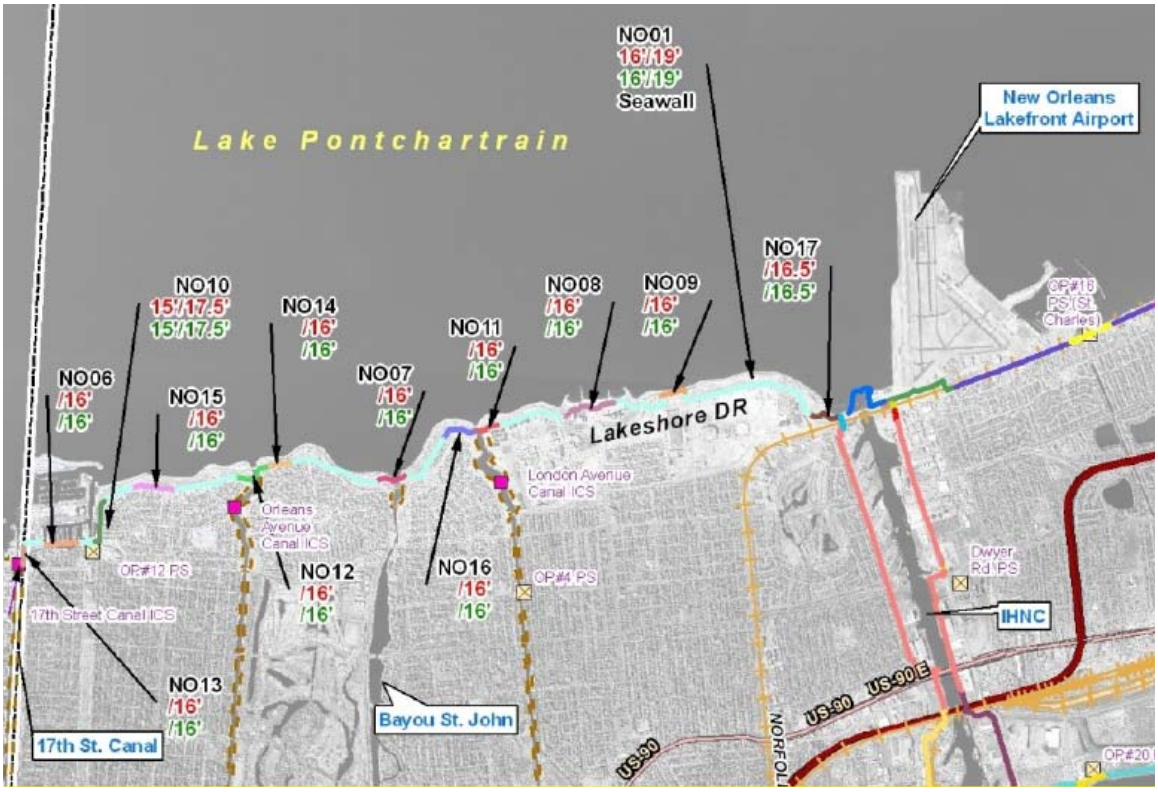

Orleans Parish Metro Lakefront Sections 1% Hydraulic boundary conditions									
				Surge level (ft)		Significant wave height (ft)		Peak period (s)	
Segment	Name	Type	Condition	Mean	Std	Mean	Std	Mean	Std
NO06	NO Marina	Structure/Wall	Future	10.2	0.7	3.3	0.3	8.0	1.4
NO10	Topaz St. Levee	Levee	Existing	8.7	0.7	2.3	0.2	7.2	1.4
NO10	Topaz St. Levee	Levee	Future	10.2	0.7	2.9	0.2	8.1	1.4
NO15	Type II Floodgate similar to Canal Blvd	Structure/Wall	Future	10.2	0.7	2.3	0.2	8.4	1.4
NO13	17th St. Outfall Canal Closure	Structure/Wall	Future	10.2	0.7	4.0	0.4	4.5	0.9
NO12	Orleans Ave Outfall Canal Closure	Structure/Wall	Future	10.2	0.8	3.0	0.3	4.0	0.8
NO14	Type I Floodgate Similar to Marconi Drive	Structure/Wall	Future	10.2	0.8	2.5	0.2	7.9	1.4
NO16	Lakeshore Drive near Rail St FG	Structure/Wall	Future	10.1	0.8	4.4	0.4	7.4	1.4
NO07	Bayou St. John	Structure/Wall	Future	10.1	0.8	3.0	0.3	4.0	0.8
NO11	London Ave Outfall Canal Closures	Structure/Wall	Future	10.1	0.8	3.0	0.3	4.0	0.8
NO08	Pontchartrain	Structure/Wall	Future	10.1	0.8	3.6	0.3	7.3	1.3
NO09	American Std FW	Structure/Wall	Future	10.1	0.8	4.4	0.4	7.1	1.3
NO01	New Orleans Lakefront Levee	Levee	Existing	8.7	0.7	5.1	0.5	7.2	1.4
NO01	New Orleans Lakefront Levee	Levee	Future	10.2	0.7	5.7	0.5	7.6	1.4
NO17	Leroy Johnson	Structure/Wall	Future	10.1	0.8	4.0	0.3	7.0	1.3

Orleans Parish Metro Lakefront Sections 1% Design heights							
						Overtopping rate	
Segment	Name	Type	Condition	Depth at toe (ft)	Height (ft)	q50 (cft/s per ft)	q90 (cft/s per ft)
NO06	NO Marina	Structure/Wall	Future	8.2	16.0	0.003	0.016
NO10	Topaz St. Levee	Levee	Existing	5.7	15.0	0.002	0.015
NO10	Topaz St. Levee	Levee	Future	7.2	17.5	0.005	0.029
NO15	Type II Floodgate similar to Canal Blvd	Structure/Wall	Future	5.7	16.0	0.000	0.001
NO13	17th St. Outfall Canal Closure	Structure/Wall	Future	10.2	16.0	0.015	0.056
NO12	Orleans Ave Outfall Canal Closure	Structure/Wall	Future	10.2	16.0	0.002	0.012
NO14	Type I Floodgate Similar to Marconi Drive	Structure/Wall	Future	6.2	16.0	0.000	0.002
NO16	Lakeshore Drive near Rail St FG	Structure/Wall	Future	11.1	16.0	0.028	0.097
NO07	Bayou St. John	Structure/Wall	Future	10.1	16.0	0.002	0.011
NO11	London Ave Outfall Canal Closures	Structure/Wall	Future	10.1	16.0	0.002	0.011
NO08	Pontchartrain	Structure/Wall	Future	9.1	16.0	0.007	0.033
NO09	American Std FW	Structure/Wall	Future	11.1	16.0	0.028	0.096
NO01	New Orleans Lakefront Levee	Levee	Existing	12.7	16.0	0.006	0.060
NO01	New Orleans Lakefront Levee	Levee	Future	14.2	19.0	0.008	0.066
NO17	Leroy Johnson	Structure/Wall	Future	10.1	16.5	0.009	0.038

Orleans Parish Metro Lakefront Sections Resiliency analysis (0.2% event)						
					Best estimates during 0.2% event	
Segment	Name	Type	Condition	Height (ft)	Surge level (ft)	Overtopping rate (cft/s per ft)
NO06	NO Marina	Structure/Wall	Future	16.0	12.8	0.244
NO10	Topaz St. Levee	Levee	Existing	15.0	11.3	0.314
NO10	Topaz St. Levee	Levee	Future	17.5	12.8	0.323
NO15	Type II Floodgate similar to Canal Blvd	Structure/Wall	Future	16.0	12.8	0.074
NO13	17th St. Outfall Canal Closure	Structure/Wall	Future	16.0	12.8	0.211
NO12	Orleans Ave Outfall Canal Closure	Structure/Wall	Future	16.0	13.1	0.076
NO14	Type I Floodgate Similar to Marconi Drive	Structure/Wall	Future	16.0	13.1	0.156
NO16	Lakeshore Drive near Rail St FG	Structure/Wall	Future	16.0	13.1	0.854
NO07	Bayou St. John	Structure/Wall	Future	16.0	13.1	0.075
NO11	London Ave Outfall Canal Closures	Structure/Wall	Future	16.0	12.9	0.059
NO08	Pontchartrain	Structure/Wall	Future	16.0	12.9	0.396
NO09	American Std FW	Structure/Wall	Future	16.0	12.8	0.648
NO01	New Orleans Lakefront Levee	Levee	Existing	16.0	11.3	0.335
NO01	New Orleans Lakefront Levee	Levee	Future	19.0	12.8	0.276
NO17	Leroy Johnson	Structure/Wall	Future	16.5	12.8	0.336

Orleans Parish East Bank, New Orleans East Lakefront, Reaches

Orleans Parish East Lakefront Sections 1% Hydraulic boundary conditions									
				Surge level (ft)		Significant wave height (ft)		Peak period (s)	
Segment	Name	Type	Condition	Mean	Std	Mean	Std	Mean	Std
NE04	NO Lakefront Airport West	Structure/Wall	Future	10.0	0.7	3.2	0.3	7.5	1.4
NE03	NO Lakefront Airport East	Structure/Wall	Future	9.9	0.7	3.2	0.3	7.4	1.3
NE09	St Charles Pump station	Structure/Wall	Future	9.9	0.7	4.0	0.3	7.3	1.3
NE07	Citrus Pump station	Structure/Wall	Future	10.0	0.7	4.0	0.3	7.2	1.3
NE01	Citrus Lakefront Levee	Levee	Existing	8.6	0.7	2.0	0.2	6.7	1.3
NE01	Citrus Lakefront Levee	Levee	Future	10.1	0.7	2.5	0.3	7.1	1.4
NE08	Jahncke Pump station	Structure/Wall	Future	10.0	0.7	4.0	0.3	7.3	1.3
NE05	Lincoln Beach	Structure/Wall	Future	10.1	0.7	2.4	0.2	7.6	1.3
NE06	Collins Pipeline Crossing	Structure/Wall	Future	10.4	0.7	3.8	0.3	7.1	1.3
NE30	Transition Reach NE01 to NE02	Levee	Existing	8.6	0.7	2.9	0.3	6.7	1.3
NE30	Transition Reach NE01 to NE02	Levee	Future	10.1	0.7	3.4	0.3	7.1	1.4
NE02	New Orleans East Lakefront Levee	Levee	Existing	8.9	0.7	3.7	0.4	6.7	1.3
NE02	New Orleans East Lakefront Levee	Levee	Future	10.4	0.7	4.3	0.4	7.1	1.4
NE31	South Point transition reach	Levee	Existing	9.0	0.8	3.7	0.4	6.7	1.3
NE31	South Point transition reach	Levee	Future	10.5	0.8	4.3	0.4	7.1	1.4

Orleans Parish East Lakefront Sections 1% Design heights							
						Overtopping rate	
Segment	Name	Type	Condition	Depth at toe (ft)	Height (ft)	q50 (cft/s per ft)	q90 (cft/s per ft)
NE04	NO Lakefront Airport West	Structure/Wall	Future	8.0	15.5	0.004	0.019
NE03	NO Lakefront Airport East	Structure/Wall	Future	7.9	15.5	0.003	0.015
NE09	St Charles Pump station	Structure/Wall	Future	9.9	15.5	0.017	0.060
NE07	Citrus Pump station	Structure/Wall	Future	10.0	15.5	0.020	0.069
NE01	Citrus Lakefront Levee	Levee	Existing	8.6	13.0	0.007	0.044
NE01	Citrus Lakefront Levee	Levee	Future	10.1	15.5	0.010	0.057
NE08	Jahncke Pump station	Structure/Wall	Future	10.0	15.5	0.020	0.069
NE05	Lincoln Beach	Structure/Wall	Future	6.1	15.5	0.000	0.003
NE06	Collins Pipeline Crossing	Structure/Wall	Future	9.4	17.5	0.003	0.012
NE30	Transition Reach NE01 to NE02	Levee	Existing	9.6	14.5	0.010	0.064
NE30	Transition Reach NE01 to NE02	Levee	Future	11.1	16.5	0.007	0.066
NE02	New Orleans East Lakefront Levee	Levee	Existing	9.9	15.5	0.003	0.033
NE02	New Orleans East Lakefront Levee	Levee	Future	11.4	17.5	0.006	0.062
NE31	South Point transition reach	Levee	Existing	9.0	16.5	0.002	0.025
NE31	South Point transition reach	Levee	Future	10.5	18.5	0.005	0.052

Orleans Parish East Lakefront Sections Resiliency analysis (0.2% event)						
					Best estimates during 0.2% event	
Segment	Name	Type	Condition	Height (ft)	Surge level (ft)	Overtopping rate (cft/s per ft)
NE04	NO Lakefront Airport West	Structure/Wall	Future	15.5	12.6	0.291
NE03	NO Lakefront Airport East	Structure/Wall	Future	15.5	12.3	0.203
NE09	St Charles Pump station	Structure/Wall	Future	15.5	12.3	0.422
NE07	Citrus Pump station	Structure/Wall	Future	15.5	12.4	0.458
NE01	Citrus Lakefront Levee	Levee	Existing	13.0	11.0	0.216
NE01	Citrus Lakefront Levee	Levee	Future	15.5	12.5	0.158
NE08	Jahncke Pump station	Structure/Wall	Future	15.5	12.4	0.456
NE05	Lincoln Beach	Structure/Wall	Future	15.5	12.5	0.101
NE06	Collins Pipeline Crossing	Structure/Wall	Future	17.5	13.0	0.136
NE30	Transition Reach NE01 to NE02	Levee	Existing	14.5	11.1	0.148
NE30	Transition Reach NE01 to NE02	Levee	Future	16.5	12.6	0.100
NE02	New Orleans East Lakefront Levee	Levee	Existing	15.5	11.5	0.065
NE02	New Orleans East Lakefront Levee	Levee	Future	17.5	13.0	0.093
NE31	South Point transition reach	Levee	Existing	16.5	11.7	0.050
NE31	South Point transition reach	Levee	Future	18.5	13.2	0.081

Orleans Parish East, New Orleans East Back Levee Reaches

GIWW Sections (outside MRGO gate) 1% Hydraulic boundary conditions									
				Surge level (ft)		Significant wave height (ft)		Peak period (s)	
Segment	Name	Type	Condition	Mean	Std	Mean	Std	Mean	Std
NE13	Highway 11 Floodgate	Structure/Wall	Future	11.1	0.9	4.4	0.4	5.8	1.1
NE10	South Point to Highway 90 Levee	Levee	Existing	10.9	0.9	4.4	0.4	5.4	1.1
NE10	South Point to Highway 90 Levee	Levee	Future	12.4	0.9	5.0	0.4	5.8	1.1
NE14	Highway 90 Floodgate	Structure/Wall	Future	12.5	0.9	5.0	0.4	5.6	1.1
NE11A	Highway 90 to CSX RR Levee	Levee	Existing	14.3	0.9	4.0	0.4	8.3	1.7
NE11A	Highway 90 to CSX RR Levee	Levee	Future	15.8	0.9	4.8	0.4	9.0	1.7
NE15	CSX RR Floodgate	Structure/Wall	Future	17.3	1.0	6.7	0.6	7.1	1.3
NE11B	CSX RR to GIWW Levee	Levee	Existing	16.2	1.0	5.9	0.6	7.7	1.5
NE11B	CSX RR to GIWW Levee	Levee	Future	17.7	1.0	6.7	0.6	8.2	1.5
NE32	Transition Levee	Levee	Existing	16.2	1.0	5.4	0.5	7.9	1.6
NE32	Transition Levee	Levee	Future	17.7	1.0	6.2	0.5	8.5	1.6
NE12A	NO East Back Levee from PS15 East along GIWW	Levee	Existing	17.4	1.0	5.4	0.5	8.0	1.6
NE12A	NO East Back Levee from PS15 East along GIWW	Levee	Future	18.9	1.0	6.2	0.5	8.6	1.6
NE16	NO East Pump Station 15	Structure/Wall	Future	18.9	1.0	5.5	0.5	7.8	1.5
NE12B	NO East Back Levee from Gate to PS15	Levee	Existing	18.4	1.0	7.1	0.7	7.9	1.6
NE12B	NO East Back Levee from Gate to PS15	Levee	Future	19.9	1.0	7.9	0.7	8.3	1.6

GIWW Sections (outside MRGO gate) 1% Design heights							
						Overtopping rate	
Segment	Name	Type	Condition	Depth at toe (ft)	Height (ft)	q50 (cft/s per ft)	q90 (cft/s per ft)
NE13	Highway 11 Floodgate	Structure/Wall	Future	11.1	18.5	0.007	0.034
NE10	South Point to Highway 90 Levee	Levee	Existing	10.9	17.0	0.006	0.063
NE10	South Point to Highway 90 Levee	Levee	Future	12.4	19.0	0.008	0.077
NE14	Highway 90 Floodgate	Structure/Wall	Future	12.5	22.0	0.004	0.016
NE11A	Highway 90 to CSX RR Levee	Levee	Existing	14.3	22.0	0.006	0.064
NE11A	Highway 90 to CSX RR Levee	Levee	Future	15.8	25.0	0.008	0.071
NE15	CSX RR Floodgate	Structure/Wall	Future	17.3	30.0	0.007	0.025
NE11B	CSX RR to GIWW Levee	Levee	Existing	16.2	25.0	0.005	0.067
NE11B	CSX RR to GIWW Levee	Levee	Future	17.7	28.0	0.005	0.056
NE32	Transition Levee	Levee	Existing	16.2	28.0	0.001	0.020
NE32	Transition Levee	Levee	Future	17.7	31.0	0.004	0.046
NE12A	NO East Back Levee from PS15 East along GIWW	Levee	Existing	17.4	28.0	0.003	0.046
NE12A	NO East Back Levee from PS15 East along GIWW	Levee	Future	18.9	31.0	0.009	0.087
NE16	NO East Pump Station 15	Structure/Wall	Future	18.9	34.0	0.000	0.002
NE12B	NO East Back Levee from Gate to PS15	Levee	Existing	18.4	29.0	0.007	0.080
NE12B	NO East Back Levee from Gate to PS15	Levee	Future	19.9	31.5	0.009	0.085

GIWW Sections (outside MRGO gate) Resiliency analysis (0.2% event)						
					Best estimates during 0.2% event	
Segment	Name	Type	Condition	Height (ft)	Surge level (ft)	Overtopping rate (cft/s per ft)
NE13	Highway 11 Floodgate	Structure/Wall	Future	18.5	14.4	0.432
NE10	South Point to Highway 90 Levee	Levee	Existing	17.0	14.2	0.933
NE10	South Point to Highway 90 Levee	Levee	Future	19.0	15.7	0.860
NE14	Highway 90 Floodgate	Structure/Wall	Future	22.0	15.7	0.160
NE11A	Highway 90 to CSX RR Levee	Levee	Existing	22.0	17.5	0.831
NE11A	Highway 90 to CSX RR Levee	Levee	Future	25.0	19.0	0.586
NE15	CSX RR Floodgate	Structure/Wall	Future	30.0	20.7	0.145
NE11B	CSX RR to GIWW Levee	Levee	Existing	25.0	19.7	0.451
NE11B	CSX RR to GIWW Levee	Levee	Future	28.0	21.2	0.282
NE32	Transition Levee	Levee	Existing	28.0	19.7	0.100
NE32	Transition Levee	Levee	Future	31.0	21.2	0.153
NE12A	NO East Back Levee from PS15 East along GIWW	Levee	Existing	28.0	20.9	0.228
NE12A	NO East Back Levee from PS15 East along GIWW	Levee	Future	31.0	22.4	0.321
NE16	NO East Pump Station 15	Structure/Wall	Future	34.0	22.4	0.024
NE12B	NO East Back Levee from Gate to PS15	Levee	Existing	29.0	22.1	0.380
NE12B	NO East Back Levee from Gate to PS15	Levee	Future	31.5	23.6	0.322

Orleans and St. Bernard Parishes East Bank, Inside IHNC and Seabrook Barriers

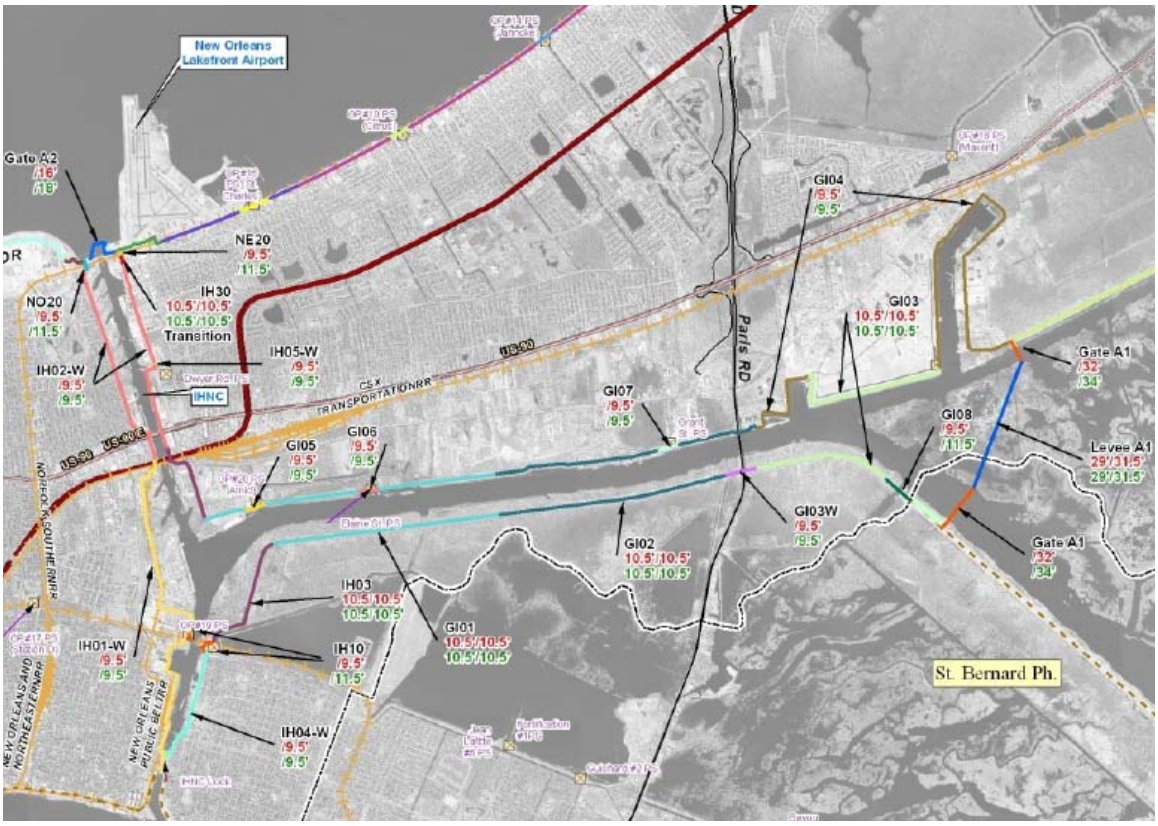

IHNC and GIWW sections (with MRGO/GIWW and Seabrook closures) 1% Hydraulic boundary conditions									
				Surge level (ft)		Significant wave height (ft)		Peak period (s)	
Segment	Name	Type	Condition	Mean	Std	Mean	Std	Mean	Std
GID8	Bienvenue Floodgate	Structure/Wall	Future	6.0	0.5	3.0	0.3	3.5	0.7
GID3	Michoud Canal to Michoud Slip and Paris Rd Bridge to Bienvenue Floodgate	Levee	Existing	6.0	0.5	3.0	0.3	3.5	0.7
GID3	Michoud Canal to Michoud Slip and Paris Rd Bridge to Bienvenue Floodgate	Levee	Future	6.0	0.5	3.0	0.3	3.5	0.7
GID4	Michoud Canal and Slip	Structure/Wall	Future	6.0	0.5	3.0	0.3	3.5	0.7
GID7	Grant Pump Station	Structure/Wall	Future	6.0	0.5	3.0	0.3	3.5	0.7
GID3-W	Floodwall under Paris Rd Bridge	Structure/Wall	Future	6.0	0.5	3.0	0.3	3.5	0.7
GID2	Paris Road to levee section GI01	Levee	Existing	6.0	0.5	3.0	0.3	3.5	0.7
GID2	Paris Road to levee section GI01	Levee	Future	6.0	0.5	3.0	0.3	3.5	0.7
GID1	Levee Section GI02 to IHNC	Levee	Existing	6.0	0.5	3.0	0.3	3.5	0.7
GID1	Levee Section GI02 to IHNC	Levee	Future	6.0	0.5	3.0	0.3	3.5	0.7
GID6	Elaine Pump Station	Structure/Wall	Future	6.0	0.5	3.0	0.3	3.5	0.7
GID5	Amid Pump Station (PS#20)	Structure/Wall	Future	6.0	0.5	3.0	0.3	3.5	0.7
IH30	Transition Reach	Levee	Existing	6.0	0.5	2.3	0.2	3.1	0.6
IH30	Transition Reach	Levee	Future	6.0	0.5	2.3	0.2	3.1	0.6
IH02-W	IHNC North of I-10	Structure/Wall	Future	6.0	0.5	2.3	0.2	3.1	0.6
IH01-W	IHNC South of I-10 to Pump Station #19	Structure/Wall	Future	6.0	0.5	3.0	0.3	3.5	0.7
IH04-W	IHNC Lock to Pump Stations (PS#5 and PS#19)	Structure/Wall	Future	6.0	0.5	2.3	0.2	3.1	0.6
IH10	Orleans Pump Stations #5 and Pump Station #19	Structure/Wall	Future	6.0	0.5	2.3	0.2	3.1	0.6
IH03	IHNC Levee South from I-10	Levee	Existing	6.0	0.5	3.0	0.3	3.5	0.7
IH03	IHNC Levee South from I-10	Levee	Future	6.0	0.5	3.0	0.3	3.5	0.7
IH05-W	Dwyer Pump Station	Structure/Wall	Future	6.0	0.5	2.3	0.2	3.1	0.6
NO20	NS Railroad gates near Seabrook (west)	Structure/Wall	Future	6.0	0.5	2.3	0.2	3.1	0.6
NE20	NS Railroad gates near Seabrook (east)	Structure/Wall	Future	6.0	0.5	2.3	0.2	3.1	0.6

IHNC and GIWW sections (with MRGO/GIWW and Seabrook closures) 1% Design heights							
						Overtopping rate	
Segment	Name	Type	Condition	Depth at toe (ft)	Height (ft)	q50 (cft/s per ft)	q90 (cft/s per ft)
GI08	Bienvenue Floodgate	Structure/Wall	Future	20.0	11.5	0.003	0.013
GI03	Michoud Canal to Michoud Slip and	Levee	Existing	6.0	10.5	0.010	0.058
GI03	Michoud Canal to Michoud Slip and	Levee	Future	6.0	10.5	0.010	0.057
GI04	Michoud Canal and Slip	Structure/Wall	Future	6.0	9.5	0.009	0.043
GI07	Grant Pump Station	Structure/Wall	Future	5.0	9.5	0.002	0.018
GI03-W	Floodwall under Paris Rd Bridge	Structure/Wall	Future	5.0	9.5	0.002	0.018
GI02	Paris Road to levee section GI01	Levee	Existing	6.0	10.5	0.010	0.057
GI02	Paris Road to levee section GI01	Levee	Future	6.0	10.5	0.009	0.055
GI01	Levee Section GI02 to IHNC	Levee	Existing	6.0	10.5	0.009	0.056
GI01	Levee Section GI02 to IHNC	Levee	Future	6.0	10.5	0.010	0.056
GI06	Elaine Pump Station	Structure/Wall	Future	7.0	9.5	0.022	0.076
GI05	Amid Pump Station (PS#20)	Structure/Wall	Future	7.0	9.5	0.021	0.075
IH30	Transition Reach	Levee	Existing	6.0	10.5	0.004	0.029
IH30	Transition Reach	Levee	Future	6.0	10.5	0.003	0.029
IH02-W	IHNC North of I-10	Structure/Wall	Future	5.0	9.5	0.002	0.015
IH01-W	IHNC South of I-10 to Pump Station #19	Structure/Wall	Future	5.0	9.5	0.002	0.017
IH04-W	IHNC Lock to Pump Stations (PS#5 and PS#19)	Structure/Wall	Future	5.0	9.5	0.002	0.015
IH10	Orleans Pump Stations #5 and Pump Station #19	Structure/Wall	Future	5.0	11.5	0.000	0.001
IH03	IHNC Levee South from I-10	Levee	Existing	6.0	10.5	0.009	0.056
IH03	IHNC Levee South from I-10	Levee	Future	6.0	10.5	0.010	0.056
IH05-W	Dwyer Pump Station	Structure/Wall	Future	5.0	9.5	0.002	0.015
NO20	NS Railroad gates near Seabrook (west)	Structure/Wall	Future	5.0	11.5	0.000	0.001
NE20	NS Railroad gates near Seabrook (east)	Structure/Wall	Future	5.0	11.5	0.000	0.001

Note. The Resiliency Analysis (0.2% Event) was not performed for the IHNC and GIWW with MRGO.GIWW and Seabrook closures.

Near IHNC and Seabrook Surge Barriers

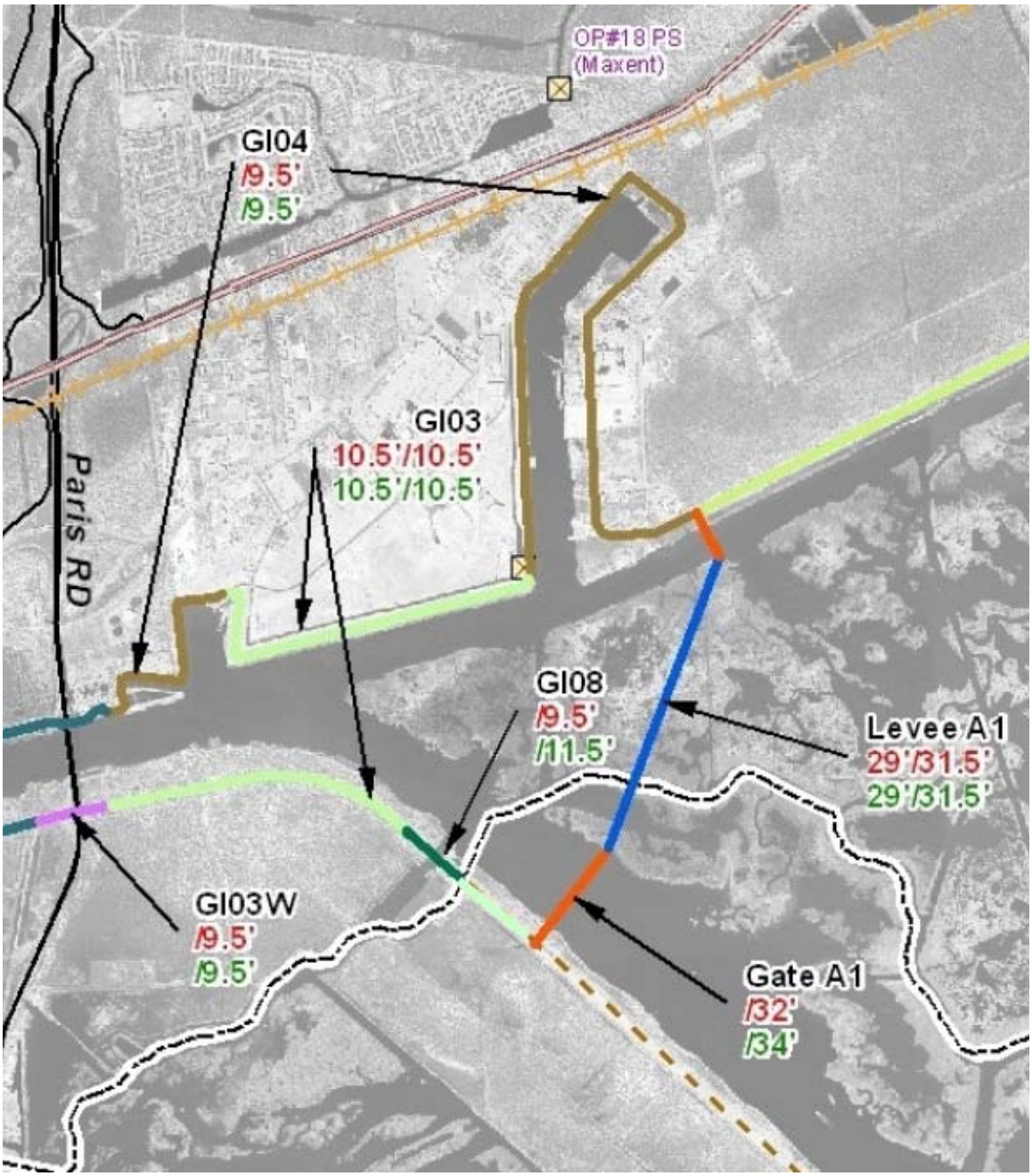


New Orleans
Lakefront Airport
Gate A2
/16'
/18'
OP#16
PS (St.
Charles)
NE20
/9.5'
/11.5'
e DR
NO20
/9.5'
/11.5'
IH30
10.5'/10.5'
10.5'/10.5'
Transition
IH05A1-W
/9.5'
/9.5'
IH02A1-W
/9.5'
/9.5'
IHNC

MRGO-GIWW and Seabrook Closure Sections
1% Hydraulic boundary conditions

				Surge level (ft)		Significant wave height (ft)		Peak period (s)	
Segment	Name	Type	Condition	Mean	Std	Mean	Std	Mean	Std
GATE-A1	Closure gate at MRGO - GIWW intersection	Structure/Wall	Future	19.9	1.0	7.2	0.6	8.4	1.6
LEVEE-A1	Closure levee at MRGO - GIWW intersection	Levee	Existing	18.4	1.0	7.1	0.7	7.9	1.6
LEVEE-A1	Closure levee at MRGO - GIWW intersection	Levee	Future	19.9	1.0	7.9	0.7	8.3	1.6
GATE-A2	Closure gate at Seabrook	Structure/Wall	Future	10.0	0.8	4.0	0.3	6.2	1.1

MRGO-GIWW and Seabrook Closure Sections
1% Design heights

						Overtopping rate	
Segment	Name	Type	Condition	Depth at toe (ft)	Height (ft)	q50 (cft/s per ft)	q90 (cft/s per ft)
GATE-A1	Closure gate at MRGO - GIWW intersection	Structure/Wall	Future	39.9	34.0	0.007	0.027
LEVEE-A1	Closure levee at MRGO - GIWW intersection	Levee	Existing	18.4	29.0	0.008	0.082
LEVEE-A1	Closure levee at MRGO - GIWW intersection	Levee	Future	19.9	31.5	0.009	0.089
GATE-A2	Closure gate at Seabrook	Structure/Wall	Future	10.0	18.0	0.002	0.009

MRGO-GIWW and Seabrook Closure Sections
Resiliency analysis (0.2% event)

					Best estimates during 0.2% event	
Segment	Name	Type	Condition	Height (ft)	Surge level (ft)	Overtopping rate (cft/s per ft)
GATE-A1	Closure gate at MRGO - GIWW intersection	Structure/Wall	Future	34.0	23.6	1.780
LEVEE-A1	Closure levee at MRGO - GIWW intersection	Levee	Existing	29.0	22.1	1.780
LEVEE-A1	Closure levee at MRGO - GIWW intersection	Levee	Future	31.5	23.6	1.780
GATE-A2	Closure gate at Seabrook	Structure/Wall	Future	18.0	12.8	1.390

St. Bernard Parish East Bank Reaches

St Bernard Parish Sections 1% Hydraulic boundary conditions									
				Surge level (ft)		Significant wave height (ft)		Peak period (s)	
Segment	Name	Type	Condition	Mean	Std	Mean	Std	Mean	Std
SB11	MRGO levee	Levee	Existing	18.4	1.0	7.1	0.7	7.9	1.6
SB11	MRGO levee	Levee	Future	19.9	1.0	7.9	0.7	8.3	1.6
SB12	MRGO levee	Levee	Existing	17.3	1.1	6.9	0.7	5.9	1.2
SB12	MRGO levee	Levee	Future	18.8	1.1	7.5	0.7	6.2	1.2
SB13	MRGO levee	Levee	Existing	16.4	1.1	6.6	0.7	6.3	1.3
SB13	MRGO levee	Levee	Future	17.9	1.1	7.2	0.7	6.6	1.3
SB15	MRGO levee	Levee	Existing	15.6	1.2	5.4	0.5	8.9	1.8
SB15	MRGO levee	Levee	Future	17.1	1.2	6.2	0.5	9.5	1.8
SB16	Caernarvon levee	Levee	Existing	17.5	1.1	5.4	0.5	8.4	1.7
SB16	Caernarvon levee	Levee	Future	19.0	1.1	6.2	0.5	8.9	1.7
SB17	Caernarvon levee	Levee	Existing	18.0	1.2	5.1	0.5	8.1	1.6
SB17	Caernarvon levee	Levee	Future	19.5	1.2	5.9	0.5	8.7	1.6
SB19	Bayou Dupre Control structure	Structure/Wall	Future	17.3	1.0	5.6	0.5	6.5	1.2
SB20	St Mary Pump Station (PS#8)	Structure/Wall	Future	18.5	1.0	6.2	0.5	8.6	1.6

St Bernard Parish Sections 1% Design heights							
						Overtopping rate	
Segment	Name	Type	Condition	Depth at toe (ft)	Height (ft)	q50 (cft/s per ft)	q90 (cft/s per ft)
SB11	MRGO levee	Levee	Existing	18.4	29.0	0.008	0.083
SB11	MRGO levee	Levee	Future	19.9	31.5	0.009	0.091
SB12	MRGO levee	Levee	Existing	17.3	27.5	0.001	0.019
SB12	MRGO levee	Levee	Future	18.8	30.0	0.002	0.022
SB13	MRGO levee	Levee	Existing	16.4	26.5	0.002	0.027
SB13	MRGO levee	Levee	Future	17.9	29.0	0.002	0.030
SB15	MRGO levee	Levee	Existing	15.6	26.5	0.005	0.062
SB15	MRGO levee	Levee	Future	17.1	29.0	0.007	0.077
SB16	Caernarvon levee	Levee	Existing	17.5	26.5	0.007	0.087
SB16	Caernarvon levee	Levee	Future	19.0	29.0	0.006	0.072
SB17	Caernarvon levee	Levee	Existing	18.0	26.5	0.002	0.040
SB17	Caernarvon levee	Levee	Future	19.5	29.0	0.009	0.097
SB19	Bayou Dupre Control structure	Structure/Wall	Future	17.3	31.0	0.001	0.004
SB20	St Mary Pump Station (PS#8)	Structure/Wall	Future	18.5	30.5	0.006	0.023

St Bernard Parish Sections Resiliency analysis (0.2% event)						
					Best estimates during 0.2% event	
Segment	Name	Type	Condition	Height (ft)	Surge level (ft)	Overtopping rate (cft/s per ft)
SB11	MRGO levee	Levee	Existing	29.0	22.1	0.374
SB11	MRGO levee	Levee	Future	31.5	23.6	0.322
SB12	MRGO levee	Levee	Existing	27.5	21.1	0.163
SB12	MRGO levee	Levee	Future	30.0	22.6	0.150
SB13	MRGO levee	Levee	Existing	26.5	20.2	2.355
SB13	MRGO levee	Levee	Future	29.0	21.7	2.284
SB15	MRGO levee	Levee	Existing	26.5	19.9	1.842
SB15	MRGO levee	Levee	Future	29.0	21.4	1.689
SB16	Caernarvon levee	Levee	Existing	26.5	21.3	1.319
SB16	Caernarvon levee	Levee	Future	29.0	22.8	0.920
SB17	Caernarvon levee	Levee	Existing	26.5	22.1	0.778
SB17	Caernarvon levee	Levee	Future	29.0	23.6	1.028
SB19	Bayou Dupre Control structure	Structure/Wall	Future	31.0	21.0	0.112
SB20	St Mary Pump Station (PS#8)	Structure/Wall	Future	30.5	21.9	0.253

St. Charles and Jefferson Parishes, Lake Cataouache Reaches

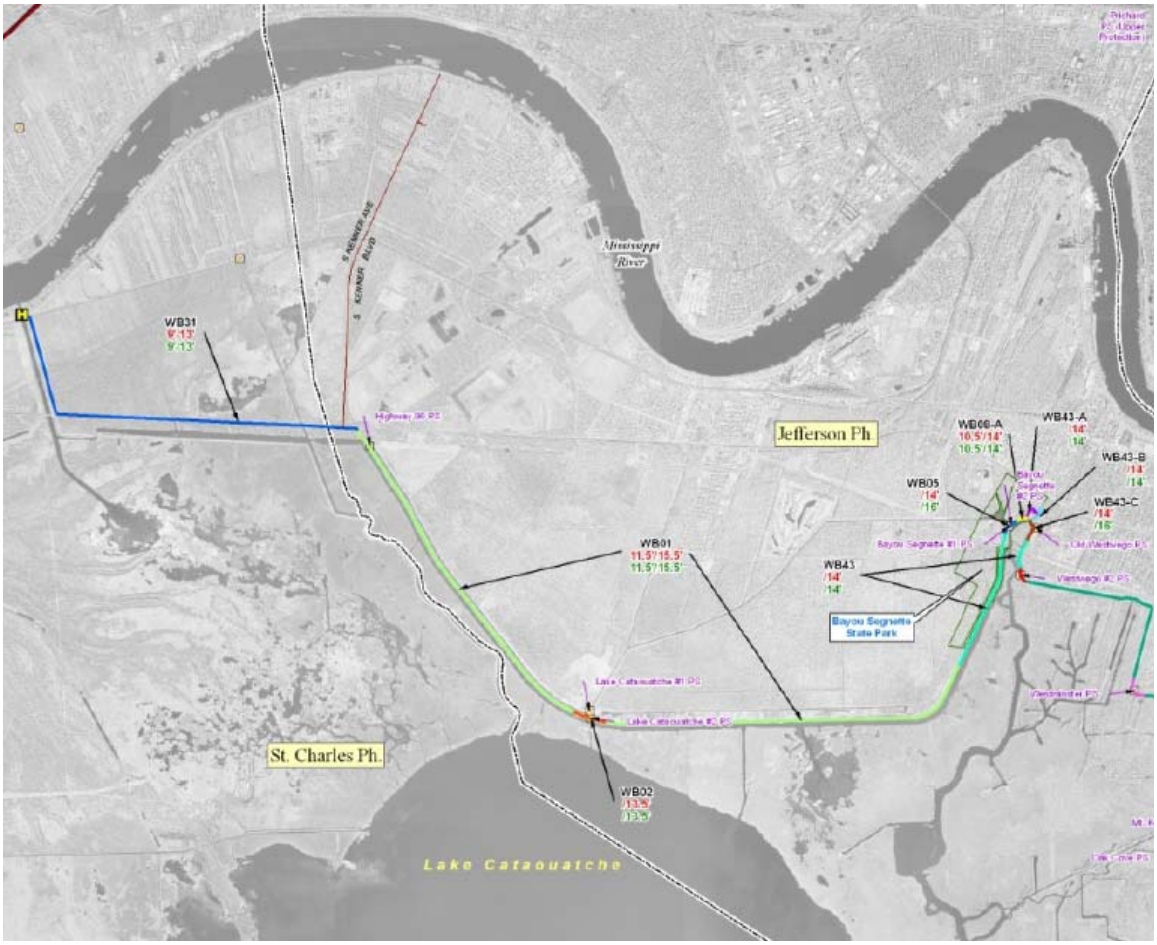

Westbank Sections (Lake Cataouache Reach) 1% Hydraulic boundary conditions									
				Surge level (ft)		Significant wave height (ft)		Peak period (s)	
Segment	Name	Type	Condition	Mean	Std	Mean	Std	Mean	Std
WB31	Mississippi River to US90 Levees	Levee	Existing	6.5	0.7	1.6	0.2	5.4	1.1
WB31	Mississippi River to US90 Levees	Levee	Future	8.5	0.7	2.6	0.2	6.9	1.1
WB01	US Highway 90 to the Bayou Segnette State Park	Levee	Existing	6.5	0.7	2.1	0.2	5.5	1.1
WB01	US Highway 90 to the Bayou Segnette State Park	Levee	Future	8.5	0.7	3.1	0.2	6.7	1.1
WB02	Lake Cataouatche Pump Station 1 and 2	Structure/Wall	Future	8.5	0.7	3.1	0.2	6.7	1.1
WB43	Bayou Segnette State Park Floodwall	Structure/Wall	Future	8.5	0.7	2.4	0.1	5.6	0.9
WB05	Bayou Segnette Pump Station 1 and 2	Structure/Wall	Future	8.5	0.7	2.4	0.1	5.6	0.9

Westbank Sections (Lake Cataouache Reach) 1% Design heights							
						Overtopping rate	
Segment	Name	Type	Condition	Depth at toe (ft)	Height (ft)	q50 (cft/s per ft)	q90 (cft/s per ft)
WB31	Mississippi River to US90 Levees	Levee	Existing	5.5	9.0	0.002	0.044
WB31	Mississippi River to US90 Levees	Levee	Future	7.5	13.0	0.003	0.030
WB01	US Highway 90 to the Bayou Segnette State Park	Levee	Existing	6.5	11.5	0.003	0.024
WB01	US Highway 90 to the Bayou Segnette State Park	Levee	Future	8.5	15.5	0.006	0.034
WB02	Lake Cataouatche Pump Station 1 and 2	Structure/Wall	Future	8.5	15.5	0.001	0.003
WB43	Bayou Segnette State Park Floodwall	Structure/Wall	Future	8.5	14.0	0.000	0.002
WB05	Bayou Segnette Pump Station 1 and 2	Structure/Wall	Future	8.5	16.0	0.000	0.000

Westbank Sections (Lake Cataouache Reach) Resiliency analysis (0.2% event)						
					Best estimates during 0.2% event	
Segment	Name	Type	Condition	Height (ft)	Surge level (ft)	Overtopping rate (cft/s per ft)
WB31	Mississippi River to US90 Levees	Levee	Existing	9.0	8.9	1.803
WB31	Mississippi River to US90 Levees	Levee	Future	13.0	10.9	0.584
WB01	US Highway 90 to the Bayou Segnette State Park	Levee	Existing	11.5	9.0	0.575
WB01	US Highway 90 to the Bayou Segnette State Park	Levee	Future	15.5	11.0	0.343
WB02	Lake Cataouatche Pump Station 1 and 2	Structure/Wall	Future	15.5	11.0	0.072
WB43	Bayou Segnette State Park Floodwall	Structure/Wall	Future	14.0	11.1	0.141
WB05	Bayou Segnette Pump Station 1 and 2	Structure/Wall	Future	16.0	11.1	0.017

Jefferson and Orleans Parishes, Westwego to Harvey Canal Reaches

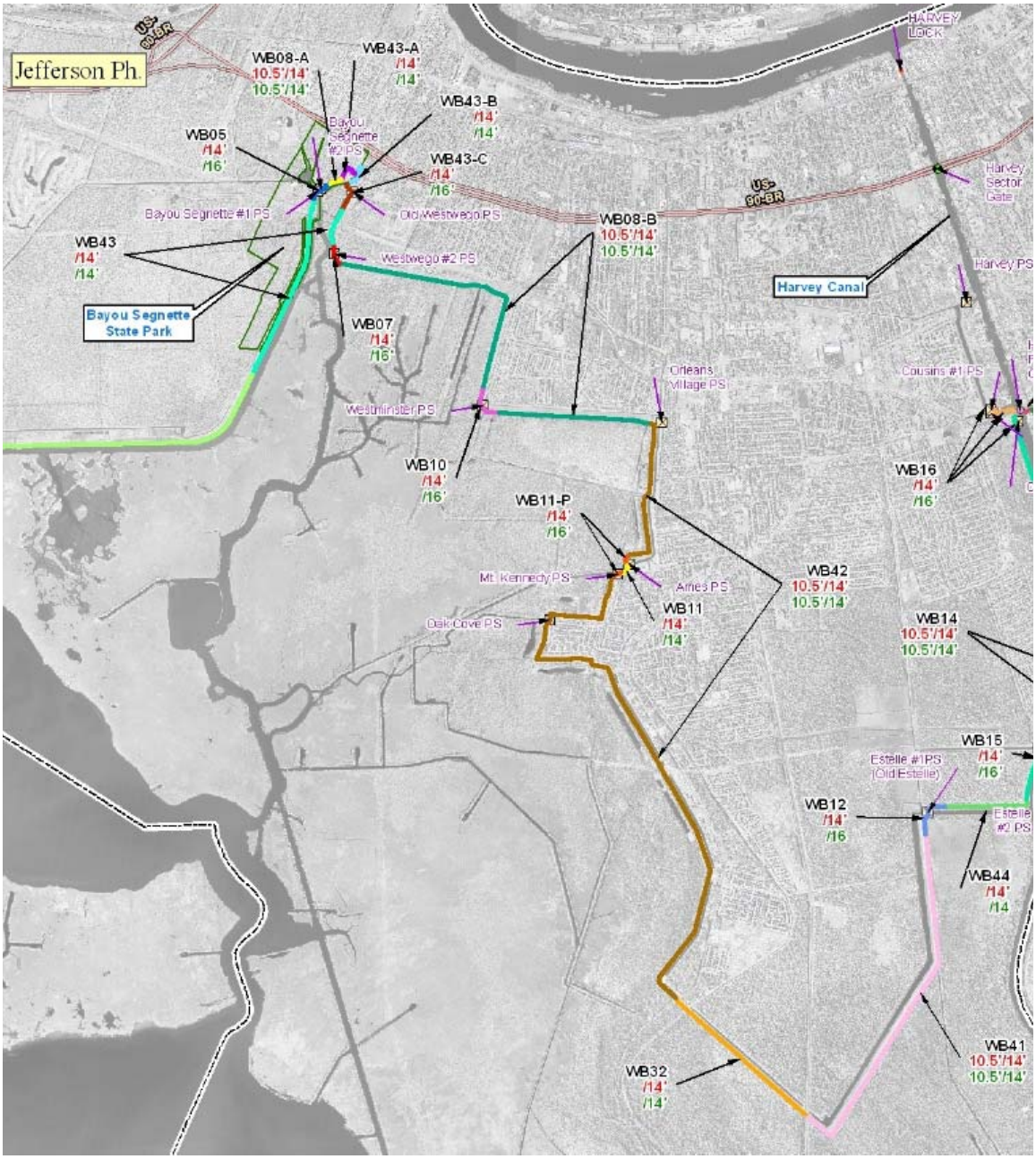

Westbank Sections (Westwego to Harvey Canal Reach) 1% Hydraulic boundary conditions									
				Surge level (ft)		Significant wave height (ft)		Peak period (s)	
Segment	Name	Type	Condition	Mean	Std	Mean	Std	Mean	Std
WB08-a	Segnette Pump Station to Company Canal Floodwall	Levee	Existing	6.5	0.7	1.4	0.1	4.3	0.9
WB08-a	Segnette Pump Station to Company Canal Floodwall	Levee	Future	8.5	0.7	2.4	0.1	5.6	0.9
WB08-b	New Westwego Pump Station to Orleans Village Levee	Levee	Existing	6.5	0.7	1.4	0.1	4.3	0.9
WB08-b	New Westwego Pump Station to Orleans Village Levee	Levee	Future	8.5	0.7	2.4	0.1	5.6	0.9
WB43-a	Segnette Pump Station to Company Canal Floodwall	Structure/Wall	Future	8.5	0.7	2.4	0.1	5.6	0.9
WB43-b	Company Canal & Westwego Floodwall	Structure/Wall	Future	8.5	0.7	2.4	0.1	5.6	0.9
WB43-c	Old Westwego Pump Station	Structure/Wall	Future	8.5	0.7	2.4	0.1	5.6	0.9
WB07	New Westwego Pump Station	Structure/Wall	Future	8.5	0.7	2.4	0.1	5.6	0.9
WB10	Westminster Pump Station	Structure/Wall	Future	8.5	0.7	2.4	0.1	5.6	0.9
WB11	Ames to Kennedy Floodwall	Structure/Wall	Future	9.3	0.9	2.3	0.1	4.9	0.7
WB11-P	Ames & Kennedy Pump Station	Structure/Wall	Future	9.3	0.9	2.3	0.1	4.9	0.7
WB42	Orleans Village to Ames Pump Station Levee	Levee	Existing	7.3	0.9	1.3	0.1	3.7	0.7
WB42	Orleans Village to Ames Pump Station Levee	Levee	Future	9.3	0.9	2.3	0.1	4.9	0.7
WB32	Highway 45 to Highway 3134	Structure/Wall	Future	9.3	0.9	2.3	0.1	4.9	0.7
WB41	Highway 3134 to Old Estelle Pump Station Levee	Levee	Existing	7.3	0.9	1.3	0.1	3.7	0.7
WB41	Highway 3134 to Old Estelle Pump Station Levee	Levee	Future	9.3	0.9	2.3	0.1	4.9	0.7
WB12	Old Estelle Pump Station	Structure/Wall	Future	9.3	0.9	2.3	0.1	4.9	0.7
WB44	Old Estelle to Robinson Point	Structure/Wall	Future	9.3	0.9	2.3	0.1	4.9	0.7

Westbank Sections (Westwego to Harvey Canal Reach) 1% Design heights							
						Overtopping rate	
Segment	Name	Type	Condition	Depth at toe (ft)	Height (ft)	q50 (cft/s per ft)	q90 (cft/s per ft)
WB08-a	Segnette Pump Station to Company Canal Floodwall	Levee	Existing	5.5	10.5	0.001	0.010
WB08-a	Segnette Pump Station to Company Canal Floodwall	Levee	Future	7.5	14.0	0.008	0.037
WB08-b	New Westwego Pump Station to Orleans Village Levee	Levee	Existing	5.5	10.5	0.001	0.010
WB08-b	New Westwego Pump Station to Orleans Village Levee	Levee	Future	7.5	14.0	0.008	0.035
WB43-a	Segnette Pump Station to Company Canal Floodwall	Structure/Wall	Future	8.5	14.0	0.000	0.003
WB43-b	Company Canal & Westwego Floodwall	Structure/Wall	Future	8.5	14.0	0.000	0.002
WB43-c	Old Westwego Pump Station	Structure/Wall	Future	8.5	16.0	0.000	0.000
WB07	New Westwego Pump Station	Structure/Wall	Future	8.5	16.0	0.000	0.000
WB10	Westminster Pump Station	Structure/Wall	Future	8.5	16.0	0.000	0.000
WB11	Ames to Kennedy Floodwall	Structure/Wall	Future	9.3	14.0	0.001	0.008
WB11-P	Ames & Kennedy Pump Station	Structure/Wall	Future	9.3	16.0	0.000	0.000
WB42	Orleans Village to Ames Pump Station Levee	Levee	Existing	7.3	10.5	0.003	0.035
WB42	Orleans Village to Ames Pump Station Levee	Levee	Future	9.3	14.0	0.010	0.063
WB32	Highway 45 to Highway 3134	Structure/Wall	Future	9.3	14.0	0.001	0.008
WB41	Highway 3134 to Old Estelle Pump Station Levee	Levee	Existing	7.3	10.5	0.003	0.034
WB41	Highway 3134 to Old Estelle Pump Station Levee	Levee	Future	9.3	14.0	0.010	0.061
WB12	Old Estelle Pump Station	Structure/Wall	Future	9.3	16.0	0.000	0.000
WB44	Old Estelle to Robinson Point	Structure/Wall	Future	9.3	14.0	0.001	0.008

Westbank Sections (Westwego to Harvey Canal Reach) Resiliency analysis (0.2% event)						
					Best estimates during 0.2% event	
Segment	Name	Type	Condition	Height (ft)	Surge level (ft)	Overtopping rate (cft/s per ft)
WB08-a	Segnette Pump Station to Company Canal Floodwall	Levee	Existing	10.5	9.1	0.945
WB08-a	Segnette Pump Station to Company Canal Floodwall	Levee	Future	14.0	11.1	0.727
WB08-b	New Westwego Pump Station to Orleans Village Levee	Levee	Existing	10.5	9.1	0.955
WB08-b	New Westwego Pump Station to Orleans Village Levee	Levee	Future	14.0	11.1	0.729
WB43-a	Segnette Pump Station to Company Canal Floodwall	Structure/Wall	Future	14.0	11.1	0.138
WB43-b	Company Canal & Westwego Floodwall	Structure/Wall	Future	14.0	11.1	0.140
WB43-c	Old Westwego Pump Station	Structure/Wall	Future	16.0	11.1	0.016
WB07	New Westwego Pump Station	Structure/Wall	Future	16.0	11.1	0.017
WB10	Westminster Pump Station	Structure/Wall	Future	16.0	11.1	0.016
WB11	Ames to Kennedy Floodwall	Structure/Wall	Future	14.0	12.4	0.434
WB11-P	Ames & Kennedy Pump Station	Structure/Wall	Future	16.0	12.4	0.047
WB42	Orleans Village to Ames Pump Station Levee	Levee	Existing	10.5	10.4	2.076
WB42	Orleans Village to Ames Pump Station Levee	Levee	Future	14.0	12.4	1.237
WB32	Highway 45 to Highway 3134	Structure/Wall	Future	14.0	12.4	0.447
WB41	Highway 3134 to Old Estelle Pump Station Levee	Levee	Existing	10.5	10.4	2.075
WB41	Highway 3134 to Old Estelle Pump Station Levee	Levee	Future	14.0	12.4	1.265
WB12	Old Estelle Pump Station	Structure/Wall	Future	16.0	12.4	0.047
WB44	Old Estelle to Robinson Point	Structure/Wall	Future	14.0	12.4	0.429

Jefferson and Orleans Parishes, East of Harvey Canal Reaches

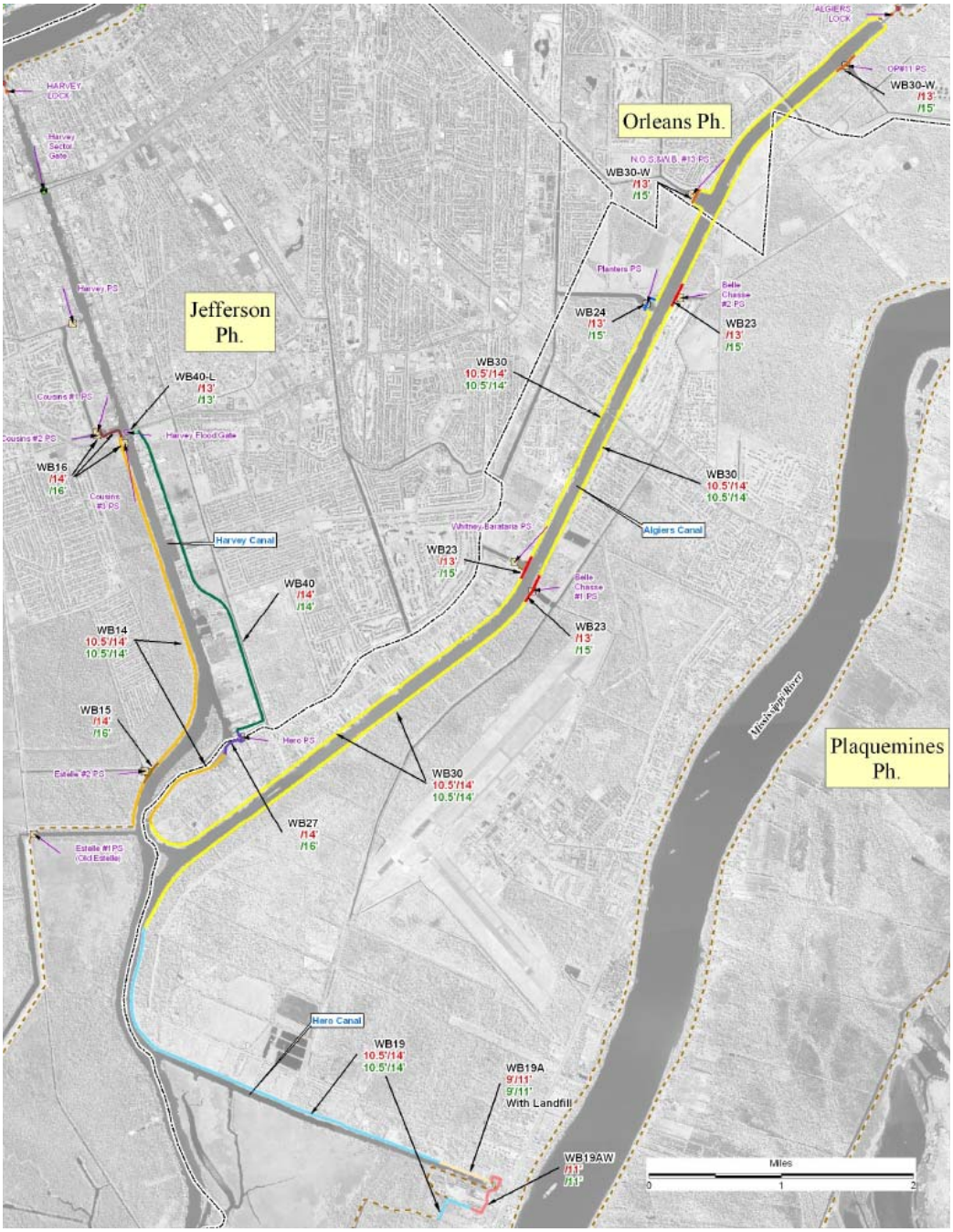

Westbank Sections (East of Harvey Canal Reach) 1% Hydraulic boundary conditions									
				Surge level (ft)		Significant wave height (ft)		Peak period (s)	
Segment	Name	Type	Condition	Mean	Std	Mean	Std	Mean	Std
WB14	Robinson Pt. to Harvey Canal W. Levee	Levee	Existing	7.8	0.9	1.3	0.1	3.7	0.7
WB14	Robinson Pt. to Harvey Canal W. Levee	Levee	Future	9.8	0.9	2.3	0.1	4.9	0.7
WB15	New Estelle Pump Station	Structure/Wall	Future	9.8	0.9	2.3	0.1	4.9	0.7
WB40	Harvey Canal Floodwall	Structure/Wall	Future	9.8	0.9	2.3	0.1	4.9	0.7
WB16	Cousins Pump Station 1, 2 and 3 (on Harvey Canal)	Structure/Wall	Future	9.8	0.9	2.3	0.1	4.9	0.7
WB40-L	Sector Gate at Lapalco Overpass on Harvey Canal	Structure/Wall	Future	9.8	0.9	2.3	0.1	4.9	0.7
WB27	Hero Pump Station (on Harvey Canal)	Structure/Wall	Future	9.8	0.9	2.3	0.1	4.9	0.7
WB30	Algiers Canal - Hero Pump Station to Algiers Lock	Levee	Existing	7.8	0.9	1.3	0.1	3.7	0.7
WB30	Algiers Canal - Hero Pump Station to Algiers Lock	Levee	Future	9.8	0.9	2.3	0.1	4.9	0.7
WB23	Whitney Barataria and Belle Chase 1 and 2 Pump Stations	Structure/Wall	Future	9.8	0.9	2.3	0.1	4.9	0.7
WB24	Planters Pump Station	Structure/Wall	Future	9.8	0.9	2.3	0.1	4.9	0.7
WB30-W	NO SBW Pump Station 11 and 13	Structure/Wall	Future	9.8	0.9	2.3	0.1	4.9	0.7
WB19	Transition Point to Hero Canal to Oakville	Levee	Existing	7.3	0.9	1.3	0.1	3.7	0.7
WB19	Transition Point to Hero Canal to Oakville	Levee	Future	9.3	0.9	2.3	0.1	4.9	0.7
WB19-A	Hero Canal-Area Behind Landfill Berm	Levee	Existing	7.3	0.9	1.0	0.1	2.0	0.4
WB19-A	Hero Canal-Area Behind Landfill Berm	Levee	Future	9.3	0.9	1.0	0.1	2.0	0.4
WB19-AW	Hero Canal Floodwall behind Landfill Berm	Structure/Wall	Future	9.3	0.9	1.0	0.1	2.0	0.4

Westbank Sections (East of Harvey Canal Reach) 1% Design heights							
						Overtopping rate	
Segment	Name	Type	Condition	Depth at toe (ft)	Height (ft)	q50 (cft/s per ft)	q90 (cft/s per ft)
WB14	Robinson Pt. to Harvey Canal W. Wall Levee	Levee	Existing	7.8	10.5	0.004	0.069
WB14	Robinson Pt. to Harvey Canal W. Wall Levee	Levee	Future	9.8	14.0	0.006	0.060
WB15	New Estelle Pump Station	Structure/Wall	Future	9.8	16.0	0.000	0.001
WB40	Harvey Canal Floodwall	Structure/Wall	Future	9.8	14.0	0.002	0.016
WB16	Cousins Pump Station 1, 2 and 3 (on Harvey Canal)	Structure/Wall	Future	9.8	16.0	0.000	0.001
WB40-L	Sector Gate at Lapalco Overpass on Harvey Canal	Structure/Wall	Future	9.8	13.0	0.011	0.073
WB27	Hero Pump Station (on Harvey Canal)	Structure/Wall	Future	9.8	16.0	0.000	0.001
WB30	Hero Pump Station to Algiers Canal Levee	Levee	Existing	7.8	10.5	0.004	0.068
WB30	Hero Pump Station to Algiers Canal Levee	Levee	Future	9.8	14.0	0.006	0.058
WB23	Whitney Barataria Pump Station	Structure/Wall	Future	9.8	15.0	0.000	0.004
WB24	Planters Pump Station	Structure/Wall	Future	9.8	15.0	0.000	0.004
WB30-W	NO SBW Pump Station 11	Structure/Wall	Future	9.8	15.0	0.000	0.004
WB19	Transition Point to Hero Canal to Oakville	Levee	Existing	7.3	10.5	0.001	0.024
WB19	Transition Point to Hero Canal to Oakville	Levee	Future	9.3	14.0	0.003	0.030
WB19-W	Hero Canal Floodwall	Structure/Wall	Future	9.3	13.0	0.005	0.033
WB19-A	Hero Canal-Area Behind Landfill Berm	Levee	Existing	7.3	9.0	0.000	0.078
WB19-A	Hero Canal-Area Behind Landfill Berm	Levee	Future	9.3	11.0	0.000	0.077
WB19-AW	Hero Canal Floodwall behind Landfill Berm	Structure/Wall	Future	9.3	11.0	0.001	0.067

Westbank Sections (East of Harvey Canal Reach) Resiliency analysis (0.2% event)						
					Best estimates during 0.2% event	
Segment	Name	Type	Condition	Height (ft)	Surge level (ft)	Overtopping rate (cft/s per ft)
WB14	Robinson Pt. to Harvey Canal W. Wall Levee	Levee	Existing	10.5	10.9	2.947
WB14	Robinson Pt. to Harvey Canal W. Wall Levee	Levee	Future	14.0	12.9	1.343
WB15	New Estelle Pump Station	Structure/Wall	Future	16.0	12.9	0.084
WB40	Harvey Canal Floodwall	Structure/Wall	Future	14.0	12.9	0.803
WB16	Cousins Pump Station 1, 2 and 3 (on Harvey Canal)	Structure/Wall	Future	16.0	12.9	0.082
WB40-L	Sector Gate at Lapalco Overpass on Harvey Canal	Structure/Wall	Future	13.0	12.9	1.671
WB27	Hero Pump Station (on Harvey Canal)	Structure/Wall	Future	16.0	12.9	0.084
WB30	Hero Pump Station to Algiers Canal Levee	Levee	Existing	10.5	10.9	3.001
WB30	Hero Pump Station to Algiers Canal Levee	Levee	Future	14.0	12.9	1.405
WB23	Whitney Barataria Pump Station	Structure/Wall	Future	15.0	12.9	0.260
WB24	Planters Pump Station	Structure/Wall	Future	15.0	12.9	0.251
WB30-W	NO SBW Pump Station 11	Structure/Wall	Future	15.0	12.9	0.259
WB19	Transition Point to Hero Canal to Oakville	Levee	Existing	10.5	10.4	1.934
WB19	Transition Point to Hero Canal to Oakville	Levee	Future	14.0	12.4	0.901
WB19-W	Hero Canal Floodwall	Structure/Wall	Future	13.0	12.4	1.202
WB19-A	Hero Canal-Area Behind Landfill Berm	Levee	Existing	9.0	10.4	8.151
WB19-A	Hero Canal-Area Behind Landfill Berm	Levee	Future	11.0	12.4	8.218
WB19-AW	Hero Canal Floodwall behind Landfill Berm	Structure/Wall	Future	11.0	12.4	8.114

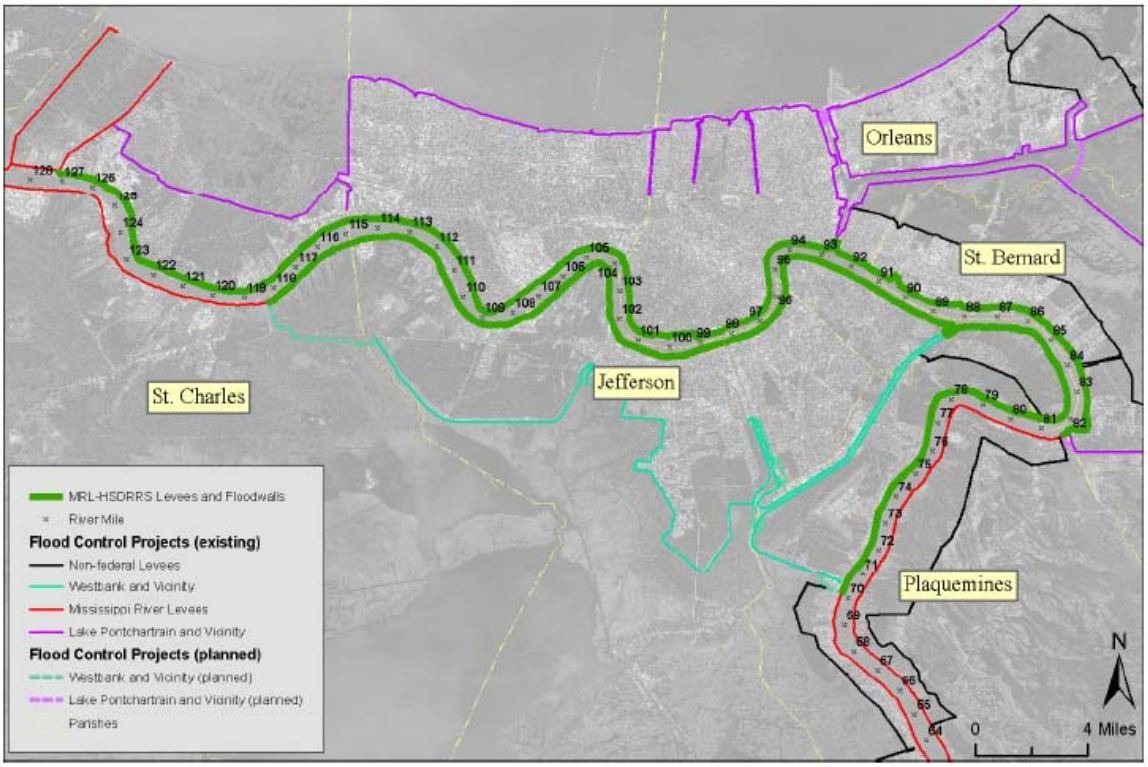

Analysis of 1% Hydraulic Conditions, Design Heights, and Resiliency have not been completed.

Part V.

Hurricane Surge Hazard Analysis for Future Conditions

Blum and Roberts 2009

As discussed in Parts I and II hurricane climatology and coastal landscapes are crucial factors in hurricane surge hazard. When these factors are subject to major trends, surge risk managers need to assess the effect of change on the estimate of surge hazard at future horizons. If rates of change are fast or accelerating—and if risk consequences are severe—horizons may be as soon as five to ten years. For slow, steady changes—and for modest impacts—horizons may be several decades.

In order to assess surge hazard at a future time quantitative trend analyses (see GTN-1 Section D) can be employed to forecast changes to key inputs in the surge hazard analysis described in Parts III and IV. For example, to forecast surge hazards in 50 years trend analyses can be used to obtain "best estimates" for a future Year 50 hurricane joint probability expression, LMMSL, ADCIRC mesh node elevations and attributes, and perimeter protection crowns. The complete surge hazard JPA with JPM-OS—as described in Parts III and IV—can then be redone to compute the Year 50 surge hazard CDFs for exterior locations and polder interiors throughout the region. If the Year 100 surge hazards are similarly computed, the three results—current, Year 50, and Year 100—can be used to evaluate trends in hurricane surge hazard.

In addition to providing a best estimate of future conditions, trend analysis also quantifies uncertainty about the estimate. Trend uncertainties can therefore be employed in the JPA—such as by expanding the Monte Carlo techniques—to quantify uncertainty about the estimate of future surge hazard.

For planning purposes, comprehensive trend analyses and JPA expansion may not be practical. This can be the case when trends are not well defined or the primary interest is only in the relative comparison of a few specific "what if" alternatives. To further simplify planning level evaluations, comparisons may be made on the basis of just a few synthetic hurricane scenarios, rather than a surge hazard derived with a full JPM-OS. These evaluations represent selected sensitivity tests of potential future conditions. However, risk managers must realize that as the analysis becomes more simplified the results become more speculative and less suitable for use in decision-making—e.g., engineering design of perimeter protection systems and coastal restoration.

This Part V reviews the current state of the practice for steps needed in hurricane surge hazard analysis for future conditions, including the following subjects:

> Section 18., research on coastal landscape trends for southeast Louisiana, including sea level rise (SLR), regional subsidence, coastal erosion, and changes in vegetation, perimeter protection, and polder interiors.
>
> Section 19., methods for addressing future hurricane climatology and coastal landscape trends, including the use of hurricane scenarios.
>
> Section 20., recent applications of hurricane surge hazard analysis for future conditions, including the USACE's 2009 LaCPR Study, Mississippi Coastal Improvement Plan (MsCIP), and HSDRRS 100-yr design for 2057; the CPRA's 2012 Master Plan; and the SLFPA-E evaluations of the Lake Pontchartrain barrier and polder compartmentalization.

These sections review approaches as presented in the current literature and project documentation, as well as discuss methodology requirements, assumptions, and limitations based on sound scientific and engineering practice. Afterwards, a list of conclusions is presented, together with recommendations for improving hurricane surge analysis for future conditions.

Section 18. Coastal Landscape Trends

This section briefly summarizes current approaches to important coastal landscape trends in southeast Louisiana that influence estimates of future surge hazard and risk. Trend information is largely derived from the extensive literature supporting Louisiana coastal protection and restoration planning—e.g., the State of Louisiana's Master Plan (2012) and the USACE's LaCPR Study (2009). The trends include SLR, regional subsidence, coastal erosion, vegetation changes, and perimeter systems and polders. Assessment of future conditions can also consider alternatives to current trends, such as proposed projects to restore coastal land elevation and vegetation or to modify perimeter protection. The steps needed to assess surge hazards associated with future conditions—based on trends or a proposed project alternative—are addressed in Section 19.

18.1 SLR

Climatologists and ocean scientists generally agree that global average temperatures and SSTs in the Atlantic Basin are both in a significant upward trend (see the website Climate Change at the National Acadamies, http://nas-sites.org/americasclimatechoices/other-reports-on-climate-change/). Coastal scientists and planners—including federal and state agencies responsible for managing coastal resources and planning for coastal infrastructure (e.g., NOAA, USGS, USACE, Louisiana Coastal Protection and Restoration Authority)—agree that current trends on global climate change and SSTs are likely to produce significant SLR due to thermal expansion and the melting of polar land ice. The scientific research on future SLR is therefore being employed by these and other agencies (see Gulf of Mexico Alliance 2011). The USACE applies a general guidance on SLR to all coastal projects (USACE 2009). For planning horizons to the year 2100 the Louisiana CPRA recommends using a SLR range of 1.6 to 4.9 ft for coastal Louisiana LMSL, with a moderate SLR value of 3.3 ft. For a 50-year horizon the recommended SLR range is 0.4 to 2.1 ft, with moderate and less optimistic values of 0.9 and 1.5 ft (see CPRA Coastal Master Plan 2012).

Adjustment for LMMSL to LMSL—i.e., the added water surface elevation for seasonal steric effect—are applied in addition to the SLR modification to LMSL.

18.2 Regional Subsidence

Southeast Louisiana experiences significant regional land subsidence (surface elevation drop with respect to the geoid, see GTN 2 and Reed et al 2009). The magnitude, timing, and rates of general regional subsidence vary under the influence of four geologic factors:

1. Deep crustal plate warping in the lower Mississippi embayment associated with millions of years of deposition (since the Cretaceious Period), as well post-glacial adjustment of the continental plate. These can be manifested in episodic slippage along active faults;
2. Deltaic loading associated with Pleistocene deposition over the past two million years;
3. Ongoing consolidation within the recent Holocene delta lobe sediments; and
4. Oil, gas, and groundwater withdrawals over recent decades.

Scientific research suggests that rates of geologic subsidence may be as high as 3 feet per century in some portions of coastal Louisiana (Reed et al 2009). Figure 18.1 depicts the 50-yr forecast of regional subsidence provided in the CPRA's 2012 Master Plan.

Combining estimates of SLR with regional subsidence yields an estimate of *relative* SLR (RSLR). Figure 18.2 shows a recent USACE estimate of variation in RSLR across southeast Louisiana. The USACE employed a RSLR estimate of 0.9 ft for the 50-year period from 2007 to 2057 in the design of the HSDRRS, which they rounded up to 1 ft (USACE 2010).

RSLR increases future surge hazard (and risk) not only because of the direct rise surge depth, but also because of effects on surge momentum. RSLR increases the cross-section flow area and conveyance, thereby facilitating greater inland movement of surge.

18.3 Coastal Erosion

Much of the southeast Louisiana delta is composed of recently deposited, poorly consolidated and only moderately cohesive fine sediments and organic matter. The coastline is highly fractal, long, and very susceptible to erosion from waves and currents. Abandoned, subsiding delta lobes—and their component barrier islands, headlands, and wetlands—naturally undergo erosion.[1]

The combination of SLR, subsidence, and erosion along shorelines of lakes, bays, and channels expands the open water area, which both

a. Enlarges fetch, thus increasing erosive currents and waves associated with the normal range of coastal winds; and

b. Raises the tidal prism, which modifies salinity and damages sensitive, soil-binding vegetation.

These further accelerate coastal land loss.

Coastal land loss trends for southeast Louisiana have been the subject of frequent research and publication. Currently, RSLR and erosion are estimated to convert about 16 square miles of subaerial land to open water each year (CPRA 2012). Figure 18.3 shows a portion of the recent USGS study depicting land loss in coastal Louisiana from 1932 through 2010 (Couvillion et al 2011). Figure 18.4 depicts the projected cumulative land loss for coastal Louisiana from 1932 through 2050 (USGS 2005).

Coastal erosion especially exacerbates surge hazard (and risk) by expanding shallow water fetch. Longer, open, shallow fetches facilitate higher wind setup force, increasing surge momentum. Expansion of open water also increases hurricane wind wave heights.

[1] Human activities have contributed significantly to erosion. These include dredging of coastal oil and gas canals and navigation channels (e.g., the MRGO); subsurface fluid extraction induced marsh subsidence (e.g., Leeville area); and modifications to natural barrier islands and shoals which prevent natural replenishment of beach/dune complexes (e.g., Caminada Pass jetty). Southeast Louisiana coastal land loss from subsidence and erosion is also exacerbated by the absence of normal Mississippi River deltaic inputs, caused by damming of the upper tributaries and confining of the delta distributaries.

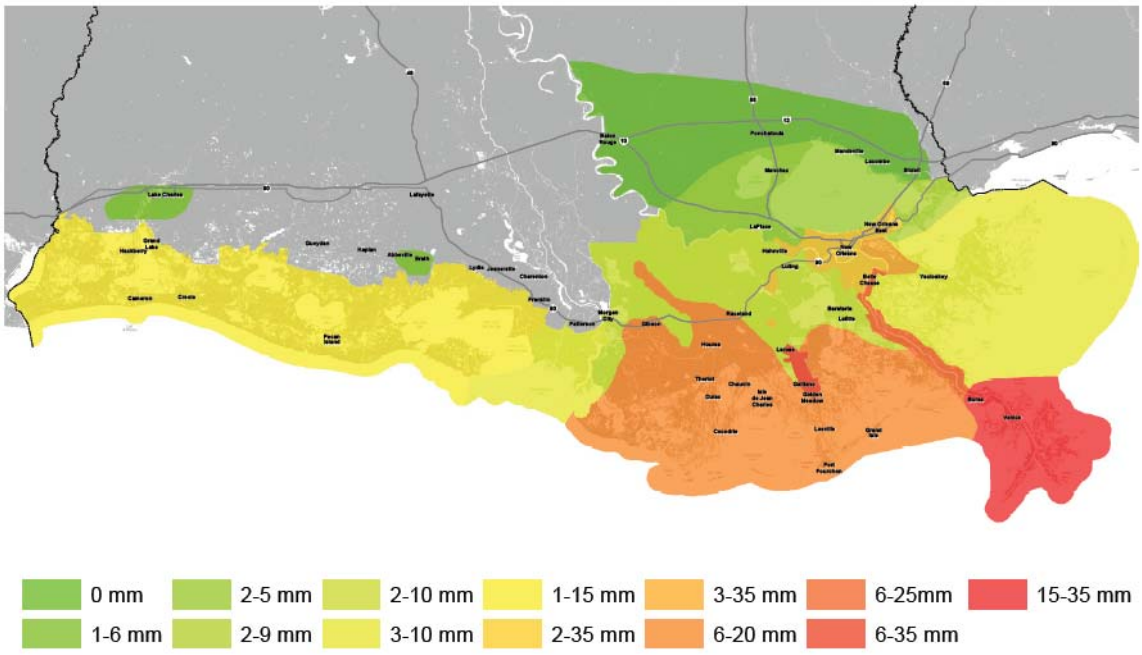

Figure 18.1. 50-Year Forecast of Regional Subsidence
CPRA 2012

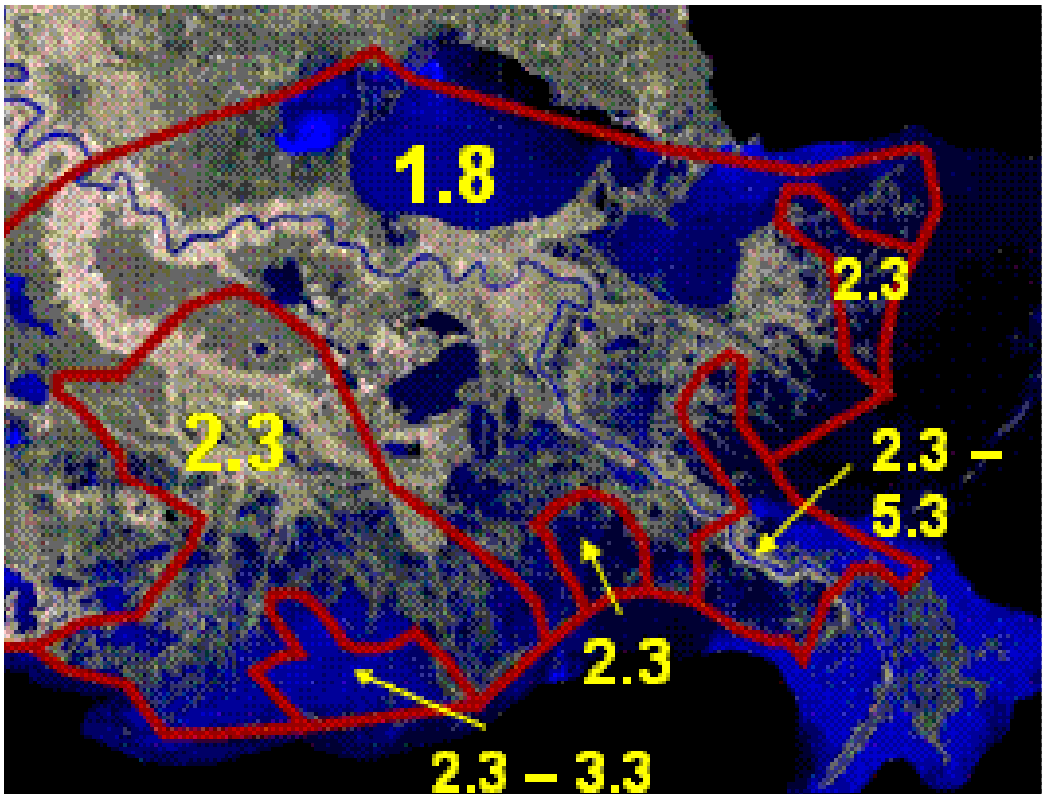

Figure 18.2. Estimates of Relative Sea Level Rise (ft per century)
USACE 2010

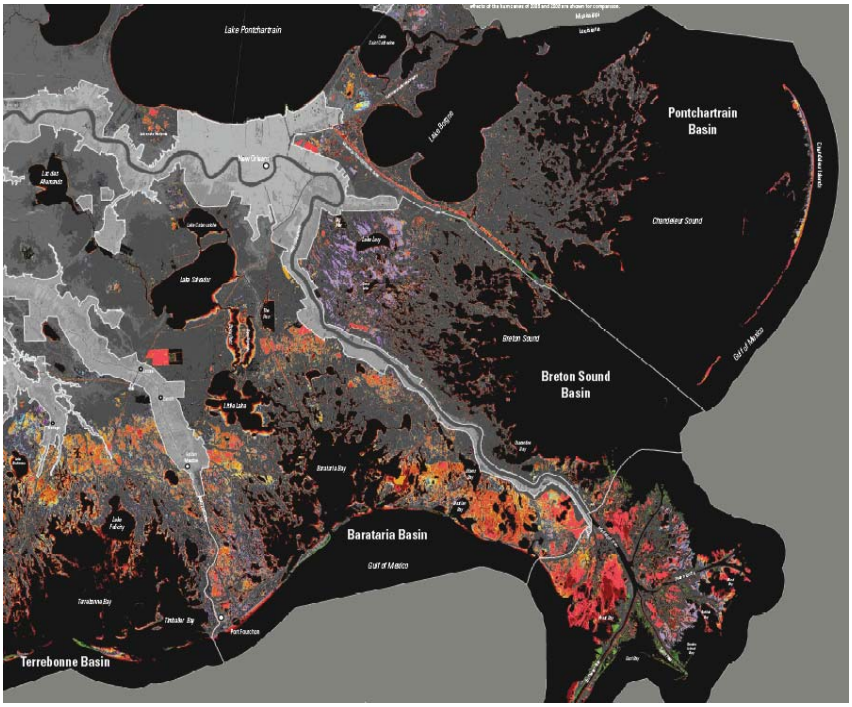

Figure 18.3. Excerpt from Land Area Change in Coastal Louisiana, 1932-2010
Couvillion et al 2011

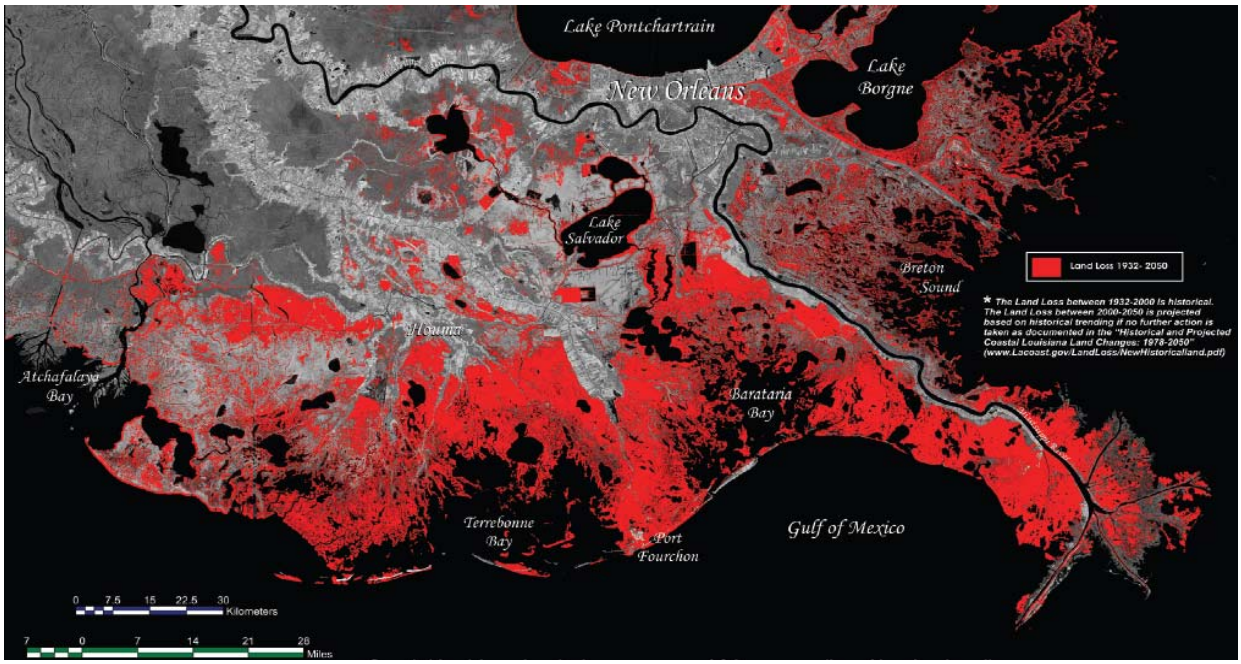

Figure 18.4. Estimated Land Loss in Coastal Louisiana, 1932-2050
USGS 2005

18.4 Vegetation Changes

In addition to direct land loss, RSLR and erosion cause key changes in the coastal land cover, including the decline of natural forested coastal ridges and cheniers and the conversion of more woody freshwater wetlands to more grassy brackish and saline marshes. Coastal wetland vegetation change—such as from woody to grassy—can increase surge hazard by reducing the friction drag which would otherwise slow down winds and the momentum of inland surges.

Historic landscape conversions are documented in updates to land cover databases, which are developed from ground-truthed satellite and aerial imagery.

Researchers have been working on combining forecasted changes to coastal hydrodynamic, sedimentation, RSLR, erosion, water quality, temperature, and other parameters to predict future habitat regimes and vegetation types (see Visser et al 2008). For the 2012 Master Plan Visser et al developed a coastal vegetation model with 500 m cells that forecasts 50 years of annual changes. The specified trends for each cell include the proportion of 19 emergent vegetation types that occupy subaerial wetland; the proportion of empty open water; and the proportion of open water occupied by submerged aquatic vegetation.

18.5 Perimeter Protection and Polders

Three important trends in perimeter protection that can affect future polder interior surge hazard (and risk) are:

- Consolidation, settlement, and subsidence of existing structures. Figure 18.5 depicts total subsidence rates—i.e., regional deltaic subsidence plus local consolidation and settlement—in the New Orleans area between 2002 and 2005. During this period rates along some HSDRRS reaches exceeded 5 ft per century (15 mm/yr). A comprehensive, reach-by-reach investigation of total subsidence rates for the recently completed HSDRRS—critical to forecasting future polder surge risk—is currently not available.
- Changes to foreshore conditions which affect wave heights, runup, and overtopping, including the loss of forested wetlands and settlement of breakwaters. For example, the presence of extensive wetlands is critical to the HSDRRS levee design height in St. Charles Parish, as are breakwaters to Jefferson Parish. A comprehensive, detailed investigation of foreshore trends for forecasting future wave overtopping is currently not available.
- Changes to the integrity and fragility of HSDRRS structures, such as corrosion of steel, deflection of walls, and the expansion of voids in soils and cracks in concrete. Mechanical structures can also experience changes in fragility due to improved or degraded operability. For example: the likelihood of a floodgate not being closed may increase under a future with restricted operations and maintenance resources. A comprehensive, detailed investigation of changing fragility conditions for forecasting future breach probabilities is currently not available.

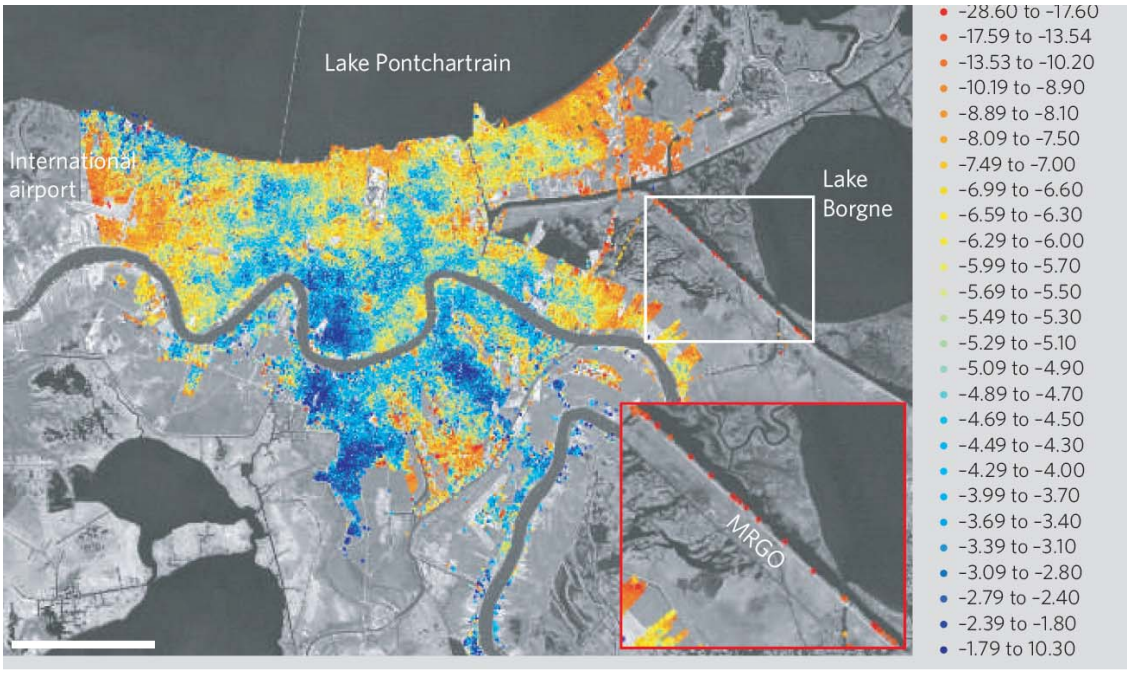

Figure 18.5. New Orleans Total Subsidence, 2002 to 2005
Dixon et al 2006

Proposed projects that can be assessed in a future conditions analysis include both new systems or system components (such as the Lake Pontchartrain Barrier across the New Orleans East Land Bridge) and enhancements to existing structures (such as a proposal to raise nearby non-federal levees). While such projects can reduce interior surge hazard, they have the potential to adversely affect exterior surge hazards—including at locations many miles away.[2]

Interior polder subsidence trends are also an important condition to the analysis of future polder inundation hazard. In addition to regional geologic subsidence, polder interior soils undergo local shrinkage and compaction due to soil drainage and oxidation. Interior subsidence increases the depth of inundation for low-lying locations and reduces the capacity of pump stations by reducing the intake head.

Portions of the New Orleans Metro Polder have experienced over 10 ft of total subsidence since forced drainage began in the early 20th Century. The 2002-05 subsidence trends shown in Figure 18.5 also illustrate the "deepening bathtub" effect facing the New Orleans area polders. More recent, detailed investigations of polder interior subsidence are not available.

Two categories of projects which can affect the interior inundation hazard include increases to interior drainage/pumping capacity and compartmentalization structures. Examples of compartmentalization projects for the New Orleans area polders include enhancing use of the Central Wetlands for diversion of water entering the IHNC/GIWW sub-basin and upgrading legacy levees along the east and west boundaries of east-bank Jefferson Parish.

[2] These projects can also have adverse environmental impacts, such as a) disrupting the local hydrology (e.g., conveyance patterns and tidal prism) and dependent coastal vegetation and habitats; and b) diverting/concentrating more surge into areas and thereby increasing salinity.

Section 19. Additional Steps for Future Hazard Analysis

This section describes the current technical approaches to incorporating trend forecasts and proposed projects into the analysis of future hurricane surge hazards.[1]

19.1. Changes in Hurricane Climatology

Section 2.3 reviewed the current scientific literature on trends in hurricane climatology, including the influence of important cycles—e.g., ENSO, AMO, and NAO—and secular global climate change. Studies of the influence of secular climate change and SST are ongoing, using both analyses of historic data on the frequency of Atlantic tropical cyclones—primarily according to their core intensity—and global climate models incorporating forecasted conditions. One challenge is discerning the possible presence of a long-term secular hurricane trend from the influence of climate cycles. Some of the research with models of global climate change and increasing SSTs portends increasing numbers of Atlantic hurricanes and/or more intense hurricanes. However, some models also indicate the potential for increased shearing conditions, which can inhibit hurricane development and intensification.

There have been no investigations to date of future hurricane climatology specific to the CN-GoM. As noted in Sections 1 and 3, the Loop Current and associated eddies are crucial to the specific high hazard of this region. Research by Liu et al (2012) suggests—consistent with other research on the Florida Straits Current and Gulf Stream—that global climate change could reduce the Loop Current by up to 25%, significantly *cooling* the GoM. This scenario could *reduce* the landfall frequency of powerful hurricanes along the CN-GoM, and particularly southeast Louisiana, and *lower* the 100-yr and higher surge hazards. More research on this and related topics—including rainfall rates associated with hurricanes—is needed.

Absent research findings on trends in GoM hurricane climatology, surge risk managers can turn to evaluating the sensitivity of surge hazard to a hypothetical future hurricane climatology. Speculative scenarios can be defined by simply proposing modifications to the hurricane joint probability expression, ***p***, shown in Figure 4.2 and discussed in Section 13.1. Various parameters in ***p*** controlling the frequency of hurricanes, CPD (or V_{max}), R_{max} , wind field distribution (e.g., Holland B), V_f, and track θ, and factors related to their uncertainty, can be adjusted.

The hypothetical ***p*** can then be used to develop a new JPM-OS representing the future joint probability. The surge JPA can then be redone to compute the future exterior surge hazard CDFs.

19.2. Coastal Landscape Trends

Section 18 reviewed the current approaches to important coastal landscape trends and discussed potential impacts on surge. Incorporating these forecasts into an estimate of future surge hazard can be accomplished with the following modifications to the storm surge/wave model—e.g., ADCIRC+SWAN:

[1] Importantly, a key step—modifying the ADCIRC+SWAN model to reflect future conditions—can also support evaluating impacts on general non-surge coastal hydrology and related ecosystem conditions. Simulations forced with basic tidal and non-hurricane meteorological conditions can be employed to evaluate the effect of RSLR, coastal erosion, landscape change, and perimeter protection system modifications on the circulation and tidal prism within complex networks of coastal water bodies. These exert significant control over critical water quality parameters (dissolved oxygen, salinity, nutrients, toxins, etc.), vegetation types, and habitat.

- Projected SLR—increase the open ocean boundary and initial domain water surface elevations, i.e., LMSL in NAVD88, in accordance with the SLR forecast. This does not change the topography/bathymetry of the domain.
- Regional subsidence—adjust the elevations assigned to nodes within mesh regions (e.g., sub-delta) for forecasted subsidence.
- Coastal erosion—further adjust mesh node elevations of barrier islands and wetlands surrounding water bodies to below LMSL to further reflect the total projected areas of land loss (as in Figure 19.1).
- Vegetation conversions—modify mesh node Manning's n and wind reduction coefficients for remaining coastal areas consistent with projected changes to land cover type.
- Perimeter protection (settlement and/or projects)—add/adjust node locations and/or internal weirs in the mesh, as needed to represent the alignment; then modify node/weir elevations to reflect forecasted crown height.

Surge risk managers can then redo the surge JPA using the future ADCIRC-SWAN model and a hypothetical JPM-OS (if appropriate) to compute the future exterior surge hazard CDFs throughout the region. Figure 19.2 is an example of a difference between a current and future conditions 100-yr surge hazard prepared for the LaCPR Study (see Section 20.1)

Figure 19.1. Louisiana Coast in 2100
Blum and Roberts 2009

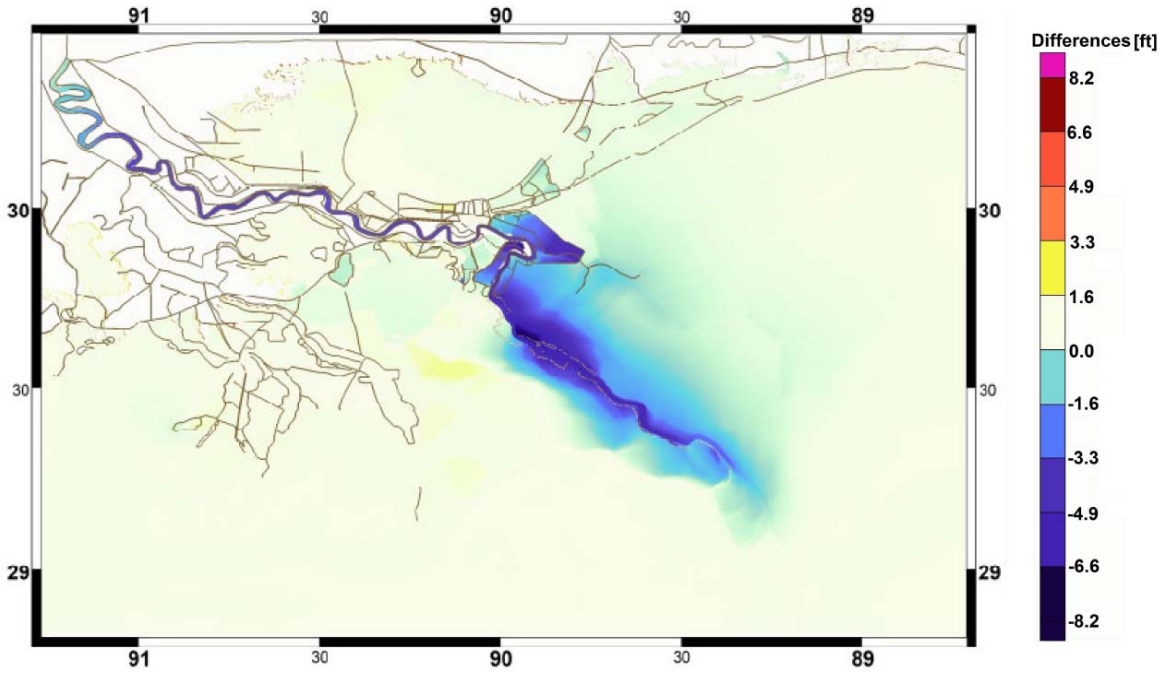

Figure 19.2. Example of Difference Between Baseline and Future Conditions 100-yr Surge Hazard

de Jong et al 2007

To assess the future polder interior hazard, the perimeter SWLs from each of the JPM-OS storms are used in an expanded JPA which includes a coupled SOBRP model, as described in Section 16. For this analysis the following steps can be added:

- Alteration of foreshore wave conditions (wetlands or breakwaters)—revise the exterior wave analysis described in Section 15.1 and use the revised wave characteristics in the overtopping calculation of the SOBRP model.
- Perimeter protection (settlement and projects)—also use the forecasted crown heights in the SOBRP overtopping calculation.
- Fragility changes—modify the breach probability parameters in the expanded joint probability expression, p^*, discussed in Section 16.2.
- Interior settlement/subsidence—adjust the interior routing model—e.g., stage storage table for level pool routing.
- Change in pumping capacity or compartmentalization projects—adjust the SOBRP and interior routing models.

With increasing HPPC speeds and declining costs, redoing expanded polder JPAs for comparing interior surge hazard CDFs under current and future conditions is becoming more practical.

19.3. Hurricane Scenarios

Despite the increasing practicality of computing future surge hazards, sensitivity analyses employing limited hurricane scenarios are often preferred for basic relative comparisons of current versus future conditions. In its 2006 Third Report of the Committee on New Orleans Regional Hurricane Protection Projects, the National Academy of Engineering/National Research Council recommended that historical and "worst-case" type scenarios be used to improve public understanding of the relative hazards and risks associated with alternative conditions.

To facilitate these comparisons five types of hurricane scenarios can be considered:

1. Important historical hurricanes;
2. The Standard Project Hurricane (SPH);
3. The Probable Maximum Hurricane (PMH);
4. The Maximum Probable/Possible Intensity (MPI) Hurricane;
5. Scenarios selected from a JPM-OS or other set; and
6. NOAA Maximum Envelope of Water (MEOW) and Maximum of the Maximums (MOM) sets.

Historical Hurricanes

Scenarios featuring powerful historical storms provide a well established frame of reference for agency officials and the general public and can often capture their interest better than abstract surge hazards. For southeast Louisiana noteworthy historical storms include Hurricanes 1915, Betsy, Katrina, Gustav, and, most recently, Isaac.

In simulating an historical hurricane GoM maximum CPD/V_{max},, R_{max}, Holland B, and V_f attributes are generally based on observations or consensus best estimates. If the simulation involves the actual historical track θ and landfall point, the observed or best estimate values are also used for pre- and post-landfall CPD/V_{max}, R_{max}, Holland B and V_f. In this case the H*Wind data is often employed to characterize the hurricane's wind field.

However, if variations in θ are being examined—e.g., modeling Hurricane Katrina on various parallel tracks—pre- and post-landfall decay in CPD/V_{max},, R_{max}, and Holland B, and changes in V_f, might be varied consistent with best judgments about the influence of the new path. In this case, a vortex model (e.g., PBL) can be employed to simulate a "Katrina-like" hurricane, coupled with a standard algorithm for decay. The results of track variations for a "Katrina-like" or other historical hurricane could be used to construct a regional MOM for the particular storm.

To date, track variations for historical hurricanes have not been employed to study future surge hazards for southeast Louisiana.

SPH

The SPH is similar in concept to a standard project flood, which was used for evaluating riverine flooding as early as the 1940s (USACE 1946). Prior to the advent of sophisticated JPA techniques, government agencies responsible for flood risk management often found it more practical to define a single flood scenario in order to simplify decision-making. For federal agencies, Congress has frequently stipulated the use of defined flood scenarios—e.g., the 100-yr flood in the NFIP.

NOAA began providing the attributes of a SPH for use by USACE and other agencies involved in surge risk management in their 1958 National Hurricane Research Project Report. In 1972 NOAA described the SPH as

> a hypothetical hurricane that is intended to represent the most severe combination of hurricane parameters that is *reasonably characteristic* of specified geographic region, excluding extremely rare combinations. The SPH is intended as practical expression of the maximum degree of protection that should be sought as a general rule in the planning and design of coastal structures for communities where protection of human life and destruction of property is involved (NOAA 1972.)

In the 1979 *Meteorological Criteria for Standard Project Hurricane and Probable Maximum Hurricane Windfields,* NOAA provided the following definition for a SPH:

> The SPH is a steady state (for several hours prior to landfall) hurricane having a severe combination of values of meteorological parameters that will give high sustained wind speeds reasonably characteristic of a specified coastal location. By reasonably characteristic is meant that only a few hurricanes of record over a large region have had more extreme values of the meteorological parameters. The "SPH wind field" is specified from the parameters. One of several uses of the wind field is to compute critical storm surge at coastal points. . . . The combined frequency for the total wind field will generally have a recurrence interval of several hundred years.

The SPH is defined in terms of CPD, R_{max}, and V_f prior to landfall, together with estimates for infilling and frictional effects on winds. In 1978 NOAA published a report estimating maximum wind fields at various locations throughout the New Orleans area for an SPH based on the above forthcoming update to SPH characteristics (NOAA 1979). Prior to Hurricane Katrina, the USACE employed these wind values—together with calculations for wind setup, barometric impacts, wave setup, and wave runup—to estimate SPH peak surge conditions for the design of southeast Louisiana surge protection systems.

Following Hurricane Katrina—and with the advances in hurricane climatology and surge JPA—surge planning, decision making. and design have relied on hazard-based criteria (e.g., 100- and 500-yr surge) instead of the SPH.

Probable Maximum Hurricane

In the 1979 report NOAA also defined a PMH—distinguished from a SPH—as one that "will give the highest sustained wind speed that can probably occur at a specific location." The report noted that various rare combinations of hurricane attributes would give different wind fields, and that the return frequency of each combination has a very large uncertainty. The 1979 report suggested that PMH CPDs for the entire Atlantic and GoM coasts were about 40 to 60 mb lower than for SPHs. Given that there were eight Category 5 hurricanes between 2003-07, this large differential now seems questionable.

Figure 19.3 presents a preliminary MOM for 10 NOAA PMHs for coastal Louisiana prepared as part of working material for the LaCPR Study by the USACE in 2006. As with the SPH, the NOAA PMH has not been used in any final post-Katrina surge evaluation studies.

Maximum Probable/Possible Intensity Hurricane

Another "worst-case" hurricane—the MPI hurricane—has been defined by the USACE for use in post-Katrina Louisiana and Mississippi coastal planning (USACE 2009a and 2009b). In each case the hurricane was defined with a minimum GoM CP of 880 mb. Interestingly, for Louisiana the MPI was assigned an R_{max} of 25 nm while for Mississippi it was 36 nm. Figure 19.4 presents the southeast Louisiana MPI MOM based on three tracks.

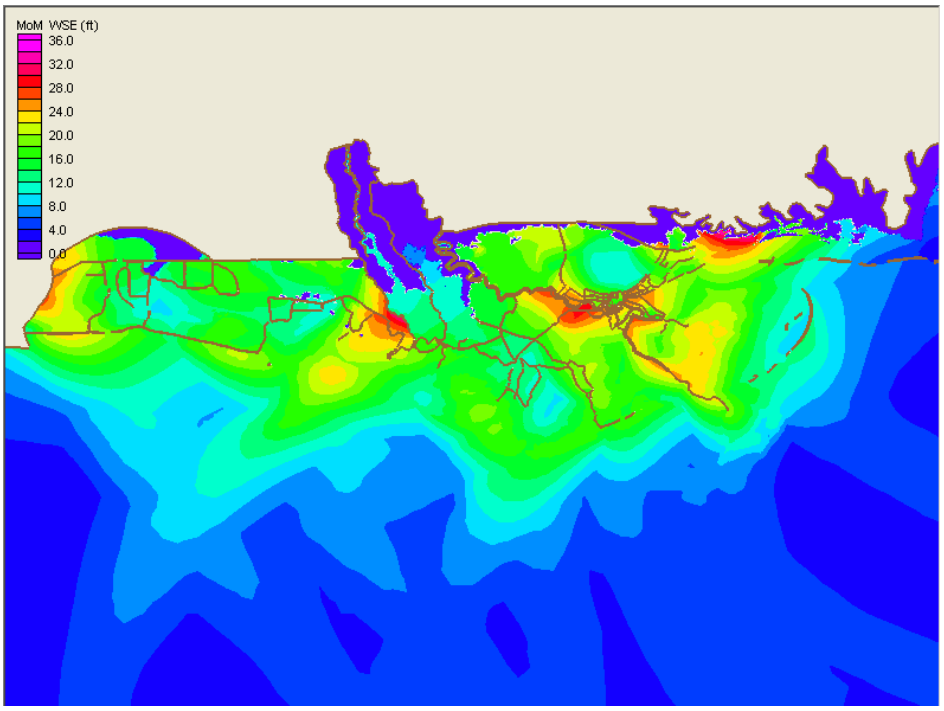

Figure 19.3. PMH MOM for Coastal Louisiana
USACE 2006

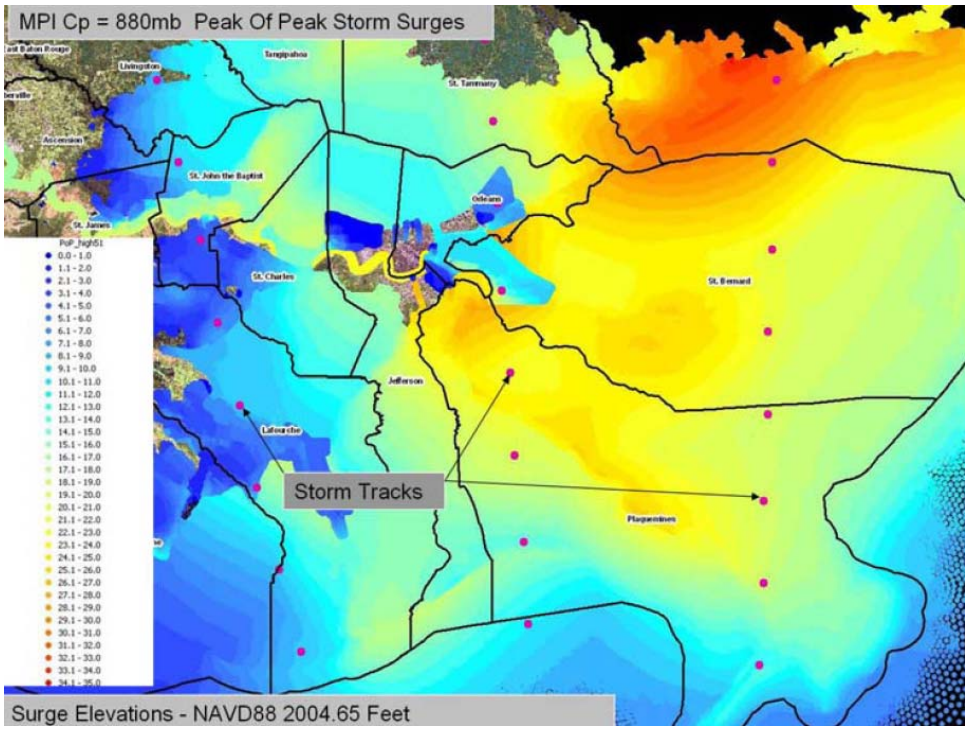

Figure 19.4. MPI MOM for Southeast Louisiana
USACE 2009a

Selected Hurricane Scenarios

Sensitivity tests can be performed for any storm of interest in a set. Figure 7.7 illustrates the surge comparisons for a hypothesized change (not tied to future time) in regional topography/bathymetry and Manning's *n* using two selected hurricanes. A hurricane that comes close to producing a targeted surge hazard—e.g., the 100- or 500-yr surge—can also be selected. Due to the importance of all attributes in effecting surge, a range of appropriate combinations need to be considered for locations of interest. For some locations both smaller more intense hurricanes and slower, larger, lower intensity hurricanes can produce the 100-yr surge.

Surge results for a selected hurricane and current conditions can be compared versus the same storm with future conditions. If there is an increase in this hurricane's probability due to changes in the hurricane climatology, then increases in surge hazard and risks associated with that storm can be computed. Similar computations for multiple locations can provide an indication of their relative vulnerability to changing conditions.

NOAA MEOWs and MOMs

To assist federal, state, and local emergency planners and responders in estimating potential surge elevations, NOAA has provided an atlas of regional maps. The atlas has included MEOW maps, each prepared using a set of synthetic hurricane scenarios for:

a. A particular category intensity (e.g., Category 3);

b. A set of parallel tracks on the same θ (e.g., northwest heading) at roughly equal spacing;

c. A particular V_f (e.g., 5 mph);

d. Some variations in size, wind field, and decay; and

e. A tide level (e.g., mean).

NOAA utilized the SLOSH model (see Section 8) to simulate the set of scenarios and compute the surge peak at locations throughout the region for each hurricane in the set. The highest peak at each location from among the scenarios was then used to create the MEOW map. Figure 19.5 illustrates a MEOW map for southeast Louisiana for the example set of hurricane scenarios. Thus, if a Category 3 hurricane is approaching the coast on a general northwest heading at 5 mph and expected to make landfall at mean tide—but with the absence of a precise forecast of landfall location—a "worst-case" surge elevation could be obtained for everywhere in the region.

For a given a. and e., NOAA combined all the regional MEOWs for b., c., and d., into one MOM map—i.e. five MOMs per tide level. Figure 19.6 presents the MOM map for southeast Louisiana for Category 3 hurricanes at high tide. The MOM represents a worst-case scenario at each location for a Category 3 hurricane making landfall at high tide.

Though MEOW and MOM maps are rapidly becoming obsolete for actual emergency response due to recent advances in real-time surge forecasting, they are still useful for planning purposes. While the SLOSH model lacks the fine resolution and wave physics of the ADCIRC+SWAN model, it can be employed to quickly generate MEOWs and MOMs for coarse assessments of future conditions. In 2012 Preston et al produced future MOMs for six SLR scenarios for SLOSH basins along the Atlantic and GoM coasts. NOAA MEOWs and MOMs have not been recently employed to assess future surge hazards for southeast Louisiana coastal erosion, landscape change, and modifications to hurricane protection systems.

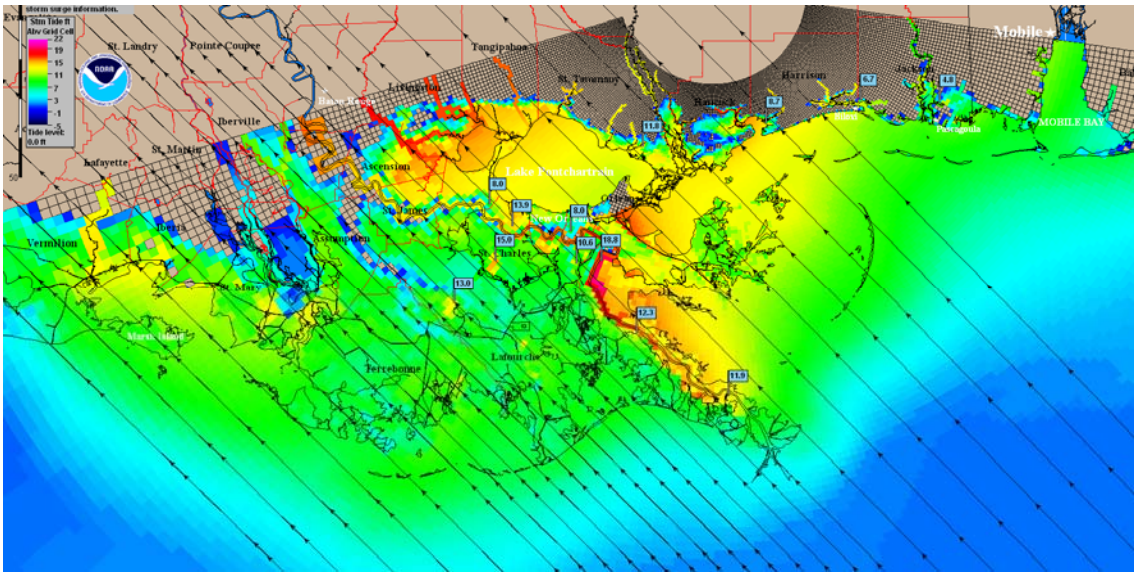

Figure 19.5. NOAA MEOW Map for Southeast Louisiana
Category 3, Northwest Heading, 5 mph Forward Speed, Landfall at Mean Tide
NOAA 2010

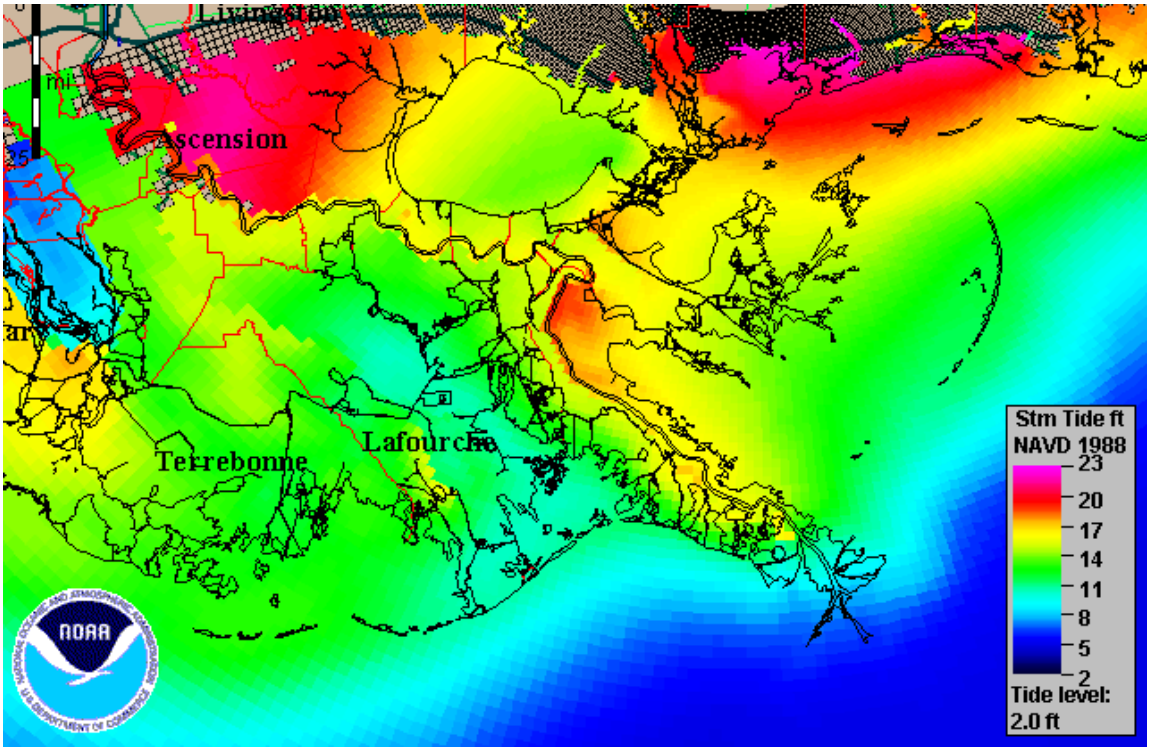

Figure 19.6. NOAA MOM Map for Southeast Louisiana
Category 3 at High Tide
NOAA 2010

Section 20. Recent Applications of Analysis for Future Conditions

In recent years investigators of future southeast Louisiana surge hazard have input forecasts of RSLR and coastal landscape conditions, as well as projects, into the additional analytical steps described in Section 19. Six major investigations include:

- USACE LaCPR Study (USACE 2009a);
- USACE MsCIP (USACE 2009b);
- USACE HSDRRS Design for RSLR (USACE 2010);
- State of Louisiana Master Plan (CPRA 2012);
- SLFPA-E New Orleans East Land Bridge Feasibility Study (Ben C. Gerwick 2012); and
- SLFPA-E Polder Compartmentalization Study (ongoing).

This section reviews the technical approaches employed in these studies, including important assumptions and limitations.

20.1 USACE LaCPR Study

The 2009 USACE LaCPR Study examined both exterior surge SWL hazard and surge-related polder inundation under many large-scale planning alternatives. Sections 14.1 and 17.2 described the USACE's development of 2007 (with post-Katrina HSDRRS improvements) and 2010 (with a nearly final 100-yr HSDRRS) ADCIRC-STWAVE models, in conjunction with a Surge Response-OS, to assess exterior 100-yr surge hazard. These two alternatives were also used to evaluate 400- and 1,000-yr hazards and polder interior scenarios. Table 20.1 lists 18 additional alternative future conditions/projects that were evaluated, a summary of the ADCIRC model changes, and the number of Surge Response-OS storms (out of a total of 152) that were rerun.

Section 17.2 noted that the 2010 alternative exterior 100-, 400-, and 1,000-yr hazards were themselves developed from the 2007 alternative by rerunning a subset of the 152 storms and applying an adjustment algorithm to the results of storms not rerun. This approach introduced additional bias and uncertainty into the 2010 analysis. The full 152-storm set was not rerun apparently due to constraints at the time on HPPC resources. Presumably a similar adjustment algorithm was employed for the various future conditions to account for the storms not rerun.

CDFs for each alternative were presumably calculated using the techniques described in Section 17.2 for the 2010 alternative, which were described as similar to those used in the 2007 FIS (Section 14.1). This approach employed bilinear interpolation, smoothing, and shifting of the CDF to account for epistemic ε.

Polder inundations for the future alternatives were assessed in a manner similar to the 2010 case (see Section 17.2). Polder inundation was evaluated for all SWLs around the entire perimeter at the exterior 100-yr value (and similarly for all SWLs at the 400- and 1,000-yr value). As noted in Section 17.2 these are not true hazards but reflect a much more unlikely "pseudo event." Wave conditions and overtopping rates for the three "pseudo events" for each alternative were estimated using the same methods described in Section 17.2.

Figures 20.1.a and b. show the difference between the 2007 condition and two future Plaquemines Parish levee alternatives, for the 100-yr surge hazard, based on the limited Surge Response-OS. The figures illustrate the kind of planning comparisons that were facilitated by the analyses of future alternatives.

In addition to future hazard analyses using limited rerunning of the Surge Response-OS, the LaCPR Study evaluated surges for the MPI hurricane. The LaCPR MPI hurricane was defined as having a GoM CP of 880 mb and an R_{max} of 25 nm (28.8 mi). The return period of a GoM hurricane with this combined CP and R_{max} was estimated at nearly 75,000 years. (Note, Part I discusses the USACE hurricane joint probability expression including several limitations.) Figure 19.4 illustrates a preliminary depiction of the southeast Louisiana MPI MOM based on three tracks.

Table 20.1. LaCPR Future Surge Hazard Analyses

USACE 2009a

Future Condition	Summary of ADCIRC Mesh Changes to 2010 Base Alternative	Surge Response-OS Storms Rerun
Lake Pontchartrain Barrier (New Orleans East Land Bridge) and West Bank (Belle Chase to Larose)	A) Full closure of Lake Pontchartrain along US90; full closure of IHNC/GIWW along west shore of Lake Borgne; full closure West Bank from between Belle Chase to Larose along GIWW.	48
	B) Weir closure of Lake Pontchartrain along US90 with structures in Chef and Rigolets tidal passes; full closure of IHNC/GIWW along west shore of Lake Borgne; weir closure West Bank from Belle Chasse to Larose along GIWW.	42 / 152
	C) Weir closure of Lake Pontchartrain along US90 without structures in Chef and Rigolets tidal passes; full closure of IHNC/GIWW along west shore of Lake Borgne; weir closure West Bank from Belle Chasse to Larose along GIWW.	48
	D) Isolating Lakes Pontchartrain and Borgne from each other by building a levee across Lake Borgne from Verret to Slidell; full closure West Bank from Belle Chasse to Larose along GIWW.	40
Larose to Golden Meadow	A). Non-overtopping levee alignment from Larose to Golden Meadow and along GIWW.	28
	B)100-year level alignment from Larose to Golden Meadow; a non-overtopping levee along the ridge and a ring levee alignment in the western part.	28
	C) Non-overtopping levee alignment from Larose to Golden Meadow and along the ridge, and an overtopping levee along GIWW with a ring levee around Lake Charles.	28
Plaquemines Parish	A) Two spillways in the levee system along Plaquemines,	17*
	B) Full removal of levee system along Plaquemines to river embankment level (for sensitivity analysis only)	17*
Landscape Conditions	1) Degraded marshes 50 years from now without increased action	174
	2) Restored marshes 50 years from now based on a hypothetical alternative (for sensitivity analysis only)	46
Sea level Rise Sensitivity Analysis	1) +1 ft sea level rise	9
	2) +2 ft sea level rise	9
	3) +3ft sea level rise	9
Barrier Islands Sensitivity Analysis	1) No barrier island	15
	2) Restored island	15
	3) Post-Katrina with forest	15
	4) Restored island with forest	15

* Note, de Jong et al 2007 describes rerunning 18 storms.

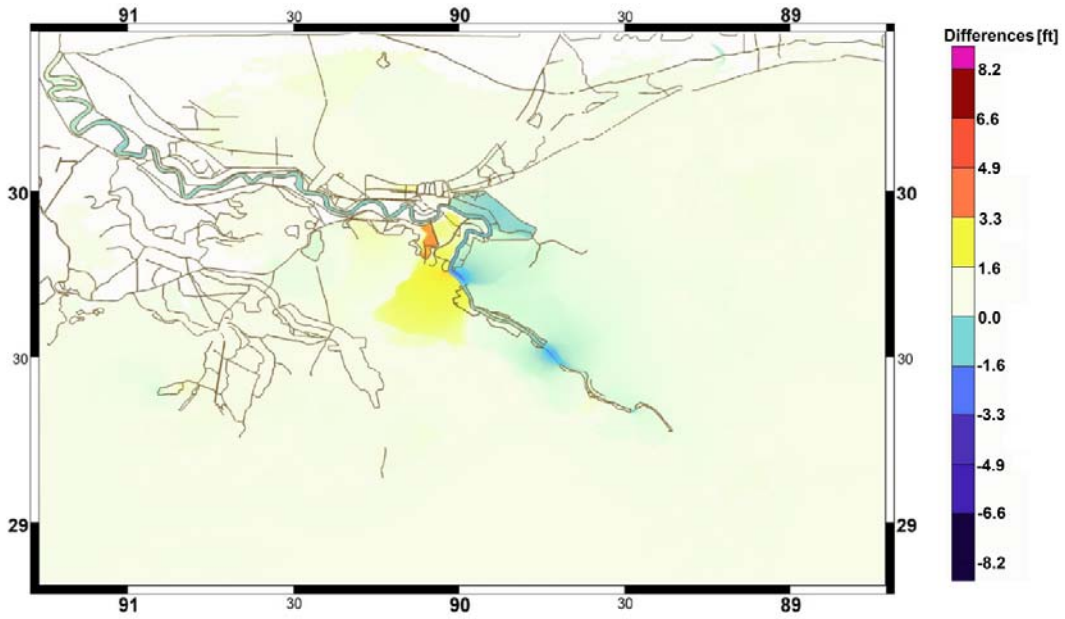

a. Difference Between 2007 and Alternative with Spillways

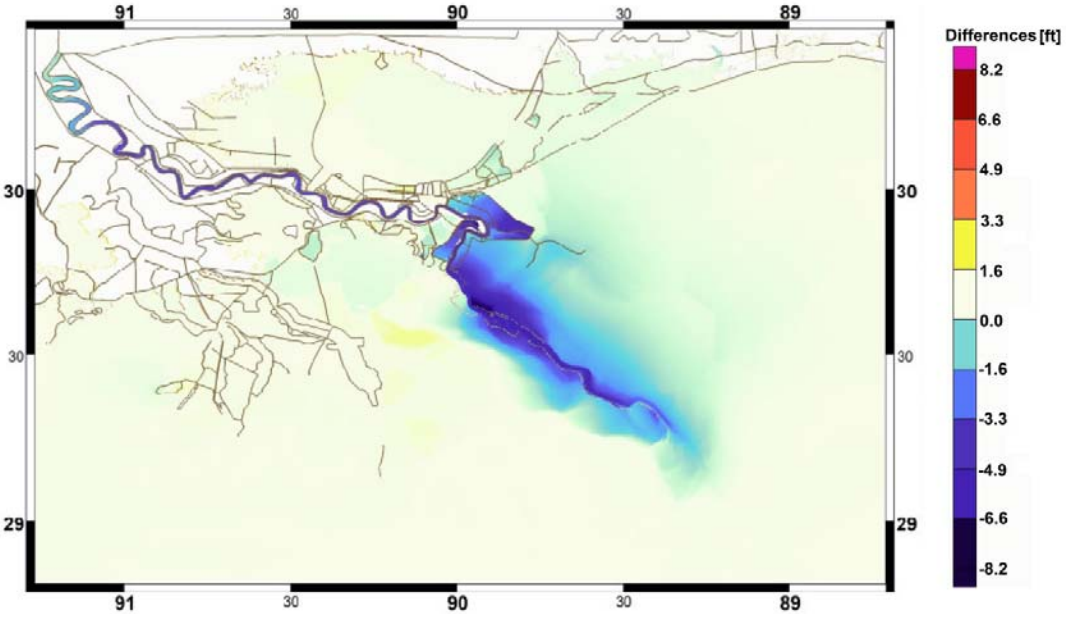

b. Difference Between 2007 and Alternative with Levees Removed

Figure 20.1. Evaluation of 100-yr Surge Hazard for Plaquemines Parish Levee Alternatives
de Jong et al 2007

20.2 USACE Mississippi CIP

Surge hazard analysis for future conditions was used in the MsCIP to evaluate two planning alternatives (Lines of Defense Nos. 3 and 4) and the extent of maximum inland surge (Line of Defense No. 5). Line of Defense No. 3 entailed modestly raising the elevations of existing roads and seawalls and adding ring levees for two communities. Line of Defense No. 4 was an inland barrier along the whole coast sufficient to prevent overtopping from several severe storms.

The MsCIP analysis was undertaken by a different team than the one that completed the Mississippi FIS described in Section 14.5. The MsCIP team used a 197-storm Surge Response-OS with a set of tracks shifted eastward to encompass the Mississippi coast.[1] Individual storms were modeled with the PBL vortex model, ADCIRC (using the SL15 mesh developed for Louisiana and modified with weirs to represent Lines of Defense Nos. 3 and 4), WAM (for offshore waves), STWAVE for propagation of waves on the continental shelf and in Mississippi Sound, and a combination of STWAVE and COULWAVE for nearshore waves.

No action exterior surge hazards (SWL, H_s, and T_p) were computed with the entire 197-storm set for the 25-, 50-, 100-, 500-, and 1,000-yr at 80 locations. (Interestingly, the 100-yr SWL hazards were not compared to those identified in the FIS). For Lines of Defense Nos. 3 and 4 a 27-storm subset was rerun to develop an adjustment algorithm (similar to LaCPR). The adjustment algorithm was then used to determine With-project 25-, 50-, 100-, 500-, and 1,000-yr SWL, H_s, and T_p at each of the 80 locations. RLSR was not incorporated into this analysis.

Eleven storms from the set were selected for testing the sensitivity of storm surge and waves to three scenarios involving the configuration of five barrier islands: No Action (post-Katrina diminished) footprint and elevation; a modest restoration; and a massive footprint and elevation expansion. Figure 20.2 illustrates the planning comparisons that were made with the Camille-like hurricane scenario.

The MsCIP also presented a sensitivity test of storm surge and waves to landscape conditions using three cases for the Biloxi Marsh in Louisiana, which front the western third of the Mississippi coast. Two storms—Hurricane Katrina and large Category 1 storm—were used to compare the base case versus an improved case. The base case assumed a degraded entire marsh area lowered to open water with elevation at -2 ft NAVD88 and reduced Manning's n, wind reduction, and sheltering coefficients. The improved case included two strips of marsh raised to 1.05 ft NAVD88 and upgraded to herbaceous wetland. Figure 20.3 illustrates the planning comparisons that were made with the Hurricane Katrina scenario.

Finally, the MsCIP evaluated Line of Defense No. 5 using an MPI MOM developed from six tracks. The MsCIP MPI hurricane was defined as having a GoM CP of 880 mb and an R_{max} of 36 nm (41.4 mi). Figure 20.4 presents the MPI MOM. Interestingly, the MPI MOMs prepared for the LaCPR Study (Figure 19.4) appear to be somewhat higher than those for the MsCIP.

[1] As discussed in Section 14.5, the Mississippi FIS used a 152-storm JPM-OS approach (not a Surge Response-OS).

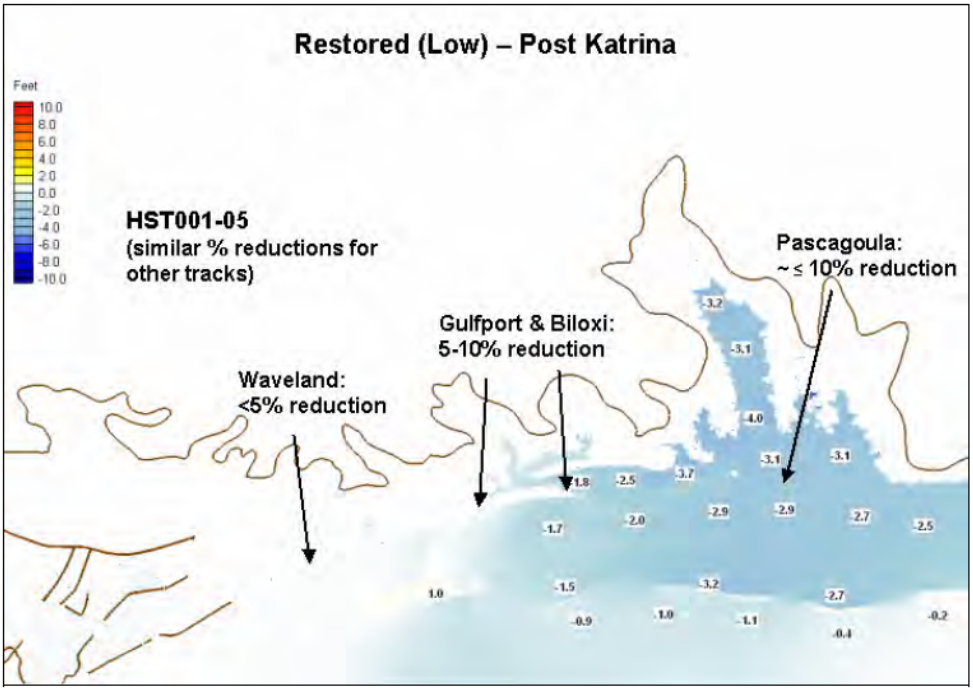

a. Modest Barrier Island Restoration versus No Action

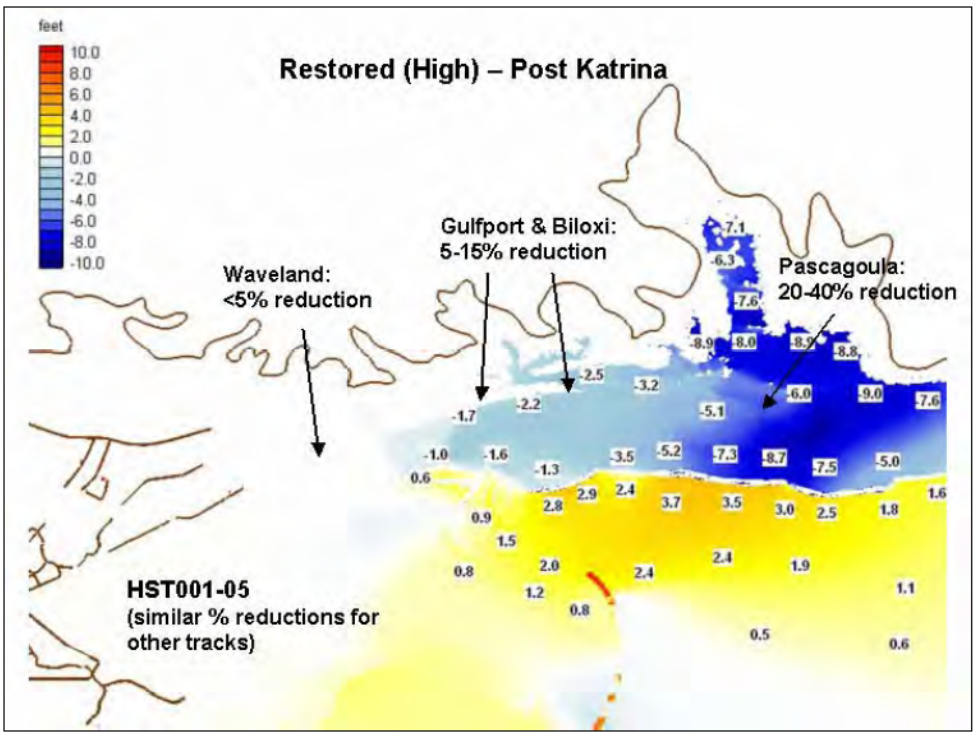

b. Massive Barrier Island Restoration versus No Action

Figure 20.2. Difference in Peak Surge for Barrier Island Restoration Alternatives Camille-Like Hurricane with Biloxi MS Landfall

USACE 2009b

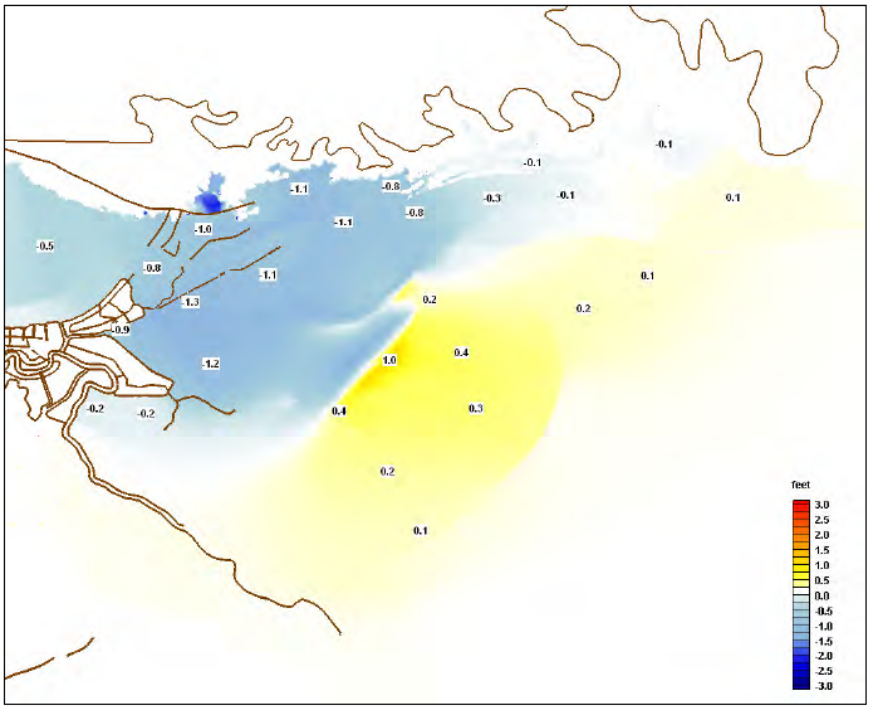

a. Improved Marsh versus No Action

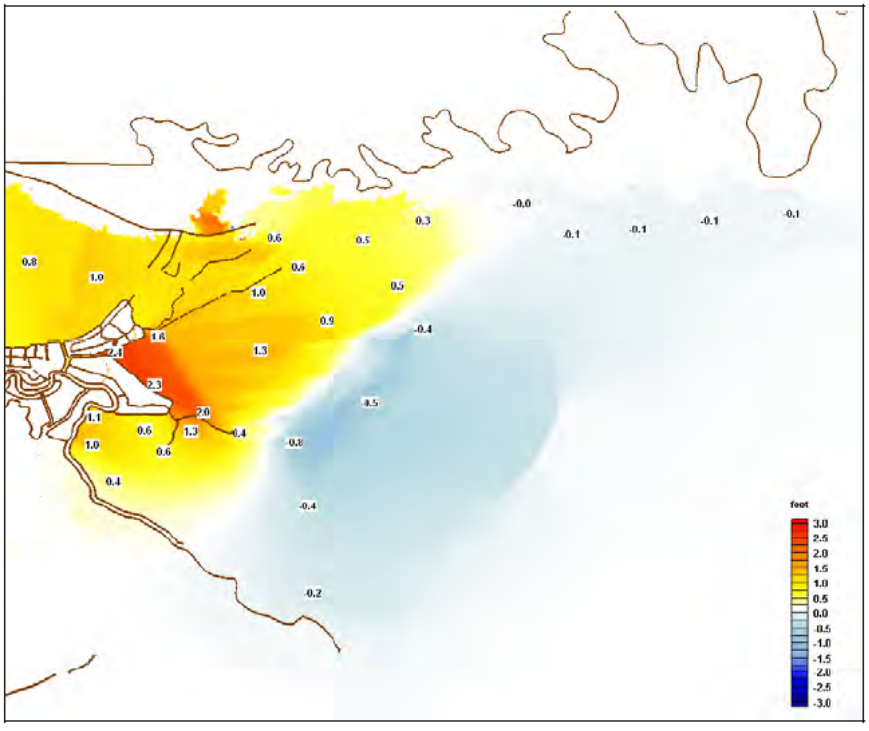

b. Degraded Marsh versus No Action

Figure 20.3. Difference in Peak Surge for Biloxi Marsh Restoration Alternatives Hurricane Katrina

USACE 2009b

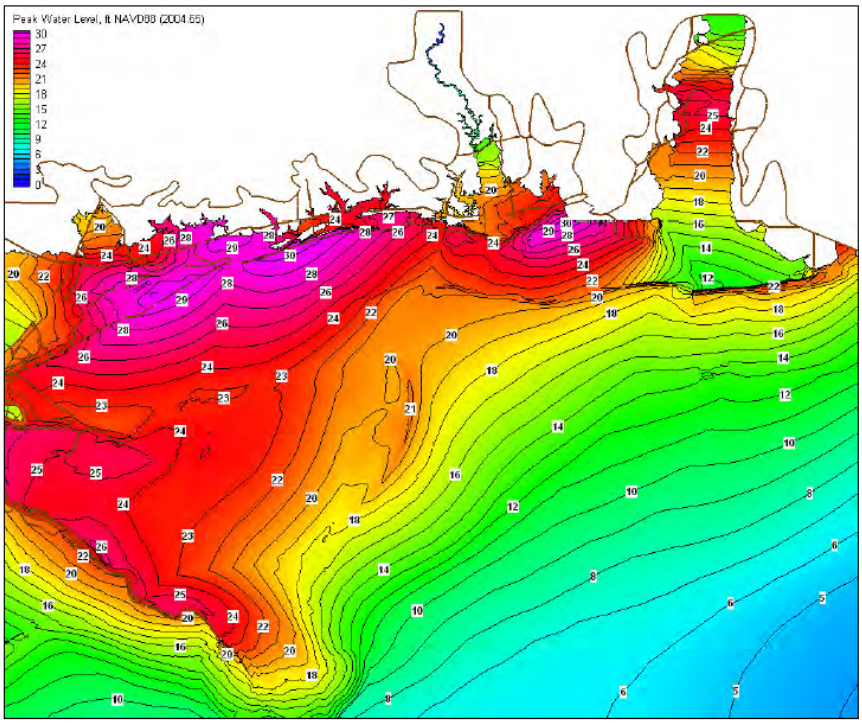

Figure 20.4. MPI MOM for Mississippi
USACE 2009b

20.3 USACE HSDRRS Design for RSLR

Section 17.3 reviewed the USACE's five step process to develop a current (2010) overtopping hazard analysis[2] and apply it to the HSDRRS 100-yr design. In addition, the USACE undertook a sixth step to evaluate future Year 50 (2057) SWL, H_S, and T_P conditions and overtopping (see USACE 2010). In assessing 2057 conditions the USACE incorporated regional forecasts for RLSR (SLR and subsidence) but not coastal erosion or large scale vegetation conversions.

To evaluate the effect of RSLR on exterior surge the USACE performed ADCIRC-STWAVE sensitivity tests with nine storms selected from the 152-storm Surge Response-OS, adjusting the LMMSL by 1.0, 2.0, and 3.0 ft. The impact of the LMMSL increases was assessed at eleven sub-regions listed in Table 20.2

Figure 20.5 shows the range in relative peak surge increase (peak surge increase divided by RSLR) for all 27 simulations for each sub-region. These results were used to estimate a single 100-yr SWL multiplier for each location—ranging from 1.2 to 2.5—provided in Table 20.2. The multiplier times a forecasted RSLR gives an estimated increase to the 100-yr SWL at that location. The USACE also used the STWAVE results to develop a multiplier applied to the 100-yr SWL increase for estimating the increase in Zone B wave heights. The wave height increase multipliers ranged from 0.12 to 0.58 and are also listed in Table 20.2.

[2] Based on the 2007 FIS analysis for exterior surge hazard, adjusted to 2010 conditions as described in Section 17.2.

Table 20.2. RLSR Sensitivity Test Results for 100-yr SWL and Zone B Waves

USACE 2010

Sub-Region	Range of Relative 100-Yr SWL Increases	100-Yr SWL Increase Multiplier	Wave Height Increase Multiplier
South Shore Lake Pontchartrain (SSP)	1.0-1.5	1.3	0.43
East Orleans (EO)	1.1-1.6	1.2	0.13
North St. Bernard (SBN)	1.2-1.6	1.3	0.17
South St. Bernard (SBS)	0.7-2.3	1.4	0.45
Caenarvon (C)	0.7-4.5	2.1	0.50
Plaquemines East (PE)	1.3-2.0	1.5	0.58
Plaquemines West (PW)	1.4-3.0	1.9	0.41
South West Bank (SWB)	1.3-3.6	2.5	0.12
North West Bank (NWB)	1.0-2.9	2.1	0.13
Golden Meadow (GM)	1.4-2.3	1.8	0.27
Morganza to the Gulf (MtG)	1.4-2.0	1.7	0.37

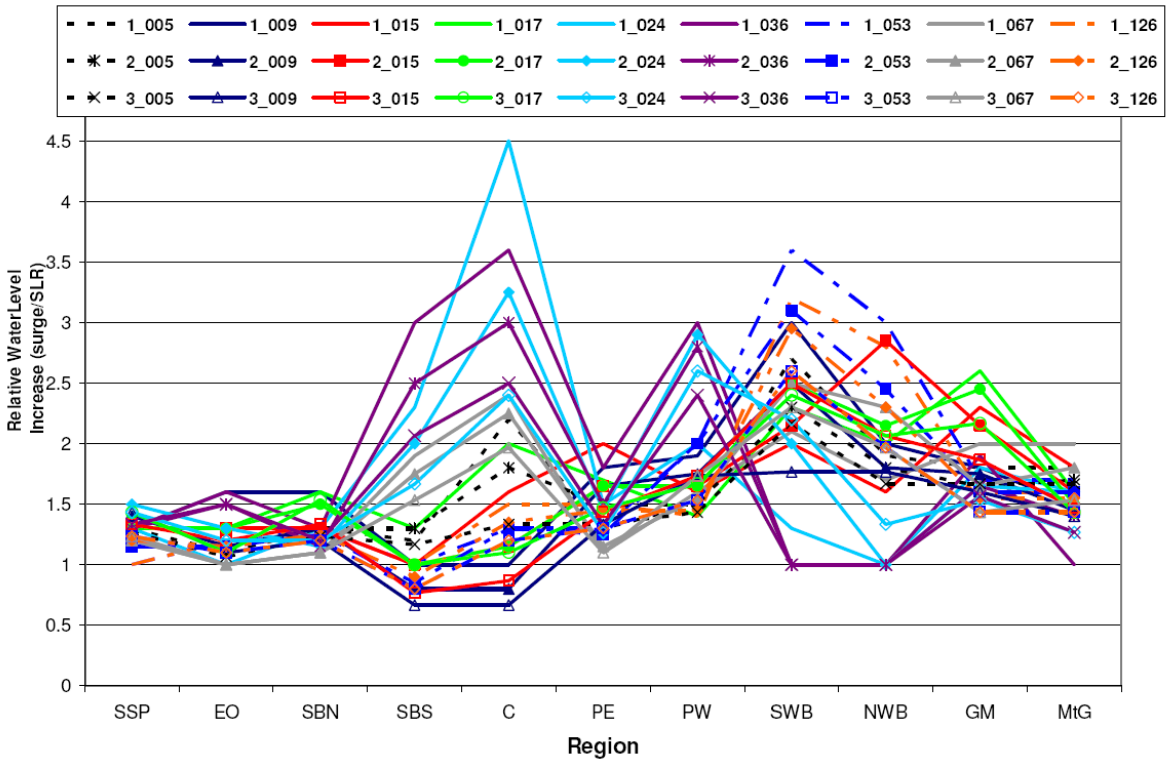

Figure 20.5. Relative Increases in Peak Surge for RSLR Sensitive Tests

USACE 2010

The USACE employed this approach apparently due to insufficient HPPC resources at the time for a complete re-running of the JPA. The USACE also estimated increases for future 500-yr SWL and wave heights with RSLR, presumably using a somewhat similar method. The limitations in this approach include:

a. Those associated with the 2010 analysis previously discussed in Section 17.3—e.g., small set size and simplifications associated with the 152-storm Surge Response-OS, particularly with regard to 500-yr conditions;

b. Not including coastal erosion and vegetation changes in the analysis of future conditions;

c. Simplifications associated with only rerunning nine storms; and

d. Generalizing the analysis to broad sub-regions—e.g., the entire south shore of Lake Pontchartrain.

Using the results of the above analysis the USACE made the following modifications to the 2010 100-yr hazard conditions to estimate 2057 100-yr hazard conditions:

- For HSDRRS reaches in the Metro New Orleans, New Orleans East, and the Lower 9th Ward/St. Bernard Polders—SWL and H_S increases of 1.5 ft and 0.75 ft, respectively.
- For West Bank Polders and the Mississippi River Levee at Caernarvon—SWL and H_S increases of 2 ft and 1 ft, respectively.
- Future increased wave T_P was computed by assuming unchanged wave steepness (i.e., the ratio of H/T^2).

The USACE then evaluated required design elevations for each HSDRRS reach at the 2057 100-yr hazard using the methods described in Section 17.3 (to reduce overtopping at the 50% and 10% Exceedance Levels to the erosion-based criteria of 0.01 and 0.1 cfs/ft). The USACE applied the 2057 100-yr design elevations in the final specifications for floodwall segments of the HSDRRS but not levees, based on considerations of the constructability and costs associated with future raising of reach crowns.[3] The 2057 100- and 500-yr hazard and HSDRRS design elevations are included in the information provided in the Part IV, Attachment 1.

20.4. State of Louisiana Master Plan

For the 2012 Master Plan (see Appendices 24 and 25, prepared by ARCADIS and RAND Corporation, respectively), CPRA evaluated coastal Louisiana (southeast and southwest) surge hazards for current versus many future conditions. As described in Section 11.4, ARCADIS developed and validated a baseline mesh (referred to as OCPR2012_S50) utilizing a tightly coupled ADCIRC+SWAN code. The 50+ day validation period in the late summer of 2008 encompassed both Hurricanes Gustav and Ike.

ARCADIS created two future Year 50 modifications to the current conditions mesh attributes and model to reflect Moderate versus Less Optimistic coastal degradation scenarios. The modifications took into account different estimates of Year 50 SLR (0.89 versus 1.48 ft), subsidence, erosion, and vegetation changes. Figures 20.6.a. and b. show the elevation difference between the current and the two future condition meshes (referred to as OCPR2012_S12_G90 and OCPR2012_S13_G90).

[3] In establishing final crown specifications for floodwalls the USACE also made reach-specific allowances for local structure settlement.

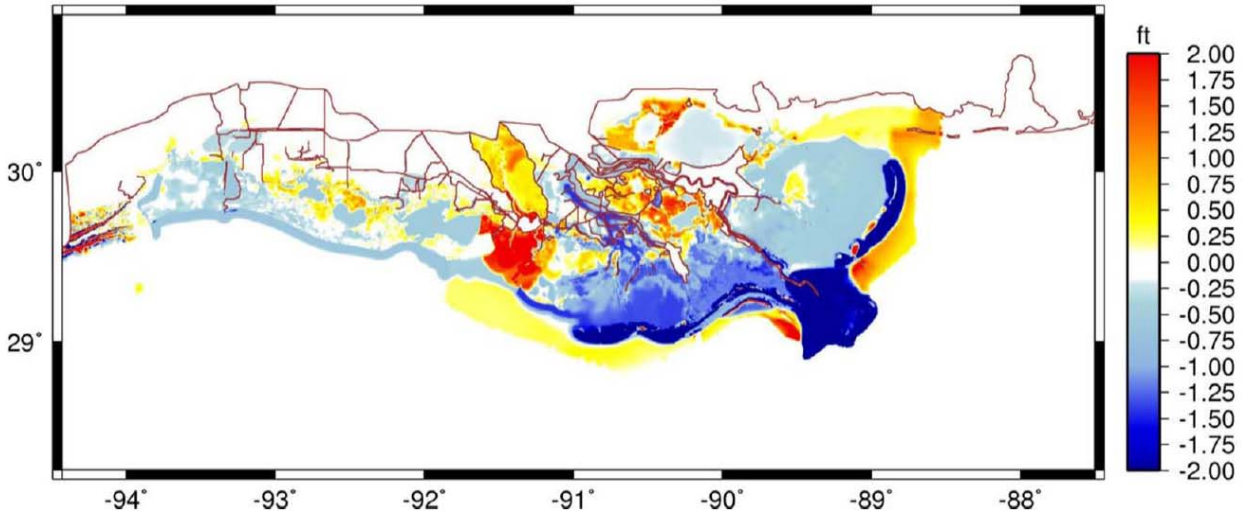

a. Current versus Moderate Coastal Degradation

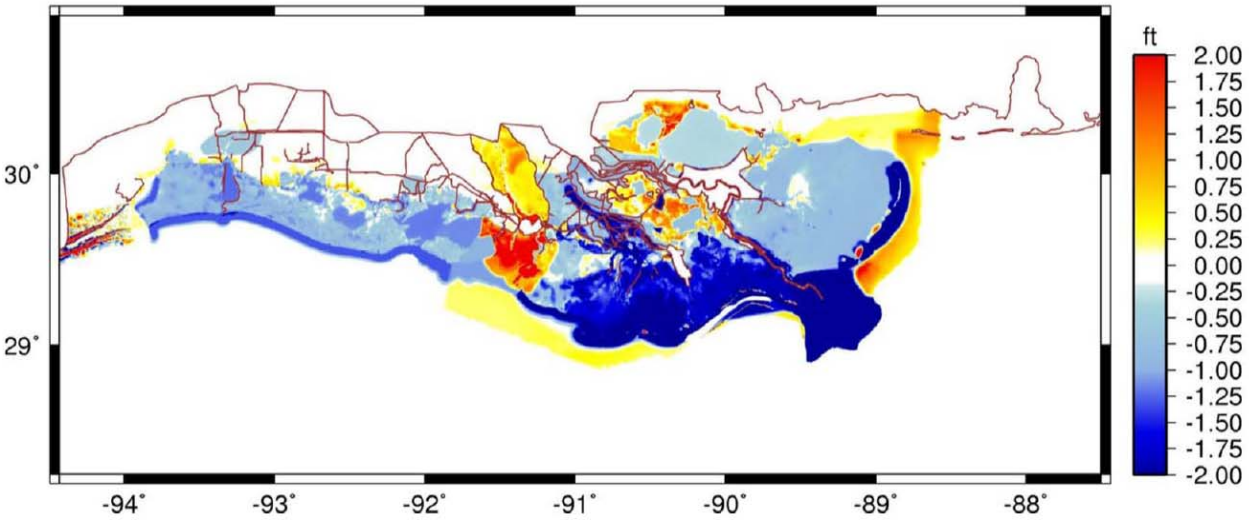

b. Current versus Less Optimistic Coastal Degradation

Figure 20.6. Elevation Difference for Future Year 50 Condition ADCIRC Meshes
CPRA 2012

Additional sub-versions of the two future condition meshes were then created to investigate 34 potential coastal restoration and surge protection projects. To minimize the number of sub-versions, multiple projects were grouped on the sub-version meshes, with projects selected for each mesh to minimize mutual interference and allow the impacts of each project to be evaluated independently. Seven sub-versions were developed for the two future meshes (G91 to G97), or a total of 14 additional meshes. Peak surge differences for selected storms and mesh subversions were included in the Master Plan Report (Appendix 24). Figures 20.7 illustrates peak surge differences for Storm 009 (a large, strong, landfalling Category 2 hurricane) for the current conditions versus a Less Optimistic future conditions mesh that included a Lake Pontchartrain Barrier project.

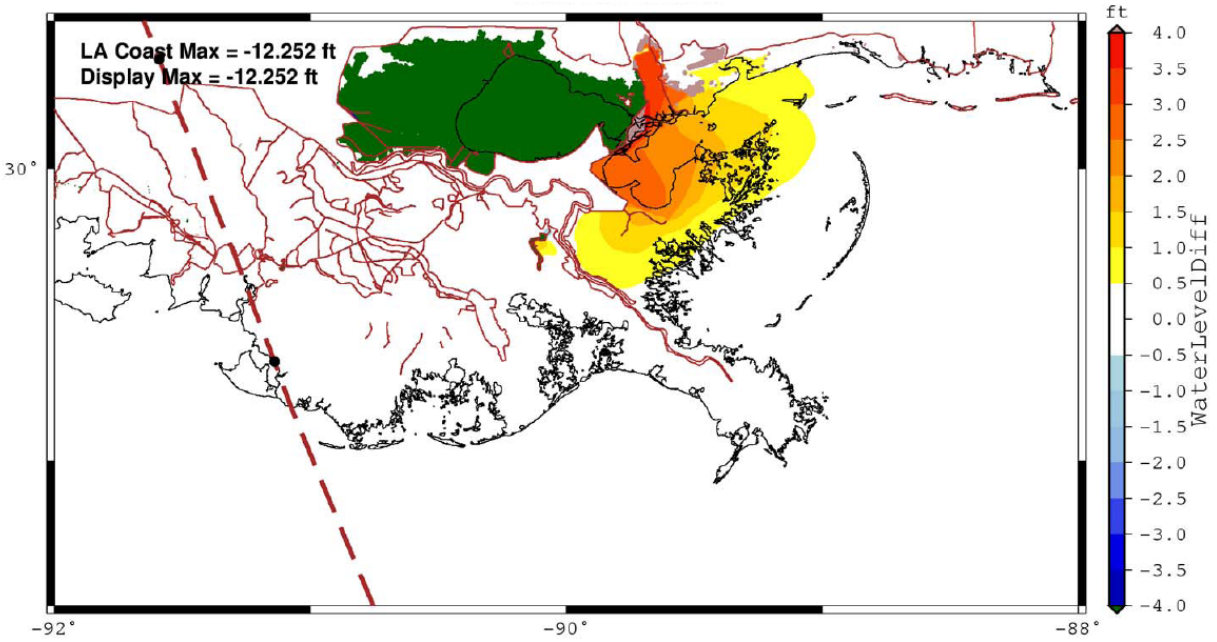

b. Current versus Less Optimistic Coastal Degradation with Lake Pontchartrain Barrier

Figure 20.7. Peak Surge Difference for Storm 009, Current Conditions versus Less Optimistic Future Conditions with Lake Pontchartrain Barrier

(green indicated surge reduced by >4 ft)
CPRA 2012

As described in Section 14.4, RAND developed a highly simplified 40-storm JPM-OS (truncated from the IPET JPM-OS, which itself was improvised from the original 152-storm Surge Response-OS). Simulation were conducted for the 40 storms with each of the 17 models—the current conditions, two future conditions, and 14 sub-versions of the future conditions. Results were used to define the exterior surge SWL hazards for each alternative (for return periods at 10-yr intervals from 10 to 150 years, and at the 400-, 500-, and 1,000-yr return periods) at locations throughout the Louisiana coast. Wave heights at each SWL hazard level at each location were defined using the SWAN results and additional interpolation techniques.

To define the interior hazard for each alternative RAND conducted a polder inundation JPA, employing a set of exterior points at roughly 300 m intervals along the perimeter of each existing or proposed project. As the 40-storm JPM-OS was too small to support a polder JPA, RAND prepared an expanded set of 720 storms by interpolating from the 40-storm JPM-OS. Each storm—with a corresponding probability—had an associated CPD, R_{max}, and track and produced a peak SWL at each perimeter location. Hydrographs were constructed at each perimeter location for the 720 storms using rising and falling limb σ_R and σ_F values determined from the 40-storm set. Exterior wave conditions for each storm were also computed using a breaking parameter.[4]

[4] The breaking parameter described in Appendix 25 appears to contain an error as it specified a foreshore maximum breaking wave height as 0.4 times the Zone B (nearshore) wave height, instead of 0.4 times the depth.

RAND evaluated SOBRP processes for their polder inundation JPA in a manner generally similar to the IPET approach (see Section 17.1): seepage inflow was ignored; overtopping was computed at each levee and floodwall perimeter location over the course of each storm using the equations described in Section 15.3; rainfall was introduced into each sub-basin based on storm intensity and distance to storm center; and pumping included the 0%, 50%, and 100% scenarios. As performed by IPET, RAND then employed level-pool routing by sub-basins, for each of the 720 storms, to determine probabilistic peak interior SWLs associated with combined overtopping, rainfall, and pumping.

Probabilistic breaching was also incorporated in the RAND polder inundation JPA using pre-defined perimeter reach segments—based on alignment and structural conditions. Each reach included at least one of the 300 m perimeter locations, but could include many more depending on length. A single, simplistic, catastrophic failure condition was defined for each whole reach: the equalization of the interior sub-basin SWL with the storm exterior peak SWL. With a failure, the exterior SWL would equalize with all interconnected sub-basins not isolated by a higher internal barrier. The probability of this failure condition occurring was then assigned based on a combined probability of failure at any location within the reach due to seepage, slope stability, or overtopping erosion.[5] Independent failure probabilities for each of these three mechanisms at each location depended only on the peak SWL, limited inputs for location-specific conditions,[6] and fairly simplistic equations. To define the probability of breach-driven interior inundation levels for each of the 720 storms, RAND conducted 100 random draws for each storm (i.e., a Monte Carlo analysis, see Section 16.4).

In order to assess surge risk associated with the 17 alternative conditions, RAND coupled the exterior and interior surge hazard results with FEMA's HAZUS model. The HAZUS model uses an input of flood depth by census block[7] to estimate damages (in dollars) for a range of assets (residential, commercial, industrial, infrastructure, etc.), together with direct economic losses. For each alternative RAND input values for 50-, 100-, 500-yr hazards for 35,500 coastal Louisiana census blocks, which make up approximately 50 exterior and polder interior communities.

The Master Plan main report and Appendix 25 do not include output from the RAND surge hazard or risk analyses—such as changes to the 100-, 500-, or 1,000 surge hazard or property/economic losses under different alternatives. The influence of future conditions and projects on surge hazard levels and property/economic risk were reportedly incorporated into the State's project evaluation but were not published.

20.5. SLFPA-E New Orleans East Land Bridge Feasibility Study

The SLFPA-E retained Ben C. Gerwick and ARCADIS to further investigate the feasibility of Lake Pontchartrain Barrier concepts—as an extension of the LaCPR Study and 2012 Master Plan assessments. As part of this investigation, ARCADIS utilized the Master Plan version of the ADCIRC+SWAN code and modified the validated Master Plan baseline mesh to examine five future scenarios:

[5] Operational failures such as an improper gate closure were not considered.

[6] For seepage failure, the conditions include the thickness and permeability of two underlying soil zones plus the slope, width, and height of the perimeter embankment; for overtopping they included the embankment soil type; and for slope stability failure they also included unit weights, friction angles, and strength of key soil components.

[7] Determined by subtracting a typical ground elevation from the surge height.

- Base Case, future regional RSLR and coastal degradation WITH a maintained natural land bridge;
- Scenario 1, future regional RSLR and coastal degradation but WITHOUT a maintained natural land bridge;
- Scenario 2, Base Case PLUS a Barrier WITH closure of the Rigolets and Chef Passes;
- Scenario 3, Base Case PLUS a Barrier WITHOUT closure of the Rigolets and Chef Passes; and
- Scenario 4, Scenario 1 PLUS a Barrier WITHOUT closure of the Rigolets and Chef Passes.

The future scenarios used a RLSR of 2.8 ft and included raising elevations for maintained roads, as well as land bridge features in Scenario 1, 3, and 4. For Scenarios 3, 4, and 5 the barrier crest was set at 22 ft NAVD88.

ARCADIS simulated eight selected storms from the 152-storm Surge Response-OS set to evaluate potential impacts on regional exterior surge hazard. A JPA of exterior hazard impacts was not utilized for the purposes of this preliminary study. ARCADIS reviewed the regional results of the individual 152-storms from the LaCPR Study and selected four storms which approximately produced the 100-yr SWL hazard and four which approximately produced the 400-yr SWL hazard.

Figure 20.8 shows the difference in the exterior surge 100-yr MOMs (from the four storms) between the Base Case and Scenario 2.

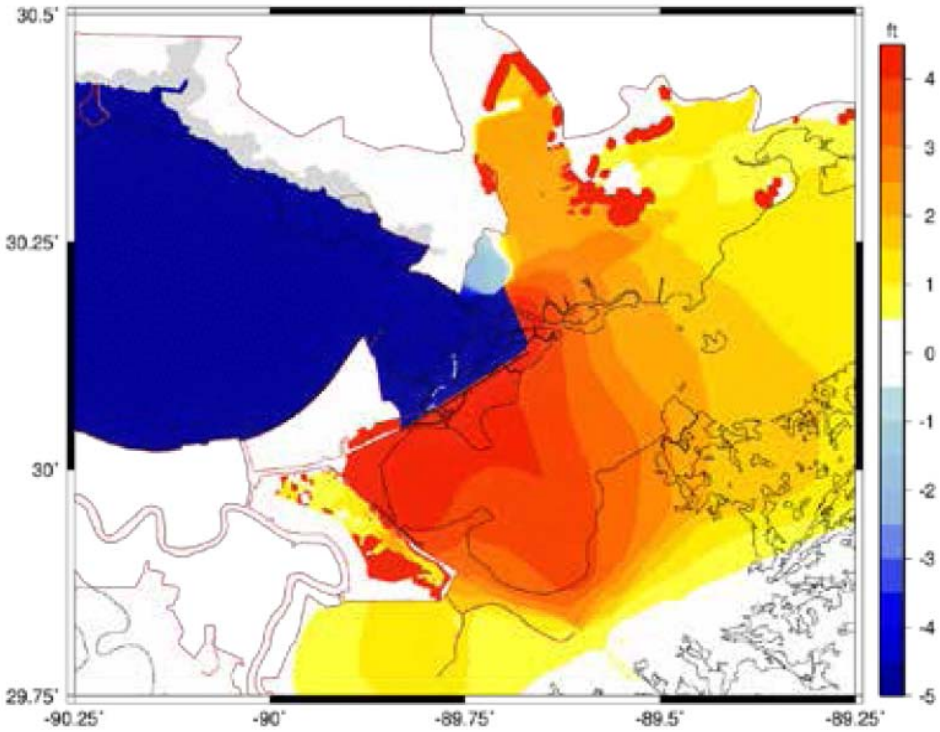

Figure 20.8. Difference in 100-yr Surge Hazard for Proposed Lake Ponchartrain Barrier

Gerwick 2012

20.6. SLFPA-E Polder Compartmentalization Study

The SLFPA-E has also initiated a study of interior polder projects to mitigate residual inundation risks associated with perimeter breaching. The study is focusing on the enhancement of legacy barriers, road and railroad embankments, and natural ridges, as well interior storage areas, to control inundation in the event of a significant perimeter failure.

The study is employing high resolution 2D HPPC ADCIRC polder models (see Figure 15.13) to study interior routing under specific breach and compartmentalization scenarios.[8] The polder meshes include detailed representation of major gravity conveyance features (canals) and pump stations. Breach scenarios—such as the one illustrated in Figure 20.9—are being evaluated at multiple locations around each polder and typically include volumes on the order of 30,000 acre-ft. Simulations are employed to compare the peak footprint and depth of inundation—as well as timing and rate of inundation—for With versus Without compartmentalization project scenarios.

An expansive JPA of interior hazard impacts is not being utilized for the purposes of this preliminary study. The HSDRRS design and IPET study of residual risk indicate that most perimeter breach scenarios generally reflect greater than 500-yr return periods. However, breach scenarios for the IHNC/GIWW sub-basin floodwalls may have a higher probability, particularly due to specific fragility issues.[9]

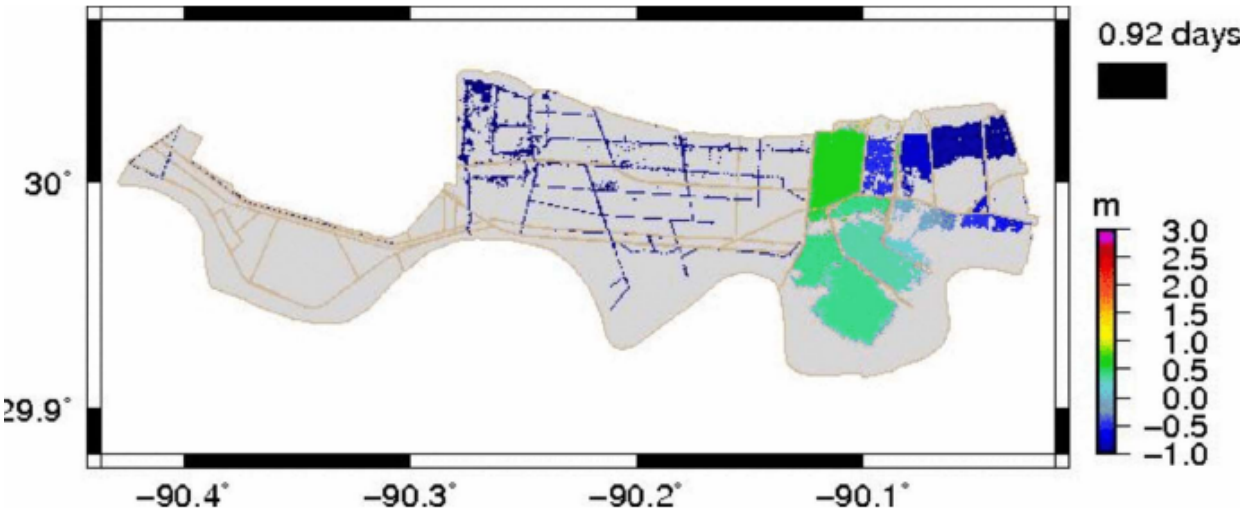

Figure 20.9. Example of Perimeter Breach Scenario for Polder Compartmentalization Study

Bob Jacobsen PE, LLC 2013

[8] In 2008 Aalberts performed a Hurricane Katrina hindcast for the New Orleans Metro Polder as part of a compartmentalization study using SOBEK (a 2D finite difference code) and simplified structured grid (164 ft square). Royal Haskoning (2009) subsequently used Aalberts model to evaluate additional compartmentalization alternatives. The SOBEK model had limited depiction of canals and other internal features.

[9] These include the vulnerability of the IHNC "I-wall" design (see Section 15.4); the potential for SWL elevations inside the IHNC/GIWW sub-basin during extreme surge events above safe levels for these floodwalls; and the additional hazard of large unsecured vessels and structures ramming these floodwalls during a surge event.

Part V. Conclusions and Recommendations

Conclusions

Part V has reviewed methodologies for analyzing hurricane surge hazards for future conditions and recent applications to southeast Louisiana. This information supports the following important findings:

1. There is currently no scientifically published trend analysis or forecast for long-term secular change to hurricane frequency, intensity, or other characteristics for the CN-GoM. Particular CN-GoM hurricane climatological factors—such as wind shear environment and the Loop Current—are likely to be important to such forecasts.
2. Coastal scientists are publishing research on several critical coastal landscape trends affecting future surge hazard—and providing forecasts for use in critical planning efforts for southeast Louisiana. These encompass SLR, regional subsidence, coastal erosion, and vegetation change.
3. Analysis of future polder inundation hazard conditions can also consider trends in perimeter protection (e.g., localized settlement/consolidation and increasing fragility) and interior subsidence. To date, evaluations for the impact of these trends have not been undertaken.
4. Forecasts of coastal landscape and perimeter system/polder change—as well as proposed projects for coastal restoration and protection—can be readily addressed through ADCIRC+SWAN mesh and code modifications. Surge hazards under these future conditions can be computed by re-running the exterior surge JPA using the modified model. Likewise, changes to perimeter systems and polders can also be incorporated into the more expansive JPA in order to evaluate future polder inundation hazards.
5. When re-running the entire JPA has not been practical, researchers have used hurricane scenarios to assess the sensitivity of surge levels to future conditions. Example include historical storms, SPHs, PMHs, MPI Hurricane, selected storms, or NOAA MEOWs and MOMs.
6. The USACE 2009 post-Katrina planning efforts for Louisiana (LaCPR Study) assessed surge hazards under 18 future conditions using modified ADCIRC-STWAVE models. However, due to limited HPPC resources, the future hazard assessments were based on only re-running a small number of storms for each future condition. The LaCPR Study did not undertake an expanded JPA for future polder inundation hazard analysis.
7. The 2009 USACE Mississippi planning study (MsCIP) applied a limited re-running of a JPA to compare surge hazards for current conditions versus two alternative Lines of Defense. The MsCIP also employed selected storms in sensitivity assessments for barrier island and marsh restoration alternatives.
8. The LaCPR Study and MsCIP both employed an MPI MOM to examine “worst case” storm surge inundation for current conditions. The reports did not provide MPI MOMs for any of the future condition alternatives.
9. The USACE HSDRRS Year 50 (2057) design evaluated the future impact of RSLR with a nine-storm sensitivity test (as opposed to re-running the entire JPA) and estimated multipliers for eleven broad sub-regions to account for increases in the 100-yr hazard under a range of forecasted RSLR. The USACE also developed multipliers for associated wave height increases. The evaluation did not address coastal erosion and vegetation changes. The USACE employed the estimated 2057 100-yr surge hazard in setting design elevations for HSDRRS floodwalls.

10. The CPRA's 2012 Master Plan created 17 ADCIRC+SWAN models: a current condition; a Moderate and a Less Optimistic coastal degradation scenario; and seven sub-versions for both degradation scenarios (14 total) to evaluate 34 potential restoration and protection projects. JPA methods—similar in many ways to those used by IPET—were developed to assess exterior and interior polder hazards. However the Master Plan JPA relied on an improvised JPM-OS with only 40 storms. Simplified breaching probabilities were incorporated into the JPA for interior hazard assessment. The Master Plan assessment of future hazards was coupled with HAZUS to examine surge risks—property and direct economic losses—under the alternatives.
11. A SLFPA-E funded study employed the Master Plan ADCIRC+SWAN model and eight storms to examine the sensitivity of regional surge SWL and wave heights under five future scenarios for the New Orleans East Land Bridge and associated Lake Pontchartrain Barrier project.
12. An ongoing SLFPA-E study is using high resolution ADCIRC-models of polders to evaluate the sensitivity of interior inundation (footprints, depth, and rates) to several potential compartmentalization projects. The study is employing scenarios reflecting significant perimeter breaching generally expected to have return periods greater than 500 years.

Recommendations

The above conclusions indicate several ways in which analyses of surge hazard for future conditions can be improved, particularly given the increasing availability and declining costs for HPPC:

1. Follow the recommendations in Parts II, III, and IV for improved model development, exterior surge hazard analysis, and polder inundation hazard analysis.
2. Re-evaluate the future conditions hazards at appropriate intervals (e.g., Years 10, 25, 50, and 100) based on *all* recognized applicable coastal landscape trends—e.g., RSLR, coastal erosion, vegetation changes, perimeter system degradation, and polder subsidence—when the current exterior surge and interior polder inundation hazards analyses are revised.
3. Re-run all JPM-OS storms for the future conditions JPAs instead of using a small subset of storms to adjust the estimate of future hazard.
4. Use specific storm scenarios—e.g., a Katrina-like hurricane—to provide additional insight and aid public understanding of impacts to future surge hazard.

The Louisiana CPRA, together with federal partners, should fund two critical research topics to improve surge hazard analysis for future conditions:

1. Assess the influence of climate cycles and secular climate change on the CN-GoM hurricane climatology, SLR, and seasonal steric conditions, including influences mediated by the Loop Current. As part of assessing future hurricane climatology for the CN-GoM provide suitable JPM-OS sets for various future surge hazard evaluations.
2. Improve trend analyses for regional subsidence, coastal erosion, and vegetation conversion; elevation changes to perimeter systems and polder interiors; and HSDRRS fragility.

The above recommendations can improve systemic and localized accuracy of surge hazard estimates for future conditions. However, it is important to recognize that the uncertainty in future hazard estimates will be even larger than the substantial uncertainty associated with estimates of current surge hazard.

Part V. References

Aalberts, M.L., The Cost Effectiveness of Compartmentation of the Orleans Metro Bowl (Master Thesis), Delft University of Technology, Faculty of Civil Engineering, Hydraulic Engineering Section, 2008.

Ben C. Gerwick, Inc., New Orleans East Land Bridge Study, for Southeast Louisiana Flood Protection Authority—East, 2012.

Blum, M. D. and H. H. Roberts, Drowning of the Mississippi Delta Due to Insufficient Sediment Supply and Global Sea-Level Rise, Nature Geoscience, Vol. 2, July 2009.

Couvillion, B. R., J. A. Barras, G. D. Steyer, W. Sleavin, M. Fischer, H. Beck, N. Trahan, B. Griffin, and D. Heckman, Land Area Change in Coastal Louisiana from 1932 to 2010, U.S. Geological Survey, 2011.

Dixon, T. H., F. Amelung, A. Ferretti, F. Novali, F. Rocca, R. Dokka4, G. Sella, S-W Kim1, S. Wdowinski, D. Whitman, Space Geodesy: Subsidence and Flooding in New Orleans. Nature Vol. 441, pp. 587-588, June 2006.

de Jong, W., , J. Westerink , M. van Ledden, The Influence of Lower Plaquemines Parish Mississippi River Levees on Storm Surge in Southern Louisiana,, Proceedings, 10th International Workshop of Wave Hindcasting and Forecasting & Coastal Hazard Symposium, November 11-16, 2007.

Liu, Yanyun, S. K. Lee, B. A. Muhling, J. T. Lamkin, D. B. Enfie, Significant reduction of the Loop Current in the 21st Century and its Impact on the Gulf of Mexico, Journal of Geophysical Research: Oceans, Vol. 117, No. C5, May 2012.

Louisiana CPRA, Louisiana's Comprehensive Master Plan for a Sustainable Coast, 2012.

National Academy of Engineering/National Research Council (NAE/NRC), Third Report of the Committee on New Orleans Regional Hurricane Protection Projects, 2006, http://www.nap.edu/catalog.php?record_id=11772

NOAA, Standard Project Hurricane Wind Fields for the New Orleans, LA. Area, November 1978.

NOAA-NWS, Meteorological Criteria for Standard Project Hurricane and Probable Maximum Hurricane Windfields, Gulf and East Coasts of the United States, NOAA Technical Report NWS 23, 1979.

Preston, B.L., M. Maloney, E. Parish, Indicators of Socioeconomic Exposure to Coastal Hazards for the U.S. Gulf Coast: Implications for Future Vulnerability, Adaptation Futures 2012 International Conference, May 29 – 31, 2012. http://adaptation.arizona.edu/files/public/post%20conference%20uploads/MeganMaloney2012PresentationRINCONupload.pdf

Reed, D. J., and B. Yuill, Understanding Subsidence in Coastal Louisiana, For the Louisiana Coastal Area Science and Technology Program, February 26, 2009, http://www.mvd.usace.army.mil/lcast/pdfs/UNO_SubsidenceinLA_09.pdf

Royal Haskoning, Polder Modeling Orleans Metro: Effects of Compartments on Flooding Extent, prepared for the Flood Protection Alliance, March 2009.

USACE, Circular Letter 4262, November 20, 1946.

USACE, Louisiana Coastal Protection and Restoration, Preliminary Technical Report to Congress, Enclosure F, Engineering Investigations, Annex 1, Hydrodynamic Modeling, June 2006.

USACE (New Orleans District), Hurricane and Storm Damage Reduction System Design Guidelines INTERIM, October 2007, Revised June 12, 2008b.

USACE, Louisiana Coastal Protection and Restoration, Final Technical Report, June 2009a.

USACE (Mobile District) Mississippi Coastal Improvement Program (MsCIP) June 2009b.

USACE (New Orleans District), Hurricane and Storm Damage Risk Reduction System, Design Elevation Report, Draft Report Version 4.0, August 18, 2010.

U.S. Geological Survey, Depicting Coastal Louisiana Land Loss, Fact Sheet 2005-3101, July 2005.

U.S. Weather Bureau, Meteorological Considerations Pertinent to Standard Project Hurricane, Atlantic and Gulf Coasts of the United States, National Hurricane Research Project Report No. 33, 1958.

Visser, J.M., C. Kaiser, and A. B. Owens. Forecasting 50-years of Habitat Switching in Coastal Louisiana: No Increased Action & Preliminary Draft Master Plan, Chapter 4. In, R.R. Twilley (ed.), Coastal Louisiana Ecosystem Assessment & Restoration (CLEAR) Program: A tool to support coastal restoration. Volume IV. Final Report to Department of Natural Resources, Coastal Restoration Division, Baton Rouge, LA. 2008.

Visser, J., S. D. Sylvester, J. Carter, and W. Broussard, Forecasting Vegetation Changes in Coastal Louisiana, Prepared for SWS/INTECOL Wetlands Meeting Orlando FL June 3-9, 2012.

General Technical Note 1.

Concepts in Flood Return Frequency Analysis

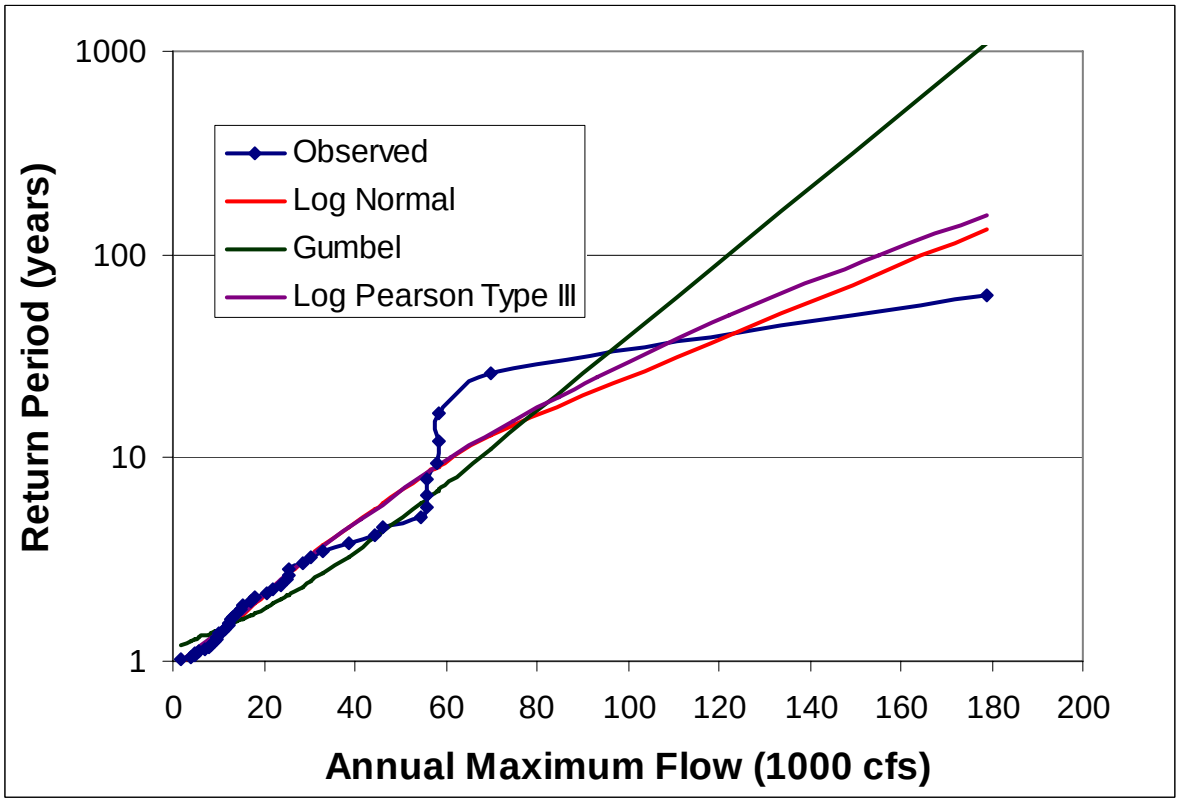

Civilizations have gradually learned the lessons of catastrophic flood sporadic recurrence, beginning with the recognition that such floods do recur and the importance of passing on warnings to descendants.[1] Over many millennia progress has been marked by several milestones:

- Detailed flood records spanning generations,
- Increasingly sophisticated measures to mitigate the consequences of infrequent floods,
- Systematic investigations of flood causes,
- Improved forecasting, and
- Finally a more scientific understanding of extreme flood recurrence.

While the timing and magnitude of individual extreme floods are random in nature, extreme flooding at a location over the long-term exhibits a general trend of increasing magnitude (either as stage or discharge) with an increase in the recurrence interval. This trend has been the subject of a sound application of basic concepts in statistics and probability. The scientific understanding of extreme flood recurrence is rooted firmly in fundamental approaches developed by hydrologists over the course of the 20th century. Hydrologists have successfully completed countless studies of riverine flooding applying these concepts and methodologies.

This General Technical Note reviews fifteen fundamental concepts in flood return frequency analysis (RFA), including important implications and limitations.

A. Probabilistic Analysis

In hydrology (as well as many other physical realms) repeated observations of phenomena can yield varying results. Many variations correlate with *deterministic* (i.e., knowable, controllable) factors and hydrologists seek to define mathematical descriptions and physical confirmation of these correlations (see Deterministic Analysis below). A basic example of a deterministic process is the variation of a river stage versus flow. Apart from deterministic variation the remaining variability in historic or experimental data is termed the *random variability*. Phenomena with appreciable randomness are termed *probabilistic processes*.[2]

When a large number of hydrologic observations for probabilistic processes are collected patterns often emerge. Figure 1a, b, and c illustrate one such pattern. Figure 1a presents a histogram of a 100-year record of highly variable observations of annual total rainfall (at a hypothetical location). Figure 1b depicts this record arranged by five-inch rainfall bins (vertical bars), with the x-axis indicating annual rainfall totals

[1] The same could be said for other directly weather-related natural disasters—e.g., droughts, blizzards, and wildfires—as well as earthquakes, plagues, and pestilence.

[2] Random variability can be associated with repeated measurement of a highly controlled experiment as well as with a series of observations of naturally occurring phenomena. In the former, deterministic variations are often term *bias* and influence the *accuracy* of the measurement—as in variations in measuring the weight of an object due to improper zeroing of the scale. Random variation describes the dispersion or spread in measurements associated with uncontrolled factors. Random variation influences the *precision* of the measurement and the number of significant digits (decimal places, order of magnitude) reported.

a) Data Record

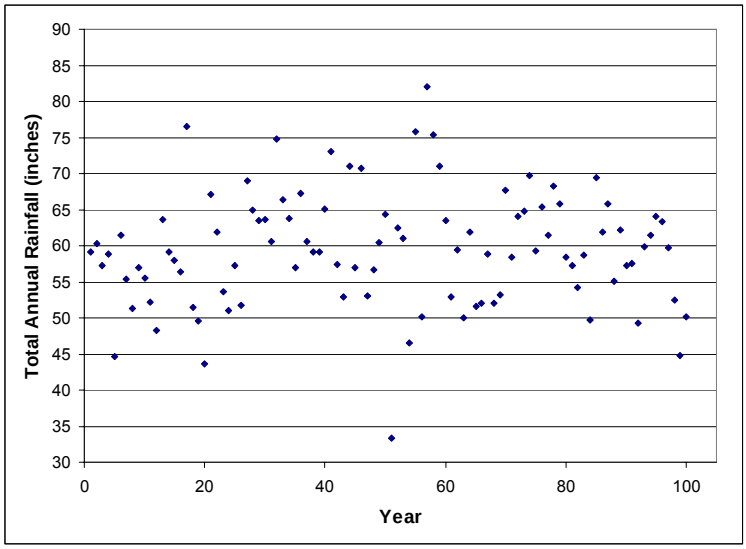

b) Data Ranges versus Percent of Records

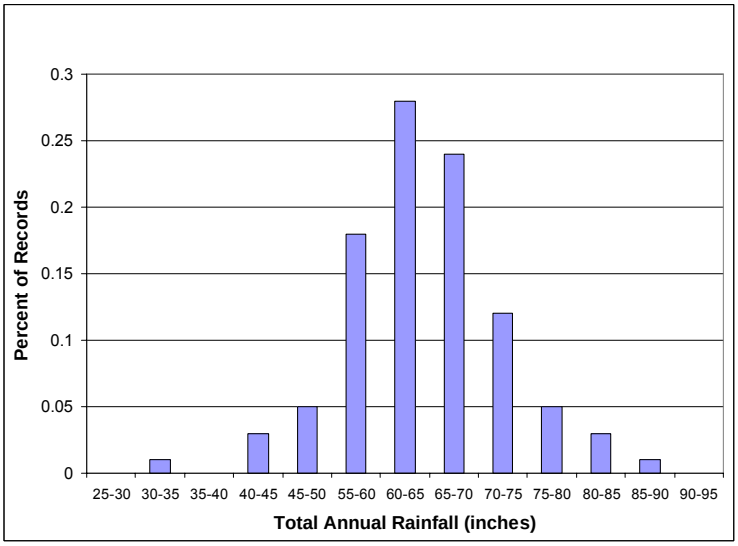

c) Data Ranges versus Cumulative Percent of Records

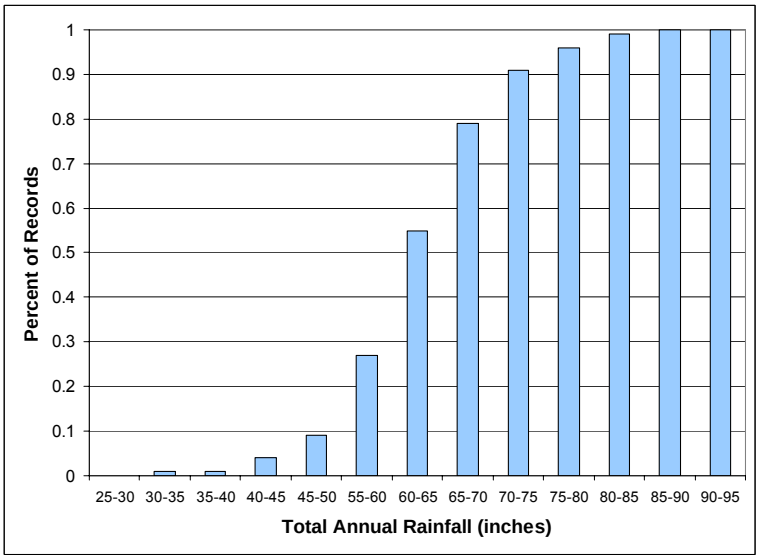

Figure 1. Variability in Total Annual Rainfall

and the y-axis indicating the fraction of total observations, or *relative frequency*, for each range. Here the x-axis spans less than one order of magnitude. Figure 1c shows the cumulative fraction of total observations. This variability pattern approaches a central peak with symmetrical tails.

Another case, shown in Figure 2a, b, and c, is the variability in a set of soil permeability (to infiltration) data. In this case, the x-axis spans nearly 3.5 orders of magnitude. These data display a very asymmetric pattern.

Mathematicians have developed idealized quantitative relationships—i.e., functions, equations—to characterize these and other patterns of relative frequency. These equations describe perfect curves and allow for precisely calculable *probabilities* for any discrete value—i.e., for each individual potential value of annual rainfall or soil permeability.

B. Normal Distribution

The most well-known symmetrical probability function is the *normal (or Gaussian) distribution Function.* Figures 3a and b illustrate the "bell curve shaped" probability density function (PDF) and the "S- shaped" cumulative distribution function (CDF) forms of the Gaussian distribution, which correspond to the relative and cumulative frequency plots in Figure 1b and c. A normal distribution function is defined by two parameters that describe two moments, i.e., points about which various considerations of the distribution "weight" are balanced. These are the *mean* (around which the two sides of the distribution balance, abbreviated as μ) and the *variance* (which describes the distribution on either side of the mean; the variance is an averaged square difference between each record and the mean). The square root of the variance is the *standard deviation* (abbreviated as σ) which is often referred to instead of the variance. The value of σ/μ is a normalized standard deviation and termed the *coefficient of variance* (CV). Figure 4 illustrates the changing shape of the normal distribution with changes in CV.

The formula for the probability density form of the normal distribution is :

$$f(x)=\frac{1}{\sigma\sqrt{2\pi}}e^{-\frac{1}{2}\left(\frac{x-\mu}{\sigma}\right)^2}$$

Figures 5a and b illustrate an important aspect of the normal distribution. For any normally distributed data, fixed percentage of data lie between μ and plus one, two, three (etc.) σ: 34.1%, 47.7%, and 49.8%, respectively. Given the symmetry of the distribution the same percentages lie below μ within multiples of minus one, two, three (etc) σ. Similarly, any percentage of values surrounding μ corresponds to a multiple of the σ. For example, 80, 90, and 95 percent of all records lie within ± 1.28σ, 1.65σ, and 1.96σ, respectively. In these cases 10%, 5%, and 2.5% of all records lie outside on the upper tail, and 10%, 5%, and 2.5% also lie on the lower tail.

In order to describe variability with a normal distribution μ and σ. are calculated for the data—in the case of Figure 1a μ and σ are 60 and 8 inches, respectively. As depicted in Figure 6, the data plot can be compared to the ideal curve (heavy blue line). Note that most of the observed relative frequencies do not line up directly on the curve and are offset by varying amounts and there is some variability in fitting the normal distribution to the data. In other words there is some *uncertainty* regarding whether this particular normal distribution curve—which is based on the estimates of μ and σ—truly reflects the random variation in annual rainfall.

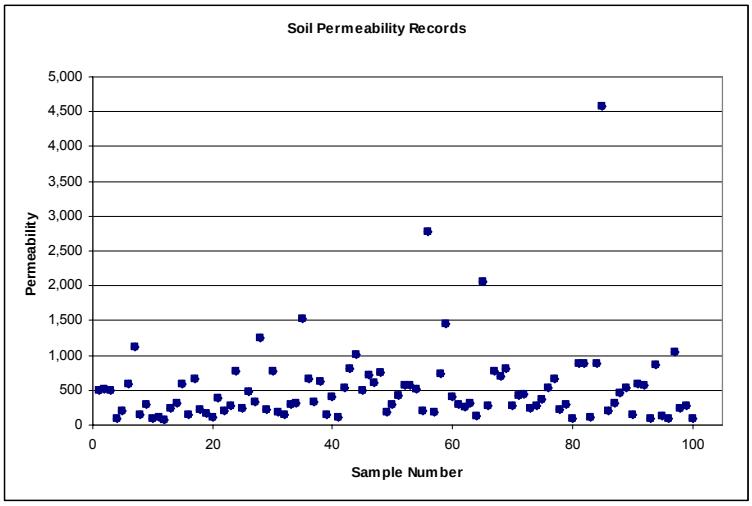

a) Data Record

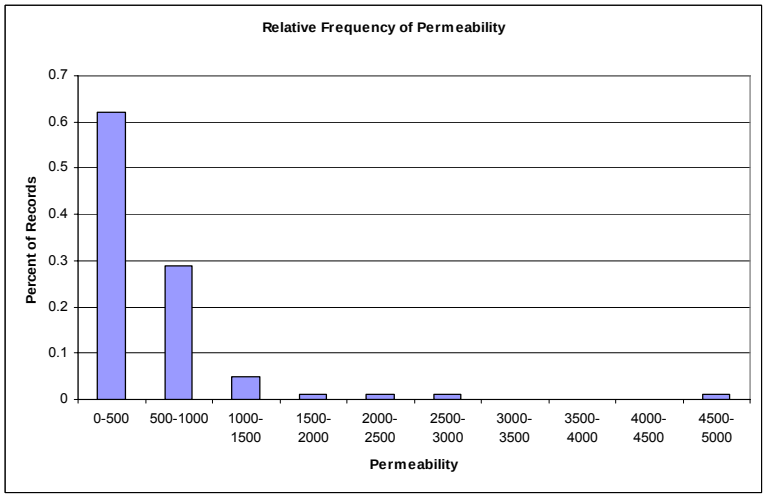

b) Data Ranges versus Percent of Records

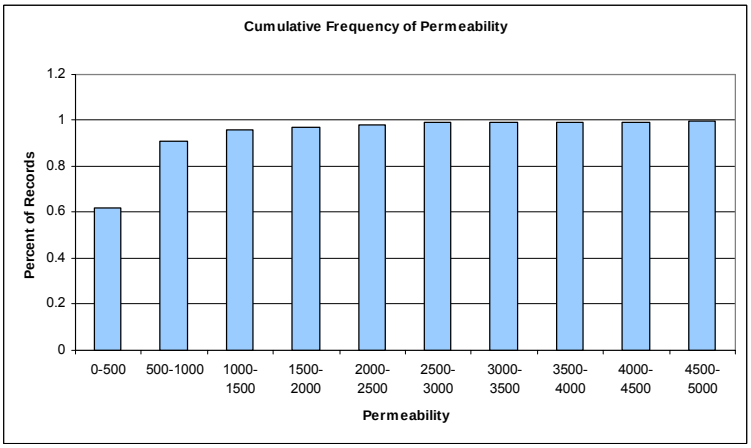

c) Data Ranges versus Cumulative Percent of Records

Figure 2. Variability in Soil Permeability
(Hypothetical Location)

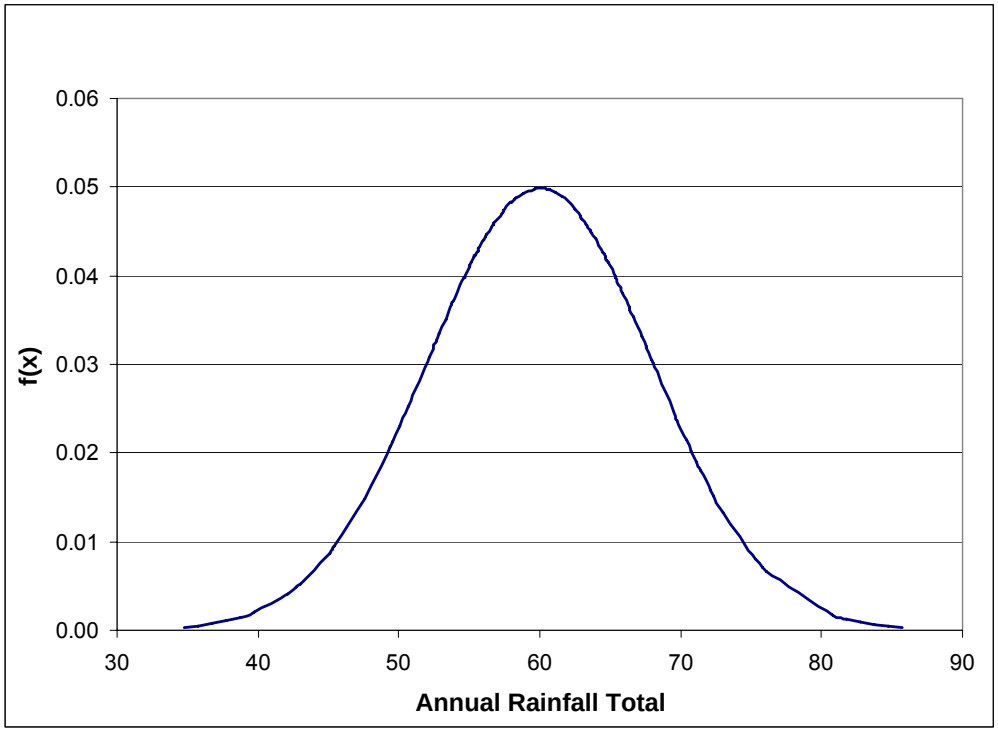

a) Probability Density Form

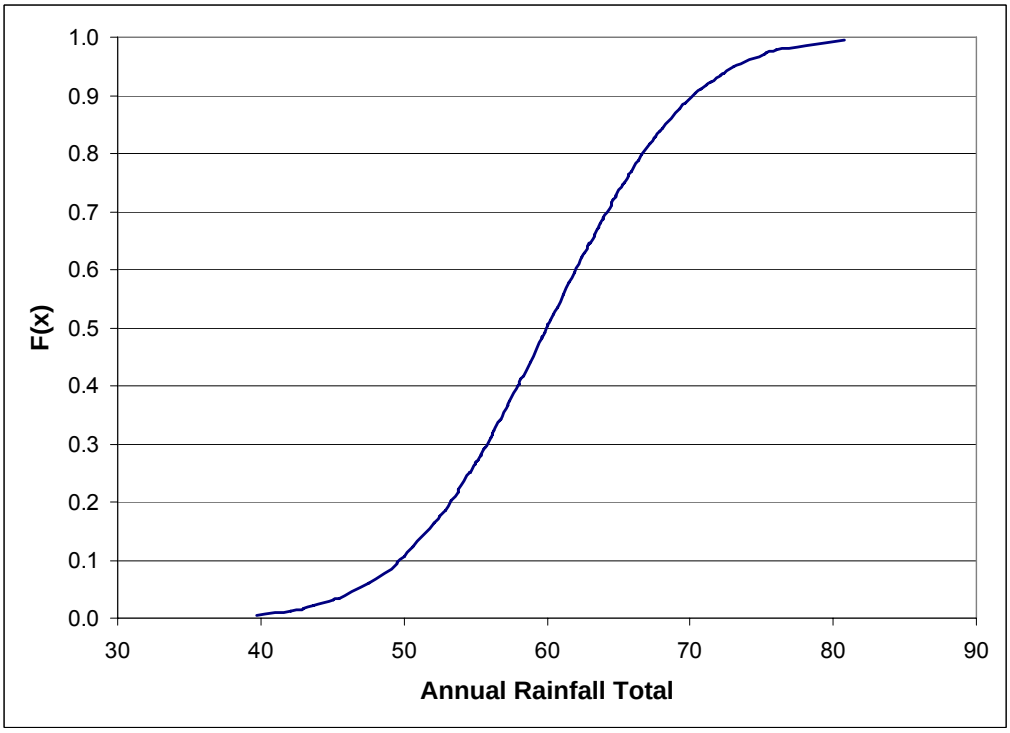

b) Cumulative Distribution Form

Figure 3. Normal Distribution Function

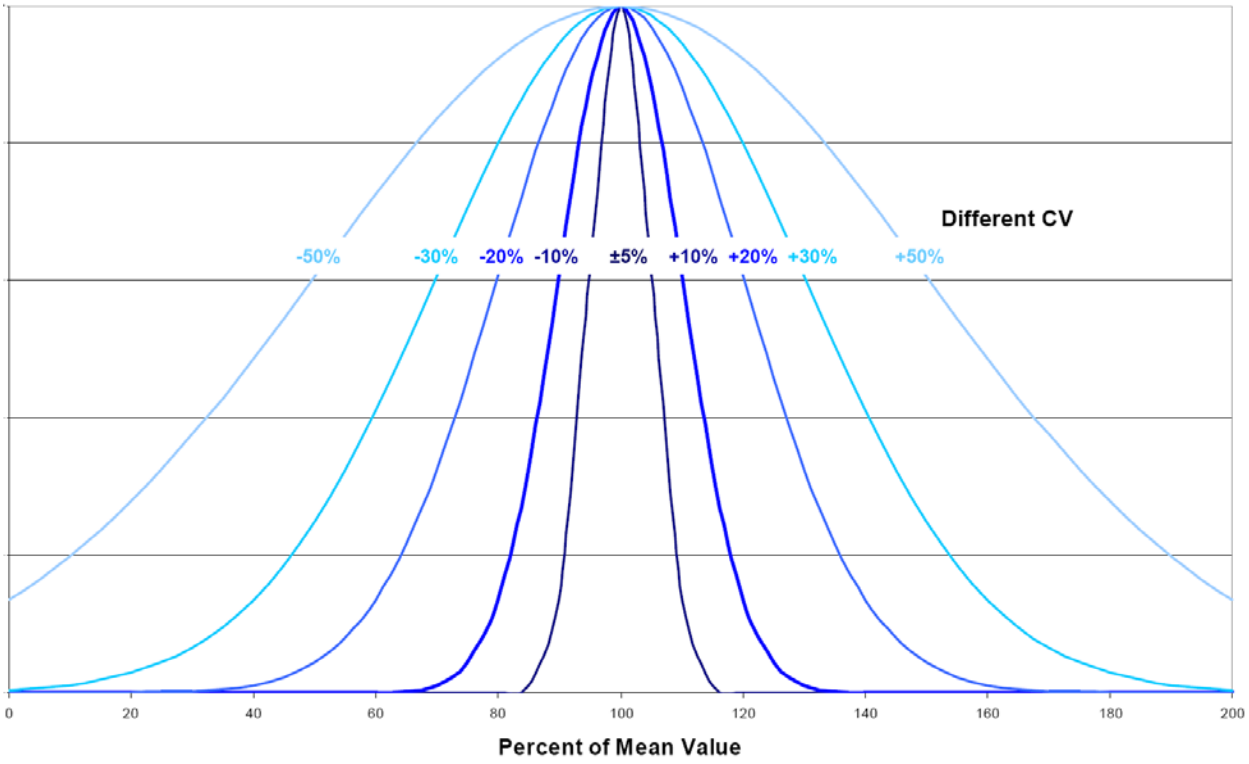

Figure 4. Changing Shape of Normal Distribution for Different CV

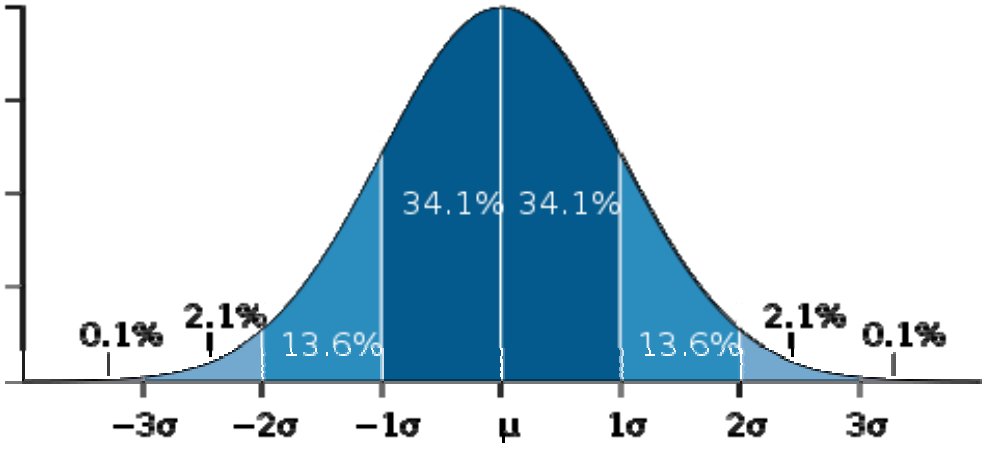

a) Percent of Data Lying Within +/- 1σ, 2σ, and 3σ From μ

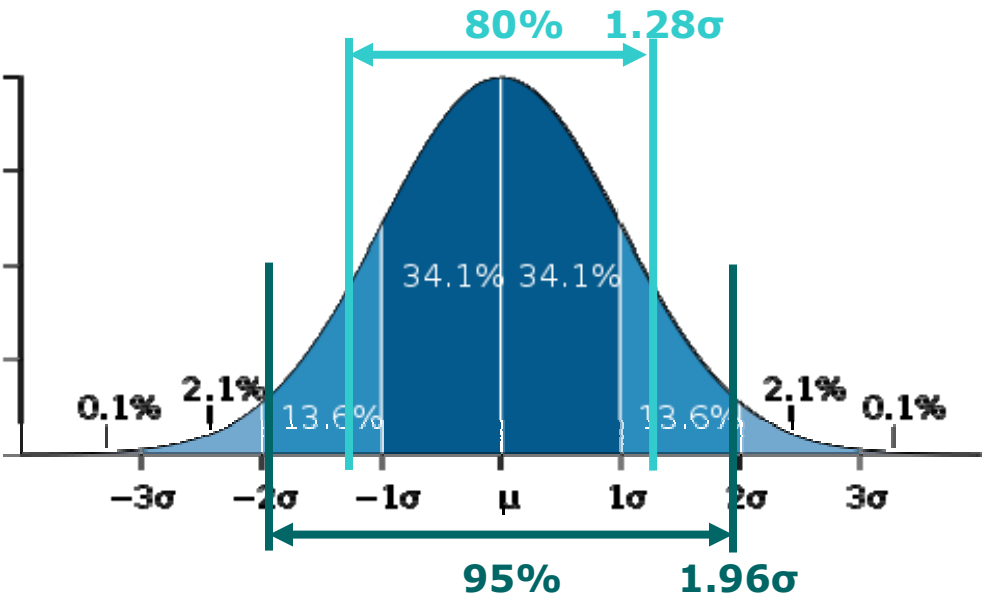

b) Values for σ Corresponding to 80% and 95% of Data

Figure 5. Percent of Data and Standard Deviation for Normal Distribution

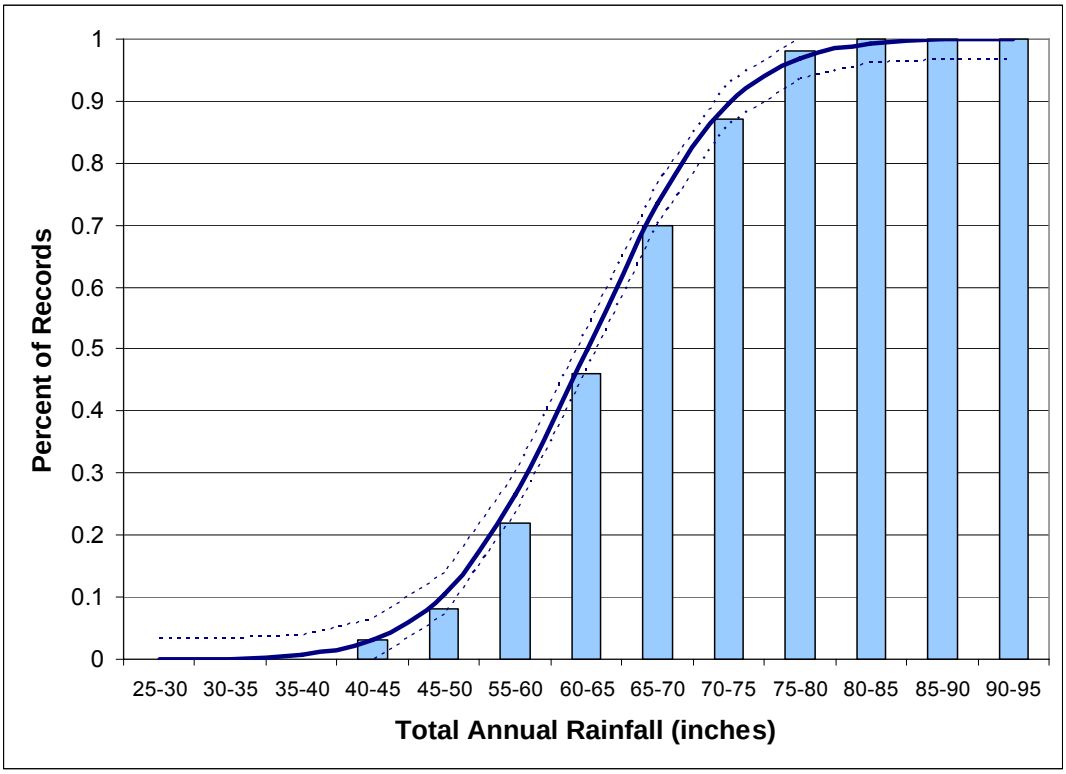

Figure 6. Cumulative Frequency Data and Cumulative Distribution Function

C. Uncertainty in Estimates

Hydrologists not only use probability distribution functions to characterize the variability of observations—such as by plugging annual rainfall record values of μ and σ into the normal distribution equations—they also use distribution equations to characterize uncertainty regarding the dataset μ and σ and the distribution. The values for μ and σ used to construct the solid blue curve in Figure 6 are the *most likely estimate of μ and σ based on the dataset*, but the actual mean and standard deviation could be expressed as a range—e.g., μ as 60 inches, ± some amount. Thus, the whole normal distribution curve could also be expressed as a range with uncertainty bands above and below the solid blue line (see Figure 6). This can seem confusing as it is basically estimating a probability for a probability estimate.

In the case of normally distributed data, the uncertainty for the estimates of *μ and 1σ* (and any point) can be calculated using well established statistical techniques. For example the ± band around the estimate of the mean uses a symmetrical distribution known as the Student's t distribution. The ± band of uncertainty for an estimate is referred to as an *Uncertainty or Confidence Interval* and the bounds are referred to as *Upper and Lower Confidence Limits, UCLs/LCLs*. UCLs/LCLs are typically set such that the Confidence Interval captures a high percentage of the possible values. For example a 95% confidence interval for the value of μ would be 60 inches ± 1.6 inches.

D. Deterministic Analysis

Hydrologists first examine data with a view toward identifying deterministic relationships, or correlations. *Correlation analysis* evaluates the variability in one dataset characteristic versus one or more physical factors, e.g., the flood stage at a point in a river versus the discharge (flow). Particular correlations between factors do not prove a specific cause-and-effect relationship—two factors may be products of a third factor—but are evidence of deterministic aspects of observed variability. For example, while flood stage and discharge at a river location are correlated, the actual physical cause-effect relationship is more complex, involving flow routing considerations over the entire river segment. A common application of correlation is *trend analysis,* which examines a characteristic versus time, termed a time-series (e.g., a stage hydrograph).

Correlation and trend analyses are usually done in conjunction with data graphs—such as Figure 7a. Using the general shape of the graph, hydrologists identify evidence for the presence of linear or other mathematical relationships—polynomial, exponential, power function, periodic oscillation, etc. In some cases the equation for a line or curve has been established—rooted in physical or mathematical theory or a large body of previous *empirical* work (experiments or observations)—and the hydrologist seeks values for the coefficients to optimize the fit. In some cases the full equation with coefficients has been established and the hydrologist will corroborate the coefficient values. In cases where a line/curve type has not been predetermined, the hydrologist relies on fundamental physical understanding to propose certain equations and then tests the equations with coefficients to fit the data. The process of fitting a line or curve to the data is known as *regression analysis*.

The fit of any proposed mathematical relationship to the data is analyzed in several ways:

- The error (difference) in the y-value for each point versus the y-value associated with the proposed line is calculated and squared (square difference or error) and then summed—referred to as the sum of the square error (SSE). The square root of the mean square error (RMSE) is analogous to a σ between the data and the proposed line/curve. RMSE for different proposed lines/curves and coefficient values can be compared. The normalized RMSE, dividing by μ, is termed the CV(RMSE) or the Scatter Index (SI).]
- The difference between each data point and the data mean, squared, and then summed is the sum of the square total, SST (analogous to the overall data variance). The difference between SST and SSE (SST – SSE) is the amount of variance in the data accounted for by the proposed line or curve. The quantity

$$R^2 = \frac{(SST - SSE)}{SST} = 1 - \frac{SSE}{SST}$$

  is the fraction of total variance explained by the proposed line/curve and is referred to as the coefficient of determination (sometimes the correlation coefficient). A high R^2 (e.g., above 0.9) is indicates that a large percentage in the data variation can be explained by the proposed line/curve. A hypothesis test is also used.[3]

[3] The probability that we can reject a hypothesis that the relationship is not valid (that we can reject the null hypothesis) is called a chi squared, χ^2, test.

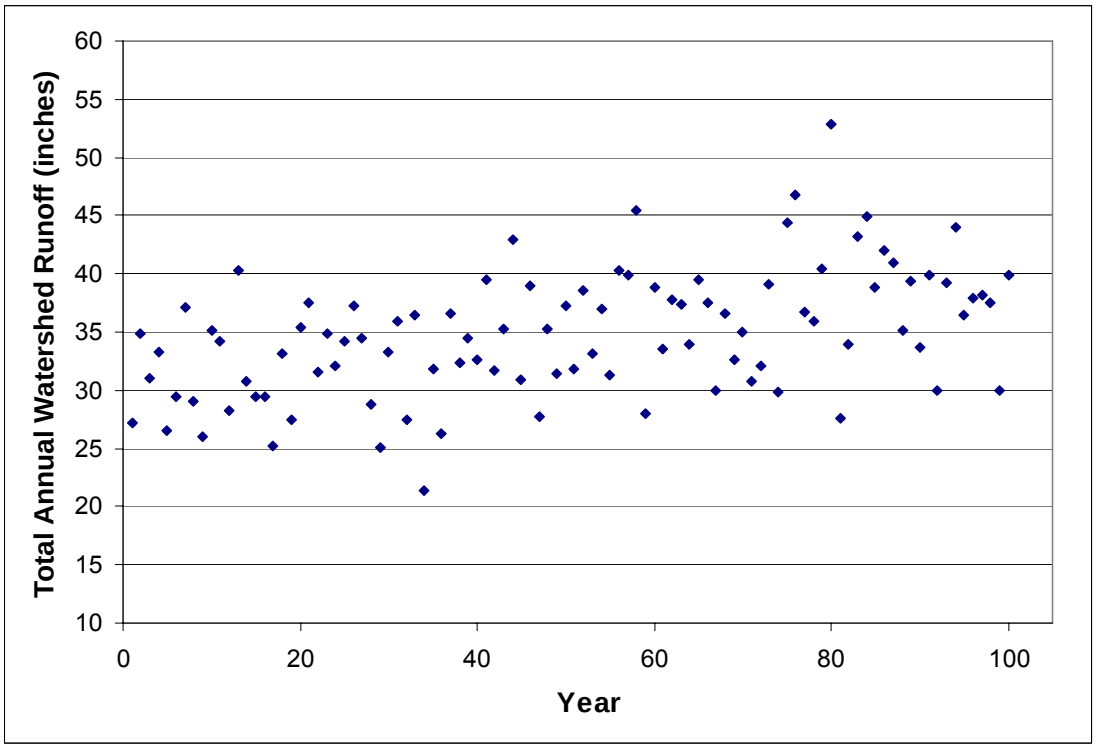

a) Data Record

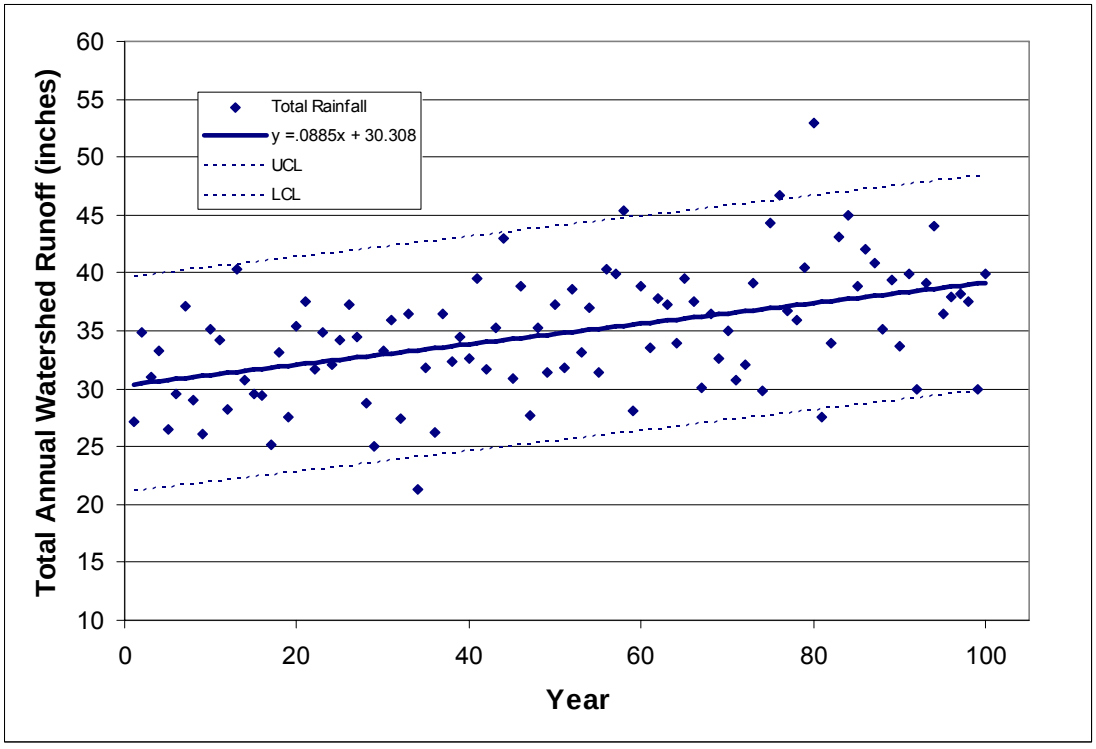

b) Data Record with Linear Trend

Figure 7. Long-Term Trend in Watershed Runoff

- The distribution of the residual error (variance) in the data apart from the variance explained by the line/curve. Often the residual error shows some evidence of a normal distribution, and RMSE (or σ for the residual error) is then used to define the UCL and LCL above and below the correlation/ trend line (or curve). The spread of UCL/LCL bands is also an indication of fitness.

Figure 7b shows the linear trend analysis for the data in Figure 7a.

Data μ	34.8	SST	2,887
Data σ	5.4	SSE	2,234
Linear Trend:	y = 0.09x +30.1	RMSE	4.73
		R^2	0.226
95% UCL/LCL	y = 0.0885x +30.308 ± 9.27		

Importantly the R^2 of 0.226 is not that high due to considerable residual variance.

The correlation of many physical factors with flood conditions—e.g., climatological, topographical, land cover, river modifications factors, etc.—is an important subject in flood hydrology, with some correlations having a direct bearing on flood forecasting. Short- or long time changes in climate e.g., El Nino, sea level rise, etc.) and floodplain and river morphodynamics (changing river shapes, depths, gradients, etc), are major subjects of flood trend analysis.

E. Conventions for Confidence Intervals

The normal distribution is used ubiquitously in scientific and engineering to evaluate random variability and estimate uncertainty. Different scientific and engineering endeavors adopt different conventions for describing variance or uncertainty. In experimental scientific literature a 95% Confidence Interval is often used to express the quality of data statistics and trend analysis. A 95% Confidence Interval has LCLs and UCLS spanning from 2.5% to 97.5% of the distribution, i.e., with 2.5% variability on each tail outside the interval.

In hydrologic design the selection of a Confidence Interval is subject to interpretations regarding risk—the consequences associated with events outside the selected interval. Goldman in 2003 (Goldman 2003) cites the use of a 90% Confidence Interval for the certification of levees along the Upper Mississippi River.

Manufacturing quality control and assurance practices often use the term Six Sigma, which refers to six standard deviations—three for each tail. Six Sigma encompasses 99.6% of the normal distribution (see Figure 5b). Manufacturing items to a tolerance of six sigma can be a rigorous quality control standard depending on the value of σ.

When uncertainty is a concern on only the upper (or lower) tail of the distribution a convention may describe the probability of values below (or above) a reference point on that tail. Figure 8 illustrates a 90% probability of values being below a point on the upper tail of a normal distribution—referred to as a 90% probability of non-exceedance. This is the same as having 10% of the values remaining on the upper tail. This 90% probability of non-exceedance is equivalent to the 80% UCL. This can be confusing as the probability of non-exceedance and the UCL are **NOT** the same number.

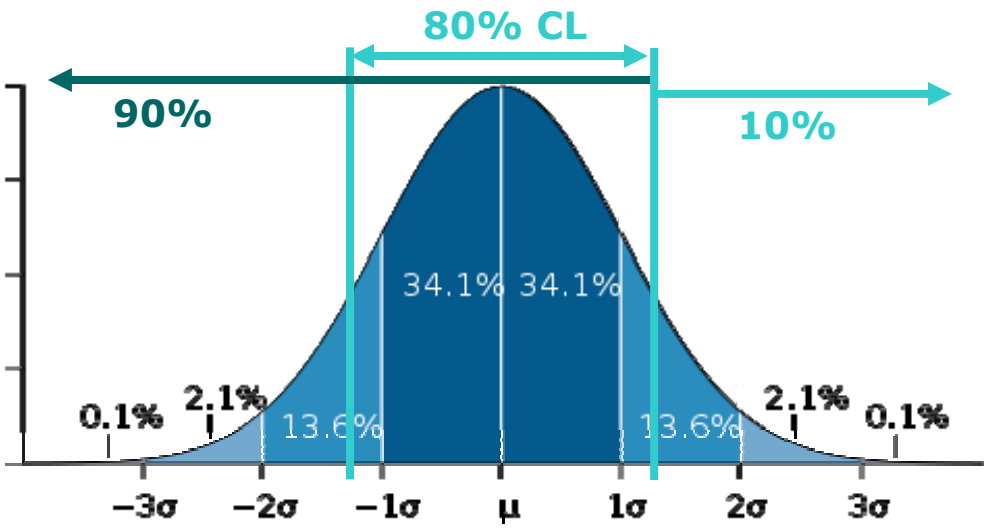

Figure 8. Probability of Non-Exceedance and Confidence Limit

F. Other Probability Distributions

The normal distribution does not adequately describe the variability of many probabilistic processes. Some common examples are:

1. Asymmetric or skewed distributions. In some data, tail observations are more prevalent and extended on one side of the distribution, resulting in differences between the mean (average), median (50th percentile) and mode (highest observed frequency). One type of asymmetric distribution is the Skewed normal distribution, which modifies the normal distribution with the addition of a third moment called the coefficient of skewness (α). Figures 9a and b show the PDFs and CDFs for the Skewed normal distribution.

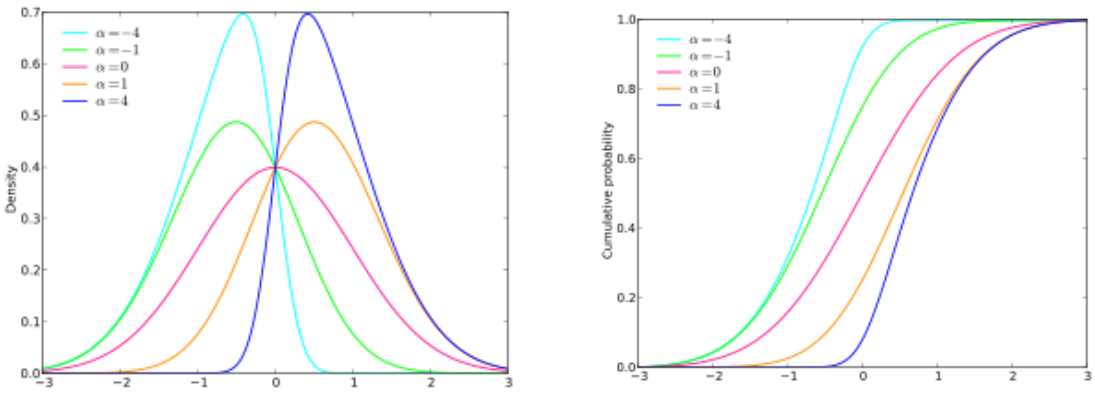

a) Probability Density b) Cumulative Distribution

Figure 9. Skewed Normal Distribution

http://en.wikipedia.org/wiki/Skew_normal_distribution

2. Log normal distribution. When data are highly skewed, with x values stretched over several orders of magnitude, similar to Figure 2, the distribution of log (x) can be evaluated. (i.e., log(10) =1, log(100) =2, log (500) = 2.699, etc.) Figures 10a and b present the untransformed and the transformed probability density functions for the data from Figure 2.
3. Pinched/rounded distributions. Figure 11 shows several symmetric distributions affected by squeezing the peak and fattening the tails (e.g., red),[4] or vice versa (e.g. blue). In these example distributions the multiples of the standard deviation do **NOT** encompass the normal distribution percentages of variability. This property can be described by adding consideration of a fourth moment of a distribution called kurtosis. In addition to kurtosis it is possible to use other shape parameters comprised of higher moments. Kurtosis and higher moments can also apply to asymmetric distributions.

Mathematicians and scientists have defined numerous distribution formulas taking into account combinations of data transformation, skewness, and shape parameters. When any probability distribution is used to describe variability in an observation, the same distribution is appropriate for characterizing the uncertainty in estimates (Chow et al.1988). Thus, if random variability is fitted to a skewed distribution, the uncertainty should also be considered to be skewed.

G. Return Frequency

As noted above, for a record of observations collected over a defined period of time[5]—such as the 100-year record of annual total rainfall—hydrologists can calculate relative frequencies and define idealized mathematical probabilities, expressed as percentage of observations. In the above case the calculated 5% relative frequency is 71.7 inches using the 95th ranked value and the estimated 5% probability is 73.0 inches using the normal distribution and dataset μ and σ. In addition, hydrologists can describe relative frequencies in terms of *return or recurrence interval* and estimate the probability of how often a particular annual rainfall magnitude can be expected to occur, or what magnitude is associated with a particular recurrence interval. To understand return frequencies and return probabilities it is important to first review four key terms.

1. The *event* is a measured or calculated data point (can be an instantaneous or cumulative measurement) with a magnitude, such as an hourly, daily, monthly, and annual rainfall accumulation; a peak flood stage or discharge (flow); a daily high tide; etc.
2. The *time-frame*, τ, is a duration under consideration over which many events of varying magnitude have or may occur (regularly or irregularly). The time-frame can be an historical record (such as 30 years, 10,950 days, of daily rainfall data) or a hypothetical (or future) time length for which recurrence is being analyzed (e.g., 100 years).

[4] The term “fat tail” has been made famous in the post-2008 discussion of the massive losses on supposedly low default probability mortgage credit instruments and the ensuing financial meltdown. Credit ratings and instrument pricing are heavily dependent on statistical analyses of default probabilities. Underestimated low probabilities have been called “black swan” events. (see Taleb, 2010)

[5] It is not necessary for the data to be collected at regular intervals, e.g., peak river flood data.

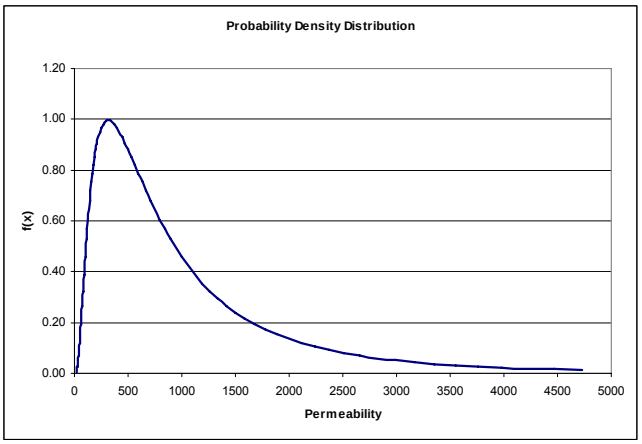

a) Probability Density for Untransformed Data

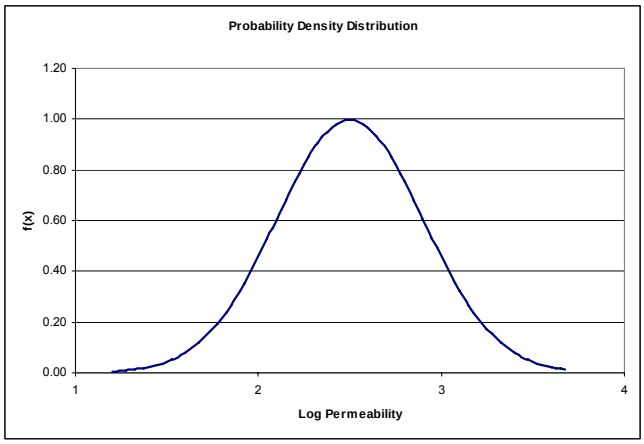

b) Probability Density for Transformed Data, log(x)

Figure 10. Log Normal Distribution (data in Figure 2)

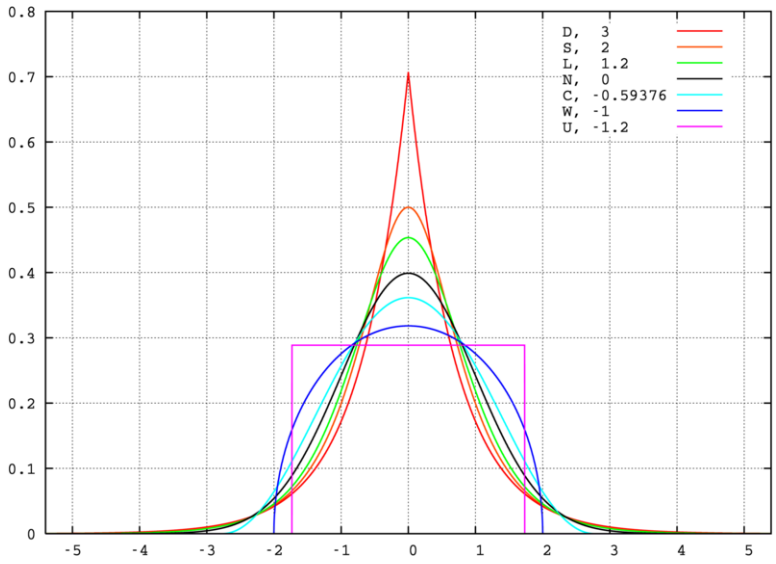

Figure 11. Distributions with Kurtosis

http://en.wikipedia.org/wiki/Kurtosis

3. The *return frequency*, F_R, for an event of *a particular magnitude or greater*. For data of duration τ the *nth* record has an *observed* F_R of n/τ . For example, if the daily rainfall has exceeded 6 inches 10 times (n = 10) during a 30-year record (τ = 10,950), F_R is 10/10,950 = 0.000913 = 0.0913% (expressed *per day*). If expressed *per year* F_R is 33.3%. The *observed* F_R is often modified as $n/(\tau +1)$ (in accordance with binomial distribution theory). In this case the F_R for a 6-inch rainfall is still 0.0913% per day. The highest ranked event for 100 years of data is 0.99% (instead of 0.1%) per year.

   For the higher ranking events, hydrologists may not consider τ to be sufficiently long enough to calculate a reasonable F_R. using $n/(\tau +1)$. To compensate hydrologists often modify *observed* F_R using $(n - a) / (\tau + 1 - 2a)$, where a is typically between 0 and 0.5. If a is taken as 0.3, the F_R of the top ranked event from a list of 100 annual records is 0.7% per year. As with the calculation of relative frequency, F_R requires a complete, accurate, representative record.

4. The *return period, T,* (or recurrence interval), is the <u>average</u> interval between the events of a particular magnitude, and equals $1/F_R$. In the above 6-inch rainfall example the *observed T* is 1095 days or 3 years. The unmodified and modified observed return periods for the top ranked flood from 100 years of data (F_R of 0.99% and 0.7%) are 101 and 143 years.

For period in years F_R is also called the annual exceedance probability, which is equal to 1- F, where F is the cumulative probability for annual non-exceedance.

Return period is a widely used term in the scientific description of flood hazards and in flood planning and engineering. The Federal Emergency Management Agency (FEMA) National Flood Insurance Program (NFIP) uses the 1% and 0.2% return frequency floods—the 100 and 500-year return period (T_{100} and T_{500}) floods—to define properties subject to various program requirements. In turn, other federal, state, and local governments use these hazard levels to manage flood mitigation and control programs (including levee design). For urban street drainage studies hydrologists often use a return frequency of 10 years. For flood safety programs involving threats to human life and critical infrastructure and population centers (e.g., dam safety analysis) hydrologists often consider a 10,000-year return period.

Conceptually, it is important to note that F_R and T are calculated averages from the record τ and not fixed values. The 30-year record noted above could contain two consecutive days of 6-inch rainfall. Following the first day, the probability of an event occurring on the succeeding day is still 0.091% based on random independent occurrence. (A rainfall *forecast*, unlike an RFA, takes into account factors other than random occurrence that might make it more likely that two events could transpire so close together). The fact that two of the ten events take place on consecutive days DOES NOT alter the overall long-term frequency and return period. Not only can hydrologic events occur at much shorter intervals than the return period, they can also occur at much longer intervals. Two of the ten rainfall events in a 30-year record could be much more than three years apart.

For any specified return period (T) flood the likely number of recurrences over any time-frame τ shorter or longer than T is provided by a probability formula—known as the *Poisson distribution*. This means, for example, that a probability can be calculated for any number of recurrences—e.g., only once, at least once, exactly three, etc.—of a 100-year (1%) flood over any given time-frame. This probability is true for any 100-year event as it is not a function of the type event, the location, or the particular 100-year event magnitude.

Figure 12a illustrates the cumulative probability for the Poisson distribution. Curves are presented for four estimated average number of recurrences (1, 2, 5, and 10) irrespective of the time-frame (τ) and show the probability of at least that number of events actually recurring in that τ. For example, the

probabilities for floods expected to occur 1, 2, 5, and 10 times over a record actually occurring that many times or more are 63, 59, 56, and 54%, respectively.

The probability *P* of *at least one T (1/F_R)* flood of occurring in a given τ can be calculated using the following version of the Poisson distribution: [6]

$$P = 1 - (1 - F_R)^{\tau}$$

For example, the probability of a 1% flood occurring during a 30-year period, the length of a typical mortgage, is 26%. Again, this is true of 100-year floods everywhere. Figures 12a and b illustrate the increasing probability of occurrence with increasing τ for T_{10} , T_{20} , T_{50} , T_{100} , T_{500} , and T_{1000}. The cumulative distributions for at least one recurrence are illustrated in Figure 12b.

Importantly, as revealed in Figure 12b, the probability of a *T* flood occurring at least once in τ equal to T is **NOT** 100%. The probability of a T_{100} flood (or greater) occurring during a given 100 year time-frame is 63%. The probabilities do not exceed 95% and 99% for at least one *T* occurrence until τ approaches 3*T* and 5T. Not illustrated on the figure but also of note, the probability for at least three *T* occurrences does not exceed 95% until τ approaches 7*T,* and 9*T* for at least five occurrences. *Thus, records for evaluating return frequency floods should be many times longer than the return periods of interest.*

H. Return Frequencies as a Function of Magnitude

In many cases sufficiently long records are not available for evaluating extreme return period floods. Furthermore, there is often reason to suspect that highly ranked floods are of much lower return frequency than would be estimated (e.g., a flood ranked 1 out of 100 years appears to be well beyond a 143-year return period based on flood records at other nearby watersheds). In these cases hydrologists need to estimate extreme *T* (or 1/F_R) as a function of flood magnitude, and vice versa. Hydrologists therefore employ probability distributions which describe (i.e., model) a correlation between the increasing flood magnitude and increasing return period (declining return frequency).

Figure 13a presents a 44-year record of annual peak river flow (Chow et al 1988). Figure 13b is a graph of the modified return period versus magnitude—thus the return period for the 1/44 ranked event is 44.4/0.7 or 63 years. Figure 13b shows that the normal distribution (using data μ and σ) is a poor fit, even below the 10-year return period. Modeling the relationship between flood magnitude and return period can usually be improved with probability distributions which accommodate combinations of a) log, exponential, or other power function transformations of the return period, b) skewness, and c) kurtosis and additional shape parameters.

---

[6] This equation is a cumulative distribution for the Poisson Distribution. Note this is the case of *at least one* recurrence and the probability is greater than for the case of *exactly one* recurrence. For a Poisson Distribution the probability of *exactly one* recurrence in T is

$$P = T * F_R * \exp(-T*F_R) \text{ OR approximately } P = T * F_R * (1 - F_R)^{T-1}$$

For a 100-year flood or greater, the probability of one and only one recurrence in 100 years is exp(-1) or 37%. Over large T, the Binomial Distribution converges to the Poisson Distribution

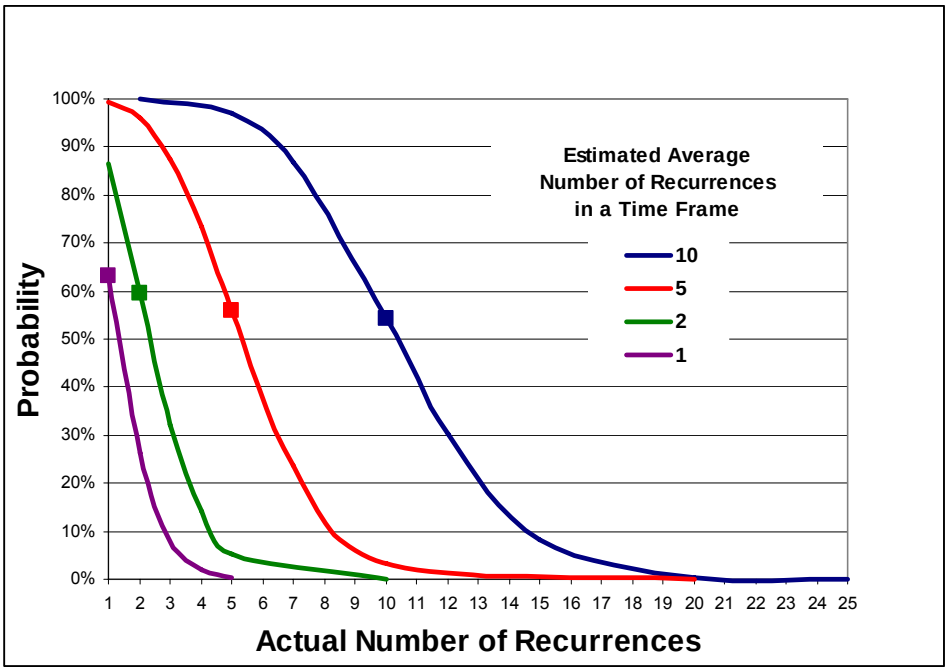

a) Cumulative Probability of Recurrences for Any Time-Frame Greater Than or Equal to Estimated Average

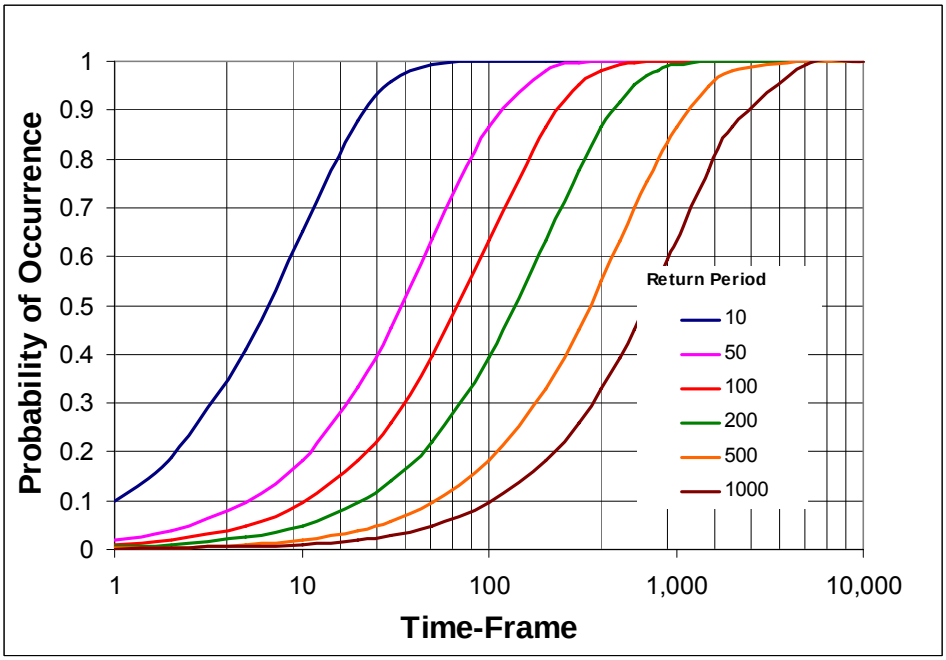

b) Cumulative Probability For At Least One Recurrence of a Return Period Event Over Different Time-Frames (Log Scale)

Figure 12. Poisson Cumulative Distribution

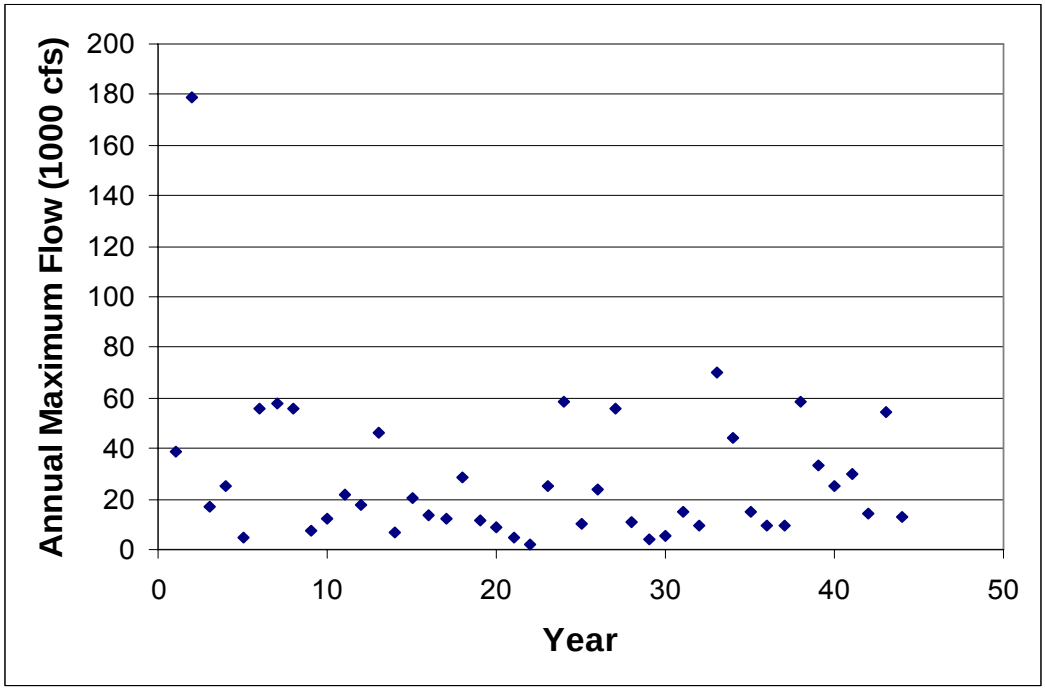

a) Data Record

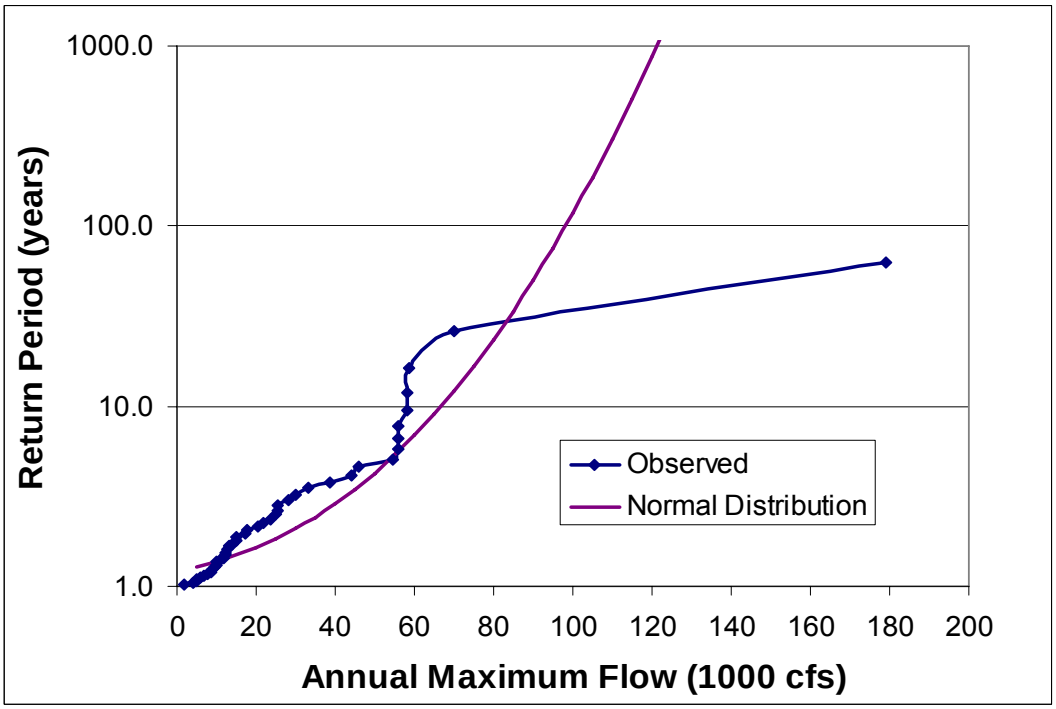

a) Observed versus Normal Distribution Return Period

Figure 13. Example Annual River Flood Data

Several common probability distributions used in describing extreme return frequencies are:

- Log-normal distribution, takes the logarithm of the return period (log (100) = 2) and uses a normal distribution of the magnitude versus log transformed return period (or return frequency); defined by two parameters, mean and the variance.
- Log Pearson Type III distribution, adds the coefficient of skewness to the log-normal distribution and reduces to the log-normal distribution when coefficient of skewness equals zero.
- Generalized Extreme Value, (GEV) distribution includes three parameters: the mean, variance, and a shape parameter in an exponential form. The shape parameter allows for a higher probability of extreme values, i.e., a"fat tail" (Gordon 2004; Zervas 2005).

  The GEV Type I, or Gumbel, distribution, has a shape parameter equal to 0, resolving to a fixed coefficient of skewness of 1.14. The GEV Type 1 is defined by two parameters, μ and σ, with a double exponential equation.

  The GEV Type II, or Frechet, distribution has an adjustable skewness and shape parameter, allowing for a fatter tail.

  The GEV Type III, or Weibull, distribution has fatter peak and the tail goes to zero at an extreme value.

  Figure 14 illustrates the three GEV type distributions.
- Generalized Pareto distribution, a three parameter power law function.

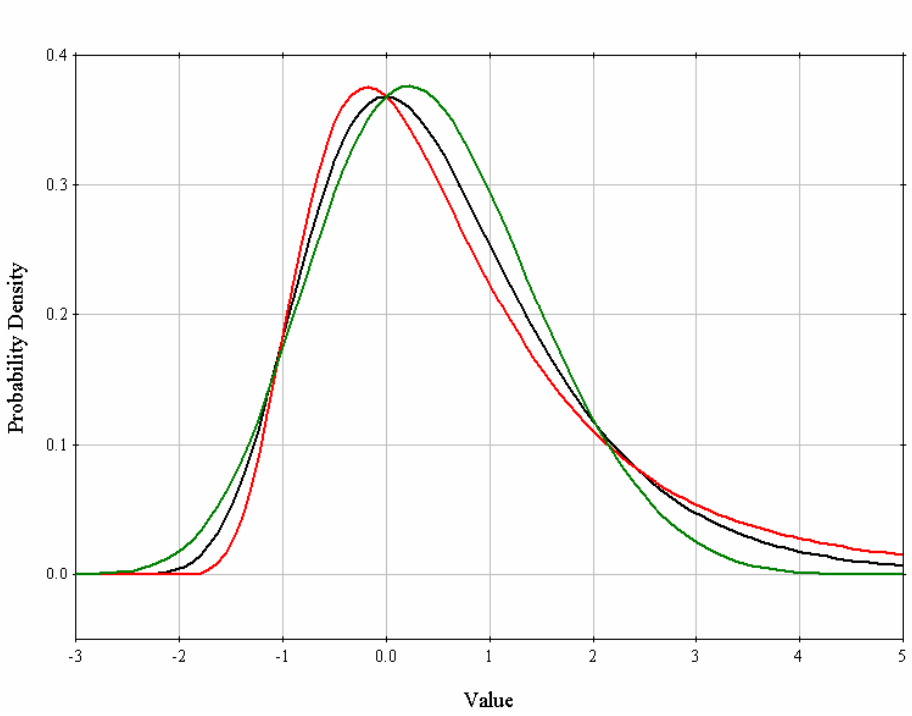

Figure 14. Example of GEV Distributions

GEV Type I (black), GEV Type II (red), GEV Type III (green). (Zervas 2005)

To apply these probability distributions to a long-term flood record hydrologists first determine dataset usability based on length, continuity, vertical accuracy (see GTN 2), and other sources of error. Next they determine dataset μ, σ, skewness, kurtosis, and other shape moments. The hydrologist then calculates values for the equation parameters using the dataset statistics. For example, the CDF, F(x), for the GEV Type I (Gumbel) distribution is:

$$F(x)=\exp\left(-\left(\exp\left(-\frac{x-u}{\alpha}\right)\right)\right)$$

$$x = flood\,magnitude$$

$$u=\mu-0.5772\alpha$$

$$\alpha=\frac{\sigma\sqrt{6}}{\pi}$$

The quality of the fit can be assessed for the lower ranked events. The purpose of using one of these distributions is that the observed return periods for the extreme events appear to be underestimated so evaluation of fit with respect to these points is not appropriate.

Figure 15 shows the observed data and log normal, Gumbel, and Log Pearson Type III distributions for the 44-year flood record given in Figure 11. As shown in Figure 14, all three distributions are better fits than the normal distribution for the 10-year return period and below. However, above the 10-year return period these equations can deviate markedly from the observations—and from each other. This is consistent with a record needing to be many times longer than the return period of interest in order to provide an accurate estimate. All three distributions indicate that the most extreme observed event (179,000 cfs) has a return period above 100 years—compared with the *observed T* of 63 years.

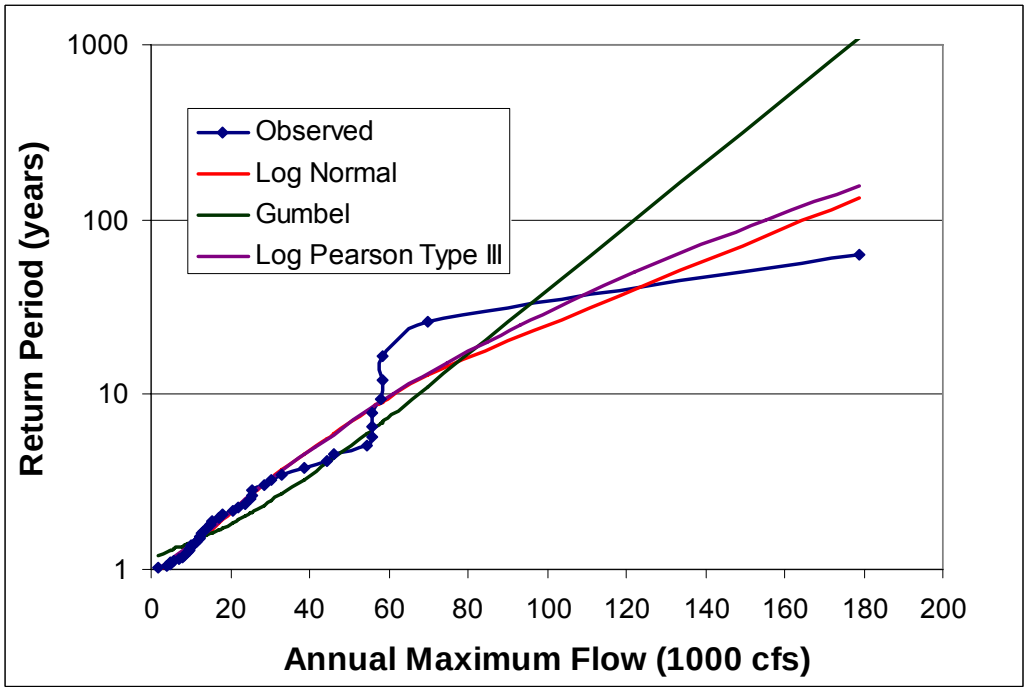

Figure 15. Frequency Distributions for Annual River Flood Data

Extreme return period flood magnitudes (e.g., 100-year or 500-year) can be estimated using a selected probability distribution. Table 1 presents the estimated 5-, 10-, 25-, 50-, 100-, 200-, and 500-year floods using the three distributions (log normal, Gumbel, and Log Pearson Type III) shown in Figure 14. These same return period floods are illustrated in Figure 16. The difference between the Log Pearson Type III and the log normal curves is a result of the skew in the log transformed record.

The estimates for the 5-, 10-, and 25-year return period floods are fairly consistent with each other and the observed return period—not surprising given the data record of 44 years. The estimates for 50-, 100-, 200-, and 500-years show increasing divergence.

Table 1. Estimated Return Period Floods for Three Distributions (1000 cfs)

Return Period (years)	Log Normal	Gumbel	Log Pearson Type III
5	41.0	49.9	41.1
10	61.7	67.5	61.3
25	95.4	89.8	93.3
50	126.3	106.2	122.1
100	162.6	122.6	155.3
200	205.0	138.9	193.3
500	271.3	160.5	251.6

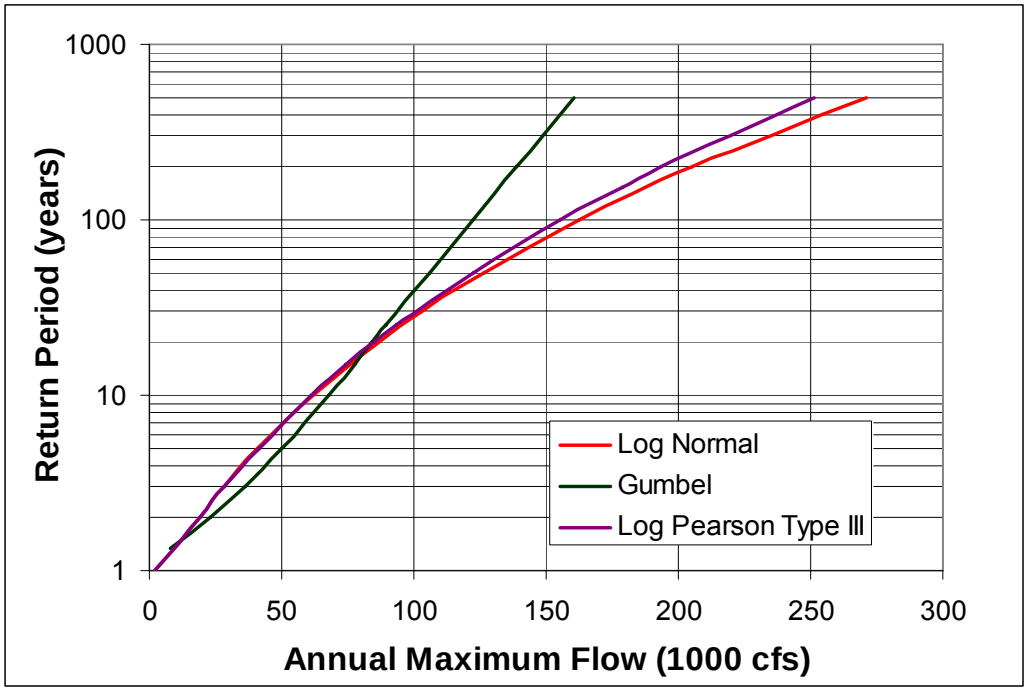

Figure 16. Estimated Return Period Floods for Three Distributions

In estimating an extreme return period flood magnitude it is important to also estimate the uncertainty of the estimate. Table 2 and Figure 17 illustrates the 90% Confidence Limits for the Log Pearson Type III distribution. Importantly, since the Log Pearson Type III distribution is skewed the confidence limits are also skewed. The interval between the mean and the UCL estimate is higher than the interval between the mean and LCL estimate.

Table 2. Confidence Limits for Estimated Return Period Floods for Log Pearson Type III Distribution (1000 cfs)

Return Period (years)	90% LCL	Mean	90% UCL
5	34.8	41.1	49.8
10	50.6	61.3	76.7
25	74.7	93.3	121.8
50	95.7	122.1	164.2
100	119.3	155.3	214.6
200	145.6	193.3	273.9
500	184.9	251.6	367.7

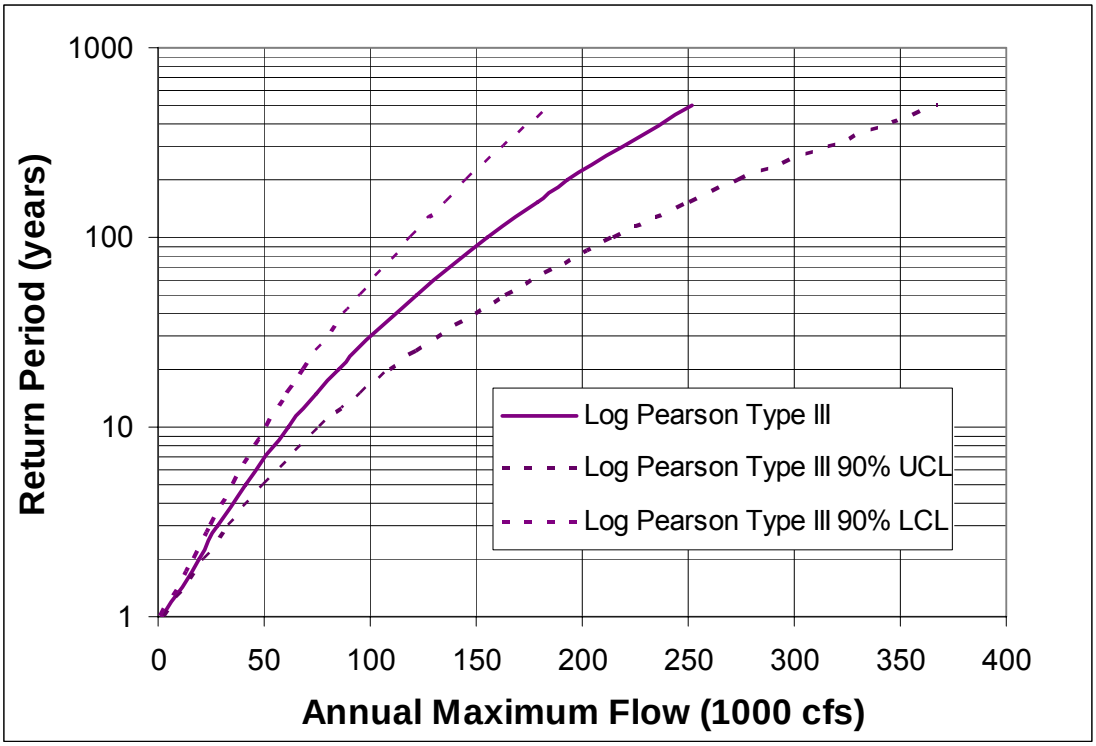

Figure 17. Confidence Limits for Estimated Return Period Floods for Log Pearson Type III Distribution

Over recent decades hydrologists around the world have used probability distributions to describe river flood return frequency, often using multi-decadal gauge records (McMahon and Srikanthan 1981; Nguyen and In-Na 1992, Karim 1995; Wang et al 2001, McCuen and Galloway 2010;), and occasionally using data on historic and paleo-floods (Kochel and Baker 1982, Benito et al 2004). Importantly, no one equation provides the best fit for all flood data, and the specific application of a particular curve type to the correlation of flood magnitude and return period could be deemed an example of "over-fitting," and is somewhat arbitrary—as the addition of more data over time could easily lead to selection of a different distribution. Any extrapolation for extreme floods also assumes that key conditions governing flood physics and meteorology during the record will remain constant. The published literature provides a basis for selecting a few probability distributions for evaluation. The Log Pearson Type III is the primary equation used by the US Geological Survey to evaluate river flood frequency (Chow et al 1988).

I. Joint and Combined Probability

When events are totally unrelated—i.e., the occurrence of one has no influence on the probability of the other—the probabilities of the two events are deemed *independent* (e.g., each successive coin toss in a series has an independent probability of 50% of turning up heads). Events can also be *dependent*, where the probability of one event depends on previous or concurrent events (e.g., drawing cards from a deck). Events are mutually exclusive if one event precludes the other from occurring.

When there is a conjunction of two or more independent events, each with its own probability distribution, joint probability is equal to the product of the individual event probabilities. When the number of independent events increases, the probability of conjunction rapidly diminishes. The joint probability for N successive coin tosses to all turn up heads is equal to 0.5^N; thus the probabilities of two through six successive tosses resulting in heads are 25%, 12.5%, 6.25%, 3.12%, and 1.56%.

Combined probabilities for multiple outcomes or multiple chances can also be computed. If the events are mutually exclusive, the combined probability is simply the sum of the event probabilities (e.g., the probability of rolling a 1 or 2 on a single dice roll is 33.3%, also the probability of rolling a 1 at least once on two rolls of a dice). When the events are not mutually exclusive the various joint probabilities must be discounted (e.g., the probability of rolling a 1 only once on two rolls of a dice). For low joint probabilities the combined probability approaches the sum of the individual probabilities. While joint probability declines with increasing number of events, the combined probability rises dramatically as the number of outcomes/chances increases. For six coin tosses, the probability of at least one heads occurring increases from 50% to 75%, 87.5%, 93.75%, 96.88%, and finally 98.4%.

The affect of uncertainty is different on joint and combined probabilities. In the former it is multiplicative whereas in the latter case it tends to be additive. If the probability of an event has been determined as a joint probability—e.g. an event has been determined to be a 100-year event as a result of the joint probability of three 21.3% events ($0.213^3 = 0.01$)—then increasing each of the three individual probabilities to 27.2% doubles the joint probability to a 50-year event.

J. Joint Probability Analysis

Joint probability analysis (JPA) becomes more complex with multiple independent events each described by a probability distribution. For example, consider a hypothetical case of three channels, with separate independent flow frequency distributions, which combine (assume steady flows) in a fourth channel. The flow frequency for the fourth channel is a joint probability of the three tributaries.

Suppose the daily flow averages range from 2,000 to 50,000 cfs for the first tributary, and from 1,000 to 20,000 and 1,000 to 18,000 cfs in the other two. If each tributary's flow is considered in 1,000 cfs increments, there are 17,640 probability combinations for the fourth channel. Any particular flow in the fourth channel—e.g., 40,000 cfs—could occur as a result of many different combinations—e.g., 20,000 plus 10,000 plus 10,000 cfs respectively; 16,000 plus 13,000 plus 11,000; etc.. If the CDFs are known for each tributary flow then their probability density forms can be used to calculated the resulting joint probability for any individual combination of tributary flows.[7] The joint probability (probability density form) for any combinations of tributary flows is the product of the corresponding probability densities.[8] To determine the flow frequency (CDF) for the fourth channel this product is integrated over the range of tributary flows.[9] Standard math software and a computer can easily calculate values for this integral using the 17,640 input combinations and thus estimate flow frequencies for the fourth channel. This approach is termed a full Joint Probability Method or Full JPM.

The flow frequency estimate (the estimate of the integral) for the fourth channel will improve with smaller input value intervals. Input values at a 100 cfs increment (17 million combinations) versus a 2,000 cfs increment (2,250 combinations) will provide a more versus less precise estimate compared to the 1,000 cfs increment. Thus, a full JPM would start with coarser inputs and then perform successive re-calculations until the resulting flow frequency estimates converge.

Another approach is the *Monte Carlo* JPM technique. This technique utilizes a large enough number of possible random combinations to satisfactorily determine the joint probability. In the Monte Carlo analysis, a frequency for each independent event is randomly drawn—for example a separate random number between 0.000 and 1.000 is selected for each tributary (three separate draws). After drawing a frequency for each tributary, the corresponding flow magnitudes for each tributary are found from the respective tributary probability distributions. These flow magnitudes are then added to give the flow in the combined (fourth) channel. The process is repeated, creating a *synthetic record* for the fourth channel, which is then evaluated using suitable probability distributions. More randomly derived records can be added until the probability distribution stabilizes. In cases where an optimal set of input combinations is difficult to determine in advance, the Monte Carlo technique can often be used to efficiently arrive at a stable estimate of the joint probability distribution.

Monte Carlo analysis can also be used to address uncertainty in the estimated magnitude associated with each individual input. For example after a frequency value is drawn for a particular tributary, an additional draw is used to determine the flow magnitude from the uncertainty distribution for possible values at that frequency—with the most likely flow value at that frequency having the highest probability of being drawn. This doubles the total draws for each calculation from three to six.

One difficulty in communicating joint probability is visualization. The joint probability "space" can be readily depicted for two independent events as a three-dimensional contour, as in Figure 18. However, for three or more events (as in the above case) such illustrations are not available.

---

[7] The cumulative frequency distribution form is referred to as F(x), where x is a particular flow and F(x) is the cumulative probability for flow equal or exceeding x with a value between 0 and 1.0, see Figure 3b for a normal Distribution. The probability density form is referred to as f(x), where f(x) is a discrete probability density value for a specific flow, x, see Figure 3a for a normal Distribution).

[8] Or $f(x_1 , x_2 , x_3) = f(x_1) * f(x_2) * f(x_3)$

[9] In calculus this is described by a triple integral, one for each tributary. $F(x) = \iiint f(x)\, dx$

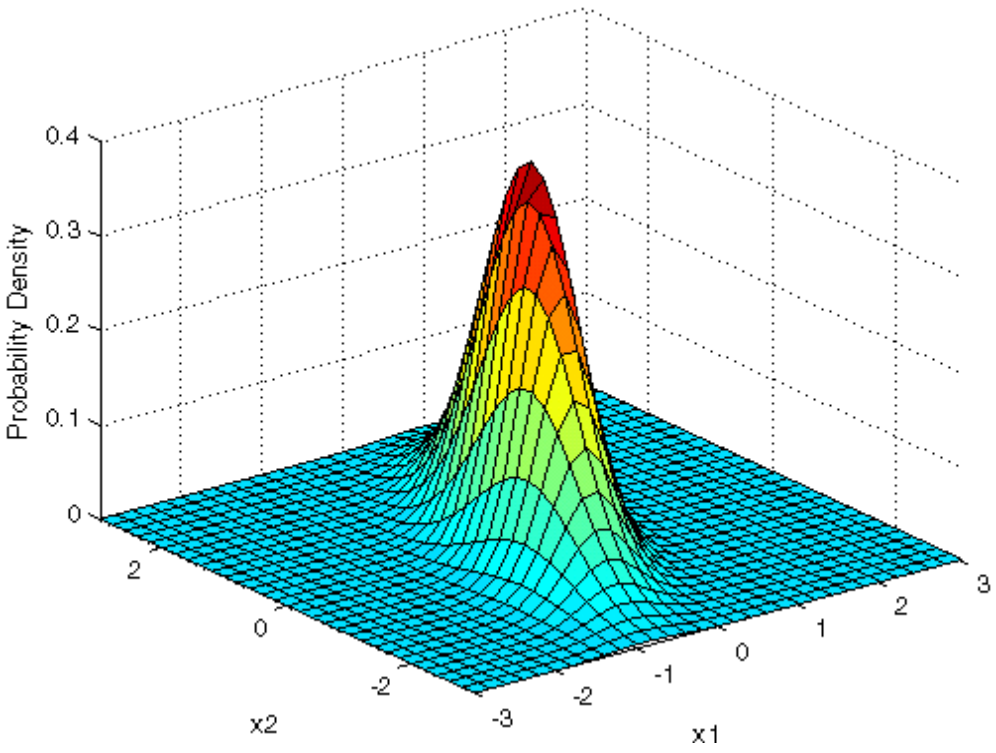

a) Probability Density

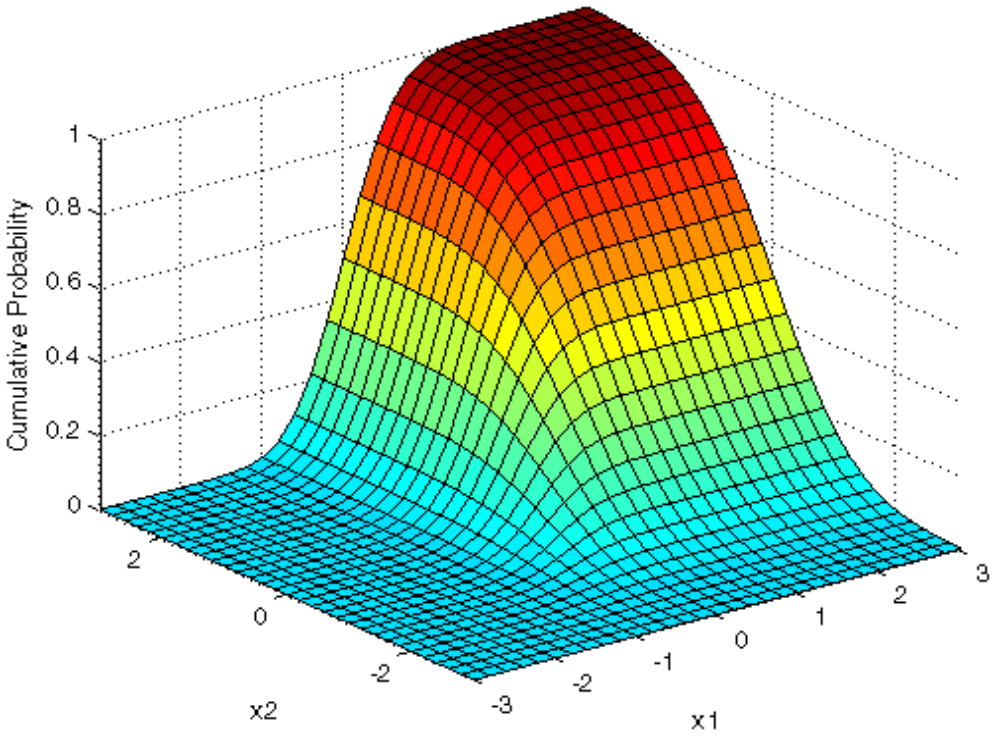

b) Cumulative Probability

Figure 18. Illustration of Joint Probability for Two Events

http://www.mathworks.com/help/toolbox/stats/brn2ivz-89.html

When the overall return frequency (probability) of a certain joint flood event is known (or reasonably estimated)—e.g., for the fourth channel say F_R of 0.02, or T_{500} , is 60,000 cfs—this return frequency can be considered the sum of all the joint probabilities for each combination of events that produces it—e.g., the three tributaries flows that can produce total flow exceeding 60,000 cfs. The joint probabilities for the various individual input combinations can then each be considered a fraction of 1 (and together they sum to 1) and the return frequency for any individual combination is thus the overall return frequency—0.02—multiplied by the fractional joint probability.

Advanced statistical techniques can be employed to select an optimal sample, or subset, of input combinations to represent the universe of combinations which sum to 0.02. For example a universe of thousands of combinations can be represented by a subset of 100 combinations. Each individual input combination is assigned a weight that is multiplied by its fractional joint probability. In this case one combination might be used to represent more than 1% of the contributing probabilities and so it could be weighted higher, e.g., at 0.015, while another representing less that 1% could be weighted lower, e.g. at 0.005. The weighted joint fractional probabilities of each combination in the subset again sum to 1, or an overall return frequency of 0.02. In this case the subset size and weightings are targeted to reduce the likelihood of error (uncertainty) in representing the joint probability "space" over a particular region—i.e., T_{500}.. This technique is known as JPM-Optimized Sample, or JPM-OS.

Depending on the number and distribution of contributing events, and the handling of uncertainty, joint probability analysis can be very computationally demanding. If conditions in one event are highly correlated to another—e.g., flow in two tributaries—these correlations can be used to reduce the number of independent events. With advances in computational resources, joint probability analysis has become a powerful tool in estimating a wide variety of recurrence events in river flood hydrology—such as the conjunction of a dam failure with extreme flood conditions.

K. Combining Deterministic and Probabilistic and Analysis

In *stochastic analysis* Hydrologists often combine deterministic and probabilistic methods. Processes that are described as *deterministic*—such as weir flow, which is a function of upstream stage, downstream stage (in the case where the weir is "drowned"), weir length, and the empirical weir crest friction coefficient—may have one or more input values and factors with appreciable random variability. Conducting a series of deterministic analyses (e.g., solutions to the weir equation) by varying an input value in accordance with its probability distribution (e.g., upstream stage) can provide the probability distribution of the output condition (weir flow). This combining of deterministic and probabilistic analysis is called *stochastic analysis*.

When more than one input value is characterized by a probability distribution, a joint probability analysis is also included. An example of stochastic analysis which also employs a joint probability analysis would be to examine the diversion flow rate at the Bonnet Carré Spillway using the defined weir length, a general value for the empirical crest friction coefficient (obtained from physical experiments on a scale model or from publications on similar weirs), and frequency distributions for the upstream and downstream stage. In this case the Monte Carlo technique could be employed to draw values for the two stages, which are then input into the weir equation to calculate the associated diversion flow. Repeating this draw hundreds of times and inputting the values into the weir equation yields a simulated record of diversion flows, which can be fitted with a probability distribution. The stochastic analysis can be expanded to also address uncertainty in the weir coefficient.

L. Flood Return Frequency Analysis

In locations with very sparse river gauge data the local flood hazard is evaluated in a flood RFA employing stochastic methods and three components:

- A rainfall return frequency probability distribution is developed using data from the nearest meteorological site, including the extrapolation of extreme rainfall return events.
- Overland flow and runoff within the basin (broken down into various sub-basins or watersheds) are analyzed for extreme rainfall events using empirical hydrologic models. In addition to the rainfall event, these models have inputs/conditions/coefficients/etc. for watershed characteristics (e.g., antecedent soil moisture, size, topography, land cover, runoff storage and losses, and distance to channel). This step translates the rainfall into input flow hydrographs at appropriate points along the overall river tributary system network.
- Flow routing within the channel network takes the set of input flow hydrographs and computes flood profiles throughout the network floodplain, using a one- or two-dimensional numerical model of the flow physics (i.e., a hydraulic model). These models require conditions/coefficients on conveyance (e.g., channel and floodplain bathymetric/ topographic data and friction—such as Manning's *n*), upstream and downstream boundary conditions, (e.g., pumping conditions for forced drainage systems), and selection of numerical settings.[10]

Local extreme (e.g., 100-year return) floods for a small basin are estimated using a single basin rainfall probability distribution input. Flood RFA for very large basins requires evaluating joint probabilities. Deterministic hydrologic and hydraulic models are employed to route a set of basin-wide rainfall events, creating a set of downstream synthetic flood events. The set of events can be developed using the full or optimized joint probability method or the Monte Carlo technique. The synthetic downstream results are then analyzed to determine the return frequency floods. The Monte Carlo technique can be used to address uncertainties for the input hydrographs, boundary conditions, conveyance properties and coefficients, and numeric parameters.

Stochastic modeling for flood RFA has been widely adopted by hydrologists throughout the world. In the U.S. most flood RFAs are performed for the federal NFIP with numerous applications in southeast Louisiana, including studies of drainage systems in the metropolitan New Orleans area. The NFIP has published guidelines for flood RFA (FEMA, 2009). The combination of rainfall RFA with deterministic hydrologic/hydraulic models can provide a very reasonable flood RFA. Three major limitations are:

a. High quality representative rainfall data from a nearby location;
b. Accurate available channel and floodplain data for setting conditions/coefficients for the hydrologic/hydraulic model; and
c. Adequate hindcast data for calibration and validation of the overall stochastic method.

[10] A discussion of river flood model numerics is beyond the scope of this General Technical Note. A discussion of numerical issues associated with two-dimensional surge modeling is presented in General Technical Note 5.

M. Sensitivity, Calibration, and Validation Tests

When hydrologists employ stochastic models—such as in a river flood RFA—the models must be tested to assess their accuracy (potential bias) and precision (uncertainty). Three types of tests are performed:

1. *Sensitivity tests* evaluate the influence of uncertainty in key input values (inflow hydrographs, boundary conditions, conveyance conditions/coefficients, numeric settings), which are not otherwise assessed (e.g., with the Monte Carlo technique). By varying an individual setting or parameter in a highly controlled way (i.e., by keeping all other inputs constant)—typically within a range of interest—a comprehensive set of sensitivity tests can rigorously evaluate the variability of model results. In practice, modelers often conduct limited sensitivity testing to assess selected variations in settings/parameters.

2. *Calibration tests* determine values for those conditions/coefficients/settings/etc. for which results are highly sensitive. The hydrologist simulate an actual historic flood—termed a *hindcast*—and compares the simulation results for flood stages and flow rates (velocities) to actual observed values. Comparing simulated versus observed peak values and/or hydrographs the hydrologist adjusts the conditions/coefficients/settings/etc. in the hydrologic and/or hydraulic model within accepted ranges to achieve a best fit. Calibration often requires judgment on whether or not to "tune" the input value to improve the simulation of a particular event. For example, it may not be appropriate to select a friction coefficient that calibrates a relatively shallow flood when many of the floods to be simulated involve deeply submerged flow. When there are multiple conditions/parameters, calibration tests must optimize the selection of values.

3. *Validation tests* assess the selected conditions/coefficients/settings/etc. for an additional separate hindcast. The results of this additional simulation are also compared to actual data. In addition to assessing the quality of hindcast values along the river network, in flood RFA an important validation test is to compare the computed flood frequency distribution with observed distributions for one or more long-term gauge stations.

The evaluation of sensitivity, calibration, and validation tests is similar to correlation and trend analysis. Graphs are usually made to compare model results versus observed data, or results from one simulation versus another in the case of sensitivity tests. These can include scatter plots of peak values across the river network and time-series hydrographs for selected locations. In the first case (see Figure 19) the test is judged by proximity of points to the line corresponding perfect agreement (slope of the line equals 1). In the second case (see Figure 20) the model hydrograph is plotted alongside the observed hydrograph.

The comparisons are then assessed for *accuracy*—bias, or deterministic variability or error—*and precision*—degree of random variation. Bias in comparing sensitivity test results (e.g., consistent offset) indicates that the model is sensitive to the input/condition/coefficient/setting/etc. being tested. Bias in a calibration or validation test—a consistent pattern of over- or under-prediction of the hindcast—indicates that the model has not captured (and may not be able to a capture) an important aspect of the physical process. Bias can be associated with local portions of the river network (e.g., along one particular reach) or they can by system-wide. Bias can arise from a limitation in the model input/conditions/coefficients/settings/etc or in the accuracy of the hindcast observations.

Bias in the results is not always easy to spot. The hydrologists must carefully review the results of calibration and validation tests to look for bias. Once UCL/LCLs are established for the random variation between model and observed results (see below), these can be used to assess the relative importance of biased results. If a sound theory on the source of bias can be identified and supported, the hydrologist can correct the model (e.g., adjusting channel depth or the friction coefficient) or the observed data (e.g., adjusting a stage observation to correct for a benchmark error). If corrections to the model and data are not supported, the data should be given priority and a method for post-simulation correction is required.

Following bias correction the random variation between two sensitivity tests, or between a calibration/validation test and the observation, is evaluated by computing RMSE and R^2 , and by examining the probability distribution for the remaining variation. The random variation distribution for a calibration/validation test is an indicator of uncertainty in the model. A normal distribution will usually be sufficient for many comparisons—such as the comparison of modeled and observed peaks and hydrographs in Figures 19 and 20. For some highly skewed comparisons—e.g., a predicted versus an observed flood return frequency distribution for a gauge station—a skewed probability distribution will be required. The distribution of uncertainty is used to determine UCL/LCLs above and below the model results.

The hydrologist may use the UCL/LCLs to note groups of points that reflect significant bias[11] or individual points that are markedly beyond the UCL/LCL—termed *outliers*. If there are reasons to believe that outliers are not valid, the hydrologist may exclude them. The uncertainty distribution and the UCL/LCLs are then recomputed following removal of bias and outliers.

The hydrologist will typically discuss the quality of test results in terms of the RMSE, R^2, and the spread of the UCL/LCL bands, and compare these values to other flood RFAs for regions with similar characteristics.

N. Application of Flood Return Frequency Analysis

Flood RFAs have five major applications:

1. *Flood Insurance Studies (FISs) under the NFIP.* Congress established the NFIP in 1968 and as part of the program set special 100- and 500-year flood hazard trigger levels for assessing insurance premiums. The NFIP establishes requirements for participating local communities to regulate floodplain development to reduce the likelihood of claims. Thus, the NFIP requires that these particular return period floods be determined and delineated on Flood Insurance Rate Maps (FIRMs).
2. *Flood Control Studies*. Flood control studies combine flood RFA—i.e., evaluation of the flood hazard—with estimates of potential consequences—e.g., property damages at the peak flood stage and lost economic production, loss of non-evacuee lives in cases of dam failure—in a *risk assessment*. Studies compare the benefits (risk reduction) associated with proposed flood control projects with the project costs. Selected projects then use the risk reduction criteria as the basis for design.

[11] Actual statistical significance of bias can be evaluated with a χ^2 Test.

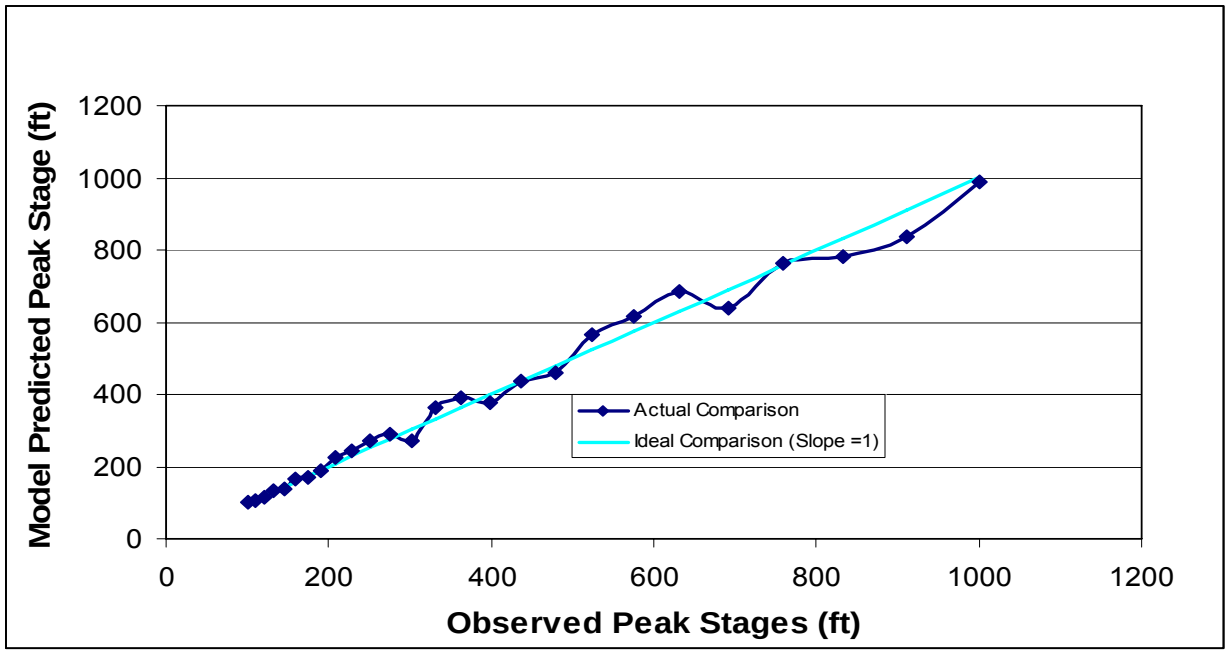

Figure 19. Example Comparison of Observed Versus Modeled Peak Stages

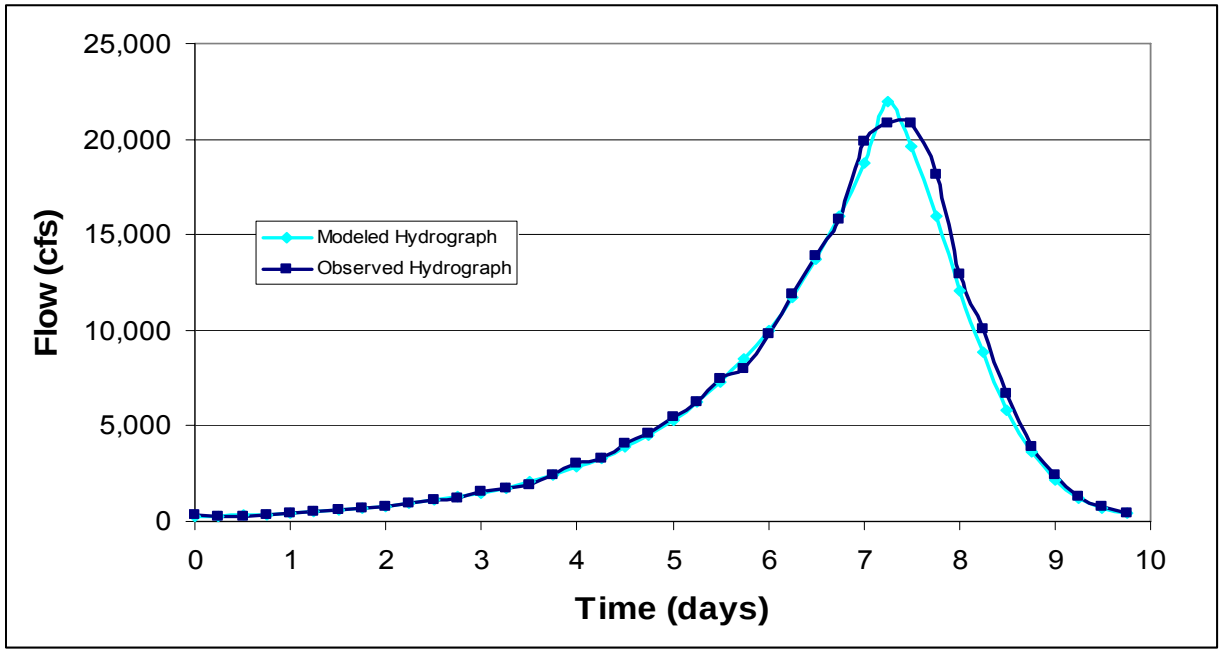

Figure 20. Example Comparison of Observed Versus Modeled Hydrograph

3. *Flood Impact Studies*. Urban and regional planners use flood RFAs to assess the potential for changing conditions to increase extreme flood returns and magnitudes. Common examples

include urbanization and regional land use changes, floodplain development, channel modifications, and flood control projects (which while reducing flooding in the target area may adversely affect flooding elsewhere). "What if" scenarios can be evaluated by changing appropriate inputs/conditions/coefficients in the flood stochastic model. The change in outcomes versus changes to the model can be examined using correlation analysis. Benefit-cost analysis is used in alternative evaluation.

4. *Flood Mitigation Studies*. Similar to flood impact studies, urban and regional planners use RFAs to assess ways of reducing extreme flood returns and magnitudes through urban runoff reduction, floodplain restoration, and channel modifications. These studies also model "what if" scenarios by changing model inputs/conditions/coefficients and examining correlations with model results. Benefit-cost analysis is used in alternative evaluation.

   Flood control, impact, and mitigation studies are strongly affected by Congress' design of the NFIP—as the benefit and costs often have abrupt discontinuities at the 100-year flood threshold. Items contributing to this threshold effect include insurance premium costs, floodplain development restrictions, property value decreases, and community growth impairment. If the NFIP addressed a comprehensive range of incremental flood hazards, then project costs and benefits would adjust more smoothly in response to a range of return period floods. Smaller communities might then opt for projects reducing 50-year floods, while larger urban areas might choose to construct 1,000-year protection (or higher).[12]

5. *Long-Term Flood Trend Studies*. Expected flood frequency distribution can be compared with actual flood recurrence at a gauge station to isolate long-term trends associated with underlying climatological, topographical, or other physical conditions. Similarly, long-term trends can be combined with the normal stochastic analysis to evaluate potential increases in return period floods. For example, the U.S. Army Corps of Engineers currently mandates use of long-term sea level rise forecasts in coastal river RFA (USACE 2009).

The treatment of bias is similar for all flood RFA applications. As previously noted, evidence of bias encountered during a flood RFA should be investigated and addressed. Recommendations for handling any significant residual bias should be explicitly discussed.

The treatment of uncertainty, however, often varies by applications of RFA. For example, FEMA NFIP guidance does not address accounting for uncertainty in the estimates of the 100-year flood elevations. This may be due, in part, to the particular actuarial approaches of the NFIP and the other tools available for management of financial risks to the program. The NFIP approach to flood thresholds and the RFA uncertainties, however, can color the treatment of uncertainty in other applications of flood RFA.

[12] The arbitrary NFIP flood insurance premium thresholds, combined with a general lack of understanding that a return period is an average recurrence interval over a much longer time-frame, contribute to distorted public perceptions of flood hazards and excessive skepticism about the science of flood RFA.

In flood control studies hydrologists may make allowances for uncertainty (e.g., use of confidence bands), and to a greater degree (e.g., wider confidence bands) consistent with considerations of

- Important gaps in model calibration/validation—e.g., lack of long-term gauge data to construct station RFAs for validating the stochastic model; and/or
- The risks associated with flooding and ramifications of uncertainty—e.g., problematic evacuation, vulnerable critical infrastructure.

Flood impact and mitigation studies may make different allowances for estimate uncertainties depending on study objectives. Thus, it is not uncommon for hydrologists to employ different estimates of the same flood hazard—e.g., the 100-year flood—depending upon the application.

O. Combined Probability of Return Floods Over Large Areas

Extreme flood events in distant river basins are basically independent events. Government agencies with large geographic jurisdictional responsibilities for flood hazards must consider the combination of return floods hazards when assessing their resources. For an agency that manages ten independent flood hazard locations (assume location floods are not mutually exclusive), the probabilities for a 100- and 500-year event occurring somewhere in a given year are 9.56% and 1.98%, respectively—not quite ten times the individual probability.

Combined probabilities can be further evaluated for longer time-frames using the Poisson distribution. Figures 21 illustrates the increasing probability of an occurrence for a 500-year return period floods with increasing time frame and increasing number of independent, not mutually exclusive, locations. For example, among 10 river basins over a 10-year time-frame there is an 18% probability for the occurrence of a 500-year event.

Uncertainty can significantly affect these combined probabilities. In the above example, if the return periods of the 500-yr events in the 10 independent river basins were really 250-yrs, the probability of one flood occurring in 10 years is 33% and not 18%.

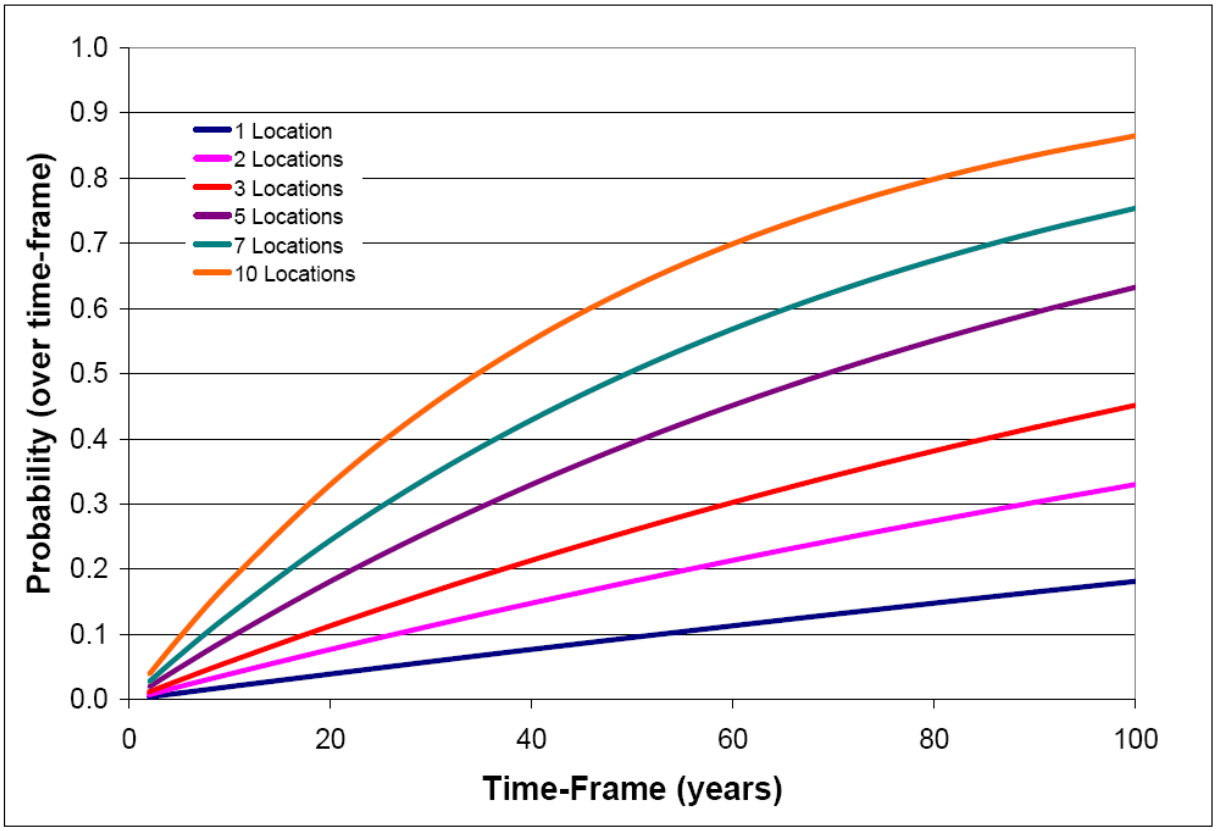

Figure 21. Return Frequency for Multiple Locations versus Time-Frame for 500-yr Flood

References

Chow, V. T., D. R. Maidment, and L. W. Mays, Applied Hydrology, McGraw-Hill, 1988.

Gerardo, B., M. Lang, M. Barriendos, M. C. Llasat, F. Francés, T. Ouarda, V. Yehouda Enzel, A. Bardossy, and A. Coeur, Use of Systematic, Palaeoflood and Historical Data for the Improvement of Flood Risk Estimation. Review of Scientific Methods, Natural Hazards Volume 31, Number 3, 623-643, 2004.

Goldman, D., Quantifying Uncertainty in Estimates of Regulated Flood Frequency Curves, Proceedings of World Water and Environmental Resources Congress 2001, Bridging the Gap: Meeting the World's Water and Environmental Resources Challenges.

Goldman, D., Upper Mississippi Flood Frequency Study, Uncertainty in Estimates of the 1% Profile, Prepared for Rock Island District, U. S. Army Corps of Engineers, Cold Regions Research and Engineering Laboratory, U.S. Army Corps of Engineers, Hanover, N.H., August 2003

Gordon, N. D., T. A. Mahon, B. L. Finlayson, C. J. Gippel, R. J. Nathan, Stream hydrology: An Introduction for Ecologists, John Wiley and Sons, 2004.

Karim, M. A., A comparison of four distributions used in flood frequency analysis in Bangladesh, Hydrological Sciences Journal, Volume 40, Issue No. 1, 1995.

Kochel, R. C., and V. R. Baker, Paleoflood Hydrology, Science, Vol. 215 no. 4531 pp. 353-361 January 22, 1982.

Mathworks, http://www.mathworks.com/help/toolbox/stats/brn2ivz-89.html

McCuen, R. H., and K.E. Galloway, Record Length Requirements for Annual Maximum Flood Series, Journal of Hydrologic Engineering Volume 15, Issue 9, Technical Notes, p. 704, 2010.

McMahon, T. A., and R. Srikanthan, Log Pearson III distribution — Is it applicable to flood frequency analysis of Australian streams? Journal of Hydrology. Volume 52, Issus 1-2, June 1981.

Nguyen, T., and N. In-Na, Plotting formula for pearson type III distribution considering historical information, Environmental Monitoring and Assessment, Volume 23, Numbers 1-3, 137-152, 1992.

Taleb, N. N., The Black Swan, The Impact of the Highly Improbable. Second Edition, Random House, 2010

U.S. Army Corps of Engineers (USACE), Incorporating Sea-Level Change Considerations in Civil Works Programs, Engineering Circular 1165-2-211, 2009.

U.S. Federal Highway Administration, HEC-19 Workshop Manual, http://www.fhwa.dot.gov/engineering/hydraulics/pubs/hec/hec19.pdf.

U.S. Federal Emergency Management Agency (FEMA), Guidelines and Specifications for Flood Hazard Mapping Partners, Appendix C: Guidance for Riverine Flooding Analyses and Mapping, November, 2009; http://www.fema.gov/library/viewRecord.do?id=2206.

U.S. Geological Survey, Guidelines for Determining Flood Flow Frequency, Bulletin 17B, 1982, http://water.usgs.gov/osw/bulletin17b/bulletin_17B.html.

Wang, H., D. Qin, J. Sun, and J. Wang, Study on the general model of hydrological frequency analysis, Science in China Series E: Technological Sciences, Volume 44, Supplement 1, 52-61, August 2001.

Zervas, C. E., Response of Extreme Storm Tide Levels to Long-term Sea Level Change, NOAA/National Ocean Service, Center for Operational Oceanographic Products and Services, 2005, http://tidesandcurrents.noaa.gov/est/050415-53.pdf.

General Note 2.
Elevation Data for
Hurricane Surge Hazard Analysis

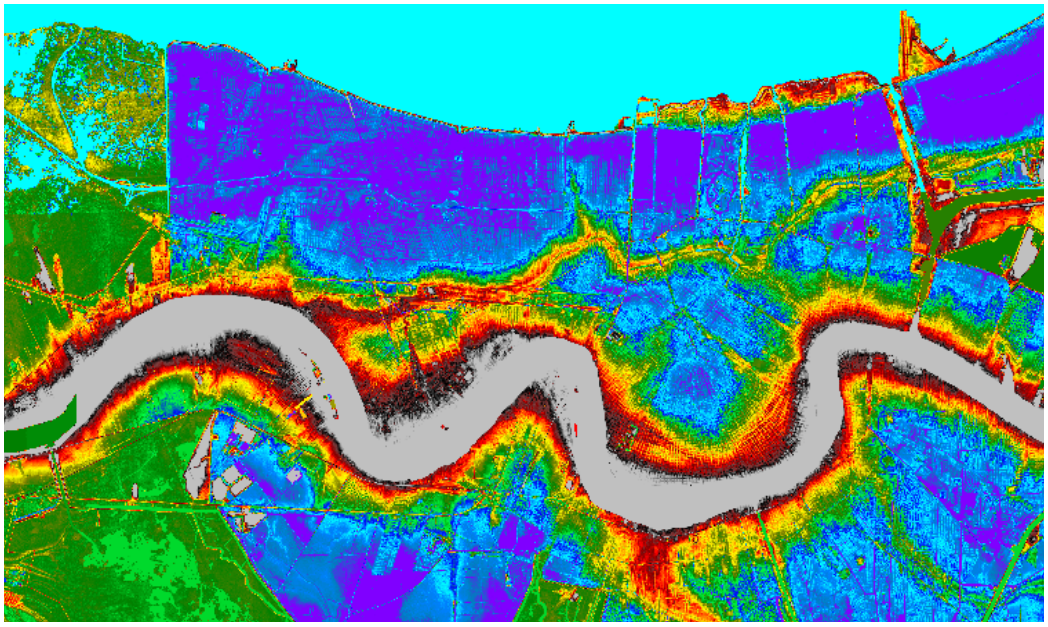

A major concern with any flood hazard analysis—including inundation from hurricane surge and associated waves—is accurate vertical data. This concern applies both to surge data (e.g., high water marks and gauge readings from past events) and to topographic and bathymetric data used in surge models and flood zone mapping. Issues include proper control, or referencing, to a uniform datum; treatment of regional and local subsidence; and development of digital elevation models (DEMs).

A. Elevation Datum

National Oceanic and Atmospheric Administration (NOAA) data are typically reported relative to a station-specific *tidal datum*—e.g., Local Mean Sea Level (LMSL), Mean Lower Low Water (MLLW), or Mean Higher High Water (MHHW) determined from the analysis of multi-decadal data at that station. U.S. Geological Survey (USGS) and U. S. Army Corps of Engineers (USACE) elevations are more commonly given relative to national references—e.g., the National Geodetic Vertical Datum of 1929 (NGVD29) or the North American Vertical Datum of 1988 (NAVD88), which until recently could only obtained by leveling (surveying) from the nearest recognized benchmarks.

NGVD29 and NAVD88 are both *geoid*-based references. The geoid is a three dimensional geometric surface where the earth's gravity has an equal given magnitude. (Gravity decreases with altitude, i.e., distance from the earth's center of mass.) The geoid represents something similar to a global MSL at which all the oceans would stabilize without winds, tides, Coriolis, and other forces. The geoid incorporates irregularities in the earth's general shape (nearly ellipsoidal but not perfectly so) and regional variations in gravity with changes in the thickness and density of the earth's crust. The most consistent and reliable geoid-based reference for hydrologic data is the NAVD88. Geodesists continue to obtain new gravitational and other information and periodically improve their model of the geoid, e.g., GEOID03, GEOID09, GEOID12, and GEOID12a.

Satellite-based global positioning system (GPS) survey methods facilitate *differential* vertical measurements (see Figure 1). The satellite locations are referenced to a perfect, idealized ellipsoid (not geoid) surrounding the earth. Surveyors use GPS to measure the ellipsoid heights of a point of interest (H_A) and a nearby location of known elevation—i.e., a benchmark (H_B). The benchmark has a previously established height with respect to the geoid—termed orthometric height (h_B). The difference at each location between the geoid and ellipsoid, termed the geoid height (N_A and N_B) is developed using the latest geoid model. With values for H_A , H_B , h_B , N_A ,and N_B , a value can be estimated for h_A .

Benchmarks in portions of the Gulf Coast are notoriously problematic due to the quality of initial leveling and subsequent aging from natural subsidence. In recent years the National Geodetic Survey (NGS) has sponsored installation of a network of Continuously Operating Reference Stations (CORS)—so-called "smart benchmarks"—to facilitate more accurate and precise differential GPS elevation measurements. The CORS network also supports *real-time kinetic* (RTK, or "on the go") GPS-based leveling with or without differential surveying of a physical benchmarks. GPS-based orthometric heights relative to the CORS network can generally be measured to within ± 1 inch with respect to the applied geoid model, with proper observation (Zilkoski 2011).

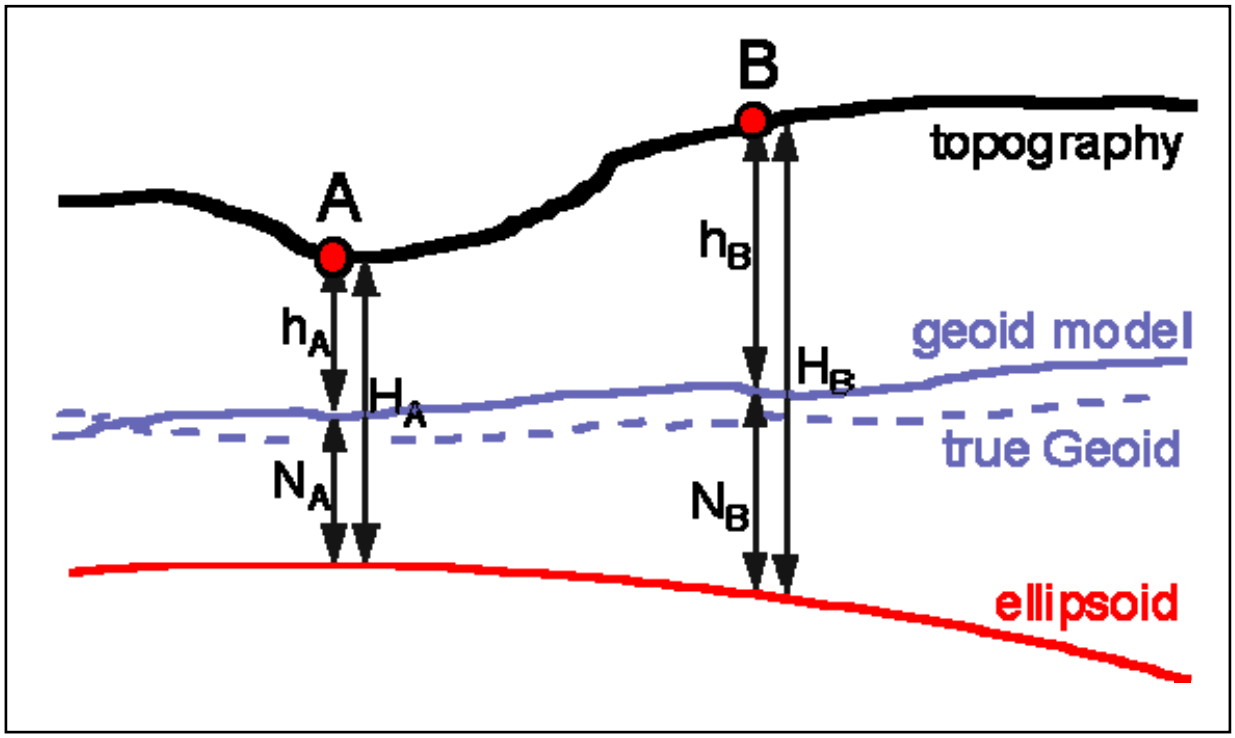

Figure 1. Illustration of Geoid and Ellipsoid
Wormley 2011

The CORS have facilitated refinements by NGS of the geoid model, significant enough to effect elevation values. Thus, references to NAVD88 should include the "epoch." "NAVD88" denotes use of older, pre-CORS control; such references are suspect as they are likely to be based on outdated benchmarks. "NAVD88-2004.65" and "NAVD88-2006.81" incorporate CORS-based control and the GEOID03 and GEOID09 models, respectively.

The LMSL reference at Grand Isle changed from 1.1 ft NAVD88, to 0.2 ft NAVD88-2004.65 with the implementation of the CORS and GEOID03, a change of 0.9 ft. Some areas were lowered even more, and a few were raised. With GEOID09, references to NAVD88-2006.81 versus NAVD88-2004.65 were generally lowered by another 0.08 to 0.16 ft (see Figure 2). Note that a change in the GEOID model is **NOT** a change in the LMSL itself. However, due to differences in the LMSL under different GEOID references it is critical that all elevation data employ the current epoch.[1]

For the purposes of hurricane surge hazard analysis, references to NAVD88-2005.65 can be readily adjusted to NAVD88-2006.81. However, data that referenced simply to NAVD88 or to NGVD29, MSL, MLLW, etc. must have their vertical control re-established. In many cases this cannot be done by a paper correction and requires resurvey of benchmarks or other approved means of re-referencing. The use of inadequately referenced vertical data, including the mixing of data of different reference quality, can contribute considerable uncertainty.

[1] The NGS and their local partner are continuing research on the GEOID model and methods of vertical control. The global error associated with the GEOID09 model is estimated to be about ± 2 inches (Zilkoski 2011).

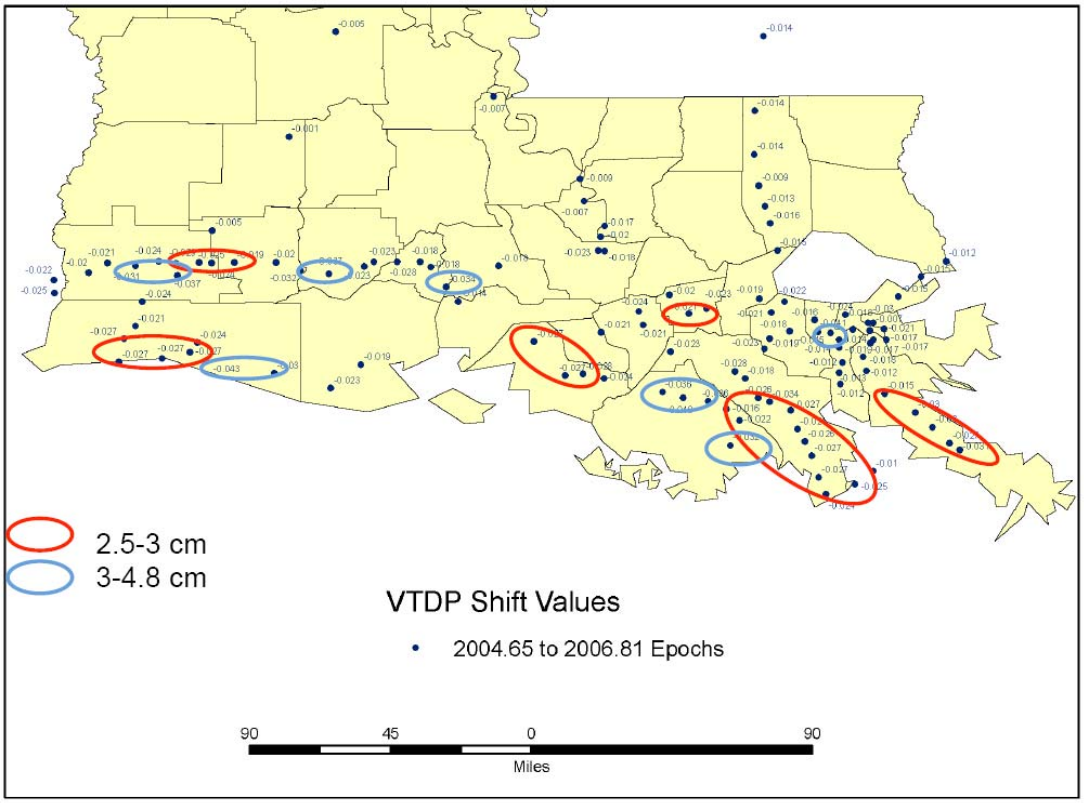

Figure 2. Differences between NAVD88-2006.81 versus NAVD88-2004.65
Shields 2011

B. Subsidence

Subsidence affects elevation measurements throughout coastal Louisiana—for land surfaces, water bottoms, roads, pile-supported structures (e.g., tide gauge structures), etc. Subsidence is influenced by numerous processes that impact different coastal regions in different ways (Reed and Yuill, 2009). These processes include:

- Tectonic subsidence
- Holocene sediment compaction
- Sediment loading
- Glacial isostatic adjustment
- Fluid withdrawal (oil and gas and groundwater)
- Surface water drainage and management

Local rates of subsidence must be considered in determining the potential for elevation data to become outdated. For example, at Grand Isle the local subsidence at the pile-supported tide station (apart from sea level rise) is on the order of 8 mm per year (Reed and Yuill 2009), or about 0.25 ft per decade. Some portions of southeast Louisiana experience higher subsidence rates. Thus, elevation data in many areas should be updated periodically to meet data quality requirements.

C. Digital Elevation Models

Hurricane surge hazard analysis makes extensive use of a regional digital elevation model (DEM), both in surge modeling and in mapping hazard areas. A DEM is a high resolution (dense pixel) representation of surface terrain and water bottoms. Figure 3 depicts a 5 meter grid (horizontal spacing) DEM for the topography of New Orleans. DEMs for surge modeling must often incorporate multiple sources of very large (terabyte) topographic and bathymetric datasets (see General Technical Note 5).

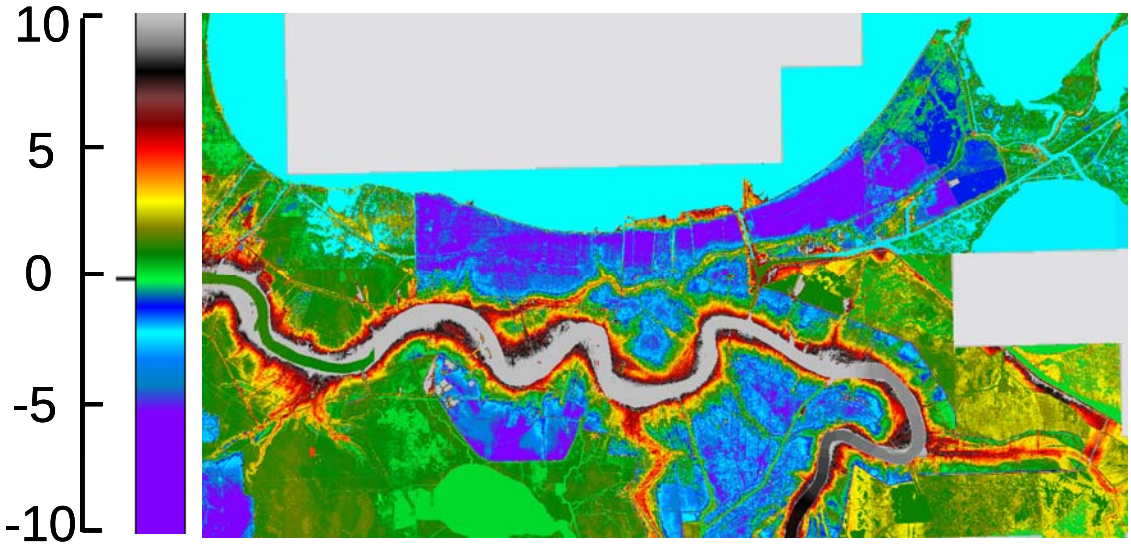

Figure 3. LIDAR DEM (ft) for New Orleans Area

Many sources of topographic data in coastal Louisiana, including numerous Light Detection and Ranging (LIDAR) data, were obtained in the 1990s and early 2000s, prior to the use of CORS corrected benchmarks and updated geoid models. Particular local and regional benchmark problems (e.g., sources of subsidence) can thus produce some significant general patterns of error in pre-CORS data. Figure 4 illustrates the discrepancies found between a 2006 CORS-based survey in Plaquemines Parish and previous pre-CORS LIDAR.

Louisiana bathymetric data sources for coastal bays, lakes, and sounds are often much older, frequently pre-dating World War II (e.g., Lake Pontchartrain). Many of these sources reference an approximate local tidal datum (e.g., local MLLW). Bathymetric data on numerous channels dredged for oil and gas activity are not even available. Some navigation channels may have initial or maintenance dredging plans but no accurate actual bank-to-bank bathymetric data.

Potential sources of data for a DEM can thus reflect widely varying accuracy (bias) and precision (uncertainty). Ultimately, all data used for a DEM should be referenced to NAVD88-2006.81 and meet objectives for accuracy and precision.[2]

[2] These objectives are set forth in project management plans consistent with particular goals of the program undertaking the hazard analysis and DEM development—e.g., a coastal Flood Insurance Study, a regional coastal planning and feasibility study, a flood control project design. DEM data quality objectives can be different under different programs.

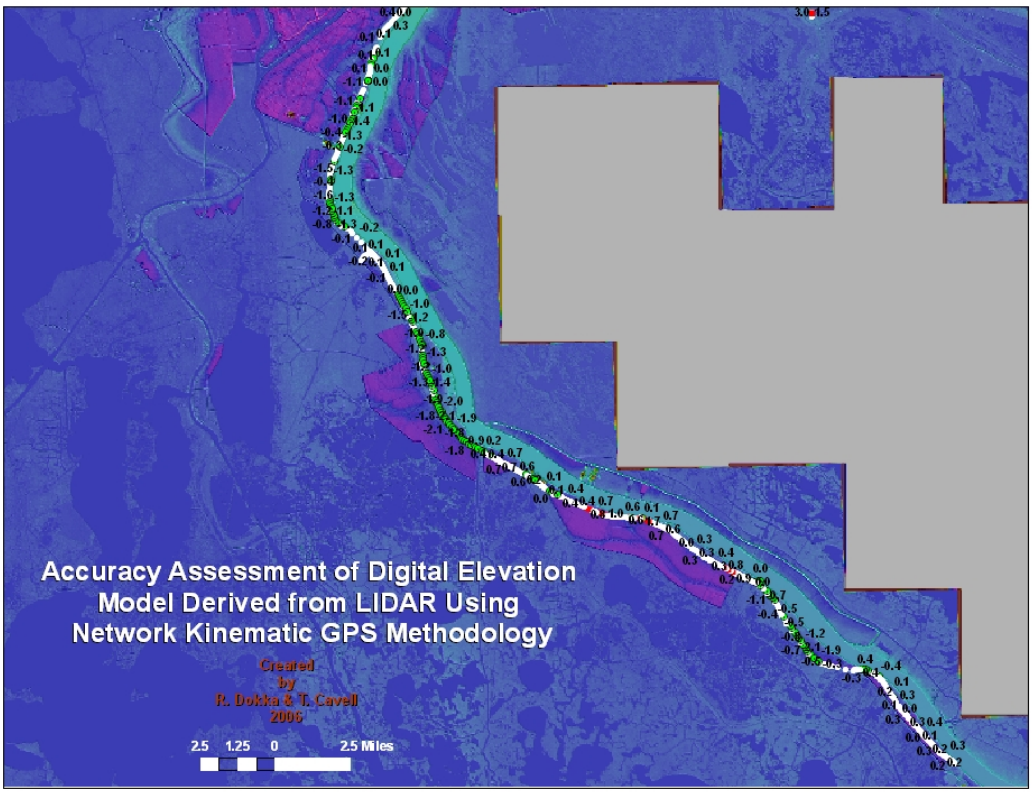

Figure 4. LIDAR DEM versus Updated Survey in Plaquemines Parish

Dokka and Cavell 2006

Green points denote (LIDAR – Current Survey) > 0.8 ft

References

Dokka, R. and T. Cavell, Accuracy Assessment of a portion of a Lidar-based Digital Elevation Model (DEM) of the Louisiana Coast—Southeast Louisiana, prepared for URS Corporation, September 21, 2006, under contract for the U.S. Army Corps of Engineers Louisiana Coastal Protection and Restoration Study.

National Oceanic and Atmospheric Administration, Tidal and Geodetic Datums: Tidal and Geodetic Relationships, http://www.laseagrant.org/pdfs/NOAA_TidalGeodeticRelationships.pdf

Reed, D. J., and B. Yuill, Understanding Subsidence in Coastal Louisiana, For the Louisiana Coastal Area Science and Technology Program, February 26, 2009, http://www.mvd.usace.army.mil/lcast/pdfs/UNO_SubsidenceinLA_09.pdf

Shields R., Vertical Geodetic Control in Southern Louisiana, in R. Dokka, T. Osborne, R. Shields, C. Mugnier, D. Zilkoski, G. Mader, and M. Schenewerk, National Static GPS/RTN Best Practices Seminar, June 20, 1011, Center for GeoInformatics, Louisiana State University, http://c4g.lsu.edu/c4g15/

Wormley, Samuel J., Orthometric Height, 2011, http://edu-observatory.org/gps/height.html

Zilkoski, D., Guidelines for Establishing GPS-Derived Ellipsoid and Orthometric Heights, in R. Dokka, T. Osborne, R. Shields, C. Mugnier, D. Zilkoski, G. Mader, and M. Schenewerk, National Static GPS/RTN Best Practices Seminar, June 20, 1011, Center for GeoInformatics, Louisiana State University, http://c4g.lsu.edu/c4g15/